



nutrients

Nutraceuticals and Human Health

Edited by

Anna Scotto d'Abusco

Printed Edition of the Special Issue Published in *Nutrients*

Nutraceuticals and Human Health

Nutraceuticals and Human Health

Editor

Anna Scotto d'Abusco

MDPI • Basel • Beijing • Wuhan • Barcelona • Belgrade • Manchester • Tokyo • Cluj • Tianjin



Editor

Anna Scotto d'Abusco
Sapienza University of Roma.P.le Aldo Moro
Italy

Editorial Office

MDPI
St. Alban-Anlage 66
4052 Basel, Switzerland

This is a reprint of articles from the Special Issue published online in the open access journal *Nutrients* (ISSN 2072-6643) (available at: https://www.mdpi.com/journal/nutrients/special_issues/nutraceuticals_health).

For citation purposes, cite each article independently as indicated on the article page online and as indicated below:

LastName, A.A.; LastName, B.B.; LastName, C.C. Article Title. *Journal Name* **Year**, *Volume Number*, Page Range.

ISBN 978-3-0365-0444-5 (Hbk)

ISBN 978-3-0365-0445-2 (PDF)

© 2021 by the authors. Articles in this book are Open Access and distributed under the Creative Commons Attribution (CC BY) license, which allows users to download, copy and build upon published articles, as long as the author and publisher are properly credited, which ensures maximum dissemination and a wider impact of our publications.

The book as a whole is distributed by MDPI under the terms and conditions of the Creative Commons license CC BY-NC-ND.

Contents

About the Editor	ix
Preface to "Nutraceuticals and Human Health"	xi
Paola De Cicco, Maria Maisto, Gian Carlo Tenore and Angela Ianaro Olive Leaf Extract, from <i>Olea europaea</i> L., Reduces Palmitate-Induced Inflammation via Regulation of Murine Macrophages Polarization Reprinted from: <i>Nutrients</i> 2020, 12, 3663, doi:10.3390/nu12123663	1
Azlinza Ibrahim, Nurul Husna Shafie, Norhaizan Mohd Esa, Siti Raihanah Shafie, Hasnah Bahari and Maizatun Atmadini Abdullah <i>Mikania micrantha</i> Extract Inhibits HMG-CoA Reductase and ACAT2 and Ameliorates Hypercholesterolemia and Lipid Peroxidation in High Cholesterol-Fed Rats Reprinted from: <i>Nutrients</i> 2020, 12, 3077, doi:10.3390/nu12103077	19
Papawee Saiki, Yasuhiro Kawano, Takayuki Ogi, Prapaipat Klungsupaya, Thanchanok Muangman, Wimonsri Phantanaprates, Papitchaya Kongchinda, Nantaporn Pinnak and Koyomi Miyazaki Purified Gymnemic Acids from <i>Gymnema inodorum</i> Tea Inhibit 3T3-L1 Cell Differentiation into Adipocytes Reprinted from: <i>Nutrients</i> 2020, 12, 2851, doi:10.3390/nu12092851	35
Małgorzata Zakłós-Szyda, Nina Pietrzyk, Marcin Szustak and Anna Podśędek <i>Viburnum opulus</i> L. Juice Phenolics Inhibit Mouse 3T3-L1 Cells Adipogenesis and Pancreatic Lipase Activity Reprinted from: <i>Nutrients</i> 2020, 12, 2003, doi:10.3390/nu12072003	49
Alcides C. de Morais Junior, Raquel M. Schincaglia, Marisa Passarelli, Gustavo D. Pimentel and João F. Mota Acute Epigallocatechin-3-Gallate Supplementation Alters Postprandial Lipids after a Fast-Food Meal in Healthy Young Women: A Randomized, Double-Blind, Placebo-Controlled Crossover Study Reprinted from: <i>Nutrients</i> 2020, 12, 2533, doi:10.3390/nu12092533	79
Marlhyn Valero-Pérez, Laura M. Bermejo, Bricia López-Plaza, Meritxell Aguiló García, Samara Palma-Milla and Carmen Gómez-Candela Regular Consumption of Lipigo® Promotes the Reduction of Body Weight and Improves the Rebound Effect of Obese People Undergo a Comprehensive Weight Loss Program Reprinted from: <i>Nutrients</i> 2020, 12, 1960, doi:10.3390/nu12071960	89
Dushyant Kshatriya, Lihong Hao, Xinyi Li and Nicholas T. Bello Raspberry Ketone [4-(4-Hydroxyphenyl)-2-Butanone] Differentially Effects Meal Patterns and Cardiovascular Parameters in Mice Reprinted from: <i>Nutrients</i> 2020, 12, 1754, doi:10.3390/nu12061754	103
Attila Biró, Arnold Markovics, Mónika Éva Fazekas, Gábor Fidler, Gábor Szalóki, Melinda Paholcsek, János Lukács, László Stündl and Judit Remenyik Allithiamine Alleviates Hyperglycaemia-Induced Endothelial Dysfunction Reprinted from: <i>Nutrients</i> 2020, 12, 1690, doi:10.3390/nu12061690	121

Alessia Mariano, Antonella Di Sotto, Martina Leopizzi, Stefania Garzoli, Valeria Di Maio, Marco Gulli, Pietro Dalla Vedova, Sergio Ammendola and Anna Scotto d'Abusco Antiarthritic Effects of a Root Extract from <i>Harpagophytum procumbens</i> DC: Novel Insights into the Molecular Mechanisms and Possible Bioactive Phytochemicals Reprinted from: <i>Nutrients</i> 2020 , <i>12</i> , 2545, doi:10.3390/nu12092545	135
Joan Cunill, Clara Babot, Liliana Santos, José C. E. Serrano, Mariona Jové, Meritxell Martin-Garí and Manuel Portero-Otín In Vivo Anti-Inflammatory Effects and Related Mechanisms of Processed Egg Yolk, a Potential Anti-Inflammatory Dietary Supplement Reprinted from: <i>Nutrients</i> 2020 , <i>12</i> , 2699, doi:10.3390/nu12092699	151
Lilia A. Koza, Aimee N. Winter, Jessica Holsopple, Angela N. Baybayon-Grandgeorge, Claudia Pena, Jeffrey R. Olson, Randall C. Mazzarino, David Patterson and Daniel A. Linseman Protocatechuic Acid Extends Survival, Improves Motor Function, Diminishes Gliosis, and Sustains Neuromuscular Junctions in the hSOD1 ^{G93A} Mouse Model of Amyotrophic Lateral Sclerosis Reprinted from: <i>Nutrients</i> 2020 , <i>12</i> , 1824, doi:10.3390/nu12061824	163
Matthew Sharp, Kazim Sahin, Matthew Stefan, Cemal Orhan, Raad Gheith, Dallen Reber, Nurhan Sahin, Mehmet Tuzcu, Ryan Lowery, Shane Durkee and Jacob Wilson Phytoplankton Supplementation Lowers Muscle Damage and Sustains Performance across Repeated Exercise Bouts in Humans and Improves Antioxidant Capacity in a Mechanistic Animal Reprinted from: <i>Nutrients</i> 2020 , <i>12</i> , 1990, doi:10.3390/nu12071990	187
Marinela Bostan, Georgiana Gabriela Petrică-Matei, Nicoleta Radu, Razvan Hainarosie, Cristian Dragos Stefanescu, Carmen Cristina Diaconu and Viviana Roman The Effect of Resveratrol or Curcumin on Head and Neck Cancer Cells Sensitivity to the Cytotoxic Effects of Cisplatin Reprinted from: <i>Nutrients</i> 2020 , <i>12</i> , 2596, doi:10.3390/nu12092596	203
Andrea Garolla, Gabriel Cosmin Petre, Francesco Francini-Pesenti, Luca De Toni, Amerigo Vitagliano, Andrea Di Nisio and Carlo Foresta Dietary Supplements for Male Infertility: A Critical Evaluation of Their Composition Reprinted from: <i>Nutrients</i> 2020 , <i>12</i> , 1472, doi:10.3390/nu12051472	227
Stefania D'Angelo, Maria Letizia Motti and Rosaria Meccariello ω -3 and ω -6 Polyunsaturated Fatty Acids, Obesity and Cancer Reprinted from: <i>Nutrients</i> 2020 , <i>12</i> , 2751, doi:10.3390/nu12092751	243
Felice Crocetto, Mariarosaria Boccellino, Biagio Barone, Erika Di Zazzo, Antonella Sciarra, Giovanni Galasso, Giuliana Settembre, Lucio Quagliuolo, Ciro Imbimbo, Silvia Boffo, Italo Francesco Angelillo and Marina Di Domenico The Crosstalk between Prostate Cancer and Microbiota Inflammation: Nutraceutical Products Are Useful to Balance This Interplay? Reprinted from: <i>Nutrients</i> 2020 , <i>12</i> , 2648, doi:10.3390/nu12092648	265
Fabiana Superti Lactoferrin from Bovine Milk: A Protective Companion for Life Reprinted from: <i>Nutrients</i> 2020 , <i>12</i> , 2562, doi:10.3390/nu12092562	287

**Mirko Magnone, Laura Sturla, Lucrezia Guida, Sonia Spinelli, Giulia Begani,
Santina Bruzzone, Chiara Fresia and Elena Zocchi**
Abscisic Acid: A Conserved Hormone in Plants and Humans and a Promising Aid to Combat
Prediabetes and the Metabolic Syndrome
Reprinted from: *Nutrients* **2020**, *12*, 1724, doi:10.3390/nu12061724 **313**

About the Editor

Anna Scotto d'Abusco Senior Scientist since 2001, researcher at the Faculty of Pharmacy and Medicine, Sapienza University of Roma

1987: Masters Degree in Biological Sciences, University of Naples "Federico II"

1995: specialization in Biotechnological Applications, University of Roma "Tor Vergata"

Research interests: The study of the onset and progression of osteoarthritis (OA), the most common rheumatic disease.

The study of the features of synoviocytes from OA joints, with particular attention to the low-grade, chronic inflammation that is typical of this pathology.

The study of some herbal extracts, with the aim to find molecules or phytocomplexes that are able to reduce the inflammation that is typical of OA.

The study of polymers, with the aim to find good substrates for tissue repair, in particular hyaluronic acid and poly L-lactide.

The study of the effects of glucosamine and its peptidyl-derivatives on intracellular pathways involved in both the inflammatory response and in the synthesis of the extracellular matrix (ECM), in OA progression using human primary chondrocytes as an experimental model.

The study of the effects of glucosamine-derivatives on osteosarcoma and prostate carcinoma cell lines as well as on ageing and skin cancer induced by UVB radiation on the skin.

Most relevant publications (last 5 years):

- Silvestro I et al. Hyaluronic Acid Reduces Bacterial Fouling and Promotes Fibroblasts' Adhesion onto Chitosan 2D-Wound Dressings. *Int J Mol Sci.* 21(6):2070, 2020. doi: 10.3390/ijms21062070.
- Lopreiato M et al. The Glucosamine-derivative NAPA Suppresses MAPK Activation and Restores Collagen Deposition in Human Diploid Fibroblasts Challenged with Environmental Levels of UVB. *Photochem Photobiol.* 96(1):74-82, 2020. doi: 10.1111/php.13185.
- Francolini I et al. Graphene Oxide Oxygen Content Affects Physical and Biological Properties of Scaffolds Based on Chitosan/Graphene Oxide Conjugates. *Materials (Basel)* 12(7). pii: E1142, 2019. doi: 10.3390/ma12071142.
- Cocchiola R et al. The Induction of Maspin Expression by a Glucosamine-Derivative has an Antiproliferative Activity in Prostate Cancer Cell Lines. *Chem Biol Interact* 300:63-72, 2019. doi: 10.1016/j.cbi.2019.01.014.
- Ammendola S et al. Effects of Nutrients, Mainly from Mediterranean Dietary Foods, on Mesenchymal Stem Derived Cells: Growth or Differentiation. *t J Clin Nutr & Diet* 4:131, 2018. doi: 10.15344/2456-8171/2018/131.
- Ammendola S et al. Olive fruit blends modulate lipid-sensing nuclear receptor PPAR γ , cell survival and oxidative stress response in human osteoblast cells. *J Am College f Nutrition* 37:589-597, 2018. doi: 10.1080/07315724.2018.1451409.
- Ammendola S et al. Modulatory effects of a nutraceutical supplement on Saos-2 cells reveal its phlebotonic activity. *J Am College f Nutrition* 36(4): 268-272, 2017. doi: 10.1080/07315724
- Leopizzi M et al. IKK α inhibition by a glucosamine derivative enhances maspin expression in osteosarcoma cell line. *Chem Biol Inter* 262:19-28, 2017. doi: 10.1016/j.cbi.2016.12.005

- Bellini D et al. PLA-grafting of collagen chains leading to a biomaterial with mechanical performances useful in tendon regeneration. *J Mech Behav Biomed Mater* 64:151-160, 2016. doi: 10.1016/j.jmbbm.2016.07.006.
- Stoppoloni et al. Effect of glucosamine and its peptidyl-derivative on the production of extracellular matrix components by human primary chondrocytes. *Osteoarthritis Cartilage* 23(1):103-113, 2015 . doi: 10.1016/j.joca.2014.09.005.

Preface to “Nutraceuticals and Human Health”

In this Special Issue of *Nutrients*, we collected papers on the health-promoting effect of nutraceuticals, taking into account both healthy individuals and patients affected by different pathologies. At present, nutraceuticals are very rarely administered to treat diseases, in contrast to their widespread utilization against aging and stress, and to serve as dietary supplements for athletes.

Several studies on compositions, formulations, and nutraceutical delivery have been conducted so far, with inconsistent outcomes. Particularly, the debate on secondary and rare adverse effects of some nutraceuticals and their safety and effectiveness is very interesting. In recent years, the health claims of a large number of nutraceuticals have not been confirmed by the FDA and EFSA agencies. Therefore, further research is required to more extensively analyze the mechanism of action of molecules that are predicted to function as useful nutraceuticals.

Anna Scotto d’Abusco

Editor

Article

Olive Leaf Extract, from *Olea europaea* L., Reduces Palmitate-Induced Inflammation via Regulation of Murine Macrophages Polarization

Paola De Cicco *, Maria Maisto, Gian Carlo Tenore and Angela Ianaro

Department of Pharmacy, School of Medicine, University of Naples Federico II, 80138 Naples, Italy; maria.maisto@unina.it (M.M.); giancarlo.tenore@unina.it (G.C.T.); ianaro@unina.it (A.I.)

* Correspondence: paola.decicco@unina.it

Received: 30 October 2020; Accepted: 23 November 2020; Published: 28 November 2020

Abstract: Olive tree (*Olea europaea* L.) leaves are an abundant source of bioactive compounds with several beneficial effects for human health. Recently, the effect of olive leaf extract in obesity has been studied. However, the molecular mechanism in preventing obesity-related inflammation has not been elucidated. Obesity is a state of chronic low-grade inflammation and is associated with an increase of pro-inflammatory M1 macrophages infiltration in the adipose tissue. In the current study, we explored *Olea europaea* L. leaf extract (OLE) anti-inflammatory activity using an in vitro model of obesity-induced inflammation obtained by stimulating murine macrophages RAW 264.7 with high dose of the free fatty acid palmitate. We found that OLE significantly suppressed the induction of pro-inflammatory mediators, tumor necrosis factor (TNF)- α , interleukin (IL)-6, IL-1 β , nitric oxide (NO), prostaglandin E2 (PGE2) and reactive oxygen species (ROS), while it enhanced the anti-inflammatory cytokine, IL-10. Moreover, we demonstrated that OLE reduced the oxidative stress induced by palmitate in macrophages by regulating the NF-E2-related factor 2 (NRF2)–Kelch-like ECH-associated protein 1 (KEAP1) pathway. Finally, we showed that OLE promoted the shift of M1 macrophage toward less inflammatory M2-cells via the modulation of the associated NF- κ B and proliferator-activated receptor gamma (PPAR γ) signaling pathways. Thereby, our findings shed light on the potential therapeutic feature of OLE in recovering obesity-associated inflammation via regulating M1/M2 status.

Keywords: obesity; nutraceuticals; olive leaf; macrophages; inflammation

1. Introduction

Obesity is one of the main threats to global human health and life expectancy. According to the World Health Organization (WHO), obesity levels have nearly tripled since 1975 and it has been estimated that in 2016 about 13% of the world's adult population (11% of men and 15% of women) were obese [1]. High-fat diet (HFD)-induced obesity is associated with a chronic state of low-grade inflammation which increases the risk of developing obesity-associated diseases such as type 2 diabetes, cardiovascular diseases, musculoskeletal disorders and cancer [2]. The major players implicated in the inflammatory response observed in the obese adipose tissue are the pro-inflammatory macrophages [3–5]. Macrophages are a heterogeneous population of cells that are instrumental in initiating the innate immune response. They represent almost the 40% of all adipose tissue cells in obese mice compared to 10% in lean mice [3]. In addition to their numbers, adipose tissue macrophages (ATMs) in lean and obese animals exhibit distinct phenotype and functions. In particular, two different macrophage populations have been found in adipose tissue: the classically activated macrophages or M1 (pro-inflammatory) and the alternatively activated macrophages or M2 (anti-inflammatory). In the lean state, M2 macrophages predominate in order to maintain tissue homeostasis and insulin

sensitivity by secreting the anti-inflammatory cytokine interleukin (IL)-10. By contrast, during weight gain, M1 macrophages proliferate greatly and replace the M2 macrophages to control and sustain a chronic inflammation state through the release of pro-inflammatory mediators, such as tumor necrosis factor (TNF)- α , IL-6, IL-1 β , reactive oxygen species (ROS), prostaglandin E2 (PGE2) and nitric oxide (NO) [6,7]. ATM numbers and/or pro-inflammatory gene expression are negatively associated with weight loss in obese subjects [8]. Moreover, the ratio of M1 to M2 cells in adipose tissue are positively correlated to the incidence of insulin resistance in obesity [9]. Diet and lifestyle may affect ATM polarization in obesity. Indeed, a saturated fatty acid (SFA)-rich diet induced upregulation of inflammatory genes and chemokines expression. Similarly, a high-carbohydrate meal also promotes inflammatory activation of macrophages [10,11]. Obese patients have significantly increased levels of free fatty acids (FFAs), in particular palmitate, in the blood [12]. Palmitate has been postulated to induce an inflammatory response mediating classical activation of macrophages in obesity by directly engaging toll-like receptors (TLR) and inducing Nuclear Factor kappa-light-chain-enhancer of activated B cells (NF- κ B)-dependent production of inflammatory cytokines such as TNF- α and IL-6 and by generation of ROS [13,14]. Accordingly, manipulation of M1/M2 homeostasis has been shown to be an effective strategy to control obesity and obesity-related diseases. Indeed, recent studies have demonstrated that infusion of IL-4, which is necessary for M2 macrophage activation, or M2 macrophages themselves could ameliorate obesity and insulin resistance in HFD mice [15,16]. Natural products provide abundant resources for anti-inflammatory compounds with potential benefits for obese patients. Various dietary components including long chain omega-3 fatty acids, antioxidant vitamins, plant flavonoids, prebiotics and probiotics have demonstrated the potential to prevent chronic inflammatory conditions [17]. *Olea europaea* L. is a fruit tree native to Asia Minor and Syria, which is now widely cultivated in the Mediterranean region. The main product extracted from the olive tree is extra-virgin olive oil (EVOO), one of the bases of the Mediterranean Diet, which is very popular for its nutritive and healthy effects particularly given the high contents of monounsaturated fatty acids as well as of other minor and worthy components like phenolics, phytosterols, tocopherols and squalene (1–2%) [18]. However, olea by-products represent rich sources of bioactive molecules; in particular, olive leaves contain phenolic compounds in amounts higher than EVOO. For example, the amount of oleuropein, which is the most abundant phenolic compound in olive leaves, ranges from 0.005% and 0.12% in EVOO while in olive leaves it ranges between 1% and 14% [19]. Among the other main polyphenols identified in olive leaf extract are hydroxytyrosol, verbascoside, apigenin and luteolin [20]. Over the centuries, extracts from olive leaves have been used for the treatment of many diseases thanks to their numerous beneficial effects to human health, such as anti-oxidant, anti-hypertensive, cardioprotective and anti-inflammatory effects [18]. Moreover, olive leaf extract has demonstrated anti-obesity effects by regulating molecular pathways involved in thermogenesis and adipogenesis [21,22]. However, the molecular mechanism of olive leaf extract in preventing obesity-related inflammation has not been elucidated. Thus, in the present study, we investigated the anti-inflammatory effects of *Olea europaea* L. leaf extract using an in vitro model of obesity-induced inflammation obtained by stimulating murine macrophages RAW 264.7 with a high dose of palmitate. Furthermore, we report novel findings relating to the ability of OLE to regulate the M1/M2 status via the modulation of the associated NF- κ B and proliferator-activated receptor gamma (PPAR γ) signaling pathways.

2. Materials and Methods

2.1. Cell Culture

RAW 264.7 macrophage cells were purchased from the American Type Culture Collection (ATCC), and cultured in Dulbecco's Modified Eagle Medium (DMEM) containing 10% fetal bovine serum (FBS), 2 mmol/L L-glutamine, penicillin (100 U/mL), streptomycin (100 μ g/mL) and 1 mmol/L sodium

pyruvate (all from Gibco, Thermo Fisher Scientific, Rodano (MI), Italy). Cells were grown at 37 °C in a humidified incubator under 5% CO₂.

2.2. Sodium Palmitate (SP) Preparation

Sodium palmitate (P9767; Sigma-Aldrich) was prepared by diluting a 200 mM stock solution in 70% ethanol into 10% fatty acid-free, low-endotoxin bovin serum albumin (BSA) (A-8806; Sigma-Aldrich; adjusted to pH 7.4) by heating at 50 °C. The palmitate-BSA stock solution was filtered using a 0.22-µm low-protein binding filter (Millipore, Billerica, MA, USA). Sodium palmitate was added at 0.5 mM. BSA/70% ethanol (10%) was used as vehicle in control cells.

2.3. Olive Leaf Extract (OLE) Preparation

Olive leaf extract was obtained by *Olea europea* L cultivar Ravece. Fresh leaves were collected from the rural region of Avellino, in the south of Italy, in the month of October 2019. 10 g of lyophilized raw material were extracted with 100 mL pure ethanol (1.59010; Sigma; food-grade solvent) for 4 h in darkness and at room temperature. The extract obtained was centrifuged (10 min at 8000 rpm) and supernatant underwent a spray-drying process with maltodextrins (Farmalabor, Canosa, Italy) as support, obtaining a fine powder, which was used for the in vitro experiments. This product was formulated by the Department of Pharmacy, University of Naples “Federico II” (Naples, Italy). Large scale production of OLE has been accomplished by MB Med Company (Turin, Italy).

2.4. High-Performance Liquid Chromatography (HPLC)/Diode-Array Detector (DAD) Analyses of OLE Polyphenols

The content of polyphenols in OLE were monitored by HPLC-DAD analysis, following the method described by Xie et al., with slight modifications. Analyses were run on a Jasco Extrema LC-4000 system (Jasco Inc., Easton, MD) provided with photo DAD. The column selected was a Kinetex[®] C18 column (250 mm × 4.6 mm, 5 µm; Phenomenex, Torrance, CA, USA). The analyses were performed at a flow rate of 1 mL/min, with solvent A (0.1% formic acid) and solvent B (0.1% formic acid in acetonitrile) and monitored at the absorbance of 280 nm, 338 nm and 360 nm. The elution gradient was performed according to the following conditions: from 15% (B) to 40% (B) in 20 min, to 95% (B) in 10 min and to 15% (B) in 2 min, followed by 8 min of maintenance. For quantitative analysis, standard curves for each polyphenol standard were prepared over a concentration range of 0.1–1.0 µg/µL with six different concentration levels and duplicate injections at each level.

2.5. Quantitative Real-Time PCR

RAW 264.7 cells (1 × 10⁶ cells/well) or Bone Marrow Derived Macrophages (BMDMs) (1 × 10⁶ cells/well) were treated with OLE (0.1 and 0.2 mg/mL) for 30 min before stimulation with SP (0.5 mM) for 6 h or 24 h. In the experiments with GW9662, cells were pre-incubate with GW9662 (Sigma-Aldrich, Milan, Italy) 1 µM for 24 h. Total RNA was extracted from macrophages by using TRI-Reagent (Sigma-Aldrich, Milan, Italy), according to the manufacturer’s instructions, followed by reverse-transcription with iScript Reverse Transcription Supermix for RT-qPCR (Bio-Rad, Milan, Italy). Quantitative Real-Time PCR (RT-PCR) was performed by using CFX384 real-time PCR detection system (Bio-Rad, Milan, Italy). mRNA expression was quantified using specific primers for mouse *Il-6*, *Il-1β*, *Tnf-α*, *Il-10*, *iNos* (*Nos2*), *Cox-2* (*Ptgs2*), *Pparγ*, *Cd206*, *Arg-1*, *Gclc*, *Gclm*, *Hmox-1*, which are listed below, with SYBR Green master mix kit (Bio-Rad, Milan, Italy). Relative gene expression was obtained by normalizing the Ct values of each experimental group against *β-actin* transcript level, using the 2-ΔCt formula. mRNA levels are expressed as arbitrary units (A.U.)

Il-6: 5'-CGGAGAGGAGACTTCACAGAG-3'; 5'-ATTCCACGATTCCAGAG-3'

Il-1β: 5'-TACCAGTTGGGAACTCTGC-3'; 5'-GGGCCTCAAAGGAAAGAATC-3'

Tnf-α: 5'-CAGTAGACAGAAGAGCGTGGT-3'; 5'-AGGCACTCCCCAAAAGA-3'

Il-10: 5'-CGGAAACAACCTCTTGAAA-3'; 5'-AAGTGTGCCAGCCTTAGAA-3'
Hmox-1: 5'-GCCGTGTAGATATGGTACAAGGA-3'; 5'-AAGCCGAGAATGCTGAGTTCA-3'
Gclm: 5'-AGGAGCTTCGGGACTGTATCC-3'; 5'-GGGACATGGTGCATCCAAAA-3'
Gclc: 5'GTTGGGTTTGTCTCTCCC-3'; 5'-GGGGTGACGAGGTGGAGTA-3'
Arg-1: 5'-CTGGTTGTCAGGGGAGTGT-3'; GTGAAGAACCCACGGTCTGT-3'
iNos: 5'-CGAAACGCTTCACTTCAA-3'; 5'-TGAGCCTATATTGCTGTGGCT-3'
Cd206: 5'-AGGACATGCCAGGGTCACCTT-3'; 5'-GTTACCTGGAGTGATGGTTCTC-3'
Cox-2: 5'-CCTGCTTGAGTATGTCGCAC-3'; 5'-TACCCTCTCACATCCCTGA-3'
Ppary: 5'-GTACTGTCGGTTTCAGAAGTGCC-3'; 5'-ATCTCCGCCAACAGCTTCTCCT-3'
β-actin: 5'-TACCACCATGTACCCAGGCA-3'; 5'-CTCAGGAGGAGCAATGATCTTGA-3'

2.6. Intracellular ROS Measurement

The generation of ROS was estimated using the fluorescence probe 2',7'-dichlorofluorescein-diacetate (H2DCF-DA). RAW 264.7 macrophage (3×10^3 cells/well) were plated in 96-multiwell black plates (Corning, USA) and incubated with OLE (0.1 and 0.2 mg/mL) for 30 min before to be stimulate with SP (0.5 mM) for 24 h. At the end of the treatment, cells were incubated with H2DCF-DA (100 μ M) for 1 h. Then, cells were washed with PBS and incubated with the Fenton's reagent (H_2O_2/Fe^{2+} 2 mM) for 3 h at 37 °C. Fluorescence generation was measured using a fluorescent microplate reader (excitation 485 nm and emission 538 nm; GloMax[®]-Multi Detection System, Promega). The intracellular ROS levels were expressed as fluorescence intensity.

2.7. Cytokines Measurement

The levels of cytokines (IL-6, IL-1 β , TNF- α and IL-10) were evaluated in cell culture supernatants obtained from RAW 264.7 cells treated with OLE (0.1 and 0.2 mg/mL) for 30 min before stimulation with SP (0.5 mM) for 24 h. Enzyme-linked immunosorbent assay (ELISA) kits were used according to the manufacturer's instructions (DuoSet ELISA, R&D systems, Minneapolis, MN, USA).

2.8. Nitrite Analysis

RAW 264.7 cells (2×10^5 cells/well) were treated with OLE (0.1 and 0.2 mg/mL) for 30 min before stimulation with SP (0.5 mM) for 24 h. After stimulation, NO levels were spectrophotometrically evaluated in culture supernatant according to the Griess reaction method. Briefly, 100 μ L of Griess reagent (0.1% naphthyl-ethylene-diamine dihydrochloride in water and 1% sulphanilamide in 5% concentrated H_3PO_4 ; vol. 1:1) was mixed with culture supernatant (100 μ L). Absorbance was measured with a microplate spectrophotometer (MultiskanTM GO Microplate Spectrophotometer) at 540 nm and nitrite concentration was calculated using a standard solutions of sodium nitrite.

2.9. PGE2 Assay

PGE2 concentration was evaluated in cell culture supernatants obtained from RAW 264.7 cells treated with OLE (0.1 and 0.2 mg/mL) for 30 min before stimulation with Sodium Palmitate (SP) (0.5 mM) for 24 h. Prostaglandin E2 Enzyme Immunoassay (EIA) kit (Cayman Chemicals) was used according to the manufacturer's instruction.

2.10. Flow cytometry

RAW 264.7 cells (5×10^5 cells/well) or BMDMs (1×10^6 cells/well) were plated into 6-well plates and allowed to adhere for 24 h. Then, cells were treated with OLE (0.1 and 0.2 mg/mL) for 30 min before stimulation with SP (0.5 mM) for 24 h. Aliquots of 5×10^5 cells were incubated with anti-Fc receptor (CD16/32) (Thermo Fisher Scientific) and then stained with the following murine monoclonal antibodies (mAbs): Phycoerythrin (PE)-Cyanine7-coniugated anti-CD206 (Thermo Fisher Scientific), Allophycocyanin (APC)-conjugated anti-arginase-1 (ARG1) (R&D System) and

PE-Cyanine7-conjugated anti-NOS2 (Thermo Fisher Scientific). For intracellular staining of ARG1 and inducible nitric oxide synthase iNOS, cells were first fixed and permeabilized with Intracellular Fixation & Permeabilization Buffer (eBiosciences). Data were analyzed using BriCyte E6 (Mindray, Shenzhen, China). Dead cells were excluded by forward and side scatter characteristics. Statistics presented are based on 20,000 events.

2.11. Western Blot Analysis

RAW 264.7 cells (2×10^6 cells/well) were plated into 6-well plates and allowed to adhere for 24 h. Then, cells were treated with OLE (0.1 and 0.2 mg/mL) for 30 min before stimulation with SP (0.5 mM) for additional 30 min (for nuclear and cytoplasmic extracts) or 24 h (for total extracts). Whole-cell or nuclear extracts were prepared as previously described [23]. Protein concentration was measured by the Bradford method (Bio-Rad, Milan, Italy). 40 μ g of proteins were separated by sodium dodecyl-sulfate polyacrylamide gel electrophoresis (SDS-PAGE) and transferred to nitrocellulose filter membranes using the Trans-Blot Turbo Transfer Starter System (Bio-Rad, Milan, Italy). Membranes were blocked with 5% low-fat milk in PBS with 0.1% Tween 20 (PBST) at room temperature for 2 h and, then, were incubated with the following primary antibodies: NF- κ B p65 XP (#8242; Cell Signaling), I κ B- α (#9242, Cell Signaling), NF-E2-related factor 2 (NRF2) (sc-722; Santa Cruz Biotechnology), KEAP1 (#4678; Cell Signaling), SOD2/MnSOD (ab13533; Abcam) iNOS (#39898; Cell Signaling), COX-2 (#4842; Cell Signaling), Glyceraldehyde 3-phosphate dehydrogenase (GAPDH) (#2118; Cell Signaling), α -TUBULIN (#3873; Cell Signaling), overnight at 4 °C. After 3 washes with PBST, the membranes were incubated with anti-mouse (Santa Cruz Biotechnology) or anti-rabbit (Jackson ImmunoResearch) secondary antibody, horseradish peroxidase (HRP) conjugate, for 2 h at room temperature. The membranes were developed with the ChemiDoc™ MP Imaging System (Bio-Rad, Milan, Italy) by the ECL chemiluminescence method. Band intensities were quantified using Image Lab Software and expressed as arbitrary units (A.U.).

2.12. MTT Assay

Cell viability was measured by 3-(4,3-(4,5-dimethylthiazol-2-yl)-2,5 diphenyltetrazolium bromide 5-dimethylthiazol-2-yl)-2, 5-diphenyltetrazolium bromide (MTT) assay. RAW 264.7 cells (0.5×10^5 cells/well) were seeded on 96-well plates and treated with OLE (0.1 and 0.2 mg/mL) for 30 min before stimulation with SP (0.5 mM) for 24 h. Then, medium was removed and 200 μ L of MTT (0.25 mg/mL) was added to each well. After 3 h incubation, the formazan crystals were solubilized in dimethyl sulfoxide (DMSO) (Merck KGaA, Darmstadt, Germany). Absorbance was measured by using a microplate spectrophotometer (Multiskan™ GO Microplate Spectrophotometer) at 490 nm.

2.13. Bone Marrow Derived Macrophages (BMDMs) Generation and Treatment

Bone marrow cells were obtained from femurs and tibias of C57BL/6 mice and cultured for 7 days in Roswell Park Memorial Institute (RPMI) 1640 medium containing 10% FBS, 10 mM HEPES buffer, penicillin (100 U/mL), streptomycin (100 μ g/mL) and 25 ng/mL of mouse M-CSF at 37 °C in 5% CO₂ atmosphere. Additional 5 mL of culture medium was added every second day. On the seventh day, BMDMs were harvested, plated at 1×10^6 cells/well and treated with OLE (0.2 mg/mL) for 30 min before stimulation with SP (0.5 mM) for 24 h.

2.14. Statistical Analysis

Data are expressed as mean \pm standard error of mean (SEM) ($n \geq 3$). Statistical analyses were performed by using GraphPad Prism 6.0 software program (GraphPad Software, Inc., San Diego, CA, USA). One-way analysis of variance (ANOVA) with post-hoc Bonferroni's test was performed to determine differences between groups. $p < 0.05$, $p < 0.01$ or $p < 0.001$ was considered statistically significant and indicated by *, ** or ***, respectively.

3. Results

3.1. Characterization of OLE Composition

The phenolic contents of OLE were calculated on the base of corresponding standard concentration–response curves obtained through HPLC-DAD analysis. The phenolic compounds identified belong to four main groups: oleuropeosides (oleuropein), flavonols (rutin), flavones (apigenin, apigenin-7-O-glucoside and luteolin), phenylethanoid (tyrosol and hydroxytyrosol). Oleuropein (174.64 mg/g) was detected at the highest concentration in OLE, followed by hydroxytyrosol (26.65 mg/g), tyrosol (0.64 mg/g) and apigenin-7-O-glucoside (0.43 mg/g). The other compounds analyzed were found only in trace amounts as shown in Table 1. Our data are in accordance with the findings reported by [24] who indicated oleuropein as a predominant phenolic compound, which represented more than 50% of the total phenolic compounds identified in alcoholic extract from olive leaves.

Table 1. Olive Leaf Extract (OLE) polyphenolic characterization.

Phenolic Compound	Calibration Curve	Content in OLE (mg/g) *
Apigenin	$Y = 4 \times 10^7 x + 118566$	0.01 ± 0.01
Apigenin-7-O-glucoside	$Y = 5 \times 10^7 x - 11131$	0.43 ± 0.02
Hydroxy-tyrosol	$Y = 650564x - 932.11$	26.65 ± 0.08
Luteolin	$Y = 6 \times 10^7 x - 2632.8$	0.36 ± 0.01
Oleuropein	$Y = 3 \times 10^6 x - 11515$	174.64 ± 2.32
Rutin	$Y = 2 \times 10^7 x + 396.8$	0.24 ± 0.02
Tyrosol	$Y = 8 \times 10^6 x - 4951.2$	0.64 ± 0.08

* Results were expressed as mg/g DW \pm SD ($n = 3$). DW: dry weight; SD: standard.

3.2. OLE Suppresses TNF- α , IL-6 and IL-1 β Production in FFAs-Stimulated RAW 264.7 Macrophages

Obesity-associated insulin resistance is associated with increased levels of pro-inflammatory cytokines, such as TNF- α , IL-1 β , and IL-6 [25]. In obese adipose tissue, excess of saturated FFAs such as palmitate was reported to activate resident macrophages with production of pro-inflammatory cytokines that compromise insulin action [26]. To determine to what extent OLE modifies the FFAs-induced inflammatory response, we first studied the mRNA expression and the amount of TNF- α , IL-6 and IL-1 β in RAW 264.7 cells exposed to 0.5 mM SP and pre-treated with OLE (0.1 and 0.2 mg/mL). The concentrations of SP used in the present study are in reference to the concentration of circulating free fatty acids in obesity [27]. The MTT assay revealed that SP 0.5 mM decreased cell viability whereas both concentrations of OLE, which was added 30' prior to SP stimulation, did not significantly affect cell viability (Supplementary Material Figure S1). RAW 264.7 macrophages stimulated with SP showed increased level of pro-inflammatory cytokines in the culture supernatant as well as of their transcriptional levels compared to vehicle-treated cells. In contrast, OLE supplementation significantly diminished the secretion of all inflammatory mediators tested and markedly reduced their mRNA expression in a concentration-dependent manner (Figure 1A–F).

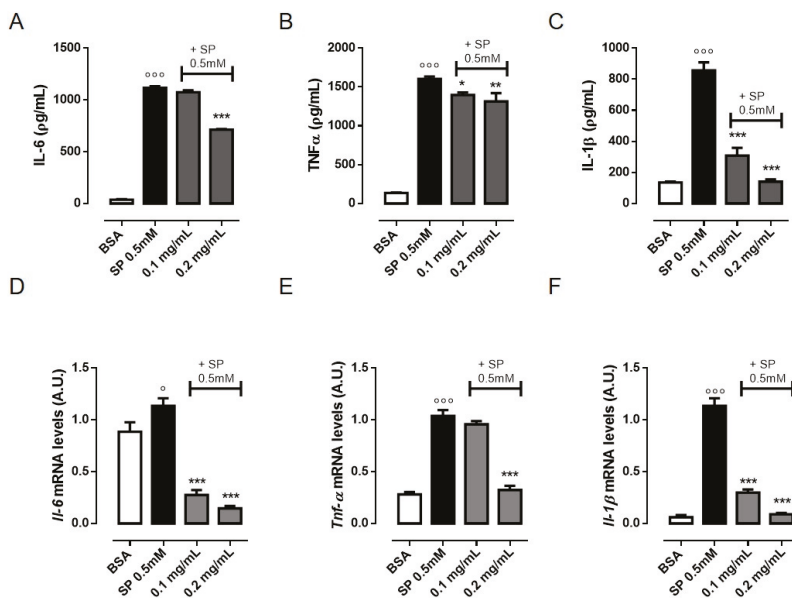


Figure 1. Olive Leaf Extract (OLE) reduces the production of pro-inflammatory cytokines in free fatty acids- (FFAs)-stimulated macrophages. RAW 264.7 cells were treated with OLE (0.1 and 0.2 mg/mL) for 30 min before stimulation with sodium palmitate (SP) 0.5 mM. (A–C) The levels of inflammatory cytokines tumor necrosis factor (TNF)- α , interleukin (IL)-6 and IL-1 β were determined in the cell culture medium after 24 h by ELISA assay. (D–F) Relative mRNA levels of *Il-6*, *Tnf- α* and *Il-1 β* in RAW 264.7 macrophages were determined by Real Time-PCR (RT-PCR) analysis after 6 h. Values are expressed as mean \pm standard error of mean (SEM) from three independent experiments. $^{\circ} p < 0.05$, $^{\circ\circ\circ} p < 0.001$ indicate significant effect of SP compared with vehicle-treated cells; $^{\circ} p < 0.05$, $^{\circ\circ} p < 0.01$, $^{\circ\circ\circ} p < 0.001$ indicate significant effect of OLE compared with SP-stimulated cells. BSA, bovin serum albumin.

3.3. OLE Attenuates FFAs-Induced Oxidative Stress in RAW 264.7 Macrophages by Activating NRF2

Accumulating evidence suggests that oxidative stress is the leading cause of adipose tissue inflammation and of the pathogenesis of obesity-associated co-morbidities [28–30]. An important source of ROS in obesity is from ATMs. Recent reports have shown that certain saturated FFAs such as palmitate cause mitochondrial dysfunction and induce ROS production [26]. To investigate the effects of OLE on cell redox homeostasis, we measured intracellular ROS levels in SP-stimulated RAW 264.7 cells pre-treated with OLE (0.1 and 0.2 mg/mL) using the fluoroprobe H2DCFDA. Exposure of macrophages to SP 0.5 mM for 24 h significantly increased intracellular ROS generation whereas pre-treatment with OLE significantly decreased it in a concentration-dependent manner bringing back ROS to the basal level (Figure 2A). The oxidative homeostasis in normal cells is regulated by several anti-oxidant enzymes, such as superoxide dismutase (SOD), catalase (CAT) and glutathione peroxidase (GSX). To evaluate macrophages' antioxidant defense capacity, we determined the expression levels of glutamate-cysteine ligase (GCL) and heme oxygenase-1 (HMOX-1) antioxidant enzymes. GCL, consisting of a catalytic (GCLC) and a modulatory (GCLM) subunits, is the rate-limiting enzyme in the glutathione (GSH) synthesis. In RAW 264.7 macrophages, OLE significantly enhanced gene expression of *Gclc*, *Gclm* and *Hmox-1* in a concentration-dependent manner (Figure 2B–D). Of interest is that increased expression of SOD can limit oxidative damage in obese mice [31]. Hence, we evaluated the protein expression of the mitochondrial SOD (SOD2). We found that SOD2 protein expression was significantly increased following OLE treatment in SP-stimulated RAW 264.7 macrophages (Figure 2E). These results suggest that OLE is able to regulate ROS production induced by SP stimulation in RAW

264.7 macrophages by promoting the expression of antioxidant proteins. Considering the indispensable role of the transcription factor NF-E2-related factor 2 (NRF2) in protecting cells from oxidative insults, we next sought to determine the involvement of NRF2 in OLE-antioxidant activity. We found that stimulation of RAW 264.7 macrophages with SP 0.5 mM promoted NRF2 protein migration into nuclei as a consequence of increased ROS level. Interestingly, OLE (0.2 mg/mL) pre-treatment significantly increased NRF2 nuclear translocation. NRF2 is predominantly degraded through the ubiquitination-mediated proteasome pathway. Under normal conditions, Kelch-like ECH-associated protein 1 (KEAP1) sequesters NRF2 into the cytosol and promotes its ubiquitination and proteasomal degradation; stimuli as ROS or electrophilic insults promote the dissociation of the NRF2-KEAP1 complex, and the subsequent NRF2 nuclear translocation [32]. Accordingly, we observed that KEAP1 protein level was significantly reduced in the cytosol of OLE treated cells (Figure 2F,G).

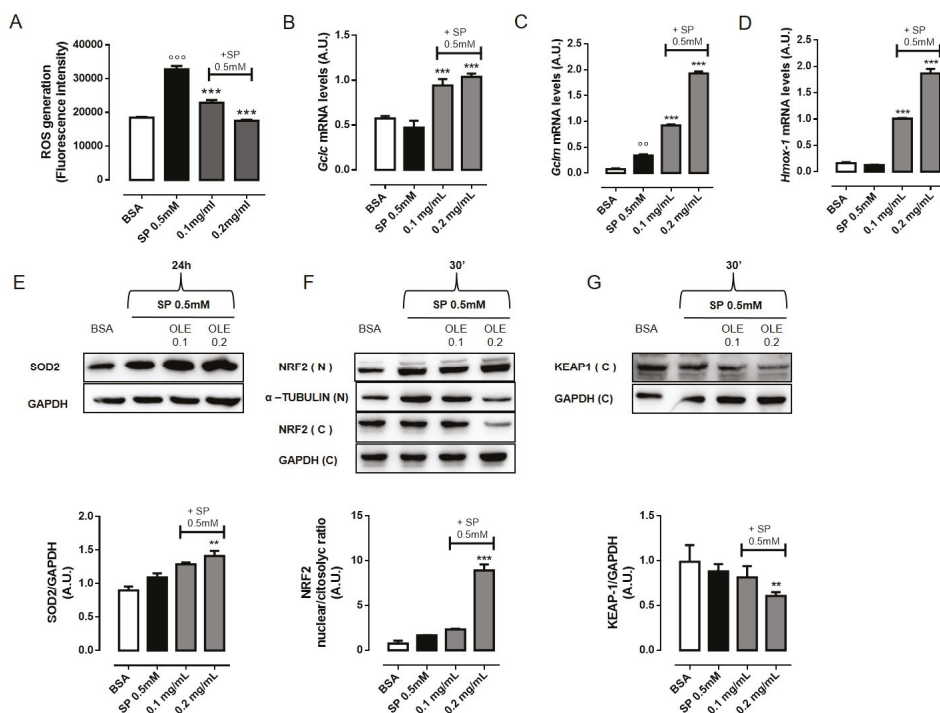


Figure 2. Olive Leaf Extract (OLE) attenuates free fatty acids (FFAs)-induced oxidative stress in macrophages by activating NF-E2-related factor 2 (NRF2) transcription factor. RAW 264.7 cells were treated with OLE (0.1 and 0.2 mg/mL) for 30 min before to stimulation with sodium palmitate (SP) 0.5 mM. (A) Intracellular reactive oxygen species (ROS) levels were measured using the fluoroprobe 2',7'-dichlorofluorescein-diacetate (H2DCF-DA) after 24 h. (B–D) Relative mRNA levels of *Gclc*, *Gclm* and *Hmox-1* in RAW 264.7 macrophages were determined by Real time-PCR (RT-PCR) after 6 h. (E) Representative image of mitochondrial superoxide dismutase (SOD2) protein expression detected by western blot and relative densitometric quantification. (F) Representative images of NRF2 detected by western blot, in nuclear (N) and cytosolic (C) extract, and densitometric quantification of the nucleus/cytosol ratio. (G) Representative images of Kelch-like ECH-associated protein 1 (KEAP1) protein detected by western blot and densitometric quantification. Glyceraldehyde 3-phosphate dehydrogenase (GAPDH) and α -tubulin were used as an internal control. Values are express as mean \pm standard error of mean (SEM) from three independent experiments. ^{oo} $p < 0.01$, ^{ooo} $p < 0.001$ indicate significant effect of SP compared with vehicle-treated cells; ^{**} $p < 0.01$, ^{***} $p < 0.001$ indicate significant effect of OLE compared with SP-stimulated cells.

3.4. OLE Suppressed M1 Pro-Inflammatory Phenotype in FFAs-Stimulated RAW 264.7 Macrophages

Macrophage M1/M2 status plays a fundamental role in the development of adipose tissue inflammation. In particular, obesity leads to a shift in ATMs phenotype from an anti-inflammatory M2-polarized state to an M1 pro-inflammatory state that supports insulin resistance [6]. M1 macrophages in obese adipose tissue express high levels of pro-inflammatory mediators, such as inducible nitric oxide synthase (iNOS), cytokines (IL-6, IL-1 β and TNF- α) and reactive intermediates [33]. Thus, we next investigated whether OLE restrained FFAs-induced inflammation via regulation of macrophages polarization. As we have already showed above, OLE reduces the release of pro-inflammatory cytokines as well as ROS generation (Figures 1 and 2). In addition, in order to detect M1 specific antigen, we performed the characterization of cell populations by flow cytometric analysis. Upon stimulation with SP 0.5 mM for 24 h, we found that the percentage of iNOS⁺ cells significantly increased from 6.9% to 78.8% compared to vehicle-treated cells. Interestingly, the pre-treatment with OLE 0.1 mg/mL and 0.2 mg/mL significantly decreased the percentage of iNOS⁺ cells to 53.4% and 40.3%, respectively (Figure 3A,B). Quantitative RT-PCR and western blot analysis also confirmed reduced expression of iNOS upon OLE treatment in SP-stimulated macrophages (Figure 3C,E). These findings were also confirmed in murine BMDMs (Supplementary Material Figure S2). Activation of M1 macrophages is normally accompanied also by increase of cyclooxygenase-2 (COX-2) expression. We found that *Cox-2* gene and protein were strongly upregulated in macrophages treated with SP. However, pre-treatment with OLE significantly and concentration-dependently reduced its expression (Figure 3D,E). In addition, the inhibitory effects of OLE on iNOS and COX-2 activity were confirmed by measuring their main products, NO and PGE₂, respectively. Consistent with the previous results, we found that OLE significantly and concentration-dependently inhibited SP-induced NO (Figure 3F) and PGE₂ (Figure 3G) production. We further examined the activation of NF- κ B, the key transcription factor that promotes the expression of pro-inflammatory genes in M1 cells [34]. NF- κ B can be activated by the SFA palmitate, through the TLR4-mediated pro-inflammatory signaling pathway leading to M1 polarization status [26,35]. To explore the effect of OLE on the regulation of NF- κ B signaling in SP-stimulated RAW 264.7 macrophages, we evaluated the nuclear translocation of NF- κ B p65 subunit by western blot analysis. We found that upon stimulation with SP, p65 nuclear level were markedly increased whereas pre-treatment with OLE (0.1 and 0.2 mg/mL) significantly reduce p65 expression into the nuclei of macrophages in a concentration dependent-manner (Figure 3H). Additionally, we evaluated I κ B- α protein expression, the inhibitor of NF- κ B that normally retains NF- κ B in the cytoplasm. We found that SP rapidly reduces I κ B- α protein level in the cytosol while pre-treatment with OLE restores normal cytoplasmatic I κ B- α level in RAW264.7 macrophages, suggesting that OLE inhibited SP-induced I κ B- α degradation and, thus, NF- κ B activation (Figure 3I).

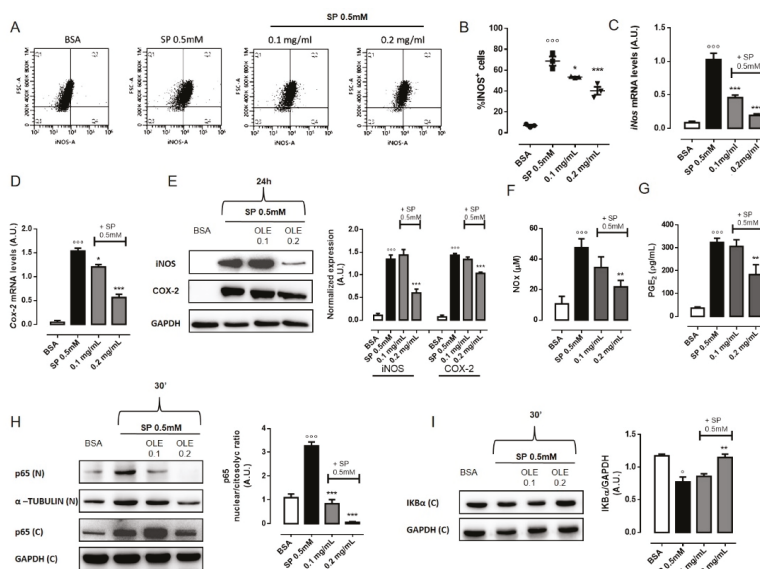


Figure 3. Olive Leaf Extract (OLE) suppresses M1 pro-inflammatory phenotype in free fatty acids (FFAs)-stimulated macrophages. RAW 264.7 cells were treated with OLE (0.1 and 0.2 mg/mL) for 30 min before stimulation with sodium palmitate (SP) 0.5 mM. (A) Representative plot and (B) relative quantitative analysis of intracellular inducible nitric oxide synthase (iNOS), expression in RAW 264.7 macrophages evaluated by flow cytometry after 24 h. Relative mRNA levels of *iNos* (C) and *Cox-2* (D) in RAW 264.7 macrophages were determined by Real Time-PCR (RT-PCR) after 24 h. (E) Representative image of iNOS and cyclooxygenase-2 (COX-2) proteins expression detected by western blot and relative densitometric quantification. Glyceraldehyde 3-phosphate dehydrogenase (GAPDH) was used as an internal control. (F) The levels of nitric oxide (NO) were measured in the cell culture medium after 24 h by the Greiss reaction. (G) The levels of prostaglandin E2 (PGE2) were measured in the cell culture medium after 24 h by the Enzyme Immunoassay (EIA). (H) Representative image of p65 detected by western blot, in nuclear (N) and cytosolic (C) extract, and densitometric quantification of the nucleus/cytoplasm ratio. (I) Representative image of IκB-α protein detected by western blot and relative densitometric quantification. α-TUBULIN and GAPDH were used as an internal control. Values are expressed as mean ± standard error of mean (SEM) from three independent experiments. ° $p < 0.05$, °° $p < 0.001$ indicate significant effect of SP compared with vehicle-treated cells; * $p < 0.05$, ** $p < 0.01$, *** $p < 0.001$ indicate significant effect of OLE compared with SP-stimulated cells.

3.5. OLE Promoted M2 Polarization in FFAs-Stimulated RAW264.7 Macrophages via PPARγ Activation

As M2 macrophages ameliorate obesity-associated inflammation and insulin resistance [6], we evaluated whether OLE had any effects on macrophage polarization toward M2 phenotype. Alternatively activated macrophages found in lean adipose tissue express specific markers, including arginase-1 (ARG-1) and the mannose receptor C type 1 (CD206) and generate high levels of the anti-inflammatory cytokine IL-10, which plays a fundamental role in potentiating insulin sensitivity of adipocytes [33]. Thus, we characterized the phenotype of RAW 264.7 macrophages after treatment with OLE by flow cytometric analysis. As shown in Figure 4, the percentage of ARG-1+ cells increased by approximately 30% 24 h post-treatment with OLE 0.2 mg/mL compared to vehicle- and SP-treated cells (Figure 4A,B). Similarly, the percentage of CD206+ cells increased by approximately 50% (Figure 4D,E). Quantitative RT-PCR also confirmed increased expression of *Arg-1* and *Cd206* mRNA upon OLE treatment (Figure 4C,F). Similar results were also confirmed in murine BMDMs (Supplementary Material Figure S2). Simultaneously, we found that SP treatment also slightly enhanced

the expression of some M2 markers including *Arg-1* and *Cd206* mRNA. However, the significant elevation of the ratio of *iNOS* versus *Arg-1* or *CD206* in response to a high dose of SP is suggestive of M1 polarization (Supplementary Material Figure S2F). Furthermore, we determined the levels of IL-10 in cell culture supernatants of RAW264.7 macrophages as well as *Il-10* mRNA expression. As shown in Figure 4G,H, OLE treatment significantly increased IL-10 expression and production in a concentration-dependent manner. Several studies have defined a key role for PPAR γ in controlling M2 macrophage polarization [36–38]. PPAR γ is a ligand-inducible transcription factor that has been well documented to have anti-inflammatory effects in macrophages [39]. Thus, we further examined the activation of PPAR γ in RAW 264.7 macrophages treated with OLE. Our data show that, OLE (0.2 mg/mL) significantly induce PPAR γ expression in SP-stimulated macrophages (Figure 5A,B). Similar results were also confirmed in murine BMDMs (Supplementary Material Figure S2). Finally, to confirm the hypothesis that OLE regulates M1/M2 status by activating PPAR γ , we used GW9662, a selective irreversible antagonist of PPAR γ , to inhibit PPAR γ transcriptional function. We found that GW9662 pre-treatment partially inhibited OLE-induced expression of M2 markers, such as *Cd206*, *Arg-1* and *Il-10* (Figure 5C) in SP-stimulated RAW 264.7 macrophages.

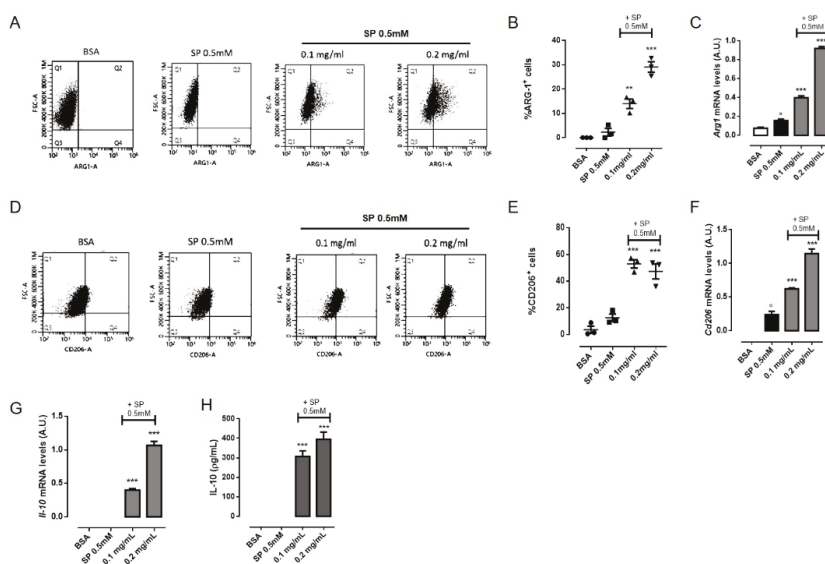


Figure 4. Olive Leaf Extract (OLE) promotes M2 polarization in free fatty acids (FFAs)-stimulated macrophages. RAW 264.7 cells were treated with OLE (0.1 and 0.2 mg/mL) for 30 min before to be stimulated with sodium palmitate (SP) 0.5 mM. (A) Representative plot and (B) relative quantitative analysis of intracellular arginase-1 (ARG-1) expression in RAW 264.7 macrophages evaluated by flow cytometry after 24 h. (C) Relative mRNA levels of *Arg-1* in RAW 264.7 macrophages were determined by Real Time-PCR (RT-PCR) after 24 h. (D) Representative plot and (E) relative quantitative analysis of mannose receptor C type 1 (CD206) expression in RAW 264.7 macrophages evaluated by flow cytometry after 24 h. (F,G) Relative mRNA levels of *Cd206* and *Il-10* mRNA in RAW 264.7 macrophages were determined by RT-PCR after 24 h and 6 h, respectively. (H) The levels of interleukin (IL)-10 cytokine were determined in the cell culture medium after 24 h by enzyme-linked immunosorbent assay (ELISA). Values are express as mean \pm standard error of mean (SEM) from three independent experiments. $^{\circ}$ $p < 0.05$ indicate significant effect of SP compared with vehicle-treated cells; ** $p < 0.01$, *** $p < 0.001$ indicate significant effect of OLE compared with SP-stimulated cells.

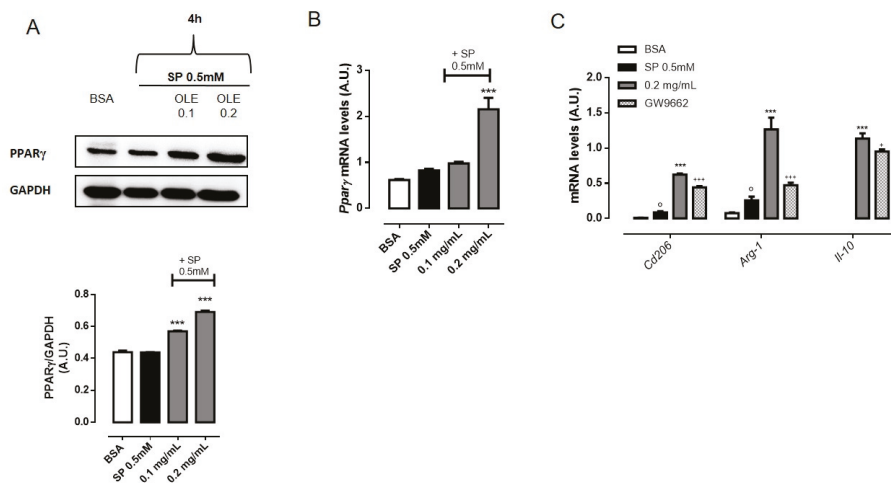


Figure 5. Olive Leaf Extract (OLE) activates peroxisome proliferator-activated receptor gamma (PPAR γ) in free fatty acids (FFAs)-stimulated macrophages. RAW 264.7 cells were treated with OLE (0.1 and 0.2 mg/mL) for 30 min before stimulation with sodium palmitate (SP) 0.5 mM. **(A)** Representative images of PPAR γ protein expression detected by western blot and relative densitometric quantification. Glyceraldehyde 3-phosphate dehydrogenase (GAPDH) was used as an internal control. **(B)** Relative mRNA levels of *Ppar γ* were determined by Real Time-PCR (RT-PCR) after 4 h. **(C)** Relative mRNA levels of *Cd206*, *Arg-1* and *Il-10* in GW9662 pre-treated RAW 264.7 macrophages were determined by RT-PCR after 24 h. Values are expressed as mean \pm standard error of mean (SEM) from three independent experiments. $^{\circ}$ $p < 0.05$ indicate significant effect of SP compared with vehicle-treated cells; *** $p < 0.001$ indicate significant effect of OLE compared with SP-stimulated cells; $^{+}$ $p < 0.05$, $^{+++}$ $p < 0.001$ indicate significant effect of GW9662 compared with OLE-treated cells.

4. Discussion

Olive leaves represent a rich source of bioactive compounds with several beneficial effects for human health [20]. Previous studies reported the anti-inflammatory effect of oleuropein, the most abundant compound of the olive leaf extract, in lipopolysaccharide (LPS)-stimulated RAW 264.7 macrophages [40,41]. In addition, olive leaf constituents have demonstrated anti-obesity activity in terms of inhibition of adipogenic differentiation, reduction of body weight and improvement of lipid metabolism [42–45]. However, any of these studies evaluated the action of olive leaf extract on obesity-associated inflammation. It has been accepted that obesity coincides with a low-grade inflammatory state, referred as meta-inflammation, that mediates insulin resistance and it is closely related to the pathogenesis of obesity-associated diseases [2]. There are extensive evidences indicating that macrophages are primarily responsible for the inflammatory response into obese adipose tissue [4,5]. ATMs can polarize into two subtypes of activated macrophages: alternatively activated M2 macrophages that attenuate obesity-induced inflammation; and classically activated M1 macrophages that promote metabolic inflammation [6]. During weight gain macrophages undergo a “phenotypic switch” from an anti-inflammatory M2 phenotype to a pro-inflammatory M1 state, which contribute to insulin resistance [46]. In particular, a continuous and excessive exposure of ATMs to saturated FFAs, such as palmitate, promotes the secretion of pro-inflammatory mediators (cytokines, ROS and NO) that further supports M1 macrophages’ polarization and aggravate inflammation in the adipose tissue [47]. Thus, restoring the M2 phenotype might reduce meta-inflammation and protect from the risk to develop obesity-related diseases [15,16]. Several studies have demonstrated that some natural compounds have the potential to alleviate obesity-related inflammation via regulation of macrophage polarization [48–50]. In the current study, we confirm previously published results on the

anti-inflammatory effect of oleuropein and showed, for the first time, the ability of OLE to induce a phenotypic switch of macrophage toward an M2-like phenotype in FFAs-stimulated macrophages. Prolonged treatment (24 h) of RAW 264.7 macrophages with high dose of SP (0.5 mM) was performed to mimic lipo-toxicity under obese condition. Consistent with many recently published studies [51,52] we found that 24 h treatment of macrophages with SP (0.5 mM) drove mouse macrophage polarization to a pro-inflammatory phenotype. Indeed, after being treated with SP, RAW 264.7 macrophages dramatically expressed several M1 markers; they exhibited increased production of ROS and inflammatory cytokines, TNF- α , IL-1 β and IL-6, and showed increased expression of COX-2 and iNOS concomitant with the release of the respectively inflammatory mediators PGE2 and NO. Secretion of these factors supports adipose tissue inflammation and promotes insulin resistance throughout the activation of several inflammatory signal transduction pathways in macrophages and adipocytes [25]. Our data showed that pre-treatment with OLE significantly suppressed the releasing of the pro-inflammatory cytokines TNF- α , IL-1 β and IL-6 in the supernatant of SP-activated RAW 264.7 cells with greater effect on IL-1 β levels and mRNA. IL-1 β is the major pro-inflammatory cytokine produced by ATMs and it is implicated in the development of obesity-associated insulin resistance [53,54]. Therefore, IL-1 β might be a therapeutic target for the improvement of insulin sensitivity at tissue and systemic levels. In fact, a neutralizing antibody for IL-1 β , Canakinumab, is currently under clinical trial for diabetes [55]. Obesity is also associated with increasing ROS levels, mainly produced by ATMs that contribute to induce insulin resistance and type 2 diabetes [29]. Indeed, exposure of RAW 264.7 cells to high concentration of SP increased ROS intracellular levels, while OLE had a remarkable suppressive effect on SP-induced ROS production. OLE-mediated suppression of oxidative stress was regulated by the transcription factor NRF2. NRF2-KEAP1 pathway is a key defense system for the protection of cells from oxidative stress [56]. To date, several natural and synthetic compounds have proven to be effective against obesity by inducing NRF2. In fact, NRF2 agonists demonstrated to reduce total body fat, plasma lipids levels, and to improve glucose tolerance and insulin resistance in HFD-fed mice [57,58]. In our experiments, we found that OLE also acts as NRF2 inducer. Indeed, it effectively reduced the abundance of KEAP1 in the cytosol and promoted the translocation of NRF2 into the nucleus of macrophages. Consequently, the activation of NRF2 correlated with the increased expression of its target antioxidant enzymes, such as HMOX-1, GCL and SOD2 responsible for ROS control in macrophages. An essential difference between M1-M2 polarization states is the metabolism of L-arginine that involves the enzymes ARG-1 and iNOS. In particular, iNOS produces reactive NO species with pro-inflammatory effects, while ARG-1 converts L-arginine to polyamines and collagen precursors that are crucial for tissue repair and remodeling [59]. In the present study, we found that OLE noticeably decreased iNOS expression and subsequent NO production induced from SP stimulation in RAW 264.7 macrophages. In addition, COX-2 and its mediator PGE2 were also significantly reduced by OLE. Concomitant with the reduction of M1 markers, RAW 264.7 macrophages treated with OLE exhibited enhanced expression of M2 specific markers including ARG-1 and CD206 as well as increased production of the anti-inflammatory cytokine IL-10. Taken together, these results demonstrated that OLE reduces M1 polarization and promote M2 remodeling of macrophages stimulated with high concentration of FFAs. The switch of macrophages from M1 to M2 phenotype was also examined by the expression of transcription factors that define macrophage profile and function. NF- κ B is the key transcription factor for M1 pro-inflammatory macrophages, while PPAR γ is considered as a master regulator of the M2 phenotype [35,38]. Several stimuli, such as ROS, TNF- α , LPS, IL-1 β and SFAs, promote NF- κ B activation and drive the expression of target genes [14]. Our data demonstrated that OLE markedly reduced the level of NF- κ B p65 subunit into the nuclei of SP-stimulated RAW 264.7 while increasing the level of I κ B α in the cytoplasm. Thus, OLE-mediated inhibition of NF- κ B translocation and activation significantly contributed to the suppression of SP-induced inflammatory responses. PPAR γ is a ligand-inducible transcription factor that regulates a variety of physiological processes, including glucose and lipid metabolism [60]. Moreover, PPAR γ is implicated in the control of immunological events, mediating the differentiation and activation of immune cells to anti-inflammatory phenotypes [61]. Due to its

role in macrophage polarization and regulation of inflammation, PPAR γ has become an attractive pharmacological target for the development of drugs used for the treatment of metabolic disease in which activated macrophages play prominent pathogenic roles. Consequently, potent full agonists of PPAR γ , thiazolidinediones, have been widely used for the treatment of type 2 diabetes in clinical practice [62]. Recently, it has been demonstrated that phenol fraction from virgin olive oil promotes M2 polarization in LPS-challenged human macrophages augmenting the transcriptional activity of PPAR γ , which contributes to lower inflammation [63]. In addition, macrophage-specific deletion of PPAR γ impairs M2 polarization and predisposes HFD-fed mice to develop obesity and insulin resistance [37]. Consistent with previous studies, we found that supplementation of OLE significantly increased the expression of PPAR γ in SP-stimulated RAW 264.7 macrophages; further, inhibition of PPAR γ with GW9662 significantly attenuated the ability of OLE to induce M2 macrophage polarization, suggesting that PPAR γ is, at least in part, required for OLE to regulate macrophage phenotype. However, other studies observed that oleuropein or OLE inhibits PPAR γ in adipocytes, which results in reduced adipogenesis and thermogenesis in vesical adipose tissue [42,64]. These contrary results might depend on the different cellular model used. Thus, oleuropein, or OLE, could be able to differently regulate PPAR γ function based on the specific cell type examined. In conclusion, our study demonstrated that OLE regulates M1/M2 macrophage polarization in conditions of FFA-induced inflammation throughout two main actions: i) suppression of M1-mediated pro-inflammatory response by inhibiting NF- κ B activity and up-regulating NRF2-dependent genes; ii) enhancement of M2 polarization in a PPAR γ -dependent manner. These findings indicate that polyphenols from olive leaves may be used as dietary supplementation for the prevention and treatment of obesity-associated inflammation and related comorbidities. However, further studies are required for a better understanding of the effects of OLE on the macrophages of the adipose tissue in diet-induced obese mice.

Supplementary Materials: The following are available online at <http://www.mdpi.com/2072-6643/12/12/3663/s1>, Figure S1: Effect of sodium palmitate (SP) on macrophages viability; Figure S2: Olive Leaf Extract (OLE) drives murine bone marrow-derived macrophages (BMDMs) towards M2 polarization.

Author Contributions: Conceptualization, P.D.C.; Methodology, P.D.C.; Formal Analysis, P.D.C. and M.M.; Investigation, P.D.C. and M.M.; Resources, A.I. and G.C.T.; Supervision, P.D.C. and A.I.; Validation, G.C.T. and A.I.; Visualization, P.D.C.; Writing—original draft, P.D.C.; Writing—review & editing, P.D.C., M.M., G.C.T. and A.I.; Project Administration, P.D.C.; Funding Acquisition, A.I. All authors have read and agreed to the published version of the manuscript.

Funding: This research received no external funding.

Conflicts of Interest: The authors declare no conflict of interest.

References

1. Available online: <http://www.who.int/news-room/fact-sheets/detail/obesity-and-overweight> (accessed on 28 May 2020).
2. Minihane, A.M.; Vinoy, S.; Russell, W.R.; Baka, A.; Roche, H.M.; Tuohy, K.M.; Teeling, J.L.; Blaak, E.E.; Fenech, M.; Vauzour, D.; et al. Low-grade inflammation, diet composition and health: Current research evidence and its translation. *Br. J. Nutr.* **2015**, *114*, 999–1012. [[CrossRef](#)] [[PubMed](#)]
3. Weisberg, S.P.; McCann, D.; Desai, M.; Rosenbaum, M.; Leibel, R.L.; Ferrante, A.W., Jr. Obesity is associated with macrophage accumulation in adipose tissue. *J. Clin. Investig.* **2003**, *112*, 1796–1808. [[CrossRef](#)] [[PubMed](#)]
4. Lauterbach, M.A.; Wunderlich, F.T. Macrophage function in obesity-induced inflammation and insulin resistance. *Pflug. Arch. Eur. J. Physiol.* **2017**, *469*, 385–396. [[CrossRef](#)] [[PubMed](#)]
5. Chawla, A.; Nguyen, K.D.; Goh, Y.P. Macrophage-mediated inflammation in metabolic disease. *Nat. Rev. Immunol.* **2011**, *11*, 738–749. [[CrossRef](#)]
6. Castoldi, A.; Naffah de Souza, C.; Camara, N.O.; Moraes-Vieira, P.M. The Macrophage Switch in Obesity Development. *Front. Immunol.* **2015**, *6*, 637. [[CrossRef](#)]
7. Thomas, D.; Apovian, C. Macrophage functions in lean and obese adipose tissue. *Metab. Clin. Exp.* **2017**, *72*, 120–143. [[CrossRef](#)]

8. Clement, K.; Viguerie, N.; Poitou, C.; Carette, C.; Pelloux, V.; Curat, C.A.; Sicard, A.; Rome, S.; Benis, A.; Zucker, J.D.; et al. Weight loss regulates inflammation-related genes in white adipose tissue of obese subjects. *FASEB J. Off. Publ. Fed. Am. Soc. Exp. Biol.* **2004**, *18*, 1657–1669. [[CrossRef](#)]
9. Fujisaka, S.; Usui, I.; Bukhari, A.; Ikutani, M.; Oya, T.; Kanatani, Y.; Tsuneyama, K.; Nagai, Y.; Takatsu, K.; Urakaze, M.; et al. Regulatory mechanisms for adipose tissue M1 and M2 macrophages in diet-induced obese mice. *Diabetes* **2009**, *58*, 2574–2582. [[CrossRef](#)]
10. van Dijk, S.J.; Feskens, E.J.; Bos, M.B.; Hoelen, D.W.; Heijligenberg, R.; Bromhaar, M.G.; de Groot, L.C.; de Vries, J.H.; Muller, M.; Afman, L.A. A saturated fatty acid-rich diet induces an obesity-linked proinflammatory gene expression profile in adipose tissue of subjects at risk of metabolic syndrome. *Am. J. Clin. Nutr.* **2009**, *90*, 1656–1664. [[CrossRef](#)]
11. Ghanim, H.; Abuaysheh, S.; Sia, C.L.; Korzeniewski, K.; Chaudhuri, A.; Fernandez-Real, J.M.; Dandona, P. Increase in plasma endotoxin concentrations and the expression of Toll-like receptors and suppressor of cytokine signaling-3 in mononuclear cells after a high-fat, high-carbohydrate meal: Implications for insulin resistance. *Diabetes Care* **2009**, *32*, 2281–2287. [[CrossRef](#)]
12. Kim, J.Y.; Park, J.Y.; Kim, O.Y.; Ham, B.M.; Kim, H.J.; Kwon, D.Y.; Jang, Y.; Lee, J.H. Metabolic profiling of plasma in overweight/obese and lean men using ultra performance liquid chromatography and Q-TOF mass spectrometry (UPLC-Q-TOF MS). *J. Proteome Res.* **2010**, *9*, 4368–4375. [[CrossRef](#)] [[PubMed](#)]
13. Shi, H.; Kokoeva, M.V.; Inouye, K.; Tzameli, I.; Yin, H.; Flier, J.S. TLR4 links innate immunity and fatty acid-induced insulin resistance. *J. Clin. Investig.* **2006**, *116*, 3015–3025. [[CrossRef](#)] [[PubMed](#)]
14. Nguyen, M.T.; Favelyukis, S.; Nguyen, A.K.; Reichart, D.; Scott, P.A.; Jenn, A.; Liu-Bryan, R.; Glass, C.K.; Neels, J.G.; Olefsky, J.M. A subpopulation of macrophages infiltrates hypertrophic adipose tissue and is activated by free fatty acids via Toll-like receptors 2 and 4 and JNK-dependent pathways. *J. Biol. Chem.* **2007**, *282*, 35279–35292. [[CrossRef](#)] [[PubMed](#)]
15. Chang, Y.H.; Ho, K.T.; Lu, S.H.; Huang, C.N.; Shiau, M.Y. Regulation of glucose/lipid metabolism and insulin sensitivity by interleukin-4. *Int. J. Obes.* **2012**, *36*, 993–998. [[CrossRef](#)] [[PubMed](#)]
16. Zhang, Q.; Hao, H.; Xie, Z.; Cheng, Y.; Yin, Y.; Xie, M.; Huang, H.; Gao, J.; Liu, H.; Tong, C.; et al. M2 macrophages infusion ameliorates obesity and insulin resistance by remodeling inflammatory/macrophages' homeostasis in obese mice. *Mol. Cell. Endocrinol.* **2017**, *443*, 63–71. [[CrossRef](#)]
17. Das, L.; Bhaumik, E.; Raychaudhuri, U.; Chakraborty, R. Role of nutraceuticals in human health. *J. Food Sci. Technol.* **2012**, *49*, 173–183. [[CrossRef](#)]
18. Romani, A.; Ieri, F.; Urciuoli, S.; Noce, A.; Marrone, G.; Nediani, C.; Bernini, R. Health Effects of Phenolic Compounds Found in Extra-Virgin Olive Oil, By-Products, and Leaf of *Olea europaea* L. *Nutrients* **2019**, *11*, 1776. [[CrossRef](#)]
19. Japon-Lujan, R.; Luque-Rodriguez, J.M.; Luque de Castro, M.D. Dynamic ultrasound-assisted extraction of oleuropein and related biophenols from olive leaves. *J. Chromatogr. A* **2006**, *1108*, 76–82. [[CrossRef](#)]
20. Zuntar, I.; Putnik, P.; Bursac Kovacevic, D.; Nutrizio, M.; Supljika, F.; Poljanec, A.; Dubrovic, I.; Barba, F.J.; Rezek Jambak, A. Phenolic and Antioxidant Analysis of Olive Leaves Extracts (*Olea europaea* L.) Obtained by High Voltage Electrical Discharges (HVED). *Foods* **2019**, *8*. [[CrossRef](#)]
21. Santiago-Mora, R.; Casado-Diaz, A.; De Castro, M.D.; Quesada-Gomez, J.M. Oleuropein enhances osteoblastogenesis and inhibits adipogenesis: The effect on differentiation in stem cells derived from bone marrow. *Osteoporos. Int.* **2011**, *22*, 675–684. [[CrossRef](#)]
22. Drira, R.; Chen, S.; Sakamoto, K. Oleuropein and hydroxytyrosol inhibit adipocyte differentiation in 3 T3-L1 cells. *Life Sci.* **2011**, *89*, 708–716. [[CrossRef](#)] [[PubMed](#)]
23. De Cicco, P.; Panza, E.; Armogida, C.; Ercolano, G.; Tagliatalata-Scafati, O.; Shokoohinia, Y.; Camerlingo, R.; Pirozzi, G.; Calderone, V.; Cirino, G.; et al. The Hydrogen Sulfide Releasing Molecule Acetyl Deacetylase Inhibits Metastatic Melanoma. *Front. Pharmacol.* **2017**, *8*, 65. [[CrossRef](#)] [[PubMed](#)]
24. Xie, P.-J. Phenolic compositions, and antioxidant performance of olive leaf and fruit (*Olea europaea* L.) extracts and their structure–activity relationships. *J. Funct. Foods* **2015**, *16*, 460–471. [[CrossRef](#)]
25. Febbraio, M.A. Role of interleukins in obesity: Implications for metabolic disease. *Trends Endocrinol. Metab.* **2014**, *25*, 312–319. [[CrossRef](#)]
26. Korbecki, J.; Bajdak-Rusinek, K. The effect of palmitic acid on inflammatory response in macrophages: An overview of molecular mechanisms. *Inflamm. Res. Off. J. Eur. Histamine Res. Soc.* **2019**, *68*, 915–932. [[CrossRef](#)]

27. Karpe, F.; Dickmann, J.R.; Frayn, K.N. Fatty acids, obesity, and insulin resistance: Time for a reevaluation. *Diabetes* **2011**, *60*, 2441–2449. [[CrossRef](#)]
28. Masschelin, P.M.; Cox, A.R.; Chernis, N.; Hartig, S.M. The Impact of Oxidative Stress on Adipose Tissue Energy Balance. *Front. Physiol.* **2019**, *10*, 1638. [[CrossRef](#)]
29. Houstis, N.; Rosen, E.D.; Lander, E.S. Reactive oxygen species have a causal role in multiple forms of insulin resistance. *Nature* **2006**, *440*, 944–948. [[CrossRef](#)]
30. Manna, P.; Jain, S.K. Obesity, Oxidative Stress, Adipose Tissue Dysfunction, and the Associated Health Risks: Causes and Therapeutic Strategies. *Metab. Syndr. Relat. Disord.* **2015**, *13*, 423–444. [[CrossRef](#)]
31. Liu, Y.; Qi, W.; Richardson, A.; Van Remmen, H.; Ikeno, Y.; Salmon, A.B. Oxidative damage associated with obesity is prevented by overexpression of CuZn- or Mn-superoxide dismutase. *Biochem. Biophys. Res. Commun.* **2013**, *438*, 78–83. [[CrossRef](#)]
32. Kobayashi, A.; Kang, M.I.; Okawa, H.; Ohtsuji, M.; Zenke, Y.; Chiba, T.; Igarashi, K.; Yamamoto, M. Oxidative stress sensor Keap1 functions as an adaptor for Cul3-based E3 ligase to regulate proteasomal degradation of Nrf2. *Mol. Cell. Biol.* **2004**, *24*, 7130–7139. [[CrossRef](#)] [[PubMed](#)]
33. Lumeng, C.N.; DelProposto, J.B.; Westcott, D.J.; Saltiel, A.R. Phenotypic switching of adipose tissue macrophages with obesity is generated by spatiotemporal differences in macrophage subtypes. *Diabetes* **2008**, *57*, 3239–3246. [[CrossRef](#)] [[PubMed](#)]
34. Liu, T.; Zhang, L.; Joo, D.; Sun, S.C. NF-kappaB signaling in inflammation. *Signal Transduct. Target. Ther.* **2017**, *2*, 1–9. [[CrossRef](#)] [[PubMed](#)]
35. Tugal, D.; Liao, X.; Jain, M.K. Transcriptional control of macrophage polarization. *Arterioscler. Thromb. Vasc. Biol.* **2013**, *33*, 1135–1144. [[CrossRef](#)]
36. Martinez, F.O.; Helming, L.; Gordon, S. Alternative activation of macrophages: An immunologic functional perspective. *Annu. Rev. Immunol.* **2009**, *27*, 451–483. [[CrossRef](#)]
37. Odegaard, J.I.; Ricardo-Gonzalez, R.R.; Goforth, M.H.; Morel, C.R.; Subramanian, V.; Mukundan, L.; Red Eagle, A.; Vats, D.; Brombacher, F.; Ferrante, A.W.; et al. Macrophage-specific PPARgamma controls alternative activation and improves insulin resistance. *Nature* **2007**, *447*, 1116–1120. [[CrossRef](#)]
38. Bouhrel, M.A.; Derudas, B.; Rigamonti, E.; Dievert, R.; Brozek, J.; Haulon, S.; Zawadzki, C.; Jude, B.; Torpier, G.; Marx, N.; et al. PPARgamma activation primes human monocytes into alternative M2 macrophages with anti-inflammatory properties. *Cell Metab.* **2007**, *6*, 137–143. [[CrossRef](#)]
39. Rigamonti, E.; Chinetti-Gbaguidi, G.; Staels, B. Regulation of macrophage functions by PPAR-alpha, PPAR-gamma, and LXRs in mice and men. *Arterioscler. Thromb. Vasc. Biol.* **2008**, *28*, 1050–1059. [[CrossRef](#)]
40. Ryu, S.J.; Choi, H.S.; Yoon, K.Y.; Lee, O.H.; Kim, K.J.; Lee, B.Y. Oleuropein suppresses LPS-induced inflammatory responses in RAW 264.7 cell and zebrafish. *J. Agric. Food Chem.* **2015**, *63*, 2098–2105. [[CrossRef](#)]
41. Mao, X.; Xia, B.; Zheng, M.; Zhou, Z. Assessment of the anti-inflammatory, analgesic and sedative effects of oleuropein from *Olea europaea* L. *Cell. Mol. Biol.* **2019**, *65*, 52–55. [[CrossRef](#)]
42. Jung, Y.C.; Kim, H.W.; Min, B.K.; Cho, J.Y.; Son, H.J.; Lee, J.Y.; Kim, J.Y.; Kwon, S.B.; Li, Q.; Lee, H.W. Inhibitory Effect of Olive Leaf Extract on Obesity in High-fat Diet-induced Mice. *In Vivo* **2019**, *33*, 707–715. [[CrossRef](#)] [[PubMed](#)]
43. Park, H.S.; Kim, S.H.; Kim, Y.S.; Ryu, S.Y.; Hwang, J.T.; Yang, H.J.; Kim, G.H.; Kwon, D.Y.; Kim, M.S. Luteolin inhibits adipogenic differentiation by regulating PPARgamma activation. *BioFactors* **2009**, *35*, 373–379. [[CrossRef](#)] [[PubMed](#)]
44. Cho, A.S.; Jeon, S.M.; Kim, M.J.; Yeo, J.; Seo, K.I.; Choi, M.S.; Lee, M.K. Chlorogenic acid exhibits anti-obesity property and improves lipid metabolism in high-fat diet-induced-obese mice. *Food Chem. Toxicol.* **2010**, *48*, 937–943. [[CrossRef](#)] [[PubMed](#)]
45. Shen, Y.; Song, S.J.; Keum, N.; Park, T. Olive leaf extract attenuates obesity in high-fat diet-fed mice by modulating the expression of molecules involved in adipogenesis and thermogenesis. *Evid. Based Complementary Altern. Med. Ecam* **2014**, *2014*, 971890. [[CrossRef](#)]
46. Lumeng, C.N.; Bodzin, J.L.; Saltiel, A.R. Obesity induces a phenotypic switch in adipose tissue macrophage polarization. *J. Clin. Investig.* **2007**, *117*, 175–184. [[CrossRef](#)]
47. Riera-Borrull, M.; Cuevas, V.D.; Alonso, B.; Vega, M.A.; Joven, J.; Izquierdo, E.; Corbi, A.L. Correction: Palmitate Conditions Macrophages for Enhanced Responses toward Inflammatory Stimuli via JNK Activation. *J. Immunol.* **2019**, *203*, 580. [[CrossRef](#)]

48. Ko, H.-J.; Lo, C.-Y.; Wang, B.-J.; Chiou, R.Y.-Y.; Lin, S.-M. Theaflavin-3, 3'-digallate, a black tea polyphenol, attenuates adipocyte-activated inflammatory response of macrophage associated with the switch of M1/M2-like phenotype. *J. Funct. Foods* **2014**, *11*, 36–48. [[CrossRef](#)]
49. Feng, X.; Weng, D.; Zhou, F.; Owen, Y.D.; Qin, H.; Zhao, J.; Wen, Y.; Huang, Y.; Chen, J.; Fu, H.; et al. Activation of PPARgamma by a Natural Flavonoid Modulator, Apigenin Ameliorates Obesity-Related Inflammation Via Regulation of Macrophage Polarization. *EBioMedicine* **2016**, *9*, 61–76. [[CrossRef](#)]
50. Feng, X.; Qin, H.; Shi, Q.; Zhang, Y.; Zhou, F.; Wu, H.; Ding, S.; Niu, Z.; Lu, Y.; Shen, P. Chrysin attenuates inflammation by regulating M1/M2 status via activating PPARgamma. *Biochem. Pharmacol.* **2014**, *89*, 503–514. [[CrossRef](#)]
51. Pardo, V.; Gonzalez-Rodriguez, A.; Guijas, C.; Balsinde, J.; Valverde, A.M. Opposite cross-talk by oleate and palmitate on insulin signaling in hepatocytes through macrophage activation. *J. Biol. Chem.* **2015**, *290*, 11663–11677. [[CrossRef](#)]
52. Xiu, F.; Diao, L.; Qi, P.; Catapano, M.; Jeschke, M.G. Palmitate differentially regulates the polarization of differentiating and differentiated macrophages. *Immunology* **2016**, *147*, 82–96. [[CrossRef](#)] [[PubMed](#)]
53. Fain, J.N. Release of interleukins and other inflammatory cytokines by human adipose tissue is enhanced in obesity and primarily due to the nonfat cells. *Vitam. Horm.* **2006**, *74*, 443–477. [[CrossRef](#)] [[PubMed](#)]
54. Wen, H.; Gris, D.; Lei, Y.; Jha, S.; Zhang, L.; Huang, M.T.; Brickey, W.J.; Ting, J.P. Fatty acid-induced NLRP3-ASC inflammasome activation interferes with insulin signaling. *Nat. Immunol.* **2011**, *12*, 408–415. [[CrossRef](#)] [[PubMed](#)]
55. Everett, B.M.; Donath, M.Y.; Pradhan, A.D.; Thuren, T.; Pais, P.; Nicolau, J.C.; Glynn, R.J.; Libby, P.; Ridker, P.M. Anti-Inflammatory Therapy With Canakinumab for the Prevention and Management of Diabetes. *J. Am. Coll. Cardiol.* **2018**, *71*, 2392–2401. [[CrossRef](#)] [[PubMed](#)]
56. Kobayashi, M.; Yamamoto, M. Molecular mechanisms activating the Nrf2-Keap1 pathway of antioxidant gene regulation. *Antioxid. Redox Signal.* **2005**, *7*, 385–394. [[CrossRef](#)] [[PubMed](#)]
57. Zhang, Y.K.; Yeager, R.L.; Tanaka, Y.; Klaassen, C.D. Enhanced expression of Nrf2 in mice attenuates the fatty liver produced by a methionine-and choline-deficient diet. *Toxicol. Appl. Pharmacol.* **2010**, *245*, 326–334. [[CrossRef](#)]
58. Yu, Z.; Shao, W.; Chiang, Y.; Foltz, W.; Zhang, Z.; Ling, W.; Fantus, I.G.; Jin, T. Oltipraz upregulates the nuclear factor (erythroid-derived 2)-like 2 [corrected](NRF2) antioxidant system and prevents insulin resistance and obesity induced by a high-fat diet in C57BL/6j mice. *Diabetologia* **2011**, *54*, 922–934. [[CrossRef](#)]
59. Bronte, V.; Zanovello, P. Regulation of immune responses by L-arginine metabolism. *Nat. Rev. Immunol.* **2005**, *5*, 641–654. [[CrossRef](#)]
60. Wahli, W.; Michalik, L. PPARs at the crossroads of lipid signaling and inflammation. *Trends Endocrinol. Metab.* **2012**, *23*, 351–363. [[CrossRef](#)]
61. Martin, H. Role of PPAR-gamma in inflammation. Prospects for therapeutic intervention by food components. *Mutat. Res.* **2009**, *669*, 57–63. [[CrossRef](#)]
62. Marciano, D.P.; Chang, M.R.; Corzo, C.A.; Goswami, D.; Lam, V.Q.; Pascal, B.D.; Griffin, P.R. The therapeutic potential of nuclear receptor modulators for treatment of metabolic disorders: PPARgamma, RORs, and Rev-erbs. *Cell Metab.* **2014**, *19*, 193–208. [[CrossRef](#)] [[PubMed](#)]
63. Aparicio-Soto, M.; Montserrat-de la Paz, S.; Sanchez-Hidalgo, M.; Cardeno, A.; Bermudez, B.; Muriana, F.J.G.; Alarcon-de-la-Lastra, C. Virgin olive oil and its phenol fraction modulate monocyte/macrophage functionality: A potential therapeutic strategy in the treatment of systemic lupus erythematosus. *Br. J. Nutr.* **2018**, *120*, 681–692. [[CrossRef](#)] [[PubMed](#)]
64. Svobodova, M.; Andreadou, I.; Skaltsounis, A.L.; Kopecky, J.; Flachs, P. Oleuropein as an inhibitor of peroxisome proliferator-activated receptor gamma. *Genes Nutr.* **2014**, *9*, 376. [[CrossRef](#)] [[PubMed](#)]

Publisher's Note: MDPI stays neutral with regard to jurisdictional claims in published maps and institutional affiliations.



© 2020 by the authors. Licensee MDPI, Basel, Switzerland. This article is an open access article distributed under the terms and conditions of the Creative Commons Attribution (CC BY) license (<http://creativecommons.org/licenses/by/4.0/>).

Article

Mikania micrantha Extract Inhibits HMG-CoA Reductase and ACAT2 and Ameliorates Hypercholesterolemia and Lipid Peroxidation in High Cholesterol-Fed Rats

Azlinna Ibrahim ¹, Nurul Husna Shafie ^{1,2,*}, Norhaizan Mohd Esa ¹, Siti Raihanah Shafie ¹, Hasnah Bahari ³ and Maizatun Atmadini Abdullah ^{4,5}

¹ Department of Nutrition and Dietetics, Faculty of Medicine and Health Sciences, Universiti Putra Malaysia, Serdang 43400, Selangor, Malaysia; azlinnaibrahim92@gmail.com (A.I.); nhaizan@upm.edu.my (N.M.E.); sitiraihanah@upm.edu.my (S.R.S.)

² Laboratory of UPM-MAKNA Cancer Research, Institute of Bioscience, Universiti Putra Malaysia, Serdang 43400, Selangor, Malaysia

³ Department of Human Anatomy, Faculty of Medicine and Health Sciences, Universiti Putra Malaysia, Serdang 43400, Selangor, Malaysia; haba@upm.edu.my

⁴ Department of Pathology, Faculty of Medicine and Health Sciences, Universiti Putra Malaysia, Serdang 43400, Selangor, Malaysia; maizatun@upm.edu.my

⁵ Institute of Bioscience, Universiti Putra Malaysia, Serdang 43400, Selangor, Malaysia

* Correspondence: nhusnashafie@upm.edu.my; Tel.: +60-39769-2470

Received: 27 July 2020; Accepted: 15 September 2020; Published: 9 October 2020

Abstract: The present study aimed to determine the effect of an ethyl acetate extract of *Mikania micrantha* stems (EAMMS) in hypercholesterolemia-induced rats. Rats were divided into a normal group (NC) and hypercholesterolemia induced groups: hypercholesterolemia control group (PC), simvastatin group (SV) (10 mg/kg) and EAMMS extract groups at different dosages of 50, 100 and 200 mg/kg, respectively. Blood serum and tissues were collected for haematological, biochemical, histopathological, and enzyme analysis. Total cholesterol (TC), triglycerides (TG), low-density lipoprotein cholesterol (LDL-C), high-density lipoprotein cholesterol (HDL-C), aspartate aminotransferase (AST), alanine aminotransferase (ALT), urea, creatinine, malondialdehyde (MDA) level, as well as enzymes of HMG-CoA reductase (HMGCR) and acetyl-CoA acetyltransferase 2 (ACAT2), were measured. Feeding rats with high cholesterol diet for eight weeks resulted in a significantly ($p < 0.05$) increased of TC, TG, LDL-C, AST, ALT and MDA levels. Meanwhile, the administration of EAMMS extract (50, 100 and 200 mg/kg) and simvastatin (10 mg/kg) significantly reduced ($p < 0.05$) the levels of TC, TG, LDL-C and MDA compared to rats in the PC group. Furthermore, all EAMMS and SV-treated groups showed a higher HDL-C level compared to both NC and PC groups. No significant difference was found in the level of ALT, AST, urea and creatinine between the different dosages in EAMMS extracts. Treatment with EAMMS also exhibited the highest inhibition activity of enzyme HMGCR and ACAT2 as compared to the control group. From the histopathological examination, liver tissues in the PC group showed severe steatosis than those fed with EAMMS and normal diet. Treatment with EAMMS extract ameliorated and reduced the pathological changes in the liver. No morphological changes showed in the kidney structure of both control and treated groups. In conclusion, these findings demonstrated that EAMMS extract has anti-hypercholesterolemia properties and could be used as an alternative treatment for this disorder.

Keywords: *Mikania micrantha*; anti-hypercholesterolemia; lipid profile; steatosis; nutraceuticals

1. Introduction

Hypercholesterolemia is a metabolic disorder that mainly results in an elevated concentration of plasma low density lipoprotein (LDL) cholesterol [1]. Hypercholesterolemia has been associated with many cardiovascular diseases, including atherosclerosis, stroke, cerebral paralysis, myocardial infarction [2] and also inflammation and cancer [3]. One of the bigger challenges in modern medicine is the identification of a cure for hypercholesterolemia which does not confer side effects. In recent times, plant-sourced products have been considered to be possible novel therapeutic agents as these are considerably less toxic, cost-effective and most importantly, they produce no or relatively lesser side effects as compared to their synthetic counterparts.

Mikania micrantha Kunth originates from the tropical central and southern part of America and is extensively spread in the Pacific region and Southeast Asian countries. *M. micrantha* is traditionally used to treat stomach aches, jaundice, respiratory diseases, dysentery and rheumatism. This perennial creeping vine is also consumed as a juice as an alternative medicine for the treatment of diabetes, hypertension and hypercholesterolemia [4,5]. *M. micrantha* were previously reported to possess many health benefits such as antioxidant [6], anti-diabetic [7], anti-cancer [8,9], antiproliferative [10], anti-dermatophytic [11], anti-inflammatory [12] and antibacterial [5] activities. These beneficial effects are related to the richness of chemical constituents such as terpenoids, flavonoids, alkaloids and vitamins [5,6,11,13].

Despite its traditional use, scientific findings to prove the traditional claims of the anti-hypercholesterolemia properties of *M. micrantha* are limited. For that reason, this study aimed to determine the hypocholesterolemic potential of an ethyl acetate extract of *M. micrantha* stems (EAMMS) on male high-cholesterol-fed rats by determining the serum lipid profile [TC, total cholesterol; TG, triglycerides; HDL-C, high-density lipoproteins cholesterol; LDL-C, low-density lipoproteins cholesterol], lipid peroxidation, enzymatic activities and histopathological evaluation.

2. Materials and Methods

2.1. Reagents and Chemicals

Ethyl acetate (HmbG Chemical, Hamburg, Germany), ethanol (R&M Chemicals), haematoxylin (Sigma-Aldrich, St Louis, MO, USA), simvastatin (Pharmaniaga Logistics (M) Sdn. Bhd, Malaysia), 10% formalin (R&M Chemicals), xylene (R&M Chemicals) and eosin (Leica Biosystems Richmond Inc., Richmond, IL, USA) were used in this study. Pierce BCA Protein Assay Kits for protein quantification were purchased from Thermo Fisher Scientific (Rockford, IL, USA). Malondialdehyde (MDA) assay kits for lipid peroxidation assays were purchased from Elabscience Biotechnology Inc. (Houston, TX, USA). ELISA Kits (HMGCR and ACAT2) were purchased from Sunlong Biotech Co. Ltd. (Zhejiang, China). High cholesterol diet (1%) was purchased from EnvigoTeklad (Cambridgeshire, UK).

2.2. Sample Preparation

Mikania micrantha was collected in August 2017 from Negeri Sembilan, Malaysia (GPS: 2.695652,102.160987) and a plant sample was deposited in the Forest Research Institute Malaysia (FRIM), Kepong, Selangor, Malaysia for taxonomic identification with a voucher specimen number of SBID 051/15. Fresh stems of *M. micrantha* was selected and washed and then dried at 35 °C for 72 h in a ventilated drying oven. *M. micrantha* powdered stems were then extracted using ethyl acetate and evaporated at 48 °C [6].

2.3. Animals

Sprague Dawley rats (male, 150–200 g weight) were purchased in this study. The rats were given tap water *ad libitum* and acclimatized under standardized laboratory circumstances (temperature 22 ± 2 °C; humidity 60 ± 4%; 12 h light-dark cycle). All animals used had received approval from the Universiti Putra Malaysia's Institutional Animal Care and Use Committee (UPM/IACUC/AUP-R081/2017).

2.4. Animal Experimental Design

The rats were divided into six groups ($n = 6$). Group 1 as normal control (NC) was fed with a normal diet for 8 weeks. Group 2 to 6 were orally administered with high cholesterol diet (1%) throughout the study for 8 weeks. After the 4th week of the induction period, Group 2 was served as cholesterol-induced rats (PC). Group 3 was treated by orally administered via gavage with an aqueous suspension of simvastatin, SV (10 mg/kg) and groups of 4, 5 and 6 were orally administered via gavage with EAMMS at the dosage of 50, 100 and 200 mg/kg, respectively, during the treatment periods. The rats were treated for 4 weeks. Upon the administration of the last treatment dose, the animals were left to fast for 18 h. Blood samples were then acquired through the cardiac puncture approach with subjects under anaesthesia (ketamine/xylazine). Then, the blood samples were centrifuged at 3000 rpm at 4 °C for 10 min and the serum was stored at a temperature of −80 °C until the point of the assay. The liver and kidney were excised, weight and also stored at a temperature of −80 °C until the point of analysis.

2.5. Liver, Kidney and Haematogram Profile Analysis

Analysis of both liver and kidney profile including aspartate aminotransferase (AST), alanine aminotransferase (ALT), urea and creatinine were analyzed using a fully automated BiOLiS 24i Premium clinical analyzer (Hitachi, Bolton, UK). The total number of red blood cells (RBC), haemoglobin (Hb), packed cell volume (PCV), mean corpuscular volume (MCV), mean corpuscular haemoglobin volume (MCHC), white blood cell (WBC), icterus index, and plasma protein concentration were analysed.

2.6. Lipid Profile Analysis

The parameters that were analysed included total cholesterol (TC), triglycerides (TG), low density lipoproteins (LDL-C) and high density lipoproteins (HDL-C). The analyses were conducted using a fully automated clinical analyser (BiOLiS 24i Premium, Hitachi).

2.7. Serum Lipid Peroxidation

MDA level was quantified in the blood serum using a rat malondialdehydes (MDA) ELISA kit from Elabscience Biotechnology Inc., (Houston, TX, USA). All the procedures were conducted carefully according to the manufacturer's instructions. The absorbance was measured at 450 nm.

2.8. Histopathological Examination

Briefly, 10% formalin buffer solution was used to fix the liver and kidney. Upon fixing, the tissues were subjected to paraffin embedding and being stained with haematoxylin and eosin (H&E) dye. The tissues of interest which have been stained were viewed and analysed using an image analyser. The histology of selected tissues was evaluated qualitatively and quantitatively. The microscopic analysis of all tissue samples was evaluated as a blind study by a pathologist and other researchers. Grading was conducted on the severity of steatosis which afflicted liver tissues and this was done according to the approach as described by Brunt et al. [14].

2.9. HMGCR and ACAT2 Activity Assays

Protein from liver tissue was homogenized in phosphate buffered saline (PBS, pH 7.4) at 4 °C. The supernatant was then centrifuged at 3500× g with 4 °C for 10 min and quantified with a BCA protein assay kit according to kit instructions. The levels of HMG-CoA reductase (HMGCR) and acetyl-CoA acetyltransferase 2 (ACAT2) enzymes were measured according to the ELISA protocol provided by the manufacturer.

2.10. Statistical Analysis

The data were expressed as mean \pm standard error of the mean (SEM) for body and organ weight, haematological parameters, liver and kidney profile, lipid profile, lipid peroxidation and enzymatic analysis. All data were analysed using one-way analysis of variance (ANOVA) and Tukey's multiple comparison tests ($p < 0.05$).

3. Results

3.1. Body and Organ Weights

The changes in body weights of rats during the experiments are presented in Figure 1. All groups showed increased body weights throughout the study. The NC group exhibited an increasing body weight throughout the experimental period. After 4 weeks of induction with high cholesterol diet (HCD), the body weight of all HCD-induced groups was increased compared to the normal group (NC) but not significantly when compared to each other (Figure 1). Besides, there was a significant increased ($p < 0.05$) in the body weight of rats fed with high cholesterol diet for 8 weeks compared to the NC group. On the other hand, after the treatment period with EAMMS at different dosages, the body weight was shown to have lower body weight but not significant ($p > 0.05$) when compared to the PC group. Among the EAMMS-treated group, 100 mg/kg showed the highest body weight increment but not significant when compared to 50 mg/kg and 200 mg/kg treatment groups. The SV-treated group was showed no significant difference ($p > 0.05$) of body weight when compared to PC and EAMMS (50, 100 and 200 mg/kg) groups.

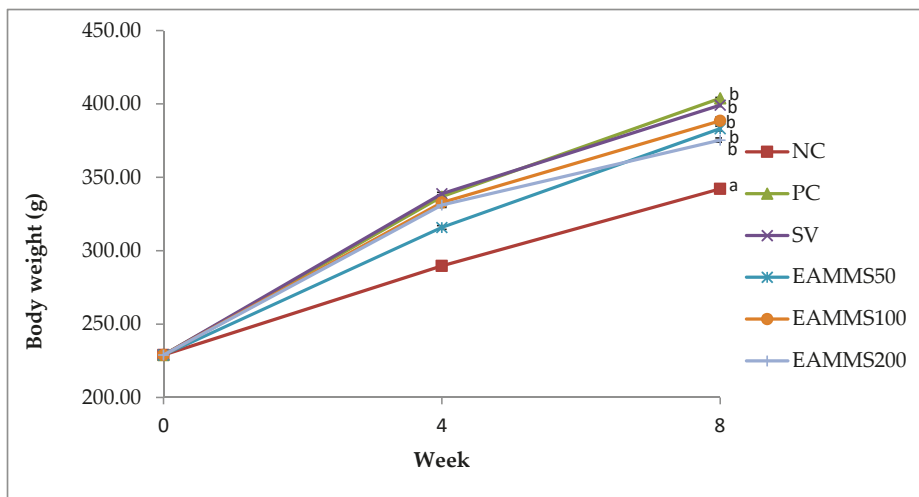


Figure 1. Effects of ethyl acetate extract of *Mikania micrantha* stems (EAMMS) on body weight in hypercholesterolemia rats. Values are expressed as mean \pm SEM ($n = 6$). Means with different superscripts (a or b) indicate statistically different at $p < 0.05$ using Tukey's multiple comparison test. NC—Normal control; PC—Positive control with high cholesterol diet (1%); SV—High cholesterol diet (1%) with simvastatin (10 mg/kg body weight); EAMMS50—High cholesterol diet (1%) with ethyl acetate *Mikania micrantha* stem extract (50 mg/kg body weight); EAMMS100—High cholesterol diet (1%) with ethyl acetate *Mikania micrantha* stem extract (100 mg/kg body weight); EAMMS200—High cholesterol diet (1%) with ethyl acetate *Mikania micrantha* stem extract (200 mg/kg body weight).

Table 1 indicates the weights of the livers and kidneys of the experimental rats. The liver weight from the PC group was significantly higher ($p < 0.05$) compared to the NC group and no difference with all EAMMS-treated groups. Meanwhile, there are no significant differences ($p > 0.05$) of kidney weight (right or left) between all groups.

Table 1. Organ weight of rats at week 8.

Group	Liver	Kidney Right	Kidney Left
NC	9.06 ± 0.20 ^a	1.12 ± 0.15 ^a	1.16 ± 0.13 ^a
PC	21.91 ± 0.39 ^b	1.19 ± 0.11 ^a	1.21 ± 0.05 ^a
SV	20.57 ± 0.60 ^b	1.22 ± 0.15 ^a	1.24 ± 0.17 ^a
EAMMS50	17.51 ± 0.83 ^b	1.13 ± 0.13 ^a	1.11 ± 0.19 ^a
EAMMS100	18.40 ± 0.72 ^b	1.18 ± 0.21 ^a	1.15 ± 0.25 ^a
EAMMS200	17.67 ± 0.45 ^b	1.16 ± 0.16 ^a	1.09 ± 0.15 ^a

Values are expressed as mean ± SEM ($n = 6$). Means with different superscripts (a or b) in a column indicate statistically different at $p < 0.05$ by Tukey's multiple comparison tests. NC—Normal control; PC—Positive control with high cholesterol diet (1%); SV—High cholesterol diet (1%) with simvastatin (10 mg/kg body weight); EAMMS50—High cholesterol diet (1%) with ethyl acetate *Mikania micrantha* stem extract (50 mg/kg body weight); EAMMS100—High cholesterol diet (1%) with ethyl acetate *Mikania micrantha* stem extract (100 mg/kg body weight); EAMMS200—High cholesterol diet (1%) with ethyl acetate *Mikania micrantha* stem extract (200 mg/kg body weight).

3.2. Effect of EAMMS on Liver, Kidney and Haematogram Parameters

Table 2 shows the serum haematological, liver and kidney profiles of rats. Rats that were fed with a diet supplemented with 1% cholesterol for 8 weeks displayed a significant ($p < 0.05$) increase in AST, ALT and MCV levels. This is apparent when the PC group is compared against the NC group. Meanwhile, the levels of urea, creatinine, RBC, MCHC, WBC from the PC group showed slight increases but these were not significant ($p > 0.05$) when compared to the NC group. After 4 weeks of treatment, the levels of AST, ALT and MCV in the EAMMS-treated groups were not significant ($p > 0.05$) when compared to the PC group whilst the RBC, MCHC, WBC and additionally the kidney profiles (urea, creatinine), showed no significant differences between all groups.

Table 2. Liver, kidney and haematology values of rats after treated with EAMMS extracts (week 8).

Parameters	NC	PC	SV	EAMMS 50	EAMMS 100	EAMMS 200
AST (U/L)	127.16 ± 1.78 ^a	222.00 ± 6.06 ^b	264.33 ± 4.72 ^c	162.83 ± 7.36 ^{a,b}	207.83 ± 3.07 ^{a,b}	148.5 ± 4.01 ^{a,b}
ALT (U/L)	71.00 ± 1.99 ^a	226.00 ± 7.21 ^b	191.00 ± 7.01 ^c	134.00 ± 4.95 ^{a,c}	194.00 ± 4.83 ^{a,c}	182.00 ± 6.36 ^{a,c}
Urea (mmol/L)	5.00 ± 0.30 ^a	6.00 ± 0.39 ^a	6.00 ± 0.21 ^a	6.00 ± 0.46 ^a	6.00 ± 0.26 ^a	7.00 ± 0.48 ^a
Creatinine (umol/L)	41.00 ± 1.10 ^a	49.00 ± 0.80 ^a	48.00 ± 0.86 ^a	48.00 ± 1.34 ^a	48.00 ± 1.07 ^a	54.00 ± 1.11 ^b
RBC ($10^{12}/L$)	7.49 ± 0.20 ^a	8.57 ± 0.29 ^a	9.26 ± 0.25 ^a	8.84 ± 0.10 ^a	9.16 ± 0.16 ^a	8.62 ± 0.17 ^a
Hb (g/L)	149.50 ± 0.59 ^a	144.83 ± 1.50 ^a	155.33 ± 0.87 ^a	152.33 ± 0.93 ^a	159.17 ± 0.44 ^a	149.67 ± 0.57 ^a
PCV (l/L)	0.42 ± 0.04 ^a	0.38 ± 0.07 ^a	0.44 ± 0.05 ^a	0.42 ± 0.03 ^a	0.43 ± 0.02 ^a	0.40 ± 0.03 ^a
MCV (fl)	55.90 ± 0.12 ^a	44.15 ± 0.37 ^b	47.59 ± 0.32 ^b	47.20 ± 0.57 ^b	46.48 ± 0.32 ^b	46.26 ± 0.13 ^b
MCHC (g/L)	358.55 ± 0.50 ^a	382.61 ± 0.52 ^a	353.25 ± 0.41 ^a	365.41 ± 0.78 ^a	374.56 ± 0.30 ^a	375.86 ± 0.48 ^a
WBC ($\times 10^9/L$)	9.62 ± 0.62 ^a	11.37 ± 1.13 ^a	13.03 ± 0.44 ^a	11.63 ± 0.73 ^a	13.13 ± 0.62 ^a	10.08 ± 0.68 ^a
Neutrophils ($\times 10^9/L$)	2.91 ± 0.36 ^a	4.19 ± 1.23 ^a	4.47 ± 0.78 ^a	3.61 ± 0.57 ^a	4.13 ± 0.45 ^a	3.22 ± 0.90 ^a
Lymphocytes ($\times 10^9/L$)	6.12 ± 0.53 ^a	6.34 ± 0.68 ^a	7.66 ± 0.52 ^a	7.15 ± 0.50 ^a	8.08 ± 0.48 ^a	6.26 ± 0.71 ^a
Monocytes ($\times 10^9/L$)	0.45 ± 0.18 ^a	0.59 ± 0.36 ^a	0.66 ± 0.19 ^a	0.59 ± 0.28 ^a	0.67 ± 0.22 ^a	0.46 ± 0.21 ^a
Eosinophils ($\times 10^9/L$)	0.04 ± 0.30 ^a	0.11 ± 0.17 ^a	0.09 ± 0.23 ^a	0.16 ± 0.31 ^a	0.13 ± 0.20 ^a	0.03 ± 0.29 ^a
Icterus index	2.00 ± 0 ^a	2.00 ± 0 ^a	2.00 ± 0 ^a	2.00 ± 0 ^a	2.00 ± 0 ^a	2.00 ± 0 ^a
Plasma protein (g/L)	73.00 ± 0.49 ^a	86.67 ± 0.68 ^b	87.00 ± 0.33 ^b	82.33 ± 0.51 ^b	80.67 ± 0.44 ^b	77.33 ± 0.40 ^b

Values are expressed as mean ± SEM ($n = 6$). Means with different superscripts (a, b or c) in the same row indicate statistically different at $p < 0.05$ by Tukey's multiple comparison test. NC—Normal control; PC—Positive control with high cholesterol diet (1%); SV—High cholesterol diet (1%) with simvastatin (10 mg/kg body weight); EAMMS50—High cholesterol diet (1%) with ethyl acetate *Mikania micrantha* stem extract (50 mg/kg body weight); EAMMS100—High cholesterol diet (1%) with ethyl acetate *Mikania micrantha* stem extract (100 mg/kg body weight); EAMMS200—High cholesterol diet (1%) with ethyl acetate *Mikania micrantha* stem extract (200 mg/kg body weight); AST—Aspartate aminotransferase; ALT—Alanine aminotransferase; RBC—Red blood cells; Hb—Haemoglobin; PCV—Packed cell volume; MCV—Mean corpuscular volume; MCHC—Mean corpuscular haemoglobin concentration; WBC—White blood cells.

However, among the different dosages of EAMMS, 200 mg/kg resulted in a significant increase ($p < 0.05$) in the level of creatinine compared to the other dosages of EAMMS-treated and NC groups. In the SV-treated group, both AST and ALT levels showed significantly increases ($p < 0.05$) when compared to PC groups. Besides, there were no significant ($p > 0.05$) differences in Hb concentration and icterus index at all EAMMS dosages and controls. The PCV level also was not affected by the treatment of EAMMS in this study. For the leukocyte parameters, no significant differences were identified in terms of WBC count as well as differential leukocyte count.

3.3. Effect of EAMMS on Lipid Profile

Table 3 shows TC, TG, LDL-C and HDL-C levels in the serum of the experimental rats. The results show that feeding rats a diet supplemented with 1% cholesterol for 8 weeks resulted in a significant ($p < 0.05$) increase in TC, TG and LDL-C levels in the PC group compared to the NC group. After 4 weeks of the treatment (EAMMS and SV) period, there were significant ($p < 0.05$) decreases in serum TC, TG and LDL-C levels observed in the EAMMS-treated and SV groups compared to the PC group (Table 3). The levels of HDL-C in all EAMMS-treated groups and SV group showed no significant ($p > 0.05$) differences when compared to control groups (NC and PC). There were no significant differences ($p > 0.05$) in the level of serum TC, TG, LDL-C and HDL-C when compared between different dosages of EAMMS extract at week 8. Besides, the level of TC, TG, LDL-C and HDL-C in all EAMMS-treated groups were comparable and not significant ($p > 0.05$) as compared to the SV-treated group.

Table 3. Serum lipid profiles of hypercholesterolemia-induced rats treated with different concentrations of *Mikania micrantha* stems (EAMMS) extracts at week 8.

Group	TC (mmol/L)	TG (mmol/L)	LDL-C (mmol/L)	HDL-C (mmol/L)
NC	1.18 ± 0.14 ^a	0.56 ± 0.11 ^a	0.24 ± 0.10 ^a	1.27 ± 0.09 ^a
PC	3.16 ± 0.39 ^b	0.73 ± 0.17 ^b	2.64 ± 0.39 ^b	1.65 ± 0.36 ^a
SV	1.45 ± 0.13 ^a	0.41 ± 0.21 ^a	1.09 ± 0.27 ^c	1.59 ± 0.17 ^a
EAMMS50	1.61 ± 0.18 ^a	0.48 ± 0.14 ^a	1.09 ± 0.28 ^c	1.60 ± 0.25 ^a
EAMMS100	1.53 ± 0.11 ^a	0.46 ± 0.29 ^a	1.12 ± 0.19 ^c	1.61 ± 0.09 ^a
EAMMS200	1.65 ± 0.38 ^a	0.46 ± 0.33 ^a	1.02 ± 0.26 ^c	1.79 ± 0.55 ^a

Values are expressed as mean ± SEM ($n = 6$). Means with different superscripts (a, b or c) in a column indicate statistically different at $p < 0.05$ by Tukey's multiple comparison tests. NC—Normal control; PC—Positive control with high cholesterol diet (1%); SV—High cholesterol diet (1%) with simvastatin (10 mg/kg body weight); EAMMS50—High cholesterol diet (1%) with ethyl acetate *Mikania micrantha* stem extract (50 mg/kg body weight); EAMMS100—High cholesterol diet (1%) with ethyl acetate *Mikania micrantha* stem extract (100 mg/kg body weight); EAMMS200—High cholesterol diet (1%) with ethyl acetate *Mikania micrantha* stem extract (200 mg/kg body weight); TC: Total cholesterol; TG: Triglyceride; LDL-C: Low density lipoprotein cholesterol; HDL-C: High density lipoprotein cholesterol.

3.4. Effect of EAMMS on Lipid Peroxidation

The levels of malondialdehyde (MDA) in the serum of experimental rats are listed in Table 4. Rats fed with a diet supplemented with 1% cholesterol over 8 weeks had significant ($p < 0.05$) increases in MDA levels when compared between the PC group and the NC group. After 4 weeks of the treatment period, there were marked and significant decreases ($p < 0.05$) in serum MDA levels observed in the EAMMS-treated and SV groups compared to the PC group but these were not significant when compared to the NC group. The comparison of different dosages of EAMMS extract did not show any significant differences ($p > 0.05$) in the serum MDA levels at week 8 (Table 4).

Table 4. Effect of ethyl acetate extract of *Mikania micrantha* stems (EAMMS) on lipid peroxidation using TBARS assay in hypercholesterolemia rats at week 8.

Group	MDA Level (ng/mL)
NC	137.71 ± 1.98 ^a
PC	247.83 ± 5.98 ^b
SV	142.06 ± 5.47 ^a
EAMMS50	157.19 ± 3.93 ^a
EAMMS100	143.54 ± 2.20 ^a
EAMMS200	152.66 ± 3.68 ^a

Values are expressed as mean ± SEM ($n = 6$). Means with different superscripts (a or b) indicate statistically different at $p < 0.05$ by Tukey's multiple comparison tests. NC—Normal control; PC—Positive control with high cholesterol diet (1%); SV—High cholesterol diet (1%) with simvastatin (10 mg/kg body weight); EAMMS50—High cholesterol diet (1%) with ethyl acetate *Mikania micrantha* stem extract (50 mg/kg body weight); EAMMS100—High cholesterol diet (1%) with ethyl acetate *Mikania micrantha* stem extract (100 mg/kg body weight); EAMMS200—High cholesterol diet (1%) with ethyl acetate *Mikania micrantha* stem extract (200 mg/kg body weight); TBARS—Thiobarbituric acid reactive substances; MDA—Malondialdehyde.

3.5. Histopathological Results

Table 5 shows the results for the liver histopathological scoring analysis of rats. Liver steatosis was absent in the NC group but observed in the PC group. There was a significant difference in steatosis between the PC group and those fed with EAMMS and NC diet. Liver tissues in the PC group showed severe diffuse steatosis within the hepatocytes and loss of single cell plates. The hepatocytes showed large cytoplasmic vacuoles due to fat deposition. However, there was no lobular or portal tract inflammation observed in the PC group. In the SV group, mild portal inflammation was observed accompanying moderate steatosis. There were expanded of losses single cell plates of hepatocytes with no significant lymphocytic infiltration in the portal tract. All EAMMS-treated liver had significantly less ($p < 0.05$) liver fat deposited than the PC group, with no inflammation, fibrosis or congestion on them that similar to that of the NC group (Table 5, Figure 2).

The effects of EAMMS in kidney tissues are illustrated in Figure 3. None of the treated and control groups showed any morphological changes in kidney structure. The sections for each group showed normal appearance with regulated nuclear arrangement of uriniferous tubules and collecting tubules with normal looking glomeruli, there was absence of sclerosis, no mesangial proliferation and no inflammation in the kidney parenchyma.

Table 5. Liver steatosis and inflammation scores in rats of different groups.

Group	Steatosis	Inflammation
NC	-	-
PC	+++	-
SV	++	+
EAMMS50	++	-
EAMMS100	++	-
EAMMS200	+	-

Normal (-): No hepatocytes; Grade 1 (+): <33% of hepatocytes; Grade 2 (++) : 33% to 66% of hepatocytes and Grade 3 (+++) : >66% of hepatocytes involved [14].

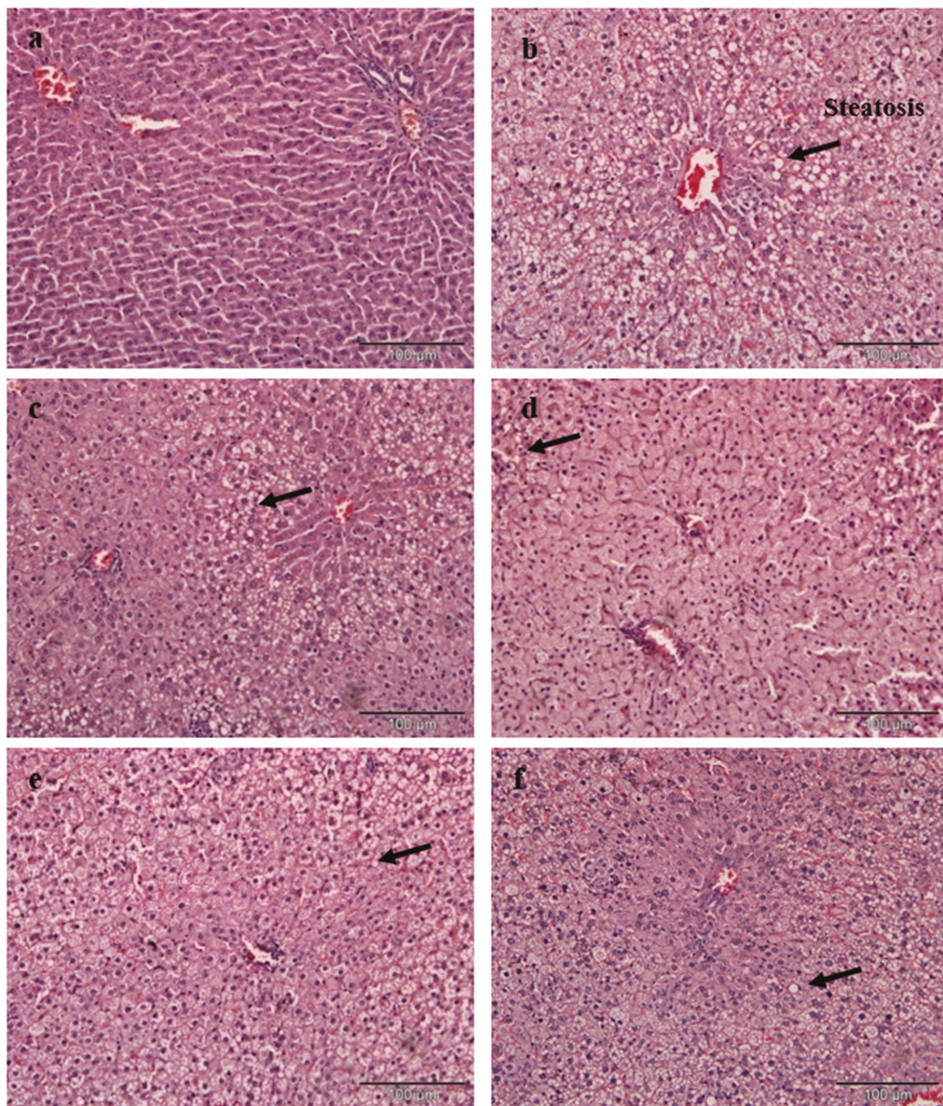


Figure 2. Histopathology of rat liver tissue in different groups. (a) NC—Normal control, (b) PC—Positive control with high cholesterol diet (1%), (c) SV—High cholesterol diet (1%) with simvastatin (10 mg/kg body weight), (d) EAMMS50—High cholesterol diet (1%) with ethyl acetate *Mikania micrantha* stem extract (50 mg/kg body weight), (e) EAMMS100 High cholesterol diet (1%) with ethyl acetate *Mikania micrantha* stem extract (100 mg/kg body weight), (f) EAMMS200—High cholesterol diet (1%) with ethyl acetate *Mikania micrantha* stem extract (200 mg/kg body weight). Livers were stained with hematoxylin and eosin (H&E) and visualized under a light microscope at 100× magnification.

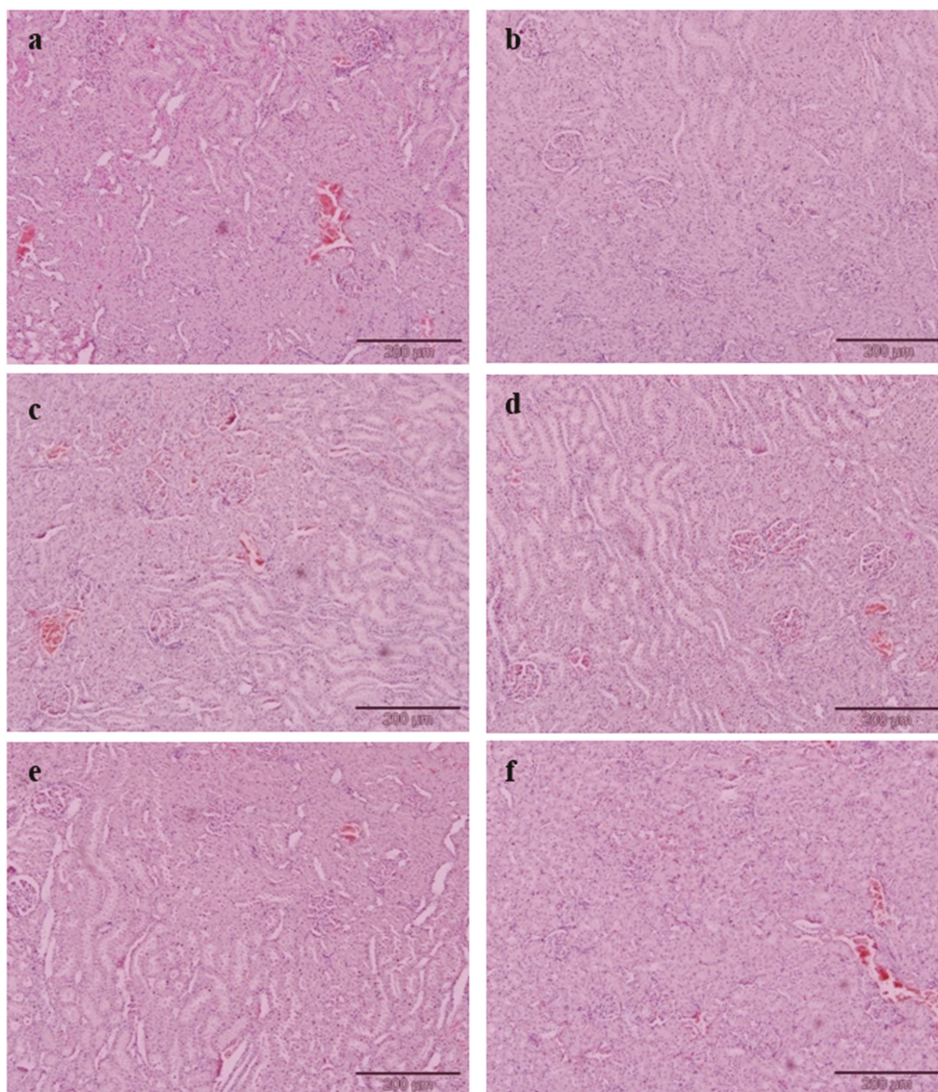


Figure 3. Histology of rat kidney tissue in different groups. (a) NC—Normal control, (b) PC—Positive control with high cholesterol diet (1%), (c) SV—High cholesterol diet (1%) with simvastatin (10 mg/kg body weight), (d) EAMMS50—High cholesterol diet (1%) with ethyl acetate *Mikania micrantha* stem extract (50 mg/kg body weight), (e) EAMMS100 High cholesterol diet (1%) with ethyl acetate *Mikania micrantha* stem extract (100 mg/kg body weight), (f) EAMMS200—High cholesterol diet (1%) with ethyl acetate *Mikania micrantha* stem extract (200 mg/kg body weight). Kidneys were stained with hematoxylin and eosin (H&E) and visualized under a light microscope at 200× g magnification.

3.6. Effect of EAMMS on HMGCR and ACAT2 Enzymes

The levels of HMG-CoA reductase (HMGCR) of experimental rats are given in Table 6. Rats that have been fed with a diet supplemented with 1% cholesterol over 8 weeks had significant ($p < 0.05$) increases in HMGCR levels when compared to the NC group. After 4 weeks of treatment, there were significant decreases ($p < 0.05$) in the HMGCR levels observed in the EAMMS-treated and SV groups compared to the PC group. Among the three different dosages of EAMMS extract, no significant difference ($p > 0.05$) was observed in the HMGCR levels at week 8 when compared to each other (Table 6).

Table 6. Effect of ethyl acetate extract of *Mikania micrantha* stems (EAMMS) on HMG-CoA reductase level in experimental rats at week 8.

Group	HMGCR (pg/mL)
NC	202.10 ± 6.68 ^a
PC	271.50 ± 11.94 ^b
SV	245.88 ± 15.94 ^c
EAMMS50	258.54 ± 13.70 ^c
EAMMS100	254.22 ± 8.64 ^c
EAMMS200	255.33 ± 21.33 ^c

Values are expressed as mean ± SEM ($n = 6$). Means with different superscripts (a, b or c) indicate statistically different at $p < 0.05$ by Tukey's multiple comparison tests. NC—Normal control; PC—Positive control with high cholesterol diet (1%); SV—High cholesterol diet (1%) with simvastatin (10 mg/kg body weight); EAMMS50—High cholesterol diet (1%) with ethyl acetate *Mikania micrantha* stem extract (50 mg/kg body weight); EAMMS100—High cholesterol diet (1%) with ethyl acetate *Mikania micrantha* stem extract (100 mg/kg body weight); EAMMS200—High cholesterol diet (1%) with ethyl acetate *Mikania micrantha* stem extract (200 mg/kg body weight).

Table 7 shows the levels of acetyl-CoA acetyltransferase 2 (ACAT2) in all experimental rats. Based on Table 7, rats that supplemented with 1% cholesterol over 8 weeks showed a significant ($p < 0.05$) increases in ACAT2 levels when compared to the NC group. After 4 weeks of treatment, rats in the EAMMS-treated and SV groups showed significantly decrease ($p < 0.05$) ACAT2 levels compared to the PC group. Among the three different dosages of EAMMS extract, the dosage of 50 mg/kg showed a slight decrease but no significant difference ($p > 0.05$) in the ACAT2 level compared to 100 mg/kg and 200 mg/kg at week 8.

Table 7. Effect of ethyl acetate extract of *Mikania micrantha* stems (EAMMS) on ACAT2 levels in all treated experimental rats at week 8.

Group	ACAT2 (pg/mL)
NC	263.07 ± 1.01 ^a
PC	529.46 ± 4.50 ^b
SV	349.07 ± 2.40 ^c
EAMMS50	405.87 ± 0.76 ^c
EAMMS100	497.96 ± 1.33 ^c
EAMMS200	454.42 ± 3.33 ^c

Values are expressed as mean ± SEM ($n = 6$). Means with different superscripts (a, b or c) indicate statistically different at $p < 0.05$ by Tukey's multiple comparison tests. NC—Normal control; PC—Positive control with high cholesterol diet (1%); SV—High cholesterol diet (1%) with simvastatin (10 mg/kg body weight); EAMMS50—High cholesterol diet (1%) with ethyl acetate *Mikania micrantha* stem extract (50 mg/kg body weight); EAMMS100—High cholesterol diet (1%) with ethyl acetate *Mikania micrantha* stem extract (100 mg/kg body weight); EAMMS200—High cholesterol diet (1%) with ethyl acetate *Mikania micrantha* stem extract (200 mg/kg body weight).

4. Discussion

Feeding with a cholesterol-enriched diet is one of the most commonly used methods for the induction of hypercholesterolemia in rats [15]. Administration of a high cholesterol diet to rats produces a marked increase of serum TC, TG and LDL-C as well as body weight when compared to a normal diet. A previous study revealed that a 1% increase in cholesterol intake by rats led to hypercholesterolemia, as evidenced by significant increases in serum TC, TG and LDL-C levels [16]. These observed changes are akin to those which could be expected when there is an excessive cholesterol load reaching the liver; a load that exceeds normal physiological limits. This will cause the inability of the liver to metabolize lipids thereby resulting in a relatively higher return of cholesterol into the blood circulation [17]. The relatively high levels of LDL which were found in rats which were fed with the cholesterol-enriched diet may be associated with the downward regulation of low density lipoprotein receptors (LDLR) by saturated fatty acids and dietary cholesterol [18]. According to Fungwe et al. [19], the elevation of triglycerides is caused by the cholesterol that was present in the diet which had been shown to diminish the oxidation of fatty acids and in the process, increase triglyceride and hepatic function levels.

Treatment with EAMMS extracts at all dosages showed marked decreases in serum TC, TG, and LDL-C levels and increases of HDL-C compared to the rats in the PC group after 4 weeks of supplementation. This phenomenon was explained by Adaramoye et al. [20] who reasoned that the decreased levels of cholesterol and triglycerides upon treatment are attributable to the lowering of the biosynthesis of hepatic triglycerides and the redeployment of cholesterol molecules between the molecules of lipoproteins. The effect of EAMMS extracts is also related to the abundance of chemical constituents' presence in EAMMS extracts such as terpenoids, flavonoids, alkaloids and vitamins [5,6,11]. Terpenoids (particularly sesquiterpene lactones) are the major compounds found in the ethyl acetate extracts of the flowers, leaves and the whole part of *M. micrantha* [11]. The chemical profile of *M. micrantha* led to the identification of terpenoids such as stigmasterol, stigmasteryl- β -D-glucopyranoside, acetyl β -amyirin and lupeol [10]. The structural similarity of stigmasterol or plant sterol with cholesterol makes plant sterols some of the best substances in reducing cholesterol levels in the blood.

Several mechanisms have been postulated to clarify the process of cholesterol reduction by phyosterols or plant sterols. Plant sterols compete with biliary and also dietary cholesterol as an inhibitor to bind with mixed micelles for solubilization of micellar in the upper intestinal lumen that leads to the general reduction in the ability of the intestinal lining in absorbing cholesterol [21,22]. This hypothesis is consistent with the postulation by Brufau et al. [23] which showed that dietary plant sterols can diminish TC and LDL-C in animal and human models. Plant sterol and stanol ester increase LDLR mRNA and ex vivo LDLR protein expression in the monocytes as well as T-lymphocytes of humans and this changes correlated negatively with the changes of concentration of LDL in the blood, it may be postulated that upregulating LDLR expression leads to decreased LDL formation along the apolipoprotein B cascade [24].

One of the more important methods for diagnosing the cause of disease and the health status of rats is the assessment of haematological parameters. In this study, no significant changes were detected in all haematological values excluding MCV between EAMMS extract, simvastatin and the control groups. However, the administration of the EAMMS caused mild microcytic anemia due to the level of MCV in rat's blood. MCV represents the average volume of the red blood cells. This abnormal blood condition could be caused by the presence of chemical constituents in plant extracts such as flavonoids and alkaloids saponins. Alkaloids have been shown to cause liver cirrhosis, liver megalocytosis and nodular hyperplasia [25] while terpenoids increase membrane permeability to divalent and monovalent ions [25].

Modern toxicology often involves the utilisation of blood sera or tissues as markers to assess damage to organs and cells besides the induction, activation and inhibition of enzymes. The kidneys and liver are organs which play major roles in the detoxification of metabolic substances [26]. AST and ALT are markers which are normally used to detect and assess injuries onto hepatocytes. It is noted that both these markers are introduced into the bloodstream following incidences where cell damage or necrosis occurs [27]. From the findings of this study, PC rats exhibited significant increases in AST and ALT levels as compared to NC rats. A similar elevation of AST and ALT levels was observed in hypercholesterolemic rats by the findings of Souza et al. [28]. In the broader sense, hypercholesterolemia is often associated with toxicity due to heightened levels of liver enzymes as well as the peroxidation of lipids that produces a lot of free radicals in blood sera and tissues [29,30].

Rats which were treated with simvastatin recorded significant elevations in AST and ALT levels. It is noteworthy that prominent adverse effects associated with the administration of the statin group are asymptomatic increases in liver transaminases as well as myopathy [31]. According to Castro et al. [32], the frequency of liver enzymes increased in a small proportion of those taking statins (2.5%). On the contrary, rats which were supplemented with EAMMS showed no differences in AST and ALT levels as compared to those in the NC group. It can, therefore, be deduced that the EAMMS treatment may suppress the level of AST and ALT in the blood and possibly help in the healing of the hepatic tissue damage, suggesting that plant extract can stabilize the plasma membrane as well as cures the damage of hepatic tissues [33].

It has been determined that one of the vital mechanisms of cellular damage that are caused by free radicals such as reactive oxygen species (ROS) is lipid peroxidation. One of the products of the peroxidation of lipid is malondialdehyde (MDA) and this is used as an index to indicate oxygen-free radicals' levels. MDA constitutes the main fraction of aldehydes that are produced upon the metabolism of lipid hydroperoxides and is extensively used to quantify and for the determination of lipid peroxidation. Elevation of serum MDA and TC in the hypercholesterolemic rats without any treatment suggested that the occurrence of lipid peroxidation eventually caused hypercholesterolemia [34]. According to Yokozawa et al. [35], decreases in lipid peroxidation could result in a reduction in the probability of hypercholesterolemia. In this present study, treatment with EAMMS extract was found to confer protection against lipid peroxidation in hypercholesterolemia-induced rats. EAMMS-treated rats were used to reduce MDA concentration nearly normal level compared to the rats with high cholesterol diet, therefore suggesting that EAMMS might possess an antioxidant activity owing to the presence of its phenol, alkane hydrocarbons, flavonoids and phytosterol [6], thus suggesting that EAMMS leads to beneficial response on oxidative stress in hypercholesterolemic rats. Many previous studies have shown that plant polyphenols, flavonoids, carotenoids, vitamins can effectively lower the level of TC, TG, LDL and MDA in hyper-cholesterolemic rodents [36–39]. The present results were following the findings of Musolino et al. [40,41] that demonstrated that bergamot polyphenolic fraction (BPF) prevented the alteration of lipid profile in hypercholesterolemic rats, counteracting oxidative stress markers and also ameliorate the dysregulation of the lipoprotein metabolism; suggesting that the richness of antioxidant properties may play an important role in improving dyslipidemia.

Cholesterol-enriched diets resulted in a remarkable change of liver histology in the PC group. A large accumulation of lipid droplets within hepatocytes of the liver is known as steatosis and has been observed microscopically. The histopathological result of liver tissue in this study is consistent with the postulation by Zheng et al. [42], who found the same hepatic architecture with the presence of large fat vacuoles in high cholesterol rats. The administration of EAMMS extracts at all dosages and simvastatin (10 mg/kg) ameliorated and reduced the hepatic lipid droplets in hepatocytes of the liver. No histological changes have been observed in the kidney tissues in all the experimental rats. These facts indicated that the EAMMS were able to inhibit the accumulation of fat in the liver due to some flavonoids in the plant extract which down-regulates the enzyme HMG-CoA reductase, the key enzyme in the process of cholesterol biosynthesis. The interaction of bioactive compounds in the plant extract with enzyme-substrate complex caused the changes of the active site of the enzyme,

thus prevents the formation of cholesterol. The bioactive compounds in *M. micrantha* may help to suppress the HMGCR activity and reduce cholesterol biosynthesis in the mevalonate pathway [43]. In agreement, the previous study was done by Gliozzi et al. [44], who also reported that the flavonoids and phenolic compounds in BPF inhibit the endogenous biosynthesis of cholesterol that mediated by HMG-CoA reductase enzyme on the mechanistic action of glycosylated polyphenols (bruteridin and melitidin), which is bind to the catalytic site of HMG-CoA reductase as an endogenous HMG-CoA substrate and causing inhibition of cholesterol synthesis.

The presence of caffeic acid ester, also known as chlorogenic acid such as 3,5-di-O-caffeoylquinic acid n-butyl ester in *M. micrantha* is reported [45,46]. The present findings suggested that these active compounds also accountable for the cholesterol-lowering activity, possibly mediated by down-regulation of HMGCR and up-regulation of LDL receptor in addition to down-regulating of ACAT2. Karthikesan et al. [47] also reported that the administration of chlorogenic acid for 45 days strongly reduced the activity of HMGCR and ACAT of lipid metabolism in rats. ACAT2 has important roles in cholesterol esterification, intestinal cholesterol absorption and ApoB-containing lipoprotein release [48]. It was reported that the inhibition of ACAT2 can effectively inhibit cholesterol absorption and reduce fat levels [49]. Phytosterols such as stigmasterol and sitosterol showed significantly reduced mRNA expression of ACAT2 activity in rodents [50]. The mechanism of the hypocholesterolemic action of *M. micrantha* extracts is summarized in Figure 4.

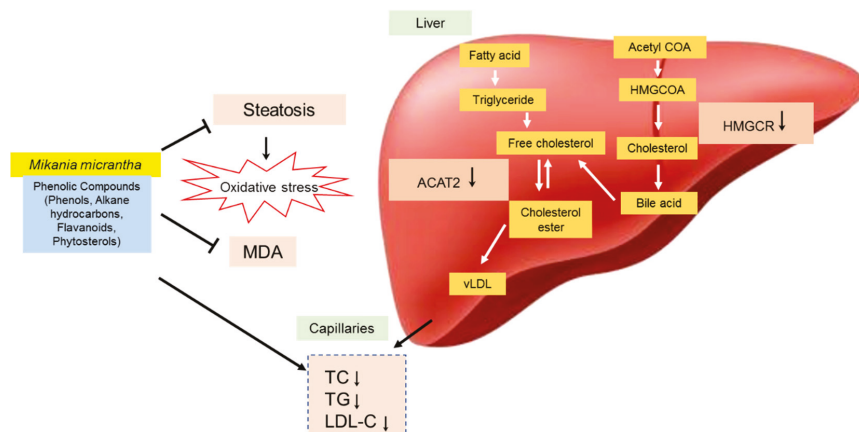


Figure 4. Proposed molecular mechanisms involved in hypocholesterolemic effects of *Mikania micrantha* stem extract (EAMMS) via inhibition of hepatic lipid accumulation, lipid peroxidation, HMG-CoA reductase (HMGCR) and ACAT2; leading to a decrease of cholesterol concentration.

5. Conclusions

The present study showed that EAMMS extracts exhibited anti-hypercholesterolemia properties by improving lipid profile, enzyme inhibitory, reducing the lipid peroxidation and lipid accumulation in combating hypercholesterolemia.

Author Contributions: Conceptualization, A.I. and N.H.S.; methodology, A.I.; validation, A.I., N.H.S., N.M.E., S.R.S., H.B. and M.A.A.; formal analysis, A.I.; investigation, A.I.; resources, A.I. and N.H.S.; data curation, A.I.; writing—original draft preparation, A.I.; writing—review and editing, A.I., N.H.S., N.M.E., S.R.S., H.B. and M.A.A.; supervision, N.H.S., N.M.E., S.R.S. and H.B.; project administration, N.H.S.; funding acquisition, N.H.S. and N.M.E. All authors have read and agreed to the published version of the manuscript.

Funding: This research was funded by Universiti Putra Malaysia (UPM). Project No. GP-IPM/2017/9524500.

Acknowledgments: The authors thank UPM for funding this research project and A.I. thanks UPM for Graduate Research Fellowship. The authors also thank Amirah Haziyah Ishak, Noor Syafiqah Aqila Mohd Rosmi, and Norain Mohd Tamsir; and the laboratory assistance from the Animal House and laboratory of the Department of Nutrition and Dietetics, Faculty of Medicine and Health Sciences, UPM for their help and guidance to the project.

Conflicts of Interest: The authors declare no conflict of interest. The funders had no role in the design of the study; in the collection, analyses, or interpretation of data; in the writing of the manuscript, or in the decision to publish the results.

References

1. Adekiya, T.A.; Shodehinde, S.A.; Aruleba, R.T. Anti-hypercholesterolemic effect of unripe *Musa paradisiaca* products on hypercholesterolemia-induced rats. *J. Appl. Pharm. Sci.* **2018**, *8*, 90–97.
2. Avci, G.; Kupeli, E.; Eryavuz, A.; Yesilada, E.; Kucukurt, I. Antihypercholesterolaemic and antioxidant activity assessment of some plants used as remedy in Turkish folk medicine. *J. Ethnopharmacol.* **2006**, *107*, 418–423. [[CrossRef](#)] [[PubMed](#)]
3. Das, S.; Vasisht, S.; Das, S.N.; Srivastava, L.M. Correlation between total antioxidant status and lipid peroxidation in hypercholesterolaemia. *Curr. Sci.* **2000**, *78*, 486–487.
4. Deori, C.; Dutta, G.; Das, S.; Phukan, D.; Gogoi, G. To evaluate the anti-inflammatory activity of ethanolic extract of leaves of *Mikania micrantha* on experimental animal models. *J. Evol. Med. Dent. Sci.* **2017**, *6*, 3818–3821. [[CrossRef](#)]
5. Chetia, J.; Upadhyaya, S.; Bora, D.K. Screening of phytochemicals, antioxidant and antimicrobial activity of some tea garden weeds of Tinsukia, Assam. *Int. J. Pharm. Sci. Rev. Res.* **2014**, *26*, 193–196.
6. Ishak, A.H.; Shafie, N.H.; Esa, N.M.; Bahari, H.; Ismail, A. From Weed to Medicinal Plant: Antioxidant Capacities and Phytochemicals of Various Extracts of *Mikania micrantha*. *Int. J. Agric. Biol.* **2018**, *20*, 561–568. [[CrossRef](#)]
7. Wan Nurhayati, W.H.; Norli Arlizan, T.; Nurdiana, S. Effect of *Mikania micrantha* leaf extract on the level of blood glucose and hepatic glycogen in the normal and alloxan-induced diabetic rats. *Nat. Prod. Indian J.* **2013**, *9*, 398–402.
8. Matawali, A.; Chin, L.P.; Eng, H.S.; Boon, L.H.; Gansau, J.A. In vitro evaluation of antikinase, antiphosphatase and cytotoxic activities of *Mikania micrantha* HBK (Asteraceae) from Malaysia. *J. Chem. Pharm. Sci.* **2016**, *9*, 696–701.
9. Dou, X.; Zhang, Y.; Sun, N.; Wu, Y.; Li, L. The anti-tumor activity of *Mikania micrantha* aqueous extract in vitro and in vivo. *Cytotechnology* **2014**, *66*, 107–117. [[CrossRef](#)]
10. Rios, E.; León, A.; Chávez, M.I.; Torres, Y.; Ramírez-Apan, M.T.; Toscano, R.A.; Delgado, G. Sesquiterpene lactones from *Mikania micrantha* and *Mikania cordifolia* and their cytotoxic and anti-inflammatory evaluation. *Fitoterapia* **2014**, *94*, 155–163. [[CrossRef](#)]
11. Jyothilakshmi, M.; Jyothis, M.; Latha, M.S. Antidermatophytic activity of *Mikania micrantha* Kunth: An invasive weed. *Pharmacogn. Res.* **2015**, *7*, S20.
12. Pérez-Amador, M.C.; Muñoz Ocotero, V.; Ibarra Balcazar, R.; Garcia Jimenez, F. Phytochemical and pharmacological studies on *Mikania micrantha* HBK (Asteraceae). *Phyton Rev. Int. Bot. Exp.* **2010**, *79*, 77.
13. Dev, U.K.; Hossain, M.T.; Islam, M.Z. Phytochemical investigation, antioxidant activity and anthelmintic activity of *Mikania micrantha* leaves. *World J. Pharm. Res.* **2015**, *4*, 121–133.
14. Brunt, E.M. Grading and staging the histopathological lesions of chronic hepatitis: The Knodell histology activity index and beyond. *J. Hepatol.* **2000**, *31*, 241–246. [[CrossRef](#)]
15. Sano, M.; Takenaka, Y.; Kojima, R.; Saito, S.I.; Tomita, I.; Katou, M.; Shibuya, S. Effects of pu-erh tea on lipid metabolism in rats. *Chem. Pharm. Bull.* **1986**, *34*, 221–228. [[CrossRef](#)]
16. Khalili, R.M.A.; Norhayati, A.H.; Rokiah, M.Y.; Asmah, R.; Muskinah, M.S.; Manaf, A.A. Hypocholesterolemic effect of red pitaya (*Hylocereus* sp.) on hypercholesterolemia induced rats. *Int. Food Res. J.* **2009**, *16*, 431–440.
17. Kushi, L.H.; Folsom, A.R.; Prineas, R.J.; Mink, P.J.; Wu, Y.; Bostick, R.M. Dietary antioxidant vitamins and death from coronary heart disease in postmenopausal women. *N. Engl. J. Med.* **1996**, *334*, 1156–1162. [[CrossRef](#)]
18. Mustad, V.A.; Etherton, T.D.; Cooper, A.D.; Mastro, A.M.; Pearson, T.A.; Jonnalagadda, S.S.; Kris-Etherton, P.M. Reducing saturated fat intake is associated with increased levels of LDL receptors on mononuclear cells in healthy men and women. *J. Lipid Res.* **1997**, *38*, 459–468.

19. Fungwe, T.V.; Cagen, L.M.; Cook, G.A.; Wilcox, H.G.; Heimberg, M. Dietary cholesterol stimulates hepatic biosynthesis of triglyceride and reduces oxidation of fatty acids in the rat. *J. Lipid Res.* **1993**, *34*, 933–941.
20. Adaramoye, O.A.; Akintayo, O.; Achem, J.; Fafunso, M.A. Lipid-lowering effects of methanolic extract of *Vernonia amygdalina* leaves in rats fed on high cholesterol diet. *Vasc. Health Risk Manag.* **2008**, *4*, 235. [[CrossRef](#)]
21. Cedó, L.; Farràs, M.; Lee-Rueckert, M. Molecular Insights into the Mechanisms Underlying the Cholesterol-Lowering Effects of Phytosterols. *Curr. Med. Chem.* **2019**, *26*, 6704–6723. [[CrossRef](#)]
22. AbuMweis, S.S.; Vanstone, C.A.; Lichtenstein, A.H.; Jones, P.J.H. Plant sterol consumption frequency affects plasma lipid levels and cholesterol kinetics in humans. *Eur. J. Clin. Nutr.* **2009**, *63*, 747. [[CrossRef](#)] [[PubMed](#)]
23. Brufau, G.; Kuipers, F.; Lin, Y.; Trautwein, E.A.; Groen, A.K. A reappraisal of the mechanism by which plant sterols promote neutral sterol loss in mice. *PLoS ONE* **2011**, *6*, e21576. [[CrossRef](#)] [[PubMed](#)]
24. Plat, J.; Mensink, R.P. Plant stanol and sterol esters in the control of blood cholesterol levels: Mechanism and safety aspects. *Am. J. Cardiol.* **2005**, *96*, 15–22. [[CrossRef](#)] [[PubMed](#)]
25. Zeinstegeer, P.A.; Romero, A.; Teibler, P.; Montenegro, M.; Rios, E.; Ciotti, E.M.; Jorge, N. Toxicity of volatile compounds of *Senecio grisebachii* Baker (margarita) Flowers, in Mice. *Rev. Investig. Agropecu.* **2003**, *32*, 125–136.
26. Heywood, R. Target organ toxicity. *Toxicol. Lett.* **1981**, *8*, 349–358. [[CrossRef](#)]
27. Suckow, M.A.; Stevens, K.A.; Wilson, R.P. *The Laboratory Rabbit, Guinea Pig, Hamster, and Other Rodents*; Academic Press: London, UK, 2012; pp. 1131–1155.
28. de Souza, M.O.; Silva, M.; Silva, M.E.; de Paula Oliveira, R.; Pedrosa, M.L. Diet supplementation with acai (*Euterpe oleracea* Mart.) pulp improves biomarkers of oxidative stress and the serum lipid profile in rats. *J. Nutr.* **2010**, *26*, 804–810. [[CrossRef](#)]
29. Suanarunsawat, T.; Ayutthaya, W.D.N.; Songsak, T.; Thirawarapan, S.; Pongshompoo, S. Antioxidant activity and lipid-lowering effect of essential oils extracted from *Ocimum sanctum* L. leaves in rats fed with a high cholesterol diet. *J. Clin. Biochem. Nutr.* **2009**, *46*, 52–59. [[CrossRef](#)]
30. Vincent, H.K.; Powers, S.K.; Dirks, A.J.; Scarpace, P.J. Mechanism for obesity-induced increase in myocardial lipid peroxidation. *Int. J. Obes.* **2001**, *25*, 378–388. [[CrossRef](#)]
31. Bellosa, S.; Paoletti, R.; Corsini, A. Safety of statins: Focus on clinical pharmacokinetics and drug interactions. *Circulation* **2004**, *109*, III-50. [[CrossRef](#)]
32. Castro, P.F.; Ribeiro, E.; Dorea, E.L.; Pinto, G.A.; Hirata, R.D.C. Factors associated with statin-related adverse muscular events in adult dyslipidemic outpatients. *Braz. J. Pharm. Sci.* **2017**, *53*, 1–10. [[CrossRef](#)]
33. Effiong, G.S.; Akpan, H.D. The effect of *Nauclea latifolia* leaf extract on some biochemical parameters in streptozotocin diabetic rat models. *J. Med. Med. Sci.* **2015**, *6*, 47–52.
34. Grotto, D.; Maria, L.S.; Valentini, J.; Paniz, C.; Schmitt, G.; Garcia, S.C.; Farina, M. Importance of the lipid peroxidation biomarkers and methodological aspects for malondialdehyde quantification. *Quim. Nova* **2009**, *32*, 169–174. [[CrossRef](#)]
35. Yokozawa, T.; Ishida, A.; Cho, E.J.; Nakagawa, T. The effects of *Coptidis rhizoma* extract on a hypercholesterolemic animal model. *Phytomedicine* **2003**, *10*, 17–22. [[CrossRef](#)] [[PubMed](#)]
36. Kai, N.S.; Nee, T.A.; Ling, E.L.C.; Ping, T.C.; Kamariah, L.; Lin, N.K. Anti-hypercholesterolemic effect of kenaf (*Hibiscus cannabinus* L.) seed on high-fat diet Sprague Dawley rats. *Asian Pac. J. Trop. Med.* **2015**, *8*, 6–13. [[CrossRef](#)]
37. Kwok, C.Y.; Wong, C.N.Y.; Yau, M.Y.C.; Yu, P.H.F.; Au, A.L.S.; Poon, C.C.W.; Chan, S.W. Consumption of dried fruit of *Crataegus pinnatifida* (hawthorn) suppresses high-cholesterol diet-induced hypercholesterolemia in rats. *J. Funct. Foods* **2010**, *2*, 179–186. [[CrossRef](#)]
38. Dianita, R.; Jantan, I.; Jalil, J.; Amran, A.Z. Effects of *Labisia pumila var alata* extracts on the lipid profile, serum antioxidant status and abdominal aorta of high-cholesterol diet rats. *Phytomedicine* **2016**, *23*, 810–817. [[CrossRef](#)]
39. Thirumalai, T.; Tamilselvan, N.; David, E. Hypolipidemic activity of *Piper betel* in high fat diet induced hyperlipidemic rat. *J. Acute Dis.* **2014**, *3*, 131–135. [[CrossRef](#)]
40. Musolino, V.; Gliozzi, M.; Scarano, F.; Bosco, F.; Scicchitano, M.; Nucera, S.; Carresi, C.; Ruga, S.; Zito, M.C.; Maiuolo, J.; et al. Bergamot polyphenols improve dyslipidemia and pathophysiological features in a mouse model of non-alcoholic fatty liver disease. *Sci. Rep.* **2020**, *10*, 2565. [[CrossRef](#)]

41. Musolino, V.; Gliozzi, M.; Nucera, S.; Carresi, C.; Maiuolo, J.; Mollace, R.; Ruga, S. The effect of bergamot polyphenolic fraction on lipid transfer protein system and vascular oxidative stress in a rat model of hyperlipemia. *Lipids Health Dis.* **2019**, *18*, 115. [[CrossRef](#)]
42. Zheng, S.; Hoos, L.; Cook, J.; Tetzloff, G.; Davis, H., Jr.; van Heek, M.; Hwa, J.J. Ezetimibe improves high fat and cholesterol diet-induced non-alcoholic fatty liver disease in mice. *Eur. J. Pharmacol.* **2008**, *584*, 118–124. [[CrossRef](#)] [[PubMed](#)]
43. Salvamani, S.; Gunasekaran, B.; Shukor, M.Y.; Shaharuddin, N.A.; Sabullah, M.K.; Ahmad, S.A. Anti-HMG-CoA reductase, antioxidant, and anti-inflammatory activities of *Amaranthus viridis* leaf extract as a potential treatment for hypercholesterolemia. *Evid-Based Complement. Altern. Med.* **2016**. [[CrossRef](#)] [[PubMed](#)]
44. Gliozzi, M.; Walker, R.; Muscoli, S.; Vitale, C.; Gratteri, S.; Carresi, C.; Aloe, A. Bergamot polyphenolic fraction enhances rosuvastatin-induced effect on LDL-cholesterol, LOX-1 expression and protein kinase B phosphorylation in patients with hyperlipidemia. *Int. J. Cardiol.* **2013**, *170*, 140–145. [[CrossRef](#)] [[PubMed](#)]
45. Wei, X.; Huang, H.; Wu, P.; Cao, H.; Ye, W. Phenolic constituents from *Mikania micrantha*. *Biochem. Syst. Ecol.* **2004**, *11*, 1091–1096. [[CrossRef](#)]
46. Ogawa, M.; Yamanashi, Y.; Takada, T.; Abe, K.; Kobayashi, S. Effect of luteolin on the expression of intestinal cholesterol transporters. *J. Funct. Foods* **2017**, *36*, 274–279. [[CrossRef](#)]
47. Karthikesan, K.; Pari, L.; Menon, V.P. Antihyperlipidemic effect of chlorogenic acid and tetrahydrocurcumin in rats subjected to diabetogenic agents. *Chem. Biol. Interact.* **2010**, *188*, 643–650. [[CrossRef](#)] [[PubMed](#)]
48. Borradaile, N.M.; de Dreu, L.E.; Barrett, P.H.R.; Huff, M.W. Inhibition of hepatocyte apoB secretion by naringenin enhanced rapid intracellular degradation independent of reduced microsomal cholesteryl esters. *J. Lipid Res.* **2002**, *43*, 1544–1554. [[CrossRef](#)]
49. Repa, J.J.; Buhman, K.K.; Farese, R.V., Jr.; Dietschy, J.M.; Turley, S.D. ACAT2 deficiency limits cholesterol absorption in the cholesterol-fed mouse: Impact on hepatic cholesterol homeostasis. *ISRN Hepatol.* **2004**, *40*, 1088–1097. [[CrossRef](#)]
50. Liang, Y.T.; Wong, W.T.; Guan, L.; Tian, X.Y.; Ma, K.Y.; Huang, Y.; Chen, Z.Y. Effect of phytosterols and their oxidation products on lipoprotein profiles and vascular function in hamster fed a high cholesterol diet. *Atherosclerosis* **2011**, *219*, 124–133. [[CrossRef](#)]



© 2020 by the authors. Licensee MDPI, Basel, Switzerland. This article is an open access article distributed under the terms and conditions of the Creative Commons Attribution (CC BY) license (<http://creativecommons.org/licenses/by/4.0/>).

Article

Purified Gymnemic Acids from *Gymnema inodorum* Tea Inhibit 3T3-L1 Cell Differentiation into Adipocytes

Papawee Saiki ^{1,*}, Yasuhiro Kawano ¹, Takayuki Ogi ², Prapaipat Klungsupya ³, Thanchanok Muangman ³, Wimonstri Phantanaprates ³, Papitchaya Kongchinda ³, Nantaporn Pinnak ³ and Koyomi Miyazaki ¹

- ¹ Cellular and Molecular Biotechnology Research Institute, National Institute of Advance Industrial Science and Technology (AIST), Tsukuba, Ibaraki 305-8566, Japan; y.kawano@aist.go.jp (Y.K.); k-miyazaki@aist.go.jp (K.M.)
 - ² Department of Environment and Natural Resources, Okinawa Industrial Technology Center, Okinawa 904-2234, Japan; ogitkyuk@pref.okinawa.lg.jp
 - ³ Research and Development Group for Bio-Industries, Thailand Institute of Scientific and Technological Research (TISTR), Techno Polis, Khlong Luang, Pathum Thani 12120, Thailand; prapaipat@tistr.or.th (P.K.); thanchanok@tistr.or.th (T.M.); Wimonstri@tistr.or.th (W.P.); papitchaya@tistr.or.th (P.K.); nantaporn_p@tistr.or.th (N.P.)
- * Correspondence: papawee-saiki@aist.go.jp; Tel.: +81-29-861-4304

Received: 20 August 2020; Accepted: 15 September 2020; Published: 17 September 2020

Abstract: *Gymnema inodorum* (GI) is an indigenous medicinal plant and functional food in Thailand that has recently helped to reduce plasma glucose levels in healthy humans. It is renowned for the medicinal properties of gymnemic acid and its ability to suppress glucose absorption. However, the effects of gymnemic acids on adipogenesis that contribute to the accumulation of adipose tissues associated with obesity remain unknown. The present study aimed to determine the effects of gymnemic acids derived from GI tea on adipogenesis. We purified and identified GiA-7 and stephanosides C and B from GI tea that inhibited adipocyte differentiation in 3T3-L1 cells. These compounds also suppressed the expression of *peroxisome proliferator-activated receptor gamma* (*Pparγ*)-dependent genes, indicating that they inhibit lipid accumulation and the early stage of 3T3-L1 preadipocyte differentiation. Only GiA-7 induced the expression of *uncoupling protein 1* (*Ucp1*) and *pparγ coactivator 1 alpha* (*Pgc1α*), suggesting that GiA-7 induces mitochondrial activity and beige-like adipocytes. This is the first finding of stephanosides C and B in *Gymnema inodorum*. Our results suggested that GiA-7 and stephanosides C and B from GI tea could help to prevent obesity.

Keywords: *Gymnema inodorum*; adipogenesis; gymnemic acid; obesity

1. Introduction

Gymnema sylvestre is a species of the genus *Gymnema* that is popular in India for reducing glucose levels, suppressing glucose absorption and preventing type 2 diabetes [1–5]. *Gymnema inodorum* (GI) is a species of same genus that is indigenous to Thailand, particularly in the northern region, where it is widely consumed. The effects of GI on glucose absorption and blood glucose levels have recently been investigated [6–8]. We previously found that extracts of GI leaves decreased blood glucose in alloxan-induced diabetic rats [9] that comprise a popular model with which to study type 1 diabetes mellitus. Alloxan selectively destroys insulin production in beta cells, which consequently results in high blood glucose levels [10]. However, about 90% of patients with diabetes have type 2 diabetes mellitus (DM) which is induced by a lack of exercise and inappropriate eating habits [11]. However, obesity is the leading risk factor for type 2 DM, and it also greatly increases the risk of

fatty liver disease, atherosclerosis, metabolic diseases, insulin resistance and hypertension [12,13]. Obesity is characterized at the cellular level as being differentiated from preadipocytes. White adipose tissue (WAT) is specialized to store excess energy as triglycerides composed of fatty acids. Inhibiting preadipocyte differentiation can prevent the initiation and progression of obesity [14,15].

The differentiation of 3T3-L1 fibroblast-like cells into adipocyte-like cells stimulated by insulin and synthetic glucocorticoids is a popular model of adipogenesis and lipid metabolism *in vitro* [16,17]. Therefore, we applied the inhibition of 3T3-L1 cell differentiation to screen gymnemic acid extracted from GI tea. Gymnemic acid is an oleanane-type triterpene glycoside [16,17] that can exist as a single entity or as a mixture of several related compounds [18,19]. The major saponin fraction in *Gymnema sylvestre* is a gymnemic acid that comprises a complex mixture of at least nine similar glycosides and aglycone derivatives [20]. Moreover, only four gymnemic acids have been identified in GI, which renders the purification and identification of gymnemic acids difficult. Furthermore, current knowledge about these compounds purified from GI is limited. We isolated and purified GiA-7, stephanoside C and stephanoside B from GI tea that inhibited 3T3-L1 cell differentiation. We also determined the expression of the *peroxisome proliferator-activated receptor gamma (Pparγ)*, *CCAAT/enhancer-binding protein alpha (Cebpa)*, *cluster of differentiation 36 (Cd36)*, *fatty acid synthase (Fasn)*, *ppary coactivator 1 alpha (Pgc1α)*, *lipin-1*, *adipose triglyceride lipase (Atgl)*, *hormone-sensitive lipase (Hsl)*, *sterol regulatory element-binding protein (Srebp)-1c*, *uncoupling protein 1 (Ucp1)*, *glucose transporter type 4 (Glut4)* and *fatty acid binding protein 4 (Fabp4)* genes to explain the signaling of adipogenesis inhibition in 3T3-L1 preadipocytes.

2. Materials and Methods

2.1. Extraction, Isolation and Purification

Fresh GI leaves (Development of Herbs and Fruit Products Community Enterprise (Chiang Mai, Thailand)) were powdered, washed, dried and then steamed for 3 min. The leaves were dried at 60 °C for 2 h, stir-fried to complete dryness and then stored in darkness.

After extracting GI tea powder with 98% methanol for 24 h, the extract was mixed with hexane in a separatory funnel. The lower solution was collected, evaporated to dryness and then the residue was washed with chloroform and methanol (2:1) to remove fat components. The washed, evaporated residue dissolved in methanol (crude gymnemic acid) was eluted through a Sep-Pak tC₁₈ cartridge (Waters Corporation, Milford, MA, USA) with a gradient of 10–100% methanol and ethanol. Six active compounds were purified from the 90% methanol fraction by high-performance liquid chromatography (HPLC) using a Model CCPD computer-controlled pump (Tosoh, Tokyo, Japan) equipped with a Capcell PAK C₁₈ 5 μm, 20-mm inner diameter (i.d.), 250-mm column (Osaka Soda Co., Ltd., Osaka, Japan) and isocratic 80% methanol with 0.1% formic acid at a flow rate of 2.5 mL/min. The compounds were detected at 254 nm using a UV wavelength detector (JASCO International Co., Ltd., Tokyo, Japan).

2.2. Mass Spectrometry

Dried purified compounds were dissolved and diluted in dimethyl sulfoxide (Fujifilm Wako Pure Chemical Industries Ltd., Osaka, Japan) at 100 ppm. The accurate molecular formula was determined by Liquid Chromatography equipped with Quadrupole Time Of Flight Mass Spectrometry (LC/Q-TOF MS) using an Agilent 6530 Accurate-Mass Q-TOF LC/MS system (Agilent Technologies Inc., Santa Clara, CA, USA) equipped with an electrospray ionization (ESI) interface. Compounds were separated by reversed-phase liquid chromatography using a photodiode array detector and monitored at a wavelength ranging from 210 to 600 nm at a flow rate of 0.4 mL/min using an ACQUITY UPLC BEH C₁₈ column (50 × 2.1 mm i.d. and 1.7 μm particle size (Waters Corp.) at 40 °C). The mobile phase consisted of a linear gradient of 0.1% formic acid:acetonitrile (1:1) to 0.1% formic acid:acetonitrile (1:19) over 3 min. The high-resolution mass spectra (HRMS) conditions were: positive ion mode; desolvation

gas, N₂; temperature 350 °C, pressure, 40 psig; flow rate, 8 L/min and capillary, fragmentary and skimmer voltages of 3500, 100 and 65 V, respectively [18].

2.3. Nuclear Magnetic Resonance (NMR) Spectroscopy

Dried compound 2 (10 mg) was exchanged into methanol-d₄, 99.8 atom% D, containing 0.05% (v/v) Tetramethylsilane (TMS) (Cambridge Isotope Laboratories Inc., Andover, MA, USA). Dried compounds 5 and 6 (10 mg each) were exchanged into pyridine-d₅, 99.5 atom% D (Cambridge Isotope Laboratories Inc.). Spectra were determined by one-dimensional (¹H NMR, ¹³C NMR and dept-135) and two-dimensional COrelated SpectroscopY (COSY), Heteronuclear Multiple Bond Correlation (HMBC) and Heteronuclear Multiple Quantum Coherence (HMQC) NMR using a Bruker 500 MHz NMR (Bruker Daltonics SPR, Hamburg, Germany).

2.4. Cell Culture

The mouse embryonic fibroblast cell line (3T3-L1 cell) was purchased from National Institutes of Biomedical Innovation, Health, and Nutrition (NIBIOHN), Osaka, Japan. These cells were cultured in low-glucose Dulbecco's modified Eagle's medium (DMEM) (Fujifilm Wako Pure Chemical Corp.) containing 10% heat-inactivated fetal bovine serum (FBS; Biowest, Tokyo, Japan) at 37 °C under a humidified 5% CO₂ atmosphere.

2.5. The Antiadipocyte Differentiation Activity

We seeded 3T3-L1 cells (1 × 10⁵/mL in 200 µL) cultured as described above into collagen-coated 96-well plates in high-glucose DMEM (Fujifilm Wako Pure Chemical Corp.) under standard conditions for 24 h, then induced their differentiation into adipocytes using 10 µg/mL insulin, 0.5 mM 3-isobutyl-1-methylxanthine (IBMX) and 1 µM water-soluble dexamethasone (Sigma-Aldrich Corp., St. Louis, MO, USA). After 1 h, the 3T3-L1 cells were incubated with samples for 7–10 days.

Cell proliferation was determined using CellTiter 96[®] Aqueous One Solution Cell Proliferation Assays (Promega Corp., Madison, WI, USA), as described by the manufacturer. The absorbance of proliferating cells determined at 490 nm using an iMark[™] Microplate Reader (Bio-Rad Laboratories Inc., Hercules, CA, USA) was compared with that of untreated differentiated 3T3-L1 cells.

Intracellular lipid accumulation was determined using a Lipid Assay Kit (Cosmo Bio Co., Ltd., Tokyo, Japan), as described by the manufacturer. Differentiated 3T3-L1 cells were washed with phosphate-buffered saline (PBS), and fixed overnight with 4% formaldehyde at room temperature. The cells were then washed twice with distilled water, incubated with Oil red O at room temperature for 15 min and washed twice with distilled water. Oil red O extraction reagent was added into cells. Absorbance was read at 540 nm using the iMark[™] Microplate Reader. Absorption due to the intracellular lipid accumulation was determined and compared with that of control-differentiated 3T3-L1 cells.

2.6. Quantitative Real-Time PCR

We incubated 3T3-L1 cells (1 × 10⁵/mL; 1 mL) seeded into collagen-coated 12-well plates in high-glucose DMEM under standard conditions for 3 days, then induced the cells to differentiate into adipocytes using 10 µg/mL insulin, 0.5 mM IBMX and 1 µM water-soluble dexamethasone for 1 h. The 3T3-L1 cells were then incubated with purified GiA-7 and stephanosides C and B from GI tea (100 µM each) for 8 days. The expression of genes associated with adipogenesis was analyzed using quantitative real-time PCR. Total RNA was extracted from the cells using RNAiso plus. Single-stranded cDNA was generated using PrimeScript[™] RT Master Mix. Quantitative real-time PCR was conducted using a SYBR[®] Premix Ex Taq[™] II (Takara Bio. Inc., Otsu, Japan) and a LightCycler[™] (Roche Diagnostics, Mannheim, Germany). The sequences of all primers (Thermo Fisher Scientific Inc) are listed in Table 1 [19]. The PCR conditions were 95 °C for 10 s, followed by 45 cycles of 95 °C for 5 s,

58 °C for 10 s and at 72 °C for 10 s. The amount of target mRNA was normalized relative to the internal standard *36b4*.

Table 1. Primer sequences for real-time reverse transcription (RT)-PCR.

Target Gene	Direction	Primer Sequence (5'–3')
<i>Pparγ</i>	Forward	AACTCTGGGAGATTCTCTGTGTA
	Reverse	TGGTAATTTCTGTGAAGTGCTCATA
<i>Fasn</i>	Forward	GGAGGTGGTGATAGCCGGTAT
	Reverse	TGGTAATCCATAGAGCCAG
<i>Cebpa</i>	Forward	AAGAAGTCGGTGGACAAGAACAG
	Reverse	GTTGCGTTGTTTGCTTTAICTC
<i>Pgc1α</i>	Forward	GTAGGCCAGGTACGACAGC
	Reverse	GCTCTTGCCGTATTCATCCC
<i>Lipin-1</i>	Forward	CCATAGAGATGAGCTCGGAT
	Reverse	AACTGGGATACGATGCTGACT
<i>Atgl</i>	Forward	CTTGAGCAGCTAGAACAAATG
	Reverse	GGACACCTCAATAATGTTGGC
<i>Hsl</i>	Forward	GCTGGAGGAGTGTTTTTTTGC
	Reverse	AGTTGAACCAAGCAGGTCACA
<i>Srebp-1c</i>	Forward	ATCGGCGCGGAAGCTGTCGGGGTAGCGTC
	Reverse	ACTGTCTTGTTGTTGATGAGCTGGAGCAT
<i>Glut4</i>	Forward	CTGTCGCTGGTTTCTCCAAC
	Reverse	CAGGAGGACGGCAAATAGAA
<i>Ucp1</i>	Forward	GGCAACAAGAGCTGACAGTAAAT
	Reverse	GGCCCTTGTAACAACAATAATAC
<i>Fabp4</i>	Forward	CCGCAGACGACAGGA
	Reverse	CTCATGCCCTTTCATAAAT
<i>36b4</i>	Forward	CTTCATTGTGGGACGACACA
	Reverse	TCTCCAGAGCTGGGTTGTTC

2.7. Statistical Analysis

Data were statistically assessed by one-way analyses of variance (ANOVAs) with Dunnett tests using EZR software version 1.52 (Jichi Medical University, Saitama, Japan), which is graphical user interface for R (The R Foundation for Statistical Computing) based on R commander [20]. Values are indicated as means ± SD. Significant differences are shown as *p*-values.

3. Results and Discussion

We measured the ability of the crude 10–100% methanol and ethanol fractions of gymnemic acid to inhibit 3T3-L1 cell differentiation. We found that the 90% methanol fraction was the most powerful inhibitor (Figure 1). We then found that compounds 2, 3, 5 and 6 among the six compounds separated by HPLC from this fraction (Figure 2) significantly inhibited 3T3-L1 cell differentiation (Figure 3). Compound 5 was the most powerful inhibitor. The inhibition of 3T3-L1 cell differentiation by compound 5 was concentration-dependent. Compound 6 also strongly inhibited 3T3-L1 cell differentiation. However, the yield of HPLC fraction 3 was very low. Therefore, HPLC fractions No. 2, 5 and 6 were further purified, and their structures were identified by NMR and mass spectrometry. The ¹³C NMR chemical shifts of compounds 2, 5 and 6 were compared with published ¹³C NMR chemical shifts of GiA-7 [6], stephanoside C and stephanoside B [21], respectively, and are shown in Tables 2–6, respectively. These findings showed that compounds 2, 5 and 6 were GiA-7, stephanoside C and stephanoside B, respectively.

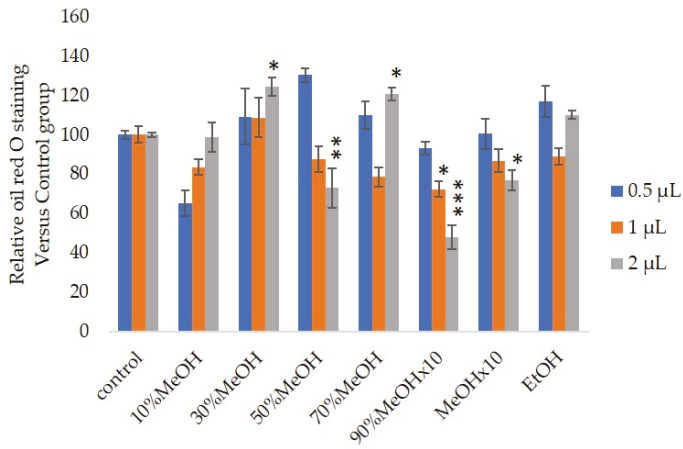


Figure 1. Effects of Sep-PaktC18 fractions on 3T3-L1 cell differentiation. We assessed the abilities of 10%MeOH, 30%MeOH, 50%MeOH, 70%MeOH and EtOH fractions at the concentration of 10 mg/mL in ethanol and 90%MeOH and MeOH fractions at the concentration of 1 mg/mL in ethanol to inhibit 3T3-L1 cell differentiation. Values are shown as means \pm SD ($n = 4$). * $p < 0.05$, ** $p < 0.01$ and *** $p < 0.001$ vs. control (ANOVA with post hoc Dunnett tests).

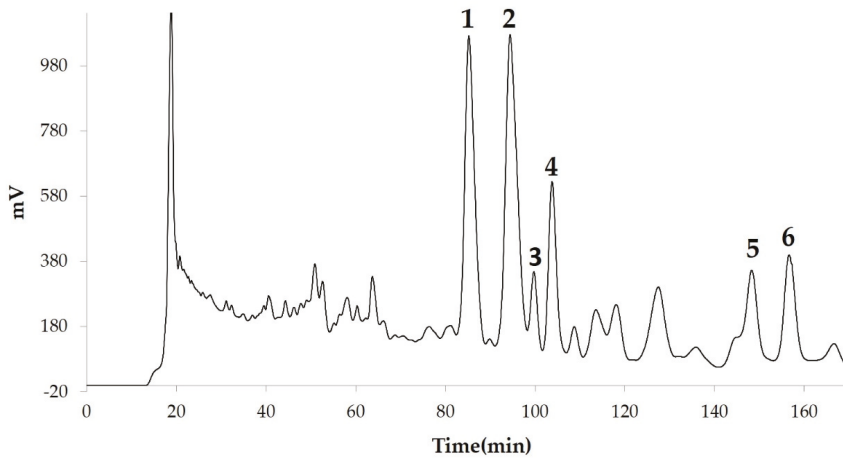


Figure 2. Compounds separated by high-performance liquid chromatography (HPLC) from 90% methanol fraction.

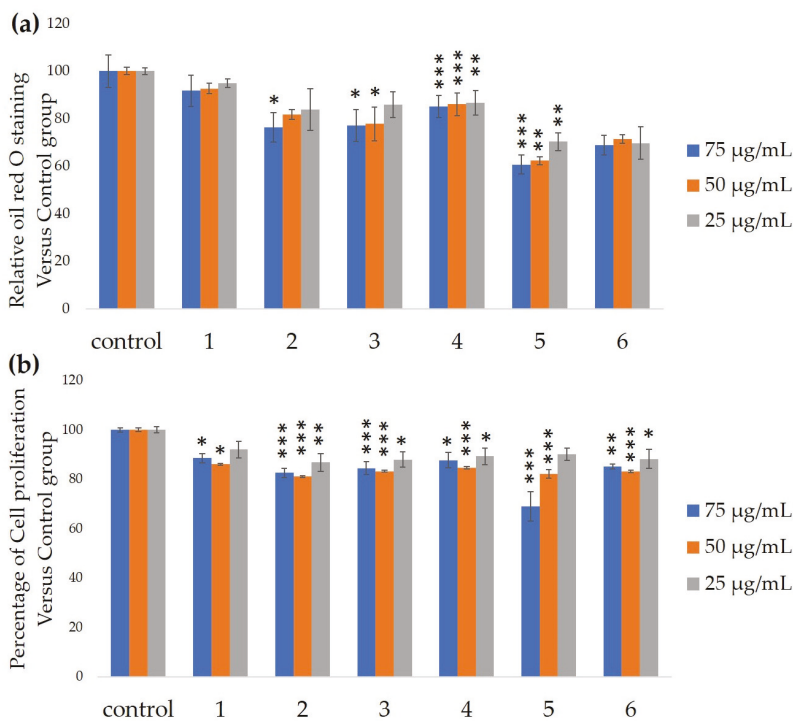


Figure 3. Ability of HPLC fractions to inhibit 3T3-L1 cell differentiation. (a) Inhibition of adipogenesis. (b) Cell proliferation. Values are shown as means \pm SD ($n = 4$). * $p < 0.05$, ** $p < 0.01$ and *** $p < 0.001$ vs. control (ANOVA and post hoc Dunnett tests).

Table 2. ^{13}C nuclear magnetic resonance (NMR) chemical shifts of GiA-7 and compound 2 (δ : ppm).

C-No.	Carbon Type	GiA-7	Compound 2
1	—CH ₂ —	39.7	39.7
2	—CH ₂ —	26.2	26.4
3	>CH—O—	82.3	82.9
4	>C<	43.9	44.0
5	>CH—	48.1	48.1
6	—CH ₂ —	18.8	18.9
7	—CH ₂ —	33.2	33.2
8	>C<	41.2	41.3
9	>CH—	48.2	48.2
10	>C<	37.5	37.5
11	—CH ₂ —	24.8	24.8
12	—CH=	124.9	125.0
13	>C=	142.8	142.8
14	>C<	43.9	44.0
15	—CH ₂ —	37.0	37.0
16	>CH—O—	66.8	66.8
17	>C<	46.5	46.5
18	>CH—	44.9	44.9
19	—CH ₂ —	47.1	47.1
20	>C<	33.0	33.1
21	—CH ₂ —	39.9	39.9
22	>CH—	74.3	74.3
23	—CH ₂ —O—	64.8	64.7
24	—CH ₃	13.4	13.4
25	—CH ₃	16.7	16.7
26	—CH ₃	17.5	17.5
27	—CH ₃	28.0	28.0
28	—CH ₂ —O—	61.2	61.1
29	—CH ₃	33.5	33.5
30	—CH ₃	25.6	25.6

Table 2. Cont.

C-No.	Carbon Type	GiA-7	Compound 2
O-NMAc			
N1	>C=O	169.6	169.7
N2	>C=	112.1	112.1
N3	>C=	153.0	153.0
N4	—CH=	111.9	112.0
N5	—CH=	135.6	135.6
N6	—CH=	115.3	115.4
N7	—CH=	133.0	133.0
N8	—CH ₃	29.7	29.7
β-glu			
1'	—O—CH—O—	105.3	105.7
2'	>CH—O—	75.0	75.2
3'	>CH—O—	78.0	78.0
4'	>CH—O—	73.5	73.5
5'	>CH—O—	76.6	78.0
6'	—COO—		

Table 3. The ¹³C NMR chemical shifts of stephanoside C and compound 5 (δ: ppm).

C-No.	Carbon Type	Stephanoside C	Compound 5
1	—CH ₂ —	38.9	38.9
2	—CH ₂ —	30.0	30.0
3	>CH—O—	77.8	77.7
4	—CH ₂ —	39.3	39.4
5	>C=	139.3	139.4
6	—CH=	119.5	119.5
7	—CH ₂ —	35.0	35.0
8	>C<	74.4	74.4
9	>CH—	44.1	44.2
10	>C<	37.3	37.4
11	—CH ₂ —	25.7	25.7
12	>CH—	74.7	74.6
13	>C<	57.0	57.0
14	>C<	89.0	89.0
15	—CH ₂ —	33.8	33.8
16	—CH ₂ —	34.0	34.0
17	>C<	87.7	87.7
18	—CH ₃	11.4	11.4
19	—CH ₃	18.1	18.1
20	>CH—O—	75.0	75.0
21	—CH ₃	15.6	15.7
12-O-Acetyl moiety			
A1	—COO—	171.5	171.4
A2	—CH ₃	22.1	22.1
20-O-N-Methylanthraniloyl moiety			
N1	—COO—	111.0	111.1
N2	>C=	152.7	152.7
N3	>C=	111.6	111.6
N4	CH=	135.1	135.2
N5	—CH=	114.8	114.8
N6	—CH=	132.7	132.7
N7	—CH=	168.3	168.3
N8	—CH ₃	29.7	29.6

Table 4. The ^{13}C NMR chemical shifts of sugar chains of stephanoside C and compound 5 (δ in ppm).

C-No.	Carbon Type	Stephanoside C	Compound 5
d-Cymarose			
1'	—O—CH—O—	96.5	96.5
2'	—CH ₂ —	37.3	37.4
3'	>CH—O—	78.0	78.0
4'	>CH—O—	83.5	83.5
5'	>CH—O—	69.1	69.1
6'	—CH ₃	18.7	18.7
O-Me	—O—CH ₃	59.0	59.0
d-Olenadrose			
1''	—O—CH—O—	102.2	102.1
2''	—CH ₂ —	37.7	37.8
3''	>CH—O—	79.3	79.3
4''	>CH—O—	83.2	83.2
5''	>CH—O—	72.1	72.2
6''	—CH ₃	19.0	19.0
O-Me	—O—CH ₃	57.4	57.4
d-Thevetose			
1'''	—O—CH—O—	104.2	104.3
2'''	>CH—O—	75.3	75.4
3'''	>CH—O—	88.2	88.3
4'''	>CH—O—	76.1	76.1
5'''	>CH—O—	72.9	73.0
6'''	—CH ₃	18.8	18.8
O-Me	—O—CH ₃	61.1	61.1

Table 5. The ^{13}C NMR chemical shifts of stephanoside B and compound 6 (δ : ppm).

C-No.	Carbon Type	Stephanoside B	Compound 6
1	—CH ₂ —	38.8	38.8
2	—CH ₂ —	30.0	29.9
3	>CH—O—	77.7	77.6
4	—CH ₂ —	39.3	39.2
5	>C=	139.3	139.2
6	—CH=	119.4	119.4
7	—CH ₂ —	34.9	34.9
8	>C<	74.3	74.3
9	>CH—	44.1	44.0
10	>C<	37.3	37.2
11	—CH ₂ —	25.6	25.6
12	>CH—	74.6	74.6
13	>C<	56.9	56.9
14	>C<	88.9	88.9
15	—CH ₂ —	33.8	33.7
16	—CH ₂ —	33.9	33.9
17	>C<	87.6	87.6
18	—CH ₃	11.3	11.3
19	—CH ₃	18.1	18.0
20	>CH—O—	74.9	74.9
21	—CH ₃	15.6	15.6
12-O-Acetyl moiety			
A1	—COO—	171.3	171.3
A2	—CH ₃	22.0	22.1
20-O-N-Methylanthraniloyl moiety			
N1	—COO—	111.0	111.0
N2	>C=	152.6	152.6
N3	>C=	111.5	111.5
N4	—CH=	135.1	135.1
N5	—CH=	114.7	114.7
N6	—CH=	132.6	132.6
N7	—CH=	168.2	168.2
N8	—CH ₂	29.6	29.5

Table 6. The ^{13}C NMR chemical shifts of sugar chains of stephanoside B and compound 6 (δ : ppm).

C-No.	Carbon Type	Stephanoside B	Compound 6
d-Cymarose			
1'	—O—CH—O—	96.4	96.4
2'	—CH ₂ —	37.3	37.2
3'	>CH—O—	77.9	77.9
4'	>CH—O—	83.5	83.5
5'	>CH—O—	69.0	68.9
6'	—CH ₃	18.7	18.7
O—Me	—O—CH ₃	58.9	58.8
d-Olenadrose			
1''	—O—CH—O—	101.9	101.9
2''	—CH ₂ —	37.5	37.6
3''	>CH—O—	79.3	79.2
4''	>CH—O—	82.8	82.9
5''	>CH—O—	72.0	72.0
6''	—CH ₃	19.0	18.9
O—Me	—O—CH ₃	57.2	57.2
d-Allomethylose			
1'''	—O—CH—O—	102.2	102.1
2'''	>CH—O—	73.2	73.3
3'''	>CH—O—	84.0	84.1
4'''	>CH—O—	74.6	74.5
5'''	>CH—O—	71.0	71.0
6'''	—CH ₃	18.7	18.7
O—Me	—O—CH ₃	62.1	62.1

The molecular formulae of purified compounds 2, 5 and 6 were determined using Q-TOF LC/MS in the positive ion mode. The molecular formula of GiA-7 was $\text{C}_{44}\text{H}_{65}\text{NO}_{12}$, according to the mass spectra (m/z 800.4580 ($\text{M} + \text{H}$)⁺, calcd. m/z 800.4582). Those of stephanoside C and stephanoside B were the same: $\text{C}_{52}\text{H}_{79}\text{NO}_{18}$, calcd. 1006.5370. The accurate masses of stephanosides C and B were m/z 1006.5383 ($\text{M} + \text{H}$)⁺ and m/z 1006.5488 ($\text{M} + \text{H}$)⁺, respectively. The molecular formulae of stephanosides C and B are the same, but their sugar chains are d-thevetose and d-allomethylose, respectively. Figure S1 shows the structures of compounds 2, 5 and 6. The NMR and mass spectrometry data confirmed that compounds 2, 5 and 6 are GiA-7, stephanoside C and stephanoside B, respectively.

We assessed the ability of purified 25, 50 and 100- μM GiA-7, stephanoside C and stephanoside B extracted from GI tea to inhibit 3T3-L1 cell differentiation. After 10 days, intercellular lipid accumulation and viable cells were determined. Each of GiA-7, stephanoside C and stephanoside B at 100 μM reduced intercellular lipid accumulation (Figure 4). Stephanoside C was the most effective inhibitor, which is the lowest concentration of significantly inhibited 3T3-L1 cell differentiation. Moreover, the inhibition of 3T3-L1 cell differentiation by GiA-7, stephanoside C and stephanoside B was concentration-dependent.

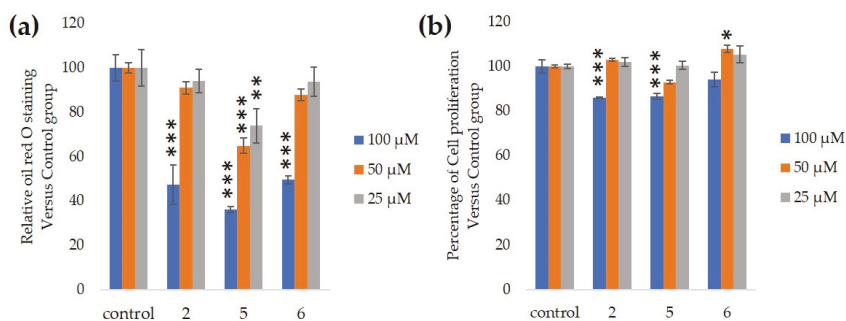


Figure 4. Effects of compounds 2 (GiA-7), 5 (stephanoside C) and 6 (stephanoside B) on 3T3-L1 cell differentiation. (a) Inhibition of adipogenesis. (b) Cell proliferation. Values are shown as means \pm SD ($n = 4$). * $p < 0.05$, ** $p < 0.01$ and *** $p < 0.001$ vs. control (ANOVA and post hoc Dunnett tests).

Several markers associated with adipogenesis control 3T3-L1 cell differentiation [22]. We assessed the expression of the *Ppar γ* , *Cebpa*, *Fasn*, *Pgc1 α* , *Cd36* and *Fabp4* genes that are associated with differentiation into adipocytes to determine the effects of GiA-7, stephanoside C and stephanoside B on adipogenesis. Figure 5 shows that GiA-7, stephanoside C and stephanoside B at 100 μ M significantly suppressed the expression of *Ppar γ* , *Cebpa*, *Fasn* and *Cd36*. Stephanoside B and GiA-7 significantly suppressed *Fabp4* expression. Stephanosides C and B also significantly suppressed *Pgc1 α* expression. These results indicated that GiA-7, stephanoside C and stephanoside B inhibited the early stage of adipogenic differentiation by inhibiting of *Ppar γ* -dependent mechanisms. Both *Hsl* and *Atgl* are phosphorylates upon appropriate physiological signaling to induce triacylglycerol (TG) lipolysis in adipocytes [23,24]. Figure 5 shows that stephanosides C, B and GiA-7 suppressed *Hsl* and *Atgl* gene expressions. These findings suggested that none of these compounds activated TG lipolysis. However, *Ppar γ* directly regulates *Hsl* and *Atgl* gene expressions in adipocytes *in vitro* [25,26]. Our results suggested that these compounds downregulated *Hsl* and *Atgl* gene expressions by inhibiting *Ppar γ* gene expression. *Lipin-1* functions in lipid droplet biogenesis during adipocyte differentiation and generates diacylglycerol for lipid synthesis [27]. *Lipin-1* is important for the process of TG accumulation during the early stage of adipogenesis. *Lipin-1* is a key factor for adipocyte maturation and maintenance by regulating *Ppar γ* and *Cebpa* [28]. *Lipin-1* expression is required to induce the transcription of adipogenic genes, including *Ppar γ* and *Cebpa* [29,30]. Figure 5 shows that stephanosides C and B and GiA-7 significantly suppressed *lipin-1* expression. These findings suggest that these compounds inhibited *Ppar γ* and *Cebpa* gene expressions by suppressing *lipin-1* gene expression. These observations confirm that GiA-7, stephanoside C and stephanoside B inhibited the early stage of adipogenesis and prevented TG accumulation. The transcriptional cofactor, *Pgc1 α* , is important for mitochondrial biogenesis. The regulation of *Pgc1 α* expression enhances mitochondrial biogenesis through *Srebp-1c* upregulation [31,32]. The present study found that only GiA-7 induced *Srebp-1c* and *Pgc1 α* . *Srebp-1c* is also a key regulator of adipocytes and is involved in lipid metabolism [33,34]. These findings suggest that GiA-7 regulates mitochondrial biogenesis through the *Srebp-1c*-dependent upregulation of *Pgc1 α* . GiA-7 also inhibits lipid accumulation in 3T3-L1 preadipocytes by downregulating adipogenic transcription factors and genes associated with lipid accumulation. Both *Pgc1 α* and *Ucp1* are brown/beige cell-specific genes. Only GiA-7 induced the expression of *Pgc1 α* and *Ucp1*. Beige adipocytes express low basal levels of *Ucp1*, whereas brown adipocytes constitutively express *Ucp1*. These findings suggest that GiA-7 inhibits the differentiation of white adipocytes and, also, induces beige-like adipocytes in 3T3-L1 mouse preadipocytes. Comprehensive profiles of gene expressions indicate that the characteristics of human brown and mouse beige adipocytes are compatible [33,34]. The activation of human brown adipocytes was recently examined as a possible novel therapeutic treatment for obesity [35]. Thus, GiA-7 might serve as a novel treatment for obesity in humans by inducing brown adipocytes.

Gymnemic acid extracted from the leaves of *Gymnema sylvestre* comprises a mixture of triterpene glycosides that can reduce glucose levels and inhibit glucose absorption [36–38]. The aqueous extract of *Gymnema sylvestre* induces insulin secretion in MIN6 cells [39]. One study found that GiA-7 from GI leaves inhibits glucose absorption in the isolated intestinal tract and suppresses blood glucose in rats [6]. However, we found here that GiA-7 purified from gymnemic acid extracted from GI tea inhibited 3T3-L1 cell differentiation into adipocytes. Stephanoside C and stephanoside B isolated from the stems of *Stephanotis lutchuensis* var. *japonica* and *Gongronema nepalense* have ant-malarial activity [21,40]. This is the first report of stephanoside C and stephanoside B isolated from *Gymnema inodorum* inhibiting 3T3-L1 cell differentiation into adipocytes. As mentioned before, obesity is characterized at the cellular level as being differentiated from preadipocytes. GiA-7, Stephanoside C and stephanoside B present in GI tea inhibited preadipocyte differentiation by suppressing the *Ppar γ* -dependent mechanisms. These findings suggest that consuming GI tea could play a role in the prevention of obesity.

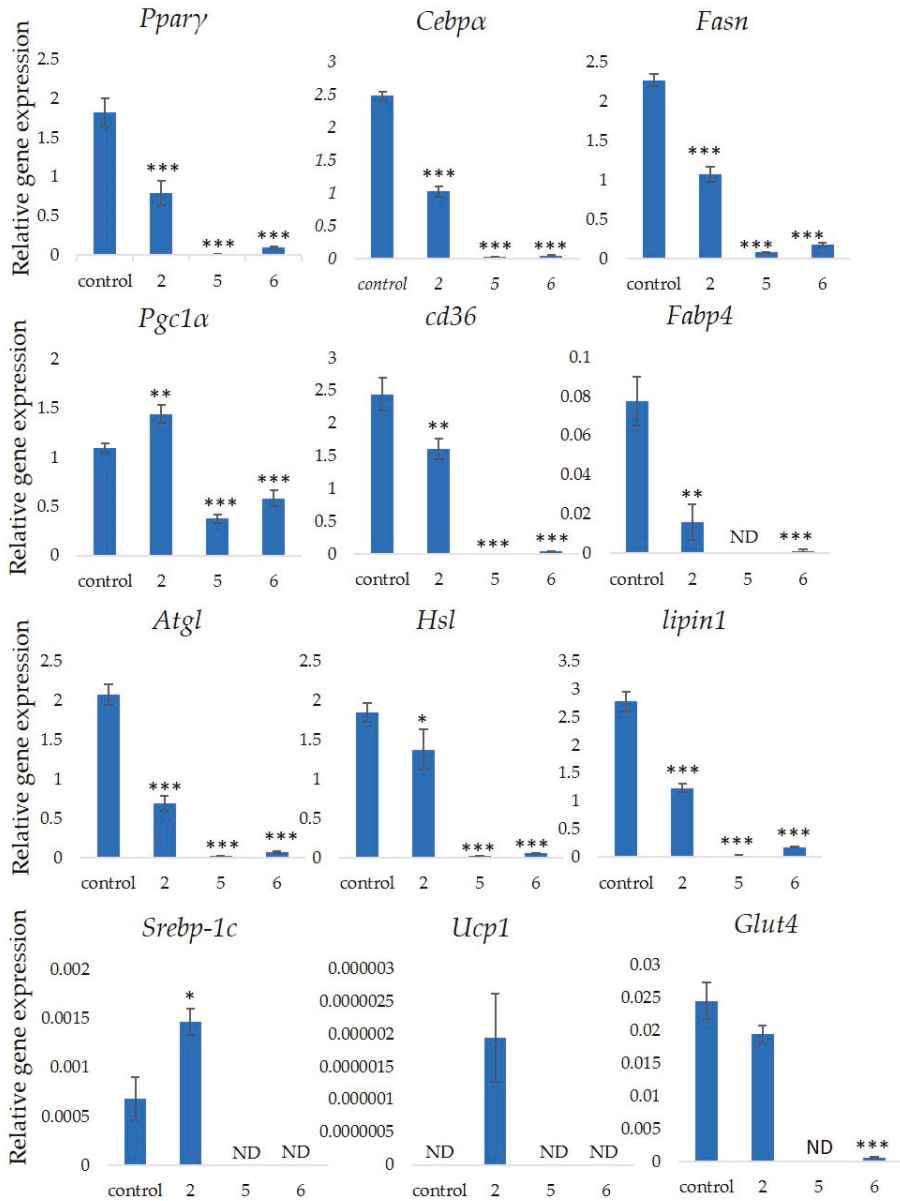


Figure 5. Effects of stephanosides C and B and GiA-7 extracted from *Gymnema inodorum* (GI) tea on gene expressions at the initial stage of 3T3-L1 cell differentiation into adipocytes. The differentiation of 3T3-L1 cells was induced, and the cells were incubated with 100 μ M GiA-7, stephanoside C and stephanoside B for 8 days; then, the gene expressions were measured. Values are shown as means \pm SD ($n = 4$). * $p < 0.05$, ** $p < 0.01$ and *** $p < 0.001$ vs. control (ANOVA with post hoc Dunnett tests). ND, not detected).

4. Conclusions

Gymnema inodorum tea has been widely applied in Thailand to control high blood glucose. Here, we screened the ability of gymnemic acids extracted from GI tea to inhibit 3T3-L1 cell differentiation into adipocytes. We isolated and purified GiA-7, stephanoside C and stephanoside B from GI tea using column chromatography and C18 HPLC, respectively, then confirmed them using NMR and mass spectrometry. All three compounds inhibited 3T3-L1 cell differentiation into adipocytes. Moreover, we determined that these compounds inhibited the early stage of adipogenesis by suppressing the *Lipin-1*, *Ppar γ* , *Cebpa*, *Fasn*, *Cd36* and *Fabp4* genes that are associated with adipogenesis. However, only GiA-7 induced *Ucp1* and *Pgc1 α* , suggesting that GiA-7 enhances mitochondrial activity and beige-like adipocytes among 3T3-L1 preadipocytes. Our findings suggest that the GiA-7, stephanoside C and stephanoside B from GI tea could help to prevent obesity.

5. Patents

Papawee Saiki and Yasuhiro Kawano, the methods of inhibiting fat synthesis, fat synthesis inhibitors and food and drink for suppressing fat synthesis, JP patent 2019-218481.

Supplementary Materials: The following is available online at <http://www.mdpi.com/2072-6643/12/9/2851/s1>, Figure S1: The structural formulae of compounds 2, 5 and 6.

Author Contributions: P.S. and P.K. (Prapaipat Klungsupaya) conceptualization; P.S., Y.K. and T.O. methodology; P.S. and Y.K. validation; P.S. formal analysis; P.S. investigation; W.P., P.K. (Papitchaya Kongchinda), N.P. and T.M. resources; P.S., Y.K. and T.O. data curation; P.S. writing—original draft preparation; P.S., Y.K., T.O., P.K. (Prapaipat Klungsupaya), T.M., W.P., P.K. (Papitchaya Kongchinda), N.P. and K.M. writing—review and editing; P.S. visualization; K.M. supervision; P.S. project administration; P.K. (Prapaipat Klungsupaya) funding acquisition. All authors have read and agreed to the published version of the manuscript.

Funding: This research was funded by the Thai Royal Government, Ministry of Higher Education, Science, Research and Innovation (MHESI) through the Thailand Institute of Scientific and Technological Research, TISTR (Grant Number: TISTR6334102122).

Acknowledgments: We thank Katsutaka Oishi and Tomoki Abe for their helpful discussions.

Conflicts of Interest: The authors declare no conflict of interest.

References

- Shanmugasundaram, E.; Rajeswari, G.; Baskaran, K.; Kumar, B.R.; Shanmugasundaram, K.R.; Ahmath, B.K. Use of *Gymnema sylvestre* leaf extract in the control of blood glucose in insulin-dependent diabetes mellitus. *J. Ethnopharmacol.* **1990**, *30*, 281–294. [CrossRef]
- Shimizu, K.; Iino, A.; Nakajima, J.; Tanaka, K.; Nakajyo, S.; Urakawa, N.; Atsuchi, M.; Wada, T.; Yamashita, C. Suppression of glucose absorption by some fractions extracted from *Gymnema sylvestre* leaves. *J. Vet. Med. Sci.* **1997**, *59*, 245–251. [CrossRef] [PubMed]
- Al-Romaiyan, A.; King, A.; Persaud, S.; Jones, P. A novel extract of *Gymnema sylvestre* improves glucose tolerance in vivo and stimulates insulin secretion and synthesis in vitro. *Phytother. Res.* **2013**, *27*, 1006–1011. [CrossRef] [PubMed]
- Paliwal, R.; Kathori, S.; Upadhyay, B. Effect of Gurmar (*Gymnema sylvestre*) powder intervention on the blood glucose levels among diabetics. *Stud. Ethno-Med.* **2009**, *3*, 133–135. [CrossRef]
- Kanetkar, P.; Singhal, R.; Kamat, M. Recent advances in indian herbal drug research guest editor: Thomas Paul Asir Devasagayam *Gymnema sylvestre*: A memoir. *J. Clin. Biochem. Nutr.* **2007**, *41*, 77–81. [CrossRef]
- Shimizu, K.; Ozeki, M.; Iino, A.; Nakajyo, S.; Urakawa, N.; Atsuchi, M. Structure-activity relationships of triterpenoid derivatives extracted from *Gymnema inodorum* leaves on glucose absorption. *Jpn. J. Pharmacol.* **2001**, *86*, 223–229. [CrossRef]
- Chiabchalard, A.; Tencomnao, T.; Santianont, R. Effect of *Gymnema inodorum* on postprandial peak plasma glucose levels in healthy human. *Afr. J. Biotechnol.* **2010**, *9*, 1079–1085.
- Shimizu, K.; Ozeki, M.; Tanaka, K.; Itoh, K.; Nakajyo, S.; Urakawa, N.; Atsuchi, M. Suppression of glucose absorption by extracts from the leaves of *Gymnema inodorum*. *J. Vet. Med. Sci.* **1997**, *59*, 753–757. [CrossRef] [PubMed]

9. Klungsupaya, P.; Muangman, T.; Theangtrong, N.; Khayungamawee, A.; Phatvej, W.; Thisayakorn, K.; Rerk-Am, U.; Sematong, T.; Trangvacharakul, S.; Arunpairajana, V. Antioxidant and antihyperglycemic activities of *Gymnema inodorum* Dence. In Proceedings of the 8th NRCT-JSPS Joint Seminar Innovative Research in Natural Products for Sustainable Development, Bangkok, Thailand, 3–5 February 2009; pp. 207–209.
10. Rohilla, A.; Ali, S. Alloxan induced diabetes: Mechanisms and effects. *Int. J. Res. Pharm. Biomed. Sci.* **2012**, *3*, 819–823.
11. Risérus, U.; Willett, W.C.; Hu, F.B. Dietary fats and prevention of type 2 diabetes. *Prog. Lipid Res.* **2009**, *48*, 44–51. [[CrossRef](#)]
12. Zeyda, M.; Stulnig, T.M. Obesity, inflammation, and insulin resistance—A mini-review. *Gerontology* **2009**, *55*, 379–386. [[CrossRef](#)] [[PubMed](#)]
13. Hotamisligil, G.S. Inflammation and metabolic disorders. *Nature* **2006**, *444*, 860–867. [[CrossRef](#)] [[PubMed](#)]
14. Farmer, S.R. Molecular determinants of brown adipocyte formation and function. *Genes Dev.* **2008**, *22*, 1269–1275. [[CrossRef](#)] [[PubMed](#)]
15. Rosen, E.D.; MacDougald, O.A. Adipocyte differentiation from the inside out. *Nat. Rev. Mol. Cell Biol.* **2006**, *7*, 885–896. [[CrossRef](#)] [[PubMed](#)]
16. Green, H.; Meuth, M. An established pre-adipose cell line and its differentiation in culture. *Cell* **1974**, *3*, 127–133. [[CrossRef](#)]
17. Rubin, C.S.; Hirsch, A.; Fung, C.; Rosen, O.M. Development of hormone receptors and hormonal responsiveness in vitro. Insulin receptors and insulin sensitivity in the preadipocyte and adipocyte forms of 3T3-L1 cells. *J. Biol. Chem.* **1978**, *253*, 7570–7578.
18. Taira, J.; Ogi, T. Induction of Antioxidant Protein HO-1 Through Nrf2-ARE Signaling Due to Pteryxin in *Peucedanum Japonicum* Thunb in RAW264. 7 Macrophage Cells. *Antioxidants* **2019**, *8*, 621. [[CrossRef](#)]
19. Oishi, K.; Ohyama, S.; Higo-Yamamoto, S. Chronic sleep disorder induced by psychophysiological stress induces glucose intolerance without adipose inflammation in mice. *Biochem. Biophys. Res. Commun.* **2018**, *495*, 2616–2621. [[CrossRef](#)]
20. Kanda, Y. Investigation of the freely available easy-to-use software “EZ” for medical statistics. *Bone Marrow Transpl.* **2013**, *48*, 452–458. [[CrossRef](#)] [[PubMed](#)]
21. Yoshikawa, K.; Okada, N.; Kann, Y.; Arihara, S. Steroidal glycosides from the fresh stem of *Stephanotis lutchuensis* var. *japonica* (Asclepiadaceae). Chemical structures of stephanosides AJ. *Chem. Pharm. Bull.* **1996**, *44*, 1790–1796. [[CrossRef](#)]
22. Drolet, R.; Richard, C.; Sniderman, A.D.; Mailloux, J.; Fortier, M.; Huot, C.; Rheaume, C.; Tchernof, A. Hypertrophy and hyperplasia of abdominal adipose tissues in women. *Int. J. Obes. (Lond.)* **2008**, *32*, 283–291. [[CrossRef](#)]
23. Xie, M.; Roy, R. AMP-Activated Kinase Regulates Lipid Droplet Localization and Stability of Adipose Triglyceride Lipase in *C. elegans* Dauer Larvae. *PLoS ONE* **2015**, *10*, e0130480. [[CrossRef](#)] [[PubMed](#)]
24. Jiang, D.; Wang, D.; Zhuang, X.; Wang, Z.; Ni, Y.; Chen, S.; Sun, F. Berberine increases adipose triglyceride lipase in 3T3-L1 adipocytes through the AMPK pathway. *Lipids Health Dis.* **2016**, *15*, 214. [[CrossRef](#)]
25. Deng, T.; Shan, S.; Li, P.P.; Shen, Z.F.; Lu, X.P.; Cheng, J.; Ning, Z.Q. Peroxisome proliferator-activated receptor-gamma transcriptionally up-regulates hormone-sensitive lipase via the involvement of specificity protein-1. *Endocrinology* **2006**, *147*, 875–884. [[CrossRef](#)] [[PubMed](#)]
26. Kershaw, E.E.; Schupp, M.; Guan, H.-P.; Gardner, N.P.; Lazar, M.A.; Flier, J.S. PPAR γ regulates adipose triglyceride lipase in adipocytes in vitro and in vivo. *Am. J. Physiol. Endocrinol. Metab.* **2007**, *293*, E1736–E1745. [[CrossRef](#)]
27. Sembongi, H.; Miranda, M.; Han, G.S.; Fakas, S.; Grimsey, N.; Vendrell, J.; Carman, G.M.; Siniosoglou, S. Distinct roles of the phosphatidate phosphatases lipin 1 and 2 during adipogenesis and lipid droplet biogenesis in 3T3-L1 cells. *J. Biol. Chem.* **2013**, *288*, 34502–34513. [[CrossRef](#)]
28. Kim, H.E.; Bae, E.; Jeong, D.-Y.; Kim, M.-J.; Jin, W.-J.; Park, S.-W.; Han, G.-S.; Carman, G.M.; Koh, E.; Kim, K.-S. Lipin1 regulates PPAR γ transcriptional activity. *Biochem. J.* **2013**, *453*, 49–60. [[CrossRef](#)]
29. Zhang, P.; Takeuchi, K.; Csaki, L.S.; Reue, K. Lipin-1 phosphatidic phosphatase activity modulates phosphatidate levels to promote peroxisome proliferator-activated receptor gamma (PPAR γ) gene expression during adipogenesis. *J. Biol. Chem.* **2012**, *287*, 3485–3494. [[CrossRef](#)] [[PubMed](#)]
30. Phan, J.; Peterfy, M.; Reue, K. Lipin expression preceding peroxisome proliferator-activated receptor-gamma is critical for adipogenesis in vivo and in vitro. *J. Biol. Chem.* **2004**, *279*, 29558–29564. [[CrossRef](#)]

31. Puigserver, P.; Spiegelman, B.M. Peroxisome proliferator-activated receptor- γ coactivator 1 α (PGC-1 α): Transcriptional coactivator and metabolic regulator. *Endocr. Rev.* **2003**, *24*, 78–90. [[CrossRef](#)]
32. Kobayashi, M.; Fujii, N.; Narita, T.; Higami, Y. SREBP-1c-Dependent Metabolic Remodeling of White Adipose Tissue by Caloric Restriction. *Int. J. Mol. Sci.* **2018**, *19*, 3335. [[CrossRef](#)] [[PubMed](#)]
33. Sharp, L.Z.; Shinoda, K.; Ohno, H.; Scheel, D.W.; Tomoda, E.; Ruiz, L.; Hu, H.; Wang, L.; Pavlova, Z.; Gilsanz, V. Human BAT possesses molecular signatures that resemble beige/brite cells. *PLoS ONE* **2012**, *7*, e49452. [[CrossRef](#)] [[PubMed](#)]
34. Wu, J.; Bostrom, P.; Sparks, L.M.; Ye, L.; Choi, J.H.; Giang, A.H.; Khandekar, M.; Virtanen, K.A.; Nuutila, P.; Schaart, G.; et al. Beige adipocytes are a distinct type of thermogenic fat cell in mouse and human. *Cell* **2012**, *150*, 366–376. [[CrossRef](#)] [[PubMed](#)]
35. Cannon, B.; Nedergaard, J. Neither brown nor white. *Nature* **2012**, *488*, 286–287. [[CrossRef](#)] [[PubMed](#)]
36. Sugihara, Y.; Nojima, H.; Matsuda, H.; Murakami, T.; Yoshikawa, M.; Kimura, I. Antihyperglycemic effects of gymnemic acid IV, a compound derived from *Gymnema sylvest*re leaves in streptozotocin-diabetic mice. *J. Asian Nat. Prod. Res.* **2000**, *2*, 321–327. [[CrossRef](#)]
37. Wang, L.; Luo, H.; Miyoshi, M.; Imoto, T.; Hiji, Y.; Sasaki, T. Inhibitory effect of gymnemic acid on intestinal absorption of oleic acid in rats. *Can. J. Physiol. Pharmacol.* **1998**, *76*, 1017–1023. [[CrossRef](#)]
38. Liu, H.-M.; Kiuchi, F.; Tsuda, Y. Isolation and structure elucidation of gymnemic acids, antisweet principles of *Gymnema sylvest*re. *Chem. Pharm. Bull.* **1992**, *40*, 1366–1375. [[CrossRef](#)]
39. Asare-Anane, H.; Huang, G.; Amiel, S.; Jones, P.; Persaud, S. Stimulation of insulin secretion by an aqueous extract of *Gymnema sylvest*re: Role of intracellular calcium. In Proceedings of the 196th Meeting of the Society for Endocrinology and Society for Endocrinology Joint Endocrinology and Diabetes Day, London, UK, 7–9 November 2005.
40. Libman, A.; Zhang, H.; Ma, C.; Southavong, B.; Sydara, K.; Bouamanivong, S.; Tan, G.T.; Fong, H.H.; Soejarto, D.D. A first new antimalarial pregnane glycoside from *Gongronema napalense*. *Asian J. Tradit. Med.* **2008**, *3*, 203.



© 2020 by the authors. Licensee MDPI, Basel, Switzerland. This article is an open access article distributed under the terms and conditions of the Creative Commons Attribution (CC BY) license (<http://creativecommons.org/licenses/by/4.0/>).



Article

Viburnum opulus L. Juice Phenolics Inhibit Mouse 3T3-L1 Cells Adipogenesis and Pancreatic Lipase Activity

Małgorzata Zakłos-Szyda *, Nina Pietrzyk, Marcin Szustak and Anna Podsedek

Department of Biotechnology and Food Sciences, Institute of Molecular and Industrial Biotechnology, Lodz University of Technology, 90-924 Łódź, Poland; nina.pietrzyk@dokt.p.lodz.pl (N.P.); marcin.szustak@p.lodz.pl (M.S.); anna.podsedek@p.lodz.pl (A.P.)

* Correspondence: malgorzata.zaklos-szyda@p.lodz.pl

Received: 4 June 2020; Accepted: 23 June 2020; Published: 6 July 2020

Abstract: *Viburnum opulus* L. fruit is a rich source of phenolic compounds that may be involved in the prevention of metabolic diseases. The purpose of this study was to determine the effects of *Viburnum opulus* fresh juice (FJ) and juice purified by solid-phase extraction (PJ) on the adipogenesis process with murine 3T3-L1 preadipocyte cell line and pancreatic lipase activity in triolein emulsion, as well as their phenolic profiles by UPLC/Q-TOF-MS. Decrease of lipids and triacylglycerol accumulation in differentiated 3T3-L1 cells were in concordance with downregulation of the expression of peroxisome proliferator-activated receptor-gamma (PPAR γ), CCAAT/enhancer-binding protein alpha (C/EBP β/α), and sterol regulatory element-binding protein 1c (SREBP-1c). Furthermore, regulation of PPAR γ -mediated β -lactamase expression by *V. opulus* components in reporter gene assay, as well as their binding affinity to ligand-binding domain of PPAR γ , were tested. In addition, the levels of enzymes involved in lipid metabolism, like fatty acid synthase (FAS) or acetyl-CoA carboxylase (ACC), were decreased, along with inflammatory cytokines, like tumor necrosis factor α (TNF α), interleukin-6 (IL-6) and leptin. Moreover, FJ and PJ were able to inhibit pancreatic lipase, which potentially could reduce the fat absorption from the intestinal lumen and the storage of body fat in the adipose tissues. Thirty-two phenolic compounds with chlorogenic acid as the dominant compound were identified in PJ which revealed significant biological activity. These data contribute to elucidate *V. opulus* juice phenolic compounds' molecular mechanism in adipogenesis regulation in 3T3-L1 cells and dietary fat lipolysis.

Keywords: *Viburnum opulus*; phenolic compounds; adipogenesis; PPAR γ ; lipase inhibition

1. Introduction

Nutrition-related chronic diseases have become the main health problem of the world of the 21st century. According to World Health Organization data based on the latest, in the European Union countries overweight and obesity affect 30–70% and 10–30% of adults, respectively [1]. Obesity is characterized as abnormal or excessive fat accumulation, which means the increase in the number (hyperplasia) and size (hypertrophy) of differentiated adipocytes [2,3]. It is known that adipose tissue is not only a reservoir of energy in the form of triacylglycerols (TAG), but it also secretes adipocytokines, growth factors, and hormones involved in energy homeostasis and insulin sensitivity maintenance. Thus, increased adiposity is regarded as one of the most important risk factors of insulin resistance, type 2 diabetes (T2D), and nonalcoholic fatty liver disease (NAFLD), which in turn may lead to hypertension, coronary heart disease, and stroke [4]. Among the most important cellular regulators of lipid metabolism are peroxisome proliferator-activated receptors (PPARs), belonging to nuclear receptors proteins [5]. There are three different receptor isotypes: PPAR α , PPAR β/δ , and

PPAR γ , among which PPAR γ is involved in the regulation of adipocyte differentiation. Ligand binding to the PPAR γ ligand-binding domain (LBD) leads to a conformational change and switching of nuclear receptor corepressors to coactivators [6]. Agonists activate PPAR γ , which, after binding with retinoic X receptor and peroxisome proliferator responsive element (PPRE) within the promoter of target genes activates their transcription [7]. Not only PPAR γ but also other transcription factors, such as CCAAT/enhancer-binding protein alpha (C/EBP β/α) and sterol regulatory element binding protein-1c (SREBP-1c), are involved in adipocyte differentiation [8]. These factors stimulate gene expression and the expression of other proteins involved in lipid synthesis and storage, such as fatty acid synthase (FAS) or acetyl-CoA carboxylase (ACC). What is more, obese adipose tissue contributes to the elevation of inflammatory cytokines, such as tumor necrosis factor α (TNF α) or interleukin-6 (Il-6), leading to chronic inflammation state promoting insulin resistance and cancer development [9]. PPAR γ agonist type of medicines, like glitazones, significantly improve glycemic control, but via promotion of free fatty acid uptake and accumulation of TAG in adipose tissue lead to weight gain, and increases in heart or renal failure [10–12]. Thus, due to the variety of induced side effects, less harmful plant-derived agents are searched as PPAR γ regulators able to prevent insulin resistance without weight obesity gaining. Other mechanisms allowing the decrease of fatty acids intestinal absorption is the usage of pancreatic lipase inhibitor, which decreases the hydrolysis of diet-originated TAG into glycerol and fatty acids. Since phenolic compounds constitute an important part in the human diet, they have recently emerged as critical phytochemicals in obesity prevention and treatment [13,14]. Among fruits rich in these secondary metabolites are those of *Viburnum opulus* L. (*V. opulus* L.), known as guelder rose, or the European cranberry bush rose [15,16]. Despite its fruit bitterness it can be found in food products such as juice, jams, jellies, marmalades, sauces, herbal tea, cordials, and liqueurs, as well as fermented drinks [17]. Our previous studies showed that due to their high antioxidant potential *V. opulus* phenolics decreased chemically generated intracellular oxidative stress under *in vitro* conditions, as well as possessed different anticancer activity with apoptosis induction and inhibition of cell migration [16,18,19]. Further studies revealed *V. opulus* fruit phenolics' impact on carbohydrate metabolism as α -amylase, α -glucosidase, protein tyrosine phosphatase-1B, and dipeptidyl peptidase-4 enzyme inhibitors [20,21]. More detailed analysis showed that *V. opulus* phenolics decreased the uptake of free fatty acids and lipids accumulation in human epithelial Caco-2 cells [15]. Nevertheless, they inhibited glucose-stimulated insulin secretion in mice insulinoma MIN6 cells, as well as increased free fatty acid uptake and lipid droplets accumulation [21]. Taking into account potent phenolics' impact on the modulation of cellular metabolism, in the present study we investigated an influence of *V. opulus* fresh juice (FJ) and purified juice (PJ) on pancreatic lipase activity and adipogenesis process in mouse preadipocyte 3T3-L1 cell line [22]. In addition, phenolic components of FJ and PJ were identified by the UPLC-MS method. Studies also assessed the influence of these preparations on the expression of transcription factors (PPAR γ , C/EBP, SREBP1c) and other proteins related to adipogenesis (FAS, ACC, TNF α , Il-6, leptin, adiponectin). Furthermore, the *V. opulus* components' influence on the regulation of PPAR γ activity was elucidated.

2. Materials and Methods

2.1. Chemicals and Reagents

Acetonitrile (Merck, Darmstadt, Germany) and formic acid (Sigma-Aldrich, Steinheim, Germany) were hyper grades for LC-MS. Folin–Ciocalteu reagent was obtained from POCH (Gliwice, Poland). The reference compounds were obtained from Sigma-Aldrich (Steinheim, Germany) ((+)-catechin, (–)-epicatechin, rutin, gallic acid), Extrasynthese (Lyon, France) (chlorogenic acid, cyanidin 3-glucoside, quercetin 3-glucoside, isorhamnetin, and isorhamnetin 3-rutinoside) and Phytolab (Vestenbergsgreuth, Germany) (neochlorogenic acid, procyanidin B1, and procyanidin B2). Ultrapure water (Simplicity®Water Purification System, Millipore, Marlborough, MA, USA) was used to prepare

all the solutions. All cell culture reagents were obtained from Life Technologies (Carlsbad, CA, USA). Other chemicals used, if not stated otherwise, were obtained from Sigma-Aldrich (Steinheim, Germany).

2.2. Preparation of *V. opulus* Samples, Identification and Quantitative Determination of Individual Phenolic Compounds by UPLC–PDA–Q/TOF-MS

Fruits of the *V. opulus* were collected from Rogów Arboretum, Warsaw University of Life Sciences (Rogów, Poland) (account number 18162). After fruit pulp homogenization and centrifugation (5000 rpm for 10 min), fresh juice (FJ) was obtained. FJ purification by solid phase extraction with C-18 Sep-Pak cartridge (10 g capacity, Waters Corp., Milford, MA, USA; 12-Port Vacuum Manifold system) and methanolic elution processes were performed. After methanol removal under reduced pressure ($T < 40\text{ }^{\circ}\text{C}$), solid residue was dissolved in water and lyophilized to purified juice (PJ). Phenolic compounds were identified using the Acquity ultraperformance liquid chromatography (UPLC) system coupled with a quadruple-time-of-flight mass spectrometry (Q/TOF-MS) instrument (Waters Corp., Milford, MA, USA) equipped with an electrospray ionization (ESI) source. The separation of individual phenolics was carried out using an Acquity UPLCR HSS T3 C18 column ($150 \times 2.1\text{ mm}$, $1.8\text{ }\mu\text{m}$; Corp., Milford, MA, USA) at $30\text{ }^{\circ}\text{C}$. The mobile phase was a mixture of 0.1% formic acid (A) and acetonitrile (B). The gradient program was as follows: initial conditions 99% (A), 12 min 65% (A), 12.5 min 100% (B), 13.5 min 99% (A). The flow rate was 0.45 mL/min and the injection volume was 5 μL . The mass spectrometer was operating in the negative mode for a mass range of 150–1500 Da, fixed source temperature at $100\text{ }^{\circ}\text{C}$, desolvation temperature $250\text{ }^{\circ}\text{C}$, desolvation gas flow of 600 L/h, cone voltage of 45 V, a capillary voltage of 2.0 kV, and a collision energy of 50 V. Leucine enkephalin was used as a lock mass. The instrument was controlled by Mass-Lynx™ V 4.1 software (Waters Corp., Milford, MA, USA). The runs were monitored at the following wavelengths: flavanols at 280 nm, hydroxycinnamic acids at 320 nm, flavonols at 360 nm, and anthocyanins at 520 nm. Photodiode detector (PDA) spectra were measured over the wavelength range of 200–600 nm. Calibration curves were run for the external standards: (+)-catechin, procyanidin C1, neochlorogenic acid, chlorogenic acid, cryptochlorogenic acid, caffeic acid, and quercetin 3-rutinoside, and quercetin 3-glucoside. Phenolic compounds were identified using their UV-Vis characteristic, MS and MS2 properties using data gathered in-house and from the literature.

2.3. Inhibition Assay for Pancreatic Lipase Activity

Inhibitory activities of FJ and PJ were expressed as the IC_{50} values (half-maximal inhibitory concentration). Orlistat was used as a positive inhibitor control. The IC_{50} value was concluded from the graph of lipase inhibition (%) versus the concentration of juices or Orlistat per 1 mL of the reaction mixture under assay conditions. The pancreatic lipase activity was tested by measuring the fatty acids released from emulsified triolein (0.6 g of triolein, 25 mL of Tris-buffer, and 0.4 g of bile acids) according to the method described previously [23]. Briefly, 0.3 mL of FJ, PJ, and orlistat solutions diluted with buffer were mixed with 0.5 mL of the triolein emulsion and pre-incubated at $37\text{ }^{\circ}\text{C}$ for 5 min before adding lipase supernatant (0.063 mL). Blanks with buffer instead of the lipase supernatant were prepared for background correction. The control consisted of all solutions without inhibitor. Finally, the reaction mixtures were incubated in a shaking bath (200 rpm) at $37\text{ }^{\circ}\text{C}$ for 30 min. The reaction was terminated by adding 0.23 mL of HCl. Then, 3 mL of isooctane was added and vortexed for 0.5 min. The upper layer (2 mL) was collected, followed by the addition of 0.4 mL copper reagent (5% copper acetate, pH 6.1 regulated by pyridine). After vortexing for 1 min, the upper layer was centrifuged at 10,000 rpm for 10 min and its absorbance (A) was measured at 720 nm against a reagent blank. All samples were assayed in triplicate. Percent inhibition of pancreatic lipase activity was calculated using the formula:

$$\text{Lipase inhibition (\%)} = [(A_c - A_{cb}) - (A_s - A_{sb})] / (A_c - A_{cb}) \times 100 \quad (1)$$

where A_c is the absorbance of the control, A_{cb} is the blank control absorbance, A_s is the sample absorbance, A_{sb} is the sample blank.

2.4. Cell Culture and Exposure Conditions

Mouse preadipocytes 3T3-L1 were supplied by ATCC (Manassas, VA, USA). Preadipocytes were grown in Dulbecco's Modified Eagle's Medium (DMEM) medium with high glucose supplemented with 10% bovine calf serum. For adipocyte differentiation a confluent culture of 3T3-L1 cells was grown for two days in a preadipocyte medium DMEM with 10% calf serum, then the cells were stimulated with a differentiation medium with DMEM containing 10% fetal bovine serum (FBS), 1 μ M dexamethasone, 0.5 mM methylisobutylxanthine (IBMX), and 1 μ g/mL insulin for two days. After 48 h of incubation, the differentiation medium was replaced with DMEM containing 10% FBS and 1 μ g/mL insulin [22]. Cell medium was replaced at 2-day intervals with the addition of compounds studied. Analyses were carried out 7 days after differentiation if not stated otherwise. To perform biological activity assays, a stock solution of PJ at concentration 100 mg/mL in 50% dimethyl sulfoxide (DMSO) was prepared and further dilutions were made with culture medium. The sample's concentrations used in biological studies are presented in the descriptions of the tests carried out. All cell culture experiments were performed in a humidified 5% CO₂ and 95% atmosphere at 37 °C. Tissue culture plastics were supplied by Greiner Bio-One GmbH (Frickenhausen, Austria). All the experimental measurements were performed using the Synergy 2 BioTek Microplate Reader (BioTek, Winooski, VT, USA). Microscopic observations were performed using contrast-phase and fluorescent microscope Nikon TS100 Eclipse (Nikon, Tokyo, Japan) under 200 \times magnification, if not stated otherwise.

2.5. Cell Viability

The effects of FJ and PJ on cell viability were assayed with the PrestoBlue reagent. The 3T3-L1 preadipocytes were seeded into a 96-well plate at a density of 10⁴ cells/well overnight. Two days after confluence, cells were treated with series of extracts concentrations for 48 hours. The final concentration of DMSO did not exceed 0.005%. Then, the PrestoBlue reagent was added for 30 min and fluorescent signal at F530/590 nm was measured. For cell visualization, 2 μ M calcein AM (Thermo Fisher Scientific, Waltham, MA, USA) was directly added to the cells.

2.6. Detection of Intracellular Reactive Oxygen Species Generation

The 3T3-L1 preadipocytes were seeded into a 96-well plate at a density of 10⁴ cells/well. After the cells' treatment with extracts, the cells were washed with phosphate buffer saline (PBS) and incubated with DMEM and 10 μ M of dichloro-dihydro-fluorescein diacetate (DCFH-DA) dye. Fluorescence intensity at F485/530 nm was determined after 30 min incubation. Five-hundred μ M *tert*-BOOH (*t*-BOOH) was used as a positive control. The intracellular fluorescence of cells was observed after cells treatment with chemicals under a fluorescence microscope.

2.7. Determination of Lipid Accumulation, Free Fatty Acid Uptake and Triglyceride Content

The 3T3-L1 preadipocytes were seeded into a 96-well plate at a density of 10⁴ cells/well for each of the experiment. The lipid content in the mature adipocytes was determined using the Nile red staining method. After cell incubation with FJ and PJ, cells were washed with cold PBS and fixed in 5% paraformaldehyde for 30 min. Then, the cells were stained with Nile red (1 μ g/mL) for 40 min and fluorescence intensity at F485/530 nm was measured. For cell nuclei visualization, to fixed cells, 1 μ g/mL 4',6-Diamidino-2'-phenylindole dihydrochloride (DAPI) stain was added. The measurement of fatty acid fluorescent probe TF2-C12 uptake by cells was performed with the Fatty Acid Uptake Kit (Sigma-Aldrich, Seinhem, Germany). After the cells' treatment with the preparations, the fluorescent signal at F485/530 nm was measured after 1 h incubation with fluorescent analogue.

Triglyceride content was measured using the Triglyceride Colorimetric Assay kit (Cayman Chemical, Ann Arbor, MI, USA). To perform the experiment cells were seeded into a 6-well plate at a

density of 2×10^5 cells/well. Following treatment, the differentiated 3T3-L1 adipocytes were rinsed with PBS, harvested with a cell scraper, lysed with 1% Triton X-100 and the total triglyceride content was assessed according to the manufacturer's instructions with an absorbance measurement at 540 nm.

2.8. Measurement of Adipolysis

To perform, the experiment cells were seeded into a 24-well plate at a density of 4×10^4 cells/well. After treatment with FJ and PJ, the cells were washed with PBS and incubated with an induction solution for 1 h. Then the medium was collected, and glycerol released into the medium was measured at 570 nm using a colorimetric assay Adipolysis Assay Kit (Sigma-Aldrich, Steinheim, Germany) and following the manufacturer's instructions. As a positive control (lipolysis inducer), $10 \mu\text{M}$ isoproterenol was used.

2.9. Gene Expression Analysis

To perform, the experiment cells were seeded into a 6-well plate at a density of 2×10^5 cells/well. After cell incubation with FJ and PJ, the total RNA was extracted with the GeneMatrix Universal RNA Purification Kit (Eurex Ltd., Gdansk, Poland) according to the manufacturer's procedure. RNA samples were purified with an amplification Grade DNase I (Sigma-Aldrich, Steinheim, Germany), and reverse transcribed with the NG dART RT Kit (Eurex Ltd., Gdansk, Poland). Real-time RT-PCR was carried out using the SG qPCR Master Mix (Eurex Ltd., Gdansk, Poland) on a BioRad CFX96 qPCR System (Bio-Rad, Hercules, CA, USA). Complementary DNA representing 6 ng of total RNA per sample was subjected to 40 cycles of PCR amplification. Samples were first incubated at 95°C for 40 s, then at 55°C for 30 s, and finally at 72°C for 30 s. To exclude non-specific products and primer-dimers, after the cycling protocol, a melting curve analysis was performed by maintaining the temperature at 52°C for 2 s, followed by a gradual temperature increase to 95°C . The threshold cycle (Ct) values for that gene did not change in independently performed experiments. The level of target gene expression was calculated as $2^{-\Delta\Delta\text{Ct}}$, where $\Delta\Delta\text{Ct} = [\text{Ct}(\text{target}) - \text{Ct}(\beta\text{actin})]_{\text{sample}} - [\text{Ct}(\text{target}) - \text{Ct}(\beta\text{actin})]$. The following primer sequences were used to determine the genes' expression: CREB-binding protein (CBP): forward primer (F) TTACAACAGGCCAGGTTTCC, reverse primer (R) GGCTGGCGACATACAGTACA; sterol regulatory element binding transcription factor 1 (SREBP1): (F) TGTTGGCATCCTGCTATCTG, (R) AGGGAAAGCTTTGGGGTCTA; β -actin: (F) CCACAGCTGAGAGGGAAATC, (R) AAGGAAGGCTGGAAAAGAGC; adiponectin: (F) AGATGGCACTCCTGGAGAGAAG, (R) ACATAAGCGGCTTCTCCAGGCT; leptin: (F) GGATCAGGTTTTGTGGTGCT, (R) TTGTGGCCATAAAGTCCTC; fatty acid synthase (FAS): (F) TTGCTGGCACTACAGAATGC, (R) AACAGCCTCAGAGCGACAAT; peroxisome proliferator activated receptor gamma (PPAR γ): (F) GCGGAAGAAGAGACCTGGG, (R) AGAACGTGACTTCTCAGCCC; interleukin-6 (Il-6): (F) GTCCTTCTACCCCAATTTCCA, (R) TAACGCACTAGGTTTGCCGA; CCAAT/enhancer binding protein (C/EBP) (F) GTGTGCACGTCTATGCTAAACCA, (R) GCCGTTAGTGAAGAGTCTCAGTTTG; tumor necrosis factor α (TNF α): (F) GGGATCTGCTCCGCGTGT, (R) TCCGCGCCAGGAGAAGTGT; acetyl-Coenzyme A carboxylase alpha (ACC): (F) GGGGATCTCTGGCTTACAGG, (R) ATCGCATGCATTTCACTGCT; fatty acid translocase (FAT/CD36), (F) TGGCCTTACTTGGGATTGG, (R) CCAGTGATATGTAGGCTCATCCA.

2.10. Western Blotting

To perform the experiment cells were seeded into a 6-well plate at a density of 2×10^5 cells/well. To prepare the total cell lysates, monolayers of 3T3-L1 adipocytes were scraped and lysed in Mammalian Protein Extraction Reagent (M-PER) containing protease and phosphatase inhibitors cocktail (Thermo Scientific, Waltham, MA, USA). Then, the lysates were centrifuged at 13,000 rpm for 5 min, and the supernatants of cell lysates were separated. The protein quantification was measured using the Protein Assay Dye Reagent Concentrate (Bio-Rad Laboratories BmbH,

München, Germany). Each 20 µg of protein samples were separated by 8% or 10% sodium dodecyl sulphate-polyacrylamide gel electrophoresis (SDS-PAGE) and transferred to 0.45 µm nitrocellulose blotting membrane (GE Healthcare, Chicago, IL, USA). The membranes were blocked using 5% bovine serum albumin (BSA) in tris-buffered saline containing 0.1% Tween-20 (TBST) for 2 h at room temperature and incubated with primary antibodies overnight at 4 °C diluted 1:1000 in the same solution. Polyclonal rabbit antibodies targeting PPAR γ (#2435), RxR α (#5388), CBP (#7389), acetyl-CoA carboxylase (#3676), phospho-acetyl-CoA carboxylase (Ser79) (#3661), phospho-AMPK α (Thr172) (#2531) and β actin (#4967) were purchased from Cell Signaling Technology (Danvers, MA, USA), SREBP-1c (14088-1-AP) from Proteintech Group (Manchester, UK), and p-IRS-1 (Ser307) from Santa Cruz Biotechnology (Dallas, TX, USA). Afterwards, the membranes were washed three times with TBST, then incubated for 1 h at room temperature with horseradish peroxidase (HRP)-conjugated secondary anti-rabbit antibody (#7074, Cell Signaling Technology, Danvers, MA, USA) diluted 1:3000 in 5% nonfat dry milk in TBST. After that membranes were re-washed three times with TBST. The proteins were visualized using an enhanced chemiluminescent SuperSignal West Pico Trial Kit (Thermo Scientific, Waltham, MA, USA). The ChemiDocTM MP Image System with Image LabTM 5.1 software (Bio-Rad Laboratories, Hercules, CA, USA) was used for acquisition and densitometric analysis of western blot images. Relative protein band intensity was normalized to β -actin and quantified with respect to control cells.

2.11. Determination of Selected Proteins Levels

To perform, the experiment cells were seeded into a 6-well plate at a density of 2×10^5 cells/well. On the last day of cells treatment the medium was collected and protein concentrations of adiponectin (Adiponectin Mouse ELISA Kit, Abcam, Cambridge, GB), leptin (Leptin Mouse ELISA Kit, Abcam, Cambridge, GB), Il6 (Mouse IL6 ELISA kit, Biorbyt Ltd., Cambridge, GB) and TNF α (Mouse TNF alpha ELISA kit, Biorbyt Ltd., Cambridge, GB), were determined using ELISA kits, following the manufacturer's instructions. The PPAR γ protein level present in the nuclear fraction of the cellular lysates was determined with the PPAR γ Transcription Factor Assay Kit (Abcam, Cambridge, GB).

2.12. Reporter Gene Assay

Cellular activation of the PPAR γ nuclear receptor was assessed in the reporter gene assay GeneBLazer[®]PPAR gamma 293HDA (Invitrogen, Carlsbad, CA, USA) according to the manufacturer's protocol. In brief, cells stably expressing specific PPAR γ ligand-binding domain fusion protein and UAS- β -lactamase reporter gene were incubated with tested extracts for 16 h, the cells were loaded with cell-permeable LiveBLazer FRET B/G substrate, after 2 h incubation fluorescence intensities at 460 and 530 nm emission following excitation at 420 nm were measured. After subtraction of fluorescence background from cell-free wells, the ratio of fluorescence intensity at 460 versus 530 nm was calculated. As the PPAR γ inhibitor 0.1 µM T0070907 was used, whereas 1 µM rosiglitazone as the activator.

2.13. Molecular Modeling

To determine the potential interaction between analyzed FJ or PJ components and the PPAR γ receptor, molecular docking simulation was performed. An X-ray crystal structure for human PPAR γ receptor in complex with rosiglitazone (5YCP) was obtained from the Protein Data Bank database (<http://www.rcsb.org/>) as a .pdb file [24]. Subsequently, the protein molecule model was prepared to docking procedure (hydrogen addition and grid box coordinates determination) with the AutoDock Tolls software. Then the protonation state of the side chains was defined with the PROPKA software (available at http://nbcrc-222.ucsd.edu/pdb2pqr_2.0.0/). Structures of rosiglitazone, chlorogenic acid, and (+)- catechin were downloaded from the ZINC database (<http://zinc.docking.org/substances/home/>). The procyanidin B1 and C1 structures were built with ChemSkech software. The obtained files were converted to .pdb file with the OPENBABEL tools <http://www.cheminfo.org/Chemistry/Cheminformatics/FormatConverter/index.html>). Then, all the ligand molecules were prepared for

further modeling (determine rotating bonds) with the AutoDock Tools and saved as .pdbqt file. The docking of the prepared ligand to PPAR γ receptor was performed with Autodock Vina docking software. [AutoDock Vina: improving the speed and accuracy of docking with a new scoring function, efficient optimization and multithreading]. The size of the grid box was set to 34 \times 30 \times 30 Å from the center of the binding pocket. The value of the exhaustiveness parameter was set to 150. Images of the docked ligands were shown with the use of the AutoDock Tools software.

2.14. Statistical Analysis

Unless stated otherwise, all the biological results are presented as means of 3–6 repeated experiments \pm SEM. All calculations were evaluated for significance using one-way ANOVA followed by Dunnett's test with the GraphPad Prism 6.0 software (GraphPad Software, Inc., La Jolla, CA, USA). $p \leq 0.05$ was considered statistically significant.

3. Results and Discussion

3.1. Identification and Content of Phenolic Compounds in *V. opulus* FJ and PJ with the UPLC–PDA-Q/TOF-MS Method

The results of the qualitative and quantitative analysis of *V. opulus* FJ and PJ determined by the UPLC/MS method are presented in Figure 1 and Tables 1 and 2. A total of 29 and 30 phenolic compounds were positively identified in FJ and PJ, respectively, on the basis of the complementary information provided by PDA and the ESI-MS detection, and literature data. The FJ and PJ showed the presence of different groups of phenolic compounds, such as hydroxycinnamic acids, flavanols, flavonols, and anthocyanins. Significant differences ($p \leq 0.05$) in the content of individual phenolic compounds between FJ and PJ were noted as a result of about a 90-fold increase in the content of phenolics in PJ (878.6342 mg/g) compared to FJ (11.508 mg/g). Thus, it could be concluded that the Solid-Phase Extraction (SPE) method on a Sep-Pak C18 column is efficient for removing non-phenolic compounds from the juice. In the published studies, total phenolic determined by the Folin-Ciocalteu method content in the *V. opulus* fruit juices varied from 5.47 to 11.70 mg/g [25].

Hydroxycinnamic acids were the most predominant phenolic group found in both samples and constituted 80.46% and 77.50% of the sum of the phenolics in PJ and FJ, respectively. Chlorogenic acid (peak 9) with the negative molecular ion $[M - H]^-$ of 353 with typical fragments of quinic acid ester (m/z at 191) showed the highest content, both among phenolic compounds and hydroxycinnamic acids. Its concentrations were 645.492 mg/g and 8.039 mg/g in PJ and FJ, respectively. Chlorogenic acid, as the main phenolic compound in fresh berries of *V. opulus* and also in fresh juice, have been reported previously, where it constituted more than 96.2% of hydroxycinnamic acid derivatives [1–4]. Quantitatively, a second compound from hydroxycinnamic acids identified in FJ and PJ was caffeoylquinic acid (peak 13) with the negative molecular ion $[M - H]^-$ of 353 and fragment ions m/z at 191, 133. Additionally, two caffeoylquinic acids with the known structures, such as neochlorogenic acid (peak 1) and cryptochlorogenic acid (peak 10), were identified. Besides, five caffeoylquinic acid derivatives (peaks 3, 4, 7, 21, 22) were present in both samples. On the other hand, feruloylquinic acids (peaks 24 and 27) were only identified in PJ. Quantitatively, the second phenolic subgroup of phenolics was flavanols, which constituted 19.52 and 16.30% of FJ and PJ total phenolics, respectively (Table 2). The main flavan-3-ol isomers were (+)-the catechin (peak 6) and procyanidin dimer B1 (peak 2). Also, the procyanidin dimer B2 (peak 11) and procyanidin trimer C1 (peak 17) were identified in both samples based on reference substances. Furthermore, other procyanidin dimer and trimer, which were identified previously, were presented in our samples [26].

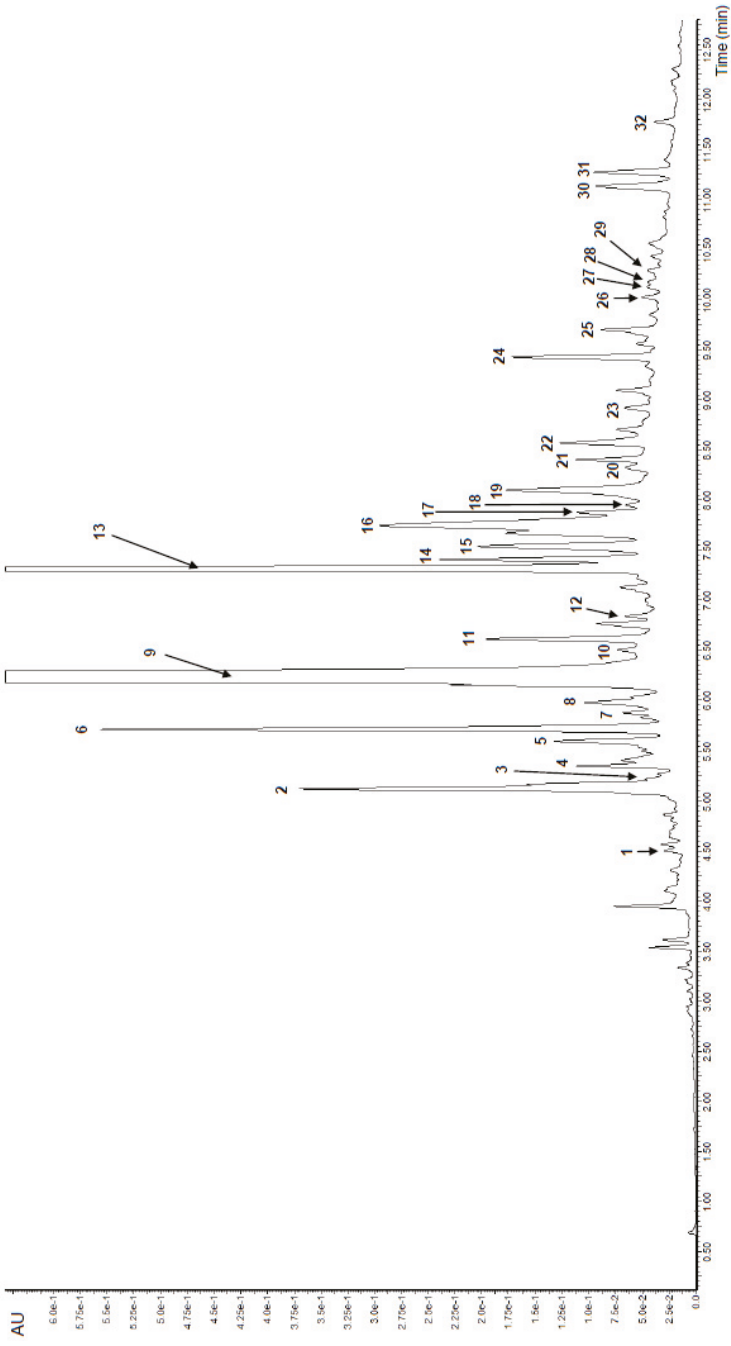


Figure 1. UPLC chromatogram of purified *V. opulus* juice (PJ) at 280 nm. Refer to Table 1 for the identification of each numbered peak.

Table 1. Retention time (Rt), wavelengths of maximum absorption (λ_{max}), mass spectral data, and the identification and quantification of phenolic compounds in fresh juice and purified juice of *Viburnum opulus* fruit.

Peak No.	Phenolic Compound	R _t (min)	λ_{max} (nm)	[M – H] [–] /[M + H] ⁺ (m/z)	Fragment(s) Ions (m/z)	Content (mg/g)	
						Fresh Juice (FJ)	Purified Juice (PJ)
1	Neochlorogenic acid ¹	4.50	318	353	191, 179	0.007 ± 0.001	0.215 ± 0.019
2	Procyanidin dimer B1 ¹	5.12	276	577	407, 289	0.759 ± 0.003	47.596 ± 0.148
3	Caffeoylquinic acid derivative I ²	5.17	323	707	191	0.015 ± 0.000	1.289 ± 0.058
4	Caffeoylquinic acid derivative II ²	5.35	323	707	191	0.024 ± 0.002	1.051 ± 0.008
5	Procyanidin trimer I ³	5.60	278	865	577, 289, 243	0.112 ± 0.001	6.866 ± 0.342
6	(+)-Catechin ¹	5.70	278	289	245, 202	0.657 ± 0.006	40.729 ± 0.596
7	Caffeoylquinic acid derivative III ²	5.74	323	707	191	0.017 ± 0.001	1.220 ± 0.020
8	Procyanidin trimer II ³	5.87	275	865	577, 289, 243	0.030 ± 0.006	2.634 ± 0.270
9	Chlorogenic acid ¹	6.20	318	353	191, 707 ^a	8.039 ± 0.145	645.492 ± 1.984
10	Cryptochlorogenic acid ¹	6.50	323	353	191, 173	0.004 ± 0.000	0.484 ± 0.023
11	Procyanidin dimer B2 ¹	6.61	278	577	407, 289	0.199 ± 0.002	11.540 ± 0.148
12	Gallocatechin gallate ⁴	6.84	280	457	169	0.031 ± 0.000	1.876 ± 0.085
13	Caffeoylquinic acid ⁴	7.31	313	353	191, 133, 707 ^a	0.745 ± 0.001	44.344 ± 0.176
14	(–)-Epicatechin ¹	7.40	278	289	245, 202	0.135 ± 0.002	8.002 ± 0.116
15	Cyanidin-3-sambubioside ¹	7.53	515	581 ⁺	287	0.093 ± 0.000	7.010 ± 0.003
16	Cyanidin-3-glucoside ¹	7.74	515	449 ⁺	287	0.139 ± 0.000	13.583 ± 0.799
17	Procyanidin dimer C1 ¹	7.86	278	865	407, 289	0.033 ± 0.001	3.212 ± 0.351
18	B-typeprocyanidin dimer derivative I ⁵	7.96	276	739	577, 289	0.016 ± 0.000	2.071 ± 0.097
19	Cyanidin-3-rutinoside ¹	8.10	516	595 ⁺	287	0.068 ± 0.001	5.072 ± 0.016
20	Procyanidin trimer III ³	8.32	278	865	577, 289, 243	0.032 ± 0.000	1.796 ± 0.053

Table 1. *Cont.*

Peak No.	Phenolic Compound	R _t (min)	λ _{max} (nm)	[M – H] [–] /[M + H] ⁺ (m/z)	Fragment(s) Ions (m/z)	Content (mg/g)	
						Fresh Juice (FJ)	Purified Juice (PJ)
21	Caffeoylquinic acid derivative IV ²	8.40	325	705	513	0.034 ± 0.000	3.306 ± 0.014
22	Caffeoylquinic acid derivative V ²	8.56	325	705	513	0.034 ± 0.000	3.268 ± 0.010
23	B-type procyanidin dimer derivative II ⁵	8.92	278	739	577, 289	0.035 ± 0.000	2.293 ± 0.094
24	Feruloylquinic acid I ³	9.43	325	367	193, 134	n.d.	5.722 ± 0.021
25	Quercetin-3-vicianoside ⁶	9.70	351	595	301, 300, 271	0.020 ± 0.000	1.266 ± 0.007
26	Procyanidin dimer ³	10.03	278	577	407, 289	0.024 ± 0.001	1.602 ± 0.258
27	Feruloylquinic acid II ³	10.13	304	367	193, 134	n.d.	0.528 ± 0.005
28	Quercetin-3-galactoside ⁴	10.18	365	463	300, 271	n.d.	0.149 ± 0.011
29	Quercetin-3-rutinoside ¹	10.29	344	609	301, 270, 151	0.016 ± 0.000	0.921 ± 0.007
30	(Epi)catechin derivative I ²	11.13	280	451	289, 161	0.103 ± 0.001	6.998 ± 0.221
31	(Epi)catechin derivative II ²	11.27	280	451	289, 161	0.080 ± 0.001	6.006 ± 0.165
32	Quercetin-3-rhamnoside ⁴	11.78	344	447	301, 270, 255, 227	0.007 ± 0.000	0.491 ± 0.002

n.d.—not detected; ^a dimeric adduct. Results are expressed as a mean ± standard deviation (*n* = 3). The values expressed differ significantly (one-way ANOVA and Duncan's test, *p* ≤ 0.05). 1—identification based on a comparison of retention time, UV-vis spectra (200–600 nm) and MS data for standards; 2, 3, 4, 5—identification based on a comparison of molecular ions and typical ion fragments with published data; 2—[6], 3—[7], 4—[8], 5—[9], 6—[10].

Table 2. The total content of the different phenolic groups in *V. opulus* fresh juice and purified juice according to UPLC–PDA-Q/TOF-MS analysis.

Group of Phenolics	Total Content (mg/g)	
	Fresh Juice (FJ)	Purified Juice (PJ)
Flavanols	2.246 ± 0.014	143.210 ± 1.377
Hydroxycinnamic acids (HCA)	8.919 ± 0.146	706.919 ± 2.119
>Flavonols	0.043 ± 0.000	2.827 ± 0.026
Anthocyanins	0.301 ± 0.002	25.665 ± 0.812
Total phenolics	11.508 ± 0.154	878.632 ± 2.722

Results are expressed as a mean ± standard deviation ($n = 3$). The values differ significantly (one-way ANOVA and Duncan's test, $p \leq 0.05$).

V. opulus fruits are characterized by varied content of anthocyanins, with cyanidin glycosides, such as glucoside, rutinoside and sambubioside as the main pigments [15,27]. In the tested FJ and PJ, cyanidin-3-glucoside (peak 16) was the main anthocyanin with the content 13.583 mg/g for PJ and 0.139 mg/g of FJ. Content of cyanidin-3-sambubioside (peak 15) and cyanidin-3-rutinoside (peak 19) were similar in both samples. The total content of anthocyanins was 0.300 mg/g of FJ and 25.665 mg/g of PJ. Perova et al. identified ten cyanidin glycoside in *V. opulus* fruits with cyanidin-3-glucoside and cyanidin-3-xylosyl-rutinoside as the main compounds [15]. Among the phenolic compounds estimated, flavonols occurred at the lowest concentration with 2.827 mg/g of PJ and only 0.043 mg/g of FJ (Table 2). *V. opulus* PJ and FJ contained quercetin-3-vicianoside (peak 25), quercetin-3-rutinoside (peak 29), quercetin-3-rhamnoside (peak 32) and quercetin-3-galactoside (peak 28), whereas the latter has not been determined in FJ. There are reports that also isorhamnetin glycosides have been found in *V. opulus* fruit and juice [15,18].

3.2. Inhibition of Pancreatic Lipase by *V. opulus* FJ and PJ

Pancreatic lipase (EC 3.1.1.3; triacylglycerol acyl hydrolase) breaks down TAG into absorbable monoacylglycerols and free fatty acids. Pancreatic lipase is responsible for the hydrolysis of 50–70% of total dietary fats in the intestinal lumen [28]; thus, its inhibition could reduce the storage of body fat in the adipose tissues. In the present study, the effect of FJ and PJ on pancreatic lipase was determined in a triolein emulsion by the spectrophotometric method with a copper reagent. This lipid substrate is a triglyceride formed by esterification of the three hydroxy groups of glycerol with oleic acid. As shown in Figure 2, both *V. opulus* samples exhibited a dose-dependent inhibitory effect on pancreatic lipase activity. The concentration of PJ inhibiting lipase activity to 50% was equal to 55.26 ± 2.54 mg/mL and showed 4.7-fold higher inhibitory activity than FJ ($IC_{50} = 261.94 \pm 2.00$ mg/mL). All these samples were less potent in pancreatic lipase inhibiting than Orlistat (a well-known anti-lipase agent). The IC_{50} value for lipase inhibition for Orlistat was 0.380 ± 0.004 μ g/mL. The lower anti-lipase activity of plant extracts than Orlistat is associated with the presence of other components in the extracts that do not affect the activity of the enzyme. In addition, fruit juice contains several classes of phenolic compounds, which in combination might differently affect the lipase activity due to the different interactions between them, as well as with other fruit components.

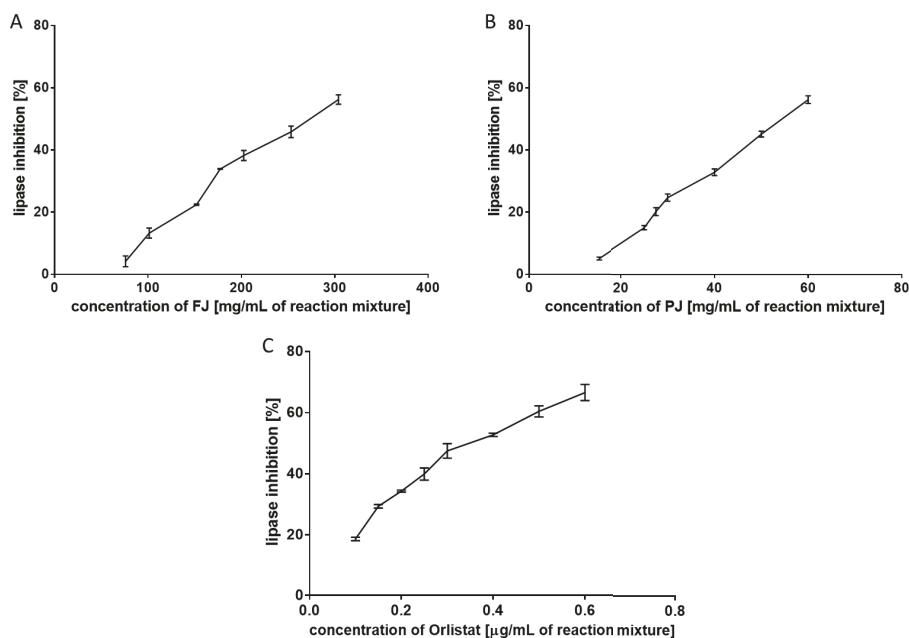


Figure 2. Inhibitory effect of fresh juice (FJ) (A), purified juice (PJ) (B), and Orlistat (C) on pancreatic lipase. Data are means of triplicate assays \pm standard deviations.

In contrast to the widely studied various fruits, literature data on the anti-lipase activity of juices and drinks are scarce. Gironés-Vilaplana et al. demonstrated a significant increase in isotonic citric acid drink and isotonic lemon juice drinkability to inhibit pancreatic lipase after enriching them in açai, blackthorn or maqui berries [29]. Magui berry exhibited the most potent inhibitory activity, and the anti-lipase properties of the drinks were positively correlated with anthocyanins amounts. A similar relationship was found by Fabroni and others [30]. Among 13 fruit extracts, juices, plant tissues, legume seeds, cereals, and vegetables, "Moro" orange juice with the highest anthocyanin content, had the strongest inhibitory effect on pancreatic lipase. The orange juice lipase inhibition IC_{50} value of 0.46 mg/mL was higher than the IC_{50} of Orlistat (0.064 mg/mL). In the present study, anthocyanins constituted only 2.61 and 2.92% of the sum of the phenolics in FJ and PJ, respectively. Chlorogenic acid, quantitatively the main phenolic compounds in both samples, has also been demonstrated as a pancreatic lipase inhibitor with an IC_{50} value of 286.5 μ M, however it has rather weak inhibitory potential compared to orlistat with an $IC_{50} = 1.2 \mu$ M [31]. On the other hand, Worsztynowicz et al. demonstrated that chlorogenic acids isolated from chokeberry fruit did not inhibit the pancreatic lipase [32]. Some authors suggest that the inhibition of the pancreatic lipase by fruits is attributed to proanthocyanidins [23,28,33]. This group of polyphenols constituted 19.52% and 16.30% of the sum of the phenolics in FJ and PJ, respectively. Most likely, the anti-lipase potential of fruit extracts and juices, which are characterized by a complex phenolic composition, is the result of their mutual interactions. Other components of the samples analyzed may also influence their inhibitory activity toward pancreatic lipase. In the present study, IC_{50} values for lipase inhibition by FJ and PJ differed almost five times, despite the fact that PJ showed almost a ninety times higher concentration of phenolic compounds than FJ.

3.3. The Effects of *V. opulus* on Cellular Viability, Adipogenesis and Adipolysis

To check the influence of *V. opulus* on the metabolic activity of 3T3-L1 cells were exposed to increasing concentrations of extracts (from 10 to 200 $\mu\text{g/mL}$) for 48 h after reaching confluence. As is presented in Figure 3A, fresh juice inhibited cell viability by almost 35% at the highest concentration used. Dosages of FJ not exceeding 100 $\mu\text{g/mL}$ had no cytotoxic effect on cells. Purified juice (PJ) showed higher cytotoxic potential, because its 100 $\mu\text{g/mL}$ concentration decreased metabolic activity by almost 65% (Figure 3B). Within the dosages studied, the IC_{50} cytotoxicity parameter was obtained only for PJ ($\text{IC}_{50} \approx 85 \mu\text{g/mL}$). The highest non-cytotoxic concentrations (IC_0) chosen for studies of adipogenesis regulation were 100 $\mu\text{g/mL}$ for FJ and 25 $\mu\text{g/mL}$ for PJ, respectively.

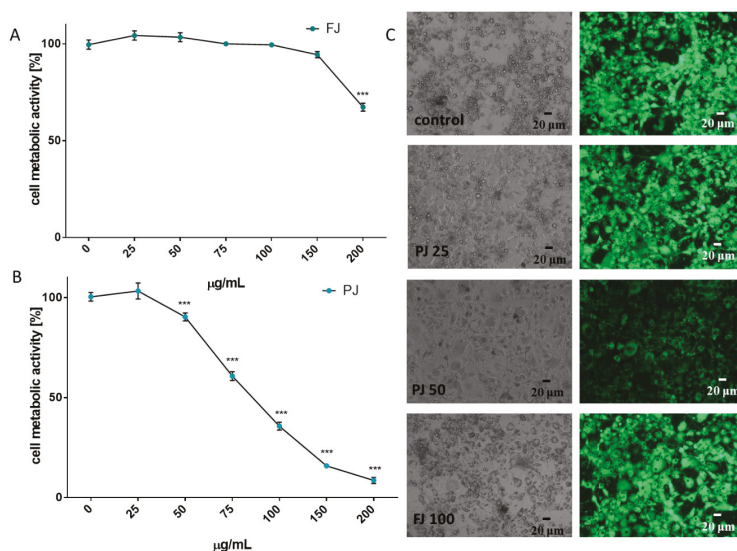


Figure 3. The influence of *V. opulus* FJ and PJ on 3T3-L1 cell metabolic activity determined by the PrestoBlue assay after 48 h exposure of FJ (A) and PJ (B); control cells were not exposed to any compound; values are means \pm standard deviations from at least three independent experiments, $n \geq 12$; statistical significance was calculated versus control cells (untreated), *** $p \leq 0.001$. Morphology of 3T3L1 cells observed on the 5th day of the cell differentiation process (C) with 25 and 50 $\mu\text{g/mL}$ of PJ, and 100 $\mu\text{g/mL}$ of FJ; randomly chosen fields were photographed at $\times 200$ phase-contrast and a fluorescent microscope (cells stained with 2 μM calcein AM).

The lack of cytotoxic effects of the *V. opulus* samples used at the IC_0 concentration was also confirmed with microscopic observations of the adipocytes performed 5 days after the initiation of their differentiation (Figure 3C). Control cells appeared more rounded, had lipid droplets visible and strong cytosolic green fluorescence of calcein after staining with calcein AM ester. Simultaneously, cells incubated with PJ used in its cytotoxic concentration (50 $\mu\text{g/mL}$) had lower cytoplasmic esterase activity; thus, decreased green fluorescence of calcein was observed, and the cells were more irregular and elongated in their shape. The IC_0 dosages obtained for FJ and PJ seem to be comparable with those previously observed for Caco-2 and MIN-6 cells; however, 3T3-L1 cells were more sensitive to the compounds studied—probably due to the longer incubation time [18,21].

The differentiation process of preadipocyte to mature adipocyte is associated with an increase of lipid droplets formation [22]. The cells staining with Nile red, a hydrophobic fluorescent dye that accumulates in neutral lipid droplets, allowed us to determine the *V. opulus* influence on cellular lipid droplets formation and accumulation (Figure 4).

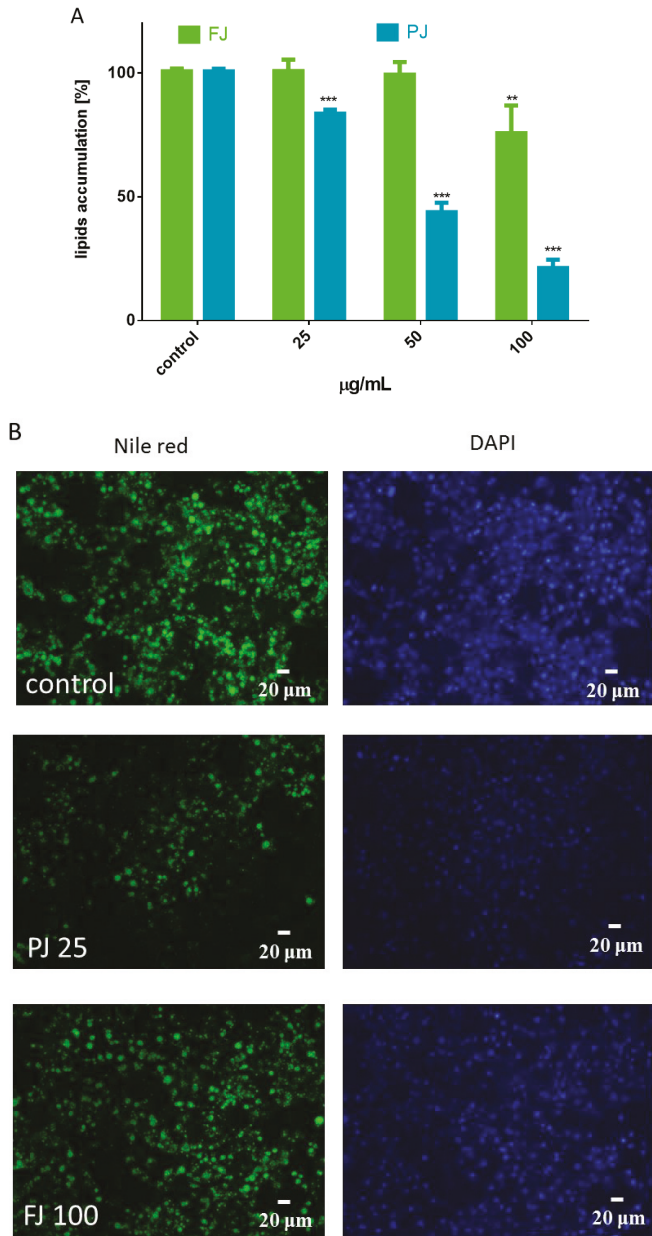


Figure 4. Influence of *V. opulus* FJ and PJ preparations on the accumulation of lipid droplets in 3T3-L1 cells stained with Nile red observed on the 7th day of differentiation (A). The control cells were not exposed to any compound; the values are means ± standard deviations from at least three independent experiments, $n \geq 12$; the statistical significance was calculated versus the control cells ** $p \leq 0.01$, *** $p \leq 0.001$. Cell lipid droplets with Nile red were visualized under a fluorescent microscope (200× magnification) (B). DAPI staining allowed for the visualization of cell nuclei with 25 µg/mL of PJ and 100 µg/mL of FJ.

As is presented in Figure 4A, the FJ at 100 µg/mL significantly reduced the formation of lipid droplets compared to the control cells, whereas PJ was able to decrease lipid accumulation by 25% at 25 µg/mL. These data were confirmed by microscopic observation (Figure 4B). As evident by Nile red staining, PJ reduced the accumulation of lipid droplets in cytoplasm, as well as the size of droplets formed was decreased. The intracellular content of TAG was also quantified. The data show that in the presence of the preparations used at IC₀ dosage the level of TAG was reduced by 20–25% (Figure 5A). It can be also seen that the PJ used at concentrations higher than 50 µg/mL was the most active inhibitor of lipid accumulation. However, it needs to be emphasized that observed lipid content reduction resulted from decreased cell viability (Figure 3B).

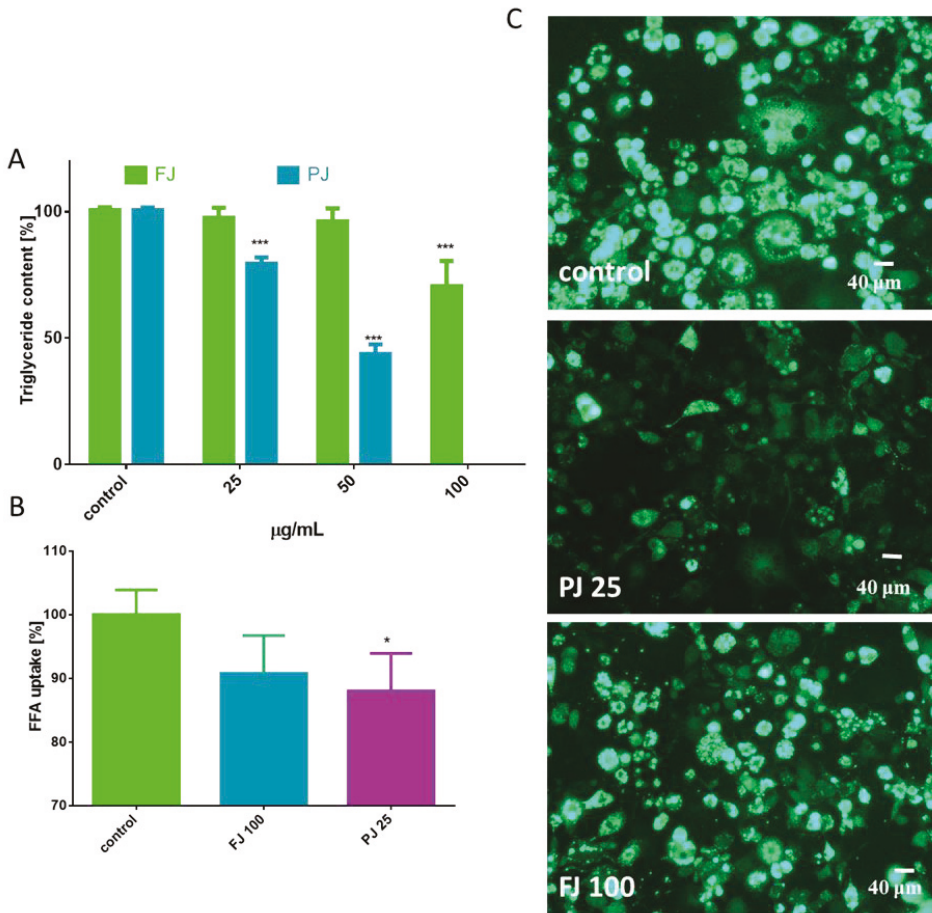


Figure 5. The influence *V. opulus* extracts on the triglyceride level (A) and fatty acid analog TF2-C12 uptake measured in 3T3L1 cells on the 7th day of differentiation (B); control cells were not exposed to any compound; values are means ± standard deviations from at least three independent experiments, $n \geq 9$; statistical significance was calculated versus control cells * $p \leq 0.05$, *** $p \leq 0.001$. Cellular uptake of FFA-C12 analogue visualized under a fluorescent microscope (400 × magnification) (C).

Simultaneously, the influence of FJ and PJ on cellular free fatty acid (FFA) uptake was determined. As shown in Figure 5B, the level of fluorescent free fatty acid analogue TF2-C12 incorporated in the presence of PJ was decreased by almost 10%. Cells treated with PJ lacked strong fluorescence of

lipid bodies, with the fluorescent analogue present mainly in the cytoplasm (Figure 5C). Collectively, it can be concluded that the purified juice of *V. opulus* (PJ) inhibited the adipogenic differentiation of 3T3-L1 cells.

Besides inhibiting lipogenesis, it is possible that *V. opulus* could influence the lipolysis process, which leads to the stored TAG breakdown to fatty acids and glycerol [34]. Cell incubation with preparations increased the amount of glycerol released from adipocytes, with maximal stimulation by 20% observed for 25 µg/mL of PJ (Figure 6), while for the FJ preparation used in 100 µg/mL concentration this increase was only 7%. The present study provides evidence that *V. opulus* components may inhibit lipogenesis and stimulate adipolysis. The decrease in lipolysis observed in the presence of elevated dosages of PJ (50 µg/mL) resulted from its cytotoxic potential. Taking into account the obtained results, it can be concluded that the *V. opulus* influence is dose dependent according to the concentration of phenolic compounds. Regardless of the 90-fold higher concentration of phenolic compounds in PJ, its IC₀ dose against 3T3-L1 cells is only 4-times lower than FJ. The most responsible for observed activity seems to be chlorogenic acid, which was identified as the main phenolic compound in probes. However, due to potential synergic activities and chemical interactions, other compounds present in juice, but lost during its purification process, such as procyanidins and proteins, are also responsible for the observed cellular effect. In this regard, the presented results are in agreement with our previous studies, where phenolic rich fraction from *V. opulus* fruit had stronger activity in Caco-2 and MIN6 cells [18,21].

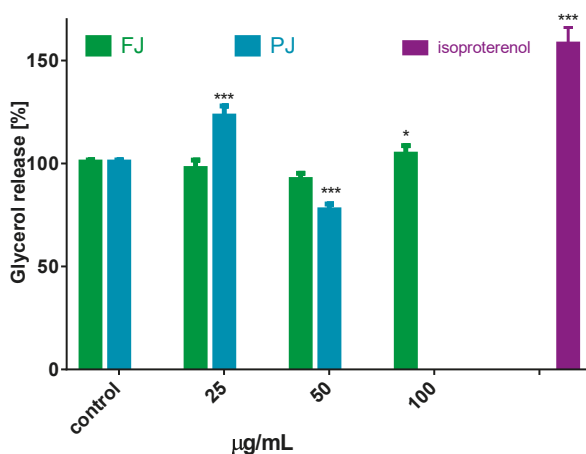


Figure 6. Lipolytic activity of *V. opulus* FJ and PJ preparations on differentiated 3T3L1; as a positive control 10 µM isoproterenol was used; control cells were not exposed to any compound; values are means ± standard deviations, $n = 6$; statistical significance was calculated versus control cells * $p \leq 0.05$, *** $p \leq 0.001$.

3.4. The Effects of *V. opulus* on Expression of Genes Associated with Adipocyte Differentiation

Differentiation of preadipocyte to adipocyte is regulated by set of transcription factors, which, upon activation, induce the expression of other adipocyte-specific genes [35]. In order to clarify the molecular effects of *V. opulus* components, the analysis of selected genes' expressions, as well as protein levels, was performed. Given the fact that *V. opulus* diminished lipid accumulation in 3T3-L1 cells, we first checked the effects of FJ and PJ used at the IC₀ concentration on the mRNA expression of master adipogenic regulators: peroxisome proliferator-activated receptor gamma (PPAR γ), CCAAT/enhancer-binding proteins (C/EBP α) and sterol regulatory element-binding protein 1c (SREBP-1c), which have a direct impact on fat cells' development [35]. As shown in Figure 7, both samples suppressed the expression of these factors compared to untreated cells. In regard to previous studies, the purified juice rich in

phenolic compounds presented a higher impact on 3T3-L1 cells than the fresh juice. Following PJ treatment, the PPAR γ mRNA level decreased to 50%, while C/EBP α , CBP and SREBP-1c mRNA levels declined by 30–40%. Among the genes studied, fresh juice had no impact on the changes of SREBP-1c mRNA expression, whereas a decrease in other genes' levels did not exceed 30%. Furthermore, we investigated the effect of tested samples on these transcription factors' protein level. Immunoblot analysis also revealed that the PJ reduced the amount of PPAR γ protein in adipocyte to 40% as compared to the control cells (Figure 8A). It is known that the activation of PPAR γ protein by specific agonists results in its translocation to the nucleus, where heterodimerizes with the retinoid x receptor alpha (RxR α) [35]. Thus, we decided to study a subcellular distribution of PPAR γ receptor. The level of protein detected in the nuclear fraction of adipocytes with ELISA technique showed that, in this regard, PJ diminished PPAR γ distribution inside the nucleus to 60% (Figure 8B). As was mentioned above, PPAR γ transcriptional activation is initiated after its binding with the RxR α receptor in the nucleus. That step of heterodimer formation describes both proteins as ligand-activated transcription factors, which coordinately regulate the gene expression of other crucial proteins involved in fatty cells differentiation, such as adipogenesis, lipid storage, lipogenesis and thermogenesis [5,6]. The results in Figure 8 show that FJ induced nearly 3-fold increase in RxR α protein. This may be caused by the presence of retinoids and 9-cis-retinoic acid in studied preparations. These compounds are known precursors of carotenoids and were found to increase RxR α expression and activity [17,36–38]. The solid-phase purification of the FJ eliminated these compounds; thus, cells' treatment with PJ showed a 20% decrease in RxR α protein. Therefore, one can conclude that the observed limitation of PPAR γ -RxR α heterodimer formation in the cells incubated with *V. opulus* may also partially reduce adipogenesis.

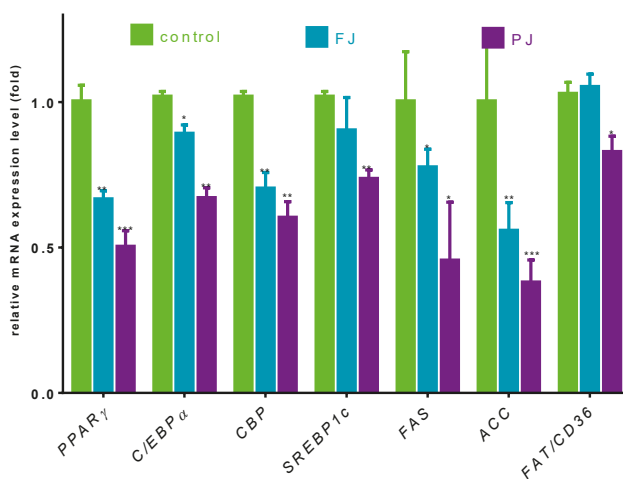


Figure 7. The influence of *V. opulus* FJ and PJ preparations on the gene expression in differentiated 3T3-L1 cells quantified by real-time PCR and normalized using β -actin as a reference gene. Control cells were not exposed to any compound; values are means \pm standard deviations, $n \geq 4$; statistical significance was calculated versus control cells (untreated), * $p \leq 0.05$, ** $p \leq 0.01$, *** $p \leq 0.001$.

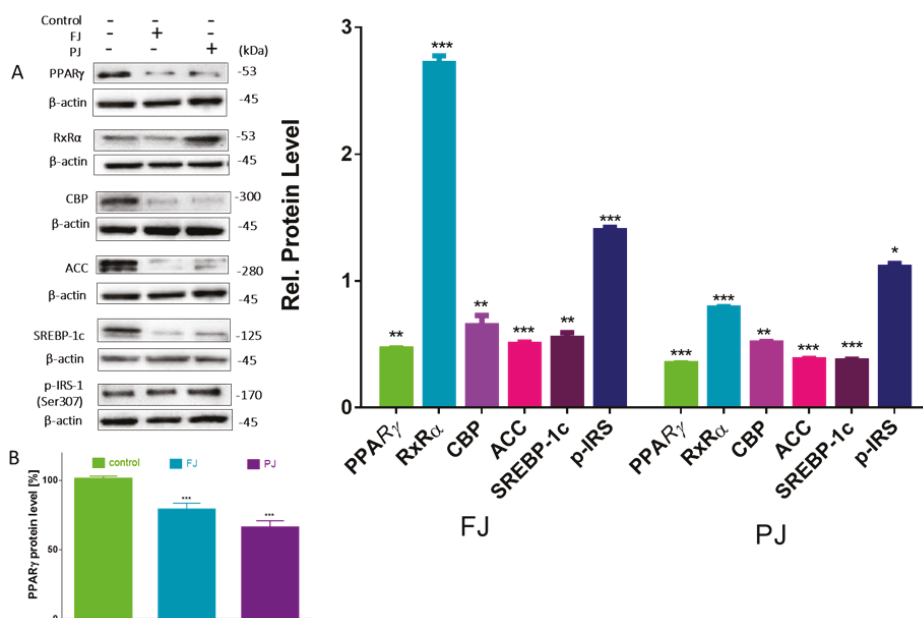


Figure 8. Effect of *V. opulus* FJ and PJ preparations on the relative protein level of crucial proteins involved in adipogenesis and lipogenesis determined by Western blot analysis in differentiated 3T3-L1 cells (A); the level of PPAR γ determined with ELISA assay in nuclear fraction (B); control cells were not exposed to any compound; the values are means \pm standard deviations, $n \geq 5$; statistical significance was calculated between treatment and control cells (untreated), * $p \leq 0.05$, ** $p \leq 0.01$, *** $p \leq 0.001$.

Regardless of this, it was also demonstrated that CREB-binding protein (CBP) after its activation binds to the promoter of the *C/EBP* gene being transcriptional coactivator that associates with PPAR γ . It has been demonstrated that IBMX and cyclic-AMP (cAMP) analogs promote adipocyte differentiation via CREB phosphorylation [39]. As before, *V. opulus* downregulated CBP on the transcriptional and translational levels (Figures 8 and 9); however potential CREB phosphorylation via the cAMP-dependent pathway needs to be further elucidated.

Next, we investigated the effect of *V. opulus* FJ and PJ on the expression of genes that are up-regulated during adipocyte differentiation and controlled by the abovementioned transcription factors. Fatty acid synthase (FAS) is involved in the *de novo* synthesis of long-chain fatty acids; thus, FAS inhibition has been considered as one of the major factors decreasing the amount of intracellular fatty acids and lipogenesis [40]. While we have not directly checked the *V. opulus* influence on FAS enzymatic activity, the significant downregulation of FAS expression by both preparations was detected (Figure 7). This effect was, again, slightly stronger for the PJ than for the FJ preparation (0.55 and 0.49, respectively). In addition, 3T3-L1 cells' incubation with PJ influenced the mRNA level of the *FAT/CD36* gene. The protein encoded by this gene is involved in the transmembrane movement of fatty acids and studies performed on *CD36* knockout mice showed decreased fatty acids uptake by adipocytes [41]. According to the data presented in Figure 7, the 3T3-L1 cells incubated with PJ showed that *FAT/CD36* expression decreased by 20%, which matches that mechanism with previously observed diminished cellular FFA uptake. Furthermore, the reduction in *SREBP-1c* protein expression results in the inhibition of the expression of the enzyme catalyzing synthesis of the malonyl-CoA involved in fatty acid and triglyceride synthesis—acetyl-CoA carboxylase (ACC) [42]. The levels of the gene and ACC protein expression were decreased by almost 50% (Figures 7 and 8) and these results are in agreement with the observed decrease in lipid and TAG content in mature 3T3-L1 cells. The results

obtained are in line with the decrease of FFA uptake observed in Caco-2 cells [18]. However, it was also presented that *V. opulus* increased FFA uptake and lipids accumulation in insulinoma MIN6 cells, which may deleteriously effect insulin secretion [19].

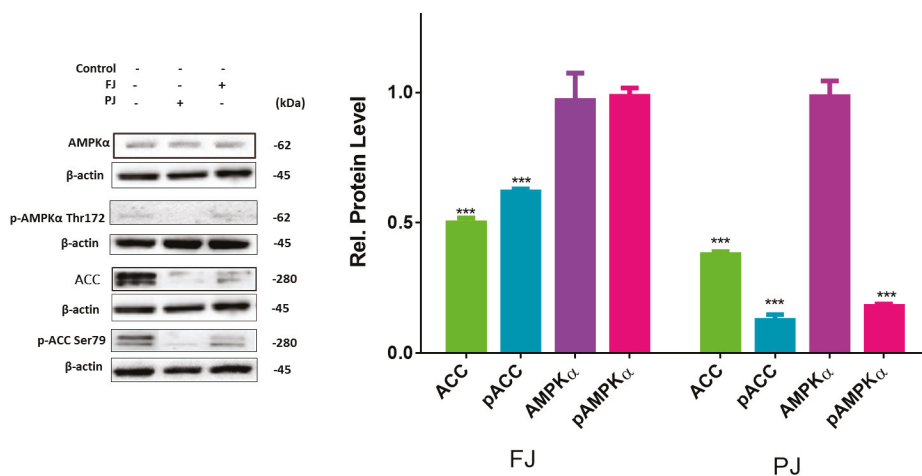


Figure 9. Effect of *V. opulus* FJ and PJ preparations on the relative levels of phosphorylated proteins involved in adipogenesis determined by Western blot analysis in differentiated 3T3-L1 cells. Control cells were not exposed to any compound; values are means \pm standard deviations, $n \geq 4$; statistical significance was calculated between treatment and control cells (untreated) with *** $p \leq 0.001$.

Previous studies showed that, despite the activation of PPAR γ , the differentiation of preadipocyte can be modulated by AMP-activated protein kinase (AMPK) involvement [43]. To clarify an influence of *V. opulus* extracts on 3T3-L1 differentiation suppression we studied whether these extracts are able to activate AMPK. One of the key factors of AMPK activation is the elevation of AMP level leading to the protein α -subunit threonine 172 phosphorylation [44]. As is shown in Figure 9, the level of total AMPK was not affected by *V. opulus* components, whereas the level of p-AMPK α was significantly decreased by the PJ preparation.

Among the AMPK substrates involved in the adipogenesis is acetyl-CoA carboxylase (ACC). The AMPK-catalyzed phosphorylation of ACC inhibits its enzymatic activity. While the mRNA and protein levels of ACC were decreased in cells treated with preparations, only the FJ elevated amount of phosphorylated ACC (Figure 9). In cells treated with the purified juice p-ACC level was notably diminished to 20% in comparison with the control cells (Figure 9), which is also in concordance with the observed decrease in p-AMPK level. In this regard it can be concluded that *V. opulus* phenolic components may inhibit activities of AMPK upstream kinases, like tumor-suppressor liver kinase B1 (LKB1), calcium-dependent calcium/calmodulin-dependent protein kinase kinase β (CaMKK β) and transforming growth factor- β activated protein kinase-1 (TAK1), or activate mechanism independent of AMPK [45].

3.5. The Effects of *V. opulus* on Intracellular Reactive Oxygen Species Production and Selected Adipokines and Cytokines Secretion

During the adipogenesis and adipocyte enlargement, the intracellular reactive oxygen species (ROS) generation by the mitochondria is intensified and contributes to energy metabolism [8]. Thus, we analyzed the influence of FJ and PJ on intracellular ROS formation. As is illustrated in Figure 10A, the *V. opulus* both samples used at the IC₀ dosages decreased oxidation status in adipocytes by 10–15% as compared to the control cells. Observations with the fluorescence microscopy of cells stained

with fluorogenic dichloro-dihydro-fluorescein diacetate (DCFH-DA) correspond to the presented quantitative results (Figure 10B). This cytoprotective activity may be related to the antioxidant properties of the components of the studied extracts. The main components identified in *V. opulus* fruit juice are phenolic compounds, which are involved in direct free radical quenching. Our previous studies revealed that the comparable dosages of *V. opulus* extracts were also able to decrease radicals generation and intracellular ROS level in Caco-2 and MIN6 cells [18,21]. Furthermore, *V. opulus* compounds were able to enhance activity of enzymes involved in cellular defense system, i.e., glutathione peroxidase (GPx). Nevertheless, the elevated dosage of PJ (50 $\mu\text{g/mL}$) increased intracellular oxidative stress as a result of the mitochondrial depolarization induced by sample components [21]. The observed reduction in ROS level for PJ at 100 $\mu\text{g/mL}$ concentration confirms its cytotoxic ability (demonstrated previously in Figure 3), leading to a decrease in cell number and the induction of cellular death.

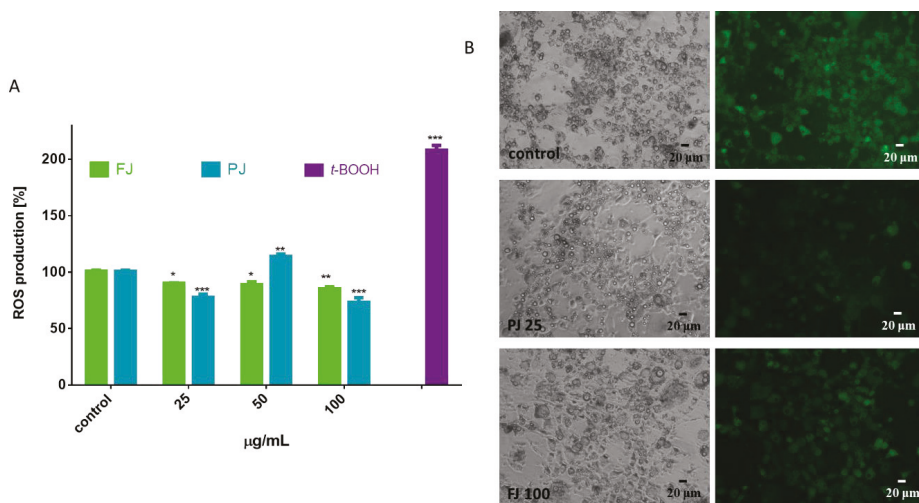


Figure 10. Influence of *V. opulus* FJ and PJ preparations on the intracellular reactive oxygen species generation analyzed by DCFH-DA assay in differentiated 3T3-L1 cells (A); control cells were not exposed to any compound; as a positive control for ROS generation, 500 μM t-BOOH was used; values are means \pm standard deviations from at least three independent experiments, $n \geq 9$; statistical significance was calculated versus control cells * $p \leq 0.05$, ** $p \leq 0.01$, *** $p \leq 0.001$. Cells visualized under phase-contrast and fluorescent microscope (200 \times magnification) (B).

Differentiated adipocytes are able to secrete proteins that are responsible for adipose tissue remodeling, as well as inflammation generation. The most abundant adipokine is adiponectin, the levels of which are decreased in subjects with diet-related diseases, such as obesity or type 2 diabetes. Activated PPAR γ , C/EBP α and SREBP1c stimulate its expression in adipocyte [7]. Adiponectin targets adiponectin receptor (AdipoR) mainly regulates energy metabolism and reveals protective insulin-sensitizing and anti-inflammatory properties. The second protein, leptin, plays role in appetite suppression and the downregulation of food intake; however, its serum concentration is increased in obesity due to observed leptin resistance [46]. As it is demonstrated in Figure 11, the incubation of differentiated 3T3-L1 cells with PJ preparation increased the expression of adiponectin gene by 15%, as well as up-regulated its extracellular secretion by 25% compared to the control cells. In the same way, there was a noticeably diminished level of lipid and TAG accumulation in 3T3-L1 cells. Despite the lack of the FJ and PJ influence on leptin mRNA expression level, there was an observed relevant decrease in leptin secretion by cells treated with these preparations (15–20%). Studies performed *in vivo* demonstrated that chlorogenic acid (dominant phenolic compound in FJ and PJ) effectively

reduced blood and liver lipid accumulation, as well as decreased amounts of leptin and insulin in plasma [47]. The enlargement of adipocytes induces the release of free fatty acids, which generate oxidative stress, leading to cellular structures damage, but also stimulate the secretion of inflammatory cytokines. Among cytokines, the most related to obesity and insulin resistance are tumor necrosis factor α (TNF α) and interleukin-6 (Il-6). Chlorogenic acid has an anti-inflammatory effect, reducing the cellular release of TNF α , Il-1 β and Il-6 cytokine [9,48–50]. Figure 11 shows that only purified juice declined the expression of TNF α mRNA by 20%. TNF α protein level was also downregulated by PJ to 70%. It is known that TNF α regulates the synthesis of pro-inflammatory cytokines, including Il-6 [51]. In concordance, both *V. opulus* preparations decreased the secretion of Il-6 protein to 40–70%. In contrast, Il-6 mRNA level was not changed. Hence, we can conclude that the FJ and PJ components could be further checked with animal models of obesity or insulin resistance as potential preventive agents against chronic inflammatory response.

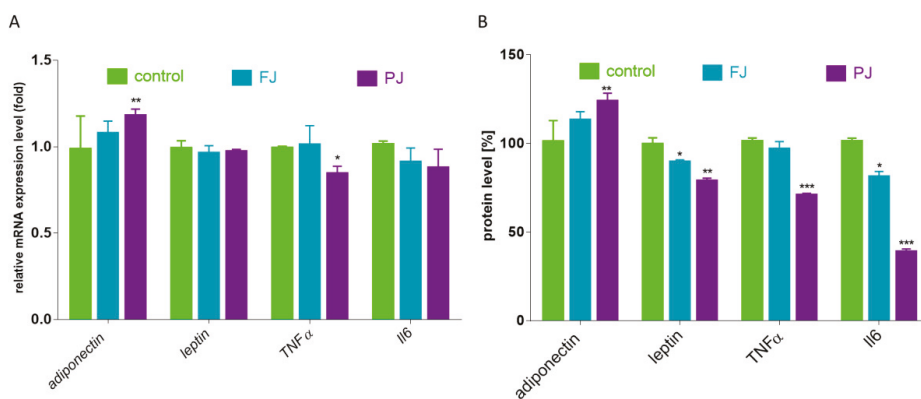


Figure 11. Influence of *V. opulus* FJ and PJ preparations on the mRNA expression (A) and protein secretion (B) of selected adipokines and cytokines in differentiated 3T3-L1 cells; control cells were not exposed to any compound; values are means \pm standard deviations, $n = 6$; statistical significance was calculated versus control cells * $p \leq 0.05$, ** $p \leq 0.01$, *** $p \leq 0.001$.

To the best of our knowledge, there are no reports on *V. opulus* fruit influence on lipid metabolism regulation with PPAR γ involvement. However, it is known that chlorogenic acid, the main phenolic constituent of *V. opulus*, was able to suppress mRNA level of Ppar γ , Cd36 and Fabp4 in liver and white adipose tissue in mice treated with a high-fat diet [49]. The results obtained by Villalpando-Arteaga et al. are comparable and show that aqueous extract from *Hibiscus sabdariffa* containing chlorogenic acid, delphinidin-3-sambubioside and cyanidin-3-sambubioside, attenuated steatosis progression and Ppar γ expression in the liver of obese mice [52]. Chlorogenic acid and rutin (quercetin-3-rutinoside) were observed as effective inhibitors of the accumulation of intracellular triglyceride content in 3T3-L1 cells [53]. They were able to down-regulate the expression of adipogenic transcription factors (PPAR γ and C/EBP) and adipocyte-specific proteins (leptin), as well as up-regulate adiponectin. In comparison, other study performed with 3T3-L1 differentiated cells identified chlorogenic acid as an agonist of PPAR γ 2, which promoted adipocyte differentiation via the elevation of PPAR γ 2, CEBP and SREBP-1 mRNA and protein level [54]. Nevertheless, the other phenolic compounds identified in *V. opulus* fruit were proved to decrease the adipogenesis process [55–57]. Cyanidin-3-glucoside was able to elevate adiponectin gene expression in human adipocytes, whereas, in C57Bl/6j mice diminished the expression of Fas and Srebp-1 and decreased body weight and hepatic lipid content [55,57]. Reduced levels of SREBP-1c, ACC and FAS were noted in 3T3-L1 cells after treatment with quercetin derivatives and rutin [58,59]. Additionally, rutin and catechin were capable of suppressing adipocyte differentiation via PPAR γ and RxR α receptor down-regulation [59–61]. Catechin effectively suppressed

3T3-L1 cells differentiation with the inhibition of the expression and protein levels of PPAR γ and FAS; however, the observed results were stronger after the cells' treatment with a combination of catechin and caffeine [62]. Procyanidin B2 and other derivatives present in FJ and PJ preparations were also confirmed as regulators of adipocyte triglyceride content with PPAR γ involvement [63,64].

3.6. The Effects of *V. opulus* on Activity of PPAR γ

Among different transcriptional activators of adipogenesis, PPAR γ , which belongs to nuclear receptors family, is considered as a master regulator of adipocytes differentiation. It interplays with other transcription factors and binds numerous proteins involved in the regulation of transcription, such as PPAR γ cofactor 1 α (PGC-1 α) [8,65]. PPAR γ activity can be regulated by ligand binding to the ligand-binding domain, inducing protein conformational changes. Among natural precursors of ligands for PPAR γ are long-chained fatty acids, as well as nitriled or oxidized lipids [66]. Thus, to detect if *V. opulus* phenolic components directly affect the activity of PPAR γ protein, we used the cell-based reporter gene assay. As a PPAR γ activator, we used rosiglitazone at 1 μ M concentration, while compound T0070967 (1 μ M) was used as an antagonist. As it is shown in Figure 12, after the cells' incubation with agonist PPAR γ , activity was elevated almost twofold compared to the control cells, whereas the antagonist decreased the receptor activity by 40%. PPAR γ activity was diminished by 25% after treatment with PJ, whereas FJ had no effect. In addition, the cells' preliminary incubation with tested preparations significantly decreased receptor activity after rosiglitazone treatment by 90% and 40% for PJ and FJ, respectively. Based on this, we can suspect that *V. opulus* juice components possess antagonist potential against PPAR γ receptor.

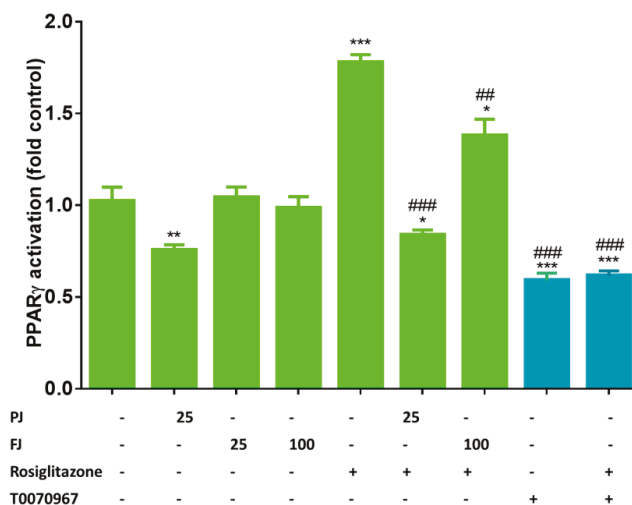


Figure 12. The effect of *V. opulus* FJ (25 and 100 μ g/mL) and PJ (25 μ g/mL) preparations on PPAR γ activation in GeneBLazer@PPAR gamma 293H DA reporter gene assay; as agonist 1 μ M rosiglitazone was used, whereas as antagonist 1 μ M T0070967; the control cells were not exposed to any compound; the values are means \pm standard deviations, $n = 4$; the statistical significance was calculated versus control cells with * $p \leq 0.05$, ** $p \leq 0.01$, *** $p \leq 0.001$; the statistical significance was calculated versus cells after rosiglitazone treatment with ## $p \leq 0.01$, ### $p \leq 0.001$.

PPAR γ protein belongs to the superfamily of nuclear receptors and possesses six domains, among which the ligand-binding domain (LBD), via interactions with ligands, is involved in the modulation of PPAR γ activity. Afterwards, the ligand binding induces a change in the receptor conformation dynamic process of corepressor dissociation, and coactivator recruitment is started [14]. To explore

the potential interaction between *V. opulus* juice components and PPAR γ protein, molecular docking simulation was performed with the binding pocket located behind the H3 helix of PPAR γ receptor. There are many PPAR γ receptor agonists that locate in this binding pocket, i.e. indol-1-yl acetic acid, nonaolic acid or amorfrutin 1 [67–69]. As an example of the PPAR γ agonist in the analyzed model, we used rosiglitazone (Figure 13), which locates deeply inside the receptor-binding pocket. The simple validation of the docking method showed slight differences between rosiglitazone in crystal structure and docked molecule in the pocket; however, this effect was acceptable for performed research with the main phenolic compounds identified in *V. opulus* juice. Molecular modeling with Autodock Vina located chlorogenic acid and (+)- catechin inside the binding pocket. Among the studied compounds, chlorogenic acid, (+)- catechin and rosiglitazone showed similar binding affinities (Figure 13). Additionally, the chlorogenic acid molecule orientation in pocket also revealed some similarity to that of rosiglitazone. Despite this, neither chlorogenic acid nor (+)- catechin did not create any possible hydrogen bond to serine 289 or tyrosine 473 of PPAR γ , which were essentially made by the rosiglitazone molecule. This gives some hint to predict that these compounds have some potential to activate PPAR γ , but their mechanism of action could be different than rosiglitazone; they could bind to a different part of the receptor and change its conformation in a similar way to the partial agonist. In contrast to these two phenolic ligands, procyanidins B1 and C1 cannot fit into the binding pocket because of their more complex structures and larger shape. In this case, estimated high binding affinity resulted from numerous hydrogen bonds created between procyanidins and the residues present in surface of receptor. Thus, procyanidins present in *V. opulus* juice could clog the entrance to the PPAR γ binding pocket and block it from a potential agonist entering, which could resemble inverse agonist behavior. As a result, the reduction of PPAR γ activity may occur despite the presence of chlorogenic acid, which was demonstrated to be a PPAR γ agonist. Among the limitations of performed basic molecular docking, there is a lack of prediction of the most favorable energetic conformation for research space, as well as kinetic data describing designed configuration. Thus, further studies with kinetic modeling or isothermal titration calorimetry would give more detailed information in this regard. Still, the results obtained with molecular docking are in agreement with the biological experiments showing a reduction of signal transduction controlled by PPAR γ , and, finally, a decrease in 3T3-L1 cells adipogenesis. Therefore, PPAR γ transcriptional potential could be modulated on different levels: by the regulation of mRNA and protein levels, as well as conformational changes made after its binding with ligands leading to protein subcellular distribution, heterodimers' formation, and, finally, binding with peroxisome proliferator hormone response elements present in promoters of PPAR-responsive genes. The studies performed recently identified chlorogenic acid as an agonist of the PPAR γ 2 receptor responsible for the enhanced differentiation of 3T3-L1 cells [54]. In the identified molecular mechanism downregulation of adipocyte differentiation-inhibitor gene, Pref1 was observed, which was accompanied by the upregulation of CEBP and SREBP-1 transcriptional factors. Microscopic observations demonstrated the elevation of PPAR γ in the nucleus fraction, as well as in total cell lysate. Based on this data and our results, we can conclude that other *V. opulus* juice components, such as proanthocyanins, may be responsible for the observed PPAR γ limitation.

To PPAR γ endoligands belong unsaturated fatty acids or eicosanoids, whereas, among synthetic ligands, the most known are thiazolidinediones, such as rosiglitazone [5]. A recent study presented chemically pure phenolic compounds' abilities to regulate the adipogenesis process and matched the obtained results with the molecular docking analysis of their binding affinity to PPAR γ LBD [70]. As it was shown, the obtained in silico binding affinities of quercetin, apigenin, resveratrol, ellagic acid and coumaric acid to PPAR γ were in agreement with these compounds' inhibition potential of 3T3-L1 cells differentiation. However, it can still be supposed that the nuclear receptor ligand activity might be limited not only by its bioavailability, but also by its intracellular uptake.

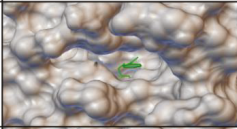
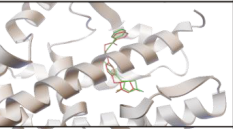
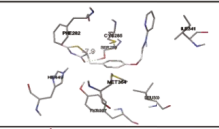
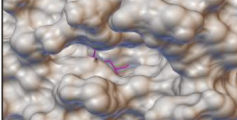
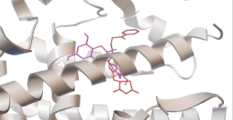
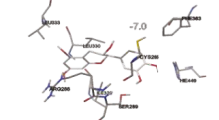
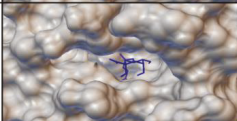
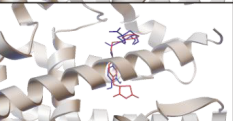
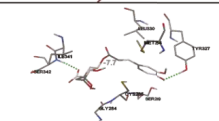
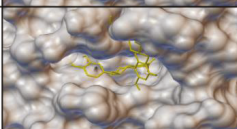
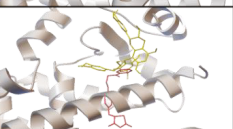
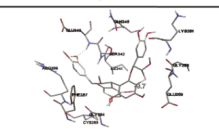
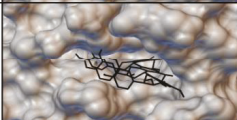
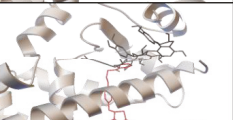
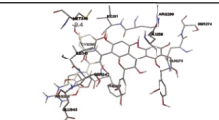
Ligand	Pocket visualization	Rosiglitazone from crystal vs ligand from molecular docking	Ligand interaction	Binding affinity [kJ/mol]
rosiglitazone				-33,91
(+)- catechin				-29,31
chlorogenic acid				-33,08
procyanidin B1				-40,61
procyanidin C1				-39,36

Figure 13. Interaction of tested phenolic compounds with PPAR γ receptor verified with molecular docking. The active site of the PPAR γ receptor is located behind the E3 helix, where a small cavity is formed. An agonist of PPAR γ , rosiglitazone, enters the receptor-active site and locates deep inside the binding pocket. Molecular models of rosiglitazone, (+)- catechin, chlorogenic acid, procyanidin B1 and procyanidin C1 are shown on the entrance of the active pocket site. Orientation of models are presented in comparison to the crystal model of rosiglitazone. Interactions of the models with corresponding binding affinities are presented in the two last columns. Molecular docking was performed with AutoDock Vina.

4. Conclusions

The present work provides direct evidence of the *V. opulus* juice effect on the adipogenesis of 3T3-L1 cells (Figure 14). Phenolic compounds identified in juice, mainly chlorogenic acid, procyanidins and catechins, were found to suppress adipogenesis by the downregulation of major regulators of adipogenesis, such as PPAR γ , C/EBP α and SREBP-1c. The regulation of PPAR γ -mediated β -lactamase expression in reporter gene assay, as well molecular docking, suggested that *V. opulus* components may work as a PPAR γ antagonist. As result, the levels of enzymes involved in lipid metabolism, such as FAS or ACC, were decreased, along with adipokine TNF α , Il-6 and leptin. Additionally, *V. opulus* juice was able to inhibit pancreatic lipase, which potentially could reduce the uptake of fatty acids in the digestive tract and the storage of body fat in the adipose tissue.

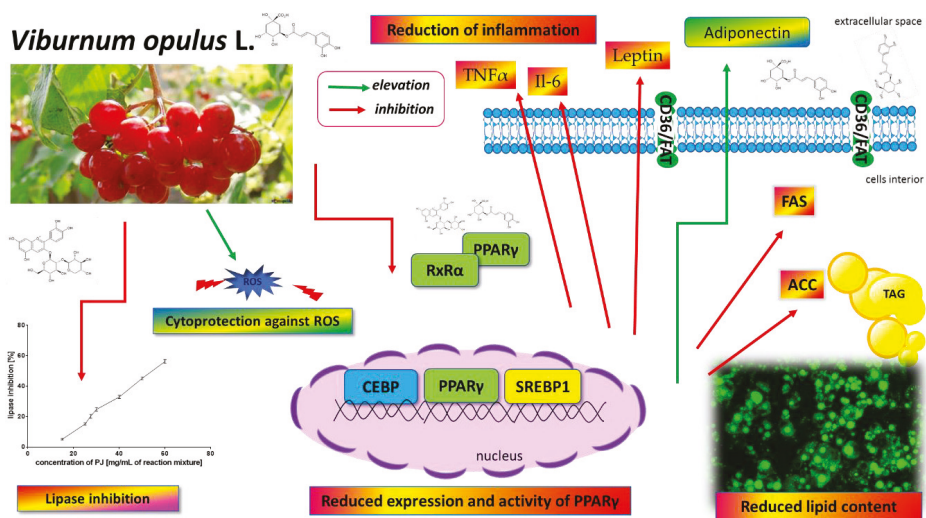


Figure 14. *V. opulus* juice phenolic compounds as modulators of lipids metabolism—the proposed mechanism of action. *V. opulus* downregulates the adipogenesis of 3T3-L1 cells, decreases the expression and activity of the PPAR γ nuclear receptor as well as PPAR γ -regulated proteins (i.e., fatty acid synthase (FAS), acetyl-CoA carboxylase (ACC)), diminishes the release of inflammatory cytokines and leptin, possesses cytoprotective activity against ROS generation and increases adiponectin secretion. *V. opulus* inhibits pancreatic-lipase and limits fatty acid release from the food matrix.

Our results contribute to elucidate *V. opulus* phenolic compounds' molecular mechanism in adipogenesis regulation. However, observed adipogenesis inhibitory outcome needs further molecular evaluation after *V. opulus* juice *in vitro* digestion and its incubation with gut microflora. These processes may greatly influence the composition of the studied phytochemicals, as well as the activity. Taking into account possible *V. opulus* cellular type-dependent *in vitro* activity, its potential usage as a diet component needs further *in vivo* studies performed with an animal obesity model to show its efficacy in the regulation of lipid metabolism at safety doses.

Author Contributions: M.Z.-S. conceptualization, supervision, methodology, lab work with cell cultures and results, writing—original draft preparation, review, and editing; N.P. lab work and results, obtaining and characterization of *V. opulus* phenolics; M.S. molecular modeling; A.P. involved in study conceptualization, lipase inhibition studies, *V. opulus* phenolics characterization; funding acquisition. All authors have read and agreed to the published version of the manuscript.

Funding: The research was supported by grant number 2016/23/B/NZ9/03629 from The National Science Centre, Poland.

Acknowledgments: Małgorzata Zakos-Szyda gratefully acknowledges Maria Koziółkiewicz for her encouragement for opening new research possibilities and critical comments.

Conflicts of Interest: The authors declare no conflict of interest.

References

1. Cataloguing, W.L. *Global Report on Diabetes*; WHO Press: Geneva, Switzerland, 2016; pp. 6–86.
2. Pascual-Serrano, A.; Arola-Arnal, A.; Suárez-García, S.; Bravo, F.I.; Suárez, M.; Arola, L.; Bladé, C. Grape seed proanthocyanidin supplementation reduces adipocyte size and increases adipocyte number in obese rats. *Int. J. Obes.* **2017**, *41*, 1246–1255. [[CrossRef](#)] [[PubMed](#)]
3. Ruiz-Ojeda, F.J.; Rupérez, A.I.; Gomez-Llorente, C.; Gil, A.; Aguilera, C.M. Cell models and their application for studying adipogenic differentiation in relation to obesity: A review. *Int. J. Mol. Sci.* **2016**, *17*, 1040. [[CrossRef](#)] [[PubMed](#)]

4. Graham, M.R.; Baker, J.S.; Davies, B. Causes and consequences of obesity: Epigenetics or hypokineses? *Diabetes Metab. Syndr. Obes. Targets Ther.* **2015**, *8*, 455–460.
5. Ma, X.; Wang, D.; Zhao, W.; Xu, L. Deciphering the roles of PPAR γ in adipocytes via dynamic change of transcription complex. *Front. Endocrinol.* **2018**, *9*, 473. [[CrossRef](#)]
6. Plutzky, J. The PPAR-RXR transcriptional complex in the vasculature: Energy in the balance. *Circ. Res.* **2011**, *108*, 1002–1016. [[CrossRef](#)]
7. Zheng, F.; Zhang, S.; Lu, W.; Wu, F.; Yin, X.; Yu, D.; Pan, Q.; Li, H. Regulation of insulin resistance and adiponectin signaling in adipose tissue by liver X receptor activation highlights a cross-talk with PPAR γ . *PLoS ONE* **2014**, *9*, e101269. [[CrossRef](#)]
8. Medina-Gomez, G.; Gray, S.; Vidal-Puig, A. Adipogenesis and lipotoxicity: Role of peroxisome proliferator-activated receptor γ (PPAR γ) and PPAR γ coactivator-1 (PGC1). *Public Health Nutr.* **2007**, *10*, 1132–1137. [[CrossRef](#)]
9. Kern, L.; Mittenbühler, M.J.; Vesting, A.J.; Ostermann, A.L.; Wunderlich, C.M.; Wunderlich, F.T. Obesity-induced TNF α and IL-6 signaling: The missing link between obesity and inflammation-driven liver and colorectal cancers. *Cancers* **2019**, *11*, 24. [[CrossRef](#)]
10. Austin, D.; Hamilton, N.; Elshimali, Y.; Pietras, R.; Wu, Y. Estrogen receptor-beta is a potential target for triple negative breast cancer treatment. *Oncotarget* **2018**, *9*, 33912–33930. [[CrossRef](#)]
11. Rigano, D.; Sirignano, C.; Tagliabatella-Scafati, O. The potential of natural products for targeting PPAR α . *Acta Pharm. Sin. B* **2017**, *7*, 427–438. [[CrossRef](#)]
12. Martens, F.M.A.C.; Visseren, F.L.J.; Lemay, J.; de Koning, E.J.P.; Rabelink, T.J. Metabolic and additional vascular effects of thiazolidinediones. *Drugs* **2002**, *62*, 1463–1480. [[CrossRef](#)] [[PubMed](#)]
13. Siriwardhana, N.; Kalupahana, N.S.; Cekanova, M.; LeMieux, M.; Greer, B.; Moustaid-Moussa, N. Modulation of adipose tissue inflammation by bioactive food compounds. *J. Nutr. Biochem.* **2013**, *24*, 613–623. [[CrossRef](#)]
14. Filho, H.V.R.; Videira, N.B.; Bridi, A.V.; Tittanegro, T.H.; Batista, F.A.H.; de Pereira, J.G.; de Oliveira, P.S.L.; Bajgelman, M.C.; Le Maire, A.; Figueira, A.C.M. Screening for PPAR non-agonist ligands followed by characterization of a hit, AM-879, with additional no-adipogenic and cdk5-mediated phosphorylation inhibition properties. *Front. Endocrinol.* **2018**, *9*, 11. [[CrossRef](#)]
15. Perova, I.B.; Zhogova, A.A.; Cherkashin, A.V.; Éller, K.I.; Ramenskaya, G.V. Biologically active substances from european guelder berry fruits. *Pharm. Chem. J.* **2014**, *48*, 332–339. [[CrossRef](#)]
16. Zakłós-Szyda, M.; Pawlik, N. The influence of *Viburnum opulus* polyphenolic compounds on metabolic activity and migration of HeLa and MCF cells. *Acta Innov.* **2019**, *33*, 33–42. [[CrossRef](#)]
17. Česonienė, L.; Daubaras, R.; Vencloviene, J.; Viškelis, P. Biochemical and agro-biological diversity of *Viburnum opulus* genotypes. *Cent. Eur. J. Biol.* **2010**, *5*, 864–871. [[CrossRef](#)]
18. Zakłós-Szyda, M.; Pawlik, N.; Polka, D.; Nowak, A.; Koziółkiewicz, M.; Podśędek, A. *Viburnum opulus* fruit phenolic compounds as cytoprotective agents able to decrease free fatty acids and glucose uptake by Caco-2 cells. *Antioxidants* **2019**, *8*, 262. [[CrossRef](#)] [[PubMed](#)]
19. Stepień, A.; Aebischer, D.; Bartusik-Aebischer, D. Anticancer properties of *Viburnum*. *Eur. J. Clin. Exp. Med.* **2018**, *1361*, 47–52. [[CrossRef](#)]
20. Zakłós-Szyda, M.; Majewska, I.; Redzynia, M.; Koziółkiewicz, M. Antidiabetic effect of polyphenolic extracts from selected edible plants as α -amylase, α -glucosidase and PTP1B inhibitors, and β pancreatic cells cytoprotective agents—A comparative study. *Curr. Top. Med. Chem.* **2015**, *15*, 2431–2444. [[CrossRef](#)]
21. Zakłós-Szyda, M.; Kowalska-Baron, A.; Pietrzyk, N.; Drzazga, A.; Podśędek, A. Evaluation of *Viburnum opulus* L. fruit phenolics cytoprotective potential on insulinoma MIN6 Cells relevant for diabetes mellitus and obesity. *Antioxidants* **2020**, *9*, 433. [[CrossRef](#)]
22. Zebisch, K.; Voigt, V.; Wabitsch, M.; Brandsch, M. Protocol for effective differentiation of 3T3-L1 cells to adipocytes. *Anal. Biochem.* **2012**, *425*, 88–90. [[CrossRef](#)] [[PubMed](#)]
23. Sosnowska, D.; Podśędek, A.; Redzynia, M.; Kucharska, A.Z. Inhibitory effect of black chokeberry fruit polyphenols on pancreatic lipase—Searching for most active inhibitors. *J. Funct. Foods* **2018**, *49*, 196–204. [[CrossRef](#)]
24. Jang, J.Y.; Bae, H.; Lee, Y.J.; Choi, Y., II; Young, I.L.; Kim, H.J.; Park, S.B.; Suh, S.W.; Kim, S.W.; Han, B.W. Structural Basis for the Enhanced Anti-Diabetic Efficacy of Lobeglitazone on PPAR γ . *Sci. Rep.* **2018**, *8*, 31. [[CrossRef](#)] [[PubMed](#)]

25. Kraujalyte, V.; Rimantas, P.; Pukalskas, A.; Laima, C. Antioxidant properties and polyphenolic compositions of fruits from different European cranberrybush (*Viburnum opulus* L.) genotypes. *Food Chem.* **2013**, *141*, 3695–3702. [[CrossRef](#)]
26. Karaçelik, A.A.; Kucuk, M.; Iskafiyeli, Z.; Aydemir, S.; De Smet, S.; Miserez, B.; Sandra, P. Antioxidant components of *Viburnum opulus* L. determined by on-line HPLC–UV–ABTS radical scavenging and LC–UV–ESI–MS methods. *Food Chem.* **2015**, *175*, 106–114. [[CrossRef](#)]
27. Velioglu, Y.S.; Ekici, L.; Poyrazoglu, E.S. Phenolic composition of European cranberrybush (*Viburnum opulus* L.) berries and astringency removal of its commercial juice. *Int. J. Food Sci. Technol.* **2006**, *9205*, 1011–1015. [[CrossRef](#)]
28. McDougall, G.J.; Kulkarni, N.N.; Stewart, D. Berry polyphenols inhibit pancreatic lipase activity in vitro. *Food Chem.* **2009**, *115*, 193–199. [[CrossRef](#)]
29. Gironés-Vilaplana, A.; Villaño, D.; Moreno, D.A.; García-Viguera, C. New isotonic drinks with antioxidant and biological capacities from berries (maqui, açai and blackthorn) and lemon juice. *Int. J. Food Sci. Nutr.* **2013**, *64*, 897–906. [[CrossRef](#)]
30. Fabroni, S.; Ballistreri, G.; Amenta, M.; Romeo, F.V.; Rapisarda, P. Screening of the anthocyanin profile and in vitro pancreatic lipase inhibition by anthocyanin-containing extracts of fruits, vegetables, legumes and cereals. *J. Sci. Food Agric.* **2016**, *96*, 4713–4723. [[CrossRef](#)]
31. Zheng, G.; Qiu, Y.; Zhang, Q.F.; Li, D. Chlorogenic acid and caffeine in combination inhibit fat accumulation by regulating hepatic lipid metabolism-related enzymes in mice. *Br. J. Nutr.* **2014**, *112*, 1034–1040. [[CrossRef](#)]
32. Worsztynowicz, P.; Napierała, M.; Białas, W.; Grajek, W.; Olkowicz, M. Pancreatic α -amylase and lipase inhibitory activity of polyphenolic compounds present in the extract of black chokeberry (*Aronia melanocarpa* L.). *Process Biochem.* **2014**, *49*, 1457–1463. [[CrossRef](#)]
33. Sugiyama, H.; Akazome, Y.; Shoji, T.; Yamaguchi, A.; Yasue, M.; Kanda, T.; Ohtake, Y. Oligomeric procyanidins in apple polyphenol are main active components for inhibition of pancreatic lipase and triglyceride absorption. *J. Agric. Food Chem.* **2007**, *55*, 4604–4609. [[CrossRef](#)] [[PubMed](#)]
34. Kowalska, K.; Olejnik, A.; Rychlik, J.; Grajek, W. Cranberries (*Oxycoccus quadripetalus*) inhibit adipogenesis and lipogenesis in 3T3-L1 cells. *Food Chem.* **2014**, *148*, 246–252. [[CrossRef](#)] [[PubMed](#)]
35. Lefterova, M.I.; Haakonsson, A.K.; Lazar, M.A.; Mandrup, S. PPAR γ and the global map of adipogenesis and beyond. *Trends Endocrinol. Metab.* **2014**, *25*, 293–302. [[CrossRef](#)]
36. Česonienė, L.; Daubaras, R.; Viškelis, P. Evaluation of productivity and biochemical components in fruit of different *Viburnum* accessions. *Biologija* **2008**, *54*, 93–96. [[CrossRef](#)]
37. Hiebl, V.; Ladurner, A.; Latkolik, S.; Dirsch, V.M. Natural products as modulators of the nuclear receptors and metabolic sensors LXR, FXR and RXR. *Biotechnol. Adv.* **2018**, *36*, 1657–1698. [[CrossRef](#)]
38. Maire, A.; Teyssier, C.; Balaguer, P.; Bourguet, W.; Germain, P. RAR-Specific Ligands and Their Combinations. *Cells* **2019**, *8*, 1392. [[CrossRef](#)]
39. Zhang, J.; Tang, H.; Deng, R.; Wang, N.; Zhang, Y.; Wang, Y.; Liu, Y.; Li, F.; Wang, X.; Zhou, L. Berberine suppresses adipocyte differentiation via decreasing CREB transcriptional activity. *PLoS ONE* **2015**, *10*, e0125667. [[CrossRef](#)]
40. Hallenborg, P.; Petersen, R.K.; Kouskoumvekaki, I.; Newman, J.W.; Madsen, L.; Kristiansen, K. The elusive endogenous adipogenic PPAR γ agonists: Lining up the suspects. *Prog. Lipid Res.* **2016**, *61*, 149–162. [[CrossRef](#)]
41. Schneider, H.; Staudacher, S.; Poppelreuther, M.; Stremmel, W.; Eehalt, R.; Füllekrug, J. Protein mediated fatty acid uptake: Synergy between CD36 / FAT-facilitated transport and acyl-CoA synthetase-driven metabolism. *Arch. Biochem. Biophys.* **2014**, *546*, 8–18. [[CrossRef](#)]
42. Crewe, C.; Zhu, Y.; Paschoal, V.A.; Joffin, N.; Ghaben, A.L.; Gordillo, R.; Oh, D.Y.; Liang, G.; Horton, J.D.; Scherer, P.E. SREBP-regulated adipocyte lipogenesis is dependent on substrate availability and redox modulation of mTORC1. *JCI Insight* **2019**, *4*. [[CrossRef](#)] [[PubMed](#)]
43. Gao, Y.; Zhou, Y.; Xu, A.; Wu, D. Effects of an AMP-activated protein kinase inhibitor, compound C, on adipogenic differentiation of 3T3-L1 cells. *Biol. Pharm. Bull.* **2008**, *31*, 1716–1722. [[CrossRef](#)] [[PubMed](#)]
44. Zakłos-Szyda, M.; Pawlik, N. Japanese quince (*Chaenomeles japonica* L.) fruit polyphenolic extract modulates carbohydrate metabolism in HepG2 cells via AMP-activated protein kinase. *Acta Biochim. Pol.* **2018**, *65*, 67–78. [[CrossRef](#)] [[PubMed](#)]

45. Li, Y.; Xu, S.; Mihaylova, M.; Zheng, B.; Hou, X.; Jiang, B.; Luo, Z.; Lefai, E.; Shyy, J.Y.; Gao, B.; et al. AMPK Phosphorylates and Inhibits SREBP Activity to Attenuate Hepatic Steatosis and Atherosclerosis in Diet-induced Insulin Resistant Mice. *Cell Metab.* **2011**, *13*, 376–388. [[CrossRef](#)] [[PubMed](#)]
46. Zhang, Y.; Dallner, O.S.; Nakada, T.; Fayzikhodjaeva, G.; Lu, Y.H.; Lazar, M.A.; Roeder, R.G.; Friedman, J.M. A noncanonical PPAR γ /RXR α -binding sequence regulates leptin expression in response to changes in adipose tissue mass. *Proc. Natl. Acad. Sci. USA* **2018**, *115*, E6039–E6047. [[CrossRef](#)]
47. Meng, S.; Cao, J.; Feng, Q.; Peng, J.; Hu, Y. Roles of chlorogenic Acid on regulating glucose and lipids metabolism: A review. *Evid. Based Complementary Altern. Med.* **2013**, *2013*. [[CrossRef](#)]
48. Gao, R.; Yang, H.; Jing, S.; Liu, B.; Wei, M.; He, P.; Zhang, N. Protective effect of chlorogenic acid on lipopolysaccharide-induced inflammatory response in dairy mammary epithelial cells. *Microb. Pathog.* **2018**, *124*, 178–182. [[CrossRef](#)]
49. Ma, Y.; Gao, M.; Liu, D. Chlorogenic acid improves high fat diet-induced hepatic steatosis and insulin resistance in mice. *Pharm. Res.* **2015**, *32*, 1200–1209. [[CrossRef](#)]
50. Liang, N.; Kitts, D.D. Role of chlorogenic acids in controlling oxidative and inflammatory stress conditions. *Nutrients* **2015**, *8*, 16. [[CrossRef](#)]
51. Naveed, M.; Hejazi, V.; Abbas, M.; Kamboh, A.A.; Khan, G.J.; Shumzaid, M.; Ahmad, F.; Babazadeh, D.; FangFang, X.; Modarresi-Ghazani, F.; et al. Chlorogenic acid (CGA): A pharmacological review and call for further research. *Biomed. Pharmacother.* **2018**, *97*, 67–74. [[CrossRef](#)]
52. Villalpando-Arteaga, E.V.; Mendieta-Condado, E.; Esquivel-Solís, H.; Canales-Aguirre, A.A.; Gálvez-Gastélum, F.J.; Mateos-Díaz, J.C.; Rodríguez-González, J.A.; Márquez-Aguirre, A.L. *Hibiscus sabdariffa* L. aqueous extract attenuates hepatic steatosis through down-regulation of PPAR- γ and SREBP-1c in diet-induced obese mice. *Food Funct.* **2013**, *4*, 618–626. [[CrossRef](#)] [[PubMed](#)]
53. Hsu, C.L.; Yen, G.C. Effects of flavonoids and phenolic acids on the inhibition of adipogenesis in 3T3-L1 adipocytes. *J. Agric. Food Chem.* **2007**, *55*, 8404–8410. [[CrossRef](#)]
54. Peng, S.G.; Pang, Y.L.; Zhu, Q.; Kang, J.H.; Liu, M.X.; Wang, Z.; Huang, Y. Chlorogenic Acid Functions as a Novel Agonist of PPAR γ 2 during the Differentiation of Mouse 3T3-L1 Preadipocytes. *BioMed Res. Int.* **2018**, *2018*. [[CrossRef](#)] [[PubMed](#)]
55. Tsuda, T.; Horio, F.; Uchida, K.; Aoki, H.; Osawa, T. Dietary Cyanidin 3-O- β -D-Glucoside-Rich Purple Corn Color Prevents Obesity and Ameliorates Hyperglycemia in Mice. *J. Nutr.* **2003**, *133*, 2125–2130. [[CrossRef](#)] [[PubMed](#)]
56. Chem, F. Regulation of Adipocyte Function by Anthocyanins. *J. Agric. Food Chem.* **2008**, *56*, 642–646.
57. Guo, H.; Xia, M.; Zou, T.; Ling, W.; Zhong, R.; Zhang, W. Cyanidin 3-glucoside attenuates obesity-associated insulin resistance and hepatic steatosis in high-fat diet-fed and db/db mice via the transcription factor FoxO1. *J. Nutr. Biochem.* **2012**, *23*, 349–360. [[CrossRef](#)] [[PubMed](#)]
58. Chyau, C.C.; Chu, C.C.; Chen, S.Y.; Duh, P. The inhibitory effects of Djulis (*Chenopodium formosanum*) and its bioactive compounds on adipogenesis in 3T3-L1 adipocytes. *Molecules* **2018**, *23*, 1780. [[CrossRef](#)]
59. Choi, I.; Park, Y.; Choi, H.; Lee, E.H. Anti-adipogenic activity of rutin in 3T3-L1 cells and mice fed with high-fat diet. *BioFactors* **2006**, *26*, 273–281. [[CrossRef](#)]
60. Nones, K.; Dommels, Y.E.M.; Martell, S.; Butts, C.; McNabb, W.C.; Park, Z.A.; Zhu, S.; Hedderley, D.; Barnett, M.P.G.; Roy, N.C. The effects of dietary curcumin and rutin on colonic inflammation and gene expression in multidrug resistance gene-deficient (mdr1a $^{-/-}$) mice, a model of inflammatory bowel diseases. *Br. J. Nutr.* **2009**, *101*, 169–181. [[CrossRef](#)]
61. Cai, Y.; Fan, C.; Yan, J.; Tian, N.; Ma, X. Effects of rutin on the expression of PPAR γ in skeletal muscles of db/db mice. *Planta Med.* **2012**, *78*, 861–865. [[CrossRef](#)]
62. Zhu, X.; Yang, L.; Xu, F.; Lin, L.; Zheng, G. Combination therapy with catechins and caffeine inhibits fat accumulation in 3T3-L1 cells. *Exp. Ther. Med.* **2017**, *13*, 688–694. [[CrossRef](#)] [[PubMed](#)]
63. Pinent, M.; Bladé, M.C.; Salvadó, M.J.; Arola, L.; Hackl, H.; Quackenbush, J.; Trajanoski, Z.; Ardévol, A. Grape-seed derived procyanidins interfere with adipogenesis of 3T3-L1 cells at the onset of differentiation. *Int. J. Obes.* **2005**, *29*, 934–941. [[CrossRef](#)] [[PubMed](#)]
64. Zhang, J.; Huang, Y.; Shao, H.; Bi, Q.; Chen, J.; Ye, Z. Grape seed procyanidin B2 inhibits adipogenesis of 3T3-L1 cells by targeting peroxisome proliferator-activated receptor γ with miR-483-5p involved mechanism. *Biomed. Pharmacother.* **2017**, *86*, 292–296. [[CrossRef](#)] [[PubMed](#)]

65. Fujisawa, K.; Nishikawa, T.; Kukidome, D.; Imoto, K.; Yamashiro, T.; Motoshima, H.; Matsumura, T.; Araki, E. TZDs reduce mitochondrial ROS production and enhance mitochondrial biogenesis. *Biochem. Biophys. Res. Commun.* **2009**, *379*, 43–48. [[CrossRef](#)]
66. Venkataraman, B.; Ojha, S.; Belur, P.D.; Bhongade, B.; Raj, V.; Collin, P.D.; Adrian, T.E.; Subramanya, S.B. Phytochemical drug candidates for the modulation of peroxisome proliferator-activated receptor γ in inflammatory bowel diseases. *Phyther. Res.* **2020**, *34*. [[CrossRef](#)]
67. Mahindroo, N.; Wang, C.C.; Liao, C.C.; Huang, C.F.; Lu, I.L.; Lien, T.W.; Peng, Y.H.; Huang, W.J.; Lin, Y.T.; Hsu, M.C.; et al. Indol-1-yl acetic acids as peroxisome proliferator-activated receptor agonists: Design, synthesis, structural biology, and molecular docking studies. *J. Med. Chem.* **2006**, *49*, 1212–1216. [[CrossRef](#)]
68. Liberato, M.V.; Nascimento, A.S.; Ayers, S.D.; Lin, J.Z.; Cvorovic, A.; Silveira, R.L.; Martínez, L.; Souza, P.C.T.; Saidenberg, D.; Deng, T.; et al. Medium chain fatty acids are selective peroxisome proliferator activated receptor (PPAR) γ activators and Pan-PPAR partial agonists. *PLoS ONE* **2012**, *7*, e36297. [[CrossRef](#)]
69. Weidner, C.; De Groot, J.C.; Prasad, A.; Freiwald, A.; Quedenau, C.; Kliem, M.; Witzke, A.; Kodelja, V.; Han, C.T.; Giegold, S.; et al. Amorfrutins are potent antidiabetic dietary natural products. *Proc. Natl. Acad. Sci. USA* **2012**, *109*, 7257–7262. [[CrossRef](#)]
70. Aranaz, P.; Navarro-herrera, D.; Migu, I.; Romo-hualde, A.; Miguel, L.; Mart, J.A.; Vizmanos, L.; Milagro, I.; Javier, C. Phenolic Compounds Inhibit 3T3-L1 Adipogenesis Depending on the Stage of Differentiation and Their Binding Affinity to PPAR γ . *Molecules* **2019**, *24*, 1045. [[CrossRef](#)]



© 2020 by the authors. Licensee MDPI, Basel, Switzerland. This article is an open access article distributed under the terms and conditions of the Creative Commons Attribution (CC BY) license (<http://creativecommons.org/licenses/by/4.0/>).

Article

Acute Epigallocatechin-3-Gallate Supplementation Alters Postprandial Lipids after a Fast-Food Meal in Healthy Young Women: A Randomized, Double-Blind, Placebo-Controlled Crossover Study

Alcides C. de Moraes Junior ¹, Raquel M. Schincaglia ¹, Marisa Passarelli ^{2,3},
Gustavo D. Pimentel ¹ and João F. Mota ^{1,*}

¹ Clinical and Sports Nutrition Research Laboratory (LABINCE), Faculty of Nutrition, Federal University of Goiás (UFG), Goiania 74690-900, GO, Brazil; allsmorais@yahoo.com.br (A.C.d.M.J.); raquelms@outlook.com (R.M.S.); gdpimentel@gmail.com (G.D.P.)

² Laboratório de Lípidos (LIM 10), Hospital das Clínicas (HCFMUSP), Faculdade de Medicina da Universidade de Sao Paulo, Sao Paulo 05403-900, Brazil; m.passarelli@fm.usp.br

³ Programa de Pós-Graduação em Medicina da Universidade Nove de Julho, Sao Paulo 01504-000, Brazil

* Correspondence: jfmota@gmail.com; Tel.: +55-(62)-3209-6270

Received: 21 July 2020; Accepted: 18 August 2020; Published: 21 August 2020

Abstract: A high-fat fast-food meal negatively impacts postprandial metabolism even in healthy young people. In experimental studies, epigallocatechin-3-gallate (EGCG), a bioactive compound present in green tea, has been described as a potent natural inhibitor of fatty acid synthase. Thus, we sought to evaluate the effects of acute EGCG supplementation on postprandial lipid profile, glucose, and insulin levels following a high-fat fast-food meal. Fourteen healthy young women 21 ± 1 years and body mass index 21.4 ± 0.41 kg/m² were enrolled in a randomized, double-blind, placebo-controlled crossover study. Participants ingested capsules containing 800 mg EGCG or placebo immediately before a typical fast-food meal rich in saturated fatty acids. Blood samples were collected at baseline and then at 90 and 120 min after the meal. The EGCG treatment attenuated postprandial triglycerides ($p = 0.029$) and decreased high-density lipoprotein cholesterol (HDL-c) ($p = 0.016$) at 120 min. No treatment \times time interaction was found for total cholesterol, low-density lipoprotein (LDL-c), and glucose or insulin levels. The incremental area under the curve (iAUC) for glucose was decreased by EGCG treatment ($p < 0.05$). No difference was observed in the iAUC for triglycerides and HDL-c. In healthy young women, acute EGCG supplementation attenuated postprandial triglycerides and glucose but negatively impacted HDL-c following a fast-food meal.

Keywords: green tea; epigallocatechin; lipid profile; high-fat diet; fast food

1. Introduction

In general, fast foods are rich in refined carbohydrates, sodium, and saturated and trans-fatty acids, and they are poor sources of vitamins, minerals, and dietary fibers [1]. The frequent consumption of fast food has been associated with overweight and obesity, cardiovascular disease, type 2 diabetes, and other metabolic disorders [2]. The acute consumption of a high-fat, energy-dense, fast-food meal promotes postprandial impairments of the lipid profile and induces oxidative stress in subjects with metabolic syndrome [3]. These acute metabolic damages are not only found in individuals with chronic diseases. In a crossover study, different types of fast-food meals negatively impacted postprandial lipids, insulin, and flow-mediated endothelium-dependent dilatation in healthy volunteers [4].

Plant polyphenols have antioxidant and anti-inflammatory properties and may be responsible for numerous beneficial effects on human health [5]. Epigallocatechin-3-gallate (EGCG) is the main

catechin present in green tea, and it is among the best-studied polyphenols [6]. It has been used in the prevention and treatment of non-communicable chronic diseases [7,8]. Treatment with EGCG for 12 weeks decreased bodyweight, total cholesterol, and low-density lipoprotein (LDL-c) in women with central obesity [8], while acute EGCG supplementation was able to delay gastric emptying and increase adiponectin levels in healthy women [9]. In addition, EGCG was observed to decrease lipid absorption from the gastrointestinal tract, which was associated with improvements in insulin resistance and liver triglyceride concentrations [10]. It is important to mention that a cup of green tea (100 mL), one of the main sources for EGCG, contains approximately 144–150 mg of EGCG [11]; nevertheless, EGCG supplements containing different amounts of this catechin are commercialized and easily found for purchase.

We hypothesized that the negative impact on the lipid profile promoted by fast-food meals, rich in saturated fatty acids, could be improved by the acute administration of EGCG. This study sought to evaluate the effects of acute EGCG supplementation on the postprandial lipid profile, glucose, and insulin levels following a fast-food meal among young healthy women. Even though chronic administration of EGCG can impact lipid profile and other metabolic markers [12], we were not aware of studies evaluating the EGCG acute impact on lipid profile after a high-fat fast-food meal in young and healthy individuals. Therefore, we believe this study may help in increasing knowledge regarding EGCG's possible effects on the human lipid profile.

2. Materials and Methods

2.1. Study Design and Participants

This was an acute, randomized, double-blind, crossover, placebo-controlled trial with healthy young women, aged 18 to 25 years old. The recruitment of the participants was carried out through social media and fliers placed on notice boards at the university campus. Exclusion criteria included smoking, diagnosis of underweight or overweight as assessed by body mass index (BMI), hypertension, diabetes mellitus, dyslipidemia, heart disease, peripheral vascular disease, a history of liver or kidney disease, the use of anti-inflammatory medications and corticosteroids, dietary restrictions related to the foods used in the study (french fries, bacon, and parmesan cheese), and pregnancy and/or breastfeeding. This study was conducted according to the Declaration of Helsinki and was approved by the Ethics Committee of the Federal University of Goiás (# 2.011.261). Written informed consent was obtained from all participants. This study was registered at [http://www.ensaiosclinicos.gov.br/](http://www ensaiosclinicos.gov.br/) as RBR-2b8p4n. All participants underwent a baseline medical history screening to determine that they were healthy.

2.2. Experimental Protocol

A fast-food meal was provided to the participants after a 12 h overnight fast. All participants were instructed to abstain from fresh fruit and vegetables, alcohol, herbal teas, fruit juices, and physical exercise for at least 24 h before the trials, but otherwise were to maintain their regular diet before the two visits, with one week of washout between the sessions [6,13]. Participants were reminded 36 h before each visit about the instructions and were questioned about compliance upon arrival at the laboratory. Right before the high-fat fast-food meal, participants ingested 800 mg, split into two capsules of 400 mg each, of either EGCG or corn starch (placebo). The capsules for the placebo and the active product were similar in appearance, smell, and taste. As presented in a review of the literature performed by our team, studies have used a very wide range regarding amounts of EGCG used in clinical trials [12]. The decision to use a high EGCG dose was based on the positive effects previously found by our research group [9] and the fact that the chronic use of this amount has not promoted harmful side effects [14]. Blood samples were collected at baseline and then 90 and 120 min after the end of the fast-food meal (Figure 1). The times at 90 and 120 min for blood collection were chosen

taking into consideration the fact that green tea polyphenols reach peak serum concentrations in the range of 1.3 to 1.6 h [6].

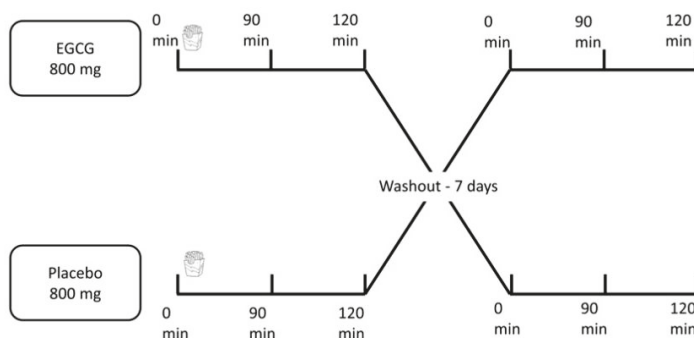


Figure 1. Study design.

The fast-food meal consisted of 80 g of McDonald's® french fries, 130 g of bacon cooked for 5 min without the addition of oil, and 60 g of grated Parmesan cheese. The meal contained 20.57 g of carbohydrate, 47.41 g of protein, and 83.90 g of fat, of which 37.17 g was saturated fat, adding to a total of 1027 kcal. This meal was chosen because of its popularity in pubs and fast-food restaurants in Brazil and other countries. Habitual dietary intake was gathered from all involved in the study using a 24 h recall including three non-consecutive days: two weekdays and one weekend day.

2.3. Anthropometric and Body Composition Assessments

Body weight, height, and waist circumference were measured according to the procedures described by Lohman (1988) [15], using a digital anthropometric scale and a stadiometer (Filizola®, São Paulo, Brazil). All of the measurements were done in duplicate, and the mean between the two findings was used. These values were used to calculate the body mass index (BMI) (kg/m^2). The estimations of their lean mass values and body fat percentage were assessed by dual-energy X-ray absorptiometry (DXA, Lunar DPX NT, GE Healthcare®) with the enCORE 2011 software (version 13.60).

2.4. Analyses of Samples

Blood samples were collected from the antecubital vein and immediately centrifuged at 4000 rpm for 10 min at 4 °C in a refrigerated centrifuge (Hitachi CF16RN, Hitachinaka, Ibaraki, Japan) to obtain the serum. The serum was immediately frozen and stored at −80 °C until analysis. Glucose concentrations were determined by the enzymatic colorimetric method. Total cholesterol (TC), high-density lipoprotein cholesterol (HDL-c), triglycerides (TG), and insulin were determined by immunoturbidimetry methods (Architect Plus®, Naperville, IL, USA). The concentration of low-density lipoprotein (LDL-c) was calculated using Friedewald's equation, and VLDL-c dividing TG by five [16].

2.5. Statistical Analyses

Sample size calculation was performed using G*Power software version 3.1.9.2, taking into consideration the effect on TG [17]. With an effect size of 1.81, a level of significance of 5%, and a statistical power of 95%, the minimum required sample was seven individuals in each treatment. Software R and RStudio were used for the statistical analyses. Values are presented as mean and standard error. The analyses were conducted considering the variations at the timepoints of 90 and 120 min after supplementation and the ingestion of the fast-food meal concerning the baseline measures of the study. The analysis of normality of the residues was performed by the Lilliefors test for the study variables. The carryover effect was analyzed as explained by Rosner (2011) [18], with no significant

values. Effect sizes (ES) were calculated using Cohen’s formula and classified as small ($d = 0.2$), medium ($d = 0.5$), or large ($d = 0.8$). Mean tests were performed by analysis of variance (factorial ANOVA) and the differentiation test of Tukey. Postprandial responses between treatments were also compared with the incremental area under the curve (iAUC) using the trapezoidal method [19]. The significance level of 5% was adopted for all tests.

3. Results

Twenty-seven participants were assessed for eligibility; however, only 25 were randomized into the treatments due to the use of anti-inflammatory drugs or BMI. During the study, nine participants dropped out due to personal reasons ($n = 7$), blood collecting difficulties ($n = 1$) and sickness ($n = 1$), and two participants were excluded from the study due to hypertriglyceridemia (Figure 2). The mean age and BMI were 21 ± 1 years of age and $21.4 \pm 0.41 \text{ kg/m}^2$, respectively. The baseline characteristics of the participants are described in Table 1.

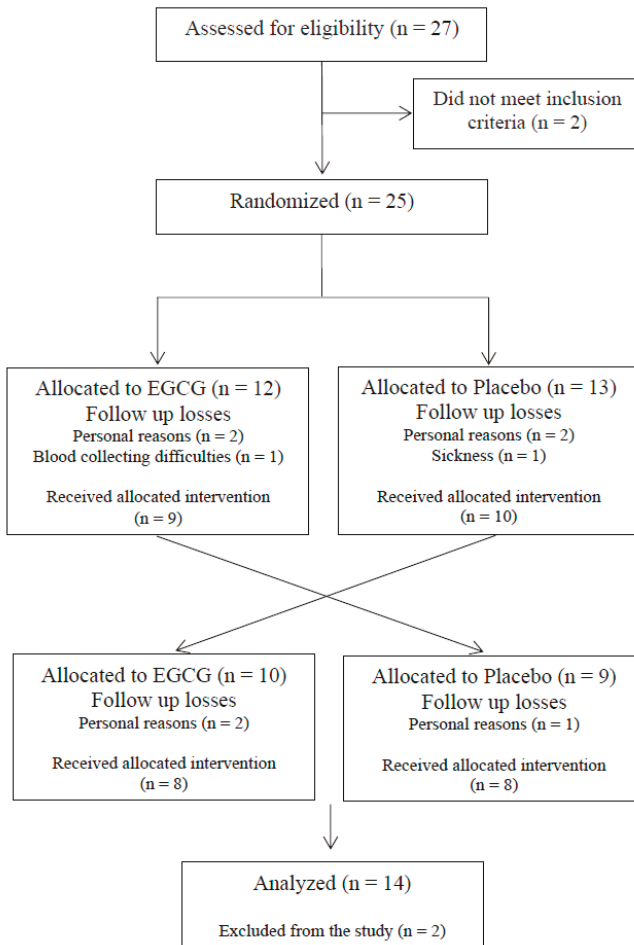


Figure 2. Flow diagram.

Table 1. Baseline characteristics of participants.

Variables	Mean \pm SEM <i>n</i> = 14
Anthropometry and Body Composition	
Height (m)	1.6 \pm 0.02
Weight (kg)	54.9 \pm 1.21
BMI (kg/m ²)	21.4 \pm 0.41
Waist circumference (cm)	67.5 \pm 0.91
Lean mass (kg)	34.4 \pm 0.99
Fat mass (kg)	16.8 \pm 0.87
Fat mass (%)	32.8 \pm 1.42
Food Intake	
Calories (kcal)	1619 \pm 138
Carbohydrate (g)	200 \pm 22.8
Carbohydrate (%)	49.1 \pm 2.33
Protein (g)	79.4 \pm 7.97
Protein (%)	22.9 \pm 2.83
Fat (g)	49.3 \pm 4.55
Fat (%)	27.98 \pm 2.02
Cholesterol (mg)	460 \pm 57.7
Total fiber (g)	16.1 \pm 2.52
Biochemical analyzes	
Total cholesterol (mg/dL)	152 \pm 7.12
HDL-c (mg/dL)	59 \pm 3.28
LDL-c (mg/dL)	76.8 \pm 6.4
Triglycerides (mg/dL)	83.3 \pm 7.17
VLDL-c (mg/dL)	16.6 \pm 1.19
Blood glucose (mg/dL)	89.5 \pm 0.89
Insulin (μ U/mL)	7.89 \pm 0.81
HOMA-IR	1.74 \pm 0.18

HOMA-IR: homeostatic model assessment for insulin resistance.

A significant treatment \times time interaction was found for TG, VLDL-c, and HDL-c ($p < 0.05$, Table 2). The EGCG group attenuated the increase in TG compared to the placebo at 120 min ($+36.1 \pm 6.25$ vs. $+45.9 \pm 6.46$ mg/dL, respectively, $p = 0.029$, ES = 0.33). VLDL-c concentrations followed the same pattern. Participants from the EGCG group also had greater reductions of HDL-c concentrations (EGCG: -6.5 ± 0.72 vs. placebo -1.50 ± 0.44 mg/dL, $p = 0.016$, ES = 0.80) compared to the placebo group at 120 min (Table 2). There was no significant difference in LDL-c. There was a marginal significance in attenuation of postprandial glucose at 90 min ($p = 0.061$, ES = 0.71) and 120 min ($p = 0.094$, ES = 0.24) in the EGCG group compared to the control. The iAUC for glucose ($p = 0.047$) was lower in the EGCG group compared to the placebo (Table 2). No unintended effects were observed throughout the experiment that were related to the ingestion of the fast-food meal or the EGCG supplementation.

Table 2. The response of the epigallocatechin-3-gallate supplementation after a high-fat fast-food meal.

	Placebo	EGCG
Total cholesterol at baseline (mg/dL)	152 ± 21.2	151 ± 5.88
Δ 90	−2.93 ± 1.34	−4.07 ± 1.65
Δ 120	−7.86 ± 1.73	−11.14 ± 1.69
iAUC	−293 ± 99.2	−411 ± 115
HDL-c at baseline (mg/dL)	59.3 ± 3.17	60 ± 3.44
Δ 90	−2.64 ± 0.47	−3.64 ± 0.68
Δ 120	−4.50 ± 0.44	−6.5 ± 0.72 *
iAUC	−226 ± 32.0	−316 ± 48.3 †
LDL-c at baseline (mg/dL)	76.2 ± 6.87	73.0 ± 6.14
Δ 90	−9.36 ± 1.37	−8.77 ± 1.13
Δ 120	−12.5 ± 1.61	−11.9 ± 1.40
iAUC	−749 ± 103	−704 ± 78.1
Triglycerides at baseline (mg/dL)	84.2 ± 7.57	89.9 ± 9.21
Δ 90	45.4 ± 5.92	41.7 ± 7.49
Δ 120	45.9 ± 6.46	36.1 ± 6.25 *
iAUC	3409 ± 446	3045 ± 518
VLDL-c at baseline (mg/dL)	16.8 ± 1.51	18.0 ± 1.84
Δ 90	9.07 ± 1.18	8.34 ± 1.50
Δ 120	9.17 ± 1.42	7.23 ± 1.16 *
iAUC	681 ± 89.4	609 ± 103
Blood glucose at baseline (mg/dL)	88.4 ± 1.19	90.8 ± 1.27
Δ 90	−0.86 ± 1.31	−5.78 ± 1.89 †
Δ 120	2.57 ± 1.59	−0.07 ± 1.58 †
iAUC	−12.86 ± 94.6	−348 ± 122 *
Insulin at baseline (μU/mL)	6.59 ± 0.77	9.59 ± 0.99 *
Δ 90	15.4 ± 2.83	10.5 ± 2.63
Δ 120	17.9 ± 3.45	13.6 ± 2.85
iAUC	1191 ± 214	835 ± 192

Values expressed as means and standard error of means ± SEM. EGCG: epigallocatechin-3-gallate. iAUC: the incremental area under the curve. † $p = 0.05$ to < 0.10 (marginal significance) and * $p < 0.05$ between treatments analyzed by factorial ANOVA test.

4. Discussion

To our knowledge, this is the first trial that evaluated the acute impact of EGCG on lipid profile after a high-fat fast-food meal in young and healthy individuals. In the present study, acute administration of EGCG attenuated postprandial TG; however, it also promoted a larger decrease in HDL-c after the high-fat fast-food meal. Considering that this type of food is frequently consumed by young people [20] and that exaggerated postprandial hypertriglyceridemia is a risk factor for cardiovascular disease [21,22], the results of this study might have important applicability in clinical practice.

Corroborating with our results, a similar finding was observed when male adults with borderline and mild hypertriglyceridemia (range 122.12–220.35 mg/dL) submitted to acute ingestion of different amounts of catechin extract from green tea (moderate dose = 224 mg and high dose = 674 mg) [23]. After a light meal, the postprandial TG curves decreased by 15.1% and 28.7%, respectively, compared to the control group [23]. Here we did not find an effect on the iAUC for triglycerides, which may be related to the fact that our study was dealing with younger and healthier individuals. This suggests that EGCG administration can be especially important for populations at high risk of coronary heart disease, considering that postprandial lipidemia is an independent risk factor for cardiovascular diseases [24] and might be predictive of an elevated risk of myocardial infarction [25].

Chronic interventions using EGCG have also shown postprandial TG decreases in mice fed a high-fat diet [26] and in obese patients [27,28]. In a randomized, double-blind, placebo-controlled study, the consumption of a green tea extract containing 208 mg of EGCG associated with minerals decreased BMI, waist circumference, TC, and LDL-c after three months in obese patients [27]. These results for the lipid profile corroborate findings obtained in our previous study with overweight women taking

1 g/day of green tea extract (560 mg polyphenols, ~224 mg of EGCG) for three months [28]. In the present study, TC and LDL-c were not acutely affected by the one-time EGCG intervention. It has been reported that a postprandial increase in TG was associated with a decrease in LDL-c among men newly diagnosed with metabolic syndrome [29], which was also observed in the current study. Thus, the effects of EGCG on LDL-c seem to occur in a chronic rather than an acute manner.

Huang et al., 2018 [30] suggested that the impact of EGCG on lipid absorption is due to a decrease in bile acid reabsorption, which is necessary for the digestion and metabolism of lipids [31]. A decrease in postprandial HDL-c may also occur when TG is reduced, and its plasma concentration should drop rapidly, considering that HDL-c concentration is dependent on the metabolism of TG-rich lipoproteins [32]. If less fat is absorbed after EGCG administration, this polyphenol may be an important tool to decrease the postprandial deleterious effects of high-fat meals.

In an experimental study conducted with male C57BL/6J mice, the benefits of EGCG for alleviating insulin resistance and liver TG concentration have been attributed to decreased lipid absorption and reduced inflammatory cytokine concentrations [10]. In our study, the iAUC for glucose decreased in the EGCG group, which was not observed for postprandial insulin concentrations. This might be due to the acute design of the study or because the participants were healthy. It has been reported that individuals with poor fasting blood glucose control show a greater decrease in glucose and insulin concentrations when submitted to dietary interventions [33]. Thus, we might speculate that the intervention attenuates negative effects of a high-fat meal, which should be confirmed in future clinical trials. In a counter-balanced crossover design with 12 healthy men, the administration of green tea extract (containing ~366 mg of EGCG) 24 h before the oral glucose tolerance test increased insulin sensitivity by 13% [34]. In addition, the consumption of 1.5 g of green tea diluted in 150 mL of hot water decreased glucose levels at 30 and 120 min after the oral glucose tolerance test in healthy humans compared to the control group [35]. The authors did not measure the EGCG amount; however, based on previous studies [36,37], it is expected to be around 663 mg of EGCG. Hence, additional studies should be conducted with different populations and EGCG doses. The results obtained in the current study may contribute to the investigation of potential acute benefits for the use of EGCG.

Concerning the limitations of this study, the lack of biomarkers of oxidative stress, measurement of lipid absorption, and postprandial lipemia up to 4 h after the meal should be mentioned. Nevertheless, Kriketos et al., 2003 [17] and Unno et al., 2005 [23] showed the largest increase in postprandial TG occurring 2 h after a high-fat meal, and no increase was found after 3 h. It is expected that the impact of EGCG may continue in the following hours since this catechin would remain at fairly high levels in the bloodstream for 4 h after consumption of 800 mg of EGCG [14]. Besides, we only tested one type of meal, and the effects of EGCG after low-fat or standard meals may differ considerably.

5. Conclusions

We found in healthy young women that EGCG attenuated postprandial TG and glucose concentrations but negatively impacted HDL-c following a high-fat fast-food meal. Our results reinforce that even when administered acutely, EGCG may have an impact on the lipid profile. However, further studies are required to elucidate the effects of EGCG after fast-food meals on cardiovascular risk markers.

Author Contributions: The authors' responsibilities were as follows—A.C.d.M.J., R.M.S., M.P., and J.F.M.: designed the research; R.M.S. and A.C.d.M.J.: performed the statistical analyses; A.C.d.M.J., R.M.S., G.D.P., and J.F.M.: analyzed and interpreted the data; A.C.d.M.J.: wrote the first draft of the manuscript and had primary responsibility for the final content; J.F.M., M.P., and G.D.P.: reviewed the manuscript, contributed to the discussion, and provided essential reagents or essential materials; and all authors were involved in editing the manuscript. All authors have read and agreed to the published version of the manuscript.

Funding: A.C.d.M.J. and R.M.S. received scholarships from the Coordination for the Improvement of Higher Education Personnel (CAPES). This research received no external funding. J.F.M. has received support from the National Council for Scientific and Technological Development (CNPq, no. 305082/2019-1).

Conflicts of Interest: The authors declare no conflict of interest.

References

- Bahadoran, Z.; Mirmiran, P.; Azizi, F. Fast Food Pattern and Cardiometabolic Disorders: A Review of Current Studies. *Heal. Promot. Perspect.* **2015**, *5*, 231–240. [[CrossRef](#)] [[PubMed](#)]
- Janssen, H.G.; Davies, I.G.; Richardson, L.D.; Stevenson, L. Determinants of takeaway and fast food consumption: A narrative review. *Nutr. Res. Rev.* **2018**, *31*, 16–34. [[CrossRef](#)]
- Devaraj, S.; Wang-Polagruto, J.; Polagruto, J.; Keen, C.L.; Jialal, I. High-fat, energy-dense, fast-food-style breakfast results in an increase in oxidative stress in metabolic syndrome. *Metabolism* **2008**, *57*, 867–870. [[CrossRef](#)] [[PubMed](#)]
- Rudolph, T.K.; Ruempler, K.; Schwedhelm, E.; Tan-Andresen, J.; Riederer, U.; Böger, R.H.; Maas, R. Acute effects of various fast-food meals on vascular function and cardiovascular disease risk markers: The Hamburg Burger Trial 1-3. *Am. J. Clin. Nutr.* **2007**, *86*, 334–374. [[CrossRef](#)] [[PubMed](#)]
- Pandey, K.B.; Rizvi, S.I. Plant polyphenols as dietary antioxidants in human health and disease. *Oxid. Med. Cell. Longev.* **2009**, *2*, 270–278. [[CrossRef](#)]
- Lee, M.-J.; Maliakal, P.; Chen, L.; Meng, X.; Bondoc, F.Y.; Prabhu, S.; Lambert, G.; Mohr, S.; Yang, C.S. Pharmacokinetics of tea catechins after ingestion of green tea and (-)-epigallocatechin-3-gallate by humans: Formation of different metabolites and individual variability. *Cancer Epidemiol. Biomark. Prev.* **2002**, *11*, 1025–1032.
- Nile, S.H.; Park, S.W. Edible berries: Bioactive components and their effect on human health. *Nutrition* **2014**, *30*, 134–144. [[CrossRef](#)]
- Chen, I.-J.; Liu, C.-Y.; Chiu, J.-P.; Hsu, C.-H. Therapeutic effect of high-dose green tea extract on weight reduction: A randomized, double-blind, placebo-controlled clinical trial. *Clin. Nutr.* **2015**, *35*, 592–599. [[CrossRef](#)]
- Fernandes, R.; Araújo, V.; Giglio, B.; Marini, A.; Mota, J.; Teixeira, K.-I.-S.; Monteiro, P.; Lira, F.; Pimentel, G. Acute Epigallocatechin 3 Gallate (EGCG) Supplementation Delays Gastric Emptying in Healthy Women: A Randomized, Double-Blind, Placebo-Controlled Crossover Study. *Nutrients* **2018**, *10*, 1122. [[CrossRef](#)]
- Chen, Y.-K.; Cheung, C.; Reuhl, K.R.; Liu, A.B.; Lee, M.-J.; Lu, Y.-P.; Yang, C.S. Effects of Green Tea Polyphenol (-)-Epigallocatechin-3-gallate on a Newly Developed High-fat/Western-style Diet-induced Obesity and Metabolic Syndrome in Mice. *J. Agric. Food Chem.* **2011**, *59*, 11862–11871. [[CrossRef](#)]
- Bhagwat, S.; Haytowitz, D.B. *USDA Database for the Flavonoid Content of Selected Foods Release 3.2*; Agricultural Research Service: Beltsville, MD, USA, 2015.
- Ferreira, M.A.; Silva, D.M.; de Moraes, A.C.; Mota, J.F.; Botelho, P.B. Therapeutic potential of green tea on risk factors for type 2 diabetes in obese adults—A review. *Obes. Rev.* **2016**, *17*, 1316–1328. [[CrossRef](#)] [[PubMed](#)]
- Chow, H.H.S.; Cai, Y.; Alberts, D.S.; Hakim, I.; Dorr, R.; Shahi, F.; Crowell, J.A.; Yang, C.S.; Hara, Y. Phase I pharmacokinetic study of tea polyphenols following single-dose administration of epigallocatechin gallate and Polyphenon E. *Cancer Epidemiol. Biomark. Prev.* **2001**, *10*, 53–58.
- Brown, A.L.; Lane, J.; Coverly, J.; Stocks, J.; Jackson, S.; Stephen, A.; Bluck, L.; Coward, A.; Hendrickx, H. Effects of dietary supplementation with the green tea polyphenol epigallocatechin-3-gallate on insulin resistance and associated metabolic risk factors: Randomized controlled trial. *Br. J. Nutr.* **2017**, *101*, 886–894. [[CrossRef](#)] [[PubMed](#)]
- Lohman, T.G.; Roche, A.F.; Martorell, R. (Eds.) *Anthropometric Standardization Reference Manual*, 1st ed.; Human Kinetics Books: Champaign, IL, USA, 1988.
- Martin, S.S.; Blaha, M.J.; Elshazly, M.B.; Toth, P.P.; Kwiterovich, P.O.; Blumenthal, R.S.; Jones, S.R. Comparison of a novel method vs the Friedewald equation for estimating low-density lipoprotein cholesterol levels from the standard lipid profile. *JAMA J. Am. Med. Assoc.* **2013**, *310*, 2061–2068. [[CrossRef](#)] [[PubMed](#)]
- Kriketos, A.D.; Sam, W.; Schubert, T.; Maclean, E.; Campbell, L.V. Postprandial triglycerides in response to high fat: Role of dietary carbohydrate. *Eur. J. Clin. Invest.* **2003**, *33*, 383–389. [[CrossRef](#)] [[PubMed](#)]
- Rosner, B. *Fundamentals of Biostatistics*, 7th ed.; Molly, T., Daniel, S., Walsh, S., Eds.; Brooks/Cole: Boston, MA, USA, 2011.
- Pruessner, J.C.; Kirschbaum, C.; Meinlschmid, G.; Hellhammer, D.H. Two formulas for computation of the area under the curve represent measures of total hormone concentration versus time-dependent change. *Psychoneuroendocrinology* **2003**, *28*, 916–931. [[CrossRef](#)]

20. Larson, N.; Neumark-Sztainer, D.; Laska, M.N.; Story, M. Young adults and eating away from home: Associations with dietary intake patterns and weight status differ by choice of restaurant. *J. Am. Diet. Assoc.* **2011**, *111*, 1696–1703. [[CrossRef](#)]
21. Rivellese, A.A.; Bozzetto, L.; Annuzzi, G. Postprandial lipemia, diet, and cardiovascular risk. *Curr. Cardiovasc. Risk Rep.* **2009**, *3*, 5–11. [[CrossRef](#)]
22. Kolovou, G.D.; Mikhailidis, D.P.; Kovar, J.; Lairon, D.; Nordestgaard, B.G.; Chye Ooi, T.; Perez-Martinez, P.; Bilianou, H.; Anagnostopoulou, K.; Panotopoulos, G. Assessment and Clinical Relevance of Non-Fasting and Postprandial Triglycerides: An Expert Panel Statement. *Curr. Vasc. Pharmacol.* **2011**, *9*, 258–270. [[CrossRef](#)]
23. Unno, T.; Tago, M.; Suzuki, Y.; Nozawa, A.; Sagesaka, Y.M.; Kakuda, T.; Egawa, K.; Kondo, K. Effect of tea catechins on postprandial plasma lipid responses in human subjects. *Br. J. Nutr.* **2005**, *93*, 543–547. [[CrossRef](#)]
24. Ebenbichler, C.F.; Kirchmair, R.; Egger, C.; Patsch, J.R. Postprandial state and atherosclerosis. *Curr. Opin. Lipidol.* **1995**, *6*, 286–290. [[CrossRef](#)] [[PubMed](#)]
25. Stampfer, M.J. A Prospective Study of Triglyceride Level, Low-Density Lipoprotein Particle Diameter, and Risk of Myocardial Infarction. *JAMA J. Am. Med. Assoc.* **1996**, *276*, 882. [[CrossRef](#)]
26. Friedrich, M.; Petzke, K.; Raederstorff, D.; Wolfram, S.; Klaus, S. Acute effects of epigallocatechin gallate from green tea on oxidation and tissue incorporation of dietary lipids in mice fed a high-fat diet. *Int. J. Obes.* **2012**, *36*, 735–743. [[CrossRef](#)] [[PubMed](#)]
27. Suliburska, J.; Bogdanski, P.; Szulinska, M.; Stepien, M.; Pupek-Musialik, D.; Jablecka, A. Effects of green tea supplementation on elements, total antioxidants, lipids, and glucose values in the serum of obese patients. *Biol. Trace Elem. Res.* **2012**, *149*, 315–322. [[CrossRef](#)] [[PubMed](#)]
28. Alves Ferreira, M.; Oliveira Gomes, A.P.; Guimarães de Moraes, A.P.; Ferreira Stringhini, M.L.; Mota, J.F.; Siqueira Guedes Coelho, A.; Borges Botelho, P. Green tea extract outperforms metformin in lipid profile and glycaemic control in overweight women: A double-blind, placebo-controlled, randomized trial. *Clin. Nutr. ESPEN* **2017**, *22*, 1–6. [[CrossRef](#)] [[PubMed](#)]
29. Skoczynańska, A.; Turczyn, B.; Wojakowska, A.; Kreczyńska, B.; Skoczynańska, M.; Wojtas, K. Postprandial decrease in LDL-cholesterol in men with metabolic syndrome. *Open Med.* **2015**, *10*, 138–151. [[CrossRef](#)]
30. Huang, J.; Feng, S.; Liu, A.; Dai, Z.; Wang, H.; Reuhl, K.; Lu, W.; Yang, C.S. Green Tea Polyphenol EGCG Alleviates Metabolic Abnormality and Fatty Liver by Decreasing Bile Acid and Lipid Absorption in Mice. *Mol. Nutr. Food Res.* **2018**, *62*. [[CrossRef](#)]
31. Molinaro, A.; Wahlström, A.; Marschall, H.U. Role of Bile Acids in Metabolic Control. *Trends Endocrinol. Metab.* **2017**, *29*, 31–41. [[CrossRef](#)]
32. Patsch, J.R.; Miesenböck, G.; Hopferwieser, T.; Mühlberger, V.; Knapp, E.; Kay Dunn, J.; Gotto, A.M.; Patsch, W. Relation of triglyceride metabolism and coronary artery disease—Studies in the postprandial state. *Arterioscler. Thromb. Vasc. Biol.* **1992**, *12*, 1336–1345. [[CrossRef](#)]
33. Livesey, G.; Taylor, R.; Hulshof, T.; Howlett, J. Glycemic response and health—a systematic review and meta-analysis: Relations between dietary glycemic properties and health outcomes 1–5. *Am. J. Clin. Nutr.* **2008**, *87*, 223S–236S. [[CrossRef](#)]
34. Venables, M.C.; Hulston, C.J.; Cox, H.R.; Jeukendrup, A.E. Green tea extract ingestion, fat oxidation, and glucose tolerance in healthy humans. *Am. J. Clin. Nutr.* **2008**, *87*, 778–784. [[CrossRef](#)] [[PubMed](#)]
35. Tsuneki, H.; Ishizuka, M.; Terasawa, M.; Wu, J.-B.; Sasaoka, T.; Kimura, I. Effect of green tea on blood glucose levels and serum proteomic patterns in diabetic (db/db) mice and on glucose metabolism in healthy humans. *BMC Pharmacol.* **2004**, *4*, 18. [[CrossRef](#)] [[PubMed](#)]
36. Balentine, D.A.; Wiseman, S.A.; Bouwens, L.C.M. The chemistry of tea flavonoids. *Crit. Rev. Food Sci. Nutr.* **1997**, *37*, 693–704. [[CrossRef](#)] [[PubMed](#)]
37. Shahidi, F. Antioxidants in food and food antioxidants. *Food Nutr.* **2000**, *44*, 158–163. [[CrossRef](#)]



Article

Regular Consumption of Lipigo[®] Promotes the Reduction of Body Weight and Improves the Rebound Effect of Obese People Undergo a Comprehensive Weight Loss Program

Marlhyn Valero-Pérez ¹, Laura M. Bermejo ^{2,*}, Bricia López-Plaza ¹, Meritxell Aguiló García ³, Samara Palma-Milla ⁴ and Carmen Gómez-Candela ⁴

¹ Nutrition Research Group, Hospital La Paz Institute for Health Research (IdiPAZ), 2804 Madrid, Spain; marlhyn.valero@idipaz.es (M.V.-P.); bricia.plaza@idipaz.es (B.L.-P.)

² Nutrition Research Group, Hospital La Paz Institute for Health Research (IdiPAZ), Complutense University of Madrid, 28040 Madrid, Spain

³ AB-BIOTICS SA, Av. Torre Blanca 57, 08172 Sant Cugat del Valles, Spain; aguilolo@ab-biotics.com

⁴ Nutrition Department, La Paz University Hospital, Nutrition Research Group, Hospital La Paz Institute for Health Research (IdiPAZ), Autonomous University of Madrid, 28046 Madrid, Spain; samara.palma@salud.madrid.org (S.P.-M.); cgcandela@salud.madrid.org (C.G.-C.)

* Correspondence: mlbermej@ucm.es; Tel.: +34-917-277-000 (ext. 42199)

Received: 10 June 2020; Accepted: 29 June 2020; Published: 30 June 2020

Abstract: Obesity is a global public health problem. Objective: To evaluate the effect of the regular consumption of the product Lipigo[®] on body weight and rebound effect on overweight/obese subjects undergoing a comprehensive weight loss program. Methods: A randomized, parallel, double-blind, placebo-controlled clinical trial was conducted with male and female subjects presenting a BMI 25–39.9 kg/m². All subjects underwent a comprehensive weight loss program (WLP) for 12 weeks, which included an individualized hypocaloric diet, physical activity recommendations, nutritional education seminars, and three times a day consumption of the product Lipigo[®] or Placebo. After-WLP, subjects continued the treatment for 9 months to assess rebound effect. Body weight (BW), BMI, and body composition were measured at the beginning and the end of the WLP, and in the follow-up. Results: A total of 120 subjects (85% women) 49.0 ± 9.5 years old and with a BW of 81.57 ± 13.26 kg (BMI 31.19 ± 3.44 kg/m²) were randomized and 73 subjects finished the study. At the end of the WLP, there was a tendency toward reduced BW ($p = 0.093$), BMI ($p = 0.063$), and WC ($p = 0.059$) in the treated group. However, subjects with obesity type 1 (OB1) from the treated group significantly reduced body weight (-5.27 ± 2.75 vs. -3.08 ± 1.73 kg; $p = 0.017$) and BMI (-1.99 ± 1.08 vs. -1.09 ± 0.55 kg/m²; $p = 0.01$) compared with placebo. They also presented a minor rebound effect after 9 months with product consumption (-4.19 ± 3.61 vs. -1.44 ± 2.51 kg; $p = 0.026$), minor BMI (-1.61 ± 1.43 vs. -0.52 ± 0.96 kg/m²; $p = 0.025$) and tended to have less fat-mass (-3.44 ± 2.46 vs. -1.44 ± 3.29 kg; $p = 0.080$) compared with placebo. Conclusions: The regular consumption of the product Lipigo[®] promotes the reduction of body weight and reduces the rebound effect of obese people after 52 weeks (12 months), mainly in obesity type 1, who undergo a comprehensive weight loss program.

Keywords: obesity; overweight; beta-glucans; chitosan; follow up study; weight loss programs; weight gain; weight loss; body weight changes

1. Introduction

Obesity is a major public health problem that has attained epidemic levels [1]. According to a recent estimate based on population analyses from 195 countries, 603.7 million adults, and 107.7 million

children suffered obesity in 2015 worldwide [2]. The mean body mass index (BMI) is calculated to increase by 0.4 and 0.5 points in men and women, respectively, every decade [3]. Metabolic complications of obesity comprise metabolic processes dysfunction such as those controlling blood glucose, lipids, and pressure.

Severe dysregulation of these pathways give rise to a cluster of conditions known as metabolic syndrome [4,5]. As a result, around 3.4 million people die each year due to an overweight or obese condition [6].

Overweight and obesity are partially derived from a dietary energy imbalance stemming from behavioral, biological, and environmental processes [7]. Although not exclusively, obesity is tightly linked with hypercaloric diets, and thus weight reduction strategies are primarily focused on reducing energy consumption (i.e., dieting and reducing fat intake) and enhancing energy expenditure (i.e., regular exercise) [8]. Nevertheless, weight lowering methods based on diet and/or physical activity often fail to ameliorate obesity condition in a long-term period. Furthermore, most studies show weight regain upon medium to long-term follow-up (rebound effect) [9–11]. This phenomenon is likely multifactorial and can be explained by a poor compliance or by behavioral or physiological adaptations and highlights the importance of extending the follow-up period in interventional trials to adequately assess efficacy.

Although a wide range of nutritional interventions pursuing weight loss are nowadays available in the market, evidence of their efficacy is fraught with uncertainty [12], and thus more adequately powered randomized trials with extended follow-up are required. Yeast-derived products as a source of biologically active oral compounds are recently gaining scientific support [13]. In vitro and in vivo data suggest that yeast-derived products, particularly of baker's and brewer's yeast *Saccharomyces cerevisiae*, harbor antioxidant, and free radical-scavenging properties besides the ability to stimulate the immune system [14,15]. Moreover, some clinical trials suggest that yeast hydrolysates may be a useful tool to help manage body weight and fat accumulation [16–18].

Lipigo® is a polysaccharide-rich fraction containing β -glucan, chitin, and chitosan, obtained by a specific hydrolysis procedure of residual *S. cerevisiae* from brewery. A previous randomized, double-blind, placebo-controlled small trial demonstrated a statistically significant benefit of Lipigo® on body weight management in overweight and obese population over 12 weeks [19,20]. In the present study, we sought to replicate the previous findings in a more robust randomized clinical trial, comprising a significantly bigger sample size, a better dietary control, and a longer treatment and follow-up periods. Moreover, we aimed to identify the population group able to obtain the greatest advantage of the oral intake of Lipigo®.

2. Materials and Methods

The present study was registered at <http://clinicaltrials.gov> under the number NCT03554525.

2.1. Study Subjects

Two hundred and twenty-four men and women aged 45–65 years were screened for the present study. Inclusion criteria were as follows: age between 18 and 65 years, BMI of ≥ 27 and < 40 kg/m², willing to follow a balanced hypocaloric diet to lose weight and perform regulated physical activity, absence of familial or social environment that prevents compliance with dietary treatment, having a suitable understanding of the clinical trial, agreeing to voluntarily participate in the study, and signing the informed consent form. The exclusion criteria were as follows: treatment for CV risk (dyslipidemia, hypertension, diabetes mellitus, and others), mental illness or low cognitive ability, history of severe liver or kidney disease or cancer, pregnancy or lactation, plans to stop smoking or to lose weight, allergy to any of the compounds of Lipigo® as well as subjects who consumed > 30 g/day alcohol, subjects were also excluded if they had participated in any program or clinical trials of weight control within the last 6 months.

The trial was approved by the Scientific Research and Ethics Committee of the HULP (Reference number: 4801) in accordance with the International Conference on Harmonization Guidelines on Good Clinical Practice and the ethical standards of the Declaration of Helsinki [21].

2.2. Study Design

This randomized, double-blinded, placebo-controlled clinical trial with two parallel arms was conducted at the Nutrition Department of La Paz University Hospital (HULP), Madrid (Spain). The total length of the intervention was 52 weeks (12 months). The intervention was divided in two phases: a weight-loss intervention phase (WLP) (12 weeks) in which all subjects were included in a dietary program controlled in 6 visits taking place every two weeks (V0–V6); and a follow-up post-weight lost intervention phase (P–WLP) (40 weeks) controlled in 3 visits taking place every three months (V7–V9). During both phases (WLP and P–WLP) participants were randomized with sex stratification to consume 3 sticks/day of Lipigo® or Placebo (2 sticks just before the lunch and 1 stick just before the dinner).

2.3. Treatments

2.3.1. Dietary Program

Hypocaloric diets (between 1500 and 3000 Kcal) were prescribed individually for all participants by a dietician expert at the Department of Nutrition of La Paz University Hospital, Madrid. Diets were designed to provide 30% less energy than the total energy expenditure (TEE) at baseline being 1500 kcal the lower limit for caloric restriction. Basal metabolic rate (BMR) was measured by bioelectric impedance Electro Fluid Graph + (EFG) (Akern s.r.l., Florence, Italy). BMR and TEE calculations were corrected according to physical activity and sex as recommended by the World Health Organization (WHO). Proposed hypocaloric diet consisted of 50–55% carbohydrates from total energy intake (added sugars <10%) and 29–34% fat (saturated fatty acids <10%, polyunsaturated fatty acids 5–10% and monounsaturated fatty acids, mainly from virgin olive oil, to complete the lipid profile), according to the recommendations of the Spanish Society of Community Nutrition (SENC, according to its Spanish initials, [22]). Proteins represented 20% of total energy intake (between 0.9–1.8 g/kg of body weight/day), based on body composition benefits observed in a recent meta-analysis [23]. The food intake was distributed in 5 meals: 3 main meals (breakfast, lunch, and dinner) and 2 snacks (mid-morning (11:00 a.m.–11:29 a.m.), and afternoon (5:00–5:29 p.m.)).

The hypocaloric dietary program was prescribed at baseline (V0) of the WLP: participants received a 7-day-meal plan as an example of the individualized diet designed for each one. Moreover, each participant received a food exchange list, allowing the personalization of diet plans according to individual preferences, but ensuring that the resulting menu would provide the individual nutritional requirements calculated. Further dietary counseling was given every two weeks (V1–V5) until the end of the WLP (12th week, V6). Dieticians used all these visits to resolve questions and to motivate participants sufficiently to comply with dietary advice. All subjects were given recommended portion sizes and information on possible food swaps. Moreover, nutrition education and motivational sessions were given by the dietician.

2.3.2. Physical Activity Recommendations

In V0 subjects were instructed to perform moderate physical activity for 1 h at least 3 times a week. The subjects began according to their level of physical activity and gradually increased until they achieved 3 sessions per week or more at the end of WLP.

2.3.3. Nutrition and Health Education Sessions

During the WLP, participants attended 5 nutrition and health education sessions (visits 1 to 5) goals to promote healthy eating and physical activity.

2.3.4. Lipigo® or Placebo

During the WLP and P-WLP, subjects consumed 3 sticks/day of Lipigo® or Placebo (2 sticks just before the lunch and 1 stick just before the dinner)

Lipigo® is a fiber combination obtained from *S. cerevisiae* from the brewery industry. Each stick contained a polysaccharide-rich fraction (909 mg β -glucan, 91 mg chitin-chitosan) and 400 mg excipients. The polysaccharide fraction was obtained by a specific hydrolysis procedure of residual *S. cerevisiae* from brewery patented by DAMM S.A (El Prat del Llobregat, Barcelona, Spain). The nutritional composition per 100 g of dry product was: protein, 1.6 g; fat, 3.7 g; carbohydrates 58.7 g; dietary fiber, 29.9 g; and sodium 0.6 g.

Placebo was composed of 1000 mg maltodextrine and 400 mg excipients.

DAMM S.A. prepared the Lipigo® and the Placebo sticks specifically for this study. Both types of sticks were packaged in box packs of 30 sticks. The packs were labeled as either L1 or L2 to maintain blinded conditions. During every visit in the WLP, subjects received all the sticks needed until the next visit every two weeks. At baseline of the P-WLP (V6) and in the V7 and V8, subjects received all the sticks need to complete three months to the next visit. The sticks received by each participant were assigned according to the randomization.

2.4. Endpoints

The following analyses and measurements were collected:

2.4.1. General Health Status Variables

During both phases (V0–V9), information about special medical conditions and drug consumption was collected. Furthermore, blood pressure and heart rate were measured using a Spot Vital Signs 420 automatic monitor (Welch Allyn, Madrid, Spain; accuracy ± 5 mmHg). Three measurements were taken at 5-min intervals, and the means were calculated. Moreover, blood sample was collected to analyze lipid profile including total cholesterol and LDL-cholesterol at the beginning and at the end of each phase (V0, V6, and V9).

2.4.2. Anthropometrics and Body Composition Variables

Anthropometric measurements were performed at the beginning and at the end of each phase (V0, V6, and V9) using standard techniques, adhering to WHO guidelines [24]. All measurements were made by trained personnel in the morning with the subject barefoot and wearing only underwear. Height was determined using a height meter with an accuracy of 1 mm (range, 80–200 cm). Body weight was measured using a TANITA BC-420 MA (Bio Lógica Tecnología Médica S.L, Barcelona, Spain). The BMI was calculated as body weight ((kg)/(height (m)²). According to their BMI, participants were classified in four categories: normal weight (BMI 18.5–24.9 kg/m²), class I overweight (BMI 25.0–27.9 kg/m²), class II overweight (BMI 28–29.9 kg/m²), class I obesity (BMI 30–34.9 kg/m²), and class II obesity (BMI 35–39.9 kg/m²). Waist circumference (WC) was measured using a Seca 201 steel tape (Quirumed, Valencia, Spain). Variables change between V0 and V6 (Dif V0–V6) and between V6 and V9 (Dif V6–V9) was calculated in order to evaluate the anthropometrics and body composition evolution during WLP and P–WLP respectively. Variables change between V0 and V9 (Dif V0–V9) was calculated to evaluate the rebound effect.

Body composition was determined using a specialized tetrapolar bioelectrical impedance analyzer, the EFG ElectroFluidGraph analyzer (Akern s.r.l., Florence, Italy): total fat mass (TFM), fat-free mass (FFM), and muscle mass (MM) were measured. These body composition data were obtained using regression validated equations of the manufacturer (Akern BodyGram Plus 1.0). These validated equations were derived from previous research [25].

All participants were instructed by the researcher to minimize the BIA affecting factors (not having used diuretic medications in the previous seven days, to have been fasting for at least four hours;

not having ingested alcohol or caffeinated beverages in the previous 48 h; having abstained from moderate-intense physical activity in the previous 24 h) [26].

The device was calibrated before measurements of each participant. All participants rested (lying on a bed) for at least five minutes prior to the measurement. Electrodes were placed on the dorsal surface of the wrist and the ankle as well as at the base of the second or third metacarpal-phalangeal joints of hand and foot after the skin was cleaned with an alcohol wipe. The lead wires were attached to the appropriate electrodes and participants were instructed to abduct their limbs from the trunk. Triplicate measurements were conducted, and a median value determined.

2.4.3. Dietary Variables

The diet of each subject was recorded during WLP and P-WLP. In V0, V6–V9 participants filled a 24-h recall over 3 consecutive days recording all food and beverages consumed inside and outside the home, including one weekend day [27]. In V2–V5 diet was recorded using a 24 h record questionnaire. Food weight or household measurements (spoonful, cups, etc.) should be self-reported in both food recording questionnaires. Subjects were previously trained by the researchers to obtain accurate data. All food records were thoroughly reviewed by a nutritionist in the presence of the subject during study visits to ensure that the information collected was complete. The energy and nutritional content of the foods consumed were then calculated using DIAL software (Alce Ingeniería, Madrid, Spain).

2.4.4. Physical Activity Variables

Physical activity was assessed using the International Physical Activity Questionnaire-Short Form (IPAQ-SF) for the Spanish population. IPAQ-SF collects the frequency and duration of vigorous-intensity activity, moderate-intensity activity, and walking activity [28]. The questionnaire was filled in V0, V6–V9. Time spent in vigorous, moderate, and walking activity was calculated by the energy spent for these categories of activity, to produce the total Metabolic Equivalent Task (MET)-minutes of physical activity/week.

2.4.5. Compliance and Adverse Events

Subjects received the exact number of sticks required for each period during study visits. Empty and non-empty sticks should be returned to the investigator in each study visit. Compliance was measured by comparing the number of sticks provided and the number of empty sticks returned. A subject was considered compliant when he/she consumed $\geq 80\%$ of the sticks provided. Adverse events were documented in all study visits (V1–V9). An adverse event was defined as any unfavorable, unintended effect. All such events were recorded along with the symptoms involved (bad breath, nausea, vomiting, diarrhea, constipation, others).

2.5. Statistical Analysis

The sample size was calculated taking into account the results obtained in a meta-analysis aiming to evaluate the effect of different non-surgical treatments on body weight maintenance in overweight/obese people [29]. Most of the studies included in such meta-analysis have a sample size of around 80 subjects. Moreover, according to these studies, a potential 33% drop-out range should be considered. Given all the above, the total sample size estimated for the present study was of 120 subjects.

The analysis population included all subjects who completed the WLP and P-WLP stages. Data is presented as mean \pm standard deviation (SD) or percent (%) and N. The Kolmogorov-Smirnov test was used to check the normal distribution of the data. Outliers (i.e., lying more than two SDs from the mean) in asymmetric distributions were deemed to reflect true results and were included in the analysis. The Levene's test was used to determine whether the variance presented by the measured variables was homogeneous. The Student t test was used to compare the mean values of normally distributed variables for the two treatment groups and the intragroup analysis. Whereas, Mann-Whitney U test

was used when data were not normally distributed. Differences within groups between V0–V6, V6–V9 and V0–V9 were examined using the Student paired t test when the distribution of the results was normal and the Wilcoxon test when it was not. Additionally, Bonferroni’s correction for multiple comparisons was performed. All tests were two-tailed.

A subgroup of analysis was also conducted based on the presence of overweight or obesity at the baseline (V0). Significance was set at two-sided $p < 0.05$. All calculations were performed using SPSS v.21.0 software (SPSS Inc.).

3. Results

3.1. Recruitment and Study Population

The study was performed between April 2017 and August 2018. One hundred and twenty apparently healthy subjects (19 men [15.8%], 101 women [84.2%]) were eligible for their inclusion in the study. Subjects were randomized into either the Placebo or Lipigo® group stratified by sex. Twenty-two subjects dropped-out during the WLP:10 in the Placebo group and 12 in the Lipigo® group. At the end of the study, a total of 47 subjects were lost to follow-up (24 in the Placebo group and 23 in the Lipigo® group) due to personal causes ($n = 27$), failure to follow treatment instructions ($n = 4$), health problems not related to clinical trial procedures ($n = 6$), loss of follow-up ($n = 9$), and low product tolerance ($n = 1$). Thus, 73 subjects (6 men [8.2%], 67 women [91.8%]) completed the 12-months study, and only their results were included in the subsequent analyses (Figure 1).

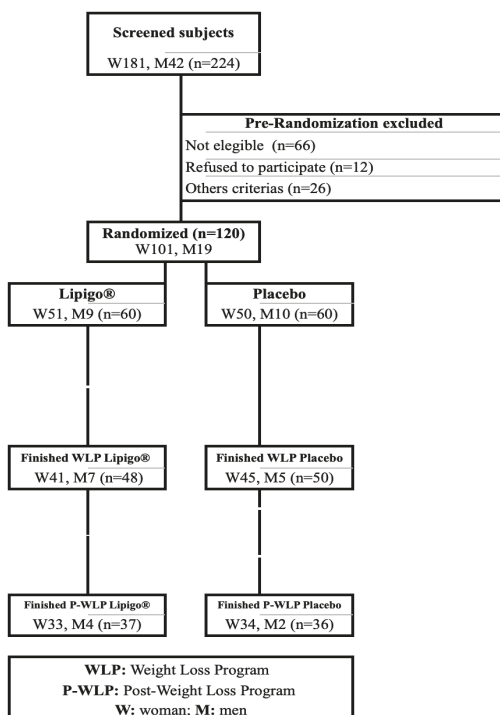


Figure 1. CONSORT diagram.

3.2. Baseline Characteristics

The mean age of the population was 50.9 ± 8.9 years old. The mean BMI was 31.2 ± 3.5 kg/m² (Obesity type 1, 39.7%). At baseline, no significant differences existed between subjects assigned to the Lipigo® and Placebo groups in terms of their anthropometric, body composition, blood pressure, and biochemical parameters or other variables such as sex, age, or smoking (Table 1).

Table 1. Baseline characteristics of the subjects.

		Total	Placebo (n = 36)	Lipigo® (n = 37)	p-Value
Gender	(Female %, n)	73	94.4 (34)	89.2 (33)	0.414
Age	(years)	50.9 ± 9.07	49.47 ± 10.4	52.3 ± 7.4	0.185
Weight	(kg)	82.85 ± 12.37	82.65 ± 12.5	83.04 ± 12.4	0.895
BMI	(kg/m ²)	31.19 ± 3.44	31.2 ± 3.6	31.2 ± 3.3	0.976
Waist circumference	(cm)	97.76 ± 11.25	97.4 ± 11.6	98.2 ± 11.0	0.765
FM	(kg)	31.51 ± 7.65	32.3 ± 7.9	30.7 ± 7.5	0.400
Lean mass	(kg)	51.25 ± 10.15	50.3 ± 9.1	52.2 ± 11.1	0.439
MM	(kg)	35.21 ± 8.03	34.3 ± 6.8	36.2 ± 9.1	0.311
SBP	(mmHg)	111.47 ± 15.13	110.7 ± 15	112.3 ± 15.5	0.666
DBP	(mmHg)	77.19 ± 9.56	77.0 ± 9.7	77.4 ± 9.6	0.864

Data is represented as mean \pm SD. BMI: Body Mass Index; FM: Fat Mass; MM: Muscle Mass; SBP: Systolic Blood Pressure; DBP: Diastolic Blood Pressure.

Despite existing differences between the number of women and men participating in the study, stratified randomization by sex allowed to obtain 2 homogeneous intervention groups.

3.3. Anthropometric and Body Composition Variables

Both treatment groups decreased body weight, BMI, and waist circumference at the end of WLP or P-WLP although no significant intra-group differences were detected in any anthropometric or body composition variables. No significant intergroup differences were obtained (Lipigo® vs. Placebo, Table 2).

Table 2. Anthropometric and body composition variables throughout the study.

		Placebo (n = 36)	Lipigo® (n = 37)	p-Value
Weight (kg)	Baseline of WLP (V0)	82.65 ± 12.48	82.65 ± 12.48	0.895
	End of WLP (V6)	79.19 ± 12.3	78.61 ± 12.56	0.842
	End of P-WLP (V9)	80.18 ± 12.49	79.67 ± 13.01	0.864
BMI (kg/m ²)	Baseline of WLP (V0)	31.21 ± 3.65	31.18 ± 3.28	0.976
	End of WLP (V6)	29.91 ± 3.54	29.39 ± 3.19	0.512
	End of P-WLP (V9)	30.27 ± 3.62	29.79 ± 3.32	0.558
Waist circumference (cm)	Baseline of WLP (V0)	97.35 ± 11.6	98.18 ± 11.05	0.765
	End of WLP (V6)	94.82 ± 11.82	93.41 ± 10.36	0.588
	End of P-WLP (V9)	91.4 ± 17.54	93.94 ± 10.66	0.456
Muscle mass (kg)	Baseline of WLP (V0)	34.25 ± 6.84	36.19 ± 9.07	0.311
	End of WLP (V6)	32.12 ± 6.55	33.23 ± 8.42	0.530
	End of P-WLP (V9)	32.51 ± 6.84	32.62 ± 6.87	0.944
Lean mass (kg)	Baseline of WLP (V0)	50.32 ± 9.12	52.19 ± 11.14	0.439
	End of WLP (V6)	48.75 ± 8.65	49.61 ± 9.01	0.680
	End of P-WLP (V9)	49.00 ± 9.11	48.92 ± 9.07	0.971
Fat mass (kg)	Baseline of WLP (V0)	32.28 ± 7.86	30.74 ± 7.48	0.400
	End of WLP (V6)	30.47 ± 7.21	29.01 ± 6.41	0.365
	End of P-WLP (V9)	31.32 ± 7.34	30.78 ± 7.17	0.755

Data is expressed as mean \pm SD. V: Visit; WLP: Weight Loss Program; P-WLP: Post-weight Loss Program; OB1: Obesity Type 1; BMI: Body Mass Index.

However, when evaluating the changes in anthropometric and body composition variables at the end of WLP (Dif. V0–V6), subjects included in the Lipigo® group showed a non-significant trend towards reducing body weight ($p = 0.093$), BMI ($p = 0.063$), and waist circumference ($p = 0.059$) when compared to Placebo (Table 3).

Table 3. Changes in anthropometric and body composition variables throughout the study.

		Placebo ($n = 36$)	Lipigo® ($n = 37$)	p -Value
Weight (kg)	Dif V0–V6	-3.46 ± 2.00	-4.43 ± 2.78	0.093
	Dif V6–V9	0.99 ± 2.35	1.06 ± 2.87	0.912
Rebound effect	Dif V0–V9	-2.47 ± 3.41	-3.36 ± 3.36	0.259
BMI (kg/m^2)	Dif V0–V6	-1.31 ± 0.77	-1.79 ± 1.35	0.063
	Dif V6–V9	0.36 ± 0.89	0.41 ± 1.09	0.831
Rebound effect	Dif V0–V9	-0.94 ± 1.32	-1.4 ± 1.58	0.178
Waist circumference (cm)	Dif V0–V6	-2.63 ± 3.1	-4.34 ± 4.13	0.059
	Dif V6–V9	-0.59 ± 3.3	0.53 ± 3.4	0.162
Rebound effect	Dif V0–V9	-3.08 ± 3.44	-3.48 ± 3.25	0.631
Muscle mass (kg)	Dif V0–V6	-2.14 ± 1.96	-2.04 ± 1.85	0.837
	Dif V6–V9	0.39 ± 1.57	-0.04 ± 1.36	0.218
Rebound effect	Dif V0–V9	-1.74 ± 2.23	-2.12 ± 1.74	0.444
Lean mass (kg)	Dif V0–V6	-1.57 ± 1.85	-1.5 ± 1.76	0.872
	Dif V6–V9	0.25 ± 1.52	-0.59 ± 1.57	0.024
Rebound effect	Dif V0–V9	-1.32 ± 1.99	-2.06 ± 1.84	0.108
Fat mass (kg)	Dif V0–V6	-1.81 ± 3.53	-2.6 ± 2.56	0.282
	Dif V6–V9	0.85 ± 2.5	1.59 ± 2.56	0.214
Rebound effect	Dif V0–V9	-0.96 ± 4.34	-1.06 ± 3.32	0.908

Data is expressed as mean \pm SD. Dif V0–V6: Difference during the WLP; Dif V6–V9: Differences during the P-WLP; Dif V0–V9: Rebound effect. WLP: Weight Loss Program; P-WLP: Post-weight Loss Program; BMI: Body Mass Index.

A significant reduction of the lean mass was observed in subjects included in the Lipigo® group when compared to Placebo during the P-WLP phase (Dif V6–V9, Lipigo®: -0.59 ± 1.57 vs. Placebo: 0.25 ± 1.52 kg; $p = 0.024$).

Next, subgroup analyses based on the presence of overweight type 2 ($n = 32$, 43.8%) or obesity type 1 ($n = 29$, 39.7%) and obesity type 2 ($n = 12$, 16.5%) was performed. Subjects with obesity type 1 and 2 enrolled in the Lipigo® group showed a non-significant higher body weight reduction compared to Placebo at the end of WLP (Dif V0–V6, -5.24 ± 2.53 vs. -3.81 ± 2.2 kg $p = 0.065$). Nevertheless, when analyzing subjects with obesity type 1, Lipigo® group, achieved a significantly higher body weight (-5.27 ± 2.75 vs. -3.08 ± 1.73 kg; $p = 0.017$) and BMI (-1.99 ± 1.08 vs. -1.09 ± 0.55 kg/m^2 ; $p = 0.010$) reduction vs. Placebo at the end of WLP (Dif V0–V6). In addition, Lipigo® group seemed to have a higher fat mass reduction than Placebo group at the end of WLP (Dif V0–V6) (-3.44 ± 2.46 vs. -1.44 ± 3.29 kg; $p = 0.080$). Moreover, intragroup difference V0 vs. V6 was observed in BMI only in Lipigo® group (Table 4).

During the P-WLP (Dif v6–v9) both groups gain weight, BMI, and fat mass but the OB1 subjects included in the Placebo group gain more in all the anthropometric and body composition variables during this period (40 weeks) than Lipigo® group, although the differences were not significant.

Moreover, obesity type 1 subjects included in the Lipigo® group presented a significant minor rebound effect (Dif V0–V9) vs. Placebo group when looking at body weight change (-4.19 ± 3.61 vs. -1.44 ± 2.51 kg; $p = 0.026$) and BMI change (-1.61 ± 1.43 vs. -0.52 ± 0.96 kg/m^2 ; $p = 0.025$). Lipigo® group seemed to have a minor rebound effect (Dif V0–V9) in fat mass when compared to Placebo group (-1.62 ± 3.45 vs. 0.62 ± 3.80 kg) although the difference is no significant ($p = 0.121$).

Table 4. Changes in body weight, BMI, and Fat mass throughout the study in overweight ($n = 32$) and obesity type 1 ($n = 29$) subjects.

		Placebo	Lipigo®	p-Value
Weight (kg) Overweight	Baseline of WLP (V0)	74.25 ± 9.22	75.31 ± 6.30	0.706
	End of WLP (V6)	71.18 ± 10.17	71.96 ± 7.77	0.810
	End of P-WLP (V9)	72.07 ± 10.41	72.65 ± 6.82	0.855
	Dif V0–V6	−2.96 ± 1.79	−3.66 ± 2.60	0.732
	Dif V6–V9	0.79 ± 1.83	0.92 ± 2.59	0.633
	Rebound effect Dif V0–V9	−2.17 ± 2.59	−2.75 ± 3.27	0.806
Weight (kg) OB1	Baseline of WLP (V0)	84.77 ± 6.18	84.98 ± 8.77	0.942
	End of WLP (V6)	81.69 ± 5.56	79.71 ± 9.53	0.503
	End of P-WLP (V9)	83.33 ± 6.66	80.79 ± 10.32	0.442
	Dif V0–V6	−3.08 ± 1.73	−5.27 ± 2.76	0.017
	Dif V6–V9	1.64 ± 1.65	1.09 ± 3.45	0.594
	Rebound effect Dif V0–V9	−1.44 ± 2.51	−4.19 ± 3.61	0.026
BMI (kg/m²) Overweight	Baseline of WLP (V0)	28.12 ± 1.14	28.34 ± 1.02	0.567
	End of WLP (V6)	26.92 ± 1.27	27.05 ± 1.63	0.790
	9 months P-WLP (V9)	27.26 ± 1.61	27.34 ± 1.48	0.881
	Dif V0–V6	0.30 ± 0.72	0.37 ± 1.03	0.860
	Dif V6–V9	−1.16 ± 0.75	−1.41 ± 1.0	0.807
	Rebound effect Dif V0–V9	−0.85 ± 1.05	−1.01 ± 1.7	0.698
BMI (kg/m²) OB1	Baseline of WLP (V0)	31.98 ± 1.33	31.91 ± 1.22	0.883
	End of WLP (V6)	30.89 ± 1.65	29.91 ± 1.78#	0.136
	End of P-WLP (V9)	31.45 ± 1.99	30.30 ± 1.87	0.120
	Dif V0–V6	−1.09 ± 0.56	−1.99 ± 1.09	0.010
	Dif V6–V9	0.56 ± 0.63	0.4 ± 1.3	0.673
	Rebound effect Dif V0–V9	−0.52 ± 0.96	−1.61 ± 1.43	0.025
Fat mass (kg) Overweight	Baseline of WLP (V0)	26.55 ± 4.58	27.62 ± 3.69	0.481
	End of WLP (V6)	24.96 ± 3.53	26.19 ± 4.42	0.391
	End of P-WLP (V9)	25.37 ± 4.55	26.94 ± 5.10	0.364
	Dif V0–V6	−1.58 ± 3.75	−1.56 ± 2.76	0.982
	Dif V6–V9	0.40 ± 1.94	0.75 ± 2.72	0.685
	Rebound effect Dif V0–V9	−1.18 ± 3.66	−0.65 ± 3.63	0.804
Fat mass (kg) OB1	Baseline of WLP (V0)	32.91 ± 3.06	30.13 ± 7.78	0.222
	End of WLP (V6)	31.48 ± 3.43	28.48 ± 5.56	0.145
	End of P-WLP (V9)	33.54 ± 3.69	31.31 ± 5.57	0.217
	Dif V0–V6	−1.44 ± 3.29	−3.44 ± 2.46	0.080
	Dif V6–V9	2.06 ± 1.62	2.02 ± 2.53	0.958
	Rebound effect Dif V0–V9	0.62 ± 3.80	−1.62 ± 3.45	0.121

Data are expressed as the means ± SDs. V0–V6: Difference during the WLP; V6–V9: Differences during the P-WLP; V0–V9: Rebound effect. WLP: Weight Loss Program; P-WLP: Post-weight Loss Program; BMI: Body Mass Index; OB1: Obesity type 1. #Intragroup difference V0 vs. V6 ($p = 0.032$).

3.4. Dietary Variables

At baseline, a mean general caloric intake of 1988.24 ± 437.13 kcal was documented. At the end of WLP both groups significantly reduced energy intake (Dif V0–V6) with no significant (NS) differences intergroup (-278.97 ± 460.7 vs. -288.82 ± 497.34 kcal; NS).

The caloric profile changed in both groups at the end of the WLP (Dif V0–V6) with no significant differences respected to baseline between Lipigo® and Placebo groups: carbohydrates (0.64 ± 8.08 vs. $2.6 \pm 5.98\%$; NS), proteins (1.56 ± 3.62 vs. $0.95 \pm 2.83\%$; NS) and lipids (-1.78 ± 7.46 vs. $-2.43 \pm 5.24\%$; NS).

At the end of the P-WLP, no significant differences (Dif V6–V9) were observed in the caloric profile between Lipigo® and Placebo groups when compared to baseline: carbohydrates (2.36 ± 7.89 vs. $-0.63 \pm 6.73\%$; NS), proteins (-1.64 ± 3.62 vs. $-0.36 \pm 3.16\%$; NS), and lipids (-0.29 ± 6.88 vs. $1.01 \pm 6.41\%$; NS).

3.5. Physical Activity Variables

Regarding physical activity (total METs), both Lipigo® and Placebo groups showed an increase in the WLP (Dif V0–V6, 530.37 ± 90.47 vs. 372.17 ± 981.91 METs; NS) and a decrease in P-WLP (Dif V6–V9, -186.48 ± 1035.93 vs. -224.89 ± 888.28 METs; NS). No significant differences were found between groups.

Specifically, sitting time was reduced in both Lipigo® and Placebo groups at the end of the WLP (Dif V0–V6, -1.05 ± 2.53 vs. -0.56 ± 2.25 h; NS). On the other hand, walking time was as increased in both groups (12.62 ± 45.05 vs. 21.71 ± 55.13 min; NS). No significant differences were found between groups.

3.6. Compliance and Adverse Events

When analyzing compliance, $88.2 \pm 8.04\%$ of the participants showed proper adherence to treatment. No serious adverse events were observed with Lipigo® consumption.

Bad breath, diarrhoea, constipation, bloating, nausea, and heartburn were documented as adverse events throughout the study. No differences were observed between treatment groups during all the study (V0–V9), except for Bloating having a significantly higher incidence in Lipigo® vs. Placebo group in V2 only (24.3 vs. 2.9% ; $p = 0.008$).

4. Discussion

This is the first randomized clinical trial conducted during 52 weeks (12 months) to study the effect of fibers combination supplement obtained from *S. cerevisiae* (Lipigo®) on weight loss after a 12 weeks Weight Loss Program (based in hypocaloric diet, physical activity recommendations, and nutritional education) and on rebound effect during 40 weeks follow-up.

The study demonstrates that three sticks/day of a polysaccharide-rich fraction (909 mg β -glucan, 91 mg chitin-chitosan) decrease significantly body weight and BMI after WLP only in OB1 subjects. Other BMI classifications (overweight or obese type II) reduce body weight and BMI classification but not significantly. Moreover, body weight, BMI, and waist circumference showed a slight reduction in Lipigo® group compared to Placebo after WLP, independently of BMI classification.

In a previous double-blinded, randomized study, Santas et al. showed that Lipigo® was beneficial in OB1 and overweight subjects. In that study, body weight and waist circumference were also reduced when compared to Placebo after 3 months of treatment. Importantly, participants were not enrolled in a body weight loss program [19]. Then, the present study results on body weight and waist circumference reduction support the efficacy of Lipigo® even when combined with a controlled diet.

Furthermore, a possible role of fiber combinations including β -glucan and chitin-chitosan on body weight loss in obese and overweight populations has been widely studied by others. Pittler et al., was the first group to perform a randomized, double-blinded, Placebo-controlled trial providing data on BMI and body weight from overweight subjects after fiber intake [30]. However, their results showed a non-significant effect for 1g/day of chitin-chitosan fibers on body weight or BMI reduction after 4 weeks of treatment. Despite that, other groups have evidenced short- and mid-term effects on body weight and BMI loss after longer administration periods of fibers combination including chitin-chitosan [31]. Two independent groups have published significant body weight and BMI reduction in obese population concomitantly following a calorie restriction and physical activity program [32,33]. The study design followed on both studies is the most similar to the present study. Nevertheless, subjects enrolled in previous studies underwent longer dietary and physical activity programs when compared to the present study (12 or 6 months vs 3 months).

The present study also showed a lean mass decrease after WLP. This result could be associated with a good adherence to the WLP and Lipigo® intake, instead of physical activity recommendations. Significant body weight loss was also achieved in other studies which provided a controlled diet but not physical activity advice [34–36]. However, the treatment period in these studies ranged from 2 to

6 months. In addition, the daily dosage of chitosan fibers (3 g) was supplemented with β -glucan and oat fibers more than betaine hydrochloride and aloe saponins in the Kaats et al. study [36]. Moreover, other studies have shown positive effects of a chitosan compound on the depletion of excess body fat under free-living conditions with minimal loss of fat-free or lean body mass [37,38]. Together, these findings suggest that β -glucan and/or chitosan combination fibers can impact body weight independently of physical activity.

To our knowledge, no previous studies have assessed the effect of β -glucan and chitosan treatments over rebound effect during a follow-up period after a weight loss program. The most highlighted result of this study is that OB1 subjects get the most benefit from consuming the product, not only during a 12 weeks weight loss program, but also decreasing the rebound effect especially in weight and BMI after 52 weeks (12 months) of starting the study including a 9 months follow-up period. This result could be due to the OB1 subjects included in the Lipigo group getting lower gain in anthropometric and body composition variables than the placebo groups during the 9 months follow-up period (P-WLP), although the differences were not significant.

OB1 subjects being the most benefited population from Lipigo[®] treatment may have several explanations. On the one hand, overweight non-obese participants have been previously associated with less interest in body weight reduction than the obese population [39,40]. This fact may lead to decreased motivation to strictly follow a calorie restriction diet. On the other hand, greater amounts of fat may increase the difficulty of losing weight [41]. This particularity might be the reason OB2 subjects are not getting a benefit from product consumption. However, the small OB2 sample size does not allow any firm conclusions to be drawn in this subgroup.

One limitation of the present study was that body composition was measured by bioimpedance electrical. This method is not a gold standard but is a method relatively simple, inexpensive, and non-invasive technique suitable in field studies. In fact, the European Society of Parenteral and Enteral Nutrition (ESPEN) suggests that BIA works well to evaluate body composition in healthy and ill subjects (including overweight and obese people), using validated BIA equation appropriate to age, sex and race [42]. This aspect has been considered in the present study.

In summary, these results support the efficacy of Lipigo[®] on body weight reduction as a concomitant and follow-up treatment to a controlled diet. Furthermore, we could for the first time demonstrate an important rebound effect reduction after 52 weeks (12 months) follow up period. Future studies with Lipigo[®] aim to investigate the ability of the product to improve serum lipid profile and other biochemical and cardiovascular risk factors.

5. Conclusions

Regular consumption of Lipigo[®] presented an adjuvant effect on body weight loss in the context of an individualized intervention, with a hypocaloric diet, physical activity practice, and nutritional education sessions. In this sense, the action of Lipigo[®] is more evident in OB1 participants undergoing a weight control program. Moreover, in OB1 subjects, Lipigo[®] intake reduced the rebound effect on body weight and BMI after 52 weeks (12 months) of starting the study including a 9 months follow-up period.

Based on the results obtained, the use of fiber mix from *S. cerevisiae* could be a complementary product to be included in weight control programs as well as in follow-up phases in obesity subjects.

Author Contributions: Conceptualization, L.M.B., B.L.-P. and C.G.-C.; Methodology, L.M.B.; Formal Analysis, M.V.-P. and B.L.-P.; Investigation, B.L.-P., L.M.B., C.G.-C. and M.V.-P.; Resources, S.P.-M.; Data Curation, M.V.-P.; Writing-Original Draft Preparation, M.V.-P., M.A.G. and L.M.B.; Writing-Review and Editing, B.L.-P., L.M.B., C.G.-C., M.V.-P. and M.A.G.; Visualization, S.P.-M., M.A.G.; Supervision, C.G.-C. and L.M.B., B.L.-P.; Project Administration, L.M.B., B.L.-P., and C.G.-C. All authors have read and agreed to the published version of the manuscript.

Funding: This study was supported by the DAMM S.A. group through the project RTC-2016-5317-1 from the RETOS COLABORACIÓN 2016 program of Economy and Competitiveness Ministry of Spain (MINECO).

Acknowledgments: We thank DAMM S.A. for the manufacture and supply of the experimental product (Lipigo®) and placebo. Also, thanks to the Biostatistics Department at the HULP for their continuous support.

Conflicts of Interest: M.A.G is a full-time employee of AB-Biotics SA, a company doing contract research work for DAMM SA. Other authors declare no conflicts of interest.

References

1. Inoue, Y.; Qin, B.; Poti, J.; Sokol, R.; Gordon-Larsen, P. Epidemiology of obesity in adults: Latest trends. *Curr. Obes. Rep.* **2018**, *7*, 276–288. [CrossRef] [PubMed]
2. GBD 2015 Obesity Collaborators; Afshin, A.; Forouzanfar, M.H.; Reitsma, M.B.; Sur, P.; Estep, K.; Lee, A.; Marcusak, L.; Mokdad, A.H.; Moradi-Lakeh, M.; et al. Health effects of overweight and obesity in 195 countries over 25 years. *N. Engl. J. Med.* **2017**, *377*, 13–27. [CrossRef] [PubMed]
3. Finucane, M.M.; Stevens, G.A.; Cowan, M.J.; Danaei, G.; Lin, J.K.; Paciorek, C.J.; Singh, G.M.; Gutierrez, H.R.; Lu, Y.; Bahalim, A.N.; et al. National, regional, and global trends in body-mass index since 1980: Systematic analysis of health examination surveys and epidemiological studies with 960 country-years and 9.1 million participants. *Lancet* **2011**, *377*, 557–567. [CrossRef]
4. Misra, A.; Khurana, L. Obesity and the metabolic syndrome in developing countries. *J. Clin. Endocrinol. Metab.* **2008**, *93*, S9–S30. [CrossRef]
5. Berger, N.A. Obesity and cancer pathogenesis. *Ann. N. Y. Acad. Sci.* **2014**, *1311*, 57–76. [CrossRef]
6. WHO. World Health Organization (WHO), Obesity and Overweight. Fact sheet. 2014. Available online: <http://www.who.int/mediacentre/factsheets/fs311/en/> (accessed on 16 January 2017).
7. Franks, P.W.; McCarthy, M.I. Exposing the exposures responsible for type 2 diabetes and obesity. *Science* **2016**, *354*, 69–73. [CrossRef] [PubMed]
8. Hooper, L.; Abdelhamid, A.; Moore, H.J.; Douthwaite, W.; Skeaff, C.M.; Summerbell, C.D. Effect of reducing total fat intake on body weight: Systematic review and meta-analysis of randomised controlled trials and cohort studies. *BMJ* **2012**, *345*, e7666. [CrossRef]
9. Kroeger, C.M.; Hoddy, K.K.; Varady, K.A. Impact of weight regain on metabolic disease risk: A review of human trials. *JObes* **2014**, *2014*, 614519. [CrossRef]
10. Loveman, E.; Frampton, G.K.; Shepherd, J.; Picot, J.; Cooper, K.; Bryant, J.; Welch, K.; Clegg, A. The clinical effectiveness and cost effectiveness of long-term weight management schemes for adults: systematic review. *Health Technol. Assess (Rockv)* **2011**, *15*, 1–6.
11. Poddar, K.; Kolge, S.; Bezman, L.; Mullin, G.E.; Cheskin, L.J. Nutraceutical supplements for weight loss: A systematic review. *Nutr. Clin. Pract.* **2011**, *26*, 539–552. [CrossRef]
12. Johansson, K.; Neovius, M.; Hemmingsson, E. Effects of anti-obesity drugs, diet and exercise on weight-loss maintenance after a very-low-calorie diet or low-calorie diet: A systematic review and meta-analysis of randomized controlled. *Am. J. Clin. Nutr.* **2014**, *99*, 14–23. [CrossRef] [PubMed]
13. Freimund, S.; Sauter, M.; Käppeli, O.; Dutler, H. A new non-degrading isolation process for 1,3- β -D-glucan of high purity from baker's yeast *Saccharomyces cerevisiae*. *Carbohydr. Polym.* **2003**, *54*, 159–171. [CrossRef]
14. El Khoury, D.; Cuda, C.; Luhovyy, B.L.; Anderson, G.H. Beta glucan: Health benefits in obesity and metabolic syndrome. *J. Nutr. Metab.* **2012**, *2012*, 851362. [CrossRef]
15. Stier, H.; Ebbeskotte, V.; Gruenwald, J. Immune-modulatory effects of dietary yeast beta-1,3/1,6-D-glucan. *Nutr. J.* **2014**, *13*, 38. [CrossRef]
16. Jung, E.Y.; Cho, M.K.; Hong, Y.H.; Kim, J.H.; Park, Y.; Chang, U.J.; Suh, H.J. Yeast hydrolysate can reduce body weight and abdominal fat accumulation in obese adults. *Nutrition* **2014**, *30*, 25–32. [CrossRef]
17. Nicolosi, R.; Bell, S.J.; Bistrian, B.R.; Greenberg, I.; Forse, R.A.; Blackburn, G.L. Plasma lipid changes after supplementation with beta-glucan fiber from yeast. *Am. J. Clin. Nutr.* **1999**, *70*, 208–212. [CrossRef] [PubMed]
18. Yanni, A.E.; Stamataki, N.S.; Konstantopoulos, P.; Stoupaki, M.; Abeliatis, A.; Nikolakea, I.; Perrea, D.; Karathanos, V.T.; Tentolouris, N. Controlling type-2 diabetes by inclusion of Cr-enriched yeast bread in the daily dietary pattern: A randomized clinical trial. *Eur. J. Nutr.* **2018**, *57*, 259–267. [CrossRef]
19. Santas, J.; Lazaro, E.; Cuñé, J. Effect of a polysaccharide-rich hydrolysate from *Saccharomyces cerevisiae* (LipiGo®) in body weight loss: Randomised, double-blind, placebo-controlled clinical trial in overweight and obese adults. *J. Sci. Food Agric.* **2017**, *97*, 4250–4257. [CrossRef]

20. Mancebo, R.; Castañé, X.; Cuñé, J.; Santas, J.; Rafecas, M.; Mirealles, M.; Mateos-Aparicio, I.; Heras, A. Fat-binder Obtained from Biomass Resulting from Beer Production. International application number: PCT/ES2013/070408. WO2014001589, 2014.
21. Puri, K.S.; Suresh, K.R.; Gogtay, N.J.; Thatte, U.M. Declaration of Helsinki, 2008: Implications for stakeholders in research. *J. Postgrad. Med.* **2009**, *55*, 131–134.
22. Spanish Society of Community Nutrition (SENC). Healthy nutrition Guide. Madrid: SENC. 2016. Available online: <https://www.nutricioncomunitaria.org/es/noticia/guias-alimentarias-senc-2016> (accessed on 29 June 2020).
23. Wycherley, T.P.; Moran, L.J.; Clifton, P.M.; Noakes, M.; Brinkworth, G.D. Effects of energy-restricted high-protein, low-fat compared with standard protein, low-fat diets: A meta-analysis of randomized controlled trials. *Am. J. Clin. Nutr.* **2012**, *96*, 1281–1298. [[CrossRef](#)]
24. WHO/FAO. *Methodology of Nutritional Surveillance. Report of a Joint FAO/UNICEF/WHO Expert Committee*; The World Health Organization Technical Report Series; WHO/FAO: Geneva, Switzerland, 1976.
25. Sun, S.S.; Chumlea, W.C.; Heymsfield, S.B.; Lukaski, H.C.; Schoeller, D.; Friedl, K.; Kuczmarski, R.J.; Flegal, K.M.; Johnson, C.L.; Hubbard, V.S. Development of bioelectrical impedance analysis prediction equations for body composition with the use of a multicomponent model for use in epidemiologic surveys. *Am. J. Clin. Nutr.* **2003**, *77*, 331–340. [[CrossRef](#)] [[PubMed](#)]
26. Dehghan, M.; Merchant, A.T. Is bioelectrical impedance accurate for use in large epidemiological studies? *Nutr. J.* **2008**, *7*, 26. [[CrossRef](#)]
27. Ortega, R.M.; Requejo, A.M.; López-Sobaler, A.M. Models of questionnaires for dietary studies, in the assessment of nutritional status. In *Nutriguía Manual of Clinical Nutrition in Primary Care*; Ortega, R.M., Requejo, A.M., Eds.; Complutense: Madrid, India, 2006; pp. 456–467.
28. Group USA Spanish Version Translated 3/2003-Short Last 7 Days Self-Administered Version of the International Physical Activity Questionnaire (IPAQ) IPAQ-Revised August 2002. Available online: www.ipaq.ki.se (accessed on 29 June 2020).
29. Dombrowski, S.U.; Knittle, K.; Avenell, A.; Araújo-Soares, V.; Sniehotta, F.F. Long term maintenance of weight loss with non-surgical interventions in obese adults: Systematic review and meta-analyses of randomised controlled trials. *BMJ* **2014**, *348*, g2646. [[CrossRef](#)]
30. Pittler, M.; Abbot, N.; Harkness, E.; Ernst, E. Randomized, double-blind trial of chitosan for body weight reduction. *Eur. J. Clin. Nutr.* **1999**, *53*, 379–381. [[CrossRef](#)] [[PubMed](#)]
31. Moraru, C.; Mincea, M.M.; Frandes, M.; Timar, B.; Ostafe, V. A Meta-Analysis on Randomised Controlled Clinical Trials Evaluating the Effect of the Dietary Supplement Chitosan on Weight Loss, Lipid Parameters and Blood Pressure. *Medicina* **2018**, *54*, 109. [[CrossRef](#)] [[PubMed](#)]
32. Cornelli, U.; Belcaro, G.; Recchia, M.; D’Orazio, N. Long-Term Treatment of Overweight and Obesity with Polyglucosamine (PG L112): Randomized Study Compared with Placebo in Subjects after Caloric Restriction. *Curr. Dev. Nutr.* **2017**, *1*, e000919. [[CrossRef](#)]
33. Pokhis, K.; Bitterlich, N.; Cornelli, U.; Cassano, G. Efficacy of polyglucosamine for weight loss-confirmed in a randomized double-blind, placebo-controlled clinical investigation. *BMC Obes.* **2015**, *2*, 25. [[CrossRef](#)]
34. Cornelli, U.; Belcaro, G.; Cesarone, M.R.; Cornelli, M. Use of polyglucosamine and physical activity to reduce body weight and dyslipidemia in moderately overweight subjects. *Minerva Cardioangiol.* **2008**, *56* (Suppl. 5), 71–78. [[PubMed](#)]
35. Trivedi, V.R.; Satia, M.C.; Deschamps, A.; Maquet, V.; Shah, R.B.; Zinzuwadia, P.H.; Trivedi, J.V. Single-blind, placebo controlled randomised clinical study of chitosan for body weight reduction. *Nutr. J.* **2016**, *15*, 3. [[CrossRef](#)]
36. Mhurchu, C.N.; Poppitt, S.D.; McGill, A.; Leahy, F.E.; Bennett, D.A.; Lin, R.B.; Ormrod, D.; Ward, L.; Strik, C.; Rodgers, A. The effect of the dietary supplement, Chitosan, on body weight: A randomised controlled trial in 250 overweight and obese adults. *Int. J. Obes. Relat. Metab. Disord.* **2004**, *28*, 1149–1156. [[CrossRef](#)]
37. Kaats, G.R.; Michalek, J.E.; Preuss, H.G. Evaluating Efficacy of a Chitosan Product Using a Double-Blinded, Placebo-Controlled Protocol. *J. Am. Coll. Nutr.* **2006**, *25*, 389–394. [[CrossRef](#)] [[PubMed](#)]
38. Woodgate, D.E.; Conquer, J.A. Effects of a stimulant-free dietary supplement on body weight and fat loss in obese adults: A six-week exploratory study. *Curr. Ther. Res. Clin. Exp.* **2003**, *64*, 248–262. [[CrossRef](#)]

39. Duncan, D.; Colin, K.; Scharoun-Lee, M.; Ding, E.; Warner, E.; Bennett, G. Does perception equal reality? Weight misperception in relation to weight-related attitudes and behaviors among overweight and obese US adults. *Int. J. Behav. Nutr. Phys. Act.* **2011**, *8*, 20. [[CrossRef](#)] [[PubMed](#)]
40. Coleman, L.; Loprinzi, P.D. The association between discrepant weight perceptions and objectively measured physical activity. *Prev. Med.* **2016**, *87*, 47–50. [[CrossRef](#)] [[PubMed](#)]
41. Rashad, N.M.; Sayed, S.E.; Sherif, M.H.; Sitohy, M.Z. Effect of a 24-week weight management program on serum leptin level in correlation to anthropometric measures in obese female: A randomized controlled clinical trial. *Diabetes Metab. Syndr. Clin. Res. Rev.* **2019**, *13*, 2230–2235. [[CrossRef](#)]
42. Kyle, U.G.; Bosaeus, I.; De Lorenzo, A.D.; Deurenberg, P.; Elia, M.; Manuel Gómez, J.; Lilienthal Heitmann, B.; Kent-Smith, L.; Melchior, J.C.; Pirlich, M.; et al. Bioelectrical impedance analysis-part II: Utilization in clinical practice. *Clin. Nutr.* **2004**, *23*, 1430–1453. [[CrossRef](#)]



© 2020 by the authors. Licensee MDPI, Basel, Switzerland. This article is an open access article distributed under the terms and conditions of the Creative Commons Attribution (CC BY) license (<http://creativecommons.org/licenses/by/4.0/>).

Article

Raspberry Ketone [4-(4-Hydroxyphenyl)-2-Butanone] Differentially Effects Meal Patterns and Cardiovascular Parameters in Mice

Dushyant Kshatriya ^{1,2}, Lihong Hao ², Xinyi Li ^{1,2} and Nicholas T. Bello ^{1,2,*}

¹ Nutritional Sciences Graduate Program, School of Environmental and Biological Sciences, Rutgers, The State University of New Jersey, New Brunswick, NJ 08901, USA; dsk118@scarletmail.rutgers.edu (D.K.); cindy.x.li@rutgers.edu (X.L.)

² Department of Animal Sciences, School of Environmental and Biological Sciences, Rutgers, The State University of New Jersey, New Brunswick, NJ 08901, USA; haoli@sebs.rutgers.edu

* Correspondence: ntbello@sebs.rutgers.edu; Tel.: +1-848-932-2966

Received: 1 May 2020; Accepted: 9 June 2020; Published: 11 June 2020

Abstract: Raspberry ketone (RK; [4-(4-hydroxyphenyl)-2-butanone]) is a popular nutraceutical used for weight management and appetite control. We sought to determine the physiological benefits of RK on the meal patterns and cardiovascular changes associated with an obesogenic diet. In addition, we explored whether the physiological benefits of RK promoted anxiety-related behaviors. Male and female C57BL/6J mice were administered a daily oral gavage of RK 200 mg/kg, RK 400 mg/kg, or vehicle for 14 days. Commencing with dosing, mice were placed on a high-fat diet (45% fat) or low-fat diet (10% fat). Our results indicated that RK 200 mg/kg had a differential influence on meal patterns in males and females. In contrast, RK 400 mg/kg reduced body weight gain, open-field total distance travelled, hemodynamic measures (i.e., reduced systolic blood pressure (BP), diastolic BP and mean BP), and increased nocturnal satiety ratios in males and females. In addition, RK 400 mg/kg increased neural activation in the nucleus of the solitary tract, compared with vehicle. RK actions were not influenced by diet, nor resulted in an anxiety-like phenotype. Our findings suggest that RK has dose-differential feeding and cardiovascular actions, which needs consideration as it is used as a nutraceutical for weight control for obesity.

Keywords: frambinone; meal frequency; open-field test; elevated plus maze; sensory motor gating; pre-pulse inhibition; c-Fos

1. Introduction

Raspberry ketone (RK; 4-(4-hydroxyphenyl)-2-butanone) is a naturally occurring phenolic compound responsible for the aroma and flavor of raspberries (*Rubus idaeus*) [1,2]. Naturally derived RK is costly to produce, therefore synthetic sources of RK are readily available [3,4]. In the United States, RK is designated as a generally recognized as safe (GRAS) food additive and is listed by the Food and Drug Administration (FDA) as a synthetic flavoring substance [5]. Recently, RK has been marketed as a weight loss agent and an appetite suppressant, and used as single- or multi-ingredient supplement [6–9].

A few studies reveal the efficacy of RK in the prevention of fat accumulation. RK has been shown to reduce lipid accumulation and alter expression of lipolytic and adipogenic genes in 3T3-L1 adipocytes [10–14]. Further, it can increase fat oxidation in vitro and the effect may be mediated by heme oxygenase-1 and brown-like adipocyte formation [13,14]. RK mitigated ovariectomy-induced weight gain [12,14], and reduced high-fat diet induced nonalcoholic steatohepatitis in rats [15]. Adulteration of diet with RK has shown to prevent weight gain [16,17], however, the strong sensory profile of RK could

have potentially affected food intake. Previous work from our lab supports the preventative actions of oral gavage administration of RK against weight gain and fat accumulation in a high-fat diet induced obesogenic environment [18]. Along with management of weight gain, RK can serve cardio protective roles. RK pretreatment reduced isoproterenol-induced cardiac tissue damage and dyslipidemia [19,20]. Because obesity therapeutic agents often are associated with adverse cardiovascular events [21], the RK doses that prevent weight gain should also be examined for their hemodynamic effects. Indeed, weight loss nutraceuticals are typically consumed on a long-term basis for several months, therefore, understanding the cardiovascular risks and benefits are critical for their assessment.

Diet-induced obesity often involves hyperphagia and changes in feeding patterns such as increased meal frequency and meal size [22,23]. Therefore, it is valuable to understand the influence of RK, as a preventative weight loss agent, on meal patterns. The present study was designed to characterize the dose-dependent effect of RK on meal microstructure in male and female mice. In addition, we assessed the interaction of diet and RK dose on hemodynamic parameters. We hypothesized that there would be a dose-dependent preventative effect of RK on the high-fat diet-induced alterations in meal patterns and cardiovascular outcomes. Because weight changes have been associated with anxiogenic or antipsychotic agents [24,25], we also conducted a series of behavioral tests to determine whether the effects were secondary to an anxiogenic effect of RK or impairments in sensory-motor gating.

Previous bioavailability studies from our laboratory have shown that oral RK is rapidly absorbed and a 200 mg/kg dose can peak in the plasma after 15 min in male and female mice [26]. In addition, RK and metabolites were detected in the brain and white adipose tissue of normal weight and diet-induced obese mice [27]. While there is accumulating evidence that RK has direct actions in adipose tissue [10,11,13], the ability of RK to activate brain areas involved in feeding and cardiovascular control has not been explored. One central site that overlaps to regulate these two physiological systems, is the nucleus of the solitary tract (NTS) in the caudal hindbrain [28–30]. Therefore, we examined whether RK, at doses that influence meal patterns and hemodynamic parameters, also activates the NTS and associated area postrema (AP).

2. Materials and Methods

2.1. Mice

A total of 270 male and female C57BL/6J mice (7 weeks old) were purchased from The Jackson Laboratory (Bar Harbor, ME, USA). Mice were fed ad libitum standard chow (Purina Mouse Diet 5015, St. Louis, MO, USA; 25.34% fat, 19.81% protein, 54.86% carbohydrate, 3.7 kcal/g) upon arrival. One week later, mice (8 weeks old) were equally divided by body weight and were switched to a high-fat diet (HFD; D12451, Research Diets, Inc., New Brunswick, NJ; 45% fat, 20% protein, 35% carbohydrate; 4.73 kcal/g) or sucrose-matched control diet (LFD; D12450H; Research Diets, Inc., New Brunswick, NJ; 10% fat, 20% protein, 70% carbohydrate; 3.85 kcal/g) and fed ad libitum. Water was available at all times. Mice were single-housed, unless otherwise noted, and maintained on a 12-h light and 12-h dark cycle with lights on from 07:00 h to 19:00 h. The animal care protocol was approved by the Institutional Animal Care and Use Committee of Rutgers University (OLAW #A3262-01). Coincident with the diet switch, daily oral dosing was initiated in mice with the following treatments: vehicle (VEH; 50% propylene glycol, 40% water, and 10% dimethyl sulfoxide (DMSO) or raspberry ketone (RK, 200 mg/kg or 400 mg/kg; (4[4-hydroxyphenyl]-2-butanone; 99%; cat#178519; Sigma Aldrich). A reference sample from each lot number of raspberry ketone batch was deposited in a secure, climate-controlled repository [31]. Oral dosing of the mice was performed using single-use, sterile plastic feeding tubes (20 ga × 30 mm; cat# FTP-20-30, Instech Laboratories, Plymouth Meeting, PA, USA). Mice were fed the individual diets and oral dosed for 2 weeks, unless otherwise noted. Daily body weight and cumulative food intake were measured throughout the entire dosing period. Daily dosing was performed between 10:00h and 12:00h. Mice were divided into six groups based on diet and

dose; HFD-Vehicle, LFD-Vehicle, HFD-RK (200 mg/kg), LFD-RK (200 mg/kg), HFD-RK (400 mg/kg), and LFD-RK (400 mg/kg), see Supplementary Materials Figure S1.

2.2. Meal Patterns and Meal Microstructures

Meal microstructures were analyzed in male and female C57BL/6J mice ($n = 4 - 16$ per group/sex) using the Biological Data Acquisition System (BioDAQ; Research Diets, New Brunswick, NJ, USA). This system utilizes standard shoe-box style cages with a gated front-mounted food hopper. The gated hopper sits upon a sensor that detects net changes in food weight per second. A feeding bout was defined as a change in stable weight of the hopper. Bouts were clustered into meals, defined by an inter-meal interval of 300 s and a minimum of 0.02 g consumed. Meal patterns were measured over the entire two-week period. Data were analyzed and averaged over the 14-day period and presented separately for the dark-cycle (nocturnal) and light-cycle (diurnal). Data recordings in the BioDAQ computer were paused when the mice were handled for measurement of body weight and dosing. Daily data were used to calculate, meal frequency (meals/day), meal size (kcal), meal duration (min/meal), eating rate (kcal/min), and satiety ratio (Inter meal interval (min)/kcal). Mice that demonstrated food shredding were not included in the analyses [18].

2.3. Anxiety-Related and Sensorimotor Gating Behavioral Testing

After the BioDAQ data collection, mice were kept in their respective diet and daily dosing groups for an additional 8 days and exposed to three behavioral tests. Mice were exposed to the following tests, one teste per day in the following order: open field test (Days 18–20), elevated plus maze (Days 19–21), and pre-pulse inhibition (Days 20–22). Daily dosing and diet regimen continued until completion of all behavioral tests. Daily testing times were staggered and were performed >1 h after mice received their respective daily dose.

2.3.1. Open Field

The open field tests took place in a brightly lit box ($40 \times 40 \times 38$ cm) with white floors and luminescent walls. Mice were placed in the center of the apparatus for a ten-minute test period. Measurements of locomotion, exploration, and anxiety were video recorded and scored offline by an individual blinded to the grouping of the study [32].

2.3.2. Elevated Plus Maze

Mice were exposed to the elevated plus maze apparatus for 5 min. The elevated plus maze apparatus has two open arms ($25 \times 5 \times 0.5$ cm) across from each other and perpendicular to two closed arms ($25 \times 5 \times 16$ cm) with a center platform ($5 \times 5 \times 0.5$ cm) and is 50 cm above the floor. At the commencement of the test, each mouse was placed at the junction of the open and closed arms and faced the open arm. The number of entries into open and closed arms, risk assessment, number of feces, and self-grooming behavior were video recorded for five minutes and scored offline by an individual blinded to the study [33].

2.3.3. Pre-Pulse Inhibition

Each pre-pulse inhibition session was conducted in a ventilated soundproof startle chamber (Med Associates Inc., Fairfax, VT, USA) and proceeds with a 5-min acclimation period with 70 dB background noise followed by five successive 110 dB trials for habituation. Six different trial types were then presented: startle pulse (ST110, 110 dB/40 ms), low prepulse stimulus given alone (P74, 74 dB/20 ms), high prepulse stimulus given alone (P90, 90 dB/20 ms), P74 or P90 given 100 ms before the onset of the startle pulse (PP74 and PP90, respectively), and finally a trial where only the background noise was presented in order to measure the baseline movement in the cylinders. All trials were applied

ten times and presented in random order (P74 and P90 were only given five times) and the average inter-trial interval was 15 s (10–20 s) [34].

2.4. Hemodynamic Measures

In a separate set of male and female C57BL/6J mice ($n = 11\text{--}12$ per group/sex) measurements of hemodynamic parameters were performed using the noninvasive blood pressure CODA system (Kent Scientific, Torrington, CT, USA) system. This computerized system measures systolic and diastolic blood pressure, mean blood pressure, and heart rate via tail volume pressure recordings. Animals were acclimated to the holder and cuff of the CODA system for 5 min before each recording trial. CODA trials were performed 1–2 h after daily dosing of either RK or vehicle. Animals were exposed to 5 consecutive days of recording trials, data from the last 2 days were used for data analysis (i.e., days 13 and 14 of the 2-week dosing period), see Supplementary Materials Figure S2.

2.5. Immunohistochemistry of Area Postrema (AP) and Nucleus of The Solitary Tract (NTS)

A separate set of male C57BL/6J mice ($n = 5\text{--}6$ per group) were dosed with RK (400 mg/kg) or vehicle for 14 days. On day 14, all mice were returned to their cage without food or water and left undisturbed for 120 min. Mice were then deeply anesthetized with 0.1% euthasol (pentobarbital sodium and phenytoin sodium) solution intraperitoneal (IP), exsanguinated with 0.9% saline, and perfused with 4% paraformaldehyde in phosphate buffered saline (PBS). Brains were extracted and post-fixed for 24 h in 4% paraformaldehyde in PBS, then switched to 20% sucrose in 4% paraformaldehyde until sectioning. Free-floating sections (40 μm) of the forebrain were obtained by using a Leica cryostat (Leica Microsystems, Rijswijk, The Netherlands). Sections were stored in cryoprotectant until immunohistochemistry was performed. Sections were transferred to a new clean plate containing PBS (10 mM phosphate, 150 mM NaCl, pH 7.5). Initial PBS was removed, sections were then washed 3×10 min in PBS. Endogenous peroxidases were neutralized with 0.3% H_2O_2 in dH_2O . After a 3×10 min PBS wash, sections were incubated in normal goat serum (PK-4001, Vectastain ABC kit, Vector Laboratories, Burlingame, CA, USA) with 0.3% Triton-X-100 in PBS for 30 min. c-Fos immunolabeling was performed with a polyclonal rabbit IgG anti c-Fos antibody (ab190289, Abcam, Cambridge, MA, USA), diluted 1:100 in PBS. Tissue sections were incubated overnight (~20 h). Sections were transferred to a new clean plate, washed 3×10 min in 0.1% Triton X-100 in PBS, then incubated for 30 min in biotinylated secondary antibody (goat IgG anti-rabbit, PK-4001, Vectastain ABC kit, Vector Laboratories) with 0.3% Triton X-100 in PBS. After 3×10 min wash in PBS, sections were incubated in an avidin-peroxidase complex (PK-4001, Vectastain ABC kit, Vector Laboratories) for 45 min. Sections were washed 3×10 min in PBS. Staining was performed using nickel diaminobenzidine tetrahydrochloride (Ni-DAB) Chromagen (SK-4100, DAB Peroxidase Substrate Kit, 3,3'-diaminobenzidine, Vector Laboratories) for approximately 30 s to stain Fos-like products black. PBS was added immediately after desired stain was reached and sections were washed in 3×10 min in PBS to halt the Ni-DAB reaction. Sections were mounted on gelatin-coated slides (Fisherbrand Double Frosted Microscope Slides, Thermo Fisher Scientific Inc., Bridgewater, NJ, USA) and dehydrated with ethanol and xylenes prior to coverslipping with permount [35], see Supplementary Materials Figure S3.

2.6. Imaging and Quantification of C-Fos Positive Nuclei

Coronal sections from area postrema (AP) and four rostrocaudal levels of the nucleus of the solitary tract (NTS) were analyzed per animal. The anterior-posterior levels were determined by coordinates from Bregma [36]. The NTS areas consisted of anatomically matched sections from caudal (cNTS; -7.92 mm), at the level of the obex, corresponding to the posterior edge of the AP; medial (mNTS; -7.48 mm) at the maximal extent of the AP; intermediate (iNTS; -7.08 mm), anterior to the AP, corresponding to the maximal extent of the gelatinous subnucleus of the NTS; rostral (rNTS; -6.84 mm) consisting of the area rostral to the gelatinous nucleus and the caudal aspect of the medial vestibular nucleus on the dorsal boundary [36]. This analysis provided a view for the rostral-caudal extent

of c-Fos activation [29]. Imaging was performed using an Olympus FSX-BSW imaging scope and FSX100 software (Olympus videoscope, Tokyo, Japan). Quantification was performed by identifying c-Fos positive black nuclei using Image J software system (NIH, Bethesda, MD, USA) image analysis software. Three anatomically matched tissue slices of each region (unilateral) of each mouse were used in data analysis. Cells were counted by two observers blinded to the experimental conditions [35].

2.7. Statistical Analyses

Data are presented as means \pm standard error of the mean (SEM). Separate two-way analysis of variance (ANOVA) or two-way ANOVA with repeated measures were performed to determine the effects of treatment conditions on individual measured parameters. When justified, Newman-Keuls post-hoc tests were performed unless otherwise specified. All statistical and power analyses were performed using Statistica 7.1 software (StatSoft; Dell Inc, Round Rock, TX, USA) and significance was set at $\alpha = 0.05$.

3. Results

3.1. Bodyweights Over 14-Day Dosing and Diet Access

At the start of the experiments and group assignment, males baseline body weights were 23.2 ± 0.3 g for HFD-Vehicle, 23.3 ± 0.5 g for HFD-RK (200 mg/kg), 23.3 ± 0.5 g for HFD-RK (400 mg/kg), 23.1 ± 0.4 g for LFD-Vehicle, 23.6 ± 0.4 g for LFD-RK (200 mg/kg), and 23.1 ± 0.6 g for LFD-RK (400 mg/kg). For body weight gain over the 14-day diet and dosing regimen, there were effects for diet ($F(1, 58) = 9.6, p < 0.005$) and dose ($F(2, 58) = 6.9, p < 0.005$), days ($F(12, 696) = 37.9, p < 0.005$) and dose \times days ($F(24, 696) = 2.2, p < 0.001$). There was increased body weight gain in the HFD fed male mice ($p < 0.05$). The 400 mg/kg dose produced an overall reduction in body weight gain over the 14-days for males ($p < 0.05$) compared with vehicle dose. There were body weight reductions with 400 mg/kg, compared with vehicle, for days 2–5 of dosing ($p < 0.05$ for all days), see Figure 1A. For females, baseline body weights were 18.3 ± 0.5 g for HFD-Vehicle, 18.1 ± 0.3 g for HFD-RK (200 mg/kg), 18.2 ± 0.4 g for HFD-RK (400 mg/kg), 18.4 ± 0.4 g for LFD-Vehicle, 17.8 ± 0.5 g for LFD-RK (200 mg/kg), and 17.9 ± 0.4 g for LFD-RK (400 mg/kg). For body weight gain there were effects for diet ($F(1, 41) = 4.2, p < 0.05$), dose ($F(2, 41) = 3.2, p < 0.05$), and days ($F(12, 492) = 43.0, p < 0.0005$). There was an increase in body weight gain in the HFD fed female mice ($p < 0.05$). The 400 mg/kg dose produced a reduction in body weight gain, compared with 200 mg/kg, over the 14-days for females ($p < 0.05$), see Figure 1B.

3.2. Meal Pattern Analysis Over 14 Days Dosing and Diet Access

For nocturnal meal frequency, in males there were diet ($F(1, 54) = 22.9, p < 0.005$) and dose ($F(1, 54) = 13.5, p < 0.005$) effects. More meals were consumed in male mice with HFD than LFD ($p < 0.001$). Fewer meals were consumed by RK 200 mg/kg ($p < 0.001$) and RK 400 mg/kg ($p < 0.05$) dosed mice, compared with vehicle. In females, there were diet ($F(1, 34) = 46.9, p < 0.001$) and dose ($F(2, 34) = 11.9, p < 0.05$) effects. More meals were consumed in female mice with HFD than LFD ($p < 0.05$). More meals were consumed with RK 200 mg/kg compared with RK 400 mg/kg ($p < 0.001$) and vehicle ($p < 0.05$), see Figure 2A. For nocturnal meal size, in males there was a dose ($F(2, 54) = 7.6, p < 0.05$) effect. Meal sizes were increased by RK 200 mg/kg ($p < 0.05$). In females, there were diet ($F(1, 34) = 9.6, p < 0.001$) and dose ($F(2, 34) = 4.3, p < 0.05$) effects. Meal sizes were increased by LFD ($p < 0.05$) and decreased by RK 200 mg/kg compared with RK 400 mg/kg and vehicle ($p < 0.05$ for both). For nocturnal meal duration, in males there were diet ($F(1, 54) = 56.5, p < 0.001$) and dose ($F(2, 54) = 11.3, p < 0.001$) effects. Meal duration was shorter with HFD compared with LFD ($p < 0.005$) and RK 200 mg/kg dose increased meal duration ($p < 0.001$). In females, there was a diet effect ($F(1, 34) = 30.7, p < 0.005$) for meal duration. Meal duration was shorter with HFD ($p < 0.05$), see Figure 2C. For nocturnal eating rate, in males there were diet ($F(1, 54) = 18.9, p < 0.001$) and

dose ($F(2, 54) = 4.9, p < 0.05$) effects. There was an increase in eating rate with HFD ($p < 0.001$), and RK 400 mg/kg had a higher eating rate compared with VEH and RK 200 mg/kg ($p < 0.05$ for both). In females, there were diet ($F(1, 32) = 43.6, p < 0.005$) and diet X dose ($F(2, 32) = 4.4, p < 0.05$) effect for eating rate. In HFD, there was increase in eating rate compared with LFD ($p < 0.005$) and 200 mg/kg had the highest eating rate of all groups ($p < 0.05$), see Figure 2D. For nocturnal satiety ratio, in males, there were diet ($F(1, 54) = 5.2, p < 0.05$) and dose ($F(2, 54) = 6.2, p < 0.005$) effects. Satiety ratio was higher in male mice fed HFD than LFD ($p < 0.05$). RK 200 mg/kg and 400 mg/kg increased satiety ratio compared with vehicle ($p < 0.05$ for both). For satiety ratio in females, there was a dose effect ($F(2, 32) = 5.9, p < 0.05$), with higher satiety ratio in female mice receiving RK 400 mg/kg ($p < 0.05$), see Figure 2E.

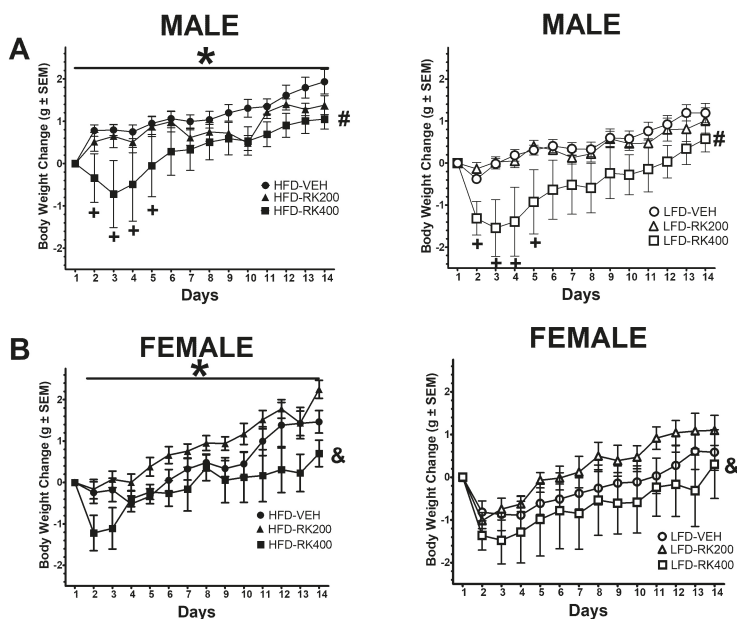


Figure 1. Body weight change in grams over the 14 days of diet access and oral RK dosing compared with baseline. Data are represented as means \pm standard error of the mean (SEM). High-fat diet (45% fat; HFD, solid symbols) and low-fat diet (10% fat; LFD, open symbols) and oral gavage with raspberry ketone (RK) or vehicle (50% propylene glycol, 40% water, and 10% dimethyl sulfoxide; DMSO) for 14 days. Comparisons are separate within each sex. (A): Males, (B): Females. * indicates overall diet difference from LFD ($p < 0.05$), # indicates overall difference from all other doses ($p < 0.05$), + indicates overall daily dose difference from VEH dose ($p < 0.05$), & indicates overall dose difference from 200 mg/kg dose ($p < 0.05$). HFD-Vehicle (males: $n = 16$, females $n = 8$), HFD-RK (200 mg/kg) (males: $n = 8$, females: $n = 8$), HFD-RK (400 mg/kg) (males: $n = 8$, females: $n = 7$), LFD-Vehicle (males: $n = 16$, females: $n = 8$) LFD-RK (200 mg/kg)(males: $n = 8$, females: $n = 8$), and LFD-RK (400 mg/kg)(males: $n = 8$, females: $n = 8$).

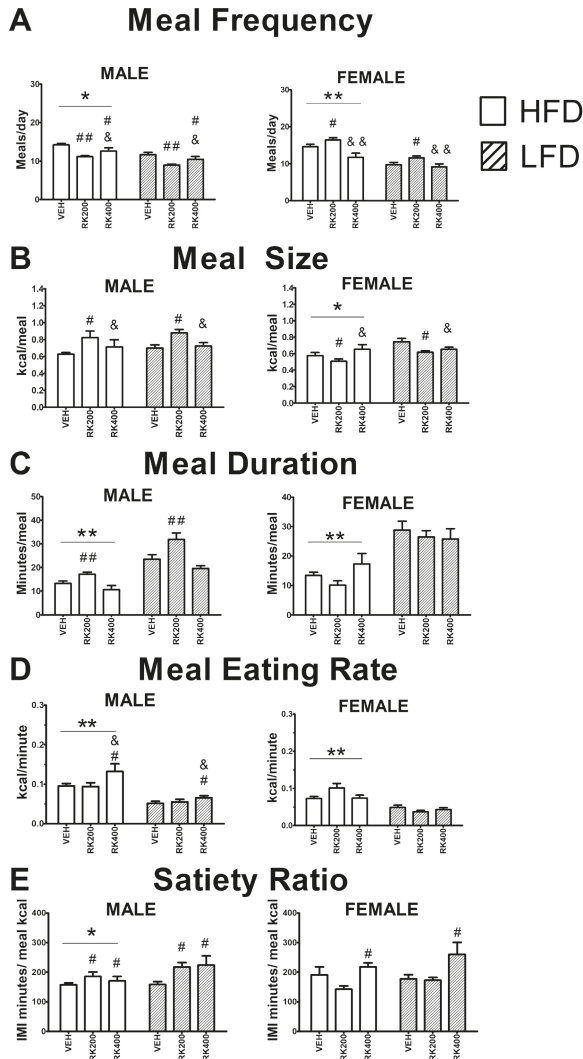


Figure 2. Average meal patterns over the 14 days of daily oral RK and diet access. Meal patterns are from the nocturnal period. Data are represented as means ± standard error of the mean (SEM). High-fat diet (45% fat; HFD, solid lines) and low-fat diet (10% fat; LFD, striped line) and oral gavage with raspberry ketone (RK) or vehicle (50% propylene glycol, 40% water, and 10% dimethyl sulfoxide; DMSO) for 14 days. Comparisons are separate within each sex. Meal patterns were averaged over fourteen days of dosing and diet exposure. (A): Meal frequency; average number of meals each day, (B): meal size (kcal), (C): meal duration (min), (D): meal eating rate (kcal/min), and (E): satiety ratio (inter meal interval in min/kcal). * indicates overall diet difference from LFD ($p < 0.05$), ** indicates overall diet difference from LFD ($p < 0.005$), # indicates overall dose difference from vehicle ($p < 0.05$), ## indicates overall dose difference from vehicle ($p < 0.01$), && indicates overall dose difference from RK200 dose ($p < 0.001$), & indicates overall dose difference from RK200 dose ($p < 0.05$). HFD-Vehicle (males: $n = 14$, females $n = 4$, HFD-RK (200 mg/kg) (males: $n = 8$, females: $n = 6$), HFD-RK (400 mg/kg) (males: $n = 7$, females: $n = 6$), LFD-Vehicle (males: $n = 16$, females: $n = 8$) LFD-RK (200 mg/kg)(males: $n = 7$, females: $n = 8$), and LFD-RK (400 mg/kg)(males: $n = 8$, females: $n = 8$).

There were no effects of treatment on diurnal meal size, meal duration, and satiety ratio, in male mice. For meal frequency, there was diet X dose ($F(2, 54) = 3.5, p < 0.05$) effect, with an increased meal number in male mice receiving HFD and RK 200 mg/kg. There was a diet effect on eating rate ($F(1, 54) = 11.6, p < 0.05$), with a higher rate in HFD fed mice. There were no effects of treatment on diurnal meal frequency, satiety ratio and eating rate in female mice. There was an effect of dose ($F(2, 34) = 6.9, p < 0.05$) on diurnal meal size, with an increase in RK 400 mg/kg compared with RK 200 mg/kg and vehicle ($p < 0.05$ for both). For diurnal meal duration in female, there was an effect of diet ($F(1, 34) = 18.7, p < 0.005$), with shorter meals in HFD compared with LFD fed mice.

At the end of the 14-day meal pattern analysis the male cumulative food intake was 147.3 ± 2.8 kcal for HFD-Vehicle, 137.3 ± 2.2 kcal for HFD-RK (200 mg/kg), 136.2 ± 4.3 kcal for HFD-RK (400 mg/kg), 130.9 ± 3.2 kcal for LFD-Vehicle, 135.5 ± 2.3 kcal for LFD-RK (200 mg/kg), and 132.1 ± 13.6 kcal for LFD-RK (400 mg/kg). The female cumulative food intake was 177.5 ± 12.3 kcal for HFD-Vehicle, 175.3 ± 4.7 kcal for HFD-RK (200 mg/kg), 156.1 ± 7.1 kcal for HFD-RK (400 mg/kg), 152.2 ± 9.4 kcal for LFD-Vehicle, 149.5 ± 3.1 kcal for LFD-RK (200 mg/kg), and 133.1 ± 6.6 kcal for LFD-RK (400 mg/kg). There was no effect of treatment on cumulative food intake.

3.3. Open-Field After 14 Days of Dosing and Diet Access

For time spent in center, in males there was an effect of dose ($F(2, 55) = 5.6, p < 0.01$). Male RK 200 mg/kg mice spent more time in the center of the open field than VEH ($p < 0.05$) and RK 400 mg/kg ($p < 0.01$), see Figure 3A. There was a significant effect of dose ($F(2, 55) = 5.8, p < 0.01$) on the number of entries into the outer zone in male mice, with RK 400 mg/kg mice entering the outer zone fewer times than VEH ($p < 0.01$). Similarly, dose ($F(2, 41) = 5.2, p < 0.05$) had a significant effect on number of entries of female mice into outer zone, with RK 400 mg/kg mice entering the outer zone fewer times than VEH ($p < 0.05$) and RK 200 mg/kg ($p < 0.05$) mice, see Figure 3B. Whereas, in male mice both dose ($F(2, 55) = 6.7, p < 0.01$) and diet ($F(1, 55) = 10.0, p < 0.01$) had an effect on total distance travelled. RK 400 mg/kg treated male mice travelled less than VEH ($p < 0.01$), and HFD mice overall travelled less than LFD mice ($p < 0.05$). Dose ($F(2, 41) = 3.4, p < 0.05$) had a significant effect on total distance travelled by female mice, with RK 400 mg/kg mice travelling less than RK 200 mg/kg, see Figure 3C.

3.4. Elevated Plus Maze After 14 Days of Dosing and Diet Access

Dose ($F(2, 56) = 4.1, p < 0.05$) had a significant effect on time spent in the open arms by male mice, with RK400 mice spending less time than VEH ($p < 0.05$) in open arms, see Figure 4A. There was a significant effect of dosing ($F(2, 56) = 6.5, p < 0.01$) on number of entries into open arms, with RK400 mice entering the open arms less frequently than VEH ($p < 0.01$), see Figure 4C. There were no significant effects of dosing or diet on elevated plus maze parameters of female mice, Figure 4A–D.

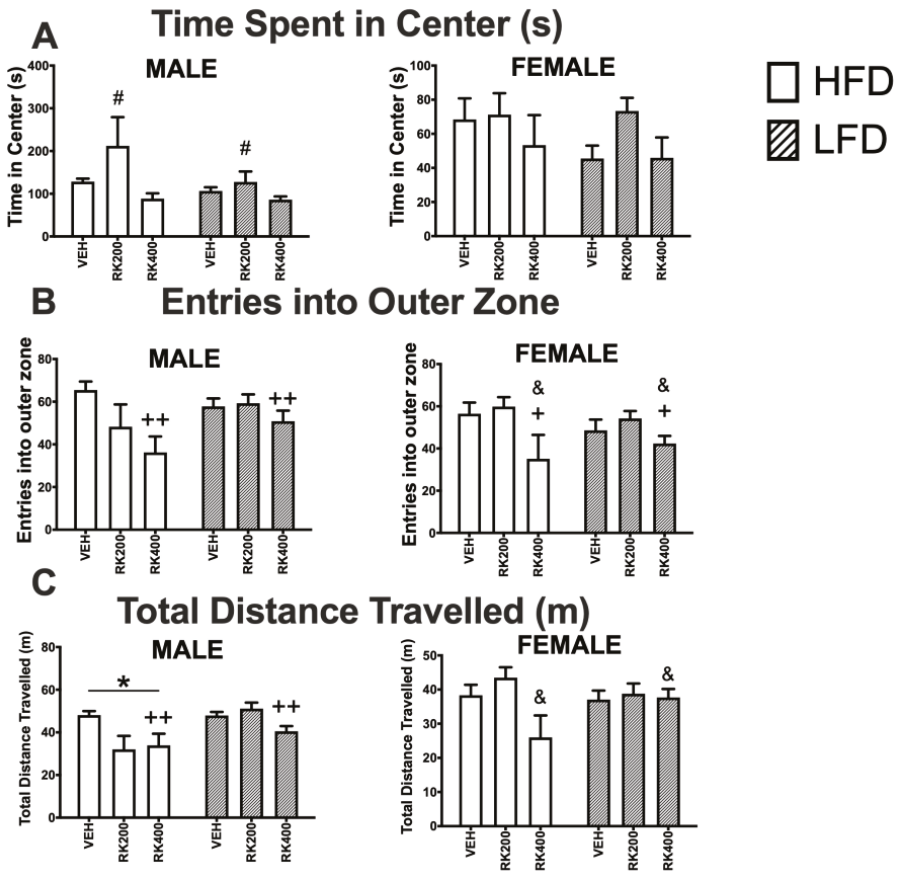


Figure 3. Open-field test during daily oral RK and diet access. Open field tests were performed during days 18–20 of daily dosing and diet access. Data are represented as means ± standard error of the mean (SEM). High-fat diet (45% fat; HFD, solid lines) and low-fat diet (10% fat; LFD, striped line) and oral gavage with raspberry ketone (RK) or vehicle (50% propylene glycol, 40% water, and 10% dimethyl sulfoxide; DMSO). Comparisons are separate within each sex. (A): Time spent in center of open field (s), (B): number of entries into outer zone, (C): total distance travelled (m). * indicates overall diet difference from LFD ($p < 0.05$), # indicates overall dose difference from all other doses ($p < 0.05$), + indicates overall dose difference from VEH dose ($p < 0.05$), ++ indicates overall dose difference from VEH dose ($p < 0.01$), & indicates overall difference from RK200 dose ($p < 0.05$). HFD-Vehicle (males: $n = 15$, females $n = 8$), HFD-RK (200 mg/kg) (males: $n = 7$, females: $n = 8$), HFD-RK (400 mg/kg) (males: $n = 8$, females: $n = 7$), LFD-Vehicle (males: $n = 16$, females: $n = 8$) LFD-RK (200 mg/kg) (males: $n = 7$, females: $n = 8$), and LFD-RK (400 mg/kg)(males: $n = 8$, females: $n = 8$).

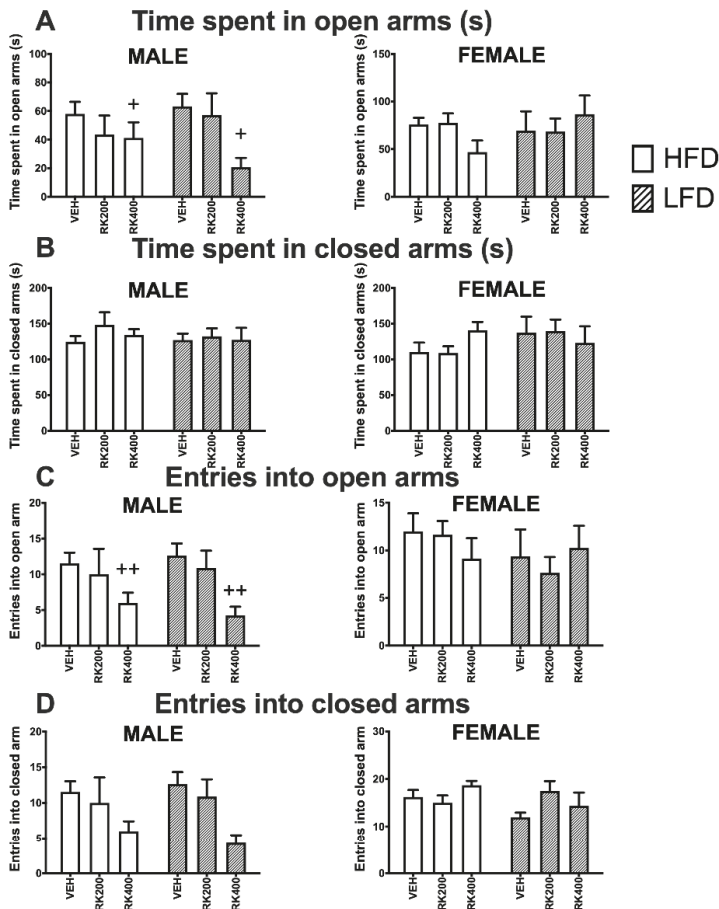


Figure 4. Elevated plus maze behavior test during daily oral RK and diet access. Elevated plus maze tests were performed during days 19–21 of daily dosing and diet access. Data are represented as means ± standard error of the mean (SEM). High-fat diet (45% fat; HFD, solid lines) and low-fat diet (10% fat; LFD, stripped line) and oral dosed with raspberry ketone (RK) or vehicle (50% propylene glycol, 40% water, and 10% dimethyl sulfoxide; DMSO). Comparisons are separate within each sex. (A): Time spent in open arms (s), (B): time spent in closed arms (s), (C): number of entries into open arms, (D): number of entries into closed arms. + indicates overall dose difference from VEH dose ($p < 0.05$), ++ indicates overall dose difference from VEH dose ($p < 0.01$). HFD-Vehicle (males: $n = 15$, females $n = 8$), HFD-RK (200 mg/kg) (males: $n = 7$, females: $n = 8$), HFD-RK (400 mg/kg) (males: $n = 8$, females: $n = 7$), LFD-Vehicle (males: $n = 16$, females: $n = 8$) LFD-RK (200 mg/kg)(males: $n = 8$, females: $n = 8$), and LFD-RK (400 mg/kg)(males: $n = 8$, females: $n = 8$).

3.5. Pre-Pulse Inhibition After 14 Days of Dosing and Diet Access

One day after completing the open field test, the mice underwent testing for the pre-pulse inhibition of an acoustic startle. This was measured in mice after three weeks of their respective daily treatment. Data were analyzed separately for each sex using a two-way ANOVA, with diet and dose as variables. There were no significant effects of diet or dose on parameters of startle response in both sexes, see Figure 5A–B.

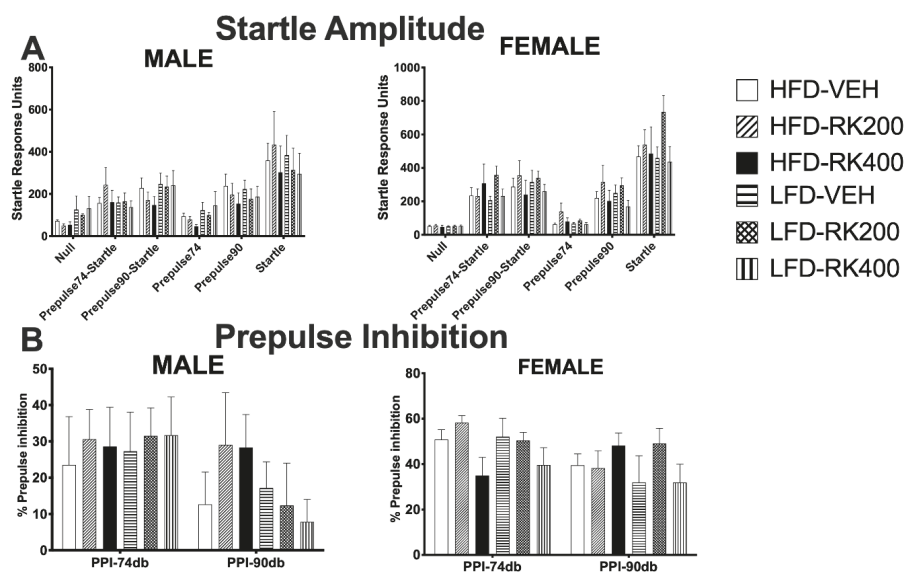


Figure 5. Pre-pulse inhibition of an acoustic startle response behavior test. Pre-pulse inhibition tests were performed during days 21–22 of daily dosing and diet access. Data are represented as means ± standard error of the mean (SEM). High-fat diet (45% fat; HFD, solid lines) and low-fat diet (10% fat; LFD, stripped line) and oral dosed with raspberry ketone (RK) or vehicle (50% propylene glycol, 40% water, and 10% dimethyl sulfoxide; DMSO). Comparisons are separate within each sex. (A): Startle amplitude, (B): pre-pulse inhibition. HFD-Vehicle (males: n = 15, females n = 8), HFD-RK (200 mg/kg) (males: n = 7, females: n = 8), HFD-RK (400 mg/kg) (males: n = 8, females: n = 7), LFD-Vehicle (males: n = 16, females: n = 8) LFD-RK (200 mg/kg)(males: n = 8, females: n = 8), and LFD-RK (400 mg/kg)(males: n = 8, females: n = 8).

3.6. Hemodynamics Differences After 14 Days of Dosing and Diet Access

For systolic blood pressure (SBP), in males, there was a dose effect ($F(2, 62) = 6.2, p < 0.005$) with a reduction in SBP with 400 mg/kg ($p < 0.05$). In females, there was a dose effect ($F(2, 62) = 5.4, p < 0.01$) for SBP. In females, the 400 mg/kg also reduced SBP ($p < 0.05$), see Figure 6A. For diastolic blood pressure (DBP), in males there was a dose effect ($F(2, 62) = 5.2, p < 0.01$) with a reduction in DBP with 400 mg/kg ($p < 0.05$). In females, there was a dose effect ($F(2, 62) = 4.0, p < 0.05$) with a reduction in DBP with 400 mg/kg ($p < 0.05$), see Figure 6B. For mean blood pressure (MBP), in males, there was a dose effect ($F(2, 62) = 5.7, p < 0.05$) with a reduction in 400 mg/kg ($p < 0.05$). Similar effects were observed with dose ($F(2, 62) = 4.4, p < 0.05$) in females with a reduction in MBP ($p < 0.05$), see Figure 6C. For heart rate, in males, there was a dose effect ($F(2, 61) = 3.4, p < 0.05$) with 400 mg/kg only different from 200 mg/kg ($p < 0.05$). In females, there was also a dose effect ($F(2, 61) = 14.9, p < 0.0005$) with 400 mg/kg reducing heart rate ($p < 0.005$), see Figure 6D.

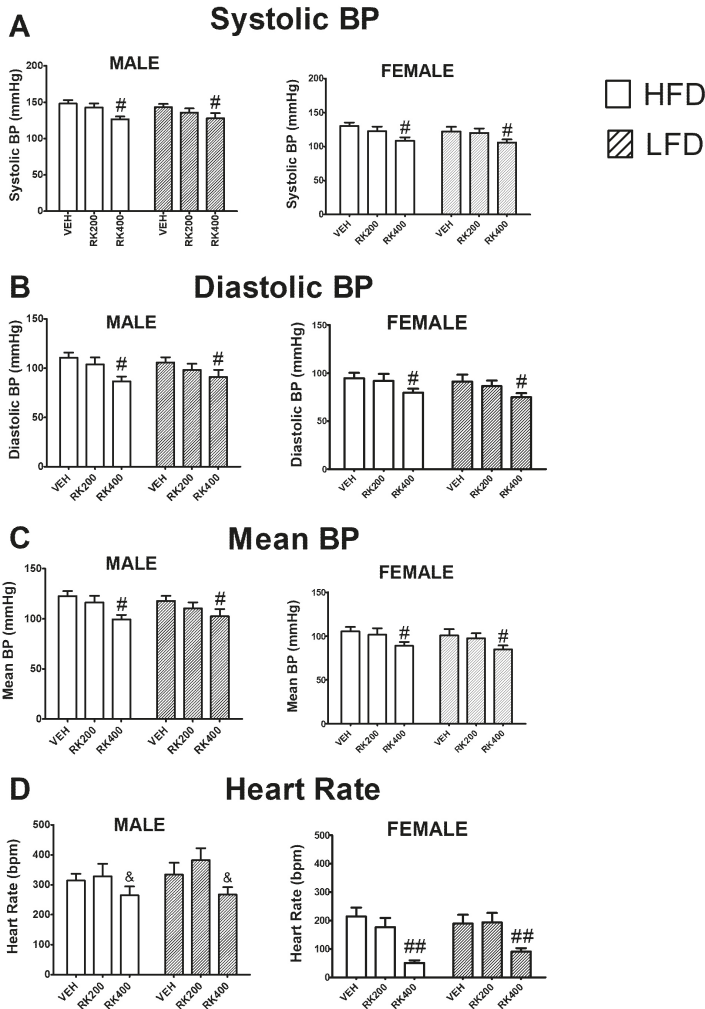


Figure 6. Hemodynamic measurements during the last two days of the 14-day daily oral RK and diet access. Blood pressure and heart rate were measured by noninvasive tail-cuff method. Data are represented as means ± standard error of the mean (SEM). High-fat diet (45% fat; HFD, solid lines) and low-fat diet (10% fat; LFD, stripped line) and oral dosed with raspberry ketone (RK) or vehicle (50% propylene glycol, 40% water, and 10% dimethyl sulfoxide; DMSO) for 14 days. Comparisons are separate within each sex. Hemodynamic measurements were averages over the last 2 days of dosing and diet exposure. (A): Systolic blood pressure (mm Hg), (B): diastolic blood pressure (mm Hg), (C): mean blood pressure (mm Hg), (D): heart rate (beats per minute; BPM). # indicates overall dose difference from vehicle and RK 200 mg/kg ($p < 0.05$), ## indicates overall dose difference from vehicle and RK 200 mg/kg ($p < 0.005$) & indicates overall dose difference from RK200 dose ($p < 0.05$). HFD-Vehicle (males: $n = 12$, females $n = 12$), HFD-RK (200 mg/kg) (males: $n = 12$, females: $n = 11$), HFD-RK (400 mg/kg) (males: $n = 11$, females: $n = 11$), LFD-Vehicle (males: $n = 11$, females: $n = 11$) LFD-RK (200 mg/kg)(males: $n = 11$, females: $n = 11$), and LFD-RK (400 mg/kg) (males: $n = 11$, females: $n = 12$).

3.7. c-Fos Immunopositive Cells of The Caudal Hindbrain in Mice Receiving Vehicle or Raspberry Ketone (400 mg/kg) and Diet Access

In the AP, there were no significant effects for dose, diet, or dose x diet, see Table 1. In the NTS, there was only a significant effect for dose ($F(1, 19) = 4.7, p < 0.05$) with mice receiving RK having a greater number of immunopositive cells ($p < 0.05$), see Table 1. The regions with the highest number of immunopositive cells were the mNTS and iNTS, see Figure 7.

Table 1. Average immunoreactive c-Fos counts in the area postrema (AP) and nucleus of the solitary tract (NTS) from mice orally dosed with vehicle or raspberry ketone (400 mg/kg). Mice were fed high-fat diet (HFD; 45% fat) or low-fat diet (LFD: 10% fat) and orally dosed vehicle (VEH) or raspberry ketone (400 mg/kg) for 14 days. Mice were euthanized on day 14, 120 min after respective dosing. Immunopositive cell counts are means \pm SEM.

Brain Region	HFD-VEH (n = 6)	HFD-RK (n = 6)	LFD-VEH (n = 5)	LFD-RK (n = 6)
AP	39 \pm 4	30 \pm 5	20 \pm 12	27 \pm 10
NTS	72 \pm 30	272 \pm 85#	15 \pm 28	184 \pm 35#

overall effect of RK (400 mg/kg) compared with vehicle; $p < 0.05$.

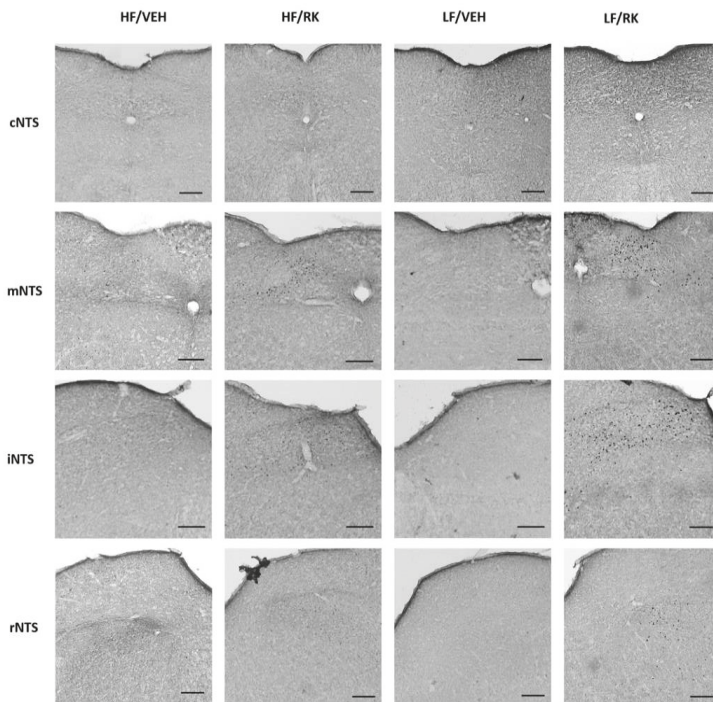


Figure 7. Representative coronal micrographs from NTS and AP in mice dosed with vehicle or raspberry ketone (400 mg/kg). Immunopositive c-Fos cells are stained black. NTS subareas are caudal (cNTS; -7.92 mm from Bregma); medial (mNTS; -7.48 mm from Bregma); intermediate (iNTS; -7.08 mm from Bregma); rostral (rNTS; -6.84 mm from Bregma). AP are located mNTS. Black bar in each image represents $153 \mu\text{m}$.

4. Discussion

RK is marketed in the United States and other countries as a nutraceutical for appetite control and weight loss [18,27,37]. This study sought to investigate the dose-dependent effects of RK on the meal patterns and hemodynamic alterations associated with an obesogenic diet. Our major finding was a dose-differential response in RK's effects on weight gain, meal patterns, and hemodynamic parameters.

RK has reported effects on weight gain due to an obesogenic diet in male mice when administered by admixture in the diet [16,17] or, in our previous studies, by oral gavage [18]. In these studies differences in weight gain were observed after three to five weeks of exposure to RK. Therefore, to understand the preceding changes that drive the reduced weight gain, we dosed animals for two weeks with a 200 mg/kg RK and high dose of RK 400 mg/kg. The dose of 400 mg/kg in a high-fat driven obesogenic environment has not been studied before. For weight gain, male mice that received 400 mg/kg RK had a reduced gain in body weight. The difference in body weight was observed on 2–5 days of the daily dosing. In females, there was a reduction in gain in body weight with RK 400 mg/kg compared with RK 200 mg/kg. These body weight differences between males and females are not surprising. Female mice are more resilient to the effect of a high-fat diet [38], and we expect to see greater differences in body weight due to RK in a longer exposure to daily dosing. Previously, we demonstrated that there was no difference in the acute oral dosed RK bioavailability in males compared with females [27]. However, metabolism of phenolic compounds can vary between males and females [39], a possibility that is currently being explored with RK.

Previously, we observed a reduction in weight gain with oral RK 200 mg/kg in males fed a high-fat diet for twice as long (i.e., 28 days) [18]. In that study, meal patterns were measured after 21 days of dosing and were not altered with RK 200 mg/kg [18]. In the present study, we analyzed meal patterns separately for dark and light cycles. We observed a dose effect with 200 mg/kg on nocturnal meal patterns in males. In males, the frequency of meals was reduced, but meal size and duration were increased. The 400-mg/kg dose increased the satiety ratio in males and females. Meal frequency was also reduced in females with 400 mg/kg compared with 200 mg/kg. Taken together, our results suggest that RK doses influence meal patterns, specifically meal frequency. Our study demonstrated an increase in meal number, size and duration associated with high-fat diet, which has been previously reported [23,40]. Similarly, diet-induced obesity susceptible rats consume more meals compared with control fed animals [22]. Therefore, nutraceuticals that mitigate the high-fat diet-induced changes in meal parameters can be useful to normalize aberrant feeding. Notably, the differences in RK-induced changes in body weight and meal patterns were not specific to the obesogenic high-fat diet condition.

Weight changes are often a secondary outcome of anxiogenic and antipsychotic agents [24, 25]. As such, we examined whether RK-induced weight loss and meal patterns alterations results in anxiety-like behaviors. The major findings were that RK 400 mg/kg decreased total distance traveled in the open field test. RK 200 mg/kg also increased time spent in the center, which is often noted with anxiolytic agents [41]. However, there were no significant findings in the elevated plus maze with 200 mg/kg. In addition, the reductions in entries into both open and closed arms are suggestive that RK 400 mg/kg reduces locomotor activity and does not promote anxiogenic behaviors. Alterations in pre-pulse inhibition have been noted with antipsychotic medications and amphetamines in rodents [34,42,43]. These compounds are also associated with adverse body weight and meal pattern alterations [44,45]. In this study, RK did not alter pre-pulse inhibition, suggesting the weight reduction was not secondary to sensorimotor gating impairments.

FDA-approved obesity medications and nutraceuticals that reduced body weight have been demonstrated to produce adverse cardiovascular outcomes [46–48]. Previous studies in rodents have suggested that RK has a cardioprotective role [19,20]. A 28-day treatment of oral RK (100–200 mg/kg) has been shown to prevent isoproterenol-induced cardiac tissue damage and dyslipidemia in rats [19,20]. That is, RK increased cardiac levels of peroxisome proliferator-activated receptor (PPAR)-alpha, and reduced markers of cell death suggesting a protective role [20]. RK shares structural similarity with synephrine [16], which is known to have an effect on hemodynamics [48,49]. As such, our study

demonstrated that RK 400 mg/kg reduced systolic blood pressure (BP), diastolic BP, and mean BP. These effects were demonstrated in males and females, regardless of diet. Future studies will examine the blood parameters, such as pro- and anti-inflammatory cytokines and lipid profiles related to these cardiometabolic parameters. Additionally, the present study demonstrated RK 400 mg/kg increased neural activation, as measured by c-Fos immunohistochemistry, of the nucleus of the solitary (NTS). The NTS receives sensory input from the vagal nerve and has been shown to be involved in meal patterns and cardiovascular control [29,30]. Future experiments will be conducted to elucidate the feeding and cardiovascular mechanisms of action and receptor activation of RK on the NTS and other brain regions.

5. Conclusions

Our study demonstrated that RK effectively reduced body weight, altered meal patterns, and reduced cardiovascular outcomes. These differences were differentially observed with dose, but they were not specific to the obesogenic diet. These studies suggest that RK might have limited use to prevent weight gain and metabolic signatures associated with high-fat diet.

Supplementary Materials: The following are available online at <http://www.mdpi.com/2072-6643/12/6/1754/s1>, Figure S1: Experimental design for measurement of meal patterns and behavioral outcomes during exposure to respective diet and dose treatments. Figure S2: Experimental design for measurement of hemodynamic parameters after 14-day exposure to respective diet and dose treatments. Figure S3: Experimental design to study activation of caudal hindbrain in response to respective diet and dose treatments.

Author Contributions: Conceptualization and experimental design, N.T.B.; experimental execution, D.K., L.H., X.L.; writing—original draft preparation, D.K.; writing—review and editing, D.K., N.T.B., X.L., L.H.; funding acquisition, N.T.B. All authors have read and agreed to the published version of the manuscript.

Funding: Research reported in this publication was supported by the NCCIH of the NIH under Award Number R01AT008933 and USDA (NIFA) NJ06280.

Acknowledgments: The authors would like to thank, Matthew Wereski, Nardine Nasr, and Gina M. Giunta for their technical assistance and Kathy Manger for her editorial assistance. The authors would especially like to thank Research Diets Inc., specifically Edward A. Ulman, Douglas Compton, and Juliet Gentile for generously providing the use of and the training with the BioDAQ system.

Conflicts of Interest: The authors declare no conflict of interest.

References

1. Borejsza-Wysocki, W.; Goers, S.K.; McArdle, R.N.; Hrazdina, G. (p-Hydroxyphenyl)butan-2-one Levels in raspberries determined by chromatographic and organoleptic methods. *J. Agric. Food Chem.* **1992**, *40*, 1176–1177. [[CrossRef](#)]
2. Borejsza-Wysocki, W.; Hrazdina, G. Biosynthesis of p-Hydroxyphenylbutan-2-one in raspberry fruits and tissue culture. *Phytochemistry* **1994**, *35*, 623–628. [[CrossRef](#)]
3. Bredsdorff, L.; Wedebye, E.B.; Nikolov, N.G.; Hallas-Moller, T.; Pilegaard, K. Raspberry ketone in food supplements—High intake, few toxicity data—A cause for safety concern? *Regul. Toxicol. Pharmacol.* **2015**, *73*, 196–200. [[CrossRef](#)] [[PubMed](#)]
4. Wang, C.; Zheng, P.; Chen, P. Construction of synthetic pathways for raspberry ketone production in engineered *Escherichia coli*. *Appl. Microbiol. Biotechnol.* **2019**, *103*, 3715–3725. [[CrossRef](#)] [[PubMed](#)]
5. U.S. Food and Drug Administration. *Code of Federal Regulations Title 21*; U.S. Food and Drug Administration: Silver Spring, MD, USA, 2019; Volume 3, pp. 1–20.
6. Lee, J. Further research on the biological activities and the safety of raspberry ketone is needed. *NFS J.* **2016**, *2*, 15–18. [[CrossRef](#)]
7. Bootsman, N.; Blackburn, D.F.; Taylor, J. The Oz craze: The effect of pop culture media on health care. *Can. Pharm. J. (Ott.)* **2014**, *147*, 80–82. [[CrossRef](#)]
8. Lopez, H.L.; Ziegenfuss, T.N.; Hofheins, J.E.; Habowski, S.M.; Arent, S.M.; Weir, J.P.; Ferrando, A.A. Eight weeks of supplementation with a multi-ingredient weight loss product enhances body composition, reduces hip and waist girth, and increases energy levels in overweight men and women. *J. Int. Soc. Sports Nutr.* **2013**, *10*, 22. [[CrossRef](#)] [[PubMed](#)]

9. Arent, S.M.; Walker, A.J.; Pellegrino, J.K.; Sanders, D.J.; McFadden, B.A.; Ziegenfuss, T.N.; Lopez, H.L. The combined effects of exercise, diet, and a multi-ingredient dietary supplement on body composition and adipokine changes in overweight adults. *J. Am. Coll. Nutr.* **2018**, *37*, 111–120. [[CrossRef](#)] [[PubMed](#)]
10. Park, K.S. Raspberry ketone increases both lipolysis and fatty acid oxidation in 3T3-L1 adipocytes. *Planta Med.* **2010**, *76*, 1654–1658. [[CrossRef](#)] [[PubMed](#)]
11. Park, K.S. Raspberry ketone, a naturally occurring phenolic compound, inhibits adipogenic and lipogenic gene expression in 3T3-L1 adipocytes. *Pharm. Biol.* **2015**, *53*, 870–875. [[CrossRef](#)] [[PubMed](#)]
12. Leu, S.Y.; Chen, Y.C.; Tsai, Y.C.; Hung, Y.W.; Hsu, C.H.; Lee, Y.M.; Cheng, P.Y. Raspberry ketone reduced lipid accumulation in 3T3-L1 cells and ovariectomy-induced obesity in Wistar Rats by regulating autophagy mechanisms. *J. Agric. Food Chem.* **2017**, *65*, 10907–10914. [[CrossRef](#)] [[PubMed](#)]
13. Tsai, Y.C.; Yang, B.C.; Peng, W.H.; Lee, Y.M.; Yen, M.H.; Cheng, P.Y. Heme oxygenase-1 mediates anti-adipogenesis effect of raspberry ketone in 3T3-L1 cells. *Phytomedicine* **2017**, *31*, 11–17. [[CrossRef](#)] [[PubMed](#)]
14. Leu, S.Y.; Tsai, Y.C.; Chen, W.C.; Hsu, C.H.; Lee, Y.M.; Cheng, P.Y. Raspberry ketone induces brown-like adipocyte formation through suppression of autophagy in adipocytes and adipose tissue. *J. Nutr. Biochem.* **2018**, *56*, 116–125. [[CrossRef](#)] [[PubMed](#)]
15. Wang, L.; Meng, X.; Zhang, F. Raspberry ketone protects rats fed high-fat diets against nonalcoholic steatohepatitis. *J. Med. Food.* **2012**, *15*, 495–503. [[CrossRef](#)]
16. Morimoto, C.; Satoh, Y.; Hara, M.; Inoue, S.; Tsujita, T.; Okuda, H. Anti-obese action of raspberry ketone. *Life Sci.* **2005**, *77*, 194–204. [[CrossRef](#)]
17. Cotten, B.M.; Diamond, S.A.; Banh, T.; Hsiao, Y.H.; Cole, R.M.; Li, J.; Simons, C.T.; Bruno, R.S.; Belury, M.A.; Vodovotz, Y. Raspberry ketone fails to reduce adiposity beyond decreasing food intake in C57BL/6 mice fed a high-fat diet. *Food Funct.* **2017**, *8*, 1512–1518. [[CrossRef](#)]
18. Kshatriya, D.; Li, X.; Giunta, G.M.; Yuan, B.; Zhao, D.; Simon, J.E.; Wu, Q.; Bello, N.T. Phenolic-enriched raspberry fruit extract (*Rubus idaeus*) resulted in lower weight gain, increased ambulatory activity, and elevated hepatic lipoprotein lipase and heme oxygenase-1 expression in male mice fed a high-fat diet. *Nutr. Res.* **2019**, *68*, 19–33. [[CrossRef](#)]
19. Khan, V.; Sharma, S.; Bhandari, U.; Ali, S.M.; Haque, S.E. Raspberry ketone protects against isoproterenol-induced myocardial infarction in rats. *Life Sci.* **2018**, *194*, 205–212. [[CrossRef](#)]
20. Khan, V.; Sharma, S.; Bhandari, U.; Sharma, N.; Rishi, V.; Haque, S.E. Suppression of isoproterenol-induced cardiotoxicity in rats by raspberry ketone via activation of peroxisome proliferator activated receptor- α . *Eur. J. Pharmacol.* **2019**, *842*, 157–166. [[CrossRef](#)] [[PubMed](#)]
21. Bramante, C.T.; Raatz, S.; Bomberg, E.M.; Oberle, M.M.; Ryder, J.R. Cardiovascular risks and benefits of medications used for weight loss. *Front Endocrinol. (Lausanne)* **2019**, *10*, 883. [[CrossRef](#)]
22. Farley, C.; Cook, J.A.; Spar, B.D.; Austin, T.M.; Kowalski, T.J. Meal pattern analysis of diet-induced obesity in susceptible and resistant rats. *Obes. Res.* **2003**, *11*, 845–851. [[CrossRef](#)] [[PubMed](#)]
23. Gotthardt, J.D.; Bello, N.T. Meal pattern alterations associated with intermittent fasting for weight loss are normalized after high-fat diet re-feeding. *Physiol. Behav.* **2017**, *174*, 49–56. [[CrossRef](#)] [[PubMed](#)]
24. Cimolai, N.; Cimolai, T. Yohimbine use for physical enhancement and its potential toxicity. *J. Diet Suppl.* **2011**, *8*, 346–354. [[CrossRef](#)] [[PubMed](#)]
25. Domecq, J.P.; Prutsky, G.; Leppin, A.; Sonbol, M.B.; Altayar, O.; Undavalli, C.; Wang, Z.; Elraiyah, T.; Brito, J.P.; Mauck, K.F.; et al. Clinical review: Drugs commonly associated with weight change: A systematic review and meta-analysis. *J. Clin. Endocrinol. Metab.* **2015**, *100*, 363–370. [[CrossRef](#)]
26. Zhao, D.; Yuan, B.; Kshatriya, D.; Polyak, A.; Simon, J.E.; Bello, N.T.; Wu, Q. Influence of diet-induced obesity on the bioavailability and metabolism of raspberry ketone (4-(4-Hydroxyphenyl)-2-Butanone) in mice. *Mol. Nutr. Food Res.* **2020**, *64*, e1900907. [[CrossRef](#)]
27. Zhao, D.; Yuan, B.; Kshatriya, D.; Polyak, A.; Simon, J.; Bello, N.; Wu, Q. Bioavailability and metabolism of raspberry ketone with potential implications for obesity prevention (OR34-05-19). *Curr. Dev. Nutr.* **2019**, *3*, nzz031. OR34-05-19. [[CrossRef](#)]
28. Baumgartner, I.; Pacheco-Lopez, G.; Ruttimann, E.B.; Arnold, M.; Asarian, L.; Langhans, W.; Geary, N.; Hillebrand, J.J. Hepatic-portal vein infusions of glucagon-like peptide-1 reduce meal size and increase c-Fos expression in the nucleus tractus solitarii, area postrema and central nucleus of the amygdala in rats. *J. Neuroendocrinol.* **2010**, *22*, 557–563. [[CrossRef](#)]

29. Bello, N.T.; Guarda, A.S.; Terrillion, C.E.; Redgrave, G.W.; Coughlin, J.W.; Moran, T.H. Repeated binge access to a palatable food alters feeding behavior, hormone profile, and hindbrain c-Fos responses to a test meal in adult male rats. *Am. J. Physiol. Regul. Integr. Comp. Physiol.* **2009**, *297*, R622–631. [[CrossRef](#)] [[PubMed](#)]
30. Blanch, G.T.; Freiria-Oliveira, A.H.; Murphy, D.; Paulin, R.F.; Antunes-Rodrigues, J.; Colombari, E.; Menani, J.V.; Colombari, D.S. Inhibitory mechanism of the nucleus of the solitary tract involved in the control of cardiovascular, dipsogenic, hormonal, and renal responses to hyperosmolality. *Am. J. Physiol. Regul. Integr. Comp. Physiol.* **2013**, *304*, R531–542. [[CrossRef](#)] [[PubMed](#)]
31. Yuan, B.; Zhao, D.; Du, R.; Kshatriya, D.; Bello, N.T.; Simon, J.E.; Li, Q. A highly sensitive ultra-high performance liquid chromatography/tandem mass spectrometry method with in-source fragmentation for rapid quantification of raspberry ketone. *J. Food Drug Anal.* **2019**, *27*, 778–785. [[CrossRef](#)] [[PubMed](#)]
32. Leitinger, B.; Poletaeva, I.; Wolfer, D.P.; Lipp, H.P. Swimming navigation, open-field activity, and extrapolation behavior of two inbred mouse strains with Robertsonian translocation of chromosomes 8 and 17. *Behav. Genet.* **1994**, *24*, 273–284. [[CrossRef](#)] [[PubMed](#)]
33. Komada, M.; Takao, K.; Miyakawa, T. Elevated plus maze for mice. *J. Vis. Exp.* **2008**, *22*, 1088. [[CrossRef](#)] [[PubMed](#)]
34. Ouagazzal, A.M.; Jenck, F.; Moreau, J.L. Drug-induced potentiation of prepulse inhibition of acoustic startle reflex in mice: A model for detecting antipsychotic activity? *Psychopharmacology (Berl)*. **2001**, *156*, 273–283. [[CrossRef](#)] [[PubMed](#)]
35. Verpeut, J.L.; DiCicco-Bloom, E.; Bello, N.T. Ketogenic diet exposure during the juvenile period increases social behaviors and forebrain neural activation in adult Engrailed 2 null mice. *Physiol. Behav.* **2016**, *161*, 90–98. [[CrossRef](#)]
36. Franklin, K.B.J.; Paxinos, G. *The Mouse Brain in Stereotaxic Coordinates*, 3rd ed.; Elsevier Inc: San Diego, CA, USA, 2008.
37. Yimam, M.; Jiao, P.; Hong, M.; Brownell, L.; Lee, Y.C.; Hyun, E.J.; Kim, H.J.; Kim, T.W.; Nam, J.B.; Kim, M.R.; et al. Evaluation of Natural Product Compositions for Appetite Suppression. *J. Diet. Suppl.* **2019**, *16*, 86–104. [[CrossRef](#)] [[PubMed](#)]
38. Huang, K.P.; Ronveaux, C.C.; Knotts, T.A.; Rutkowsky, J.R.; Ramsey, J.J.; Raybould, H.E. Sex differences in response to short-term high fat diet in mice. *Physiol. Behav.* **2020**, *221*, 112894. [[CrossRef](#)] [[PubMed](#)]
39. Margalef, M.; Pons, Z.; Iglesias-Carres, L.; Arola, L.; Muguerza, B.; Arola-Arnal, A. Gender-related similarities and differences in the body distribution of grape seed flavanols in rats. *Mol. Nutr. Food. Res.* **2016**, *60*, 760–772. [[CrossRef](#)] [[PubMed](#)]
40. Bake, T.; Murphy, M.; Morgan, D.G.A.; Mercer, J.G. Large, binge-type meals of high fat diet change feeding behaviour and entrain food anticipatory activity in mice. *Appetite* **2014**, *77*, 60–71. [[CrossRef](#)]
41. Heredia, L.; Torrente, M.; Colomina, M.T.; Domingo, J.L. Assessing anxiety in C57BL/6J mice: A pharmacological characterization of the open-field and light/dark tests. *J. Pharmacol. Toxicol. Methods* **2014**, *69*, 108–114. [[CrossRef](#)]
42. Flood, D.G.; Zuvich, E.; Marino, M.J.; Gasior, M. Prepulse inhibition of the startle reflex and response to antipsychotic treatments in two outbred mouse strains in comparison to the inbred DBA/2 mouse. *Psychopharmacology (Berl)*. **2011**, *215*, 441–454. [[CrossRef](#)] [[PubMed](#)]
43. Moy, S.S.; Perez, A.; Koller, B.H.; Duncan, G.E. Amphetamine-induced disruption of prepulse inhibition in mice with reduced NMDA receptor function. *Brain Res.* **2006**, *1089*, 186–194. [[CrossRef](#)] [[PubMed](#)]
44. Albaugh, V.L.; Henry, C.R.; Bello, N.T.; Hajnal, A.; Lynch, S.L.; Halle, B.; Lynch, C.J. Hormonal and metabolic effects of olanzapine and clozapine related to body weight in rodents. *Obesity (Silver Spring)*. **2006**, *14*, 36–51. [[CrossRef](#)] [[PubMed](#)]
45. Bauer, W.S.; Perley, J.E. Diurnal variation of hepatic amphetamine concentrations in mice fed freely and fed single daily meals. *J. Pharm. Pharmacol.* **1971**, *23*, 976–977. [[CrossRef](#)] [[PubMed](#)]
46. Gotthardt, J.D.; Bello, N.T. Can we win the war on obesity with pharmacotherapy? *Expert. Rev. Clin. Pharmacol.* **2016**, *9*, 1289–1297. [[CrossRef](#)] [[PubMed](#)]
47. Ray, S.; Phadke, S.; Patel, C.; Hackman, R.M.; Stohs, S. Short-term and long-term in vivo exposure to an ephedra- and caffeine-containing metabolic nutrition system does not induce cardiotoxicity in B6C3F1 mice. *Arch. Toxicol.* **2005**, *79*, 330–340. [[CrossRef](#)]

48. Verpeut, J.L.; Walters, A.L.; Bello, N.T. Citrus aurantium and Rhodiola rosea in combination reduce visceral white adipose tissue and increase hypothalamic norepinephrine in a rat model of diet-induced obesity. *Nutr. Res.* **2013**, *33*, 503–512. [[CrossRef](#)]
49. Hansen, D.K.; George, N.I.; White, G.E.; Abdel-Rahman, A.; Pellicore, L.S.; Fabricant, D. Cardiovascular toxicity of Citrus aurantium in exercised rats. *Cardiovasc. Toxicol.* **2013**, *13*, 208–219. [[CrossRef](#)]



© 2020 by the authors. Licensee MDPI, Basel, Switzerland. This article is an open access article distributed under the terms and conditions of the Creative Commons Attribution (CC BY) license (<http://creativecommons.org/licenses/by/4.0/>).

Article

Allithiamine Alleviates Hyperglycaemia-Induced Endothelial Dysfunction

Attila Biró¹, Arnold Markovics¹, Mónika Éva Fazekas¹, Gábor Fidler², Gábor Szalóki³, Melinda Paholcsek², János Lukács⁴, László Stündl¹ and Judit Remenyik^{1,*}

¹ Institute of Food Technology, Faculty of Agricultural and Food Sciences and Environmental Management, University of Debrecen, H-4032 Debrecen, Hungary; biro.attila@agr.unideb.hu (A.B.); arnoldmarkovics@gmail.com (A.M.); fazekas.monika@agr.unideb.hu (M.É.F.); stundl@agr.unideb.hu (L.S.)

² Department of Human Genetics, Faculty of Medicine, University of Debrecen, H-4032 Debrecen, Hungary; fidler.gabor@med.unideb.hu (G.F.); paholcsek.melinda@med.unideb.hu (M.P.)

³ 1st Department of Pathology and Experimental Cancer Research, Semmelweis University, H-1085 Budapest, Hungary; szaloki.gabor@med.semmelweis-univ.hu

⁴ Department of Obstetrics and Gynaecology, University of Debrecen, H-4032 Debrecen, Hungary; lukacs.janos@med.unideb.hu

* Correspondence: remenyik@agr.unideb.hu; Tel.: +36-52-518-600

Received: 8 May 2020; Accepted: 29 May 2020; Published: 5 June 2020

Abstract: Diabetes mellitus-related morbidity and mortality is a rapidly growing healthcare problem, globally. Several nutraceuticals exhibit potency to target the pathogenesis of diabetes mellitus. The antidiabetic effects of compounds of garlic have been extensively studied, however, limited data are available on the biological effects of a certain garlic component, allithiamine. In this study, allithiamine was tested using human umbilical cord vein endothelial cells (HUVECs) as a hyperglycaemic model. HUVECs were isolated by enzymatic digestion and characterized by flow cytometric analysis using antibodies against specific marker proteins including CD31, CD45, CD54, and CD106. The non-cytotoxic concentration of allithiamine was determined based on MTT, apoptosis, and necrosis assays. Subsequently, cells were divided into three groups: incubating with M199 medium as the control; or with 30 mM/L glucose; or with 30 mM/L glucose plus allithiamine. The effect of allithiamine on the levels of advanced glycation end-products (AGEs), activation of NF- κ B, release of pro-inflammatory cytokines including IL-6, IL-8, and TNF- α , and H₂O₂-induced oxidative stress was investigated. We found that in the hyperglycaemia-induced increase in the level of AGEs, pro-inflammatory changes were significantly suppressed by allithiamine. However, allithiamine could not enhance the activity of transketolase, but it exerts a potent antioxidant effect. Collectively, our data suggest that allithiamine could alleviate the hyperglycaemia-induced endothelial dysfunction due to its potent antioxidant and anti-inflammatory effect by a mechanism unrelated to the transketolase activity.

Keywords: allithiamine; garlic; hyperglycaemia; advanced glycation end-products; cytokines

1. Introduction

In recent decades, several research have focused on the pharmacologically active, plant-derived compounds [1]. Extensive research on physiological effects of nutraceuticals is expected to continue in the near future. A recently published review unequivocally declared that the ongoing discovery of naturally occurring drugs stands as a major contributor to cope with diseases, reaching high prevalence, globally [2].

Among plants having significant pharmacological activity, garlic (*Allium sativum* L.) is among the most studied ones [3]. Several studies have shown that garlic exerts antioxidant, antimicrobial [4], anti-inflammatory, immunomodulatory [5], antithrombotic [6], anti-atherosclerotic [7], antihypertensive [8],

and anti-carcinogenic [9] effects. The biological effects of garlic are mainly attributed to its characteristic organosulfur compounds, including alliin, alliin, ajoene, S-allylmercaptocysteine, diallyl disulfide, and S-allyl-cysteine, among others. [10]. Limited data in the scientific literature are available on the biological effects of another garlic component, allithiamine, which is a less polar thiamine (B₁-vitamin) derivative and, similar to the molecules mentioned above, has a prop-2-en-1-yl disulfanyl moiety. According to a recent study, allithiamine is also accumulated in red sweet pepper (*Capsicum annuum* L.) seeds, implying that its occurrence is more frequent than as thought until now. Nevertheless, several studies revealed that numerous garlic compounds have beneficial effects on hyperglycaemia in diabetes mellitus [11].

Diabetes mellitus is a rapidly growing public health burden, particularly in developed countries [12]. Diabetes mellitus is a metabolic, endocrine disorder, which can cause an acute life-threatening homeostasis imbalance as well as chronically developing micro- and macrovascular complications (blindness, neuropathy, myocardial infarction, stroke, etc.) [13]. There is a common agreement that endothelial dysfunction precedes the development of micro- and macrovascular complications associated with diabetes mellitus [14]. These complications are caused—at least partially—by the detrimental effects of hyperglycaemia, which affects endothelial cell biology by accelerating the formation of advanced glycation end-products (AGEs), thereby increasing pro-inflammatory signaling and resulting in oxidative stress [15].

Glucose reacts with an amino group of the circulating proteins during the formatting of AGEs. The level of AGEs elevates heavily in the presence of chronic hyperglycaemia to evoke both damaging biological functions of glycosylated molecules, resulting in altered intracellular signaling, gene expression, release of pro-inflammatory molecules, and enhanced oxidative stress by bonding to cell surface receptors (RAGE), and so consequently, AGEs play a major role in diabetic microvascular complications [16]. Hyperglycaemia, alone can trigger inflammation by activating the pro-inflammatory transcription factor nuclear κ B (NF- κ B), resulting in an increased inflammatory chemokine and cytokine release including interleukin-6 (IL-6), interleukin-8 (IL-8), and tumor necrosis factor- α (TNF- α), among others. [17]. A recent study reported that alleviating the release of pro-inflammatory cytokines has a beneficial effect in chronic hyperglycaemia [18]. In addition, a high level of glucose enhances oxidative stress, when the rate of oxidant production exceeds the rate of oxidant scavenging [19]. In the case of hyperglycaemia, there are both enhanced oxidant production and impaired antioxidant defenses by multiple interacting pathways [20]. Studies have demonstrated that compounds with a strong antioxidant property can potentially be effective in delaying diabetes-related complications.

To date, there is no preclinical evidence for the antidiabetic effect of allithiamine, therefore, the main objective of our current research was to study whether this compound is able to exert a beneficial effect on diabetes. Primary cultured human umbilical cord vein endothelial cells (HUVECs) were used as a unique hyperglycaemic model, which appeared to be ideally capable to investigate the level of AGEs, antioxidant status, and pro-inflammatory cytokines.

2. Materials and Methods

2.1. Materials

Chemicals

All reagents were obtained from the distributor of iBioTech Hungary Ltd. (Budapest, Hungary) and DIAGON Ltd. Hungary (Budapest, Hungary).

2.2. Methods

2.2.1. Preparation and Purification of Allithiamine

Preparation and purification of allithiamine were carried out based on the method of our recent allithiamine-oriented study [21]. Briefly, allyl thiosulphate and thiamine hydrochloride with an opening thiazole ring were reacted. As a result of the reaction, many organosulfur compounds were

formed, including allithiamine. Reaction products were separated and allithiamine was purified by reversed-phase chromatography using LaChrom HPLC equipped with a diode array detector. (Hitachi, Osaka, Japan). To confirm the accuracy and efficiency of the allithiamine synthesis and purification, matrix-assisted laser desorption/ionization mass spectrometric (MALDI-MS) analysis and HPLC-MS/MS fragmentation were performed applying a Bruker Biflex MALDI-TOF mass spectrometer (Bruker, Billerica, MA, USA) and Thermo Scientific Q Exactive Orbitrap mass spectrometer (Thermo Fisher Scientific Inc., Waltham, MA, USA).

2.2.2. Isolation and Treatment of Primary HUVECs

The HUVECs were isolated from human umbilical cords and maintained according to the method previously described [22]. In our experiments, supplemented M199 medium was used as a control and had 5.6 mMol/L glucose. To create a hyperglycaemic model, glucose was added to M199 for a final concentration of 30 mMol/L.

2.2.3. Characterization of HUVECs by Flow Cytometry

HUVECs were incubated with four fluorescent dye-labeled antibodies, involving fluorescein-isothiocyanate (FITC)-labeled mouse anti-human CD31, phycoerythrin (PE)-labeled anti-human CD54, allophycocyanin (APC)-labeled mouse anti-human CD106, and PerCP-Cy5.5-labeled mouse anti-human CD45 (BD Biosciences, Franklin Lakes, NJ, USA), and then characterized by using a FACS Aria III Cell Sorter (Becton Dickinson, Mountain View, CA, USA) [22].

2.2.4. Determination of Cellular Viability

Cell viability was determined by an MTT (3-[4,5-dimethylthiazol-2-yl]-2,5 diphenyltetrazolium bromide) assay. Cells were plated into 96-well plates at a density of 20,000 cells per well in quadruplicates and treated with allithiamine of different concentrations (0.1, 0.5, 1, 5, 10, and 50 µg/mL) and without allithiamine (control group) for 24, 48, and 72 h. The medium was removed and incubated with 100 µL of MTT solution (0.5 mg/ml dissolved in Dulbecco's modified Eagle's medium) for 3 h. Subsequently, the formazan crystals were dissolved in 100 µL solubilizing solution (81% (v/v) isopropyl alcohol, 9% (v/v), 1 M HCl, 10% (v/v) Triton X-100) and the absorbance was measured at 465 nm by using a Clariostar microplate reader (BMG Labtech, Ortenberg, Germany). Cell viability at different allithiamine concentrations was expressed relative to 100% of the control group.

2.2.5. Determination of Apoptosis

The mitochondrial membrane potential of the HUVECs was determined by using 1,1',3,3',3',3'-hexamethylindodicarbocyanin iodide (DiIC₁(5)) dye. The decrease in the DiIC₁(5) intensity indicated mitochondrial depolarization, i.e., the onset of early apoptotic processes of HUVECs [23,24]. Cells were seeded to 96-well plates at a density of 20,000 cells per well treated with allithiamine of different concentrations (0.1, 0.5, 1, 5, 10, and 50 µg/mL). After the removal of the medium, the cells were incubated for 30 min with 50 µL/well DiIC₁(5) working solution (50 nM dissolved in Dulbecco's modified Eagle's medium). After incubation, cells were washed twice with PBS and the fluorescence of DiIC₁(5) was measured at 630 nm excitation and 670 nm emission wavelengths by using a Clariostar microplate reader (BMG Labtech, Ortenberg, Germany). The results were expressed relative to 100% of the control group.

2.2.6. Determination of Necrosis

Necrotic processes were evaluated by SYTOX Green staining. The dye is able to penetrate only necrotic cells with ruptured plasma membranes and then binds to the nucleic acids, whereas intact cells with unimpaired surface membranes show a negligible SYTOX Green staining intensity [23,24]. Cells were cultured in 96-well plates, and treated as indicated in Section 2.2.5. After the removal

of medium, cells were incubated for 30 min with 50 μL /well SYTOX Green dye (1 μM dissolved in Dulbecco's modified Eagle's medium) and then washed with PBS. The fluorescence of SYTOX Green was measured at 490 nm excitation and 520 nm emission wavelengths by using a Clariostar microplate reader (BMG Labtech, Ortenberg, Germany). The results were expressed relative to 100% of the control group.

2.2.7. Performing ELISAs

Measurement of Advanced Glycation End-Products

The assay was performed according to the manufacturer's instructions by using an OxisSelect™ Advanced Glycation End Product (AGE) Competitive ELISA Kit (Cell Biolabs Inc., San Diego, CA, USA).

Measurement of NF- κ B

The assay was performed according to the manufacturer's instructions by using a Human NF- κ B p65 Sandwich ELISA Kit (Fine Biological Technology Ltd., Wuhan, China)

2.2.8. Determination of Cytokine Release

HUVECs were seeded into a 6-well plate (500,000 cells/well), and were incubated in 5 mM/L glucose and 30 mM/L glucose with or without 5 $\mu\text{g}/\text{mL}$ allithiamine for 6, 12, or 24 h. Supernatants were collected, centrifuged for 10 min 10,000 $\text{r}\cdot\text{min}^{-1}$ and the released amount of IL-6, IL-8, and TNF- α was determined by using a MILLIPLEX MAP Human cytokine/chemokine Magnetic Bead Panel (EMD Millipore Corp., Billerica, MA, USA) based on the manufacturer's recommendation.

2.2.9. Measurement of Transketolase Activity

Transketolase activity was measured by adding 100 μL cytosolic fraction to 200 μL reaction mixture containing 14.8 mM/L ribose-5-phosphate, 253 $\mu\text{M}/\text{L}$ NADH, 185 U/mL triosephosphate isomerase, and 21.5 U/mL glycerol-3-phosphate dehydrogenase in Tris buffer (pH = 7.9). The optical density was measured at 340 nm immediately and then every 10 min for 2 h by using a Clariostar microplate reader (BMG Labtech, Ortenberg, Germany). The activity was calculated from the difference in the optical density readings at 10 and 80 by min using the extinction coefficient of NADH. Results are expressed in nMol/min/mg protein.

2.2.10. Determination of Protein Content

The protein concentrations were determined in the cell lysate by using a Pierce BCA Protein assay (Pierce Biotechnology Inc., Rockford, IL, USA). Protease inhibitor cocktail (Pierce Biotechnology Inc., Rockford, IL, USA) was added to the cell lysate prior to its storage or measurement.

2.2.11. Determination of ROS Production

The cells were seeded in a 24-well plate and exposed to 100 $\mu\text{M}/\text{L}$ 2',7'-dichlorofluorescein diacetate (DCFDA) for 1 h at 37 °C to label the intracellular ROS. After incubation, the cells were washed twice with PBS and divided into three groups: incubating with M199 medium as control; or with 100 $\mu\text{M}/\text{L}$ H_2O_2 ; or with 100 $\mu\text{M}/\text{L}$ H_2O_2 plus 5 $\mu\text{g}/\text{mL}$ allithiamine. Fluorescence (excitation = 485 nm; emission = 530 nm) was assessed by using a Clariostar microplate reader (BMG Labtech, Ortenberg, Germany).

2.2.12. Statistical Analysis

For multiple comparisons, results were analyzed by an ANOVA followed by a modified *t*-test for repeated measures according to Bonferroni's method. Data were presented as mean \pm SEM. Differences were considered statistically significant, when $p < 0.05$.

2.3. Ethics

The study was conducted in accordance with the Declaration of Helsinki, and the protocol was approved by the Ethics Committee of the University of Debrecen (registration number RKEB/IKEB 3712-2012).

3. Results

3.1. Purification and Verification of Allithiamine

Since allithiamine is not commercially available and that isolation from the plant does not work in large amounts, chemically prepared and purified allithiamine was applied for our experiments. The synthesis of allithiamine resulted in a wide variety of organosulfur compounds, which were separated by using the reversed-phase chromatographic method. After the chromatographic separation and purification of allithiamine, a fraction of allithiamine was verified by using the MALDI-MS and HPLC-MS/MS techniques. These methods clearly indicated that the chromatographic purification of allithiamine was accurate and efficient. The chromatogram (Supplementary Figure S1) of the synthetic mixture and MALDI-MS spectrum (Supplementary Figure S2) as well as the MS² spectrum (Supplementary Figure S3) of purified allithiamine can be seen in the Supplemental Materials.

3.2. Flow Cytometric Studies

Isolated HUVECs were characterized to positive and negative marker expressions by applying flow cytometry and antibodies against specific marker proteins, a routinely used method in our recent HUVEC-oriented study [22]. CD106, CD45, CD31, and CD54 were applied to label the cells. As shown in Figure 1, the isolated HUVECs showed a high CD31 and CD54 positive marker expression, while approximately 93% of the cells did not express CD45 and CD106 (negative markers). These results suggest that the isolation of HUVECs was sufficiently accurate and efficient.

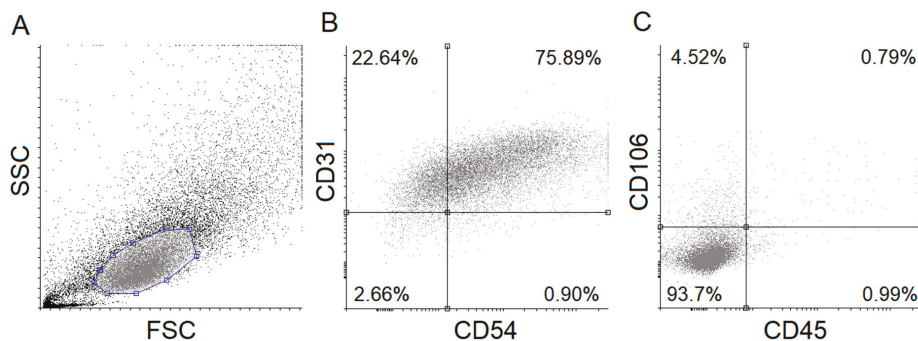


Figure 1. Flow cytometric analysis of human umbilical cord vein endothelial cells (HUVECs). Isolated HUVECs were verified using specific fluorescent-labeled antibodies. Forward- and side-scatter plot and dot-plots (A) of HUVEC positive (CD54, CD31) (B) and negative (CD45, CD106) (C) markers are shown. FSC: Forward scatter, SSC: Side scatter.

3.3. Determination of Optimal Concentration of Allithiamine

Up to 5 µg/mL, Allithiamine Treatment Has No Effect on Survival Rate of HUVECs

At first, the effect of allithiamine on cell viability was evaluated by using an MTT assay. HUVECs were exposed to allithiamine at different concentrations (0.1–50 µg/mL) for 24, 48, and 72 h. We found that up to 5 µg/mL allithiamine did not decrease the viability of HUVECs in this time window (Figure 2).

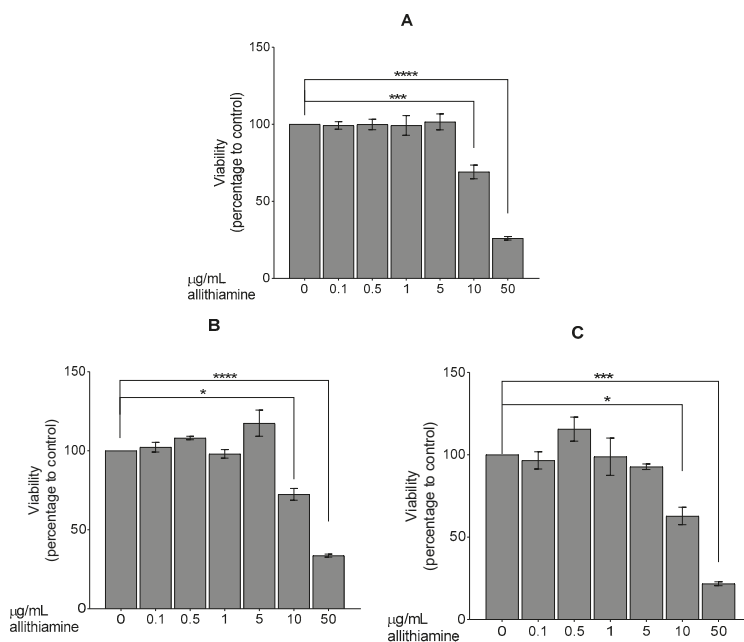


Figure 2. Viability of HUVECs was examined after 24 (A), 48 (B), or 72 (C) h. Results are expressed in the percentage of the control (0 µg/mL allithiamine). Data are expressed as the mean \pm SEM of three individual experiments. Two additional experiments yielded similar results. *, ***, and **** mark significant ($p < 0.05$, 0.0005, and 0.0001, respectively) differences compared with control.

In order to exclude the possibility of early apoptotic and necrotic events, which are not obvious alterations in the MTT assay, we further evaluated the effect of allithiamine whilst performing fluorescent labeling (DiI_{C1}(5) and SYTOX Green dyes). The results show that allithiamine, in line with the MTT data, did not induce a necrotic and apoptotic process and can be used without the risk of any biologically relevant cytotoxic actions in this concentration range (≤ 5 µg/mL; 24–72 h; Figure 3). Based on these preliminary experiments, a concentration of 5 µg/mL allithiamine was selected for further investigations.

3.4. Allithiamine Can Reduce the Level of Advanced Glycation End-Products (AGEs)

In cases of chronic hyperglycaemia, cells are exposed to prolonged elevated glucose concentrations leading to an excessive formation of AGEs [25]. Several studies have reported the positive effect of garlic sulfur compounds on the level of AGEs [26,27]. Therefore, we aimed to study the effects of allithiamine on the level of AGEs after one-day and one-week exposure to hyperglycaemia. As expected, 30 mMol/L glucose significantly increased the level of AGEs in HUVECs (Figure 4). We found that this hyperglycaemia-induced nearly 2-fold increase was significantly suppressed by the above-revealed non-cytotoxic concentration (5 µg/mL) of allithiamine.

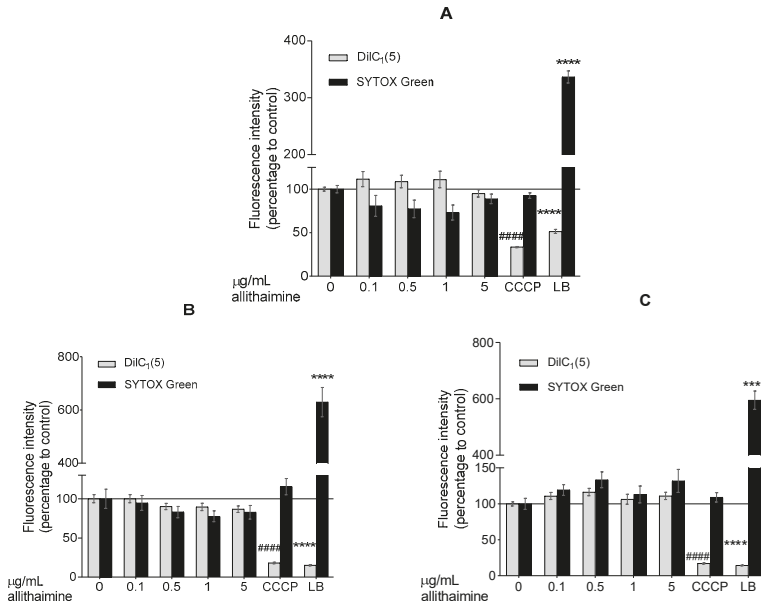


Figure 3. Fluorescent DiIC₁(5) and SYTOX Green labeling. Effect of allithiamine on apoptosis and necrosis after 24 (A), 48 (B), or 72 (C) h. Results (intensity of fluorescence) are expressed in the percentage of the control (0 μg/mL allithiamine; 100% is represented by the solid lines). Apoptosis is indicated by a decrease in fluorescence of DiIC₁(5), and necrosis is indicated by an increase in fluorescence of SYTOX Green. Data are expressed as the mean ± SEM of three individual experiments. Two additional experiments yielded similar results. **** and ##### mark significant (*p* < 0.0001 in both cases) differences compared with the control group (0 μg/mL allithiamine). CCCP: carbonyl cyanide *m*-chlorophenyl hydrazone (positive control for apoptosis); LB: lysis buffer (positive control for necrosis). SYTOX Green: non-permeable fluorescent nucleic acid dye; DiIC₁(5): 1,1',3,3',3',3'-hexamethylindodicarbocyanin iodide dye.

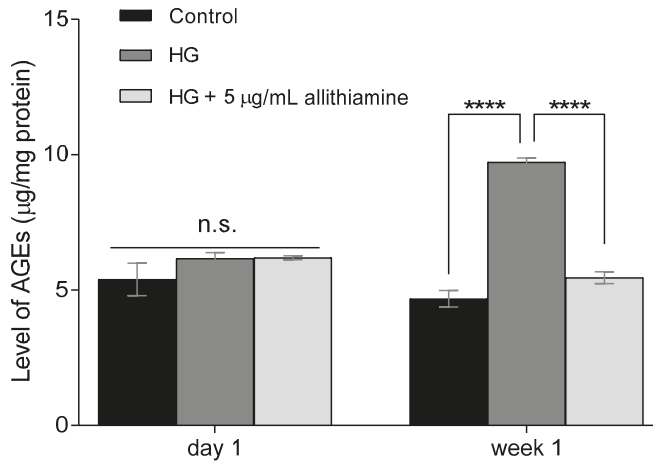


Figure 4. Effect of allithiamine on level of advanced glycation end-products (AGEs) in HUVECs after one day and one week. Data are expressed as the mean ± SEM of three individual experiments. **** marks a significant (*p* < 0.0001) difference between the control and HG, and between HG and HG+5 μg/mL allithiamine after one week. n.s.: not significant. HG: hyperglycaemia (30 mMol/L glucose).

3.5. Allithiamine Can Alleviate the Hyperglycaemia-Induced Inflammatory Response in HUVECs

Several studies reported the close relationship between hyperglycaemia and the inflammatory response of endothelium. In order to get a deeper insight into the effects of allithiamine on these inflammatory reactions, we assessed the activation of NF- κ B in the cell lysate after 6 and 12 h and the release of TNF- α , IL-6, and IL-8 in the cell supernatant after 6, 12, and 24 h incubation in 5 mM/L glucose and 30 mM/L glucose with or without 5 μ g/mL allithiamine. We found that the hyperglycaemic condition was able to trigger the inflammatory processes at an early time. The activation of NF- κ B was significantly increased after the hyperglycaemic treatments in all the sampling times. Allithiamine was able to decrease this increment (Figure 5). The secretion of IL-6 and IL-8 was significantly increased after the hyperglycaemic treatments in all the sampling times. The TNF- α secretion significantly increased after the hyperglycaemic treatment at 6 and 12 h. At 24 h, a statistically not significant but marked biological change was observed. We found that allithiamine could alleviate the hyperglycaemia-induced inflammatory response by suppressing the pro-inflammatory cytokines mentioned above (Figure 6).

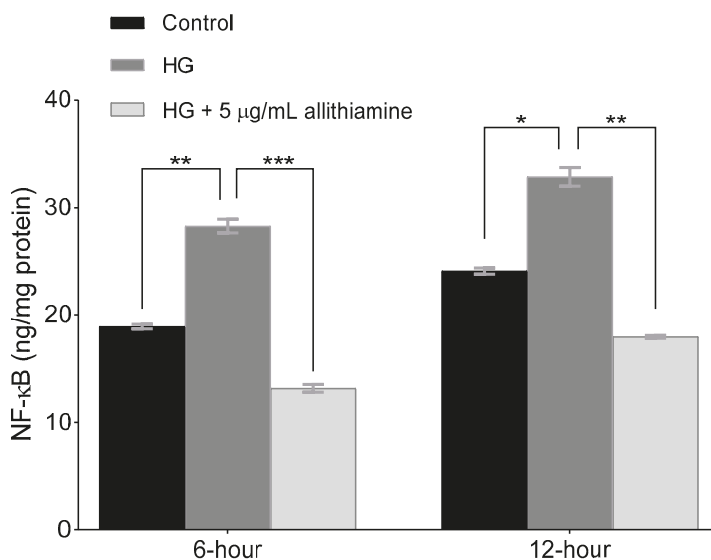


Figure 5. Effect of allithiamine on the activation of NF- κ B in HUVECs after 6 and 12 h. Data are expressed as the mean \pm SEM of three individual experiments *, **, and *** mark significant ($p < 0.05$, $p < 0.005$, and $p < 0.0005$) differences between the control and HG, and between HG and HG+5 μ g/mL allithiamine, HG: hyperglycaemia (30 mM/L glucose).

3.6. Allithiamine Has No Effect on Transketolase Activity

Considering the encouraging results presented above, we assayed to determine which mechanism may be responsible for the positive biological changes. First, we assumed that allithiamine, similar to thiamine derivatives, is able to enhance the activity of transketolase, a key enzyme in the pentose phosphate pathway. Benfothiamine is a potent transketolase activator [28], therefore, we applied it as a positive control in our experiments involving transketolase. The enzyme activity was evaluated in HUVECs after 6, 12, and 24 h of incubation. In the 6-h sample, we observed that 20 μ g/mL benfothiamine increased significantly the transketolase activity in cells incubated in 30 mM glucose compared with cells incubated in 5 mM glucose and 30 mM glucose. However, 5 μ g/mL allithiamine in cells incubated in 30 mM glucose did not change the transketolase activity significantly (Figure 7). Further incubations did not result in a significant increase in the transketolase activity (data not shown).

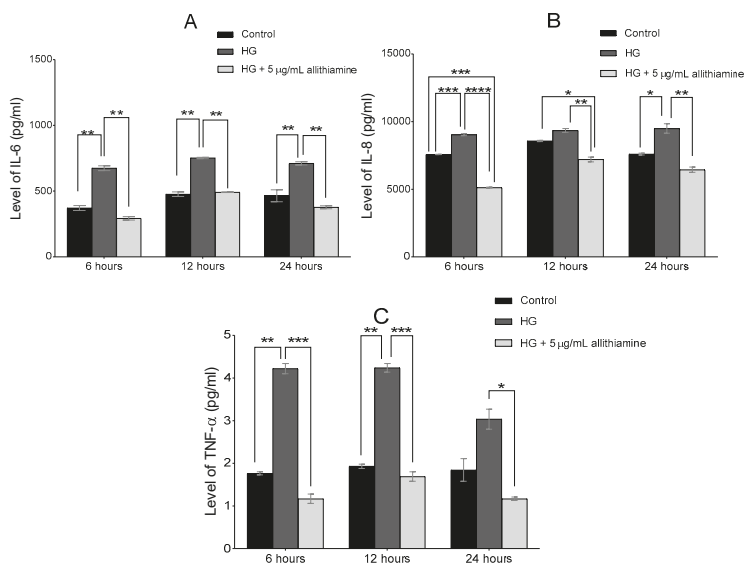


Figure 6. Effect of allithiamine on the level of pro-inflammatory cytokines including IL-6 (A), IL-8 (B), and TNF- α (C) in HUVECs after 6, 12, and 24 h. Data are expressed as the mean \pm SEM of three individual experiments. *, **, ***, and **** mark significant ($p < 0.05$, $p < 0.005$, $p < 0.0005$, and $p < 0.0001$) differences between the control and HG, between HG and HG+5 $\mu\text{g/mL}$ allithiamine, and between control and HG+5 $\mu\text{g/mL}$ allithiamine. HG: hyperglycaemia (30 mMol/L glucose).

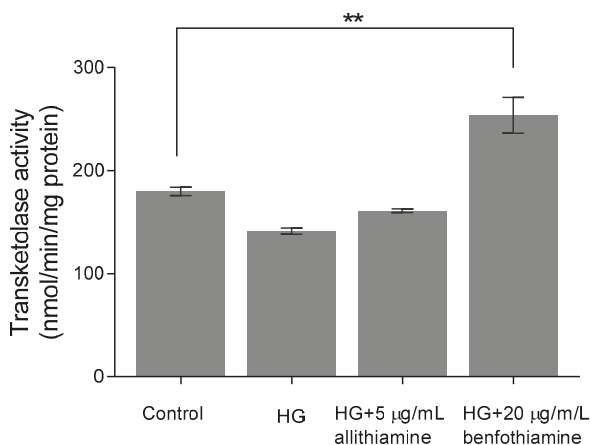


Figure 7. Effect of allithiamine on the transketolase activity in HUVECs after 6 h of incubation. Data are expressed as the mean \pm SEM of three individual experiments. Two additional experiments yielded similar results. ** marks a significant ($p < 0.005$) difference between the control and HG+20 $\mu\text{g/mL}$ benfotiamin. HG: hyperglycaemia (30 mMol/L glucose).

3.7. Allithiamine Exerts a Potent Antioxidant Effect

As small molecule organosulfur compounds with a prop-2-en-1-yl disulfanyl moiety of garlic have strong antioxidant properties [29], we further intended to investigate the potential antioxidant effect of allithiamine. To assess the antioxidant capacity of allithiamine, hydrogen-peroxide (H_2O_2), a routinely used oxidative agent [30], was applied in our HUVEC model, ensuring an enhanced ROS

production and imbalance in the oxidative status of cells. As expected, the administration of H_2O_2 significantly increased the production of ROS. Allithiamine was able to eliminate a significant part of this increment, indicating the potent antioxidant effect of allithiamine (Figure 8).

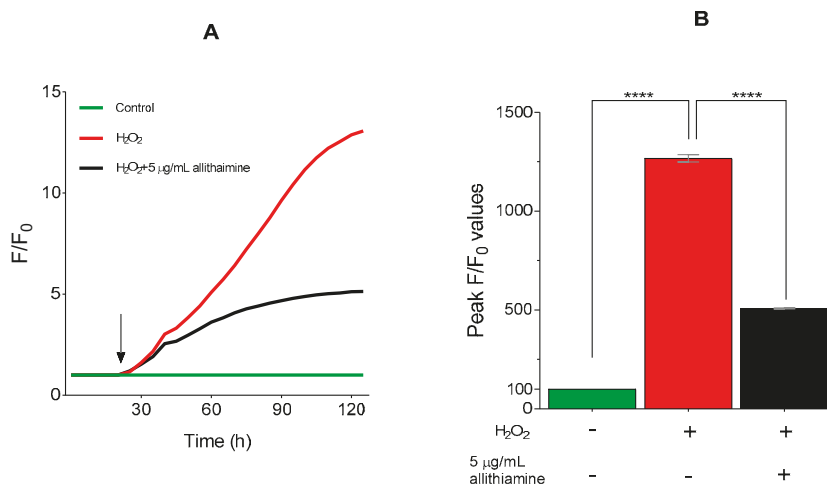


Figure 8. Antioxidative effect of allithiamine in HUVECs incubated with or without 100 μ Mol/L H_2O_2 . Fluorescent intensity was normalized to the baseline (A). H_2O_2 was administrated as indicated by the arrow. Statistical analysis was performed at the peak fluorescence (F/F_0) values (B). Data are expressed as the mean \pm SEM of three individual experiments. Two additional experiments yielded similar results. **** marks a significant ($p < 0.0001$) difference between the control and H_2O_2 , and between H_2O_2 and H_2O_2 +5 μ g/mL allithiamine. H_2O_2 : hydrogen-peroxide. – indicates the absence of treatment substance; + indicates the presence of treatment substance.

4. Discussion

In recent years, several research indicate that plant-derived compounds will be among the most important sources of new drugs [31]. Plants tend to produce several chemically highly diverse secondary metabolites, which may be suitable for exerting positive effects in human diseases [32]. Numerous studies have shown that garlic compounds (ajoene, alliin, allicin, diallyl disulfide S-allyl-cystein, etc.) are particularly valuable in this regard [33]. An experiment with mice demonstrated that hyperglycaemia was suppressed by ajoene treatment [34]. Another study revealed that allicin had a protective effect on hyperglycaemia-induced injury in aortic endothelial cells [35]. Findings of a study in rats suggest that S-allyl-Cystein treatment exerts a therapeutic protective effect on diabetes by decreasing oxidative stress [36]. Furthermore, comprehensive studies on garlic showed its therapeutic potential in various diseases accompanied by hyperglycaemia, including diabetes mellitus [37]. Our objective was to investigate the effect of allithiamine, a less-studied garlic component, on hyperglycaemia-induced endothelial pathologic changes (AGEs yielding, inflammatory processes, ROS production) in a HUVEC model.

Primarily, HUVECs were characterized by flow cytometric analysis using antibodies against specific marker proteins including CD31, CD45, CD54, and CD106. The results proved that the cells used in our experiments were endothelial cells, indeed. Subsequently, the non-cytotoxic concentration of allithiamine was determined by using an MTT assay and fluorescent labeling with DiIC₁(5) (examination of apoptosis) and SYTOX Green (investigation of necrosis) dyes. The viability tests of HUVECs after exposure to allithiamine at different concentrations (0.1–5 μ g/mL) for up to 72 h indicate that cells were not significantly affected.

In parallel with the research on the garlic component which showed a suppressed formation of AGEs [27], excellent markers of tissue damage caused by persistent hyperglycaemia [38], we examined

the effect of allithiamine on the level of AGEs. We found that a prolonged (one week) hyperglycaemia-induced increase in the level of AGEs was significantly suppressed by allithiamine.

In order to investigate the effects of allithiamine on inflammatory processes, we examined NF- κ B which has been proven to be upregulated under hyperglycaemic conditions. NF- κ B has a pivotal role in the inflammatory process as a transcriptional factor of several pro-inflammatory cytokines [39]. We found that allithiamine alleviated the expression of NF- κ B caused by an elevated glucose level. We also assessed the release of several cytokines including IL-6, IL-8, and TNF- α , which faithfully reflect the inflammatory state of HUVECs [40]. To observe the early release of the preformed cytokine pool and secretion of de novo-synthesized cytokines, we measured the level of the abovementioned molecules after 6, 12, and 24 h of treatment. We also revealed that allithiamine was able to significantly decrease the level of the investigated cytokine at the time of sampling.

Seeking possible reasons behind the positive effect of allithiamine, two plausible explanations were raised. At first, we assumed that allithiamine is able to enhance the transketolase activity, resulting in a decreased flux of hyperglycaemia-induced pathologic pathways involving the polyol, AGEs, PKC, and hexosamine pathways, similar to thiamine [41] and benfothiamine [28]. However, we found that 5 μ g/mL allithiamine did not change the transketolase activity significantly. We assumed that this non-toxic concentration may be rather negligible to increase the transketolase activity. At second, the widely researched garlic compounds having prop-2-en-1-yl moiety, as a two-edged sword, are able to attenuate the oxidative damage [29] and exert a beneficial anti-inflammatory effects as a slow H₂S donor [42,43]. Allithiamine possesses a prop-2-en-1-yl moiety, as well. In order to get a deeper insight into the putative antioxidant effect of allithiamine, an experiment was performed to verify the eliminating ability of ROS using H₂O₂ as an oxidative agent. Allithiamine was able to eliminate the significant part of ROS after the administration of H₂O₂. Consequently, our results clearly indicate that allithiamine exhibits a potent antioxidant effect, which may be responsible for the improvement in hyperglycaemia-induced endothelial dysfunction.

5. Conclusions

Collectively, in this study, we observed that—without influencing the viability, necrosis, or apoptosis of HUVECs—allithiamine was able to attenuate particular negative effects of an elevated glucose level by its potent antioxidant effect and a mechanism unrelated to the transketolase activity. Further studies are needed to elucidate the mechanisms of action of allithiamine as well as its supposed beneficial role in the spectrum of plant-derived bioactive molecules. However, our results contribute to a better understanding of this relatively less-researched compound, with particular respect to its beneficial effects on hyperglycaemia.

Supplementary Materials: The following are available online at <http://www.mdpi.com/2072-6643/12/6/1690/s1>, Figure S1: HPLC chromatogram of allithiamine at 250 nm, Figure S2: MALDI-TOF spectrum of purified allithiamine, Figure S3: MS² spectrum of allithiamine.

Author Contributions: J.R., A.B., conceived and designed the experiments, A.B., A.M., M.É.F., M.P. and G.F. performed the experiments. A.B., A.M., G.S., L.S. and J.L. analyzed the data. A.B. and J.R. wrote the paper. All authors have read and agreed to the published version of the manuscript.

Funding: This research received no external funding.

Acknowledgments: The work is supported by the GINOP-2.3.2-15-2016-00042 project. This project is co-financed by the European Union and the European Social Fund. The authors are grateful for the generous help of the Hungarian Academy of Sciences-University of Debrecen (HAS-UD) Vascular Biology and Myocardial Pathophysiology Research Group, Faculty of Medicine, Nephrology Division, Debrecen, Hungary, for the human umbilical vein endothelial cell isolation. The authors would like to thank Ádám Biró for helpful advice and corrections.

Conflicts of Interest: The authors declare no conflicts of interest.

References

- Dias, D.A.; Urban, S.; Roessner, U. A historical overview of natural products in drug discovery. *Metabolites* **2012**, *2*, 303–336. [[CrossRef](#)] [[PubMed](#)]
- Thomford, N.E.; Senthelane, D.A.; Rowe, A.; Munro, D.; Seele, P.; Maroyi, A.; Dzobo, K. Natural Products for Drug Discovery in the 21st Century: Innovations for Novel Drug Discovery. *Int. J. Mol. Sci.* **2018**, *19*, 1578. [[CrossRef](#)] [[PubMed](#)]
- Bayan, L.; Koulivand, P.H.; Gorji, A. Garlic: A review of potential therapeutic effects. *Avicenna J. Phytomed.* **2014**, *4*, 1–14. [[PubMed](#)]
- Jang, H.-J.; Lee, H.-J.; Yoon, D.-K.; Ji, D.-S.; Kim, J.-H.; Lee, C.-H. Antioxidant and antimicrobial activities of fresh garlic and aged garlic by-products extracted with different solvents. *Food Sci. Biotechnol.* **2017**, *27*, 219–225. [[CrossRef](#)] [[PubMed](#)]
- Arreola, R.; Quintero-Fabián, S.; López-Roa, R.I.; Flores-Gutiérrez, E.O.; Reyes-Grajeda, J.P.; Carrera-Quintanar, L.; Ortuño-Sahagún, D. Immunomodulation and anti-inflammatory effects of garlic compounds. *J. Immunol. Res.* **2015**, *2015*, 401630. [[CrossRef](#)] [[PubMed](#)]
- Ariga, T.; Seki, T. Antithrombotic and anticancer effects of garlic-derived sulfur compounds: A review. *BioFactors* **2006**, *26*, 93–103. [[CrossRef](#)]
- Sobenin, I.A.; Andrianova, I.V.; Lakunin, K.Y.; Karagodin, V.P.; Bobryshev, Y.V.; Orekhov, A.N. Anti-atherosclerotic effects of garlic preparation in freeze injury model of atherosclerosis in cholesterol-fed rabbits. *Phytomed. Int. J. Phytother. Phytopharmacol.* **2016**, *23*, 1235–1239. [[CrossRef](#)]
- Ried, K.; Fakler, P. Potential of garlic (*Allium sativum*) in lowering high blood pressure: Mechanisms of action and clinical relevance. *Integr. Blood Press Control* **2014**, *7*, 71–82. [[CrossRef](#)]
- Dorant, E.; van den Brandt, P.A.; Goldbohm, R.A.; Hermus, R.J.; Sturmans, F. Garlic and its significance for the prevention of cancer in humans: A critical view. *Br. J. Cancer* **1993**, *67*, 424–429. [[CrossRef](#)]
- Omar, S.H.; Al-Wabel, N.A. Organosulfur compounds and possible mechanism of garlic in cancer. *Saudi Pharm. J.* **2010**, *18*, 51–58. [[CrossRef](#)] [[PubMed](#)]
- Wang, J.; Zhang, X.; Lan, H.; Wang, W. Effect of garlic supplement in the management of type 2 diabetes mellitus (T2DM): A meta-analysis of randomized controlled trials. *Food Nutr. Res.* **2017**, *61*, 1377571. [[CrossRef](#)]
- Animaw, W.; Seyoum, Y. Increasing prevalence of diabetes mellitus in a developing country and its related factors. *PLoS ONE* **2017**, *12*, e0187670. [[CrossRef](#)] [[PubMed](#)]
- Fowler, M.J. Microvascular and Macrovascular Complications of Diabetes. *Clin. Diabetes* **2008**, *26*, 77. [[CrossRef](#)]
- Domingueti, C.P.; Dusse, L.M.S.A.; Carvalho, M.d.G.; de Sousa, L.P.; Gomes, K.B.; Fernandes, A.P. Diabetes mellitus: The linkage between oxidative stress, inflammation, hypercoagulability and vascular complications. *J. Diabete Complicat.* **2016**, *30*, 738–745. [[CrossRef](#)] [[PubMed](#)]
- Ren, X.; Ren, L.; Wei, Q.; Shao, H.; Chen, L.; Liu, N. Advanced glycation end-products decreases expression of endothelial nitric oxide synthase through oxidative stress in human coronary artery endothelial cells. *Cardiovasc. Diabetol.* **2017**, *16*, 52. [[CrossRef](#)] [[PubMed](#)]
- Rhee, S.Y.; Kim, Y.S. The Role of Advanced Glycation End Products in Diabetic Vascular Complications. *Diabetes Metab. J.* **2018**, *42*, 188–195. [[CrossRef](#)] [[PubMed](#)]
- Suryavanshi, S.V.; Kulkarni, Y.A. NF- κ B: A Potential Target in the Management of Vascular Complications of Diabetes. *Front. Pharmacol.* **2017**, *8*, 798. [[CrossRef](#)]
- Sun, Q.; Li, J.; Gao, F. New insights into insulin: The anti-inflammatory effect and its clinical relevance. *World J. Diabetes* **2014**, *5*, 89–96. [[CrossRef](#)]
- Birben, E.; Sahiner, U.M.; Sackesen, C.; Erzurum, S.; Kalayci, O. Oxidative stress and antioxidant defense. *World Allergy Organ. J.* **2012**, *5*, 9–19. [[CrossRef](#)]
- Matough, F.A.; Budin, S.B.; Hamid, Z.A.; Alwahaibi, N.; Mohamed, J. The role of oxidative stress and antioxidants in diabetic complications. *Sultan Qaboos Univ. Med. J.* **2012**, *12*, 5–18. [[CrossRef](#)]
- Biro, A.; Gál, F.; Hegedűs, C.; Batta, G.; Cziáky, Z.; Peitl, B.; Stündl, L.; Gyémánt, G.; Remenyik, J. Isolation of allithiamine from Hungarian red sweet pepper seed (*Capsicum annuum* L.). *Heliyon* **2018**, *4*, e00997. [[CrossRef](#)] [[PubMed](#)]
- Biro, A.; Markovich, A.; Homoki, J.R.; Szöllösi, E.; Hegedűs, C.; Tarapcsák, S.; Lukács, J.; Stündl, L.; Remenyik, J. Anthocyanin-Rich Sour Cherry Extract Attenuates the Lipopolysaccharide-Induced Endothelial Inflammatory Response. *Molecules* **2019**, *24*, 3427. [[CrossRef](#)] [[PubMed](#)]

23. Markovics, A.; Tóth, K.F. Nicotinic acid suppresses sebaceous lipogenesis of human sebocytes via activating hydroxycarboxylic acid receptor 2 (HCA(2)). *J. Cell. Mol. Med.* **2019**, *23*, 6203–6214. [[CrossRef](#)] [[PubMed](#)]
24. Oláh, A.; Markovics, A.; Szabó-Papp, J.; Szabó, P.T.; Stott, C.; Zouboulis, C.C.; Bíró, T. Differential effectiveness of selected non-psychotropic phytocannabinoids on human sebocyte functions implicates their introduction in dry/seborrheic skin and acne treatment. *Exp. Dermatol.* **2016**, *25*, 701–707. [[CrossRef](#)] [[PubMed](#)]
25. Huebschmann, A.G.; Regensteiner, J.G.; Vlassara, H.; Reusch, J.E. Diabetes and advanced glycoxidation end products. *Diabetes Care* **2006**, *29*, 1420–1432. [[CrossRef](#)] [[PubMed](#)]
26. Elostá, A.; Slevin, M.; Rahman, K.; Ahmed, N. Aged garlic has more potent antiglycation and antioxidant properties compared to fresh garlic extract in vitro. *Sci. Rep.* **2017**, *7*, 39613. [[CrossRef](#)]
27. Ahmad, M.S.; Pischetsrieder, M.; Ahmed, N. Aged garlic extract and S-allyl cysteine prevent formation of advanced glycation endproducts. *Eur. J. Pharmacol.* **2007**, *561*, 32–38. [[CrossRef](#)]
28. Hammes, H.P.; Du, X.; Edelstein, D.; Taguchi, T.; Matsumura, T.; Ju, Q.; Lin, J.; Bierhaus, A.; Nawroth, P.; Hannak, D.; et al. Benfotiamine blocks three major pathways of hyperglycemic damage and prevents experimental diabetic retinopathy. *Nat. Med.* **2003**, *9*, 294–299. [[CrossRef](#)]
29. Chung, L.Y. The antioxidant properties of garlic compounds: Allyl cysteine, alliin, allicin, and allyl disulfide. *J. Med. Food* **2006**, *9*, 205–213. [[CrossRef](#)]
30. Kaczara, P.; Sarna, T.; Burke, J.M. Dynamics of H₂O₂ availability to ARPE-19 cultures in models of oxidative stress. *Free Radic. Biol. Med.* **2010**, *48*, 1064–1070. [[CrossRef](#)]
31. Atanasov, A.G.; Waltenberger, B.; Pferschy-Wenzig, E.-M.; Linder, T.; Wawrosch, C.; Uhrin, P.; Temml, V.; Wang, L.; Schwaiger, S.; Heiss, E.H.; et al. Discovery and resupply of pharmacologically active plant-derived natural products: A review. *Biotechnol. Adv.* **2015**, *33*, 1582–1614. [[CrossRef](#)] [[PubMed](#)]
32. Ncube, B.; Van Staden, J. Tilting Plant Metabolism for Improved Metabolite Biosynthesis and Enhanced Human Benefit. *Molecules* **2015**, *20*, 12698–12731. [[CrossRef](#)] [[PubMed](#)]
33. Shang, A.; Cao, S.-Y.; Xu, X.-Y.; Gan, R.-Y.; Tang, G.-Y.; Corke, H.; Mavumengwana, V.; Li, H.-B. Bioactive Compounds and Biological Functions of Garlic (*Allium sativum* L.). *Foods* **2019**, *8*, 246. [[CrossRef](#)] [[PubMed](#)]
34. Hattori, A.; Yamada, N.; Nishikawa, T.; Fukuda, H.; Fujino, T. Antidiabetic effects of ajoene in genetically diabetic KK-A(y) mice. *J. Nutr. Sci. Vitaminol.* **2005**, *51*, 382–384. [[CrossRef](#)] [[PubMed](#)]
35. Wang, S.-L.; Liu, D.E.S.; Liang, E.-S.; Gao, Y.-H.; Cui, Y.; Liu, Y.-Z.; Gao, W. Protective effect of allicin on high glucose/hypoxia-induced aortic endothelial cells via reduction of oxidative stress. *Exp. Ther. Med.* **2015**, *10*, 1394–1400. [[CrossRef](#)] [[PubMed](#)]
36. Saravanan, G.; Ponnurugan, P. Beneficial effect of S-allylcysteine (SAC) on blood glucose and pancreatic antioxidant system in streptozotocin diabetic rats. *Plant Foods Hum. Nutr.* **2010**, *65*, 374–378. [[CrossRef](#)] [[PubMed](#)]
37. Ashraf, R.; Khan, R.A.; Ashraf, I. Garlic (*Allium sativum*) supplementation with standard antidiabetic agent provides better diabetic control in type 2 diabetes patients. *Pak. J. Pharm. Sci.* **2011**, *24*, 565–570.
38. Perkins, B.A.; Rabbani, N.; Weston, A.; Ficociello, L.H.; Adaikalakoteswari, A.; Niewczas, M.; Warram, J.; Krolewski, A.S.; Thornalley, P. Serum levels of advanced glycation endproducts and other markers of protein damage in early diabetic nephropathy in type 1 diabetes. *PLoS ONE* **2012**, *7*, e35655. [[CrossRef](#)]
39. Liu, T.; Zhang, L.; Joo, D.; Sun, S.-C. NF- κ B signaling in inflammation. *Signal Transduct. Target. Ther.* **2017**, *2*, 17023. [[CrossRef](#)]
40. Zhang, C. The role of inflammatory cytokines in endothelial dysfunction. *Basic Res. Cardiol.* **2008**, *103*, 398–406. [[CrossRef](#)]
41. Berrone, E.; Beltramo, E.; Solimine, C.; Ape, A.U.; Porta, M. Regulation of intracellular glucose and polyol pathway by thiamine and benfotiamine in vascular cells cultured in high glucose. *J. Biol. Chem.* **2006**, *281*, 9307–9313. [[CrossRef](#)] [[PubMed](#)]
42. Rios, E.C.; Szczesny, B.; Soriano, F.G.; Olah, G.; Szabo, C. Hydrogen sulfide attenuates cytokine production through the modulation of chromatin remodeling. *Int. J. Mol. Med.* **2015**, *35*, 1741–1746. [[CrossRef](#)] [[PubMed](#)]
43. Melino, S.; Leo, S.; Toska Papajani, V. Natural Hydrogen Sulfide Donors from *Allium* sp. as a Nutraceutical Approach in Type 2 Diabetes Prevention and Therapy. *Nutrients* **2019**, *11*, 1581. [[CrossRef](#)] [[PubMed](#)]



Article

Antiarthritic Effects of a Root Extract from *Harpagophytum procumbens* DC: Novel Insights into the Molecular Mechanisms and Possible Bioactive Phytochemicals

Alessia Mariano ¹, Antonella Di Sotto ², Martina Leopizzi ³, Stefania Garzoli ⁴, Valeria Di Maio ³, Marco Gulli ², Pietro Dalla Vedova ⁵, Sergio Ammendola ⁶ and Anna Scotto d'Abusco ^{1,*}

¹ Department of Biochemical Sciences, Sapienza University of Roma, P.le Aldo Moro 5, 00185 Roma, Italy; alessia.mariano@uniroma1.it

² Department of Physiology and Pharmacology, Sapienza University of Rome, P.le Aldo Moro 5, 00185 Rome, Italy; antonella.disotto@uniroma1.it (A.D.S.); marco.gulli@uniroma1.it (M.G.)

³ Department of Medico-Surgical Sciences and Biotechnologies, Polo Pontino-Sapienza University, 04100 Latina, Italy; martina.leopizzi@uniroma1.it (M.L.); dimaiovaleria@libero.it (V.D.M.)

⁴ Department of Drug Chemistry and Technologies, Sapienza University of Rome, P.le Aldo Moro 5, 00185 Rome, Italy; stefania.garzoli@uniroma1.it

⁵ UOC di Ortopedia e Traumatologia, Ospedale Santa Scolastica di Cassino, ASL di Frosinone, Via S. Pasquale, 03043 Cassino, Italy; pietro.dallavedova@aslfrosinone.it

⁶ Ambiotec S.A.S. Via Appia Nord 47, 04012 Cisterna di Latina (LT), Italy; ambiotec@libero.it

* Correspondence: anna.scottodabusco@uniroma1.it; Tel.: +39-06-4991-0947

Received: 28 July 2020; Accepted: 21 August 2020; Published: 23 August 2020

Abstract: *Harpagophytum procumbens* (Burch.) DC. ex Meisn. is a traditional remedy for osteoarticular diseases, including osteoarthritis (OA), although the bioactive constituents and mechanisms involved are yet to be clarified. In the present study, an aqueous *H. procumbens* root extract (HPE; containing 1.2% harpagoside) was characterized for its effects on synoviocytes from OA patients and phytochemical composition in polyphenols, and volatile compounds were detected. HPE powder was dissolved in different solvents, including deionized water (HPE_{H2O}), DMSO (HPE_{DMSO}), 100% *v/v* ethanol (HPE_{EiOH100}), and 50% *v/v* ethanol (HPE_{EiOH50}). The highest polyphenol levels were found in HPE_{DMSO} and HPE_{EiOH50}, whereas different volatile compounds, mainly β -caryophyllene and eugenol, were detected in all the extracts except for HPE_{H2O}. HPE_{H2O} and HPE_{DMSO} were able to enhance CB2 receptor expression and to downregulate PI-PLC β 2 in synovial membranes; moreover, all the extracts inhibited FAAH activity. The present results highlight for the first time a multitarget modulation of the endocannabinoid system by HPE, likely ascribable to its hydrosoluble compounds, along with the presence of volatile compounds in *H. procumbens* root. Although hydrosoluble compounds seem to be mainly responsible for endocannabinoid modulation by HPE, a possible contribution of volatile compounds can be suggested, strengthening the hypothesis that the entire phytocomplex can contribute to the *H. procumbens* healing properties.

Keywords: osteoarthritis; nutraceuticals; polyphenols; volatile compounds; β -caryophyllene; eugenol; FAAH; cannabinoid receptors; phospholipases

1. Introduction

Osteoarthritis (OA) is a pathology of the whole joint structure, involving several cellular and molecular processes, in different types of cells, such as chondrocytes, osteoblasts, synoviocytes, and immune cells [1]. The clinical symptoms include pain as well as joint dysfunction and deformity, often leading to joint replacement surgery, with high costs for healthcare [2].

Recently, an association between inflammation and endocannabinoid receptors has been described [3]. In particular, the role of CB2 receptors seems very interesting in OA inflammation. CB2 is a peripheral cannabinoid receptor and has been found in immune system cells, raising the possibility that the endocannabinoid system could have a role in immunomodulatory processes [3]. In this respect, several studies reported that mice lacking CB2 receptors showed an exacerbated inflammatory phenotype [4]. Moreover, CB2 receptors are involved also in inhibiting nociceptive transmission [5]. CB2 receptor signaling has been associated with phospholipase C (PI-PLC) activation in calf pulmonary endothelial cells and in mast cells [6,7]. Moreover, the inhibition of inflammatory pathways, such as NF- κ B nuclear translocation, has been obtained by inhibiting the PI-PLC β pathway in osteoblast-like cells [8]. The presence of CB2 in articular joints has been explored, mainly in animal models, and it has been highlighted in chondrocytes and in synoviocytes [9,10]. Thus, therapeutic strategies able to modulate CB2 signaling could be considered as a novel approach.

OA is treated with analgesic agents and anti-inflammatory and painkiller drugs, mainly non-steroidal anti-inflammatory drugs (NSAIDs), with the aim of alleviating symptoms [11]. Structure-modifying agents, such as nutraceuticals, are also administered to OA patients, with the aim of preventing or delaying cartilage degradation, even though further studies are required to confirm their effectiveness [12–14]. ARTRIT DOL, an Italian food supplement (Italian Minister of Health food supplement no. 71362 since 2013), is a composition containing glucosamine, chondroitin sulfate, extracts from *Harpagophytum procumbens* DC. and *Glycyrrhiza glabra* L., *Curcuma longa* L. roots, manganese, and copper in traces. Although this work does not focus on ARTRIT DOL, it is interesting to note that, as stated by the manufacturer, this nutritional supplement obtained good feedback from OA patients, in particular for the reduction of pain.

Harpagophytum procumbens (Burch.) DC. ex Meisn. (Fam. Pedaliaceae), commonly known as devil's claw, is a plant used worldwide as a traditional remedy for joint pain associated with OA and mild rheumatic ailments [15,16]. Moreover, it has been described to have analgesic effects on neuropathic pain in rats [17]. The harpagoside, one of the characteristic constituents of *H. procumbens* root, has been shown to be effective for osteoarthritis and low back pain [18].

The pharmacological activity of devil's claw root is attributed to the whole phytocomplex containing iridoid glucosides, such as harpagoside, phenolic glycosides (acteoside and isoacteoside), mono- and polysaccharides, triterpenes (mainly oleanolic acid, 3 β -acetyloleanolic acid, and ursolic acid), phytosterols, phenolic acids (caffeic, cinnamic, and chlorogenic acids), flavonoids, and minor components such as volatile compounds [15]. A number of studies have been conducted in order to characterize the analgesic and anti-inflammatory activities of *H. procumbens* and its secondary metabolites. An *in vitro* study showed that *H. procumbens* was able to decrease the production of proinflammatory cytokines and inhibit metalloprotease activity in human monocytes [19]. Studies conducted in animals showed that an aqueous *H. procumbens* extract showed dose-dependent analgesic and anti-inflammatory activity, but the purified harpagoside did not effectively inhibit the inflammatory pathways, at least at the dosage used in that study [20]. However, human clinical studies showed that the administration of *H. procumbens* root extract was able to improve the clinical picture of OA patients, in terms of pain and limitation of movements [21–23], suggesting that the phytocomplex may contribute to observed effects [20]. The biological effects of volatile compounds have not been extensively studied. Recently, the combination of purified β -caryophyllene with curcumin was shown to reduce the inflammation pathway through inhibition of NF- κ B in OA primary chondrocytes [24]. Purified β -caryophyllene has been described to mitigate pain in a mouse model of arthritis through a mechanism involving CB2 receptors [25]. Moreover, the volatile eugenol, a known dentistry analgesic, has been shown to be effective in a monoiodoacetate-induced rat model of osteoarthritis [26].

In the present study, an *H. procumbens* root extract was studied for its effects on human primary synoviocytes, with particular attention to the expression of CB2 receptors; furthermore, the extract was characterized for its polyphenol and volatile phytochemical content, in order to highlight possible novel bioactive compounds.

2. Materials and Methods

2.1. *Harpagophytum Procumbens* Extract

The dry aqueous extract from *H. procumbens* root (HPE) was provided by Ambiotec S.A.S. It was obtained starting from 300 g of root slices, which were repeatedly washed with cold ethanol 99% (*v/v*). After being washed, the slices were reduced by grinding with an electric miller for 10 min, and the powder was recovered by a sieve, with 4 mm holes. This powder was dissolved in ethanol/water solution (1:5 *w/v*) in the dark, shaking at 58 °C for 24 h, and then, it was filtered using 0.45 µm membrane. The retained fraction was air dried at 80 °C in a static dryer and in the presence of 5% maltodextrin (as carrier). The powder was again screened by a certified sieve (diameter 200 µm, mesh 100; net light 0.150 µm). The final yield of this preparation was 70% (drug-extract ratio, DER 1.4) of the initial root slices. The extract was a fine brown-colored powder with characteristic smell and taste, containing 1.2% (*w/w*) harpagoside. The powder was stored at room temperature in dry and dark conditions until use.

In order to evaluate antiarthritic activity and to highlight possible bioactive constituents, HPE was further dissolved in different solvents, including dimethyl sulfoxide (DMSO), 100% *v/v* ethanol (EtOH), 50% *v/v* EtOH, and deionized water. These solvents were chosen on the basis of their biocompatibility and ability to dissolve different classes of phytochemicals, mainly focusing on volatile compounds and polyphenols. Particularly, DMSO possesses high solubilizing properties for both polar and nonpolar compounds, thus, being able to dissolve the entire phytocomplex. Conversely, deionized water and ethanol recover mainly polar and nonpolar molecules, respectively, whereas 50% *v/v* ethanol is able to collect compounds dissolved by both solvents.

2.2. Phytochemical Analysis

2.2.1. Determination of Total Polyphenols, Tannins, and Flavonoids

Total amounts of polyphenols and tannins in the tested extracts were determined spectrophotometrically by the Folin–Ciocalteu method, as previously reported [27]. For both polyphenols and tannins, the absorbance was measured at 765 nm, and the amount was calculated as tannic acid equivalent (TAE) per milligram of dry HPE extract. Furthermore, total flavonoids and its subclass flavonols were measured by applying the aluminum chloride method with minor changes [27]. Specifically, total flavonoids were measured after mixing equal volumes of each extract (2 mg/mL) and aluminum trichloride (2% *w/v* in methanol), whereas the content of flavonols was determined by mixing 50 µL extract (4 mg/mL), 20 µL aluminum trichloride (10% *w/v* in methanol), 60 µL sodium hydroxide (1 M), 10 µL sodium nitrite (5% *w/v* in deionized water), and 70 µL deionized water. After a 10-min incubation, the absorbance was measured at 415 nm, and the total contents of flavonoids and flavonols were determined and expressed as quercetin equivalent (QE) per milligram of dry HPE extract.

2.2.2. Solid-Phase Microextraction (SPME)

For the extraction of volatile compounds, solid-phase microextraction (SPME) holders and coating fibers (Supelco; Bellefonte, PA, USA) were used. The sampling was performed with an SPME fiber (50/30 µm divinylbenzene/carboxen/polydimethylsiloxane—DVB/CAR/PDMS). Before sampling, the SPME fiber was conditioned by heating in the injector of a gas chromatograph at 270 °C for 30 min in order to remove traces of contaminants. Prior to analysis, a fiber blank was run to confirm the absence of contaminant peaks. To obtain a better extraction, SPME conditions, such as the most suitable temperature and equilibration time, were adjusted. Each sample (0.5 mL) was placed in a septum-sealed glass vial. The fiber was exposed to the headspace of the sample for 20 min at 40 °C. During this time, samples were stirred with a magnetic stirrer. After equilibration, the fiber

was removed from the sample and immediately inserted into the GC injection port for the thermal desorption (2 min) at 270 °C.

2.2.3. Gas Chromatography–Mass Spectrometry (GC–MS)

The extracts were analyzed using a GC–MS Perkin Elmer Clarus 500 instrument (Perkin Elmer, Waltham, MA, USA) equipped with a flame ionization detector (FID). Chromatographic separations were performed on a Varian FactorFour VF-1 fused-silica capillary column (length 60 m × 0.32 mm ID × 1.0 µm film thickness). The oven temperature program was as follows: 60 °C for two min, then, a gradient of 6 °C/min to 250 °C for 10 min, and an injector temperature of 270 °C. Helium was used as the carrier gas with a flow rate of 1.0 mL/min. Split injection with a split ratio of 1:20 was used. The electron-impact ionization mass spectrometer was operated as follows: ionization voltage, 70 eV; ion source temperature, 200 °C; scan mode, 30.0 to 500.0 mass range. The volatile compounds were identified by comparing mass spectra with those in the NIST02 and Wiley libraries. Furthermore, linear retention indices (LRIs) of each compound were calculated using a mixture of n-alkane hydrocarbons (C8–C30, Ultrasci, Ultra Scientific Italia, Bologna, Italy) injected directly into GC injector using the same temperature program reported above. Semiquantitative analysis was performed by normalizing the peak area generated in the FID (%) without using correction factors (relative response factors, RRFs). All analyses were repeated twice.

2.3. Human Tissue

Human synovial membranes were isolated from 6 OA patients and 5 non-OA (fractured) patients that underwent surgical treatment. Full ethical consent was obtained from all donors and the Research Ethics Committee, Sapienza University of Roma (#290/07, 29 March 2007), and ASL Lazio 2 (#005605/2019, 3 March 2019) approved the study. The tissues were fixed in 4% paraformaldehyde in 0.1 M phosphate buffer pH 7.2 immediately after removal from patients.

2.4. Immunohistochemistry

Histological sections were deparaffinized and rehydrated in graded ethanol. Endogenous peroxidase activity was blocked by 3% hydrogen peroxide for 10 min. Antigen retrieval was performed in 10 mM sodium citrate buffer (pH 6.0) for 15 min. The sections were then incubated with anti-CB1, anti-CB2, anti-PI PLC β2, and anti-PI PLC β3 (Santa Cruz Biotechnology, Inc., Dallas, TE, USA), all diluted 1:50, overnight at 4 °C. After incubation, specimens were washed and incubated with the secondary-biotinylated antibody and subsequently, with streptavidin–biotin–peroxidase (DAKOLSAB Kit peroxidase; DAKO, Carpinteria, CA, USA). The signals were developed by incubating with freshly prepared 3,3'-diaminobenzidine (DAB) substrate–chromogen buffer at room temperature. Slides were counterstained with hematoxylin and mounted with permanent mounting media. Negative controls were used in each experiment. The samples were scored semiquantitatively using a score based on the intensity and distribution: 0, undetectable; 1+, weak staining; 2+, medium staining; 3+, strong staining [28].

2.5. Human Primary Cell Isolation

Human primary synoviocytes (FLSs) were isolated from synovial membranes, obtained, as above described, from patients who underwent a total knee and hip arthroplasty. In brief, the synovial membrane fragments were minced and treated with 1 mg/mL collagenase type IV and 0.25% trypsin for 1 h, at 37 °C in agitation. Then, FLSs were grown to 80% confluence in DMEM (HyClone, Logan, UT, USA) supplemented with L-glutamine, penicillin/streptomycin (Sigma-Aldrich, St. Louis, MO, USA), and 10% fetal bovine serum (FBS) and cultured at 37 °C and 5% CO₂. All experiments were carried out with synoviocytes at first passage (p1), isolated from at least 3 different donors.

2.6. Immunofluorescence

Vimentin, CB2, and PI-PLC β 2 were visualized by immunofluorescence. Cells were plated at a density of $8 \times 10^3/\text{cm}^2$ and cultured for 48 h and then, washed in PBS, fixed in 4% paraformaldehyde in PBS for 15 min at 4 °C, and permeabilized with 0.5% Triton-X 100 in PBS for 10 min at room temperature. After blocking with 3% bovine serum albumin (BSA) in PBS for 30 min at room temperature, cells were incubated at 1 h, at room temperature, with mouse monoclonal anti-vimentin antibody (Proteintech Group, Manchester, UK) 1:50, mouse monoclonal anti-CB2 antibody 1:150, and mouse monoclonal anti-PI-PLC β 2 antibody (Santa Cruz Biotechnology) 1:50. Cells were washed with PBS and then, incubated for 1 h, at room temperature, with Alexa Fluor 488 donkey anti-rabbit antibody 1:300 (Invitrogen, Thermo Fisher Scientific, Waltham, MA, USA), to stain vimentin green; with Alexa Fluor 488 donkey anti-goat antibody 1:600 (Invitrogen, Thermo Fisher Scientific), to stain CB2 receptors green; and Alexa Fluor 595 donkey anti-rabbit antibody 1:300 (Invitrogen, Thermo Fisher Scientific), to stain PI-PLC β 2 red. Slides were washed and then, stained with DAPI (Invitrogen, Thermo Fisher Scientific) to visualize the nuclei. The images were captured by a Leica DM IL LED optical microscope, using an AF6000 modular microscope (Leica Microsystem, Milan, Italy).

2.7. Densitometric Analysis

The free software ImageJ (<https://imagej.nih.gov/ij/>) was used to perform the densitometric analysis of protein production. For each cell culture condition, the integrated density values of fluorescence were considered.

2.8. Cell Treatment

Cells were left untreated (CTL) or treated, for the required time, with 0.1 mg/mL of *Harpagophytum procumbens* root extract (HPE) dissolved in deionized water (HPE_{H2O}), DMSO (HPE_{DMSO}), 100% *v/v* EtOH (HPE_{EtOH100}), and 50% *v/v* EtOH (HPE_{EtOH50}). Experiments were independently repeated at least three times.

2.9. Cell Viability

To assess a potential cytotoxic effect of *H. procumbens* extracts on FLSs at different concentrations and time points, an MTS (3-(4,5-dimethylthiazol-2-yl)-5-(3-carboxymethoxyphenyl)-2-(4-sulfophenyl)-2H-tetrazolium)-based colorimetric assay was performed (Promega Corporation, Madison, WI, USA). Briefly, 8×10^3 cells per well were seeded in a 96-well plate. The day after seeding, cells were starved overnight in reduced serum medium, in order to align cell cycle progression. Cells were then left untreated (CTL) or treated with *H. procumbens* extracts for 24, 48, and 72 h. After each time point, 100 μ L MTS solution was added to the wells. Spectrophotometric absorbance was directly measured at 492 nm after 3 h incubation.

2.10. RNA Extraction and Reverse Transcription

Total RNA was extracted with TRIZOL (Invitrogen, Thermo Fisher Scientific), purified using a micro RNeasy column (Qiagen, Valencia, CA, USA), and reverse transcribed by Improm II enzyme, (Promega Corporation, Madison, WI, USA), according to the manufacturers' instructions.

2.11. Quantitative Real-Time PCR

Quantitative real-time PCR analysis was performed using an ABI Prism 7300 (Applied Biosystems, Thermo Fisher Scientific). Amplification was carried out using SensimixPlus SYBR master mix (Bioline, London, UK). Primers were designed using Primer Express software (Applied Biosystems) and were synthesized by Biofab Research (Rome, Italy). Primers' sequences are reported in Table 1.

Table 1. Sequences of the primers used in RT-PCR analysis.

Gene	Primer Sequences
CB1 NM_016083	Forward: 5'-TTCCTTCTGTGAAGGCACTG-3' Reverse: 5'-TCTTGACCGTGCTCTTGATGC-3'
CB2 NM_001841	Forward: 5'-ATGCTGTGCCTCATCAACTC-3' Reverse: 5'-CTCACACACTTCTCCAGTG-3'
FAAH NM_001441	Forward: 5'-CAGCTTTCCTCAGCAACATG-3' Reverse: 5'-CAATCACGGTTTGCGGTAC-3'
18S NM_003286	Forward: 5'-CGCCGCTAGAGGTGAAATTC-3' Reverse: 5'-CATTCTTGGCAAATGCTTTCG-3'

Data were analyzed by the $2^{-\Delta\Delta C_t}$ method, which determines the transcript abundance relative to the 18S housekeeping gene [29].

2.12. FAAH Inhibition

The potential ability of the tested extract to inhibit fatty acid amide hydrolase (FAAH) was evaluated using a commercial fluorescence-based kit (Cayman's FAAH Inhibitor Screening Assay Kit, Vinci Biochem, Vinci (FI), Italy), according to the manufacturer's instructions. The fluorescence of the FAAH-catalyzed product was measured at an excitation wavelength of 340 to 360 nm and an emission wavelength of 450 to 465 nm by a BD Accuri™ C6 flow cytometer (BD Biosciences, Milan, Italy). Suitable control wells treated with vehicles (maximum FAAH activity) and with the known FAAH inhibitor JZL 195 (maximum FAAH inhibition) were included. Each treatment was assayed at least in triplicate and at least in two different experiments. The enzyme activity was evaluated as % inhibition with respect to the vehicle.

2.13. Statistical Analysis

All data were obtained from at least three independent experiments, each performed either in duplicate or in triplicate ($n = 6$ or $n = 9$). Data were statistically analyzed with two-way repeated measures analysis of variance (ANOVA) with Bonferroni's multiple comparison test using Prism 5.0 software (GraphPad Software, San Diego, CA, USA). The p value < 0.05 was considered significant.

The Hill equation $E = E_{\max}/(1 + (10^{\log EC_{50}/A})^{\text{HillSlope}})$ (E , effect at a given concentration; E_{\max} , maximum activity; EC_{50} or IC_{50} , concentration giving a 50% inhibition; A , concentration of agonist; HillSlope, slope of the agonist curve) was applied to obtain a concentration–response curve.

3. Results

3.1. Phytochemical Characterization

The highest levels of total polyphenols were extracted by DMSO and 50% *v/v* EtOH, followed by deionized water and pure ethanol. Indeed, their levels in HPE_{DMSO} and HPE_{EtOH50} were 1.2- to 1.4-fold higher than in $HPE_{\text{H}_2\text{O}}$ and HPE_{EtOH100} (Table 2). Tannins were mainly recovered by H_2O and DMSO, their amount in $HPE_{\text{H}_2\text{O}}$ and HPE_{DMSO} being 1.5- to 1.9-fold higher than that found in HPE_{EtOH100} and HPE_{EtOH50} (Table 2). Regarding flavonoids and flavonols, the highest extraction power was exhibited by DMSO; HPE_{DMSO} exhibited about 1.5- to 3-fold and 1.5- to 1.7-fold higher concentrations of total flavonoids and flavonols than HPE_{EtOH50} or HPE_{EtOH100} and $HPE_{\text{H}_2\text{O}}$, respectively (Table 2).

Table 2. Amounts of total polyphenols, tannins, flavonoids, and flavonols in the extract from *Harpagophytum procumbens* root (HPE) dissolved in DMSO (HPE_{DMSO}), 100% *v/v* EtOH (HPE_{EtOH100}), 50% *v/v* EtOH (HPE_{EtOH50}), and deionized water (HPE_{H2O}). Data are the mean \pm SE of at least three independent experiments with three replicates for each experiment (n = 9).

Compounds	HPE _{DMSO}	HPE _{EtOH100}	HPE _{EtOH50}	HPE _{H2O}
	$\mu\text{g}/\text{mg}$ of Dry Extract (Mean \pm SE)			
Polyphenols (TAE)	99.6 \pm 0.05 ***§	69.6 \pm 0.05	97.9 \pm 0.01 ***§	84.2 \pm 0.04 **
Tannins (TAE)	14.2 \pm 0.02 **	9.2 \pm 0.04	9.2 \pm 0.02	17.9 \pm 0.03 ***
Flavonoids (QE)	113.0 \pm 5.1 ***§§	71.3 \pm 6.6 §§	75.1 \pm 6.1 §§	37.6 \pm 4.3
Flavonols (QE)	43.8 \pm 2.4 ***§§	27.6 \pm 3.2	30.1 \pm 2.0 §	25.1 \pm 2.0

TAE—tannic acid equivalent. QE—quercetin equivalent. ** $p < 0.01$ and *** $p < 0.01$ significantly higher than HPE_{EtOH100} (ANOVA followed by Bonferroni's multiple comparison post hoc test). § $p < 0.05$ and §§ $p < 0.01$ significantly higher than HPE_{H2O} (ANOVA followed by Bonferroni's multiple comparison post hoc test).

Altogether, these results revealed that DMSO is the most suitable for recovering total polyphenols, including tannins, flavonoids, and flavonols, followed by 50% *v/v* EtOH, especially for total flavonoids and flavonols. Pure ethanol extract possesses similar features compared to 50% *v/v* EtOH regarding total flavonoids and flavonols, with a lower recovery of total polyphenols. Finally, pure deionized water was able to better extract tannins, with significantly lower flavonoid levels.

The SPME–GC–MS analysis highlighted the presence of different volatile compounds in all the samples except for the aqueous HPE_{H2O} extract. Among them, eight compounds, listed in Table 3, were identified and their relative percentage amounts were calculated. Eugenol and β -caryophyllene were the main volatile phytochemicals in all extracts. Eugenol achieved a maximum 51.6% amount in HPE_{EtOH50}, while HPE_{DMSO} and HPE_{EtOH100} contained the highest percentages of β -caryophyllene (i.e., 77.4% and 77.1%, respectively). Moreover, β -pinene (5.1%) and isoeugenol (1.0%) were found in HPE_{EtOH50}, while thymol (0.8%) was found in HPE_{DMSO}. α -copaene was also identified in ethanolic extracts HPE_{EtOH100} and HPE_{EtOH50} (6.3% and 3.7%, respectively). On the other hand, α -humulene (10.0%; 0.8%) and δ -cadinene (5.8%; 1.3%) were detected in HPE_{DMSO} and HPE_{EtOH100}, respectively.

Table 3. Volatile compounds (relative percentage in the volatile fraction) detected in *Harpagophytum procumbens* root extract (HPE) dissolved in DMSO (HPE_{DMSO}), 100% *v/v* EtOH (HPE_{EtOH100}), 50% *v/v* EtOH (HPE_{EtOH50}), and deionized water (HPE_{H2O}).

No. ¹	Compound ²	LRI ³	LRI ⁴	MS ⁵	HPE _{DMSO} (%)	HPE _{EtOH100} (%)	HPE _{EtOH50} (%)	HPE _{H2O} (%)
1	β -pinene	978	974	+	-	-	5.1	-
2	thymol	1308	1310	+	0.8	-	-	-
3	eugenol	1339	1344	+	6.0	14.6	51.6	-
4	α -copaene	1381	1387	+	-	6.3	3.7	-
5	β -caryophyllene	1412	1416	+	77.4	77.1	38.6	-
6	isoeugenol	1432	1439	+	-	-	1.0	-
7	α -humulene	1450	1454	+	10.0	0.8	-	-
8	δ -cadinene	1528	1530 ⁺	+	5.8	1.3	-	-
	Total (%)				100.0	100.0	100.0	

¹ Compound identification number; ² compounds are reported according their elution order on column; ³ linear retention indices measured on apolar columns; ⁴ linear retention indices from literature; ⁺ normal alkane RI; ⁵ identification by MS spectra, tr < 0.1%.

3.2. Expression of Cannabinoid Receptors in OA Synovial Membrane

The presence of CB1 and CB2 receptors and PI-PLC β 2 and β 3 was detected by immunohistochemistry in synovial membranes isolated both from non-OA and OA patients. CB1 receptors were expressed in both normal and pathological tissues but with different scores; they were moderately present in non-OA patients (score 1+), while strongly present in OA patients (score 3+) (Figure 1, left-upper panel). CB2 receptors were detected only in non-OA tissue (score 2+) (Figure 1,

left-bottom panel). Regarding the presence of PI-PLC $\beta 2$ and $\beta 3$, we found that the expression of PI-PLC $\beta 2$ showed a lesser staining in non-OA (score 2+) than OA tissue (score 3+), and it was localized in the cytoplasm of both tissues (Figure 1, right-upper panel). PI-PLC $\beta 3$ was equally expressed in tissues from non-OA (score 3+) and OA patients (score 3+) (Figure 1, right-bottom panel). We also analyzed PI-PLC $\beta 1$ and PI-PLC $\beta 4$, finding that were both barely expressed both in non-OA and OA synovial membranes.

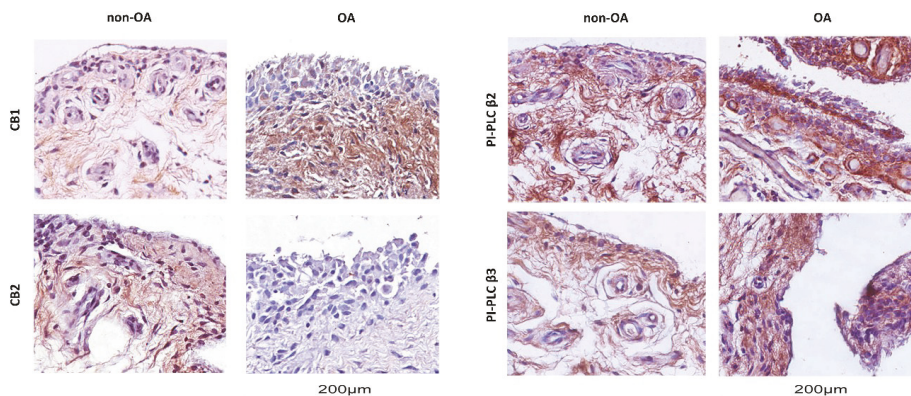


Figure 1. Immunohistochemical analysis of synovial membranes from OA (osteoarthritis) and non-OA patients. Left panel: Slices were stained with anti-CB1 and anti-CB2 receptor antibodies. Right panel: Slices were stained with anti-PI-PLC $\beta 2$ and anti-PI-PLC $\beta 3$ antibodies. Slides were counterstained with hematoxylin and mounted with permanent mounting media. This figure shows representative images of different experiments ($n = 5$ non-OA and $n = 6$ OA).

3.3. Effects of *Harpagophytum* Extracts on Synoviocyte Cell Viability

Synoviocytes were isolated by both OA and non-OA tissues. Two types of synoviocytes are present in the synovial membrane, A and B. The synoviocytes A are macrophage-like and the synoviocytes B are fibroblast-like synoviocytes (FLSs). The latter are characterized by their elongated shape and the expression of vimentin [30]; we verified the expression of this protein in our cells, finding that they were able to produce vimentin (Figure 2A).

The effects of *Harpagophytum procumbens* extracts on FLS cell viability were determined by the MTS colorimetric method. The extracts, tested at 1 mg/mL, 0.5 mg/mL, and 0.1 mg/mL for 24, 48, and 72 h, did not show detrimental effects at any analyzed concentration or time point (Figure 2B). We decided to use the 0.1 mg/mL concentration for further experiments.

3.4. Mechanism of Action of *Harpagophytum* Extracts on FLSs

In order to assay the effects of the different extracts on cannabinoid receptor expression, they were added to cell culture medium at a concentration of 0.1 mg/mL for 24 h, then, the mRNA expression level of CB1 and CB2 receptors was analyzed. The HPE_{H₂O} and HPE_{DMSO} and to a lesser extent, HPE_{E_tOH₅₀}, were able to increase the CB2 mRNA expression level, whereas HPE_{E_tOH₁₀₀} did not show any effect (Figure 3). CB1 receptor mRNA expression level was increased by HPE_{H₂O} and HPE_{DMSO} and to a lesser extent by HPE_{E_tOH₁₀₀}, whereas it was decreased by HPE_{E_tOH₅₀} (Figure 3).

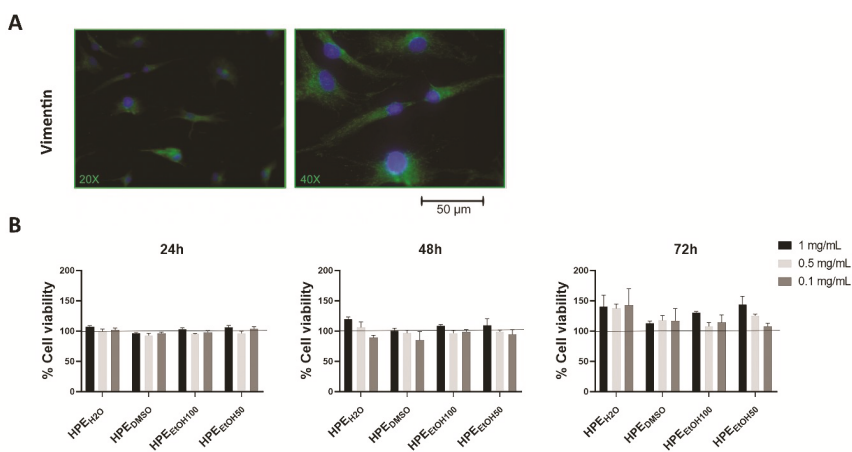


Figure 2. Characterization of human primary synoviocytes (FLSs) and analysis of cell viability. (A) Human primary FLSs, isolated by synovial membranes and cultured in vitro, were stained with anti-vimentin primary antibody and with Alexa Fluor 488 (green) secondary antibody. (B) Cell viability was assessed by the MTS colorimetric method, and FLSs were treated with three concentrations, 1, 0.5, and 0.1 mg/mL of *Harpagophytum procumbens* root extract (HPE) dissolved in deionized water (HPE_{H2O}), DMSO (HPE_{DMSO}), 100% v/v EtOH (HPE_{EtOH100}), and 50% v/v EtOH (HPE_{EtOH50}), for 24, 48, and 72 h. Cell viability of treated samples was normalized to the untreated cells, which is reported as 100% and represented by a horizontal line.

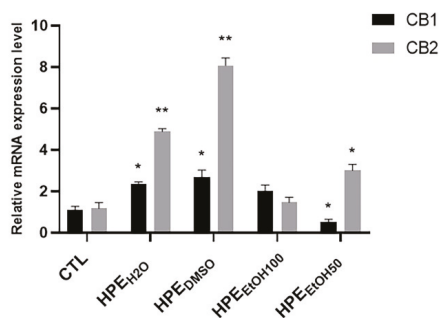


Figure 3. Effects of all HPE extracts on CB1 and CB2 mRNA expression level in human primary FLSs. After 24 h treatment with 0.1 mg/mL of *Harpagophytum procumbens* root extract (HPE) dissolved in deionized water (HPE_{H2O}), DMSO (HPE_{DMSO}), 100% v/v EtOH (HPE_{EtOH100}), and 50% v/v EtOH (HPE_{EtOH50}), cells were harvested and mRNA was extracted and analyzed by RT-PCR. CB1 and CB2 receptor mRNA levels were reported as relative mRNA expression level with respect to 18S mRNA ($2^{-\Delta\Delta C_t}$ method). Results are expressed as mean \pm S.E.M. of data obtained by three different experiments. Statistical significance was * $p < 0.05$; ** $p < 0.01$.

Considering that only CB2 receptors are associated with inflammation and pain in peripheral tissues, we verified whether the CB2 receptors also increased at the protein level by immunofluorescence staining. FLSs were treated with 0.1 mg/mL extracts for 24 and 48 h, then, the cells were stained with antibody anti-CB2. We found that HPE_{H2O} and HPE_{DMSO} extracts were able to stimulate the exposure in membrane of CB2 receptors, both at 24 and 48 h, whereas HPE_{EtOH50} and HPE_{EtOH100} did not stimulate CB2 receptor expression at any analyzed time (Figure 4 and Figure S1). Taking into account that the expression of PI-PLC β 2 was increased in synovial membranes from OA patients, we verified whether the HPE extracts were able to reduce the production of this phospholipase. HPE_{H2O}

and HPE_{DMSO} were able to inhibit the expression of PI-PLC β2, whereas HPE_{EtOH50} and HPE_{EtOH100} did not show effects (Figure 4).

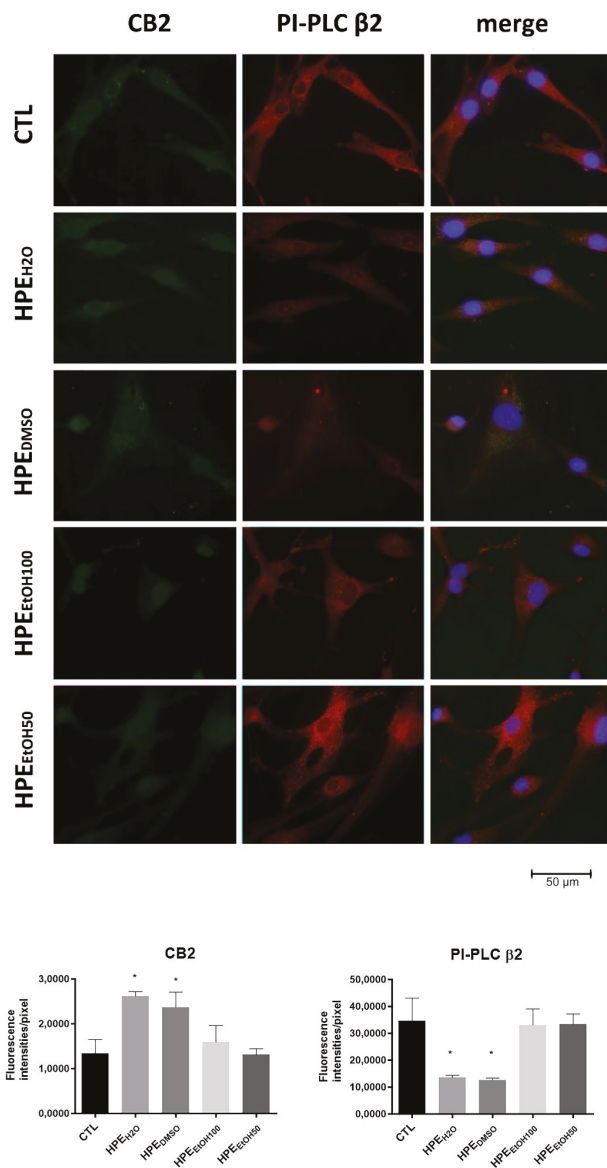


Figure 4. Effects of all HPE extracts on CB2 receptor and PI-PLC β2 protein production. Upper panel: Cells were treated with 0.1 mg/mL of *Harpagophytum procumbens* root extract (HPE) dissolved in deionized water (HPE_{H2O}), DMSO (HPE_{DMSO}), 100% *v/v* EtOH (HPE_{EtOH100}), and 50% *v/v* EtOH (HPE_{EtOH50}), for 24 h and then, analyzed by immunofluorescence using anti-CB2 and anti-PI-PLC β2 primary antibodies and Alexa Fluor 488 (green, CB2) and Alexa Fluor 568 (red, PI-PLC β2) secondary antibodies, respectively. Nuclei were stained with DAPI (original magnification 40×). Lower panel: The pixel intensities in the region of interest were obtained by ImageJ. * *p* < 0.05.

3.5. Inhibition of Fatty Acid Anandamide Hydrolase

In order to check whether the HPE extracts were able to affect the fatty acid amide hydrolase (FAAH), we analyzed both the FAAH mRNA expression level and enzymatic activity. HPE_{H2O} was able to decrease the FAAH mRNA level even if the downregulation was not statistically significant, whereas all other extracts were ineffective (Figure 5A). Interestingly, under our experimental conditions, all the extracts were able to interfere with the FAAH activity, although with different efficacy and potency (Figure 5B). Particularly, HPE_{H2O} was the least effective sample, achieving a maximum 58.5% enzyme inhibition at the highest concentration of 2500 µg/mL. Conversely, the other extracts could completely inhibit the FAAH enzyme, HPE_{EtOH100} being slightly more potent than HPE_{DMSO} and HPE_{EtOH50}, which displayed similar potencies. Indeed, the IC₅₀ value of HPE_{EtOH100} was about 1.2- to 1.5-fold lower than those of HPE_{EtOH50} and HPE_{DMSO} (Table 4). Under the same experimental conditions, 100 µg/mL harpagoside (corresponding to 200 µM) was found to be ineffective in the inhibition of the FAAH enzyme (about 9% inhibition compared the control). Conversely, the positive control JZL 195 (20 µM corresponding to 8.7 µg/mL) produced a maximum 90% enzyme inhibition (Table 4). As expected, the positive control was significantly more potent than the HPE extracts (Table 4).

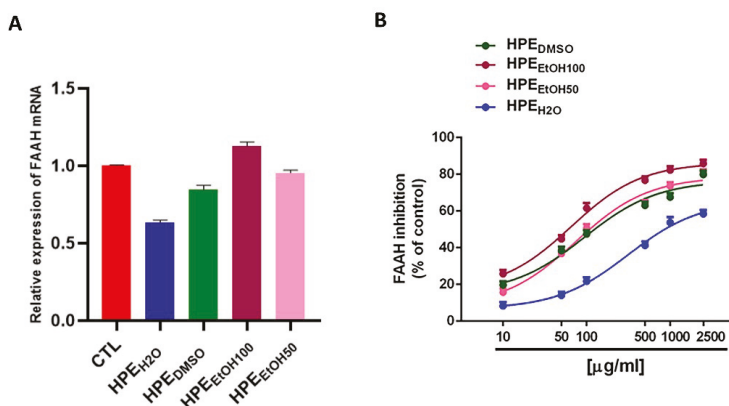


Figure 5. Effects of *Harpagophytum procumbens* root extract (HPE) on fatty acid anandamide hydrolase (FAAH) expression and enzymatic activity. (A) Cells were treated with 0.1 mg/mL of *Harpagophytum procumbens* root extract (HPE) dissolved in deionized water (HPE_{H2O}), DMSO (HPE_{DMSO}), 100% *v/v* EtOH (HPE_{EtOH100}), and 50% *v/v* EtOH (HPE_{EtOH50}), for 24 h. Cells were then harvested, and mRNA was extracted and analyzed by RT-PCR. FAAH mRNA levels were reported as relative mRNA expression level with respect to 18S mRNA ($2^{-\Delta\Delta C_t}$ method). Results are expressed as mean \pm S.E.M. of data obtained by three different experiments. (B) Concentration–response curves showing the inhibitory effects on FAAH from HPE_{DMSO}, 100% *v/v* HPE_{EtOH100}, 50% *v/v* HPE_{EtOH50}, and HPE_{H2O}. Data are the mean \pm SE of at least three independent experiments with two replicates for each experiment (n = 6).

Table 4. IC₅₀ values of *Harpagophytum procumbens* root extract (HPE) dissolved in DMSO (HPE_{DMSO}), 100% *v/v* EtOH (HPE_{EtOH100}), 50% *v/v* EtOH (HPE_{EtOH50}), and deionized water (HPE_{H2O}) and the positive control JZL 195 in the FAAH inhibition assay.

<i>Harpagophytum procumbens</i> Root Extract	IC ₅₀ (CL) µg/mL
HPE _{DMSO}	94.7 (23.8–97.5)
HPE _{EtOH100}	65.5 (19.2–87.9) *
HPE _{EtOH50}	73.8 (24.5–94.3)
HPE _{H2O}	-
JZL 195	0.03 (0.01–0.06) *

Not evaluable being lower than 80% inhibition achieved. * $p < 0.05$ significantly lower than HPE_{DMSO} (ANOVA followed by Bonferroni’s multiple comparison post hoc test).

4. Discussion

The aim of this study was to investigate the effects of *Harpagophytum procumbens* extract (HPE) on fibroblast-like synoviocytes (FLSs) from osteoarthritis patients, with particular attention on the endocannabinoid-mediated mechanisms. Osteoarthritis (OA) is characterized by chronic inflammation, and it is currently treated with anti-inflammatory drugs, which are only able to counteract the symptoms [2,31]. Several nutraceuticals, such as glucosamine, chondroitin sulfate, and curcumin, are administered with the aim of delaying the cartilage degradation, with inconsistent results [32]. Extracts from plants are also traditionally used to treat OA [16]. Among them, *H. procumbens* DC. has been studied for its chondroprotective activities, mainly for the ability to inhibit the production of proinflammatory mediators, such as TNF α and IL-1 β , and enzymes able to hydrolyze the extracellular matrix components, metalloproteases, and elastase [19].

Iridoid glycosides have received major attention as possible bioactive compounds of *H. procumbens* secondary metabolites [33]. Harpagoside is the most investigated one, and it is considered a reference standard of *H. procumbens* for titration purposes [15]. The anti-inflammatory activity of harpagoside has been found to be mediated by the inhibition of COX-1 and COX-2 enzymes along with by a lowered cytokine and NO release [33]. It was also able to counteract inflammation in primary human osteoarthritic chondrocytes through the suppression of c-FOS/AP-1 signal and the inhibition of proinflammatory cytokine and fibrinogenic factor production [23]. Moreover, harpagoside requires hydrolysis to a bioactive metabolite to exert its anti-inflammatory activity [34].

Despite this promising evidence, the anti-inflammatory properties of harpagoside cannot fully explain those of the entire *H. procumbens* phytocomplex, thus, suggesting that other compounds can contribute to the activity of the plant [15,33]. In the phytocomplex, some phenylpropanoids were reported to contribute to the *H. procumbens* anti-inflammatory effects [15].

Some studies have highlighted that plant roots can release volatile compounds as a defense strategy to counteract pathogen and fungal infections and to mediate the interaction between plant and soil bacteria [35–37]. Accordingly, our SPME–GC–MS analysis of HPE extracts highlighted the presence of several volatile compounds, mainly recovered by HPE_{DMSO}, 100% *v/v* HPE_{EtOH}, and 50% *v/v* HPE_{EtOH}. Among these volatile compounds, β -caryophyllene and eugenol were identified to be the major sesquiterpene and monoterpene present, followed by the sesquiterpenes α -humulene and α -copaene. Previously, 31 different volatile compounds, obtained by an heptanoic extraction, were characterized in *H. procumbens* root, although neither sesquiterpenes nor monoterpenes were detected [38]. In several preclinical models, β -caryophyllene, α -humulene, and eugenol have been shown to possess anti-inflammatory activities, affecting proinflammatory cytokine secretion and inhibiting inducible nitric oxide synthase (iNOS) and cyclooxygenase (COX-2) expression [39,40]. β -caryophyllene acts as an agonist of the endocannabinoid CB2 receptor, which is involved in the modulation of inflammation and the immune system and inhibits the fatty acid amide hydrolase enzyme [41,42]. Recent evidence highlighted the ability of this sesquiterpene to reduce articular and systemic inflammation in several animal models of arthritis [25,43,44]. Particularly, its antiarthritic effects in human articular chondrocytes were mediated by a crosstalk between CB2 and PPAR- γ receptors [25].

In articular joints, FLSs are involved both in supporting health chondrocytes and the immune system during inflammation [45]. In this study, we decided to use FLSs isolated from human synovial membranes as an *in vitro* model to study the effects of *H. procumbens* extracts. Preliminarily, the expression of CB2 receptors was checked in synovial membranes from OA and non-OA joints, and we found that it was expressed only in non-OA joints and was completely absent in OA. This finding agrees with the observations of Fukuda and coworkers, who found that CB2 receptors are expressed in rheumatoid arthritis (RA) synovial membranes and not in OA synovial membranes [46]. Moreover, they showed that CB2 plays an anti-inflammatory role in RA, and the treatment of RA synoviocytes with an agonist of CB2 blocked the production of proinflammatory mediators, through the inhibition of adenylyl cyclase, which, in turn, did not produce cAMP. Thus, protein kinase A was not activated,

finally leading to failure of the activation of NF- κ B [46]. Accordingly, the absence of CB2 in OA synovial membranes, which has been observed in our samples, can be associated with the activated inflammatory pathways present in joints of OA patients. Several studies showed the activation of NF- κ B in OA joints [34,47]; thus, the activation of pathways or molecules that can downregulate NF- κ B activity is very desirable [48,49]. Moreover, Sophocleous and coworkers showed that CB2^{-/-} mice had a greater susceptibility to OA [4].

The phosphoinositide (PI)-dependent signal plays important roles in many cellular processes, among them proinflammatory pathways, the alteration of which is involved in the onset and progression of several diseases [50]. The PI-phospholipase C (PI-PLC) β 1 isoform has been described as differently modulated in osteoblasts from OA and RA patients [51]. We analyzed the synovial membranes from OA and non-OA patients for the presence of PI-PLC β 1– β 4, finding that β 1 and β 4 were almost unexpressed both in OA and non-OA tissues, whereas β 3 was equally expressed in both tissues. Interestingly, β 2 was highly expressed in OA and poorly expressed in non-OA, suggesting that only β 2 is related to injured OA tissue. These findings prompted us to evaluate whether the *H. procumbens* extracts were able to modulate both CB2 and PI-PLC β 2 in isolated human primary FLSs, finding that HPE_{H₂O} and HPE_{DMSO} stimulated the expression of CB2 receptors and decreased the expression of PI-PLC β 2, whereas the HPE_{E_tO_H50} had a weak effect and HPE_{E_tO_H100} was completely ineffective on the expression of these two molecules. Thus, the ability of HPE_{H₂O} and HPE_{DMSO} to increase the expression of CB2 receptors may explain the anti-inflammatory and antinociceptive activity of this plant. The role of PI-PLC β 2 in inflammatory pathways has not been described so far; for this reason, the inhibition of its expression needs to be explored more in depth. We suppose that its expression in OA tissue could be associated with stimulation of the proinflammatory pathway through the activation of protein kinase C.

Moreover, further anti-inflammatory mechanisms are affected, as shown by the inhibition of FAAH in all the analyzed HPE extracts. The best inhibition was shown by HPE_{E_tO_H100} and HPE_{E_tO_H50}, so we can hypothesize that volatile compounds, such as β -caryophyllene, eugenol, and α -humulene, can be involved in these HPE effects.

5. Conclusions

Harpagoside, harpagide, and procumbide are present in all extracts, and ethnopharmacology considers them primarily responsible for *H. procumbens* activity. However, several studies, performed at the molecular level, showed that the administration of these purified compounds cannot justify the analgesic activity of the whole phytocomplex. The present study showed that further extractions with deionized water or DMSO can recover some bioactive compounds able to increase the synthesis of CB2 receptors, which are unexpressed in the osteoarthritic tissues. Moreover, the deionized water and DMSO extracts decrease the expression of the PI-PLC β 2 isoform, which, in turn, could inhibit the FAAH synthesis of endocannabinoids. Interestingly, DMSO, 50% ethanolic, and to a greater extent, 100% ethanolic extracts, were able to inhibit FAAH activity.

Further studies in vitro cell models and in vivo animal models are needed to support the hypothesis that *H. procumbens* root can be effective in controlling osteoarthritic pain, through the modulation of endocannabinoid system. The specific contribution of iridoid glucosides, polyphenols, and terpenes deserve to be further investigated too.

Supplementary Materials: The following materials are available online at <http://www.mdpi.com/2072-6643/12/9/2545/s1>, Figure S1: Effects of all HPE extracts on CB2 receptor and PI-PLC β 2 protein production after 48 h treatment.

Author Contributions: Conceptualization, A.S.d., A.D.S. and S.A.; methodology and investigation, A.M., A.D.S., M.L., S.G., V.D.M., M.G., P.D.V.; data curation, A.S.d., A.M., A.D.S.; writing—original draft preparation, A.S.d., S.A. and A.D.S. All authors have read and agree to the published version of the manuscript.

Funding: This research was partially funded by “Progetto di Facoltà 2019”.

Acknowledgments: We would like to thank Ssa E. Biscicchia for helpful discussion. A.D.S. fellowship was funded by grants from Sapienza University, “Progetto di Ateneo 2019”.

Conflicts of Interest: The authors declare no conflict of interest.

References

1. Robinson, W.H.; Lepus, C.M.; Wang, Q.; Raghu, H.; Mao, R.; Lindstrom, T.M.; Sokolove, J. Low-grade inflammation as a key mediator of the pathogenesis of osteoarthritis. *Nat. Rev. Rheumatol.* **2016**, *12*, 580–592. [[CrossRef](#)] [[PubMed](#)]
2. Goldring, S.R.; Goldring, M.B. Changes in the osteochondral unit during osteoarthritis: Structure, function and cartilage bone crosstalk. *Nat. Rev. Rheumatol.* **2016**, *12*, 632–644. [[CrossRef](#)] [[PubMed](#)]
3. Turcotte, C.; Blanchet, M.R.; Laviolette, M.; Flamand, N. The CB2 receptor and its role as a regulator of inflammation. *Cell. Mol. Life Sci.* **2016**, *73*, 4449–4470. [[CrossRef](#)]
4. Sophocleous, A.; Börjesson, A.E.; Salter, D.M.; Ralston, S.H. The type 2 cannabinoid receptor regulates susceptibility to osteoarthritis in mice. *Osteoarthr. Cartil.* **2015**, *23*, 1586–1594. [[CrossRef](#)] [[PubMed](#)]
5. Chiou, L.C.; Hu, S.S.J.; Ho, Y.C. Targeting the cannabinoid system for pain relief? *Acta Anaesthesiol. Taiwanica* **2013**, *51*, 161–170. [[CrossRef](#)]
6. Zoratti, C.; Kipmen-Korgun, D.; Osibow, K.; Malli, R.; Graier, W.F. Anandamide initiates Ca²⁺ signaling via CB2 receptor linked to phospholipase C in calf pulmonary endothelial cells. *Br. J. Pharmacol.* **2003**, *140*, 1351–1362. [[CrossRef](#)]
7. Ferrara, A.L.; Piscitelli, F.; Petraroli, A.; Parente, R.; Galdiero, M.R.; Varricchi, G.; Marone, G.; Triggiani, M.; Di Marzo, V.; Loffredo, S. Altered metabolism of phospholipases, diacylglycerols, endocannabinoids, and N-Acylethanolamines in patients with mastocytosis. *J. Immunol. Res.* **2019**. [[CrossRef](#)]
8. Nagao, M.; Tanabe, N.; Manaka, S.; Naito, M.; Sekino, J.; Takayama, T.; Kawato, T.; Torigoe, G.; Kato, S.; Tsukune, N.; et al. LIPUS suppressed LPS-induced IL-1 α through the inhibition of NF- κ B nuclear translocation via AT1-PLC β pathway in MC3T3-E1 cells. *J. Cell. Physiol.* **2017**, *232*, 3337–3346. [[CrossRef](#)]
9. Dunn, S.L.; Wilkinson, J.M.; Crawford, A.; Bunning, R.A.D.; Le Maitre, C.L. Expression of Cannabinoid Receptors in Human Osteoarthritic Cartilage: Implications for Future Therapies. *Cannabis Cannabinoid Res.* **2016**, *1*, 3–15. [[CrossRef](#)]
10. Richardson, D.; Pearson, R.G.; Kurian, N.; Latif, M.L.; Garle, M.J.; Barrett, D.A.; Kendall, D.A.; Scammell, B.E.; Reeve, A.J.; Chapman, V. Characterisation of the cannabinoid receptor system in synovial tissue and fluid in patients with osteoarthritis and rheumatoid arthritis. *Arthritis Res. Ther.* **2008**. [[CrossRef](#)]
11. McAlindon, T.E.; Bannuru, R.R. Latest advances in the management of knee OA. *Nat. Rev. Rheumatol.* **2018**, *14*, 73–74. [[CrossRef](#)] [[PubMed](#)]
12. Scotto d’Abusco, A.; Politi, L.; Giordano, C.; Scandurra, R. A peptidyl-glucosamine derivative affects IKK α kinase activity in human chondrocytes. *Arthritis Res. Ther.* **2010**, *12*. [[CrossRef](#)]
13. D’Adamo, S.; Cetrullo, S.; Panichi, V.; Mariani, E.; Flamigni, F.; Borzi, R.M. Nutraceutical Activity in Osteoarthritis Biology: A Focus on the Nutrigenomic Role. *Cells* **2020**, *9*, 1232. [[CrossRef](#)] [[PubMed](#)]
14. Stoppoloni, D.; Politi, L.; Leopizzi, M.; Gaetani, S.; Guazzo, R.; Basciani, S.; Moreschini, O.; De Santi, M.; Scandurra, R.; Scotto d’Abusco, A. Effect of glucosamine and its peptidyl-derivative on the production of extracellular matrix components by human primary chondrocytes. *Osteoarthr. Cartil.* **2015**, *23*, 103–113. [[CrossRef](#)]
15. Committee on Herbal Medicinal Products (HMPC). *Community Herbal Monograph on Harpagophytum Procumbens Dc. and/or Harpagophytum Zeyheri Decne, Radix*; European Medicines Agency: Amsterdam, The Netherlands, 2008.
16. Dragos, D.; Gilca, M.; Gaman, L.; Vlad, A.; Iosif, L.; Stoian, I.; Lupescu, O. Phytomedicine in joint disorders. *Nutrients* **2017**, *9*, 70. [[CrossRef](#)] [[PubMed](#)]
17. Lim, D.W.; Kim, J.G.; Han, D.; Kim, Y.T. Analgesic effect of harpagophytum procumbens on postoperative and neuropathic pain in rats. *Molecules* **2014**, *19*, 1060–1068. [[CrossRef](#)]
18. Gagnier, J.J.; Chrubasik, S.; Manheimer, E. Harpagophytum procumbens for osteoarthritis and low back pain: A systematic review. *BMC Complement. Altern. Med.* **2004**, *4*, 13. [[CrossRef](#)]

19. Fiebich, B.L.; Fiebich, B.L.; Heinrich, M.; Hiller, K.O.; Kammerer, N. Inhibition of TNF- α synthesis in LPS-stimulated primary human monocytes by Harpagophytum extract SteiHap 69. *Phytomedicine* **2001**, *8*, 28–30. [[CrossRef](#)]
20. Akhtar, N.; Haqqi, T.M. Current nutraceuticals in the management of osteoarthritis: A review. *Ther. Adv. Musculoskelet. Dis.* **2012**, *4*, 181–207. [[CrossRef](#)]
21. Wegener, T.; Lüpke, N.P. Treatment of Patients with Arthrosis of Hip or Knee with an Aqueous Extract of Devil's Claw (*Harpagophytum procumbens* DC.). *Phyther. Res.* **2003**, *17*, 1165–1172. [[CrossRef](#)] [[PubMed](#)]
22. Chantre, P.; Cappelaere, A.; Leblan, D.; Guedon, D.; Vandermander, J.; Fournie, B. Efficacy and tolerance of Harpagophytum procumbens versus diacerhein in treatment of osteoarthritis. *Phytomedicine* **2000**, *7*, 177–183. [[CrossRef](#)]
23. Haseeb, A.; Ansari, M.Y.; Haqqi, T.M. Harpagoside suppresses IL-6 expression in primary human osteoarthritis chondrocytes. *J. Orthop. Res.* **2017**, *35*, 311–320. [[CrossRef](#)] [[PubMed](#)]
24. D'Ascola, A.; Irrera, N.; Ettari, R.; Bitto, A.; Pallio, G.; Mannino, F.; Atteritano, M.; Campo, G.M.; Minutoli, L.; Arcoraci, V.; et al. Exploiting curcumin synergy with natural products using quantitative analysis of dose-effect relationships in an experimental in vitro model of osteoarthritis. *Front. Pharmacol.* **2019**, *10*, 1347. [[CrossRef](#)]
25. Irrera, N.; D'ascola, A.; Pallio, G.; Bitto, A.; Mazzon, E.; Mannino, F.; Squadrito, V.; Arcoraci, V.; Minutoli, L.; Campo, G.M.; et al. β -Caryophyllene Mitigates Collagen Antibody Induced Arthritis (CAIA) in Mice Through a Cross-Talk between CB2 and PPAR- γ Receptors. *Biomolecules* **2019**, *9*, 326. [[CrossRef](#)]
26. Ferland, C.E.; Beaudry, F.; Vachon, P. Antinociceptive effects of eugenol evaluated in a monoiodoacetate-induced osteoarthritis rat model. *Phyther. Res.* **2012**, *26*, 1278–1285. [[CrossRef](#)]
27. Di Sotto, A.; Di Giacomo, S.; Amatore, D.; Locatelli, M.; Vitalone, A.; Toniolo, C.; Rotino, G.L.; Lo Scalzo, R.; Palamara, A.T.; Marcocci, M.E.; et al. A polyphenol rich extract from solanum melongena L. DR2 peel exhibits antioxidant properties and anti-herpes simplex virus type 1 activity In Vitro. *Molecules* **2018**, *23*, 2066. [[CrossRef](#)]
28. Krenn, V.; Morawietz, L.; Häupl, T.; Neidel, J.; Petersen, I.; König, A. Grading of chronic synovitis—A histopathological grading system for molecular and diagnostic pathology. *Pathol. Res. Pract.* **2002**, *198*, 317–325. [[CrossRef](#)]
29. Schmittgen, T.D.; Livak, K.J. Analyzing real-time PCR data by the comparative CT method. *Nat. Protoc.* **2008**, *3*, 1101–1108. [[CrossRef](#)]
30. Li, F.; Tang, Y.; Song, B.; Yu, M.; Li, Q.; Zhang, C.; Hou, J.; Yang, R. Nomenclature clarification: Synovial fibroblasts and synovial mesenchymal stem cells. *Stem Cell Res. Ther.* **2019**, *10*, 260. [[CrossRef](#)]
31. Scanzello, C.R. Role of low-grade inflammation in osteoarthritis. *Curr. Opin. Rheumatol.* **2017**, *29*, 79–85. [[CrossRef](#)] [[PubMed](#)]
32. Honvo, G.; Reginster, J.Y.; Rabenda, V.; Geerinck, A.; Mkinsi, O.; Charles, A.; Rizzoli, R.; Cooper, C.; Avouac, B.; Bruyère, O. Safety of Symptomatic Slow-Acting Drugs for Osteoarthritis: Outcomes of a Systematic Review and Meta-Analysis. *Drugs Aging* **2019**, *36*, 65–99. [[CrossRef](#)] [[PubMed](#)]
33. Mncwangi, N.; Chen, W.; Vermaak, I.; Viljoen, A.M.; Gericke, N. Devil's Claw—A review of the ethnobotany, phytochemistry and biological activity of Harpagophytum procumbens. *J. Ethnopharmacol.* **2012**, *143*, 755–771. [[CrossRef](#)]
34. Zhang, L.; Feng, L.; Jia, Q.; Xu, J.; Wang, R.; Wang, Z.; Wu, Y.; Li, Y. Effects of β -glucosidase hydrolyzed products of harpagide and harpagoside on cyclooxygenase-2 (COX-2) in vitro. *Bioorg. Med. Chem.* **2011**, *19*, 4882–4886. [[CrossRef](#)] [[PubMed](#)]
35. Pichersky, E.; Gershenzon, J. The formation and function of plant volatiles: Perfumes for pollinator attraction and defense. *Curr. Opin. Plant Biol.* **2002**, *5*, 237–243. [[CrossRef](#)]
36. Wenke, K.; Kai, M.; Piechulla, B. Belowground volatiles facilitate interactions between plant roots and soil organisms. *Planta* **2010**, *231*, 499–506. [[CrossRef](#)]
37. Gfeller, V.; Huber, M.; Förster, C.; Huang, W.; Köllner, T.G.; Erb, M. Root volatiles in plant–plant interactions I: High root sesquiterpene release is associated with increased germination and growth of plant neighbours. *Plant Cell Environ.* **2019**, *42*, 1950–1963. [[CrossRef](#)]
38. Kriukova, A.; Vladimirova, I. The GC-MS determination of chemical constituents from harpagophytum procumbens dc roots. *Technol. Transf. Innov. Solut. Med.* **2017**, 52–54. [[CrossRef](#)]

39. Fernandes, E.S.; Passos, G.F.; Medeiros, R.; da Cunha, F.M.; Ferreira, J.; Campos, M.M.; Pianowski, L.F.; Calixto, J.B. Anti-inflammatory effects of compounds alpha-humulene and (-)-trans-caryophyllene isolated from the essential oil of *Cordia verbenacea*. *Eur. J. Pharmacol.* **2007**, *569*, 228–236. [[CrossRef](#)]
40. Barboza, J.N.; da Silva Maia Bezerra Filho, C.; Silva, R.O.; Medeiros, J.V.R.; de Sousa, D.P. An overview on the anti-inflammatory potential and antioxidant profile of eugenol. *Oxid. Med. Cell. Longev.* **2018**, *2018*, 3957262. [[CrossRef](#)]
41. Gertsch, J.; Leonti, M.; Raduner, S.; Racz, I.; Chen, J.Z.; Xie, X.Q.; Altmann, K.H.; Karsak, M.; Zimmer, A. Beta-caryophyllene is a dietary cannabinoid. *Proc. Natl. Acad. Sci. USA* **2008**, *105*, 9099–9104. [[CrossRef](#)] [[PubMed](#)]
42. Chicca, A.; Caprioglio, D.; Minassi, A.; Petrucci, V.; Appendino, G.; Tagliabatella-Scafati, O.; Gertsch, J. Functionalization of β -caryophyllene generates novel polypharmacology in the endocannabinoid system. *ACS Chem. Biol.* **2014**, *107*, 1499–1507. [[CrossRef](#)] [[PubMed](#)]
43. Ames-Sibin, A.P.; Barizão, C.L.; Castro-Ghizoni, C.V.; Silva, F.M.S.; Sá-Nakanishi, A.B.; Bracht, L.; Bersani-Amado, C.A.; Marçal-Natali, M.R.; Bracht, A.; Comar, J.F. β -Caryophyllene, the major constituent of copaiba oil, reduces systemic inflammation and oxidative stress in arthritic rats. *J. Cell. Biochem.* **2018**, *119*, 10262–10277. [[CrossRef](#)] [[PubMed](#)]
44. El-Sheikh, S.M.A.; Abd El-Alim, A.E.A.F.; Galal, A.A.A.; El-Sayed, R.G.; El-naseery, N.I. Anti-arthritis effect of β -caryophyllene and its ameliorative role on methotrexate and/or leflunomide-induced side effects in arthritic rats. *Life Sci.* **2019**, *233*, 116750. [[CrossRef](#)]
45. Scanzello, C.R.; Goldring, S.R. The role of synovitis in osteoarthritis pathogenesis. *Bone* **2012**, *51*, 249–250. [[CrossRef](#)]
46. Fukuda, S.; Kohsaka, H.; Takayasu, A.; Yokoyama, W.; Miyabe, C.; Miyabe, Y.; Harigai, M.; Miyasaka, N.; Nanki, T. Cannabinoid receptor 2 as a potential therapeutic target in rheumatoid arthritis. *BMC Musculoskelet. Disord.* **2014**, *15*, 275. [[CrossRef](#)]
47. Marcu, K.B.; Otero, M.; Olivotto, E.; Maria Borzi, R.; Goldring, M.B. NF- κ B Signaling: Multiple Angles to Target OA. *Curr. Drug Targets* **2010**, *11*, 599–613. [[CrossRef](#)]
48. Scotto d'Abusco, A.; Corsi, A.; Grillo, M.G.; Cicione, C.; Calamia, V.; Panzini, G.; Sansone, A.; Giordano, C.; Politi, L.; Scandurra, R. Effects of intra-articular administration of glucosamine and a peptidyl-glucosamine derivative in a rabbit model of experimental osteoarthritis: A pilot study. *Rheumatol. Int.* **2008**, *28*, 437–443. [[CrossRef](#)]
49. Veronesi, F.; Giavaresi, G.; Maglio, M.; Scotto d'Abusco, A.; Politi, L.; Scandurra, R.; Olivotto, E.; Grigolo, B.; Borzi, R.M.; Fini, M. Chondroprotective activity of N-acetyl phenylalanine glucosamine derivative on knee joint structure and inflammation in a murine model of osteoarthritis. *Osteoarthr. Cartil.* **2017**, *25*, 589–599. [[CrossRef](#)]
50. Suh, P.G.; Park, J.I.; Manzoli, L.; Cocco, L.; Peak, J.C.; Katan, M.; Fukami, K.; Kataoka, T.; Yun, S.; Sung, H.R. Multiple roles of phosphoinositide-specific phospholipase C isozymes. *J. Biochem. Mol. Biol.* **2008**, *41*, 415–434. [[CrossRef](#)]
51. Zini, N.; Lisignoli, G.; Solimando, L.; Bavelloni, A.; Grassi, F.; Guidotti, L.; Trimarchi, C.; Facchini, A.; Maraldi, N.M. IL1- β and TNF- α induce changes in the nuclear polyphosphoinositide signalling system in osteoblasts similar to that occurring in patients with rheumatoid arthritis: An immunocytochemical and immunocytochemical study. *Histochem. Cell Biol.* **2003**, *120*, 243–250. [[CrossRef](#)] [[PubMed](#)]



Article

In Vivo Anti-Inflammatory Effects and Related Mechanisms of Processed Egg Yolk, a Potential Anti-Inflammaging Dietary Supplement

Joan Cunill ^{1,*}, Clara Babot ¹, Liliana Santos ², José C. E. Serrano ², Mariona Jové ², Meritxell Martin-Garí ² and Manuel Portero-Otín ^{2,*}

¹ Ovivity Group, c/Angli 66 (torre), E08017 Barcelona, Spain; clarababot@ovivity.com

² Metabolic Pathophysiology Research Group/Nutren-Nutrigenomics, University of Lleida-Lleida Biomedical Research Institute's Pifarré Foundation (IRBLleida), Avda Rovira Roure, 80 E-25196 Lleida, Spain; ltsantos@ua.pt (L.S.); jcserrano@udl.cat (J.C.E.S.); mariona.jove@udl.cat (M.J.); meritxell.martin@udl.cat (M.M.-G.)

* Correspondence: joancunill@excelvit.com (J.C.); manuel.portero@udl.cat (M.P.-O.); Tel.: +34-69-641-9428 (J.C.); +34-97-370-2408 (M.P.-O.); Fax: +34-93-212-0130 (J.C.); +34-97-370-2426 (M.P.-O.)

Received: 28 July 2020; Accepted: 30 August 2020; Published: 4 September 2020

Abstract: Egg-yolk based supplements have demonstrated biological effects. We have developed a novel processed egg-yolk (PEY) complement, and we have tested whether it has inflammation modulatory properties. These were evaluated in a lipopolysaccharide (LPS)-challenge in 1-month male rats by in vivo circulating cytokine profiles measured by multiplexing techniques. Cell culture was used to explore ex vivo properties of derived serum samples. We explored growth factor composition, and mass-spectrometry metabolome and lipidome analyses of PEY to characterize it. PEY significantly prevented LPS-induced increase in IL-1 β , TNF- α , and MCP-1. Further, serum from PEY-treated animals abrogated LPS-induced iNOS build-up of the Raw 264.7 macrophage-like cell line. Immunochemical analyses demonstrated increased concentrations of insulin-like growth factor 1 (IGF-1), connective tissue growth factor (CTGF), and platelet-derived growth factor (PDGF) in the extract. PEY vs. egg-yolk comparative metabolomic analyses showed significative differences in the concentrations of at least 140 molecules, and in 357 in the lipidomic analyses, demonstrating the complexity of PEY. Globally, PEY acts as an orally-bioavailable immunomodulatory extract that may be of interest in those conditions associated with disarranged inflammation, such as inflammaging.

Keywords: fecundation; inflammation; cytokine; growth factors; metabolomics; lipidomics

1. Introduction

Inflammaging is a chronic increase in the body's pro-inflammatory status with advancing age in some tissues [1]. As inflammatory reactions increase, neurohormonal signaling (e.g., renin-angiotensin, adrenergic, insulin-IGF1 signaling) tends to be deregulated, immunosurveillance against pathogens and premalignant cells declines, and the composition of the peri- and extracellular environment changes, thereby affecting the mechanical and functional properties of tissues involved [2]. With the rise of this aging characteristic, a new concept of "anti-inflammaging" was also proposed, which influences progressive pathophysiological changes, as well as lifespan, and acts along with inflammaging [1]. In physiological conditions, the immune system helps to maintain homeostasis by mounting nonspecific innate and specific adaptive responses (inflammation) against potential aggressions. The inflammatory response is driven by a complex network of mediators and signaling pathways and is the net effect of interactions between pro-inflammatory and anti-inflammatory molecules (cytokines) that determines the immune response [3]. A properly functioning and reliable immune system is essential

for maintaining health. When the expression of cytokines is chronically altered, it can lead to chronic inflammation, tumorigenesis, and autoimmunity. Inflammaging comprises the phenomena explaining the age-related trend towards increasing pro-inflammatory cytokine concentrations, more pronounced for IL-6, IL-8, IL-2, IFN- γ , and TNF- α [4], which is an indicator of the inflammation. It is logical to think, thus, that adequating the wrong cytokine profile, can prevent or slow down over some of the harmful consequences of the aging process.

Among the measures addressed to this rearrangement, pharmacological treatments can be found—statins to improve cardiac health [5]; also, nutritional approaches like caloric restriction [5]. Also, dietary supplements have emerged as potential anti-aging treatments, like antioxidants (curcumin, polyphenols), vitamins, and probiotics. The NIH defines dietary supplements as “substances you might use to add nutrients to your diet or to lower your risk of health problems, like osteoporosis or arthritis” [6]. Raising health concerns, changing lifestyles, and dietary habits, are driving increased attention to these products. In this line, there is ample scientific evidence that eggs contain biologically active compounds that may have a role in the therapy and prevention of chronic and infectious diseases. Several dietary supplements derived from eggs can be found in the market, broadly divided into unfertilized (commercialized), and fertilized. Commercialized hen eggs are highly nutritious food; its macronutrient content includes low carbohydrates and about 12 g per 100 g of protein and lipids (most of which are monounsaturated) as well as several nutrients such as zinc, selenium, retinol, and tocopherols. It is known that regular commercialized egg yolk contains proteins and peptides with biological activity. For example, it has been seen that whole egg yolk in the native form as a potential source of angiotensin converting enzyme-inhibitory peptides, or that yolk lipoproteins are important for lipid-mediated antimicrobial activity; also, a protein called γ -livetin, also referred to as immunoglobulin Y, exerts the same immunomodulatory activity as immunoglobulin G, and has been shown to have immunoregulatory effects [7]. In fact, *in vivo* anti-inflammatory and analgesic effects of nonfertilized egg yolk have been reported [8]. Based on preclinical studies, egg phosphatidylcholine and sphingomyelin species appear to regulate cholesterol absorption and inflammation; in clinical studies, egg phospholipid intake is associated with beneficial changes in biomarkers related to HDL reverse cholesterol transport [9]. Fertilized eggs contain every nutrient essential to sustaining a new life, in a closed shell that only permits O₂, CO₂ and H₂O gas exchange [10], and its composition changes as the embryo develops. The screening of the bioactive components in the different development stages has attracted researcher’s attention, and important differences have been observed, showing very interesting potential applications. However, reports on the immune mechanism and the related bioactive components are limited.

Furthermore, to our knowledge, there are no studies regarding the effects of the intake of fertilized eggs *in vivo*. We have obtained, by a patented process [11], an extract of fertilized eggs, termed here patented egg yolk (PEY). To shed light over its effects in the inflammaging context, we explored its potential anti-inflammatory effect in comparison with the commercial egg yolk, and we characterized its composition in order to establish further screening protocols of the potential mechanisms of action, with the final goal of establishing the basis for potential interventional inflammaging studies.

2. Materials and Methods

2.1. Chemicals

Unless stated otherwise, all chemicals were obtained from indicated major commercial suppliers. PEY consists of an egg preparation obtained through a patented process [11]. It comprises a mixture of yolk and white extracted from a fertilized egg which has been incubated for a short period, which then is lyophilized to obtain a commercial product called Excelvit®.

2.2. Animals

One-month-old male Wistar rats (initial weight 75–100 g, $n = 10$ per group in the 5 day treatment regime, and $n = 5$ in the two or one day-treatment regime) obtained from Harlan Laboratories (Catalunya, Spain) were maintained at 23 ± 2 °C under a 12:12 h light-dark cycle (lights on from 07:00 to 19:00). All rats were allowed unlimited access to Harlan Teklad 14% protein rodent maintenance diet during the whole experimental period. After one week of acclimation to animal facilities, the animals were weighed and divided into two groups (PEY and egg yolk group) with equal bodyweight. Experimental treatment consisted of a 4-h fast (8:00–12:00 a.m.), where further a daily dose of 2000 mg/kg of PEY or egg yolk during one, two or five days was administered by oro-gastric gavage. Bodyweight and signs of toxicity were recorded daily during the treatment period, in which all treated animals showed adequate health. After the designated duration (one, two or five days), 2-h after the oro-gastric gavage of PEY or egg yolk, all animals were intraperitoneally injected with a 2.5 mg/kg dose of lipopolysaccharide (LPS, Sigma-Aldrich, Sant Louis, MO, USA). One hour after LPS injection, all animals were sacrificed by cervical displacement, and blood samples were collected by cardiac puncture. Serum from blood samples was collected within 30 min by centrifugation and immediately frozen with liquid nitrogen, and stored at -80 °C until further analyses. The study was conducted in accordance with the Declaration of Helsinki, and the protocol was approved by the University of Lleida Institutional Animal Care Committee (Project Code CEEA 03/03-12).

2.3. Cytokine Analysis

Cytokines were determined by Milliplex RECYMAG65K27PMX magnetic bead immunology multiplex assay (Merck-Millipore, Burlington, MA, USA) following the manufacturer's instructions.

2.4. Cell Culture and Treatments

Mouse RAW 264.7 macrophages (ATCC TIB-71) were grown in a humidified incubator containing 5% CO₂ and 95% air at 37 °C. Cells were grown in DMEM medium supplemented with 10% of heat-inactivated fetal bovine serum, 100 UI/mL of penicillin, and 100 µg/mL of streptomycin. In all experiments, cells were grown until confluence and then transferred to 6-well plates. On the day of the assay, the medium was changed to serum-free medium for 4 h, and further cells were exposed to DMEM medium supplemented with 10% rat serum obtained from rats exposed to a dose of 2000 mg/day (for five days) of PEY or egg yolk, or fetal bovine serum. For iNOS activation, a dose of 0.1 microgram/mL of LPS was added to selected wells. After 24-h, cells were collected and lysed using RIPA buffer with protease and phosphatase inhibitors. Protein concentrations were measured using the Bradford assay (BioRad Laboratories, München, Germany) with bovine serum albumin as a standard, and further cell-lysates were frozen a -80 °C for further analyses.

2.5. Western Blot Analysis

Total protein (15–40 µg) was resolved by SDS-PAGE and electroblotted onto polyvinylidene difluoride membranes (Immobilon-P Millipore, Bedford, MA, USA). Immunodetection was performed using primary antibodies anti-iNOS (Cell Signaling Technologies #2977), PDGF (RD Systems, AB23NA), NGF (Abcam Ab6199), CTGF (Genetex, GTX37727), and IGF-1 (Abcam, Ab106838). A monoclonal antibody to β -actin (Sigma, Saint Louis, MO, USA) was used to control protein loading from cell culture samples. Protein bands were visualized with the chemiluminescence ECL[®] method (Millipore Corporation, Billerica, MA, USA). Luminescence was recorded and quantified in Lumi-Imager equipment (Boehringer, Mannheim, Germany), using the Quantity One 4.6.5. software (Bio-Rad, Hercules, CA, USA).

2.6. Lipidomic and Metabolomic Analyses

Metabolites and lipids in PEY and egg yolk were analyzed by liquid chromatography coupled to mass spectrometry as previously described [12]. For metabolomics, samples were depleted of proteins

by methanol addition [13]. The resulting metabolites were separated using a reverse-phase column (Zorbax SB-Aq 1.8 μm 2.1 \times 50 mm; Agilent Technologies, Barcelona, Spain). We employed a gradient of water to methanol (all with 0.2% acetic acid) in a chromatograph (LC Agilent 1290) coupled to a mass spectrometry system (time of flight (TOF) mass spectrometer Agilent 6520). Mass spectra were collected in both negative and positive ionization modes, scanning from m/z values from 50 to 1600, at 1.5 scans/s. For lipidomic analyses, lipids were obtained by chloroform:methanol extraction, internal standards added, and processed as described [14,15] employing the same system as above (Agilent Technologies, Santa Clara, CA, USA) with adequate solvents [14]. This method allows the orthogonal characterization (based on exact mass (<10 ppm) and on retention time) of lipids. When combined with internal standards, this strategy is useful for proposing potential identities with low uncertainty [14,16]. In this case, data were collected in both positive and negative electrospray ionization in full-scan mode at 100–3000 m/z in an extended dynamic range (2 GHz).

2.7. Statistical Analyses and Data Annotation

Statistic calculations were performed using SPSS (IBM SPSS v 25, Armonk, NY, USA) and GraphPad Prism 8 (GraphPad Software, San Diego, CA, USA). The Kolmogorov–Smirnov test checked the normality of the distribution of variables. For metabolomics and lipidomic analyses, only common features (found in $\geq 75\%$ of the replicas of PEY and egg yolk samples) were taken into account, to correct for individual bias. Principal component analysis (PCA), partial least squares discrimination analysis (PLS-DA), and hierarchical clustering analysis were performed using MassHunter Mass Profiler Professional (Agilent Technologies, Barcelona, Spain) after the transformation of chromatographic results to the CEF[®] format. Analyses (Volcano plots, PCA and PLS-DA reported here) were performed employing the Metaboanalyst 3.0 platform [17].

Annotations of metabolites were produced based on an accurate mass-retention time algorithm (Agilent[®], MassHunter Mass Profiler Professional) and for lipids on the comparison with the retention time of internal standards. Therefore, the level of evidence of annotation is 2 (i.e., putatively annotated compounds, without chemical reference standards, based upon physicochemical properties and spectral similarity with public/commercial spectral libraries), according to [18]. A level of $p < 0.05$ was selected as the point of minimal statistical significance in every comparison. Pathway analyses were produced according to these putatively annotated compounds by employing the ConsensusPathDataBase platform [19].

3. Results

As expected, LPS injection induced an increase in plasma levels of cytokines (Supplemental Figure S1A), increasing ca 43% circulating levels of TNF- α after 2 h. To study the systemic anti-inflammatory effects of PEY, plasmatic concentrations of cytokines of animals feed during five days with PEY were measured after 2 h of performing the inflammatory stimulus (LPS injection) (Figure 1A). Compared with egg-yolk, the PEY group presented a significant reduction in plasmatic concentrations of IL-1 β (Figure 1B), TNF- α (Figure 1C), and MCP-1 (Figure 1D). Interestingly, shorter times of treatment also sufficed to abrogate LPS-induced buildup of circulating cytokines (1 day, Supplemental Figure S1A; or 2 days, Supplemental Figure S1B).

Demonstrating the bioavailability of PEY and the solubility of PEY-induced effects, the anti-inflammatory effect was confirmed ex-vivo using Raw 264.7 cells treated with the serum of the animals exposed during five days to PEY and egg-yolk (Figure 1E). RAW 264.7 cells were treated with LPS to stimulate their inflammatory response, and i-NOS content was measured. A significant difference in the iNOS immunoreactivity between the LPS group and the other groups, showing the different inflammatory responses of the cells, was observed (Figure 1E). iNOS production by the cells treated with the serum of the egg yolk group was significantly lower than control, and the serum of rats treated with PEY had the highest anti-inflammatory effect, significantly lower than the egg yolk.

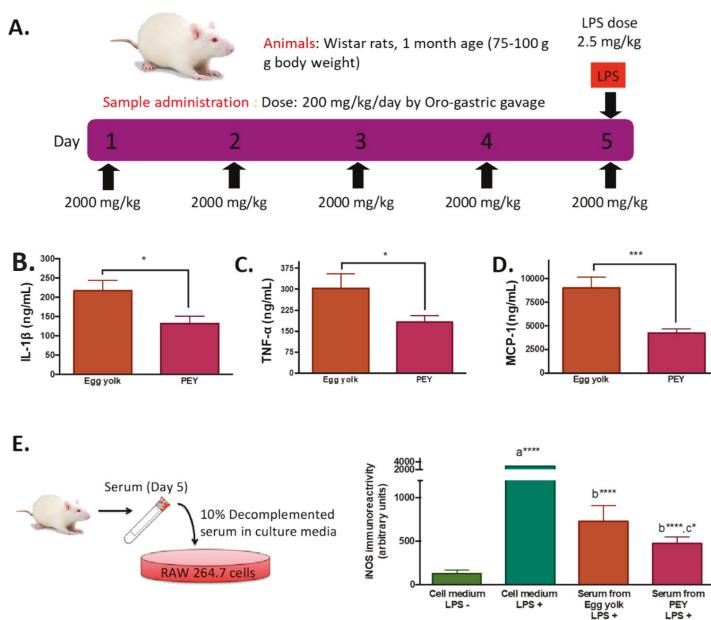


Figure 1. Characterization of the anti-inflammatory effects of processed egg-yolk in vivo. (A) Oral administration of processed egg-yolk (PEY) during five days and application of inflammatory aggression the 5th day by lipopolysaccharide (LPS). (B–D) Plasmatic concentrations of cytokines IL-1 β , TNF- α , and MCP-1 in the control group (egg yolk) and treated group (PEY) after 2 h of the administration of lipopolysaccharide (LPS) (* $p < 0.05$, *** $p < 0.001$). (E) iNOS immunoreactivity of Raw 264.7 cell culture exposed to 0.1 $\mu\text{g/mL}$ of LPS after the application of standard cell medium (no treatment), blood serum from rats treated with egg yolk (control) and serum from rats treated with PEY; a **** significant difference with cell medium LPS- $p < 0.001$; b **** significant difference with cell medium LPS+ $p < 0.0001$; c * significant difference with serum from egg yolk LPS+ $p < 0.05$. One-way ANOVA or Student's *t*-test was used for statistical analyses. In vitro experiments were performed in triplicate, while as treatments were delivered to $n = 10$ animals per group.

The composition of PEY was studied to explore the origin of the anti-inflammatory effects observed. We evaluated the presence of growth factors (Figure 2), as well as the comparative metabolomics and lipidomics (Figure 3) of egg yolk and PEY.

It was observed that PEY contained 2.5 more connective tissue growth factor (CTGF), 1.7 more platelet-derived growth factor (PDGF), 1.3 more nerve growth factor (NGF) and 8.6 more insulin-like growth factor (IGF-1) than egg yolk (see Figure 2). All the increases were significant, but NGF. The presence of growth factors has been previously described [20]. The results of liquid chromatography coupled to mass spectrometry indicate (Figure 3) that PEY contains a non-negligible number of methanol-soluble (metabolites) and organic solvent-soluble (lipids) differing from egg yolk. Interestingly, lipidomic profiles allow a more thorough differentiation in comparison to metabolomics (Figure 3A,E). Even applying a Benjamini–Hochberg correction for false discovery rate, a total of 357 differential lipids were found (231 increased in PEY and 126 increased in PEY, FDR = 0.05; Supplemental Dataset). A total number of 140 metabolites differentially present in the extract were also found (16 increased in egg yolk and 124 increased in PEY, FDR = 0.05; Supplemental Dataset). Collectively, regarding putative identifications, these lipids clustered among different sphingolipid-related pathways, as well as some immune-related pathways (Figure 3D). Interestingly, differential metabolites were also present in pathways related to omega-3 fatty acids, among many other metabolic nodes (Figure 3H). All differential metabolites and lipids, including exact mass, chromatographic behavior (retention

time in respective systems), composite spectrum, fold-change and *p*-values (both raw and adjusted for false-discovery rate) are available as a Supplemental Dataset in Excel® file in Supplemental materials, found online. Similarly, the individual levels of metabolites and lipids employed for pathway analyses (Figure 3D,H) can be found in an ad-hoc designed web page (<https://excelv.herokuapp.com/>).

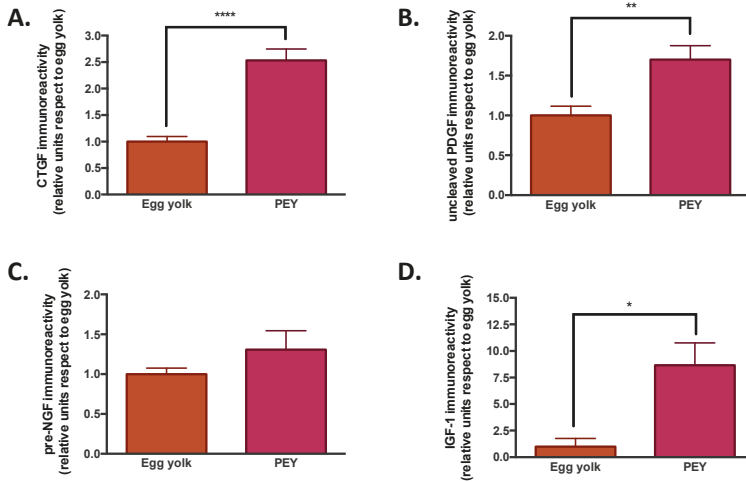


Figure 2. PEY contains a significant amount of growth factors. (A). Connective tissue growth factor (CTGF) immunoreactivity in egg yolk and PEY, showing a difference between them with a *p* < 0.0001 significance. (B). Platelet-derived growth factor (PDGF) immunoreactivity in egg yolk and PEY, showing the difference between them with a *p* < 0.01 significance. (C). Nerve growth factor (NGF) immunoreactivity in egg yolk and PEY, showing no significant difference between them. (D). Insulin-like growth factor 1 (IGF-1) immunoreactivity in egg yolk and PEY, showing a significant difference between them (* *p* < 0.05, ** *p* < 0.01, **** *p* < 0.0001).

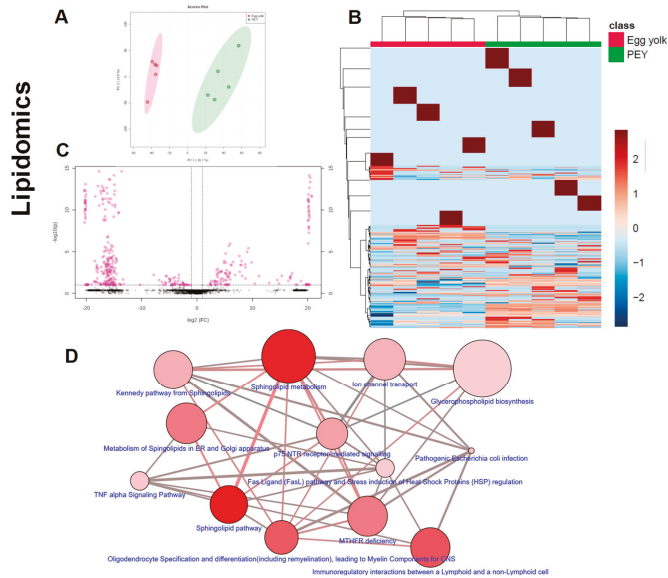


Figure 3. Cont.

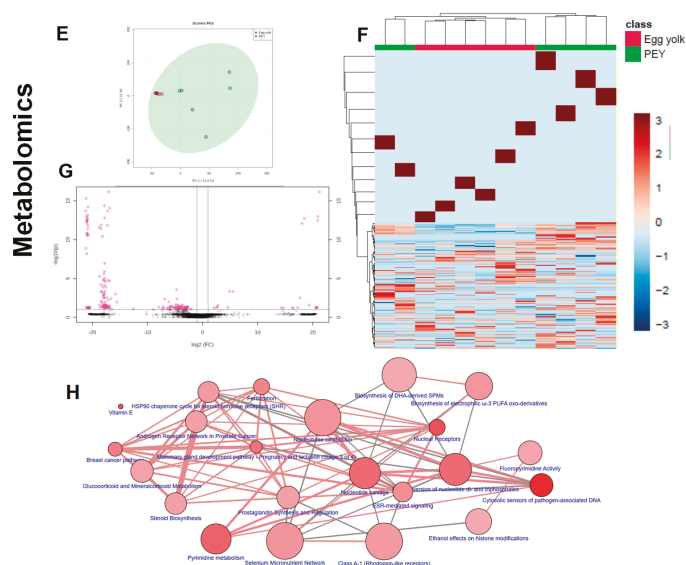


Figure 3. PEY exhibits a differential lipidomic and metabolomic profile. Lipidome (A–D) and metabolome (F–H) profiles of PEY and egg yolk were analyzed by liquid chromatography coupled to mass spectrometry. As shown by principal component analyses graphs, PEY and egg yolk show different lipidome (A) and metabolome (E) signatures. This is reinforced by hierarchical clustering analyses which show a perfect clustering in lipidomics (B), but not in metabolomics (F). Univariate statistics such as a Volcano plot are shown, indicating that there are marked differences in a high number of molecules both in the lipidome (C) and metabolome (G). Pathway analyses, shown in (D) for lipidomics and in H for metabolomics, indicate the pathways where putatively annotated molecules are located—network neighborhood-based entity sets of lipidomic and metabolomics differences between PEY and egg yolk. Differential lipids (D) and metabolites (H) (see main text) were entered into the ConsensusPathDB platform, and nodes, representing neighborhood-based entity sets (whose size is proportional to the number of metabolites/lipids of the set, and color intensity denote p -value for hypergeometric tests) are linked by interactions consisting of the number of metabolites shared by nodes. The type of network chosen was 2-next neighbors, with a minimum number of 1 metabolite overlap with members of the entity set (and a $p < 0.05$ for lipidomics and a $p < 0.01$ for metabolomics as the cutoff). The sets were obtained, considering only Wikipathway based ones. Lipids included were C21480, C21481, C00350, C02737, C13883, C00195, C12126, C00550, C01190, and C02686. Metabolites used were C01179, C06104, C06425, C00239, C00364, C00984, C14214, C02043, C06429, C08491, C00256, C05332, C00410, C05441, and C02477 (KEGG nomenclature). Individual levels of metabolites and lipids employed for pathway analyses are available in <https://excelv.herokuapp.com/>.

4. Discussion

It is known that nutrition can affect the functioning of various immune parameters, and the immunomodulation through dietary supplements is not new; e.g., linoleic acid promotes the production of leukotrienes and prostaglandins, or that arginine and glutamine enhance macrophage phagocytosis [21]. Also, epidemiological studies show that both overall diet or specific dietary components like polyphenols can reduce inflammatory cytokines in animal and cell culture models [22]. Then, it was expectable that a dietary component so rich in biomolecules as egg yolk would lead to some effects in the immunity. What it was not predictable, is the fact that PEY would significantly improve these effects.

In our view, PEY optimizes the immune response. This effect means that, more than down-regulating hyperactive immune functions or up-regulating suppressive immune functions, PEY strengthens the resilience of immune functions to respond to external ‘stressors’ [21]. The results of this work agree

with PEY intake induced changes at the systemic level that led to a less aggressive immune response in rodents since a lower induction of pro-inflammatory cytokines was observed after an inflammatory stimulus. PEY, like any biological extract, is a complex matrix containing thousands of molecules with biological activity, in a vast range of concentrations; thus, elucidating its mechanism of action is not an easy task. The individual effects of single compounds can be easily studied *in vitro*. However, synergisms and antagonisms, as well as metabolic reactions, take place when a food, as a complex matrix, is ingested, digested, and processed by a living being. Accounting for cytokine blood levels, it was clear that some differences in the composition between PEY and egg yolk must exist, and screening these differences could give some clues.

The increased presence of growth factors (CTGF, PDGF, IGF-I and NGF) on PEY, when compared with egg yolk, is not surprising from a biological point of view. Growth factors play a vital role in the evolution and resolution of inflammatory reactions [22]. Thus the presence of these proteins leads to thinking that they could be related to the different immune responses observed *in vivo*. CTGF is a critical player in connective tissue homeostasis since it helps to maintain extracellular matrix remodeling in normal physiological processes such as wound healing, and it has also been shown to possess apoptotic and nonmitogenic properties [23]. PDGF has a vital role in the early differentiation of hematopoietic/endothelial precursors; it has been used in clinical trials as a topical treatment for healing chronic neuropathy, as well as to improve periodontal regeneration in severe periodontal disease [24]. Insulin-like growth factor I (IGF-I) is a polypeptide hormone secreted by multiple tissues in response to growth hormone (GH). It is partly responsible for GH activity, and also has anabolic effects. NGF is a neurotrophic factor that promotes the growth and survival of peripheral sensory and sympathetic nerve cells. It is a pleiotropic factor, since it produced and utilized by several cell types, including structural (epithelial cells, fibroblasts/myofibroblasts, endothelial cells, smooth muscle cells and hepatocytes), accessory (glial cells, astrocytes and Muller cells) and immune (antigen presenting cells, lymphocytes, granulocytes, mast cells and eosinophils) cells [25], having neuroprotective and tissue repairing properties. Strikingly, since PEY is administered orally, it must be assumed that there exists bioavailability of these molecules. PEY effects could be explained through absorption in the digestive tract by indirect interaction with the host's microbiota. Previous studies showed how the Platelet-Rich Plasma rich in growth factors (PDGF, IGF, VEGF, TGF β) promoted the regenerative processes inhibiting the macrophage activation and the release of cytokines (TNF α , MCP-1, and RANTES) [26] *in vitro*. However, another study showed that orally administered IGF-I mainly acts at the intestine, a portion of ingested IGF-I is absorbed into the general circulation to enhance the growth of selective organs/tissue [27]. As indicated, interaction with microbiota cannot be excluded—for instance, Padlyia et al. [28] analyzed fertilized eggs, finding that the proteins that increased in abundance play a role in angiogenesis (pleiotrophin, histidine-rich glycoprotein), in defending the developing embryo against microbial pathogens (avian β -defensin 11, polymeric immunoglobulin receptor, serum amyloid P-component, ovostatin and mannose-binding ligand) and in augmenting the structural integrity of the egg shell (ovo-calyxin-32), necessary to provide a substantial barrier against microbial infection.

The action of PEY is not only due to the presence of growth factors. The lipids and metabolites that were found increased in PEY clustered among different sphingolipid-related pathways, as well as some immune-related pathways. A plethora of cell biological processes are critically modulated by bioactive sphingolipids, including growth regulation, cell migration, adhesion, apoptosis, senescence, and inflammatory responses [29]. Similarly, Duan et al. [30] reported that fertilized eggs exhibited higher essential fatty acids (EFAA) and monounsaturated (MUFA) fatty acids levels than unfertilized eggs, and lower cholesterol concentrations, having the potential of being utilized as an EFAA/MUFA-rich, low-cholesterol dietary supplement for the aged and people with special dietary requirements. There are also *in vitro* experiments demonstrating the pharmacological effects of these bioactive molecules; Xi Li et al. [31] observed that 12-day chicken embryo extracts enhanced spleen lymphocyte proliferation (and IL-2 production), and macrophage function (phagocytosis and NO production). Accounting the high bioavailability of lipids, we cannot discard a role of lipids in PEY in the immune optimization.

Globally, the observed decrease in LPS-induced increase in circulating TNF α , IL1 β , and MCP-1 could be related with the complex PEY composition. Growth factors, together with a vibrant matrix of bioactive lipids and metabolites, are promoting a less aggressive immune response, which means better maintenance of homeostasis. Further, these responses can be ascribed to a change in the M1-M2 macrophage status, favoring the resolutive (M2) phase, a thread that will be the focus of future studies.

As for the limitations of our work, we acknowledge that a single nutrient cannot explain observed effects; that the oral bioavailability of the compounds present in PEY can be limited; and that perhaps the system is limited to preclinical studies. Further, we think that measurement of systemic cytokine data induced by PEY treatment, as well as its surrogate metabolome and lipidome changes, the focus of future studies, could offer more light on the potential mechanisms behind this. However, we think that the demonstration that PEY is a complex of bioactive molecules (growth factors, lipids, metabolites) that encloses the molecules that an embryo needs to develop a whole organism affects the host's immunity is clear. It is reasonable to think that these active compounds are bioavailable even if orally administered since a systemic effect has been observed. These active molecules probably act together; this differentiates it from a single active ingredient since possibly this set of molecules produces a series of simultaneous effects that include synergies and antagonisms, promoting an anti-inflammatory microenvironment and leading to a state of homeostasis. Since chronic inflammation contributes to the development of chronic diseases (cancer, cardiovascular disease, and diabetes) and aging, consumption of PEY could effectively reduce the incidence and the progression of these processes.

Supplementary Materials: The following are available online at <http://www.mdpi.com/2072-6643/12/9/2699/s1>, Supplemental Dataset, which is an Excel[®] file containing differential molecules between PEY and egg yolk in the metabolomics and lipidomics analyses, and Supplemental Figure S1. Individual levels of metabolites and lipids employed for pathway analyses are present in <https://excelv.herokuapp.com/>.

Author Contributions: Conceptualization, J.C., C.B. and J.C.E.S.; Methodology, J.C.E.S., M.M.-G., L.S., M.J. and C.B.; Validation, M.M.-G., J.C.E.S., L.S., M.J. and M.P.-O.; Formal analysis, M.M.-G., J.C.E.S., C.B. and J.C.; Investigation, J.C. and M.P.-O.; Resources, J.C.; Data curation, M.M.-G. and J.C.E.S.; Writing—original draft preparation, C.B. and J.C.E.S.; Writing—review and editing, M.P.-O., C.B. and J.C.; Visualization and supervision, J.C.E.S.; Project administration and funding acquisition, J.C. All authors have read and agreed to the published version of the manuscript.

Funding: This research received no external funding.

Acknowledgments: Support from Generalitat de Catalunya, 2017SGR696.

Conflicts of Interest: Authors J.C.E.S., M.J., L.S. and M.P.-O. declare no conflict of interest. J.C. is the inventor of the patent protecting PEY obtention. J.C. and C.B. are employees of Ovovity s.l., which is the owner of the patent protecting PEY obtention. The funders (Ovovity s.l.) had no role in the design of the study; in the collection, analyses, or interpretation of data; in the writing of the manuscript, or in the decision to publish the results.

References

- Xia, S.; Zhang, X.; Zheng, S.; Khanabdali, R.; Kalionis, B.; Wu, J.; Wan, W.; Tai, X. An Update on Inflamm-Aging: Mechanisms, Prevention, and Treatment. *J. Immunol. Res.* **2016**, *2016*, 8426874. [[CrossRef](#)] [[PubMed](#)]
- López-Otín, C.; Blasco, M.A.; Partridge, L.; Serrano, M.; Kroemer, G. The hallmarks of aging. *Cell* **2013**, *153*, 1194–1217. [[CrossRef](#)] [[PubMed](#)]
- Opal, S.M.; DePalo, V.A. Anti-inflammatory cytokines. *Chest* **2000**, *117*, 1162–1172. [[CrossRef](#)] [[PubMed](#)]
- Koelman, L.; Pivovarova-Ramich, O.; Pfeiffer, A.F.H.; Grune, T.; Aleksandrova, K. Cytokines for evaluation of chronic inflammatory status in ageing research: Reliability and phenotypic characterisation. *Immun. Ageing* **2019**, *16*, 11. [[CrossRef](#)] [[PubMed](#)]
- Vaiserman, A.; Lushchak, O. Implementation of longevity-promoting supplements and medications in public health practice: Achievements, challenges and future perspectives. *J. Transl. Med.* **2017**, *15*, 160. [[CrossRef](#)]
- Tyrovolas, S.; Haro, J.M.; Foscolou, A.; Tyrovolas, D.; Mariolis, A.; Bountziouka, V.; Piscopo, S.; Valacchi, G.; Anastasiou, F.; Gotsis, E.; et al. MEDIS Study Group Anti-Inflammatory Nutrition and Successful Ageing in Elderly Individuals: The Multinational MEDIS Study. *Gerontology* **2018**, *64*, 3–10. [[CrossRef](#)]
- Zambrowicz, A.; Dąbrowska, A.; Bobak, Ł. Egg yolk proteins and peptides with biological activity. *Adv. Hygiene* **2014**, *68*, 1524–1529. [[CrossRef](#)]

8. Pourmorad, F.; Rezaie, N.; Mahmoudi, M.A. Anti-inflammatory and analgesic effects of egg yolk: A comparison between organic and machine made. *Eur. Rev. Med.* **2013**, *17*, 472–476.
9. Blesso, C.N. Egg phospholipids and cardiovascular health. *Nutrients* **2015**, *7*, 2731–2747. [[CrossRef](#)]
10. Rahn, H.; Ar, A. Gas exchange of the avian egg time, structure, and function. *Am. Zool.* **1980**, *20*, 477–484. [[CrossRef](#)]
11. WO2013053503 Egg Preparation with Regenerating, Analgesic and/or Anti-Inflammatory Properties. Available online: https://patentscope.wipo.int/search/en/detail.jsf?docId=WO2013053503&_cid=P10-KD4QQJ-57854-1 (accessed on 27 July 2020).
12. Jové, M.; Serrano, J.C.E.; Ortega, N.; Ayala, V.; Anglès, N.; Reguant, J.; Morelló, J.R.; Romero, M.P.; Motilva, M.J.; Prat, J.; et al. Multicompartmental LC-Q-TOF-based metabolomics as an exploratory tool to identify novel pathways affected by polyphenol-rich diets in mice. *J. Proteome Res.* **2011**, *10*, 3501–3512. [[CrossRef](#)] [[PubMed](#)]
13. Wikoff, W.R.; Pendyala, G.; Siuzdak, G.; Fox, H.S. Metabolomic analysis of the cerebrospinal fluid reveals changes in phospholipase expression in the CNS of SIV-infected macaques. *J. Clin. Investig.* **2008**, *118*, 2661–2669. [[CrossRef](#)] [[PubMed](#)]
14. Sandra, K.; Pereira, A.D.S.; Vanhoenacker, G.; David, F.; Sandra, P. Comprehensive blood plasma lipidomics by liquid chromatography/quadrupole time-of-flight mass spectrometry. *J. Chromatogr. A* **2010**, *1217*, 4087–4099. [[CrossRef](#)] [[PubMed](#)]
15. Portero-Otín, M.; Fernández-Real, J.M. Human omental and subcutaneous adipose tissue exhibit specific lipidomic signatures. *FASEB* **2014**, *28*, 1071–1081.
16. Sana, T.R.; Roark, J.C.; Li, X.; Waddell, K.; Fischer, S.M. Molecular formula and METLIN Personal Metabolite Database matching applied to the identification of compounds generated by LC/TOF-MS. *J. Biomol. Tech.* **2008**, *19*, 258–266. [[PubMed](#)]
17. Xia, J.; Sinelnikov, I.V.; Han, B.; Wishart, D.S. MetaboAnalyst 3.0—Making metabolomics more meaningful. *Nucleic Acids Res.* **2015**, *43*, W251–W257. [[CrossRef](#)]
18. Sumner, L.W.; Amberg, A.; Barrett, D.; Beale, M.H.; Beger, R.; Daykin, C.A.; Fan, T.W.-M.; Fiehn, O.; Goodacre, R.; Griffin, J.L.; et al. Proposed minimum reporting standards for chemical analysis Chemical Analysis Working Group (CAWG) Metabolomics Standards Initiative (MSI). *Metabolomics* **2007**, *3*, 211–221. [[CrossRef](#)]
19. Kamburov, A.; Pentchev, K.; Galicka, H.; Wierling, C.; Lehrach, H.; Herwig, R. ConsensusPathDB: Toward a more complete picture of cell biology. *Nucleic Acids Res.* **2011**, *39*, D712–D717. [[CrossRef](#)]
20. Nakane, S.; Tokumura, A.; Waku, K.; Sugiura, T. Hen egg yolk and white contain high amounts of lysophosphatidic acids, growth factor-like lipids: Distinct molecular species compositions. *Lipids* **2001**, *36*, 413–419. [[CrossRef](#)]
21. Abood, W.N. Immunomodulatory and natural immunomodulators. *J. Allergy Inflamm.* **2017**, *1*, e101.
22. Hardman, W.E. Diet components can suppress inflammation and reduce cancer risk. *Nutr. Res. Pract.* **2014**, *8*, 233–240. [[CrossRef](#)] [[PubMed](#)]
23. Moussad, E.E.; Brigstock, D.R. Connective tissue growth factor: What's in a name? *Mol. Genet. Metab.* **2000**, *71*, 276–292. [[CrossRef](#)] [[PubMed](#)]
24. Andrae, J.; Gallini, R.; Betsholtz, C. Role of platelet-derived growth factors in physiology and medicine. *Genes Dev.* **2008**, *22*, 1276–1312. [[CrossRef](#)]
25. Aloe, L.; Rocco, M.L.; Balzamino, B.O.; Micera, A. Nerve growth factor: A focus on neuroscience and therapy. *Curr. Neuropharmacol.* **2015**, *13*, 294–303. [[CrossRef](#)]
26. El-Sharkawy, H.; Kantarci, A.; Deady, J.; Hasturk, H.; Liu, H.; Alshahat, M.; Van Dyke, T.E. Platelet-rich plasma: Growth factors and pro- and anti-inflammatory properties. *J. Periodontol.* **2007**, *78*, 661–669. [[CrossRef](#)]
27. Kim, W.K.; Ryu, Y.H.; Seo, D.S.; Lee, C.Y.; Ko, Y. Effects of oral administration of insulin-like growth factor-I on circulating concentration of insulin-like growth factor-I and growth of internal organs in weanling mice. *Neonatology* **2006**, *89*, 199–204. [[CrossRef](#)] [[PubMed](#)]
28. Padliya, N.D.; Qian, M.; Roy, S.M.; Chu, P.; Zheng, H. The impact of fertilization on the chicken egg yolk plasma and granule proteome 24 hours post-lay at room temperature: Capitalizing on high-pH/low-pH. *Food Funct.* **2015**, *6*, 2303–2314. [[CrossRef](#)]
29. Trayssac, M.; Hannun, Y.A.; Obeid, L.M. Role of sphingolipids in senescence: Implication in aging and age-related diseases. *J. Clin. Investig.* **2018**, *128*, 2702–2712. [[CrossRef](#)]

30. Duan, X.; Li, M.; Wu, F.; Yang, N.; Nikoo, M.; Jin, Z.; Xu, X. Postfertilization changes in nutritional composition and protein conformation of hen egg. *J. Agric. Food Chem.* **2013**, *61*, 12092–12100. [[CrossRef](#)]
31. Li, X.; Su, Y.; Sun, J.; Yang, Y. Chicken embryo extracts enhance spleen lymphocyte and peritoneal macrophages function. *J. Ethnopharmacol.* **2012**, *144*, 255–260. [[CrossRef](#)]



© 2020 by the authors. Licensee MDPI, Basel, Switzerland. This article is an open access article distributed under the terms and conditions of the Creative Commons Attribution (CC BY) license (<http://creativecommons.org/licenses/by/4.0/>).



Article

Protocatechuic Acid Extends Survival, Improves Motor Function, Diminishes Gliosis, and Sustains Neuromuscular Junctions in the hSOD1^{G93A} Mouse Model of Amyotrophic Lateral Sclerosis

Lilia A. Koza ^{1,2}, Aimee N. Winter ¹, Jessica Holsopple ¹, Angela N. Baybayon-Grandgeorge ¹, Claudia Pena ^{1,2}, Jeffrey R. Olson ^{1,2}, Randall C. Mazzarino ^{1,2}, David Patterson ^{1,2,3} and Daniel A. Linseman ^{1,2,3,*}

¹ Department of Biological Sciences, F. W. Olin Hall, Room 102, University of Denver, 2190 E. Iliff Ave, Denver, CO 80208, USA; lilia.koza@du.edu (L.A.K.); anwinter@usf.edu (A.N.W.); jessie.h511@gmail.com (J.H.); bg.angela1@gmail.com (A.N.B.-G.); claudia.pena@du.edu (C.P.); jeffrey.olson.du@gmail.com (J.R.O.); randall.mazzarino@du.edu (R.C.M.); david.patterson@du.edu (D.P.)

² Knoebel Institute for Healthy Aging, Engineering Computer Science, Suite 579, University of Denver, 2155 E. Wesley Ave, Denver, CO 80208, USA

³ Eleanor Roosevelt Institute, University of Denver, 2101 E. Wesley Ave, Denver, CO 80210, USA

* Correspondence: daniel.linseman@du.edu; Tel.: +1-(303)-871-4663

Received: 4 May 2020; Accepted: 15 June 2020; Published: 18 June 2020

Abstract: Amyotrophic lateral sclerosis (ALS) is a devastating disorder characterized by motor neuron apoptosis and subsequent skeletal muscle atrophy caused by oxidative and nitrosative stress, mitochondrial dysfunction, and neuroinflammation. Anthocyanins are polyphenolic compounds found in berries that possess neuroprotective and anti-inflammatory properties. Protocatechuic acid (PCA) is a phenolic acid metabolite of the parent anthocyanin, kuromanin, found in blackberries and bilberries. We explored the therapeutic effects of PCA in a transgenic mouse model of ALS that expresses mutant human Cu, Zn-superoxide dismutase 1 with a glycine to alanine substitution at position 93. These mice display skeletal muscle atrophy, hindlimb weakness, and weight loss. Disease onset occurs at approximately 90 days old and end stage is reached at approximately 120 days old. Daily treatment with PCA (100 mg/kg) by oral gavage beginning at disease onset significantly extended survival (121 days old in untreated vs. 133 days old in PCA-treated) and preserved skeletal muscle strength and endurance as assessed by grip strength testing and rotarod performance. Furthermore, PCA reduced astrogliosis and microgliosis in spinal cord, protected spinal motor neurons from apoptosis, and maintained neuromuscular junction integrity in transgenic mice. PCA lengthens survival, lessens the severity of pathological symptoms, and slows disease progression in this mouse model of ALS. Given its significant preclinical therapeutic effects, PCA should be further investigated as a treatment option for patients with ALS.

Keywords: amyotrophic lateral sclerosis; anti-inflammatory; antioxidant; phenolic acid; neuroprotective; neurodegeneration

1. Introduction

Amyotrophic lateral sclerosis (ALS), also known as Lou Gehrig's disease, is a devastating, progressive, and fatal neurodegenerative disease that affects motor neurons of the central nervous system. ALS patients exhibit a median survival of only 2–3 years following diagnosis, with death typically caused by respiratory failure [1]. ALS presents as either a sporadic or familial disease. Sporadic ALS cases account for approximately 90% of all patients and do not have an obvious genetic

cause. Familial ALS accounts for the remaining 10% of patients and has been linked to mutations in genes such as Cu, Zn-superoxide dismutase 1 (SOD1), chromosome 9 open reading frame 72 (C9orf72), fused in sarcoma, and TAR DNA-binding protein 43 (TDP-43) [2]. Although ALS is classified as a rare disease, with a prevalence of 5 in 100,000 people living in the United States, the effects of the disease are calamitous for those who are afflicted [1]. ALS is characterized pathologically by the death of motor neurons, axonal retraction away from the neuromuscular junctions (NMJs), skeletal muscle atrophy, and ultimately, death.

The pathogenesis underlying both familial and sporadic forms of ALS has been extensively studied but is still not completely understood. Protein aggregation, disrupted axonal transport, perturbed RNA metabolism, excitotoxicity, neuroinflammation, mitochondrial dysfunction, and oxidative stress have all been identified as underlying mechanisms and contributing factors in ALS. In the context of motor neuron degeneration, neuroinflammation and oxidative stress appear to be major pathogenic mechanisms. Both astrocytes and microglia can adopt distinct anti- or pro-inflammatory phenotypes, depending on signals from the surrounding environment. These anti- or pro-inflammatory phenotypes are neuroprotective or neurotoxic to motor neurons, respectively. Astrocytes, although beneficial to neurons in their resting state, become reactive and contribute to motor neuron death in various models of ALS [3–6]. Reactive astrocytes have also been shown to impair the process of autophagy in motor neurons, resulting in increased protein aggregation and reduced motor neuron health in *in vivo* and *in vitro* models of ALS [7–9]. Microglia also contribute significantly to the neuroinflammation in ALS. Microglia have been shown to induce astrocyte reactivity by releasing pro-inflammatory cytokines, resulting in an inability of astrocytes to protect motor neurons [10,11]. Microglia also become pro-inflammatory and have been found to display an ALS-specific phenotype that contributes to rapid disease progression and increased motor neuron loss [12–15].

Oxidative stress is another mechanism that has been identified as a causative factor in ALS. Increased oxidative stress burden correlates positively with disease severity [16,17]. Superoxide and nitric oxide have been found to be elevated in ALS [18,19]. Oxidative stress markers such as glutathione peroxidase, malondialdehyde, glutathione status, and 8-oxodeoxyguanosine demonstrate significant alterations in ALS patients [20,21]. Furthermore, mitochondrial dysfunction and mutations in genes that affect mitochondrial processes have been linked to ALS [22–26]. Specifically, in the case of ALS caused by mutations in SOD1, the mutant SOD1 protein has been shown to aggregate within mitochondria, resulting in mitochondrial dysfunction and mitochondrial oxidative stress [24,27]. Given the above findings, a beneficial therapeutic approach for ALS may be to reduce both neuroinflammation and oxidative stress.

Currently, only two drugs, Riluzole and Edaravone, have been approved by the U.S. Food and Drug Administration (FDA) to treat ALS. Riluzole is administered orally, only has a modest effect on slowing disease progression, and shows an extension of life of only a few months [2]. Edaravone has been shown to delay disease progression by only 33% when compared to a placebo, is costly, and must be administered intravenously [28]. Unfortunately, both Riluzole and Edaravone have only modest effects on disease progression and survival. Furthermore, both drugs are expensive and display substantial side effects. Many other therapeutics have failed in the clinic or are still undergoing clinical trials. However, no new pharmacological therapies are immediately on the horizon for ALS patients.

Nutraceuticals, natural bioactive compounds found in foods, may be safe, easy to administer, and cost-effective therapeutic treatments for ALS. More specifically, anthocyanins, a type of flavonoid, may be beneficial to ALS patients due to their substantial antioxidant and anti-inflammatory properties [29]. Anthocyanins vary in color from red to blue and are responsible for the vibrant coloring of many fruits and vegetables [30]. We have previously demonstrated a therapeutic effect of an anthocyanin-enriched strawberry extract in a transgenic mouse model of ALS that expresses mutant human SOD1 with a glycine to alanine substitution at position 93 (hSOD1^{G93A}) [31]. This strawberry extract is enriched in callistephin, an anthocyanin derived from pomegranates and strawberries [29,32]. We have also shown that callistephin suppresses apoptosis induced by mitochondrial oxidative stress

and protects neurons from glutamate excitotoxicity *in vitro* [29,32]. *In vivo*, we found that hSOD1^{G93A} mice treated with strawberry anthocyanin extract beginning at 60 days old showed delayed disease onset, improved grip strength throughout the disease, and significantly extended survival when compared to untreated hSOD1^{G93A} littermate mice. Furthermore, treated mice displayed significantly decreased astrogliosis in the spinal cord and preserved NMJs in gastrocnemius muscle when compared to untreated littermate mice [31]. These findings indicate that anthocyanin compounds may have therapeutic potential in ALS. However, despite their potential benefits, parent anthocyanins suffer from poor bioavailability. In contrast, their phenolic acid metabolites typically display much higher bioavailability and most can readily cross the blood brain barrier [33].

Here, we examined the therapeutic potential of protocatechuic acid (PCA) in the hSOD1^{G93A} preclinical mouse model of ALS. PCA is a phenolic acid metabolite of kuromanin, the parent anthocyanin found in blackberries, bilberries, and black rice. We have previously shown that kuromanin protects neurons from oxidative stress induced by glutamate excitotoxicity, nitrosative stress induced by nitric oxide, and it also suppresses mitochondrial oxidative stress and the consequent apoptosis by preserving mitochondrial glutathione [29,32]. In a similar manner, PCA protects neurons against nitrosative and oxidative stress and reduces nitric oxide production in microglial cells treated with lipopolysaccharide, demonstrating both antioxidant and anti-inflammatory activities [34]. Based on our previous findings, we tested the therapeutic effects of PCA in the hSOD1^{G93A} mouse model of ALS.

2. Materials and Methods

2.1. The hSOD1^{G93A} Mouse Model of ALS

FVB/NJ mice harboring a human transgene coding for a mutated form of SOD1 with a glycine to alanine substitution at position 93 were obtained from The Jackson Laboratory (Bar Harbor, ME, USA). Mice were bred and maintained at the University of Denver animal facility under a standard 12 h light/dark cycle with food and water provided *ad libitum*. Genotyping to identify transgenic mice was carried out by a third-party company, Transnetyx Inc. (Cordova, TN, USA). All procedures were performed in accordance with two protocols approved by the institutional animal care and use committee at the University of Denver. The initial protocol (927091) was approved on 21 July 2016 and the second protocol (1454889) was approved on 12 July 2019.

2.2. Survival Data

For the survival study, mice were divided into four groups consisting of 15 mice each. The first group consisted of non-transgenic wild-type (WT) age- and sex-matched littermate controls. The other three groups consisted of age- and sex-matched transgenic hSOD1^{G93A} littermate mice, either untreated or treated with either 50 or 100 mg/kg PCA. PCA was dissolved in sterile deionized water and was administered once per day as a 0.25 mL dose by oral gavage 5 days/week. Oral gavage treatment of PCA began at disease onset (90 days of age) and continued until mice reached end stage, defined as the point at which a mouse no longer had the ability to right itself within 15 s after being placed on its side. PCA-treated and untreated hSOD1^{G93A} littermate mice were euthanized at end stage by an overdose of inhaled isoflurane (Vet One, Boise, ID, USA). The WT littermate control mouse was euthanized at end stage of whichever hSOD1^{G93A} littermate mouse lived the longest, regardless of treatment.

2.3. Paw Grip Endurance and Rotarod Testing

Hind limb strength was assessed by paw grip endurance (PaGE) testing twice per week beginning at disease onset. Briefly, mice were placed on top of a standard wire cage lid which was suspended a few inches above the bench top. Mice were briefly allowed to acclimate before the cage lid was smoothly inverted to prompt the mouse to grip the wire with both its fore and hind limbs. A stopwatch was started as soon as the cage lid was inverted and the time was measured to determine how long

the mouse could hold on before its hind legs released their grip from the cage lid, expressed as latency to fall. Care was taken not to jostle the lid during this time. The stopwatch was stopped at a maximum of 30 s. Mice were given five scored attempts and the highest and lowest scores were excluded from the final score. Final scores are reported as an average of the three remaining scored attempts \pm standard error of the mean (SEM) for each time point. Time points correspond to the age of the animal at the time that testing was performed and are reported as a range of several days since multiple sets of animals having slightly different ages were tested concomitantly.

Motor function and endurance were assessed by accelerating rotarod testing once per week beginning at disease onset. Mice were placed on a rod, 30 mm in diameter, rotating at 4 rpm. Each animal was placed in one lane and subjected to three trials. The lane was cleaned before the next mouse was tested to prevent interference. Once the mice were acclimated to the initial speed of 4 rpm, the rod was accelerated from 4 to 40 rpm over the course of 5 min. The time was stopped when the mouse fell off the rotating rod, expressed as latency to fall. Mice were given three scored attempts reported as an average \pm SEM for each time point. Time points correspond to the age of the animal at the time that testing was performed and are reported as a range of several days since multiple sets of animals having slightly different ages were tested concomitantly.

2.4. Analysis of Mice at End Stage of the Untreated hSOD1^{G93A} Littermate Mouse

For assessment of Nissl-stained motor neuron counts, glial fibrillary acidic protein (GFAP) and ionized calcium-binding adapter molecule 1 (Iba-1) staining, NMJ area, perimeter, and Sholl analysis, mice were divided into three groups consisting of approximately 10 mice per group. The first group consisted of non-transgenic WT age- and sex-matched littermate controls. The other two groups consisted of age- and sex-matched transgenic hSOD1^{G93A} littermate mice, either untreated or treated with 100 mg/kg PCA orally as described above. PCA treatment continued until the untreated hSOD1^{G93A} littermate mouse reached end stage. At that point, mice from all 3 groups were euthanized and spinal cord and gastrocnemius muscles were collected.

2.5. Analysis of Mice at 105 Days of Age

We observed the greatest improvements in motor function as assessed by rotarod and PaGE testing between 97 and 114 days of age in PCA-treated hSOD1^{G93A} mice. Therefore, we analyzed the gastrocnemius muscle wet weight, vesicular acetylcholine transporter (VACHT) and alpha-bungarotoxin (BTx) co-stained gastrocnemius muscle, and 4-hydroxynonenal (4-HNE)-stained spinal cord ventral horn from a separate cohort of mice at 105 days of age. This cohort consisted of both WT and hSOD1^{G93A} mice with or without PCA treatment, with each treatment group containing approximately 10 mice. Mice receiving PCA were given a daily dose of 100 mg/kg beginning at 90 days of age and continuing until the mice reached 105 days of age. At 105 days of age, mice from all 3 groups were euthanized and gastrocnemius muscles and lumbar spinal cord were collected.

2.6. Tissue Preparation and Cryosectioning

Following euthanasia, the thoracolumbar portion of the spinal column, containing the lumbar spinal cord, and gastrocnemius muscle were removed. Each specimen was washed with 1 \times phosphate-buffered saline (PBS, pH 7.4), and placed in 4% paraformaldehyde at 4 °C overnight. Each specimen was then washed again and allowed to sit in 1 \times PBS for 20 min. Gastrocnemius muscle was placed in 30% sucrose in 1 \times PBS and allowed to sink for cryoprotection. The lumbar spinal cord was placed in 6% trichloroacetic acid (Sigma-Aldrich, St. Louis, MO, USA) in deionized water for 6 days for decalcification. Following decalcification, the lumbar spinal cord was placed in 30% sucrose until saturated. Both gastrocnemius muscle and spinal cord were frozen rapidly in optimal cutting temperature (OCT) compound with liquid nitrogen and stored at -80 °C until sectioning took place. Prior to sectioning, tissue was allowed to acclimate in the microtome cryostat for at least 20 min. For gastrocnemius muscle and spinal cords, sections of 30 μ m in length were cut and

every viable tissue section was collected onto the surface of Fisherbrand Superfrost Colorfrost Plus coated slides (Fisher Scientific, Pittsburgh, PA, USA). Slides were stored at -20°C until subjected to immunohistochemistry.

2.7. Immunohistochemistry of Spinal Cord Sections

Prior to staining, slides were allowed to equilibrate at room temperature for at least 30 min. Tissue sections on the slides were then outlined with a hydrophobic pen (Liquid Blocker Super PAP Pen; Daido Sangyo Co., Tokyo, Japan) and washed twice with $1\times$ PBS to remove any residual OCT. Tissue was then incubated at room temperature in blocking buffer, containing 5% (*w/v*) bovine serum albumin (BSA) and $1\times$ PBS containing 0.2% triton-X 100 for 90 min. For astrocyte staining, primary antibody to GFAP (Abcam, Cambridge, MA, USA) was then prepared as a 1:500 dilution in $1\times$ PBS containing 0.2% triton-X 100 and 2% BSA (*w/v*). For microglial staining, primary antibody to Iba-1 (Abcam, Cambridge, MA, USA) was prepared as a 1:167 dilution in PBS containing 0.2% triton-X 100 and 2% BSA (*w/v*). For 4-HNE staining, primary antibody to 4-HNE (Alpha Diagnostic Intl. Inc., San Antonio, TX, USA) was prepared as a 1:500 dilution in PBS containing 0.2% triton-X 100 and 2% BSA (*w/v*). Tissue was incubated in primary antibody overnight at 4°C . Tissue was washed 3–4 times with $1\times$ PBS to remove any unbound primary antibody. FITC-conjugated donkey anti-rabbit antibody (Jackson ImmunoResearch Laboratories, West Grove, PA, USA) or Alexa Fluor 488-conjugated donkey anti-goat antibody (Jackson ImmunoResearch Laboratories, West Grove, PA, USA) were then prepared at 1:500 dilutions (*v/v*) in $1\times$ PBS containing 0.2% triton-X100 and 2% BSA (*w/v*) and Hoechst nuclear stain (Sigma-Aldrich, St. Louis, MO, USA) at a 1:500 dilution to detect GFAP and Iba-1, and to label nuclei, respectively. For 4-HNE staining, FITC-conjugated donkey anti-rabbit antibody (Jackson ImmunoResearch Laboratories, West Grove, PA, USA) was prepared at 1:500 dilution (*v/v*) in $1\times$ PBS containing 0.2% triton-X100 and 2% BSA (*w/v*) and Hoechst nuclear stain (Sigma-Aldrich, St. Louis, MO, USA) at a 1:500 dilution to detect 4-HNE and to label nuclei, respectively. Sections were incubated with secondary antibodies at room temperature for 90 min, then washed 3–4 times with $1\times$ PBS. ProLong Gold anti-fade reagent (Thermo Fisher Scientific, Eugene, OR, USA) was used as mounting medium and slides were sealed with coverslips. Stained slides were stored in the dark at -20°C until imaging took place. Twelve sections of spinal cord were stained for Iba-1, GFAP, and 4-HNE per mouse.

2.8. Imaging and Quantification of Spinal Cord Sections Stained for Iba-1 and GFAP at End Stage of the Untreated $\text{hSOD1}^{\text{G93A}}$ Littermate Mouse

Tissue was imaged using a Zeiss Axio Observer epifluorescence microscope to capture a single image of each ventral horn on the $20\times$ objective. Imaging was performed by blinded researchers. For Iba-1 and GFAP, images were captured on the Alexa Fluor 488 channel and the exposure time was set appropriately for the untreated $\text{hSOD1}^{\text{G93A}}$ littermate and kept constant when imaging the PCA-treated $\text{hSOD1}^{\text{G93A}}$ and WT littermate mice. At least 6 ventral horns per animal were imaged and analyzed for fluorescence intensity using Adobe Photoshop CC software for both Iba-1 and GFAP staining. For both Iba-1 and GFAP quantification, the ventral horn image of the untreated $\text{hSOD1}^{\text{G93A}}$ littermate control mouse with the most background was chosen, and the green channel input level was adjusted so that background staining was best eliminated. This value was recorded and used for each subsequent image, including those taken from the WT control littermate and the PCA-treated $\text{hSOD1}^{\text{G93A}}$ littermate mice such that all images were adjusted by an equivalent amount. After the channel levels were adjusted, the ventral horn was outlined using the lasso tool and green channel values for mean pixel intensity and pixel area were recorded for each ventral horn image. Total pixel intensity of the green channel was obtained by multiplying the pixel intensity and pixel area. An average of the total pixel intensity was taken for each mouse. Quantification was performed twice by two different and blinded researchers. An average of the pixel intensities for each mouse was obtained. For analysis, the average total pixel intensity for the WT littermate control mouse

for each group was set at 100% and the average total pixel intensities for the untreated hSOD1^{G93A} littermate control and PCA-treated hSOD1^{G93A} littermate mice were calculated as percentages relative to the WT littermate control mouse. Mean raw GFAP and Iba-1 fluorescence intensity in the lumbar spinal cord ventral horn in the untreated hSOD1^{G93A} littermate mice and WT littermate mice were also counted and statistically compared to verify a significant disease effect.

2.9. Nissl Staining of Spinal Cord Sections

Prior to staining, slides were allowed to equilibrate at room temperature for at least 30 min. Slides were then washed twice with 1× PBS to remove any residual OCT. Tissue was then incubated in 70% ethanol and then 95% ethanol for 3 min each. Slides were then incubated in 100% ethanol for 3 min and then 5 min, changing the ethanol between each incubation. Slides were then washed in deionized water 3–4 times. A Cresyl Violet Counterstain Solution (Bioenno Tech, Santa Anna, CA, USA) was applied to each slide for 3 min. De-staining was then performed by washing briefly in 70 mM acetic acid solution. Slides were rinsed in deionized water 3 times. Lastly, slides were incubated sequentially in solutions of 70%, 95%, and 100% ethanol as described above. Slides were mounted with ProLong Gold anti-fade reagent and were sealed with coverslips. Stained slides were stored in the dark at −20 °C until imaging took place. Two slides from each mouse spinal cord were stained for Nissl with 6 sections per slide.

2.10. Imaging and Quantification of Nissl-Stained Spinal Cord Sections at End Stage of the Untreated hSOD1^{G93A} Littermate

A single image of each ventral horn was captured on the 20× objective using bright field by blinded researchers. At least six ventral horns for each mouse were imaged. Any neuron greater than 20 μm in length along its longest axis was considered to be a viable alpha motor neuron. Using Adobe Photoshop CC, the contrast was set to the WT littermate and kept the same within the group to ensure consistency in staining. Next, the ruler tool was used to measure all motor neurons greater than 20 μm. For each mouse, the average number of alpha motor neurons was taken. Quantification was performed twice by two different and blinded researchers. Each average of the untreated hSOD1^{G93A} littermate and 100 mg/kg PCA-treated hSOD1^{G93A} littermate mouse were calculated as a percent of the average of the WT littermate control mouse (set at 100%). The mean numbers of alpha motor neurons in the lumbar spinal cord ventral horn in the untreated hSOD1^{G93A} littermate mice and WT littermate mice were also statistically compared to verify a significant disease effect.

2.11. Alpha-Bungarotoxin and VACHT Staining of Gastrocnemius Sections

Prior to staining, slides were allowed to equilibrate at room temperature for at least 30 min. Tissue sections on the slides were then outlined with a hydrophobic pen and washed twice with 1× PBS to remove any OCT. Tissue was then incubated at room temperature in blocking buffer, containing 5% (*w/v*) BSA and 0.2% triton-X 100 in 1× PBS for 90 min. For analysis of NMJ area, perimeter, and complexity, the slides were then incubated for 90 min with alpha-BTx conjugated to Alexa Fluor® 594 (ThermoFisher Scientific Inc., Rockford, IL, USA) at a 1:200 dilution in blocking buffer containing Hoechst nuclear stain at a dilution of 1:500. For analysis of NMJ innervation, slides were stained with primary antibody to VACHT (C-terminal) (Sigma-Aldrich, St. Louis, MO, USA) which was prepared as a 1:500 dilution in PBS containing 0.2% triton-X 100 and 2% BSA (*w/v*). Tissue was incubated in primary antibody overnight at 4 °C. FITC-conjugated donkey anti-rabbit antibody (Jackson ImmunoResearch Laboratories, West Grove, PA, USA) was then prepared at a 1:500 dilution (*v/v*) and alpha-BTx conjugated to Alexa Fluor® 594 (ThermoFisher Scientific Inc., Rockford, IL, USA) was prepared at a 1:200 dilution in 1× PBS containing 0.2% triton-X100 and 2% BSA (*w/v*) and Hoechst nuclear stain (Sigma-Aldrich, St. Louis, MO, USA) at a 1:500 dilution to detect VACHT on the presynaptic axon terminal, NMJs, and to label nuclei, respectively. Slides were washed with 1× PBS 3–4 times and then

mounted using ProLong Gold anti-fade reagent and sealed with coverslips. Stained slides were stored in the dark at -20°C until imaging took place.

2.12. Imaging and Area, Perimeter, and Sholl Analysis Quantification of Gastrocnemius Sections Stained with Alpha-Bungarotoxin at End Stage of the Untreated hSOD1^{G93A} Littermate Mouse

Neuromuscular junctions (20–25) were imaged for each mouse by blinded researchers on the 40^X objective for all mice that were euthanized at end stage of the untreated hSOD1^{G93A} littermate control mice. Using the magic wand tool in Adobe Photoshop CC, the area was measured, in pixels, for each NMJ. This was achieved by outlining the outside of each NMJ, pressing “Record Measurements”, and taking the provided “Area” value. The perimeter, in pixels, of each NMJ was also measured by tracing the NMJ inside and outside, pressing “Record Measurements”, and taking the provided “Perimeter” value. An average perimeter and area were calculated for each mouse from all the values recorded for the mouse. Quantification was performed twice by two different and blinded researchers. The untreated hSOD1^{G93A} and 100 mg/kg PCA-treated hSOD1^{G93A} littermate mice averages were calculated as a percent of the WT littermate mouse, which was set at 100%. Mean NMJ pixel area and perimeter in the untreated hSOD1^{G93A} littermate mice and WT littermate mice were also statistically compared to verify a significant disease effect. The Sholl analysis was also performed on the same NMJ images that were used to analyze area and perimeter. Briefly, using ImageJ, the red (BTx) channel was separated from all channels and the NMJ was isolated using the plugins “Despeckle” and “Find Edges”. The edges of the NMJ were traced with “Simple Neurite Tracer” and “Analyze Skeleton” plugins. Each NMJ was circled by hand and pasted into a new image. The plugin “Skeletonize” was run to draw a line around the border of the NMJ. The “Sholl Analysis” plugin was run to decide a point in the center of the NMJ and to draw concentric circles around that point at a radius increasing by 10 pixels. Mean Sholl analysis values of NMJ complexity, or the number of intersections formed between the concentric circles and the skeleton of the NMJ, were reported for each untreated hSOD1^{G93A} and 100 mg/kg PCA-treated hSOD1^{G93A} littermate mouse to be taken as a percent of the WT littermate control mouse (set at 100%). Mean Sholl analysis values from untreated hSOD1^{G93A} littermate mice and WT littermate mice were also statistically compared to verify a significant disease effect.

2.13. Analysis of Gastrocnemius Muscle Wet Weight at 105 Days of Age

Gastrocnemius muscle from all 105-day-old mice were placed into a tared weigh boat on a standard analytical balance to obtain muscle wet weight. Weights of gastrocnemius muscle were taken from WT, 100 mg/kg PCA-treated hSOD1^{G93A}, and untreated hSOD1^{G93A} littermate mice. Each gastrocnemius muscle wet weight from the untreated hSOD1^{G93A} littermate mouse and 100 mg/kg PCA-treated hSOD1^{G93A} littermate mouse was calculated as a percent of the average of the WT littermate control mouse (set at 100%).

2.14. Imaging of Gastrocnemius Sections Stained with Alpha-BTx and VAcHt at 105 Days of Age

Neuromuscular junctions (20–25) were captured on the Rhodamine channel for each mouse by blinded researchers on the 20^X objective for all mice that were euthanized at 105 days of age. VAcHt was captured on the Alexa Fluor 488 channel for each NMJ. Representative images are shown from a WT, untreated hSOD1^{G93A} mouse, and a 100 mg/kg PCA-treated hSOD1^{G93A} mouse.

2.15. Imaging of Quantification of 4-HNE-Stained Spinal Cord Sections at 105 Days of Age

A single image of each ventral horn on the 20^X objective was captured for each mouse. Imaging was performed by blinded researchers. Images were captured on the Alexa Fluor 488 channel (pseudo-colored red) and the exposure time was set appropriately for the untreated hSOD1^{G93A} littermate and kept constant when imaging the PCA-treated hSOD1^{G93A} and WT littermate mice. Two littermate groups were analyzed and 6 ventral horns per animal were imaged and analyzed for

fluorescence intensity using Adobe Photoshop CC software. The ventral horn image of the untreated hSOD1^{G93A} littermate control mouse with the most background was chosen, and the red channel input level was adjusted so that background staining was best eliminated. This value was recorded and used for each subsequent image, including those taken from the WT control littermate and the PCA-treated hSOD1^{G93A} littermate mice such that all images were adjusted by an equivalent amount. After the channel levels were adjusted, the ventral horn was outlined using the lasso tool and red channel values for mean pixel intensity and pixel area were recorded for each ventral horn image. Total pixel intensity of the red channel was obtained by multiplying the pixel intensity and pixel area. An average of the total pixel intensity was taken for each mouse. Quantification was performed once by a blinded researcher. An average of the pixel intensities for each mouse was obtained. For analysis, the average total pixel intensity for the WT littermate control mouse for each group was set at 100% and each individual total pixel intensity for each ventral horn for the untreated hSOD1^{G93A} littermate control and PCA-treated hSOD1^{G93A} littermate mice were calculated as percentages relative to the average total pixel intensity of the WT littermate control mouse. Mean raw 4-HNE fluorescence intensity in the lumbar spinal cord ventral horn in the untreated hSOD1^{G93A} littermate mice and WT littermate mice were also counted and statistically compared to verify a significant disease effect.

2.16. Statistical Analysis

Histological analyses were performed on at least 6 mice per treatment group. Differences between untreated and PCA-treated hSOD1^{G93A} littermate mice for Iba-1, GFAP, and 4-HNE intensity, NMJ area and perimeter, Nissl-stained counts, and gastrocnemius muscle wet weight were analyzed using a paired *t*-test. PaGE and rotarod were analyzed using an unpaired *t*-test at each time point. Correlation analysis of PaGE data and survival were analyzed using a Pearson correlation. Mean NMJ Sholl analysis values were analyzed using a one-way analysis of variance (ANOVA) with post-hoc Tukey's test. Survival Kaplan–Meier curves and body weight data were analyzed using a log-rank test. For all analyses, differences were statistically significant when $p < 0.05$.

3. Results

3.1. PCA Orally Administered Beginning at Disease Onset Results in a Significant Extension of Survival but Does Not Preserve Body Weight in the hSOD1^{G93A} Mouse Model of ALS

In order to determine the therapeutic benefit of PCA in an ALS mouse model, we first evaluated the ability of PCA to extend the lifespan of hSOD1^{G93A} mice. Mice were dosed by oral gavage with either 50 or 100 mg/kg PCA beginning at 90 days of age. This time point corresponds with average disease onset. At this age, mice typically display gait disturbances, decreased weight, and lower limb tremors [35]. Mice were dosed by oral gavage with PCA until end stage, assessed by the ability of the mouse to right itself to sternum when placed on its side. Administration of both 50 and 100 mg/kg PCA significantly extended median survival in hSOD1^{G93A} mice to 129 and 133 days, respectively, when compared to untreated hSOD1^{G93A} mice, which exhibited a median survival of 121 days ($p = 0.0025$; Figure 1A). This impressive extension of survival indicates that PCA is slowing the disease progression in hSOD1^{G93A} ALS mice. Body weight of the hSOD1^{G93A} mice was assessed twice per week and is expressed as a percentage of peak body weight at each time point. Despite significantly extended survival, administration of PCA had no significant effect on the decline in body weight in the hSOD1^{G93A} mouse model of ALS (Figure 1B).

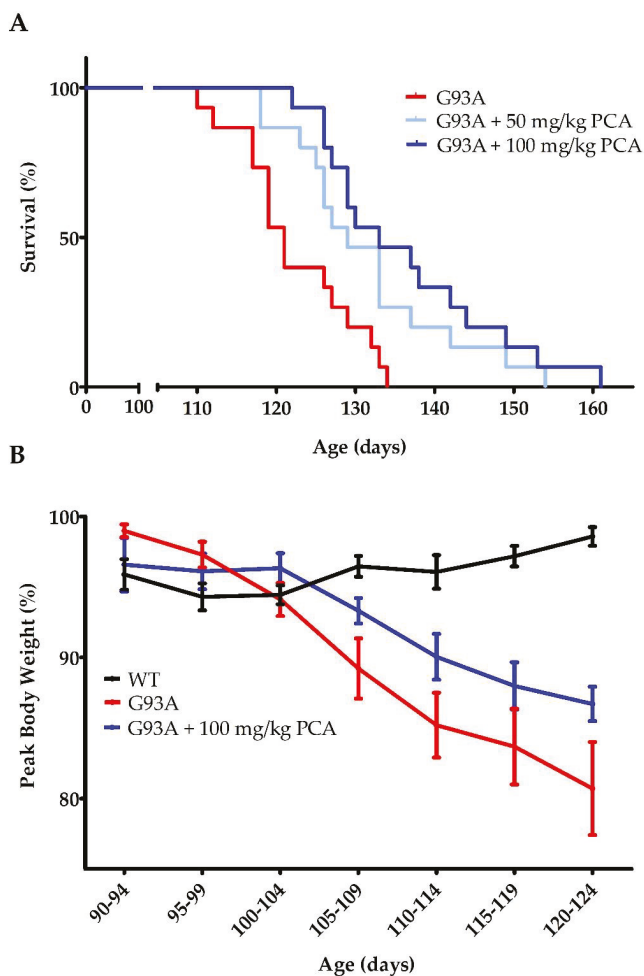


Figure 1. PCA treatment extends survival in the hSOD1^{G93A} mouse model of ALS. **(A)** Survival of hSOD1^{G93A} mice (untreated or treated with 50 or 100 mg/kg PCA) and wildtype mice (WT). Oral administration of either 50 or 100 mg/kg PCA beginning at disease onset (90 days of age) significantly extended median survival in hSOD1^{G93A} mice to 129 and 133 days, respectively, when compared to untreated hSOD1^{G93A} mice, which exhibited a median survival of 121 days. Curves are significantly different as determined by log-rank (Mantel–Cox) test ($p = 0.0025$; $n = 15$ mice per group). **(B)** Body weight of hSOD1^{G93A} mice (untreated or treated with 100 mg/kg PCA) and WT mice. Body weight was assessed twice per week and is expressed as the percent of peak body weight at each time point. Data are displayed as the mean \pm SEM with $n = 15$ mice for each group.

3.2. PCA Treatment Improves Grip Strength and Motor Performance in the hSOD1^{G93A} Mouse Model of ALS

Since the dose of 100 mg/kg PCA had a more pronounced effect on survival than the 50 mg/kg PCA dose, grip strength and motor function were assessed in mice dosed with 100 mg/kg PCA. hSOD1^{G93A} mice treated with 100 mg/kg PCA were further evaluated using PaGE testing and rotarod testing in order to assess motor function [36]. PaGE testing was performed twice a week beginning at disease onset until end stage of disease to assess grip strength. Administration of 100 mg/kg PCA beginning at disease onset significantly increased the latency to fall as assessed by PaGE testing at 100 to 114 days of

age when compared to the untreated hSOD1^{G93A} littermate controls ($p < 0.05$, Figure 2A). PaGE data were also analyzed for differences between male and female mice. PCA-treated male hSOD1^{G93A} mice did not show a significantly increased latency to fall at any time points when compared to the untreated male hSOD1^{G93A} littermate controls (Figure 2B). However, PCA-treated male hSOD1^{G93A} mice did trend towards a significant increase in latency to fall at 95–99 ($p = 0.118$, Figure 2B) and 100–104 days of age ($p = 0.115$). PCA-treated female hSOD1^{G93A} mice displayed a significantly increased latency to fall as assessed by PaGE testing at 105–109 ($p < 0.001$, Figure 2C) and 110–114 ($p < 0.05$, Figure 2C) days of age when compared to untreated female hSOD1^{G93A} littermate controls. Lastly, we sought to understand the relationship between PaGE testing and survival in PCA-treated hSOD1^{G93A} mice. We averaged latency to fall as assessed by PaGE testing at 100–114 days of age from male and female hSOD1^{G93A} mice treated with 100 mg/kg PCA beginning at disease onset. The latency to fall at these time points was chosen to be averaged because PCA-treated hSOD1^{G93A} displayed an increased latency to fall as assessed by PaGE testing at these time points when compared to untreated hSOD1^{G93A} littermate mice. The average latency to fall over these time points was correlated with the days lived for each mouse. Average latency to fall at 100–114 days and days lived was positively and significantly correlated in PCA-treated hSOD1^{G93A} mice ($r = 0.558$, $p < 0.05$, Figure 2D).

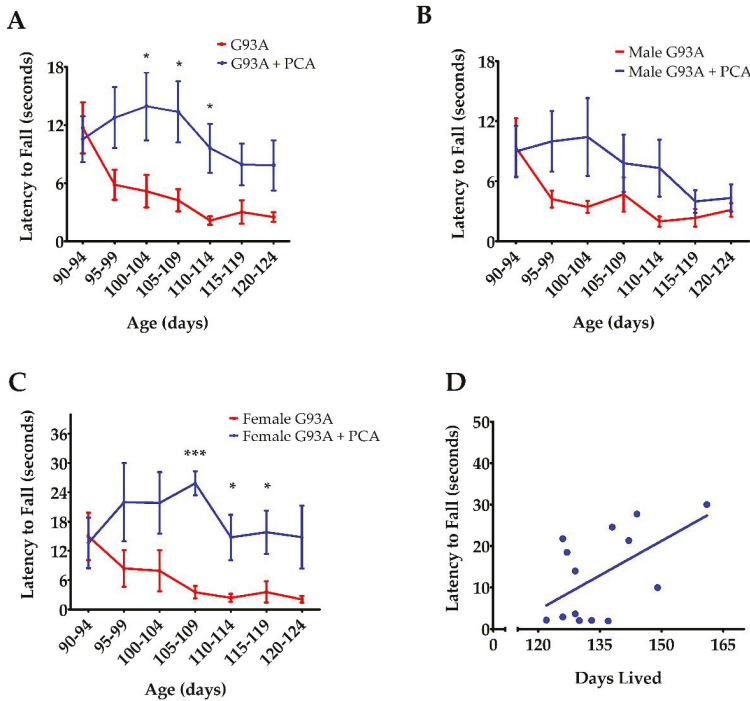


Figure 2. PCA treatment improves grip strength as assessed by PaGE in the hSOD1^{G93A} mouse model of ALS. (A) PaGE testing of hSOD1^{G93A} mice (untreated or treated with 100 mg/kg PCA) beginning at disease onset. PaGE testing was performed twice a week beginning at 90 days of age and is expressed as latency to fall. PaGE data are expressed as the mean \pm SEM for each time point; $n = 15$ mice per group. * indicates $p < 0.05$ in comparison to untreated hSOD1^{G93A} littermate controls. All data were analyzed using an unpaired t -test at each time point. (B) PaGE testing of male hSOD1^{G93A} mice (untreated or treated with 100 mg/kg PCA) beginning at disease onset. PaGE data are expressed as the mean \pm SEM for each time point; $n = 9$ mice per group. All data were analyzed using an unpaired t -test at each time point. (C) PaGE testing of female hSOD1^{G93A} mice (untreated or treated with 100 mg/kg PCA)

beginning at disease onset. PaGE data are expressed as the mean \pm SEM for each time point; $n = 6$ mice per group. All data were analyzed using an unpaired t -test at each time point. * indicates $p < 0.05$ in comparison to untreated hSOD1^{G93A} littermate controls. *** indicates $p < 0.001$ in comparison to untreated hSOD1^{G93A} littermate controls. (D) Increased average PaGE latency to fall between 100 and 114 days of age is significantly correlated with longer survival of 100 mg/kg PCA-treated hSOD1^{G93A} mice. PaGE data from 100–114 days of age are expressed as the mean for each mouse; $n = 14$ mice. All data were analyzed using a Pearson correlation ($r = 0.558, p < 0.05$).

For further motor function analysis, rotarod testing was performed once a week beginning at disease onset until end stage of disease. This behavioral assay also showed an impressive enhancement in the motor function of PCA-treated hSOD1^{G93A} mice when compared to untreated hSOD1^{G93A} littermates. Administration of 100 mg/kg PCA beginning at disease onset significantly but transiently increased the latency to fall as measured by rotarod testing at 97 and 104 days of age when compared to the untreated hSOD1^{G93A} littermate control mice ($p < 0.001$, Figure 3A). The results of these behavioral tests indicate that oral administration of PCA beginning at disease onset significantly improves balance, grip strength, and motor coordination in the hSOD1^{G93A} mouse model of ALS.

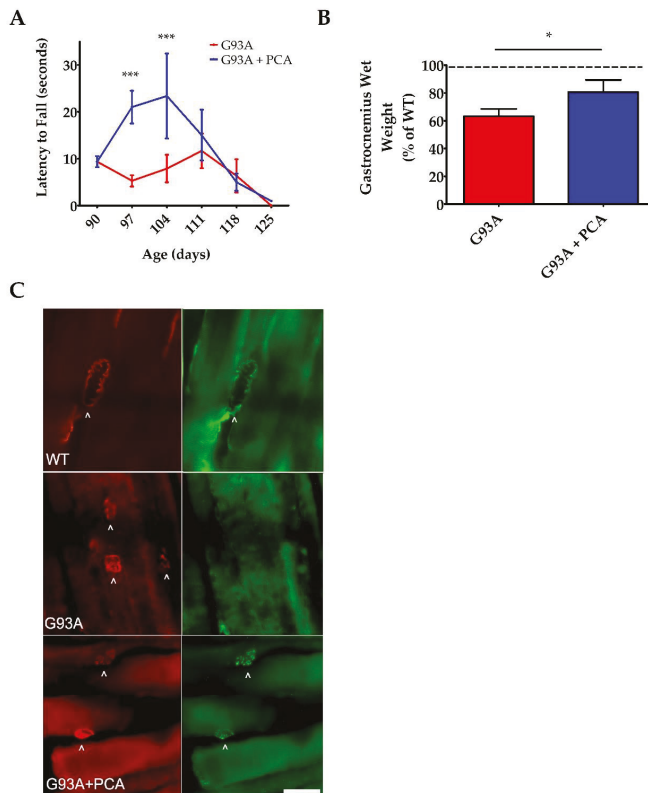


Figure 3. PCA treatment improves motor function as assessed by rotarod and also preserves gastrocnemius muscle weight and neuromuscular junction (NMJ) innervation at 105 days of age in the hSOD1^{G93A} mouse model of ALS. (A) Rotarod testing of hSOD1^{G93A} mice (untreated or treated with 100 mg/kg PCA beginning at disease onset). Rotarod testing was performed beginning at 90 days of age and extending through end stage and is expressed as latency to fall. Rotarod data are represented as the mean \pm SEM for each time point; $n = 10$ mice per group. *** indicates $p < 0.001$ in

comparison to untreated hSOD1^{G93A} littermate controls. All data were analyzed using an unpaired *t*-test at each time point. (B) Quantification of gastrocnemius muscle weights. Data are expressed as a percent of the wildtype (WT) littermate mouse muscle weight and are shown as the mean \pm SEM; *n* = 7 mice per group. * indicates *p* < 0.05 compared to untreated hSOD1^{G93A} control mice (paired *t*-test). Mean gastrocnemius wet weight for the untreated hSOD1^{G93A} mouse (0.0912 \pm 0.0070) is significantly decreased when compared to the WT littermate control mouse (0.1433 \pm 0.0055) (*p* = 0.0002; *n* = 7 mice per group). (C) Representative images of gastrocnemius muscle from wildtype control mice (WT), untreated hSOD1^{G93A} mice (G93A), and hSOD1^{G93A} mice treated orally with 100 mg/kg PCA beginning at disease onset (G93A+PCA). Mice were euthanized at 105 days of age and gastrocnemius muscles were stained with alpha-BTx (red) and VAcHT (green) to label NMJs and innervation of NMJs, respectively. Scale bar = 20 μ m. Arrowheads point to NMJs stained positively with alpha-BTx and VAcHT.

3.3. PCA Treatment Preserves Gastrocnemius Muscle Wet Weight, Protects NMJ Innervation, and Reduces Oxidative Stress in the hSOD1^{G93A} Mouse Model of ALS at 105 Days of Age

We observed the greatest improvements in motor function as assessed by rotarod and PaGE testing between 97 and 114 days of age in PCA-treated hSOD1^{G93A} mice. Therefore, we next analyzed gastrocnemius muscle weight at 105 days of age, the time point at which we saw the greatest behavioral therapeutic effect of PCA. Wet muscle weight isolated from untreated hSOD1^{G93A} mice (0.091 g \pm 0.007) was significantly decreased when compared to WT littermate mice (0.143 g \pm 0.006) (*p* < 0.01, Figure 3B). PCA-treated mice exhibited a significant preservation of gastrocnemius muscle wet weight when compared to untreated hSOD1^{G93A} littermate mice. PCA-treated hSOD1^{G93A} mice had a mean muscle wet weight of 80% of the WT littermate mice, while untreated hSOD1^{G93A} mice had a mean muscle weight of only 63% of WT littermate mice (*p* < 0.05, Figure 3B). These results show that PCA treatment significantly delayed atrophy of the gastrocnemius muscle in the hSOD1^{G93A} mouse model of ALS. To support these findings, we stained gastrocnemius muscle isolated at 105 days of age with alpha-BTx and VAcHT in order to visualize innervated NMJs. Although these findings are preliminary, they indicate that PCA-treated mice exhibit a protection of NMJ innervation when compared to untreated hSOD1^{G93A} littermate mice, as evidenced by retention of the overlapping staining of alpha-BTx and VAcHT in the treated mouse NMJs (Figure 3C).

Oxidative stress is an underlying pathology of ALS and contributes to motor neuron death and subsequent skeletal muscle atrophy and deficits in motor function [16,17]. Therefore, we also analyzed the effect of PCA on the production of 4-HNE in the lumbar spinal cord ventral horn of the hSOD1^{G93A} mouse model of ALS. Lumbar spinal cord isolated at 105 days of age from two littermate groups was stained with antibodies against 4-HNE to measure lipid peroxidation. Untreated hSOD1^{G93A} mice in both groups exhibit significantly higher raw 4-HNE fluorescence units (((11.70 \pm 0.78) \times 10⁶) and ((6.56 \pm 0.88) \times 10⁶)) when compared to their WT littermate control mice (((7.83 \pm 0.16) \times 10⁶) and ((4.17 \pm 0.24) \times 10⁶)), respectively. These data indicate profound lipid peroxidation in the ventral horn (*p* < 0.01 and *p* < 0.05, Figure 4A and C, respectively). Administration of 100 mg/kg PCA beginning at disease onset significantly reduced lipid peroxidation in the ventral horn of the lumbar spinal cord in the hSOD1^{G93A} mouse model of ALS relative to the untreated littermate control (*p* < 0.01 and *p* < 0.05, Figure 4B and D, respectively).

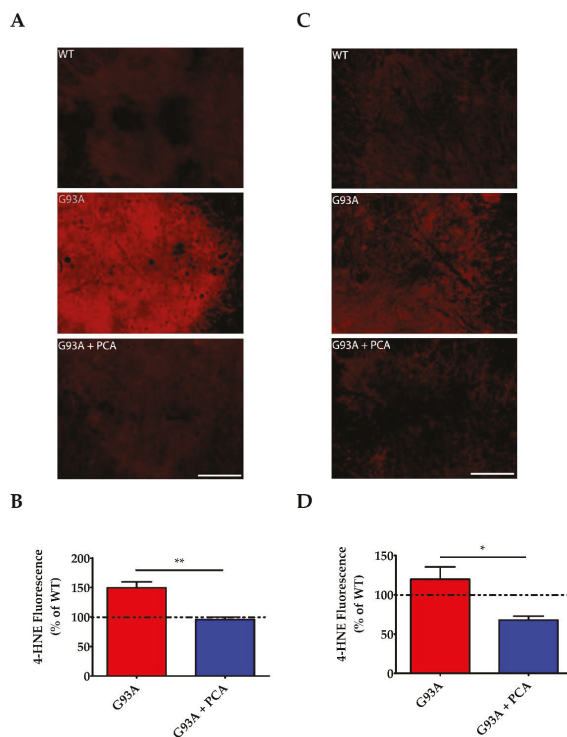


Figure 4. PCA treatment significantly reduces lipid peroxidation in the ventral horn of the spinal cord in the hSOD1^{G93A} mouse model of ALS. (A,C) Representative images of lumbar spinal cord ventral horns stained for 4-HNE from two littermate groups of wildtype control mice (WT), untreated hSOD1^{G93A} mice (G93A), and hSOD1^{G93A} mice treated orally with 100 mg/kg PCA beginning at disease onset (G93A+PCA). Mice were euthanized at 105 days of age and ventral horns were stained with an antibody to 4-HNE to measure lipid peroxidation. Scale bar = 70 μ m. (B) Quantification of spinal cord ventral horns stained with 4-HNE as described and shown in A. The 4-HNE fluorescence intensity of untreated and PCA-treated hSOD1^{G93A} littermate mice were normalized and expressed as a percentage of mean 4-HNE fluorescence measured in the WT littermate control mouse. Data are expressed as the mean \pm SEM; 6 ventral horns were imaged per mouse. ** indicates $p < 0.01$ compared to the untreated hSOD1^{G93A} control littermate (paired *t*-test). Raw mean 4-HNE fluorescence units for the untreated hSOD1^{G93A} mouse (11.70 ± 0.78) $\times 10^6$ are significantly higher than the WT littermate mouse (7.83 ± 0.16) $\times 10^6$ ($p < 0.01$). (D) Quantification of spinal cord ventral horns stained with 4-HNE as described and shown in C. The 4-HNE fluorescence intensity of untreated and PCA-treated hSOD1^{G93A} littermate mice were normalized and expressed as a percentage of mean 4-HNE fluorescence measured in the WT littermate control mouse. Data are expressed as the mean \pm SEM; 6 ventral horns were imaged per mouse. * indicates $p < 0.05$ compared to the untreated hSOD1^{G93A} control littermate (paired *t*-test). Raw mean 4-HNE fluorescence units for the untreated hSOD1^{G93A} mouse (6.56 ± 0.88) $\times 10^6$ are significantly higher than the WT (4.17 ± 0.24) $\times 10^6$ ($p < 0.05$).

3.4. PCA Treatment Significantly Preserves Motor Neurons in the Ventral Horn of the Spinal Cord in the hSOD1^{G93A} Mouse Model of ALS

It was evident that PCA had a beneficial therapeutic effect, as evidenced by the extension of survival and motor function improvements in the hSOD1^{G93A} mouse model of ALS. However, the effects of PCA on inflammation, motor neuron preservation, and neuromuscular junction integrity needed to be

studied in order to support the survival and behavioral assay results. Lumbar spinal cord was isolated at end stage of the untreated hSOD1^{G93A} littermate control mouse and Nissl staining was performed so that neuronal cell bodies could be identified. The number of alpha motor neurons, with somas typically greater than 20 μm along the longest axis, were counted in the ventral horn of the lumbar spinal cord of untreated and PCA-treated hSOD1^{G93A} littermate mice. These values were normalized and expressed as a percentage of the number of alpha motor neurons counted in the WT littermate control mouse. The cell bodies of alpha motor neurons are located in the ventral horn of the lumbar spinal cord and their axons project to innervate skeletal muscle fibers of the leg muscles including the gastrocnemius muscle. The hSOD1^{G93A} mouse model of ALS exhibits a rapidly progressive lower limb muscular atrophy and subsequent paralysis as a result of alpha motor neuron death in the ventral horn of the spinal cord and retraction of motor axons away from the NMJs [35]. As anticipated, untreated hSOD1^{G93A} mice exhibited nearly 60% fewer alpha motor neurons in the lumbar spinal cord ventral horn than their healthy WT littermates (Figure 5A). However, when 100 mg/kg PCA was administered beginning at disease onset, the average alpha motor neuron count in the ventral horn of the lumbar spinal cord was significantly increased in comparison to the untreated hSOD1^{G93A} littermate mouse ($p < 0.05$, Figure 5B). These findings may contribute to the observed improvements in motor function as assessed by rotarod and PaGE testing.

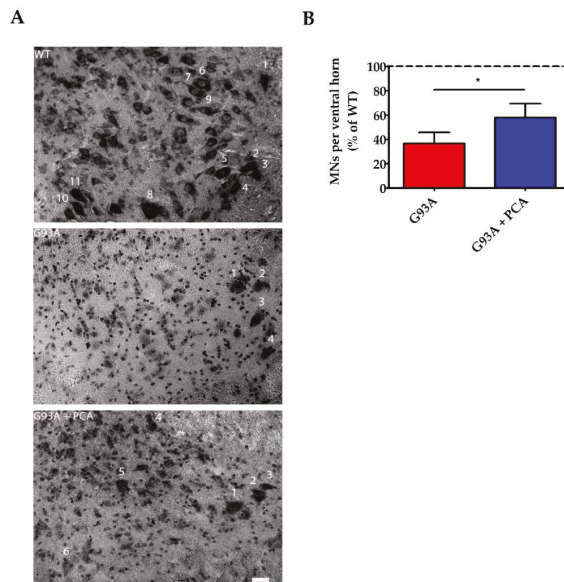


Figure 5. PCA treatment significantly preserves motor neurons in the ventral horn of the spinal cord in the hSOD1^{G93A} mouse model of ALS. **(A)** Representative images of lumbar spinal cord ventral horns from wildtype control mice (WT), untreated hSOD1^{G93A} control mice (G93A) and hSOD1^{G93A} mice treated orally with 100 mg/kg PCA beginning at disease onset (G93A+PCA). Mice were euthanized at end stage of the untreated hSOD1^{G93A} littermate control mouse and ventral horns were Nissl stained to label neuronal cell bodies. Stained soma were measured along the longest axis and cells were considered alpha motor neurons if the length was greater than 20 μm . Scale bar = 20 μm . **(B)** Quantification of Nissl-stained alpha motor neurons as described in A. The number of alpha motor neurons in the ventral horns of lumbar spinal cord of untreated and PCA-treated hSOD1^{G93A} littermate mice were normalized and expressed as a percentage of the number of alpha motor neurons measured in the WT littermate control mouse. Data are expressed as the mean \pm SEM; $n = 7$ mice per group; 4–6 ventral

horns were imaged per mouse. * indicates $p < 0.05$ compared to untreated hSOD1^{G93A} littermate controls (paired *t*-test). Mean number of alpha motor neurons present in the ventral horn lumbar spinal cord for the untreated hSOD1^{G93A} littermate mouse (1.92 ± 0.47) is significantly less than that of the WT (5.55 ± 0.57) ($p = 0.004$; $n = 7$ mice per group). Abbreviations used: MNs = motor neurons.

3.5. PCA Treatment Significantly Reduces Astrogliosis and Microgliosis in the Ventral Horn of the Spinal Cord in the hSOD1^{G93A} Mouse Model of ALS

A robust neuroinflammatory response in the central nervous system of the hSOD1^{G93A} mouse model contributes to the motor neuron death and muscle atrophy producing the ALS-like phenotype [35]. Therefore, we next analyzed the effect of PCA on astrogliosis and microgliosis in the lumbar spinal cord ventral horn of the hSOD1^{G93A} mouse model of ALS. Lumbar spinal cord isolated at end stage of the untreated hSOD1^{G93A} littermate mouse was stained with antibodies against GFAP and Iba-1 to identify astrocytes and microglia, respectively. Untreated hSOD1^{G93A} mice exhibit significantly higher raw mean GFAP fluorescence units ($(3.21 \pm 0.46) \times 10^6$) when compared to WT littermate control mice ($(0.97 \pm 0.16) \times 10^6$) indicating profound astrogliosis in the ventral horn ($p = 0.001$, Figure 6A). Microgliosis is also present in the lumbar spinal cord ventral horn of untreated hSOD1^{G93A} mice, as these mice exhibited significantly higher raw mean Iba-1 fluorescence units ($(3.41 \pm 0.52) \times 10^6$) when compared to healthy WT littermate control mice ($(1.56 \pm 0.29) \times 10^6$) ($p < 0.05$, Figure 7A). Administration of 100 mg/kg PCA beginning at disease onset significantly reduced astrogliosis in the ventral horn of the lumbar spinal cord in the hSOD1^{G93A} mouse model of ALS from a mean 394% increase to a mean 258% increase in GFAP fluorescence units relative to the WT littermate control ($p < 0.05$, Figure 6B). Administration of PCA also significantly reduced microgliosis in the ventral horn lumbar spinal cord in the hSOD1^{G93A} mouse model of ALS from a mean 248% increase to a mean 156% increase in Iba-1 fluorescence units relative to the WT littermate control ($p < 0.05$, Figure 7B). From these data, we conclude that PCA significantly reduces gliosis which may ultimately protect alpha motor neurons in the ventral horn of the lumbar spinal cord in the hSOD1^{G93A} mouse model of ALS.

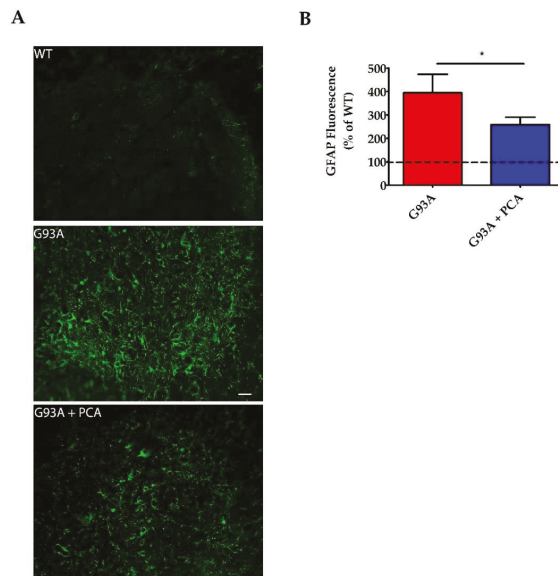


Figure 6. PCA treatment significantly reduces astrogliosis in the ventral horn of the spinal cord in the hSOD1^{G93A} mouse model of ALS. (A) Representative images of lumbar spinal cord ventral horns

stained for GFAP from wildtype control mice (WT), untreated hSOD1^{G93A} mice (G93A), and hSOD1^{G93A} mice treated orally with 100 mg/kg PCA beginning at disease onset (G93A+PCA). Mice were euthanized at end stage of the untreated hSOD1^{G93A} littermate control mouse and ventral horns were stained with an antibody to GFAP to label astrocytes. Scale bar = 20 μ m. (B) Quantification of spinal cord ventral horns stained with GFAP as described in A. GFAP fluorescence intensity of untreated and PCA-treated hSOD1^{G93A} littermate mice were normalized and expressed as a percentage of GFAP fluorescence measured in the WT littermate control mouse. Data are expressed as the mean \pm SEM; $n = 10$ mice per group; 4–6 ventral horns were imaged per mouse. * indicates $p < 0.05$ compared to untreated hSOD1^{G93A} controls (paired t -test). Raw mean GFAP fluorescence units for the untreated hSOD1^{G93A} mice ($(3.21 \pm 0.46) \times 10^6$) are significantly higher than the WT ($(0.97 \pm 0.16) \times 10^6$) ($p = 0.001$; $n = 10$ mice per group).

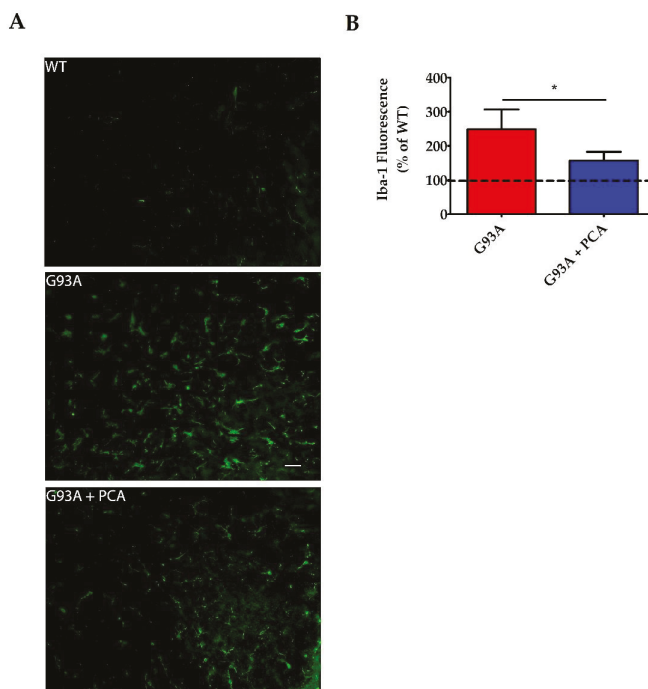


Figure 7. PCA treatment significantly reduces microgliosis in the ventral horn of the spinal cord in the hSOD1^{G93A} mouse model of ALS. (A) Representative images of lumbar spinal cord ventral horns stained for Iba-1 from wildtype control mice (WT), untreated hSOD1^{G93A} mice (G93A), and hSOD1^{G93A} mice treated orally with 100 mg/kg PCA beginning at disease onset (G93A+PCA). Mice were euthanized at end stage of the untreated hSOD1^{G93A} littermate mouse and ventral horns were stained with an antibody to Iba-1 to label microglia. Scale bar = 20 μ m. (B) Quantification of spinal cord ventral horns stained with Iba-1 as described in A. Iba-1 fluorescence intensity of untreated and PCA-treated hSOD1^{G93A} littermate mice were normalized and expressed as a percentage of Iba-1 fluorescence measured in the WT littermate control mouse. Data are expressed as the mean \pm SEM; $n = 6$ mice per group; 4–6 ventral horns were imaged per mouse. * indicates $p = 0.05$ compared to untreated hSOD1^{G93A} controls (paired t -test). Raw mean Iba-1 fluorescence units for the untreated hSOD1^{G93A} mouse ($(3.41 \pm 0.52) \times 10^6$) are significantly higher than the WT ($(1.56 \pm 0.29) \times 10^6$) ($p < 0.05$; $n = 6$ mice per group).

3.6. PCA Treatment Significantly Preserves Neuromuscular Junctions of the Gastrocnemius Muscle in the hSOD1^{G93A} Mouse Model of ALS

After determining that PCA has neuroprotective and anti-inflammatory effects in the ventral horn of the lumbar spinal cord isolated from hSOD1^{G93A} mice, we sought to analyze NMJs in gastrocnemius muscle in order to further elucidate how administration of PCA improved motor deficits. Neuromuscular junctions represent the synapse between the alpha motor neuron axon terminal and the gastrocnemius muscle fiber. In the hSOD1^{G93A} mouse model of ALS, NMJs become weakened and break down as the alpha motor neuron cell body dies and the axon retracts away from the muscle. This results in skeletal muscle atrophy and paralysis characteristically seen in this mouse model [35]. To analyze the NMJs, gastrocnemius muscle was isolated at end stage of the untreated hSOD1^{G93A} littermate mouse and stained with alpha-bungarotoxin. Alpha-bungarotoxin binds to nicotinic acetylcholine receptors found on the gastrocnemius muscle. Mean NMJ area, perimeter, and Sholl analysis values of untreated and PCA-treated hSOD1^{G93A} littermate mice were normalized and expressed as a percentage of the corresponding NMJ values measured in the WT littermate control mouse. Untreated hSOD1^{G93A} mice exhibited an overall decreased NMJ pixel area ($11,842 \pm 1204$) when compared to WT littermate control mice ($17,966 \pm 818$) ($p = 0.01$, Figure 8A). Furthermore, untreated hSOD1^{G93A} mice also exhibited an overall decreased NMJ pixel perimeter (731 ± 40) when compared to the healthy WT littermate control mice (1141 ± 95) ($p = 0.0007$, Figure 8A). Administration of 100 mg/kg PCA beginning at disease onset significantly preserved NMJ area yielding an average NMJ pixel area of 79% of the WT littermate mice compared to the untreated hSOD1^{G93A} littermate mice, which had an average area of 61% of the WT littermate mice ($p < 0.05$, Figure 8B). Furthermore, PCA significantly preserved NMJ perimeter in the hSOD1^{G93A} mouse model of ALS. PCA-treated hSOD1^{G93A} mice exhibited a mean NMJ pixel perimeter of 81% of WT littermate mice versus untreated hSOD1^{G93A} littermate mice, which exhibited a mean of 64% of WT littermate mice ($p < 0.05$, Figure 8C). Untreated hSOD1^{G93A} mice also exhibited an overall decreased NMJ mean Sholl analysis value (62 ± 1.6) when compared to WT littermate mice (97 ± 4.3) ($p < 0.001$, Figure 8D). More importantly, PCA-treated hSOD1^{G93A} littermates exhibited a significantly greater mean Sholl analysis value (79 ± 6.8) when compared to untreated hSOD1^{G93A} littermate mice ($p < 0.05$, Figure 8D). These findings indicate that PCA protects the synapse between the alpha motor neuron axon and the gastrocnemius muscle, ultimately allowing for improved motor function and mobility.

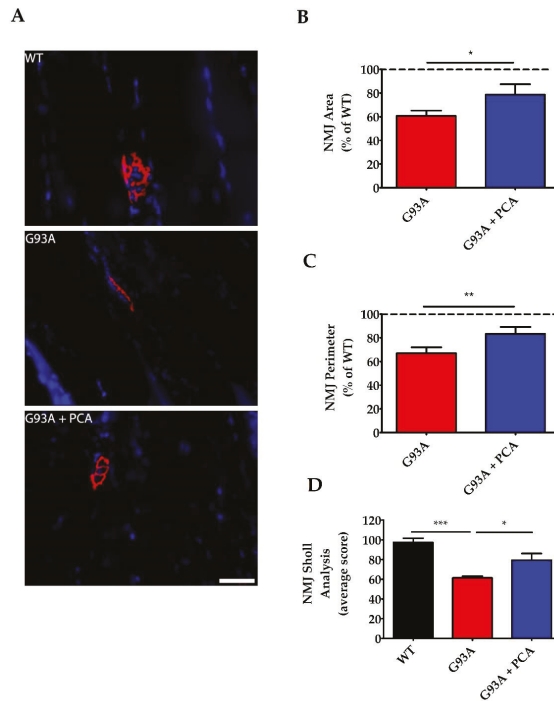


Figure 8. PCA treatment significantly preserves neuromuscular junctions (NMJ) in the gastrocnemius muscle in the hSOD1^{G93A} mouse model of ALS. (A) Representative images of gastrocnemius muscle from wildtype control mice (WT), untreated hSOD1^{G93A} mice (G93A), and hSOD1^{G93A} mice treated orally with 100 mg/kg PCA beginning at disease onset (G93A+PCA). Mice were euthanized at end stage of the untreated hSOD1^{G93A} littermate mouse and gastrocnemius muscles were stained with alpha-BTx (red) and Hoechst (blue) to label NMJs and nuclei, respectively. Scale bar = 40 μ m. (B) Quantification of gastrocnemius NMJ area stained with alpha bungarotoxin as described in A. The NMJ area, measured in pixels by tracing the outside of the neuromuscular junction, of untreated and PCA-treated hSOD1^{G93A} littermate mice were normalized and expressed as a percentage of NMJ area measured in the WT littermate control mouse. Data are expressed as the mean \pm SEM; $n = 8$ mice per group; 20–25 NMJs were imaged per mouse. * indicates $p < 0.05$ compared to untreated hSOD1^{G93A} control mice (paired t -test). Mean NMJ pixel area for the untreated hSOD1^{G93A} littermate mouse ($11,842 \pm 1204$) is significantly less than the WT littermate control mouse ($17,966 \pm 818$) ($p = 0.01$; $n = 8$ mice per group). (C) Quantification of gastrocnemius NMJ perimeter stained with alpha bungarotoxin as described in A. The NMJ perimeter, measured in pixels by tracing the inside and outside of the NMJ, of untreated and PCA-treated hSOD1^{G93A} littermate mice were normalized and expressed as a percentage of NMJ perimeter measured in the WT littermate control mouse. Data are expressed as the mean \pm SEM; $n = 9$ mice per group; 20–25 neuromuscular junctions were imaged per mouse. ** indicates $p < 0.01$ compared to untreated hSOD1^{G93A} controls (paired t -test). Mean NMJ pixel perimeter for the untreated hSOD1^{G93A} littermate mouse (730.9 ± 39.37) is significantly less than the WT littermate control mouse (1141 ± 94.52) ($p = 0.0007$; $n = 9$ mice per group). (D) Quantification of gastrocnemius NMJ Sholl analysis stained with alpha bungarotoxin as described in A. WT, untreated, and PCA-treated hSOD1^{G93A} littermate mice were given a mean Sholl analysis value, which represents the number of intersections that the NMJ makes with concentric circles every 10 pixels from a center point. Data are expressed as the mean \pm SEM; $n = 8$ mice per group; 20–25 neuromuscular junctions were imaged per mouse. * indicates $p < 0.05$ and *** indicates $p < 0.001$ compared to WT littermate control mice (one-way ANOVA with post-hoc Tukey's test).

4. Discussion

Plant-derived polyphenolic compounds exhibit anti-inflammatory, antioxidant, and neuroprotective capabilities; therefore, they have the potential to be safe, cost-effective, and successful agents in treating neurodegenerative diseases such as ALS. The catechol, protocatechuic acid (PCA), is a phenolic acid metabolite of kuromanin, an anthocyanin found in foods such as blackberries, bilberries, and black rice. Here, we demonstrate that PCA extends survival, improves motor function, reduces gliosis, protects motor neurons, and preserves NMJs in the hSOD1^{G93A} mouse model of ALS.

To ensure that PCA was non-toxic and had therapeutic potential, we first studied the effects of PCA on survival. We found that daily administration of 100 mg/kg PCA by oral gavage beginning at disease onset significantly extended survival of hSOD1^{G93A} mice when compared to untreated hSOD1^{G93A} littermate control mice. PCA-treated hSOD1^{G93A} mice also exhibited significantly improved motor function as assessed by rotarod and PaGE testing when compared to untreated hSOD1^{G93A} littermate control mice. To supplement these findings, we also analyzed gastrocnemius muscle weight at 105 days of age, a time point at which we observed significant peak motor performance in PCA-treated hSOD1^{G93A} mice. We found a preservation of muscle wet weight in PCA-treated hSOD1^{G93A} littermate mice when compared to untreated littermate controls at 105 days of age. At this time point, we also observed that PCA-treated hSOD1^{G93A} mice seemed to display a preservation of NMJ innervation in gastrocnemius muscle when compared to untreated hSOD1^{G93A} mice. Indeed, PCA administration preserved motor function and muscle weight well into the disease course, indicating that this compound was able to slow the progression of motor symptoms, which could indicate improved quality of life.

We next sought to determine how PCA was able to elicit a significant improvement in survival and motor function. We analyzed the ventral horn of the lumbar spinal cord at end stage of untreated hSOD1^{G93A} littermate mice and found that PCA-treated hSOD1^{G93A} mice had significantly reduced astrogliosis, microgliosis, and increased motor neuron count when compared to untreated hSOD1^{G93A} littermate control mice. Furthermore, we analyzed NMJs within the gastrocnemius muscle isolated from PCA-treated hSOD1^{G93A} mice at end stage of the untreated hSOD1^{G93A} littermate control mice and measured them in terms of overall area, perimeter, and complexity (via Sholl analysis). We found that oral treatment with PCA significantly preserved NMJ area, perimeter, and complexity when compared to untreated hSOD1^{G93A} littermate control mice. Furthermore, at 105 days of age, we analyzed gastrocnemius muscle stained with alpha-BTx along with antibodies against VACHT. We wanted to visualize the NMJs and their innervation by presynaptic cholinergic neurons. Representative images indicate that administration of PCA was able to protect the innervation of the NMJ at this time point. Although we did not quantitatively assess NMJ innervation, the combined results of preserved NMJ size and complexity at end stage of the untreated hSOD1^{G93A} littermate control mice, along with a preservation of gastrocnemius muscle wet weight and improved motor performance at 105 days of age, indicate that PCA has a beneficial effect on preserving skeletal muscle performance. Taken together, these findings indicate that PCA exhibits neuroprotective properties while also reducing gliosis *in vivo* and therefore, should be further explored as a therapeutic for ALS.

In future studies, we plan to further examine the mechanism of action of PCA in mitigating the deleterious effects of ALS. We have previously shown that PCA exhibits antioxidant activity due to its catechol structure. PCA has the ability to chelate metal ions, act as a reducing agent, and scavenge free radical species including nitric oxide [29,32]. In the current study, we performed a preliminary analysis and explored the effect of PCA on lipid peroxidation in the ventral horn of lumbar spinal cord isolated at 105 days of age from two groups of WT, untreated hSOD1^{G93A}, and PCA-treated hSOD1^{G93A} littermate mice. Ventral horn was stained with 4-HNE, a byproduct of lipid peroxidation, and fluorescence intensity was measured. These data show that untreated hSOD1^{G93A} mice had significantly higher levels of 4-HNE fluorescence intensity in the ventral horn when compared to their WT littermates, a result that has previously been shown by others [37]. Furthermore, PCA-treated hSOD1^{G93A} mice exhibited significantly lower levels of 4-HNE fluorescence intensity when compared to their untreated hSOD1^{G93A} littermate controls. These data are further supported by previous

research indicating that PCA has the ability to protect cells from mitochondrial dysfunction and apoptosis in vitro and in vivo [38,39]. Furthermore, PCA is able to increase glutathione and superoxide dismutase activity and decrease lipid peroxidation in vitro [40,41]. An increase in free radical species, release of pro-inflammatory cytokines by microglia and astrocytes, and mitochondrial dysfunction all contribute to the oxidative stress burden seen in ALS patients [18,23,24,42]. Consequently, markers such as glutathione peroxidase and malondialdehyde have been found to be elevated in the serum, plasma, and urine of ALS patients [20,21]. Research has demonstrated that oxidative stress heavily contributes to motor neuron death in ALS and PCA has been studied for its antioxidant properties. Therefore, it is possible that PCA is aiding in the preservation of motor neuron viability by reducing the oxidative stress burden through free radical scavenging or by an upregulation of endogenous antioxidant activity. Each of these potential mechanisms should be evaluated in future studies.

Acting in parallel with oxidative stress in the pathogenesis of ALS is neuroinflammation. For example, mutant SOD1 contributes to the death of motor neurons and promotes microgliosis and astrogliosis in the spinal cord. In the hSOD1^{G93A} mouse model of ALS, glial cells, such as astrocytes and microglia, overexpress mutant SOD1. This is toxic to motor neurons and causes an accelerated disease progression. It is theorized that ALS disease onset induced by expression of mutant SOD1 is non-cell autonomous and that glial cells play a central role in motor neuron death [43,44]. Microglial cells expressing mutant SOD1 become activated and release pro-inflammatory cytokines and free radical species [10,45]. Furthermore, mutant SOD1-expressing microglia release increased nitric oxide, superoxide, and decreased insulin-like growth factor-1 when compared to WT microglia in the presence of lipopolysaccharide [12]. Neuroinflammatory microglia also contribute to the activation of astrocytes. Activated astrocytes lose the ability to promote motor neuron survival, phagocytosis, and synaptogenesis [11]. Furthermore, activated astrocytes expressing mutant SOD1 contribute to the death of primary spinal motor neurons [46]. In vitro, PCA has the ability to reduce pro-inflammatory cytokines and nitric oxide production in lipopolysaccharide treated microglial cultures [34,47]. In vivo, PCA treatment reduces cyclooxygenase-2, interleukin-1 β , interleukin-6, tumor necrosis factor- α , and prostaglandin E2 expression in inflammatory models in rats and mice [40,47,48]. In the hSOD1^{G93A} mouse model of ALS, we have found that PCA significantly reduces both astrogliosis and microgliosis in the ventral horn of the lumbar spinal cord. While further study is required to determine whether reducing the presence of these cells also reduces the release of pro-inflammatory factors, our data suggest that the reduction in the presence of reactive astrocytes and microglia could be a principal mechanism by which PCA preserves motor neuron survival and overall motor function in hSOD1^{G93A} mice.

In the hSOD1^{G93A} mouse model of ALS, NMJs become weakened and break down as the alpha motor neuron cell body dies and the axon retracts away from the muscle. This results in skeletal muscle atrophy and paralysis characteristically seen in this mouse model. Since PCA-treated hSOD1^{G93A} mice exhibited neuroprotection in the ventral horn of the lumbar spinal cord, we aimed to explore the preservation of the NMJ which represents the synapse between the alpha motor neuron axon terminal and the gastrocnemius muscle fiber. In the hSOD1^{G93A} mouse model of ALS, detachment of nerve terminals from the neuromuscular junction can be seen as early as 10 weeks of age [49]. Although no previous research has explored the effect of PCA treatment on NMJs in mice, we found that PCA was able to preserve the size and complexity of NMJs in hSOD1^{G93A} mice. These findings help further explain the improved motor function measured by rotarod and PaGE testing in PCA-treated hSOD1^{G93A} mice. However, the precise mechanism by which PCA protects the NMJs is currently unknown.

This study is valuable in that it highlights the ability of PCA to significantly reduce neuronal death and gliosis in a mouse model of ALS. However, the therapeutic benefits of PCA are not limited to ALS. Oxidative stress and neuroinflammation contribute to the pathology and subsequent neuronal death observed in many neurodegenerative diseases such as Alzheimer's disease (AD) and Parkinson's disease (PD). PCA has been previously studied in mouse models of AD and was able to improve spatial learning, decrease inflammatory cytokine expression, and increase expression of brain-derived

neurotrophic factor in the APP/PS1 mouse model of familial AD [50]. Furthermore, a diet high in date palm fruits, which contain high amounts of phenolic compounds, including PCA, improved spatial learning deficits, and resulted in a reduction in lipid peroxidation and restoration of antioxidant enzymes in the [APPsw]/Tg2576 mouse model of AD [51,52]. In cell models of PD, PCA treatment resulted in a significant upregulation of antioxidant enzymes and inhibited the activation of nuclear factor- κ B and expression of inducible nitric oxide synthase [53]. PCA was also able to prevent apoptosis, reduce reactive oxygen species (ROS) production, decrease activation of caspase-3, and enhance SOD activity in in vitro models of PD [54,55]. In vivo, PCA was able to improve motor function and ameliorate PD pathology in the substantia nigra in both MPTP and 6-hydroxydopamine mouse models of PD [53,56]. Interestingly, PCA has been shown in vitro to inhibit aggregation of pathogenic proteins including amyloid beta peptide and alpha-synuclein [57]. Therefore, it will be of interest in future studies to determine whether PCA attenuates aggregation of mutant SOD1 or TDP-43 in models of ALS.

5. Conclusions

This preclinical study is the first to explore the therapeutic benefits of PCA in a mouse model of ALS. Our findings of the neuroprotective and anti-inflammatory effects of PCA in the hSOD1^{G93A} mouse model of ALS are supported by previous studies showing similar effects of PCA in other models of neurodegeneration. Although PCA has been well studied in other disease models (e.g., AD and PD), it should be further studied in additional models of ALS, such as C9orf72 and TDP-43 ALS, to further elucidate its benefit for treating ALS in a diverse patient population. A thorough analysis of the effect of PCA treatment on levels of biomarkers relating to oxidative stress and neuroinflammation should also be performed. It would be important to measure the effect of PCA treatment on levels of pro-inflammatory cytokines and intracellular levels of ROS (superoxide anion, nitric oxide) in lumbar spinal cord and gastrocnemius muscle in the hSOD1^{G93A} model and other mouse models of ALS, and to analyze these levels over the time course of the disease. Such an analysis would allow for identification of predictive biomarkers for the efficacy of PCA treatment and ALS disease progression. Furthermore, other phenolic acid metabolites of anthocyanin compounds (e.g., 4-hydroxybenzoic acid, gallic acid, and syringic acid) should be studied for similar benefits in ALS and other neurodegenerative diseases. Our findings indicate that nutraceutical phenolic compounds, such as PCA, have the potential to help treat patients with ALS and should be investigated as possible therapeutics for this devastating disorder.

Author Contributions: D.P. and D.A.L. conceptualization; L.A.K. and D.A.L. data curation; L.A.K., J.R.O. and D.A.L. formal analysis; D.A.L. funding acquisition; L.A.K., A.N.W., J.H., A.N.B.-G. and C.P. investigation; D.P. and D.A.L. methodology; L.A.K., A.N.W. and D.A.L. project administration; R.C.M., D.P. and D.A.L. resources; L.A.K., A.N.W., R.C.M. and D.A.L. supervision; L.A.K., A.N.W., J.H., A.N.B.-G., C.P. and J.R.O. validation; L.A.K. and D.A.L. visualization; L.A.K. writing—original draft; A.N.W. and D.A.L. writing—review and editing. All authors have read and agreed to the published version of the manuscript.

Funding: This research received funding from the Ralph L. Smith Foundation.

Acknowledgments: We would like to thank the Ralph L. Smith Foundation for the funds and support for this project.

Conflicts of Interest: The authors declare no conflict of interest.

References

- Oskarsson, B.; Gendron, T.F.; Staff, N.P. Amyotrophic lateral sclerosis: An update for 2018. *Mayo Clin. Proc.* **2018**, *93*, 1617–1628. [[CrossRef](#)] [[PubMed](#)]
- Kumar, V.; Kashav, T.; Hassan, M.I. Amyotrophic Lateral Sclerosis: Current Therapeutic Perspectives. In *Pathology, Prevention and Therapeutics of Neurodegenerative Disease*; Singh, S., Joshi, N., Eds.; Springer: Singapore, 2019; pp. 207–224.

3. Diaz-Amarilla, P.; Olivera-Bravo, S.; Trias, E.; Cragolini, A.; Martinez-Palma, L.; Cassina, P.; Beckman, J.; Barbeito, L. Phenotypically aberrant astrocytes that promote motoneuron damage in a model of inherited amyotrophic lateral sclerosis. *Proc. Natl. Acad. Sci. USA* **2011**, *108*, 18126–18131. [[CrossRef](#)] [[PubMed](#)]
4. Haidet-Phillips, A.M.; Hester, M.E.; Miranda, C.J.; Meyer, K.; Braun, L.; Frakes, A.; Song, S.; Likhite, S.; Murtha, M.J.; Foust, K.D.; et al. Astrocytes from familial and sporadic ALS patients are toxic to motor neurons. *Nat. Biotechnol.* **2011**, *29*, 824–828. [[CrossRef](#)]
5. Ramírez-Jarquín, U.N.; Rojas, F.; van Zundert, B.; Tapia, R. Chronic infusion of SOD1 (G93A) astrocyte-secreted factors induces spinal motoneuron degeneration and neuromuscular dysfunction in healthy rats. *J. Cell Physiol.* **2017**, *232*, 2610–2615. [[CrossRef](#)]
6. Tyzack, G.E.; Hall, C.E.; Sibley, C.R.; Cymes, T.; Forostyak, S.; Carlino, G.; Meyer, I.F.; Schiavo, G.; Zhang, S.C.; Gibbons, G.M.; et al. A neuroprotective astrocyte state is induced by neuronal signal EphB1 but fails in ALS models. *Nat. Commun.* **2017**, *8*, 1164. [[CrossRef](#)] [[PubMed](#)]
7. Madill, M.; McDonagh, K.; Ma, J.; Vajda, A.; McLoughlin, P.; O'Brien, T.; Hardiman, O.; Shen, S. Amyotrophic lateral sclerosis patient iPSC-derived astrocytes impair autophagy via non-cell autonomous mechanisms. *Mol. Brain.* **2017**, *10*, 22. [[CrossRef](#)]
8. Rudnick, N.D.; Griffey, C.J.; Guarnieri, P.; Gerbino, V.; Wang, X.; Piersaint, J.A.; Tapia, J.C.; Rich, M.M.; Maniatis, T. Distinct roles for motor neuron autophagy early and late in the SOD1^{G93A} mouse model of ALS. *Proc. Natl. Acad. Sci. USA* **2017**, *114*, E8294–E8303. [[CrossRef](#)]
9. Tripathi, P.; Rodriguez-Muela, N.; Klim, J.R.; de Boer, A.S.; Agrawal, S.; Sandoe, J.; Lopes, C.S.; Oglari, K.S.; Williams, L.A.; Shear, M.; et al. Reactive astrocytes promote ALS-like degeneration and intracellular protein aggregation in human motor neurons by disrupting autophagy through TGF- β 1. *Stem Cell Rep.* **2017**, *9*, 667–680. [[CrossRef](#)]
10. Meissner, F.; Molawi, K.; Zychlinsky, A. Mutant superoxide dismutase 1-induced IL-1 accelerates ALS pathogenesis. *Proc. Natl. Acad. Sci. USA* **2010**, *107*, 13046–13050. [[CrossRef](#)]
11. Liddelov, S.A.; Guttenplan, K.A.; Clarke, L.E.; Bennett, F.C.; Bohlen, C.J.; Schirmer, L.; Bennett, M.L.; Münch, A.E.; Chung, W.S.; Peterson, T.C.; et al. Neurotoxic reactive astrocytes are induced by activated microglia. *Nature* **2017**, *541*, 481–487. [[CrossRef](#)]
12. Xiao, Q.; Zhao, W.; Beers, D.R.; Yen, A.A.; Xie, W.; Henkel, J.S.; Appel, S.H. Mutant SOD1(G93A) microglia are more neurotoxic relative to wild-type microglia. *J. Neurochem.* **2007**, *102*, 2008–2019. [[CrossRef](#)] [[PubMed](#)]
13. Graber, D.J.; Hickey, W.F.; Harris, B.T. Progressive changes in microglia and macrophages in spinal cord and peripheral nerve in the transgenic rat model of amyotrophic lateral sclerosis. *J. Neuroinflamm.* **2010**, *7*, 8. [[CrossRef](#)] [[PubMed](#)]
14. Brettschneider, J.; Toledo, J.B.; Van Deerlin, V.M.; Elman, L.; McCluskey, L.; Lee, V.M.; Trojanowski, J.Q. Microglial activation correlates with disease progression and upper motor neuron clinical symptoms in amyotrophic lateral sclerosis. *PLoS ONE* **2012**, *7*, e39216. [[CrossRef](#)] [[PubMed](#)]
15. Chiu, I.M.; Morimoto, E.T.; Goodarzi, H.; Liao, J.T.; O'Keeffe, S.; Phatnani, H.P.; Muratet, M.; Carroll, M.C.; Levy, S.; Tavazoie, S.; et al. A neurodegeneration-specific gene-expression signature of acutely isolated microglia from an amyotrophic lateral sclerosis mouse model. *Cell Rep.* **2013**, *4*, 385–401. [[CrossRef](#)] [[PubMed](#)]
16. D'Amico, E.; Factor-Litvak, P.; Santella, R.M.; Mitsumoto, H. Clinical perspective on oxidative stress in sporadic amyotrophic lateral sclerosis. *Free Radic. Biol. Med.* **2013**, *65*, 509–527. [[CrossRef](#)]
17. Ikawa, M.; Okazawa, H.; Tsujikawa, T.; Matsunaga, A.; Yamamura, O.; Mori, T.; Hamano, T.; Kiyono, Y.; Nakamoto, Y.; Yoneda, M. Increased oxidative stress is related to disease severity in the ALS motor cortex. *Neurology* **2015**, *84*, 2033–2039. [[CrossRef](#)]
18. Almer, G.; Vukosavic, S.; Romero, N.; Przedborski, S. Inducible nitric oxide synthase up-regulation in a transgenic mouse model of familial amyotrophic lateral sclerosis. *J. Neurochem.* **1999**, *72*, 2415–2425. [[CrossRef](#)]
19. Lee, J.; Ryu, H.; Kowall, N.W. Differential regulation of neuronal and inducible nitric oxide synthase (NOS) in the spinal cord of mutant SOD1 (G93A) ALS mice. *Biochem. Biophys. Res. Commun.* **2009**, *387*, 202–206. [[CrossRef](#)]
20. Mitsumoto, H.; Santella, R.M.; Liu, X.; Bogdanov, M.; Zipprich, J.; Wu, H.C.; Mahata, J.; Kilty, M.; Bednarz, K.; Bell, D.; et al. Oxidative stress biomarkers in sporadic ALS. *Amyotroph Lateral Scler* **2008**, *9*, 177–183. [[CrossRef](#)]

21. Blasco, H.; Garcon, G.; Patin, F.; Veyrat-Durebex, C.; Boyer, J.; Devos, D.; Vourc'h, P.; Andres, C.R.; Corcia, P. Panel of oxidative stress and inflammatory biomarkers in ALS: A pilot study. *Can. J. Neurol. Sci.* **2017**, *44*, 90–95. [[CrossRef](#)]
22. Palomo, G.M.; Manfredi, G. Exploring new pathways of neurodegeneration in ALS: The role of mitochondria quality control. *Brain Res.* **2015**, *1607*, 36–46. [[CrossRef](#)] [[PubMed](#)]
23. Lopez-Gonzalez, R.; Lu, Y.; Gendron, T.F.; Karydas, A.; Tran, H.; Yang, D.; Petrucelli, L.; Miller, B.L.; Almeida, S.; Gao, F.B. Poly(GR) in C9ORF72-related ALS/FTD compromises mitochondrial function and increases oxidative stress and DNA damage in iPSC-derived motor neurons. *Neuron* **2016**, *92*, 383–391. [[CrossRef](#)] [[PubMed](#)]
24. Pickles, S.; Semmler, S.; Broom, H.R.; Destroismaisons, L.; Legroux, L.; Arbour, N.; Meiering, E.; Cashman, N.R.; Vande Velde, C. ALS-linked misfolded SOD1 species have divergent impacts on mitochondria. *Acta Neuropathol. Commun.* **2016**, *4*, 43. [[CrossRef](#)] [[PubMed](#)]
25. Carri, M.T.; D'Ambrosi, N.; Cozzolino, M. Pathways to mitochondrial dysfunction in ALS pathogenesis. *Biochem. Biophys. Res. Commun.* **2017**, *483*, 1187–1193. [[CrossRef](#)]
26. Walczak, J.; Dębska-Vielhaber, G.; Vielhaber, S.; Szymański, J.; Charzyńska, A.; Duszyński, J.; Szczepanowska, J. Distinction of sporadic and familial forms of ALS based on mitochondrial characteristics. *FASEB J.* **2018**, *33*, 4388–4403. [[CrossRef](#)]
27. Abu-Hamad, S.; Kahn, J.; Leyton-Jaimes, M.F.; Rosenblatt, J.; Israelson, A. Misfolded SOD1 accumulation and mitochondrial association contribute to the selective vulnerability of motor neurons in familial ALS: Correlation to human disease. *ACS Chem. Neurosci.* **2017**, *8*, 2225–2234. [[CrossRef](#)]
28. Bhandari, R.; Kuhad, A.; Kuhad, A. Edaravone: A new hope for deadly amyotrophic lateral sclerosis. *Drugs Today* **2018**, *54*, 349–360. [[CrossRef](#)]
29. Kelsey, N.; Hulick, W.; Winter, A.; Ross, E.; Linseman, D.A. Neuroprotective effects of anthocyanins on apoptosis induced by mitochondrial oxidative stress. *Nutr. Neurosci.* **2011**, *14*, 249–259. [[CrossRef](#)]
30. Murukan, G.; Murugan, K. Anthocyanin content of teak and its potential therapeutic traits: Some observations. *World J. Pharm. Res.* **2018**, *7*, 977–985.
31. Winter, A.N.; Ross, E.K.; Wilkins, H.M.; Stankiewicz, T.R.; Wallace, T.; Miller, K.; Linseman, D.A. An anthocyanin-enriched extract from strawberries delays disease onset and extends survival in the hSOD1G93A mouse model of amyotrophic lateral sclerosis. *Nutr. Neurosci.* **2018**, *21*, 414–426. [[CrossRef](#)]
32. Winter, A.N.; Ross, E.K.; Khatter, S.; Miller, K.; Linseman, D.A. Chemical basis for the disparate neuroprotective effects of the anthocyanins, callistephin and kuromanin, against nitrosative stress. *Free Radic. Biol. Med.* **2017**, *103*, 23–34. [[CrossRef](#)] [[PubMed](#)]
33. Losada-Barreiro, S.; Bravo-Díaz, C. Free radicals and polyphenols: The redox chemistry of neurodegenerative diseases. *Eur. J. Med. Chem.* **2017**, *133*, 379–402. [[CrossRef](#)]
34. Winter, A.N.; Brenner, M.C.; Punessen, N.; Snodgrass, M.; Byars, C.; Arora, Y.; Linseman, D.A. Comparison of the neuroprotective and anti-inflammatory effects of the anthocyanin metabolites, protocatechuic acid and 4-hydroxybenzoic acid. *Oxid. Med. Cell Longev.* **2017**, *2017*, 6297080. [[CrossRef](#)] [[PubMed](#)]
35. Mancuso, R.; Oliván, S.; Osta, R.; Navarro, X. Evolution of gait abnormalities in SOD1(G93A) transgenic mice. *Brain Res.* **2011**, *1406*, 65–73. [[CrossRef](#)] [[PubMed](#)]
36. Weydt, P.; Hong, S.; Kliot, M.; Möller, T. Assessing disease onset and progression in the SOD1 mouse model of ALS. *NeuroReport* **2003**, *14*, 1051–1054. [[CrossRef](#)]
37. Seo, J.S.; Baek, I.S.; Leem, Y.H.; Kim, T.K.; Cho, Y.; Lee, S.M.; Park, Y.H.; Han, P.L. SK-PC-B70M alleviates neurologic symptoms in G93A-SOD1 amyotrophic lateral sclerosis mice. *Brain Res.* **2011**, *1368*, 299–307. [[CrossRef](#)] [[PubMed](#)]
38. Liu, Y.M.; Jiang, B.; Bao, Y.M.; An, L.J. Protocatechuic acid inhibits apoptosis by mitochondrial dysfunction in rotenone-induced PC12 cells. *Toxicol In Vitro* **2008**, *22*, 430–437. [[CrossRef](#)]
39. Semaming, Y.; Sripetchwandee, J.; Sa-Nguanmoo, P.; Pintana, H.; Pannangpetch, P.; Chattipakorn, N.; Chattipakorn, S.C. Protocatechuic acid protects brain mitochondrial function in streptozotocin-induced diabetic rats. *Appl. Physiol. Nutr. Metab.* **2015**, *40*, 1078–1081. [[CrossRef](#)]
40. Nakamura, Y.; Torikai, K.; Ohigashi, H.A. A catechol antioxidant protocatechuic acid potentiates inflammatory leukocyte-derived oxidative stress in mouse skin via a tyrosinase bioactivation pathway. *Free Radic. Biol. Med.* **2001**, *30*, 967–978. [[CrossRef](#)]

41. Lende, A.B.; Kshirsagar, A.D.; Deshpande, A.D.; Muley, M.M.; Patil, R.R.; Bafna, P.A.; Naik, S.R. Anti-inflammatory and analgesic activity of protocatechuic acid in rats and mice. *Inflammopharmacology* **2011**, *19*, 255–263. [[CrossRef](#)]
42. McGeer, P.L.; McGeer, E.G. Inflammatory processes in amyotrophic lateral sclerosis. *Muscle Nerve* **2002**, *26*, 459–470. [[CrossRef](#)]
43. Di Giorgio, F.P.; Carrasco, M.A.; Siao, M.C.; Maniatis, T.; Eggen, K. Non-cell autonomous effect of glia on motor neurons in an embryonic stem cell-based ALS model. *Nat. Neurosci.* **2007**, *10*, 608–614. [[CrossRef](#)]
44. Yamanaka, K.; Boillee, S.; Roberts, E.A.; Garcia, M.L.; McAlonis-Downes, M.; Mikse, O.R.; Cleveland, D.W.; Goldstein, L.S. Mutant SOD1 in cell types other than motor neurons and oligodendrocytes accelerates onset of disease in ALS mice. *Proc. Natl. Acad. Sci. USA* **2008**, *105*, 7594–7599. [[CrossRef](#)] [[PubMed](#)]
45. Zhao, W.; Beers, D.R.; Henkel, J.S.; Zhang, W.; Urushitani, M.; Julien, J.P.; Appel, S.H. Extracellular mutant SOD1 induces microglial-mediated motoneuron injury. *Glia* **2010**, *58*, 231–243. [[CrossRef](#)] [[PubMed](#)]
46. Nagai, M.; Re, D.B.; Nagata, T.; Chalazonitis, A.; Jessell, T.M.; Wichterle, H.; Przedborski, S. Astrocytes expressing ALS-linked mutated SOD1 release factors selectively toxic to motor neurons. *Nat. Neurosci.* **2007**, *10*, 615–622. [[CrossRef](#)]
47. Min, S.W.; Ryu, S.N.; Kim, D.H. Anti-inflammatory effects of black rice, cyanidin-3-O-beta-D-glucoside, and its metabolites, cyanidin and protocatechuic acid. *Int. Immunopharmacol.* **2010**, *10*, 959–966. [[CrossRef](#)] [[PubMed](#)]
48. Tsai, S.J.; Yin, M.C. Anti-glycative and anti-inflammatory effects of protocatechuic acid in brain of mice treated by D-galactose. *Food Chem. Toxicol.* **2012**, *50*, 3198–3205. [[CrossRef](#)]
49. Narai, H.; Manabe, Y.; Nagai, M.; Nagano, I.; Ohta, Y.; Murakami, T.; Takehisa, Y.; Kamiya, T.; Abe, K. Early detachment of neuromuscular junction proteins in ALS mice with SODG93A mutation. *Neurol. Int.* **2009**, *1*, e16. [[CrossRef](#)] [[PubMed](#)]
50. Song, Y.; Cui, T.; Xie, N.; Zhang, X.; Qian, Z.; Liu, J. Protocatechuic acid improves cognitive deficits and attenuates amyloid deposits, inflammatory response in aged A β PP/PS1 double transgenic mice. *Int. Immunopharmacol.* **2014**, *20*, 276–281. [[CrossRef](#)] [[PubMed](#)]
51. Subash, S.; Essa, M.M.; Al-Asmi, A.; Al-Adawi, S.; Vaishnav, R.; Guillemin, G.J. Effect of dietary supplementation of dates in Alzheimer’s disease APPsw/2576 transgenic mice on oxidative stress and antioxidant status. *Nutr. Neurosci.* **2015**, *18*, 281–288. [[CrossRef](#)]
52. Subash, S.; Essa, M.M.; Braidy, N.; Awlad-Thani, K.; Vaishnav, R.; Al-Adawi, S.; Al-Asmi, A.; Guillemin, G.J. Diet rich in date palm fruits improves memory, learning and reduces beta amyloid in transgenic mouse model of Alzheimer’s disease. *J. Ayurveda Integr. Med.* **2015**, *6*, 111–120. [[PubMed](#)]
53. Zhang, Z.; Li, G.; Szeto, S.S.W.; Chong, C.M.; Quan, Q.; Huang, C.; Cui, W.; Guo, B.; Wang, Y.; Han, Y.; et al. Examining the neuroprotective effects of protocatechuic acid and chrysin on in vitro and in vivo models of Parkinson disease. *Free Radic. Biol. Med.* **2015**, *84*, 331–343. [[CrossRef](#)] [[PubMed](#)]
54. An, L.J.; Guan, S.; Shi, G.F.; Bao, Y.M.; Duan, Y.L.; Jiang, B. Protocatechuic acid from *Alpinia oxyphylla* against MPP⁺-induced neurotoxicity in PC12 cells. *Food Chem. Toxicol.* **2006**, *44*, 436–443. [[CrossRef](#)] [[PubMed](#)]
55. Guan, S.; Jiang, B.; Bao, Y.M.; An, L.J. Protocatechuic acid suppresses MPP⁺-induced mitochondrial dysfunction and apoptotic cell death in PC12 cells. *Food Chem. Toxicol.* **2006**, *44*, 1659–1666. [[CrossRef](#)] [[PubMed](#)]
56. Zhang, H.N.; An, C.N.; Zhang, H.N.; Pu, X.P. Protocatechuic acid inhibits neurotoxicity induced by MPTP in vivo. *Neurosci. Lett.* **2010**, *474*, 99–103. [[CrossRef](#)]
57. Hornedo-Ortega, R.; Álvarez-Fernández, M.A.; Cerezo, A.B.; Richard, T.; Troncoso, A.M.; Garcia-Parrilla, M.C. Protocatechuic acid: Inhibition of fibril formation, destabilization of preformed fibrils of amyloid- β and α -synuclein, and neuroprotection. *J. Agric. Food Chem.* **2016**, *64*, 7722–7732. [[CrossRef](#)]



© 2020 by the authors. Licensee MDPI, Basel, Switzerland. This article is an open access article distributed under the terms and conditions of the Creative Commons Attribution (CC BY) license (<http://creativecommons.org/licenses/by/4.0/>).

Article

Phytoplankton Supplementation Lowers Muscle Damage and Sustains Performance across Repeated Exercise Bouts in Humans and Improves Antioxidant Capacity in a Mechanistic Animal

Matthew Sharp ^{1,*}, Kazim Sahin ², Matthew Stefan ¹, Cemal Orhan ², Raad Gheith ¹, Dallen Reber ¹, Nurhan Sahin ², Mehmet Tuzcu ², Ryan Lowery ¹, Shane Durkee ³ and Jacob Wilson ¹

¹ The Applied Science & Performance Institute, Research Division, Tampa, FL 33607, USA; mstefan@theaspi.com (M.S.); rgheith@theaspi.com (R.G.); dreber@theaspi.com (D.R.); rlowery@theaspi.com (R.L.); jwilson@theaspi.com (J.W.)

² Animal Nutrition Department, School of Veterinary Medicine, Firat University, Elazig 23200, Turkey; nsahinkm@yahoo.com (K.S.); corhan@firat.edu.tr (C.O.); nsahin@firat.edu.tr (N.S.); mtuzcu@firat.edu.tr (M.T.)

³ Lonza Consumer Health Inc., Morristown, NJ 07960, USA; shane.durkee@lonza.com

* Correspondence: msharp@theaspi.com

Received: 15 May 2020; Accepted: 1 July 2020; Published: 4 July 2020

Abstract: The purpose of this study was to investigate the impact of antioxidant-rich marine phytoplankton supplementation (Oceanix, OCX) on performance and muscle damage following a cross-training event in endurance-trained subjects. Additionally, an animal model was carried out to assess the effects of varying dosages of OCX, with exercise, on intramuscular antioxidant capacity. **Methods:** In the human trial, endurance-trained subjects (average running distance = 29.5 ± 2.6 miles \times week⁻¹) were randomly divided into placebo (PLA) and OCX (25 mg) conditions for 14 days. The subjects were pre-tested on a one-mile uphill run, maximal isometric strength, countermovement jump (CMJ) and squat jump (SJ) power, and for muscle damage (creatine kinase (CK)). On Day 12, the subjects underwent a strenuous cross-training event. Measures were reassessed on Day 13 and 14 (24 h and 48 h Post event). In the animal model, Wistar rats were divided into four groups ($n = 7$): (i) Control (no exercise and placebo (CON)), (ii) Exercise (E), (iii) Exercise + OCX 1 (Oceanix, 2.55 mg/day, (iv) Exercise + OCX 2 (5.1 mg/day). The rats performed treadmill exercise five days a week for 6 weeks. Intramuscular antioxidant capacity (superoxide dismutase (SOD), catalase (CAT), glutathione peroxidase (GSH-Px)) and muscle damage (CK and myoglobin (MYOB)) were collected. The data were analyzed using repeated measures ANOVA and *t*-test for select variables. The alpha value was set at $p < 0.05$. **Results:** For the human trial, SJ power lowered in PLA relative to OCX at 24 h Post (-15% , $p < 0.05$). Decrements in isometric strength from Pre to 48 h Post were greater in the PLA group (-12% , $p < 0.05$) than in the OCX. Serum CK levels were greater in the PLA compared to the OCX ($+14\%$, $p < 0.05$). For the animal trial, the intramuscular antioxidant capacity was increased in a general dose-dependent manner ($E + Oc2 > E + Oc1 > E > CON$). Additionally, CK and MYOB were lower in supplemented compared to E alone. **Conclusions:** Phytoplankton supplementation (Oceanix) sustains performance and lowers muscle damage across repeated exercise bouts. The ingredient appears to operate through an elevating oxidative capacity in skeletal muscle.

Keywords: phytoplankton; antioxidants; muscle damage; muscle recovery; muscle soreness

1. Introduction

Sport performance depends on the ability of an athlete to produce and sustain high levels of physical, technical, decision-making, and psychological skills throughout competition. The deterioration of any of these skills could appear as a symptom of fatigue. The phenomenon of fatigue is complex, with the underlying processes developing as exercise proceeds to ultimately manifest as a decline of performance. The issue of fatigue is compounded when there is an imbalance between recovery and exertion. Recent research has demonstrated that endurance and cross-training athletes partake in multiple high-intensity competition events, which limits the recovery opportunities. The result is extreme stress to the body which is not counterbalanced by proper rest [1]. The lack of rest between intra-competition bouts impairs regeneration and leads to decrements in strength, power, and endurance-based performance [2,3]. Previous research has demonstrated that functional impairments are strongly associated with an increase in oxidative stress [4,5], defined as disturbances in the homeostatic balance where oxidant capacity exceeds the antioxidant capacity, causing the redox state to be more pro-oxidizing [6]. Mechanistically, extreme exercise can elevate oxygen consumption by up to 20-fold over resting levels [7]. The heightened use of oxygen may result in a leakage of reactive oxygen species (ROS) such as superoxide dismutase (SOD). If not properly regulated, these changes can alter cellular structure and function, leading to performance declines [4,5].

While athletes find it challenging to change the demands of competition, they may improve their recovery in response to exercise through the consumption of nutraceuticals that are rich in antioxidants. In fact, it is commonplace for athletes to supplement with antioxidants under the conviction that they will enhance the recovery of muscle function and performance [8,9]. As a result, a fair amount of attention has been given to antioxidant supplements for exercise recovery, which is largely due to their capacity to enhance the endogenous support in diminishing oxidative damage by discarding ROS [10,11]. The majority of studies investigating the impact of antioxidant supplementation on exercise report that antioxidants can reduce oxidative stress [12]; however, the physiological implications of this effect are not well known in more practical competition environments. Furthermore, strong evidence supporting antioxidant supplementation as a protectant against muscle damage is incomplete, as most investigations do not consider oxidative stress makers and intramuscular enzymes in conjunction with the functional indices of muscle damage (e.g., losses in force and power) [12,13].

Dieticians have made a push for natural and sustainable super foods, which contain an array of performance aids [14]. In response, scientists have isolated a unique source of marine phytoplankton, microalga *Tetraselmis chuii* (Oceanix (OCX), Lonza Consumer Health, Morristown, NJ, USA). This microalga contains highly active antioxidant enzymes, particularly superoxide dismutase (SOD), which speeds the reaction that converts superoxide into ordinary molecular oxygen, thereby protecting cells from oxidative damage [15]. The ingredient was also found to upregulate glutathione peroxidase and catalase enzymes in human skeletal muscle myoblasts in vitro [15]. When isolated, antioxidants have been shown to aid in recovery [16–19]. However, the effects on recovery of a marine-derived, SOD-rich ingredient remains to be investigated on high-intensity, cross-training events. Therefore, the purpose of this study was to investigate the targeted marine phytoplankton supplementation on recovery across repeated bouts of activity encompassing endurance, strength, and power and to investigate its effects on intramuscular antioxidant capacity using human and animal models. We hypothesized that marine phytoplankton would better reduce muscle damage while sustaining endurance and strength, which collectively indicates improved recovery. We also hypothesized that the ingredient would improve antioxidant capacity and lower oxidative stress in our mechanistic animal model.

2. Materials and Methods

2.1. Human Modal

2.1.1. Subjects

Subjects were recruited by word of mouth, email contact, and direct contact with the local runner's clubs. Subjects were excluded from the study if they: had a body mass index (BMI) ≥ 30 kg/m², had allergies to fish, shellfish, algae, or seaweed; had any cardiovascular, metabolic, or endocrine disease; had undergone surgery that affects digestion and absorption, smoke, drink heavily (>7 and >14 drinks per week for women and men, respectively), were pregnant or planning to be pregnant, were on medication to regulate blood glucose, lipids, and/or blood pressure; had used anabolic-androgenic steroids, were currently using antioxidant supplements, non-steroidal anti-inflammatory drugs, or nutritional supplements known to stimulate recovery or muscle mass gains. A total of 20 subjects volunteered for participation in the study. Eighteen of the enrolled subjects completed the study and two subjects withdrew from the study due to work or family requirements. Prior to engaging in any study procedures, the subjects signed a written informed consent form that was approved by an Institutional Review Board (IntegReview, Austin, TX; Protocol # 1219) for study participation. Subjects in the study were considered active athletes who could withstand multiple endurance bouts (i.e., at least ran 20 miles \times week⁻¹). The self-reported weekly running mileage ranged from 20–60 miles (mean \pm SD = 29.5 \pm 10.9 miles \times week⁻¹). The subject characteristics are reported in Table 1 as the mean \pm standard error.

Table 1. Subject characteristics.

Variable	OCX (n = 9)	PLA (n = 9)
Age (years)	38 \pm 1	36 \pm 2
Height (cm)	171.3 \pm 3.6	168.5 \pm 2.8
Body Mass (kg)	73.0 \pm 4.5	69.1 \pm 3.3
BMI (kg/m ²)	24.8 \pm 1.0	24.4 \pm 1.1
Body Fat (%)	27.2 \pm 2.4	26.7 \pm 2.4
VO ₂ max (mL/kg/min)	46.0 \pm 2.5	47.7 \pm 2.9

OCX = Oceanix; PLA = Placebo; BMI = body mass index

2.1.2. Study Protocol

This study was carried out in a randomized, double-blind, placebo-controlled and parallel manner. Prior to allocation into conditions, the subjects were assessed for maximal oxygen uptake (VO₂max) on a graded treadmill test. The subjects were then classified into quartiles according to the VO₂max values, and then subjects forming each quartile were randomly assigned to conditions. Following the condition allocation, the subjects underwent baseline testing on day 0 (Pre) which included: salivary cortisol, serum creatine kinase, maximal isometric strength, maximal muscle power, one-mile timed run, and perceptual measures using visual analog scales (VAS). Immediately following pre-testing, the subjects were given their respective condition (Oceanix (OCX) or microcrystalline cellulose-based placebo (PLA)). The OCX ingredient was independently examined by Brunswick Laboratories (Southborough, MA, USA) for oxygen radical absorbance capacity (ORAC) expressed in micromole Trolox equivalency (μ mole TE) per gram. The results indicated that the values were high for hydroxyl radicals at 178.71 μ mole TE/gram and super oxide anions at 348.11 μ mole TE/gram, moderate in peroxynitrite and peroxy radicals at 8.65 and 29.65 μ mole TE/gram, respectively, and not detectable in singlet oxygen and hypochlorite. The ORAC values for the super oxide anion corresponded with high total values (38,000 IU per 100 g) of SOD in the raw powder measured.

The conditions were stored in visually identical capsules and containers. The subjects were required to consume one serving (25 mg) a day, either 30 min prior to exercise or with the first meal

of the day on non-exercise days. Supplement compliance was assessed by supplement logs and the collection of supplement containers. The subjects were instructed to refrain from consuming any nutritional supplements for the duration of the study. Additionally, the subjects were informed to follow their habitual routine regarding exercise and diet for days 1–9 of the supplement period; however, the subjects were instructed to refrain from exercise on days 10 and 11 to avoid a potential interference effect from the cross-training bout on day 12. On the twelfth day of supplementation, the subjects returned to the laboratory to complete a supervised cross-training, muscle damage protocol. The subjects continued to supplement for two days after completing the supervised training protocol. Approximately 24 h and 48 h post training (days 13 and 14), the subjects were retested in a manner identical to the Pre to assess the changes in endurance, strength, power, and muscle damage. Study procedures are further described below.

2.1.3. Maximal Oxygen Uptake (VO_2max)

Subjects began the assessment at a velocity of 3 mph with a grade of 0%. The velocity was increased by 1 mph at the top of each min, and the rating of perceived exertion (RPE) was recorded using the Borg Scale [20]. Once an RPE of 12 was reached, the velocity increments ceased, and the grade was increased by 1% at the top of each min. This process continued until volitional fatigue was reached or if two of the three following criteria was reached: (1) leveling off (plateau) of oxygen uptake with an increase in work rate [21], (2) respiratory exchange ratio (VCO_2/VO_2) greater than 1.10 [22], or (3) 90% of the age-predicted maximum heart [23]. The Cardio Coach CO_2 metabolic analyzer (Korr Medical Technologies Inc., Salt Lake City, UT, USA) was used for the collection and analysis of respiratory gases. This device has been validated for assessing maximal and submaximal VO_2 [24]. The samples of respiratory gases were sampled every 15 s and measured using a 5 L mixing chamber technique. A Hans Rudolph one-way valve and silicone face mask was used for the gas collection. A 6-foot breathing tube connected the non-breathing valve to the mixing chamber inlet. Ventilatory oxygen was calculated using modified Haldane equations while the CO_2 was measured directly by the analyzer.

2.1.4. Salivary Cortisol (sCT)

Salivary cortisol samples were collected using IPRO Oral Fluid Collector (OFC) Kits (Soma Bioscience; Wallingford, UK). The OFC kits collect 0.5 mL of oral fluid and contain a color-changing volume adequacy indicator within the swab, giving collection times typically in the range of 20–50 s [25]. All samples were collected following a 10 h overnight fast. The samples were analyzed using an IPRO POC Lateral Flow Device (LFD), specific for cortisol, in an IPRO LFD Reader. Two drops of saliva/buffer mix from the OFC were added to the sample window of the LFD. The liquid runs the length of the test strip via lateral flow, creating a control and test line visible in the test window. Ten min after the sample was added, the test line intensity was measured in an IPRO LFD Reader and converted into a quantitative value.

2.1.5. Serum Creatine Kinase (CK)

Venous blood was extracted by the venipuncture of the antecubital vein using a 21-gauge syringe and collected into a 10 mL ethylenediaminetetraacetic acid (EDTA) vacutainer tube (BD Vacutainer, Becton, Dickinson and Company, Franklin Lakes, NJ, USA) by a certified phlebotomist. Afterward, the blood samples were centrifuged at 2500 rpm for 10 min at 4 °C. The resulting serum were then aliquoted and stored at -80 °C until further analysis. The serum creatine kinase was assayed via commercially available ELISA kits. The samples were thawed once and analyzed in duplicate in the same assay for each analyte to avoid compounded inter-assay variance.

2.1.6. Maximal Isometric Muscle Strength

Each subject was tested for maximal isometric strength using isometric mid-thigh pull (IMTP) performed in an Olympic style half rack to allow the fixation of the bar at any height. Subjects were

secured to the bar using lifting straps and athletic tape. Utilizing a pronated clean grip, the subjects were instructed to assume a body position similar to the second pull of the snatch and clean. Knee angle was confirmed between 125° and 135° using a hand-held goniometer and the hip angle was approximately set at 175°. Once the body positioning was stabilized, the subject was given a countdown. Minimal pre-tension was allowed to eliminate slack prior to the initiation of the IMTP. Each subject performed two warm-up reps, one at 50% and one at 75% of the perceived maximum effort. Thereafter, subjects completed 2 maximal IMTPs separated by 2–3 min rest. Subjects were instructed to pull fast and hard and were given strong verbal encouragement during the assessment. Peak isometric force production was recorded using a linear position transducer [26].

2.1.7. Maximal Muscle Power

Maximal muscle power was assessed via a countermovement jump (CMJ) and squat jump (SJ) on a dual force plate platform (Leonardo Mechanograph GRFP XL; Novotec Medical GmbH, Pforzheim, Germany). The platform was composed of two symmetrical force plates that separated the platform into a left and a right half. The resonance frequency of each plate was at 150 Hz. Each plate contained four strain gauge force sensors (the whole platform thus had eight force sensors). The sensors were connected to a laptop computer via a USB 2.0 connection. The signal from the force sensors was sampled at a frequency of 800 Hz and was analyzed using the Leonardo Mechanography GRFP Research Edition software (in this study version 4.2-b05.53-RES was used).

Prior to the test, the subjects completed a warm-up of 10 body weight squats and two submaximal effort CMJs. The subjects were instructed to stand in a comfortable and upright position with the feet about shoulder width apart and parallel to each other. The subjects then performed a countermovement by flexing the hips and knees. Once the subjects reached a preferred countermovement depth, they explosively extended their hip, knee, and ankle joints to perform a maximal vertical jump. Subjects performed 3 hands-free, maximal effort CMJs with 30 s rest between jumps. After completing 3 CMJs, the subjects rested for 2 min and performed 3 hands-free, maximal effort SJs separated by 30 s rest. The SJ started from a similar upright position as the CMJ and subjects were instructed to lower into a squat position (90° knee angle). The subjects held their squat position for approximately 3 s until a “jump” command was announced by the researcher. Immediately following the command, the subjects jumped as high as possible from the squat position without reloading or further descent.

2.1.8. One-Mile Timed Run

As a warm-up, the subjects walked on a treadmill for 3 min at 4.8 km/h. Afterward, the subjects ran on the treadmill for 1 min at 9.7 km/h. Immediately following the warm-up, the subjects were allotted a 2 min period to rest or stretch. Thereafter, the treadmill grade and velocity settings were adjusted to a 1% incline and 4.8 km/h, respectively. The subjects maintained this velocity until the distance covered reached 0.05 miles. Upon reaching this distance, the subjects could control the velocity on the treadmill to complete one mile (marked as 1.05 miles) as fast as possible. Control panel placements displaying speed and time were covered to block the subject view. Time was kept by a research technician using a stopwatch. One-mile completion time was recorded to the nearest whole second.

2.1.9. Perceptual Measures

The perceptual measures collected for the study were the perceived recovery status (PRS) scale, rating of perceived soreness (RPS), and the rating of perceived exertion (RPE). PRS was collected in a manner describe by Laurent et al. [27]. The PRS and RPS scales consist of a scalar representation numbering from 0–10. On the PRS scale, the visual descriptors of “very poorly recovered”, “adequately recovered” and “very well recovered” for perceived recovery are presented at numbers 0, 5, and 10, respectively. On the RPS scale, the visual descriptors of “no soreness at all”, “moderate soreness”, and “extreme soreness” are presented at numbers 0, 5, and 10, respectively. The subjects provided PRS at baseline (Pre), immediately before the training protocol (Pre2), and prior to the performance testing at

24 h and 48 h post-workout (24 h Post and 48 h Post) and the RPS was collected at Pre2, 24 h Post, and 48 h Post. The standard 6–20 Borg Scale was used to assess the RPE [20], and the RPE was collected four times: immediately after the 1 mile timed run at baseline (Pre), immediately after the training protocol, and immediately after the 1-mile timed run at 24 h Post and 48 h Post training protocol. Each perceptual measure was recorded as an arbitrary unit (au).

2.1.10. Cross-Training Muscle Damaging Event

Prior to the muscle-damaging session, the subjects completed a dynamic warm-up. Following the warm-up, the subjects completed a cross-training obstacle style program, which was anticipated to induce fatigue and muscle damage. The protocol consisted of 2 separate “blocks”. Each block contained 2 exercise stacks, with each stack containing 3 movements (e.g., A1, A2, and A3). The total amount of exercises performed during the training session was 12. Each exercise consisted of 10 reps per set, except for a sled push (45 meters push) and a rowing machine (300 m meters row). Each exercise stack was performed 3 times before moving on to the second stack of each block. Once Block 1 was completed, subjects moved to Block 2. Up to 2 min of rest was allowed between stacks, and then between blocks. However, it was at the discretion of the subject whether they used the full 2 min to rest. Minimal rest was given between exercises within a superset. The subjects were instructed to attempt to finish each stack in as little time as possible with compromising exercise form. An overview is provided in Table 2.

Table 2. Warm-up and cross-training protocol.

Warm-up	Block 1	Block 2
World’s Greatest Stretch 45 m	A1. Bulgarian Split Squat × 10e	A1. Goblet Squat × 10
Hamstring Scoops 45 m	A2. 45 m Sled Push	A2. 300 m Row
Lunge w/Overhead Reach 45 m	A3. Unilateral BW Calf Raise × 20e	A3. KB Swing × 10
High Knees 45 m		
Butt Kicks 45 m	B1. Med Ball Slam × 10	B1. DB Squat Thrusters × 10
Lateral Shuffle 45 m	B2. Inverted BW Row × 10	B2. 35 cm Drop Jump × 10
Shoulder Bilateral “T”, “W”, “Y” × 10	B3. 45 cm Step-up × 10e	B3. Reverse Lunge × 10e

m = meters; cm = centimeters; e = each leg; BW = bodyweight; DB = dumbbell; KB = kettlebell; W = prone shoulder internal/external rotation; T = prone horizontal shoulder abduction; Y = prone shoulder extension.

2.1.11. Statistical Analysis

Prior to carrying out inferential statistics, normality was assessed via Shapiro–Wilk testing and the visual inspection of box plots. All data passed normality testing except for CK, which was logged transformed ($y = \log(y)$) and reported as an arbitrary unit (au). Dependent variables were scrutinized using a two-way mixed analysis of variance (ANOVA) with the condition as the “between-group” factor, time as the “within-group” factor, and the subjects as a random factor. Whenever a significant F -value was obtained, post-hoc testing was performed with a Bonferroni correction for multiple comparisons. Additionally, the absolute mean differences ($\text{Time}_2 - \text{Time}_1$) were analyzed using a two-tailed, unpaired t -test. The alpha level was set at $p < 0.05$ for statistical significance. For significant within- and between group differences, the mean difference ($\text{mean}_{\text{diff}}$), 95% confidence interval (95% CI), and p -value were reported in text. The data are presented as the mean \pm standard error.

2.2. Animal Model

2.2.1. Animals and Protocol

Male Wistar albino rats ($n = 28$, 8 weeks old) were provided from the Laboratory Animal Research Center, Firat University (Elazig, Turkey). The animals were kept in a room with standard conditions (22 ± 2 °C temperature, $55 \pm 5\%$ humidity, a 12 h light–12 h dark cycle). The ethical permission of the experiment was obtained from the Animal Experimentation Ethics Committee of Firat University (2019/139–206) according to the relevant laws, guidelines, and restrictions.

Rats were randomly divided into four groups ($n = 7$): (i) Control (no exercise and placebo), (ii) Exercise (E), (iii) Exercise + Oceanix 1 (2.55 mg/day, (E + Oc1)), and (iv) Exercise + Oceanix 2 (5.1 mg/day (E + Oc2)). Oceanix and placebo (physiological saline) were administered orally via gavage every day before exercise during the experiment period (6 weeks).

The rats were subjected to treadmill exercise on a motorized rodent treadmill (Commat Limited, Ankara, Turkey). The treadmill contained a stimulus grid at the back end of the treadmill giving an electric shock when the animal placed its paw on the grid. The apparatus had a 5-lane animal exerciser utilizing a single belt unit divided with walls suspended over the tread surface. In order to eliminate the diurnal variations, all the exercise tests were applied during the same time of the day. A week of adaptation was provided as pre-training practice for the animals in order to get familiar with the treadmill equipment and handling. In doing so, the rats in the exercise training groups were accustomed to treadmill exercise over a 5 day period such that: (i) first day, 10 m/min, 10 min, (ii) second day, 20 m/min, 10 min, (iii) third day, 25 m/min, 10 min, (iv) fourth day, 25 m/min, 20 min and (v) fifth day, 25 m/min, 30 min. Upon the adaptation of a week to the treadmill system for the novel and stress impacts, the rats in the treadmill exercise groups ran on the treadmill 25 m/min, 45 min/day and five days per week for 6 weeks according to the protocol described by Liu et al. [28]. The exercise model was chosen because it is the most common procedure to carry out animal exercise training from weeks to months at 45 min⁻¹ h/day and 5 days/week. In addition, the exercise model provides adaptations to the cardiovascular system including the physiological remodeling of the heart representative with the increased O₂ consumption, the improvement of cardiac contractile function, and calcium handling [29]. The chosen long-term animal exercise model fits an effective program to benefit both healthy and individuals at cardiovascular risk [30].

2.2.2. Biochemical Analysis

Serum samples were obtained by taking blood samples to gel biochemical tubes after centrifugation (5000 rpm at 4 °C for 10 min). For the assays, the muscle tissue samples were homogenized within 10 min in 10 volumes of cold Tris 10 mM (pH 7.4). The serum concentrations of creatine kinase (CK) were assayed using a portable automated chemistry analyzer (Samsung LABGEO PT10, Samsung Electronics Co., Suwon, Korea). ELISA was also used in measuring the serum myoglobin (MyBioSource, San Diego, CA, USA). Tissue homogenates (10%, *w/v*) were prepared in 10 mM phosphate buffer and centrifuged at 13,000× *g* for 10 min at 4 °C. The muscle activities of superoxide dismutase (SOD), catalase (CAT) and glutathione peroxidase (GSH-Px) were determined using the commercially available kits (Cayman Chemical, Ann Arbor, MI, USA) according to the manufacturer's procedure.

2.2.3. Statistical Analysis

Data were presented as the mean ± standard error. All the tests were performed with the SPSS software program (IBM SPSS, Version 21.0; Chicago, IL, USA). Significance was determined by one-way ANOVA. Whenever a significant *F*-value was obtained, the Tukey HSD post-hoc test was applied for comparisons. Statistical significance for the data was defined as $p < 0.05$.

3. Results

3.1. Human Trial

3.1.1. Salivary Cortisol and Serum Creatine Kinase

There was no significant between-group difference for any dependent variable at Pre ($p > 0.05$). No significant differences were detected for sCT ($p > 0.05$). A significant group-by-time interaction was demonstrated for CK ($p < 0.05$). The post-hoc analysis indicated that both groups had higher CK levels at 24 h Post (OCX: $\text{mean}_{\text{diff}} = 0.395$ au, 95% CI: 0.153 to 0.637 au, $p < 0.001$; PLA: $\text{mean}_{\text{diff}} = 0.759$ au, 95% CI: 0.517 to 1.00 au, $p < 0.0001$) and 48 h Post (OCX: $\text{mean}_{\text{diff}} = 0.364$ au, 95% CI: 0.122 to 0.606

au, $p < 0.005$; PLA: $\text{mean}_{\text{diff}} = 0.554$ au, 95% CI: 0.312 to 0.796 au, $p < 0.0001$). However, 24 h Post levels were significantly higher in the PLA compared to the OCX ($\text{mean}_{\text{diff}} = 0.354$ au, 95% CI: 0.026 to 0.715 au, $p < 0.05$; Figure 1).

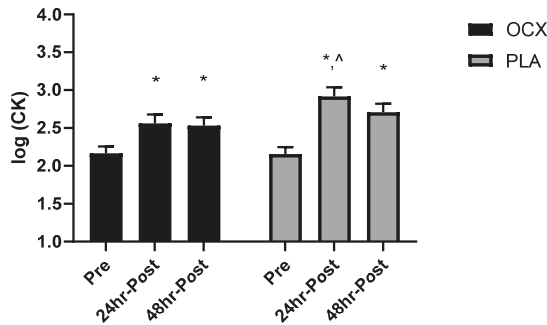


Figure 1. Bar charts displaying the mean and standard error for the log transformation of the plasma creatine kinase (CK) in the Oceanix (OCX) and placebo (PLA) conditions collected prior to the supplement period (Pre), one day, and two days following the supervised cross-training bout (24 h Post and 48 h Post, respectively). * = significantly greater than Pre ($p < 0.05$). ^ = significantly greater than OCX ($p < 0.05$).

3.1.2. Muscle Strength and Power

The absolute mean difference in IMTP strength from Pre to 48 h Post was significantly lower in the PLA group ($\text{mean}_{\text{diff}} = -9.01$ kg, 95% CI: -17.6 to -0.4 kg, $p < 0.05$; Figure 2). A significant main effect of time was detected for the CMJ relative power ($p < 0.05$) in which levels at 24 h Post ($\text{mean}_{\text{diff}} = -1.63$ W kg^{-1} , 95% CI: 0.27 to 2.99 W kg^{-1} , $p < 0.05$ and 48 h Post ($\text{mean}_{\text{diff}} = -2.07$ W kg^{-1} , 95% CI: 0.71 to 3.43 W kg^{-1} , $p < 0.01$) were significantly lower than Pre. A significant group-by-time interaction was demonstrated for the SJ relative power ($p < 0.05$). The post-hoc analysis revealed that the PLA was significantly lower than OCX at 24 h Post ($\text{mean}_{\text{diff}} = -5.93$ W kg^{-1} , 95% CI: -14.32 to -0.31 W kg^{-1} , $p < 0.05$; Figure 3).

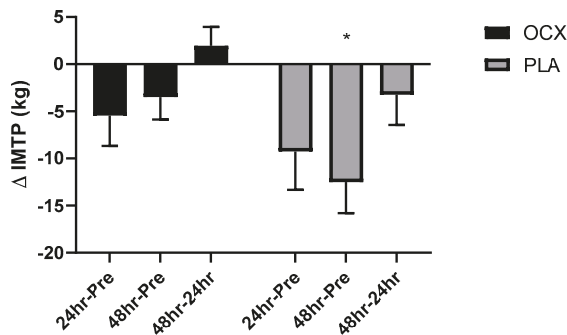


Figure 2. Bar charts displaying the mean and standard error for the absolute mean difference in maximal strength assessed by the isometric mid-thigh pull (IMTP) in the Oceanix (OCX) and placebo (PLA) conditions from Pre to 1 day following the cross-training bout (24 h Pre), Pre to 2 days following the cross-training bout (48 h Pre), and 1 day to 2 days following the cross-training bout (48 h–24 h). * = significantly lower than OCX ($p < 0.05$).

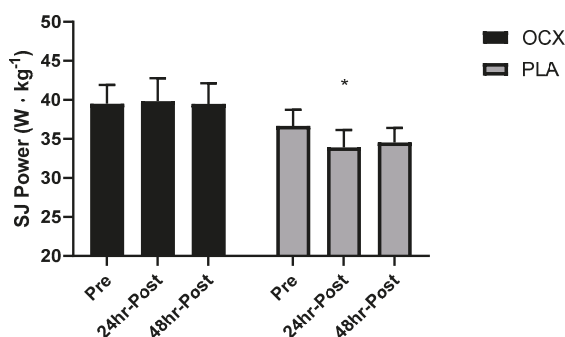


Figure 3. Bar charts displaying the mean and standard error for the relative power output during the squat jump (SJ) in the Oceanix (OCX) and placebo (PLA) conditions collected prior to the supplement period (Pre), one day, and two days following the supervised cross-training bout (24 h Post and 48 h Post, respectively). * = significantly lower than OCX ($p < 0.05$).

3.1.3. One Mile Timed Run

A significant main effect for time was detected for the one mile timed run ($p < 0.0001$) whereby times at 24 h Post (mean_{diff} = 79 s, 95% CI: 45 to 113 s, $p < 0.0001$) and 48 h post (mean_{diff} = 70 s, 95% CI: 36 to 104 s, $p < 0.0001$) were greater than Pre.

3.1.4. Perceptual Measures

A significant main effect of time was detected for Soreness ($p < 0.0001$). The post-hoc analysis indicated that Soreness levels were elevated at 24 h Post (mean_{diff} = 2.3 au, 95% CI: 0.9 to 3.8 au, $p < 0.01$) and 48 h Post (mean_{diff} = 3.8 au, 95% CI: 2.4 to 5.3, $p < 0.0001$) compared to Pre. Additionally, the levels were elevated at 48 h Post compared to 24 h Post (mean_{diff} = 1.5 au, 95% CI: 0.1 to 3.0 au, $p < 0.05$). A significant main effect of time was detected for the PRS ($p < 0.0001$). The post-hoc analysis revealed that the PRS was lower at 24 h Post (mean_{diff} = -2.3 au, 95% CI: -3.9 to -0.7 au, $p < 0.01$) and 48 h Post (mean_{diff} = -3.5 au, 95% CI: -5.2 to -1.9 au, $p < 0.0001$) compared to Pre. Moreover, 48 h Post was significantly lower than Pre2 (mean_{diff} = -2.7 au, 95% CI: -4.3 to -1.0 au, $p < 0.001$). No significant differences were detected for RPE.

3.2. Animal Modal

3.2.1. Muscle Damage

For the exercise arm and both supplement arms, the CK was significantly greater than the control (Figure 4a). However, the CK in both supplement arms were lower than in the exercise arm, and E + Oc2 was lower than E + Oc1 ($p < 0.05$). The myoglobin concentration was significantly greater in the exercise and supplement arms compared to the control (Figure 4b). Additionally, both supplement arms were lower than the exercise arm ($p < 0.05$).

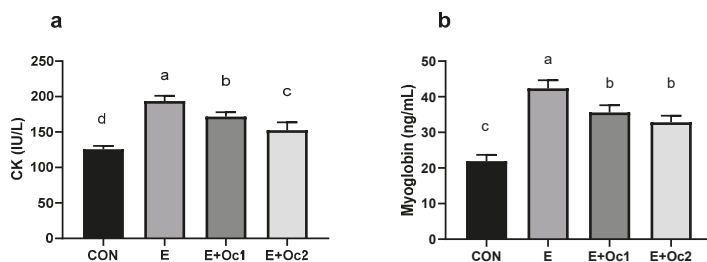


Figure 4. Bar charts displaying the mean and standard error for serum creatine kinase (a) and myoglobin (b) following the 6-week motorized rodent treadmill exercise protocol described in Section 3.1. Conditions are: Control (CON), Exercise (E), Exercise + Oceanix 1 (2.55 mg day/rat, (E + Oc1)), and Exercise + Oceanix 2 (5.1 mg day/rat (E + Oc2)). Conditions without a common letter differ significantly ($p < 0.05$).

3.2.2. Intramuscular Antioxidant Enzymes

Serum malonaldehyde (MDA) was lowered by exercise and exercise plus supplementation compared to control, and levels in E + Oc2 was significantly lower than E + Oc1 and E ($p < 0.05$). The exercise and supplement arms demonstrated higher SOD and GSH-Px relative to the control ($p < 0.05$). Furthermore, the supplement arms demonstrated higher levels compared to the exercise arm in a dose-dependent manner (i.e., E + Oc2 > E + Oc1 > E). Catalase was significantly greater in the exercise and supplement arms compared to the control, and both supplement arms were greater than the exercise arm ($p < 0.05$). The raw mean and standard error data for these biochemical measures are provided in Table 3.

Table 3. Intramuscular activity of MDA, SOD, CAT, and GSH-Px across conditions.

Sample	Groups			
	Control	Exercise	E + Oc1	E + Oc2
MDA ($\mu\text{mol/L}$)	0.76 ± 0.02^a	0.68 ± 0.01^b	0.61 ± 0.03^b	0.46 ± 0.02^c
SOD (U/mL)	70.88 ± 1.57^d	82.28 ± 1.82^c	97.68 ± 2.36^b	113.46 ± 1.26^a
CAT (U/mL)	140.82 ± 2.80^c	153.00 ± 2.85^b	164.92 ± 2.12^a	175.79 ± 3.91^a
GSH-Px (U/mL)	71.13 ± 1.97^d	82.00 ± 2.61^c	95.29 ± 1.52^b	107.10 ± 1.77^a

Data are presented as mean and standard error a–d: Means in the same line without a common superscript differ significantly ($p < 0.05$). MDA = malonaldehyde; SOD = superoxide dismutase; CAT = catalase; GSH-Px = glutathione peroxidase.

4. Discussion

The purpose of this study was to investigate targeted marine phytoplankton supplementation (Oceanix, OCX) on recovery across repeated bouts of activity encompassing endurance, strength, and power, and to investigate its effects on intramuscular antioxidant capacity using human and animal models. We hypothesized that OCX would better reduce muscle damage and sustain endurance and strength, which collectively indicates improved recovery. We also hypothesized that the ingredient would improve the antioxidant capacity and lower oxidative stress in our mechanistic animal model. The primary findings of this study supported four out of our five major hypotheses. Specifically, OCX was able to lower muscle damage, sustain power and prevent declines in strength across repeated endurance and cross-training bouts. Mechanistically, the ingredient appears to operate through elevating oxidative capacity in skeletal muscle, which led to decreased oxidative stress and muscle damage.

Excessive exercise during competitions may contribute to disturbances in biological function through a physiological deregulation that leads to impairments in performance and recovery [31].

While athletes find it challenging to change the demands of a competition, they may alter their responses through the consumption of supplements that are rich in ingredients capable of influencing recovery. Previous investigations have taken an isolated approach to supplement research by determining their effects on recovery from either aerobic or anaerobic activities. However, many sports (e.g., soccer, basketball, and hockey) require individuals to be exposed to concurrent training stimuli [32]. Moreover, the emergence of CrossFit as a sport has driven athletes to excel across multiple physiological domains [33]. The uniqueness of the present study was that subjects participated in two endurance uphill runs, one cross-training event, and six maximal strength and power bouts (three maximal attempts on two occasions). We feel that this protocol allows researchers to truly determine the ecological validity of the present nutraceutical-based intervention.

Strength and power are two of the most critical attributes underlying success in competitions [32,34]. These variables are intimately related and allow athletes to be successful in their respective sport [35]. Moreover, the ability to sustain repeated outputs over distances is commonly referred to as endurance [32]. In the short term, these opposite spectrum attributes appear to compete with one another [32]. For example, just 25 min of endurance exercise ranging from 40 to 100% VO_2 max acutely decreased power and strength by 19–36% [36]. From another perspective, resistance training acutely impairs endurance in a volume and intensity-dependent manner [37]. The present study found that repeated concurrent bouts of strength, power, and endurance decreased the majority of performance metrics examined in this study and resulted in noticeable muscle damage.

When observing CMJ power, it was found that performance dropped equally in both groups. Intriguingly, however, SJ power declined more in the PLA compared to the OCX group (−15% at 24 h Post). These differences were paralleled by greater increases in muscle damage in the PLA (+14% at 24 h Post) compared to the OCX. The ability of OCX to improve power in the SJ but not the CMJ may be due to the differences in mechanics between the two exercises [38]. Specifically, athletes may be able to better use passive elastic components of connective tissue and tendons to overcome muscle damage in a CMJ relative to a SJ, which removes much of the ability to store and release elastic energy [39]. Intriguingly, the ability to use elastic energy increases as the stretch-shorten cycle time decreases [39]. Correspondingly, the high intensity run in our study would demonstrate the shortest stretch shortening cycle in all the measures examined. Thus, the lack of differences in endurance between conditions despite greater muscle damage in the PLA may be explained by similar reasons to the CMJ. In support, we found that decrements in our isometric measure of strength from Pre to 48 h Post were greater in the PLA group (−12%) than OCX.

Since improving recovery through lowering muscle damage is of great interest to athletes, it is worth exploring how OCX may influence these outcomes. To begin to answer this question, it is important to understand the contribution of reactive oxygen species (ROS) to exercise-induced muscle damage. This topic has been addressed in impactful reviews [40]. Briefly, exercise elevates metabolism, and the use of oxygen is heightened [41]. The result is a leakage of ROS from the mitochondria [41]. Superoxide is a major ROS produced as a by-product of oxygen metabolism and, if not regulated, causes many types of cell damage [42]. As such, ROS alters cell structure and function, and contributes to muscle damage causing performance declines [42].

The ingredient administered in this study was derived from the microalga *Tetraselmis chuii*. This microalga contains highly active antioxidant enzymes, particularly superoxide dismutase (SOD), which speeds the reaction that converts superoxide into ordinary molecular oxygen, thereby protecting cells from oxidative damage [15]. The ingredient was also found to upregulate glutathione peroxidase and catalase enzymes in human skeletal muscle myoblasts in vitro [15]. Research has shown that antioxidant supplementation can protect against exercise-induced muscle damage [43,44] and as a result, reduce muscle performance loss and fatigue [45,46]. Our human and animal trials demonstrated that exercise increased muscle damage (e.g., elevated CK and myoglobin levels). Moreover, in both studies, muscle damage was lowered by supplementation. An independent analysis of the present ingredient demonstrated high antioxidant capacity via high concentrations of SOD (38,000 IU per 100 g)

with robust corresponding ORAC values for the enzymes' corresponding anion. These properties led us to explore multiple intramuscular antioxidant enzymes in exercise alone and exercise with OCX supplementation. We found that the ingredient improved measures of antioxidant capacity in a generally dose-dependent fashion.

The results of our study agreed with the past literature demonstrating that exercise alone increases antioxidant capacity, likely as an adaptation to increased oxidative stress [47]. Our animal study also found that exercise combined with the administration of the SOD rich ingredient further decreased oxidative stress. Our findings agreed with a number of antioxidant supplement studies, which demonstrated decreased oxidative stress. These studies include positive effects with vitamin E [48–50], vitamin C [10,51], polyphenolic compounds [52], β -carotene [53], and different antioxidant combinations [54]. These changes occurred as result of elevations in antioxidant capacity as indicated by greater levels of the three intramuscular enzymes measured. The increased capacity found agreed with the past research demonstrating that antioxidant supplementation can increase antioxidant enzyme activity both at rest [55] and in combination with exercise [51,54].

While the mechanism of action still needs exploring, previous in vitro research with the ingredient in human skeletal muscle myoblasts observed that the changes in the proteins studied in our research occurred via the transcriptional responses of genes encoding the antioxidant enzymes and the further regulation of the polypeptide translation downstream of these events [15]. Specifically, a parallel and positive response in enzyme activities and transcripts for SOD, CAT and GSH-Px encoding genes in myoblasts, as a consequence of microalga *Tetraselmis chuii* treatment, was found [15]. This previous finding appears to unravel the potential molecular basis of the cytoprotective effect of the studied ingredient in relation to the primary antioxidant enzymes investigated.

5. Conclusions

We can conclude that the training program was effective at inducing high levels of neuromuscular fatigue. However, marine phytoplankton supplementation (Oceanix, OCX) was able to improve recovery, sustain power, and prevent declines in strength across repeated endurance and cross-training bouts. Since recovery can be defined as, "returning what was lost due to exercise," [56], we demonstrated that OCX supplementation can improve recovery from intense competitions. Moreover, we present for the first time mechanistic data, which support the OCX role in improving intramuscular antioxidant capacity when combined with exercise.

These findings may allow practitioners to better recommend supplementation for athletes competing under high stress scenarios. While no person should be expected to maximally display every skill of athleticism on a daily basis, OCX supplementation may assist in improving recovery during demanding training or competition periods.

Author Contributions: Conceptualization, M.S., K.S., R.Y., S.D., and J.W.; data curation, M.S., M.S., C.O., R.G., D.R., N.S., and M.T.; formal analysis, M.S., C.O., N.S., M.T., J.W.; investigation, M.S., M.S., C.O., R.G., D.R., N.S., M.T.; methodology, M.S., K.S., M.S., C.O., R.G., D.R., N.S., M.T.; supervision, M.S. and J.W.; writing—original draft, M.S., K.S., J.W.; writing—review and editing, M.S., K.S., R.L., J.W. All authors have read and agreed to the published version of the manuscript.

Funding: All projects reported in this manuscript was supported by Lonza Consumer Health Inc. (Morrison, NJ, USA).

Conflicts of Interest: S.D. is an employee of Lonza Consumer Health Inc. Other authors have no other relevant affiliations or competing financial involvement with the subject matter or materials in this manuscript.

Abbreviations

OCX	Oceanix
MDA	Malonaldehyde
TE	Trolox equivalency
CK	Creatine kinase
MYOB	Myoglobin
IMTP	Isometric mid-thigh pull
CMJ	Countermovement jump
SJ	Squat jump
E	Exercise
E + Oc1	Exercise + Oceanix 1 (2.55 mg d/rat)
E + Oc2	Exercise + Oceanix 2 (5.1 mg d/rat)
SOD	Superoxide dismutase
CAT	Catalase
GSH-Px	Glutathione peroxidase
PLA	Placebo
sCT	Salivary cortisol
BMI	Body mass index
RPE	Rating of perceived exertion
PRS	Perceived recovery status
ANOVA	Analysis of variance
ROS	Reactive oxygen species
EDTA	Ethylenediaminetetraacetic acid
m	Meters
cm	Centimeters
e	Each leg
DB	Dumbbell
KB	Kettlebell
W	Prone shoulder internal/external rotation
T	Prone horizontal shoulder abduction
Y	Prone shoulder extension

References

1. Bandyopadhyay, A.; Bhattacharjee, I.; Sousana, P.K. Physiological perspective of endurance overtraining—A comprehensive update. *Al Ameen J. Med. Sci.* **2012**, *5*, 7–20.
2. Meeusen, R.; Watson, P.; Hasegawa, H.; Roelands, B.; Piacentini, M.F. Central fatigue: The serotonin hypothesis and beyond. *Sports Med.* **2006**, *36*, 881–909. [[CrossRef](#)] [[PubMed](#)]
3. Moreira, A.; Nosaka, K.; Nunes, J.A.; Viveiros, L.; Jamurtas, A.Z.; Aoki, M.S. Changes in muscle damage markers in female basketball players. *Biol. Sport* **2014**, *31*, 3–7. [[CrossRef](#)] [[PubMed](#)]
4. Margonis, K.; Fatouros, I.G.; Jamurtas, A.Z.; Nikolaidis, M.G.; Douroudos, I.; Chatzinikolaou, A.; Mitrakou, A.; Mastorakos, G.; Papassotiropoulos, I.; Taxildaris, K.; et al. Oxidative stress biomarkers responses to physical overtraining: Implications for diagnosis. *Free Radic. Biol. Med.* **2007**, *43*, 901–910. [[CrossRef](#)] [[PubMed](#)]
5. Tanskanen, M.; Atalay, M.; Uusitalo, A. Altered oxidative stress in overtrained athletes. *J. Sports Sci.* **2010**, *28*, 309–317. [[CrossRef](#)]
6. Sies, H. Oxidative stress: From basic research to clinical application. *Am. J. Med.* **1991**, *91*, 315–385. [[CrossRef](#)]
7. Sen, C.K. Oxidants and antioxidants in exercise. *J. Appl. Physiol.* **1995**, *79*, 675–686. [[CrossRef](#)]
8. Maughan, R.J.; Depiesse, F.; Geyer, H.; International Association of Athletics Federations. The use of dietary supplements by athletes. *J. Sports Sci.* **2007**, *25* (Suppl. 1), S103–S113. [[CrossRef](#)]
9. Sobal, J.; Marquart, L.F. Vitamin/mineral supplement use among athletes: A review of the literature. *Int. J. Sport Nutr.* **1994**, *4*, 320–334. [[CrossRef](#)]
10. Alessio, H.M.; Goldfarb, A.H.; Cao, G. Exercise-induced oxidative stress before and after vitamin C supplementation. *Int. J. Sport Nutr.* **1997**, *7*, 1–9. [[CrossRef](#)]

11. Meydani, M.; Evans, W.J.; Handelman, G.; Biddle, L.; Fielding, R.A.; Meydani, S.N.; Burrill, J.; Fiatarone, M.A.; Blumberg, J.B.; Cannon, J.G. Protective effect of vitamin E on exercise-induced oxidative damage in young and older adults. *Am. J. Physiol.* **1993**, *264*, R992–R998. [[CrossRef](#)] [[PubMed](#)]
12. Peternelj, T.-T.; Coombes, J.S. Antioxidant supplementation during exercise training: Beneficial or detrimental? *Sports Med.* **2011**, *41*, 1043–1069. [[CrossRef](#)] [[PubMed](#)]
13. McGinley, C.; Shafat, A.; Donnelly, A.E. Does antioxidant vitamin supplementation protect against muscle damage? *Sports Med.* **2009**, *39*, 1011–1032. [[CrossRef](#)] [[PubMed](#)]
14. Graeff-Hönninger, S.; Khajehei, F. The Demand for Superfoods: Consumers' desire, production viability and bio-intelligent transition. In *Food Tech Transitions: Reconnecting Agri-Food, Technology and Society*; Piatti, C., Graeff-Hönninger, S., Khajehei, F., Eds.; Springer International Publishing: Cham, Switzerland, 2019; pp. 81–94, ISBN 978-3-030-21059-5.
15. Ramirez, P.; Torres, S.; Lama, C.; Mantecón, L.; Unamunzaga, C.; Infante, C. TetraSOD activates the antioxidant response pathway in human cells: An in vitro approach. *AJB* **2020**, *19*, 367–373. [[CrossRef](#)]
16. Dekkers, J.C.; van Doornen, L.J.; Kemper, H.C. The role of antioxidant vitamins and enzymes in the prevention of exercise-induced muscle damage. *Sports Med.* **1996**, *21*, 213–238. [[CrossRef](#)]
17. Jakeman, J.R.; Lambrick, D.M.; Wooley, B.; Babraj, J.A.; Faulkner, J.A. Effect of an acute dose of omega-3 fish oil following exercise-induced muscle damage. *Eur. J. Appl. Physiol.* **2017**, *117*, 575–582. [[CrossRef](#)]
18. Urso, M.L.; Clarkson, P.M. Oxidative stress, exercise, and antioxidant supplementation. *Toxicology* **2003**, *189*, 41–54. [[CrossRef](#)]
19. Wilson, J.; Wilson, S.; Loenneke, J.; Wray, M.; Norton, L.; Campbell, B.; Lowery, R.; Stout, J. Effects of amino acids and their metabolites on aerobic and anaerobic sports. *Strength Cond. J.* **2012**, *34*, 33–48. [[CrossRef](#)]
20. Borg, G.A.V. *Physical Performance and Perceived Exertion*; University Lund: Oxford, UK, 1962.
21. Howley, E.T.; Bassett, D.R.; Welch, H.G. Criteria for maximal oxygen uptake: Review and commentary. *Med. Sci. Sports Exerc.* **1995**, *27*, 1292–1301. [[CrossRef](#)]
22. Koutlianos, N.A.; Kouidi, E.J.; Metaxas, T.I.; Deligiannis, A.P. Non-invasive cardiac electrophysiological indices in soccer players with mitral valve prolapse. *Eur. J. Cardiovasc. Prev. Rehabil.* **2004**, *11*, 435–441. [[CrossRef](#)]
23. Gibson, T.M.; Harrison, M.H.; Wellicome, R.M. An evaluation of a treadmill work test. *Br. J. Sports Med.* **1979**, *13*, 6–11. [[CrossRef](#)] [[PubMed](#)]
24. Dieli-Conwright, C.M.; Jensky, N.E.; Battaglia, G.M.; McCauley, S.A.; Schroeder, E.T. Validation of the CardioCoachCO2 for submaximal and maximal metabolic exercise testing. *J. Strength Cond. Res.* **2009**, *23*, 1316–1320. [[CrossRef](#)] [[PubMed](#)]
25. Jehanli, A.; Dunbar, J.; Skelhorn, S. Development and validation of an oral fluid collection device and its use in the immunoassay of salivary steroids and immunoglobulins in sports persons. In Proceedings of the International Society of Exercise Immunology Symposium, Oxford, UK, 11–13 June 2011.
26. Garnacho-Castaño, M.V.; López-Lastra, S.; Maté-Muñoz, J.L. Reliability and validity assessment of a linear position transducer. *J. Sports Sci. Med.* **2015**, *14*, 128–136. [[PubMed](#)]
27. Laurent, C.M.; Green, J.M.; Bishop, P.A.; Sjökvist, J.; Schumacker, R.E.; Richardson, M.T.; Curtner-Smith, M. A practical approach to monitoring recovery: Development of a perceived recovery status scale. *J. Strength Cond. Res.* **2011**, *25*, 620–628. [[CrossRef](#)]
28. Liu, Y.-F.; Chen, H.; Yu, L.; Kuo, Y.-M.; Wu, F.-S.; Chuang, J.-I.; Liao, P.-C.; Jen, C.J. Upregulation of hippocampal TrkB and synaptotagmin is involved in treadmill exercise-enhanced aversive memory in mice. *Neurobiol. Learn. Mem.* **2008**, *90*, 81–89. [[CrossRef](#)]
29. Rivas-Estany, E.; Sixto-Fernández, S.; Barrera-Sarduy, J.; Hernández-García, S.; González-Guerra, R.; Stusser-Beltranena, R. Effects of long-term exercise training on left ventricular function and remodeling in patients with anterior wall myocardial infarction. *Arch. Cardiol. Mex.* **2013**, *83*, 167–173. [[CrossRef](#)]
30. Feng, R.; Wang, L.; Li, Z.; Yang, R.; Liang, Y.; Sun, Y.; Yu, Q.; Ghartey-Kwansah, G.; Sun, Y.; Wu, Y.; et al. A systematic comparison of exercise training protocols on animal models of cardiovascular capacity. *Life Sci.* **2019**, *217*, 128–140. [[CrossRef](#)]
31. Slattery, K.; Bentley, D.; Coutts, A.J. The role of oxidative, inflammatory and neuroendocrinological systems during exercise stress in athletes: Implications of antioxidant supplementation on physiological adaptation during intensified physical training. *Sports Med.* **2015**, *45*, 453–471. [[CrossRef](#)]

32. Wilson, J.M.; Marin, P.J.; Rhea, M.R.; Wilson, S.M.C.; Loenneke, J.P.; Anderson, J.C. Concurrent training: A meta-analysis examining interference of aerobic and resistance exercises. *J. Strength Cond Res.* **2012**, *26*, 2293–2307. [[CrossRef](#)]
33. Smith, M.M.; Sommer, A.J.; Starkoff, B.E.; Devor, S.T. Crossfit-based high-intensity power training improves maximal aerobic fitness and body composition. *J. Strength Cond. Res.* **2013**, *27*, 3159–3172. [[CrossRef](#)]
34. Robbins, D.W.; Docherty, D. Effect of loading on enhancement of power performance over three consecutive trials. *J. Strength Cond. Res.* **2005**, *19*, 898–902. [[CrossRef](#)]
35. Cormie, P.; McGuigan, M.R.; Newton, R.U. Developing maximal neuromuscular power: Part 1—biological basis of maximal power production. *Sports Med.* **2011**, *41*, 17–38. [[CrossRef](#)] [[PubMed](#)]
36. Leveritt, M.; Abernethy, P.J. Acute effects of high-intensity endurance exercise on subsequent resistance activity. *J. Strength Cond. Res.* **1999**, *13*, 47–51.
37. Brentano, M.A.; Martins Kruehl, L.F. A review on strength exercise-induced muscle damage: Applications, adaptation mechanisms and limitations. *J. Sports Med. Phys. Fitness* **2011**, *51*, 1–10. [[PubMed](#)]
38. Harrison, A.J.; Gaffney, S.D. Effects of muscle damage on stretch-shortening cycle function and muscle stiffness control. *J. Strength Cond. Res.* **2004**, *18*, 771–776. [[CrossRef](#)] [[PubMed](#)]
39. Wilson, J.M.; Flanagan, E.P. The role of elastic energy in activities with high force and power requirements: A brief review. *J. Strength Cond. Res.* **2008**, *22*, 1705–1715. [[CrossRef](#)] [[PubMed](#)]
40. Finaud, J.; Lac, G.; Filaire, E. Oxidative stress: Relationship with exercise and training. *Sports Med.* **2006**, *36*, 327–358. [[CrossRef](#)]
41. Nikolaidis, M.G.; Jamurtas, A.Z. Blood as a reactive species generator and redox status regulator during exercise. *Arch. Biochem. Biophys.* **2009**, *490*, 77–84. [[CrossRef](#)]
42. Sakellariou, G.K.; Jackson, M.J.; Vasilaki, A. Redefining the major contributors to superoxide production in contracting skeletal muscle. The role of NAD(P)H oxidases. *Free Radic. Res.* **2014**, *48*, 12–29. [[CrossRef](#)]
43. Bryer, S.C.; Goldfarb, A.H. Effect of high dose vitamin C supplementation on muscle soreness, damage, function, and oxidative stress to eccentric exercise. *Int. J. Sport Nutr. Exerc. Metab.* **2006**, *16*, 270–280. [[CrossRef](#)]
44. Silva, L.A.; Pinho, C.A.; Silveira, P.C.L.; Tuon, T.; De Souza, C.T.; Dal-Pizzol, F.; Pinho, R.A. Vitamin E supplementation decreases muscular and oxidative damage but not inflammatory response induced by eccentric contraction. *J. Physiol. Sci.* **2010**, *60*, 51–57. [[CrossRef](#)] [[PubMed](#)]
45. Bowtell, J.L.; Sumners, D.P.; Dyer, A.; Fox, P.; Mileva, K.N. Montmorency cherry juice reduces muscle damage caused by intensive strength exercise. *Med. Sci. Sports Exerc.* **2011**, *43*, 1544–1551. [[CrossRef](#)] [[PubMed](#)]
46. Nakazato, K.; Ochi, E.; Waga, T. Dietary apple polyphenols have preventive effects against lengthening contraction-induced muscle injuries. *Mol. Nutr. Food Res.* **2010**, *54*, 364–372. [[CrossRef](#)] [[PubMed](#)]
47. Powers, S.K.; Ji, L.L.; Leeuwenburgh, C. Exercise training-induced alterations in skeletal muscle antioxidant capacity: A brief review. *Med. Sci. Sports Exerc.* **1999**, *31*, 987–997. [[CrossRef](#)] [[PubMed](#)]
48. Dillard, C.J.; Litov, R.E.; Savin, W.M.; Dumelin, E.E.; Tappel, A.L. Effects of exercise, vitamin E, and ozone on pulmonary function and lipid peroxidation. *J. Appl. Physiol. Respir. Environ. Exerc. Physiol.* **1978**, *45*, 927–932. [[CrossRef](#)]
49. Jessup, J.V.; Horne, C.; Yarandi, H.; Quindry, J. The Effects of Endurance Exercise and Vitamin E on Oxidative Stress in the Elderly. *Biol. Res. Nur.* **2003**, *5*, 47–55. [[CrossRef](#)]
50. Satchek, J.M.; Milbury, P.E.; Cannon, J.G.; Roubenoff, R.; Blumberg, J.B. Effect of vitamin E and eccentric exercise on selected biomarkers of oxidative stress in young and elderly men. *Free Radic. Biol. Med.* **2003**, *34*, 1575–1588. [[CrossRef](#)]
51. Tauler, P.; Aguiló, A.; Gimeno, I.; Fuentespina, E.; Tur, J.A.; Pons, A. Influence of vitamin C diet supplementation on endogenous antioxidant defences during exhaustive exercise. *Pflugers Arch.* **2003**, *446*, 658–664. [[CrossRef](#)]
52. Di Giacomo, C.; Acquaviva, R.; Sorrenti, V.; Vanella, A.; Grasso, S.; Barcellona, M.L.; Galvano, F.; Vanella, L.; Renis, M. Oxidative and antioxidant status in plasma of runners: Effect of oral supplementation with natural antioxidants. *J. Med. Food* **2009**, *12*, 145–150. [[CrossRef](#)]
53. Sumida, S.; Doi, T.; Sakurai, M.; Yoshioka, Y.; Okamura, K. Effect of a single bout of exercise and beta-carotene supplementation on the urinary excretion of 8-hydroxy-deoxyguanosine in humans. *Free Radic. Res.* **1997**, *27*, 607–618. [[CrossRef](#)]

54. Ryan, M.J.; Dudash, H.J.; Docherty, M.; Geronilla, K.B.; Baker, B.A.; Haff, G.G.; Cutlip, R.G.; Alway, S.E. Vitamin E and C supplementation reduces oxidative stress, improves antioxidant enzymes and positive muscle work in chronically loaded muscles of aged rats. *Exp. Gerontol.* **2010**, *45*, 882–895. [[CrossRef](#)] [[PubMed](#)]
55. Shireen, K.F.; Pace, R.D.; Mahboob, M.; Khan, A.T. Effects of dietary vitamin E, C and soybean oil supplementation on antioxidant enzyme activities in liver and muscles of rats. *Food Chem. Toxicol.* **2008**, *46*, 3290–3294. [[CrossRef](#)] [[PubMed](#)]
56. Sands, W.A. Thinking sensibly about recovery. In *Strength and Conditioning for Sports Performance*; Routledge: New York, NY, USA, 2016; Chapter 18; pp. 451–483.



© 2020 by the authors. Licensee MDPI, Basel, Switzerland. This article is an open access article distributed under the terms and conditions of the Creative Commons Attribution (CC BY) license (<http://creativecommons.org/licenses/by/4.0/>).



Article

The Effect of Resveratrol or Curcumin on Head and Neck Cancer Cells Sensitivity to the Cytotoxic Effects of Cisplatin

Marinela Bostan ^{1,2,†}, Georgiana Gabriela Petrică-Matei ^{3,†}, Nicoleta Radu ^{4,5}, Razvan Hainarosie ⁶, Cristian Dragos Stefanescu ⁶, Carmen Cristina Diaconu ^{7,*} and Viviana Roman ^{1,*}

¹ Center of Immunology, Stefan S. Nicolau' Institute of Virology, 030304 Bucharest, Romania; marinela.bostan@virology.ro

² Department of Immunology, Victor Babeş' National Institute of Pathology, 050096 Bucharest, Romania

³ Personal Genetics-Medical Genetics Center, Department of Cytogenetics, 010987 Bucharest, Romania; gabryela.matei@gmail.com

⁴ Department of Biotechnology, University of Agronomic Sciences and Veterinary Medicine of Bucharest, 011464 Bucharest, Romania; nicolbiotec@yahoo.com

⁵ Biotechnology Department, National Institute for Chemistry and Petrochemistry R&D of Bucharest, 060021 Bucharest, Romania

⁶ Otorhinolaryngology and Head and Neck Surgery Department-University of Medicine and Pharmacy "Carol Davila", 020021 Bucharest, Romania; razvan@riacclinic.com (R.H.); cristiandragos@hotmail.com (C.D.S.)

⁷ Department of Cellular and Molecular Pathology, Stefan S. Nicolau Institute of Virology, 030304 Bucharest, Romania

* Correspondence: directie@virology.ro (C.C.D.); viviana.roman@virology.ro (V.R.)

† Equal contribution with the first author.

Received: 31 July 2020; Accepted: 21 August 2020; Published: 26 August 2020

Abstract: Natural compounds can modulate all three major phases of carcinogenesis. The role of the natural compounds such as resveratrol (RSV) and curcumin (CRM) in modulation of anticancer potential of platinum-based drugs (CisPt) is still a topic of considerable debate. In order to enhance head and neck cancer (HNSCC) cells' sensitivity to the cytotoxic effects of CisPt combined treatments with RSV or CRM were used. The study aim was to evaluate how the RSV or CRM associated to CisPt treatment modulated some cellular processes such as proliferation, P21 gene expression, apoptotic process, and cell cycle development in HNSCC tumor cell line (PE/CA-PJ49) compared to a normal cell line (HUVEC). The results showed that RSV or CRM treatment affected the viability of tumor cells more than normal cells. These natural compounds act against proliferation and sustain the effects of cisplatin by cell cycle arrest, induction of apoptosis and amplification of P21 expression in tumor cells. In conclusion, using RSV or CRM as adjuvants in CisPt therapy might have a beneficial effect by supporting the effects induced by CisPt.

Keywords: resveratrol; curcumin; cisplatin; head and neck cancer; cell cycle; apoptosis

1. Introduction

The heterogeneous nature, at the molecular level, of many types of cancer has hindered both the identification of specific targets and development of efficient therapeutic strategies against tumours. The most common types of treatment for cancer include surgery, radiation and chemotherapy, which can be used either alone or in combination. But these approaches are associated with significant morbidity and a dramatic reduction in quality of life. Head and neck squamous cell carcinomas (HNSCCs) affect different regions of the head and neck, including the tongue, pharynx, larynx, the nasal

cavity and salivary glands. The HNSCC is one of the most aggressive cancers, with a complex etiology and pathophysiology [1,2] and these aspects make finding an optimal treatment strategy relatively difficult. Moreover, regardless of the specificity and efficiency of monotherapy, it is difficult to obtain optimal cytotoxic effects on cancer cells because of their molecular adaptability [3]. The poor prognosis of HNSC is due to the occurrence of recurrence or metastasis in many patients after radiation or chemotherapy. Cisplatin (*cis*-diamminedichloroplatinum; CisPt) is the most effective and widely spread chemotherapy choice of treatment available for patients with recurrent and metastatic HNSCC [4]. Unfortunately, there is a high rate of clinical failure of CisPt due to intrinsic or acquired resistance which may lead to therapy discontinuation [5,6]. Tumor cells' CisPt resistance could occur by reduction of intracellular CisPt accumulation, changes in DNA repair or in the apoptotic cell death pathways [7,8].

In the past few decades, efforts to improve efficacy of cancer treatment have been largely without success, highlighting the need for finding new solutions such as complementary treatment approaches in order to improve the response to chemotherapy [9]. Many natural herbal compounds have attracted the attention of both researchers and clinicians for their use in preventing or improving the current treatment of various chronic diseases, including different types of cancer [10–13]. Natural compounds are able to interact with multiple cellular targets associated with tumor growth, drug resistance, and metastasis, simultaneously making them a potential source of synergistic cancer treatments. It is possible that, through their multi-targeting activity, natural compounds have the potential to enhance the efficacy of current cancer treatments or to reduce the treatment resistance. The main aim of cancer treatment is to remove or destroy the tumor cells without killing normal cells. Most of the natural compounds have less toxicity, a low cost, are associated with limited side effects and many studies described their effects on the process of carcinogenesis. Due to side effects and drug resistance appearance during conventional therapy, it is becoming obvious that natural compounds have potential to demonstrate anticancer activities or can be used as adjuvants in chemotherapy [14–16].

Curcumin (CRM) is a natural compound extracted from the rhizome of turmeric (*Curcuma longa* L.) with reported antiproliferative, antitumoral, antioxidant, anti-inflammatory and chemo-preventive properties and no apparent side effects. In some clinical trials [17–19] curcumin use showed low toxicity and good tolerability. CRM exerts anti-carcinogenic activity against a wide variety of human cancers by regulation of various signaling pathways involved in tumorigenesis, gene expression, cell cycle regulation and apoptosis. Curcumin can influence the expression of various protein kinases, transcription factors, inflammatory cytokines and other oncogenic proteins [20–23].

Resveratrol (3,5,4'-trihydroxystilbene, RSV) is a phytoalexin produced by a wide variety of plants, such as grapes, peanuts and mulberries. This natural compound is one of the most studied compounds for its anti-cancer properties besides its other biological properties such as anti-diabetic, anti-platelet, cardioprotective, neuroprotective, anti-aging, antioxidant and anti-inflammatory activity [24–26]. Resveratrol appears to be an important player in the fight against cancer, as it may influence the mechanisms responsible for inducing the suppression of tumor cell proliferation, as well as the mechanisms involved in sensitization to chemotherapy [27–29]. Rigorous control of cell proliferation and differentiation are necessary to ensure the normal growth and development. Any disorder of the cell division pathways leads to the amplification of the cell division process, the formation of tumors and the appearance of the carcinogenesis process. The carcinogenesis of HNSCC is characterized by multiple events such as activation or suppression of tumour suppressor genes, cell cycle phases disruption, increasing of cell proliferation associated with the decreasing of the apoptotic process [30]. Tumor cells are able to bypass the control point of cell cycle in G1, do not respond to internal regulation and continue to proliferate. It is possible that there are changes in the other phases of the cell cycle, which could be responsible for generating an exaggerated cell proliferation. The balance between cell growth and cell death is influenced by the various molecule regulators like cyclins, cyclin dependent kinases, oncogenes and tumour suppressor genes [31]. One of gene known as a key regulator of the cell cycle as well as cell death and DNA repair is P21 (WAF1/CIP1) a tumor suppressor gene located on chromosome 6 [32,33]. P21 is a cyclin-dependent kinase inhibitor, which is active in response to

cellular and environmental signals to develop tumor suppressor activity. In addition, P21 may act as a key mediator of cell cycle arrest after DNA damage [34]. Many studies suggest that P21 gene by direct association with the promoter region of individual genes or by binding to specific transcription factors/coactivators, contribute to modulation of their activity [35,36]. P21 can exert either positive or negative activities toward a specific cellular response in a context-dependent manner, including the cell type and the source of stress signals. Although abnormal expression of P21 gene has been found in various types of malignancy, current views on the role of P21 as a tumor suppressor or tumor-promoting protein remain ambiguous [37–41]. Our study aimed to define the role of P21 on cell control of the cell cycle progression, programmed cell death and response to cisplatin in tumor line PE/CA-PJ49 comparatively with normal cell line HUVEC. Despite invasive treatment protocols that comprise surgical resection of the tumor, radiotherapy, chemotherapy and often in combination, the 5-years survival rate of HNSCC patients remain around 40–50% [42]. New therapy approaches are awaited to reduce toxicities, improve survival rates, and quality of life. Natural compounds could be used as adjuvants in HNSCC therapy, due to their good tolerability and low toxicity, as well as their acceptance as dietary supplements [43]. Moreover, numerous studies have displayed the potential utility of natural compounds against HNSCC [44,45]. Currently, there is a great concern about finding natural compounds to support the effects of conventional therapy used in the treatment of HNSCC. The results of this study will provide additional information about P21 gene or protein expression in response to cisplatin mediated by natural compounds (CRM or RSV). Extensive knowledge regarding the molecular mechanisms of natural compounds induced apoptosis, cell cycle regulation and influence on cisplatin response is indispensable for the development of improved therapeutic strategies. In this study we have analyzed the influence of CRM or RSV treatment on protein (p21) or gene expression in HNSCC line (PE/CA-PJ49) treated or not with CisPt, compared to a normal cell line (HUVEC). In addition, we tried to analyze how the CRM or RSV treatment influences the apoptotic processes and the tumor cells arrest in different phases of the cell cycle and the proliferation activity of tumor cells in response to cisplatin therapy. Data analysis was performed in order to investigate possible correlation between the expression level of p21 and the apoptotic process or cell cycle progression in PE/CA-PJ49 tumor cells treated with CisPt in the presence or absence of CRM or RSV compared to the normal HUVEC cell line. The results of this study suggest the use of natural compounds CRM or RSV, as adjuvants in order to improve the response to CisPt therapy.

2. Materials

Dulbecco's modified Eagle's medium (DMEM), fetal bovine serum (FBS), glutamine, cisplatin (*cis*-diammineplatinum (II) dichloride, DDP), resveratrol (3,5,4'-trihydroxystilbene), curcumin, 0.9% sodium chloride (NaCl), dimethyl sulfoxide (DMSO), trypsin-EDTA (0.25% trypsin, 0.03% ethylenediaminetetraacetic acid), phosphate buffer solution (PBS) and 3-(4,5 dimethylthiazol-2-yl)-2,5 di-phenyltetrazolium bromide (MTT), propidium iodide (PI) stock solution (4 mg/mL PI in PBS); and RNase A stock solution (10 mg/mL RNase A) were purchased from Sigma-Aldrich (St. Louis, MO, USA). CellTiter 96[®] AQueous One Solution Cell Proliferation Assay (G3580) was from Promega (Madison, WI, USA). RIPA buffer was obtained from Pierce (Rockford, IL, USA), protease inhibitor cocktail and phosphatase inhibitor were from Roche (Rockford, IL, USA); BCA protein assay kit was from Thermo Scientific (Waltham, MA, USA); DuoSet[®] IC ELISA Intracellular Human Total p21/CIP1/CDKN1A (DYC1047-2) and stop solution–2 N H₂SO₄ were purchased from R&D Systems Inc. (Minneapolis, MI, USA); the Annexin V-FITC kit was from BD Pharmingen (San Jose, CA, USA); TRIzol reagent was from Invitrogen (Carlsbad, CA, USA); 96-well plates, micropipettes, special tips, Eppendorf tubes; High-capacity cDNA Reverse Transcription Kits (Applied Biosystems, Foster City, CA, USA) contained the following components: RT-Buffer 10×, 1 mL; RT-10× random primers, 1 mL; 25× dNTP mix (100 mM); MultiScribe[™] Reverse Transcriptase, 50 U/μL; RNase inhibitor 100 uL; ultrapure water; TagMan validate Hs00355782_m1 gene CDKN1A and Hs02800695_m1 gene HPRT1; QPCR master mix; plates (MicroAmp Fast Optical 96-Well Reaction Plate, 0.1 mL).

3. Methods

3.1. Cell Lines and Treatment

The cell lines were obtained from European Collection of Authenticated Cell Cultures (ECACC, Salisbury, UK). The squamous carcinoma cell line PE/CA-PJ49 (ECACC cat. no. 0060606) was obtained from a 57-year old male patient with tongue carcinoma. The PE/CA-PJ49 cell line was grown and maintained in DMEM supplemented with 10% FBS, 2 mM glutamine, at 37 °C in 5% CO₂.

Human Umbilical Vein Endothelial Cells line (HUVEC, ECACC cat. no.06090720) was maintained at 37 °C and 5% CO₂ in complete endothelial cell growth medium (ECACC cat. no.06091509). The sub-confluent cultures of both cell lines (70–80%) were split 1:4–1:8 (i.e., seeding at 1–3 × 10,000 cells/cm²) using trypsin-EDTA (0.25% trypsin, 0.03% EDTA) according to the manufacturer's instructions [46].

3.1.1. Preparation of Stock Solution

CRM and RSV were dissolved in DMSO to make a stock solution of 10 mM. Cisplatin was prepared as a 10 mM stock in 0.9% sodium chloride (NaCl). The solutions stock were filtered through a 0.22 μm membrane, aliquoted and stored at –20 °C until further use. The cisplatin, curcumin or resveratrol stock was used to obtain the working concentrations related to the treatment by performing dilutions in the culture medium [47].

3.1.2. Cell Cultures Treatment

Cells were cultured in specific cell line medium supplemented with 10% inactivated FBS, 2 mM L-glutamine and incubated at 37 °C and in 5% CO₂ humid atmosphere for 24 h to achieve around 60–70% confluence, and then treated with various concentrations of CisPt, CRM or RSV for different periods of time (6, 24, 48 h). After treatments, adherent cells were detached from flasks with a trypsin-EDTA solution, washed twice in PBS. PE/CA=PJ49 and HUVEC cells were used for the evaluation of cytotoxicity capacity, apoptosis, distribution of cell cycle phases or for storing as cell pellets at –80 °C for preparation of cell lysates for further use in ELISA or PCR assays. In all experiments described in this study, all untreated cells were designated as control cells. For treated cells, the conditions (dose and treatment duration) and reagents that were used together at specific dose, were indicated in the figure legends. Non-treated cells were used as controls throughout the experiments.

3.2. Drug Sensitivity Assay (MTT)

The MTT assay is based on the ability of viable cells to reduce the reagent 3-(4,5-dimethylthiazol-2-yl)-2,5-diphenyltetrazolium bromide to colored formazan compounds [48]. Because the transformation is only possible in viable cells, the amount of blue formazan is proportional to the number of viable cells and thus, a linear dependence exists between cell activity and absorbance. Cells were seeded in triplicate in 96-well plates at a density of 5000 cells/well, incubated at 37 °C for 24 h. Then cells were treated with or without different concentrations of CisPt (1–80 μM) and CRM or RSV (1–160 μM) for the different time period (6, 24, and 48 h). After the incubation period, 20 μL MTT (5 mg/mL in PBS) was added and further incubated for 4 h. The supernatant was removed, and the formazan product was analyzed spectrophotometrically (570 nm) after dissolution in DMSO. Wells without cells serve as a blank, and their absorbance was subtracted from the other results. Untreated cells were used as control and their viability was assumed as 100%. Results were expressed as mean values of three determinations ± standard deviation (SD). Data are presented as percent of cell viability and compared to untreated [Viability% = (T – B)/(U – B) × 100, {where T = absorbance of treated cells; U = absorbance of untreated cells, B = absorbance of blank}]. Once percent viability was obtained, the drug response curve was generated, and inhibitory concentration (IC₅₀ and IC₂₅) was calculated using GraphPad Prism version 5.01 [49].

In the present study, the degrees of selectivity of the CisPt, RSV or CRM are expressed as a selectivity index (SI): $SI = IC_{50}$ of compound in a normal cell line/ IC_{50} of the same compound in cancer cell line, where IC_{50} is the concentration required to kill 50% of the cell population. SI values of more than 2 were considered as indicative of high selectivity [50,51].

3.3. Cell Proliferation Assay

In order to determine the effect of CRM or RSV on proliferative activity of cisplatin treated cells was used the Promega CellTiter 96[®] Aqueous One Solution Cell Proliferation Assay, a test that is based on the reduction of yellow MTS tetrazolium salt by the viable cells and generation of colored formazan soluble in the culture medium. The product was spectrophotometrically quantified by measuring the absorbance at $\lambda = 490$ nm using a Dynex plate reader (DYNEX Technologies-MRS, Chantilly, VA, USA) [52,53]. Results were expressed as mean values of three determinations \pm standard deviation (SD). Untreated cells served as control and considered to have a proliferation index (PI = absorbance of treated cells/absorbance of untreated cells) equal to 1.

3.4. Cell Lysates

Cells were treated for 24 h with CisPt, RSV and CRM at the indicated concentrations. After incubation, cells were washed twice with ice-cold PBS, scraped, pelleted and lysed in RIPA buffer (Pierce) supplemented with protease inhibitor cocktail (Roche) and phosphatase inhibitor (Roche) for 30 min on ice. The lysates were transferred into microcentrifuge tubes and centrifuged at $14,000 \times g$ for 5 min at 4 °C followed by sonication (10–15 s \times 3). The supernatants were collected into clean microcentrifuge tubes and stored at -80 °C. Lysates protein concentration were quantified by BCA protein assay kit (Thermo Scientific) and aliquots of 50 μ g of total cell lysate were used for ELISA assay [54].

3.5. ELISA Assay

DuoSet[®] IC ELISA-Human Total p21/CIP1/CDKN1A(: DYC1047-2) was purchased from R&D Systems Inc. and contains the basic components required for the development of sandwich ELISAs to measure human p21 protein also known as CIP1 and CDKN1A in cell lysates. An immobilized capture antibody specifically binds human p21. After washing away unbound material, a biotinylated detection antibody specific for human p21 is used to detect the captured protein, utilizing a standard Streptavidin-HRP format [55]. All experiments were performed in triplicates and absorbance was measured at $\lambda = 450$ nm using a Dynex plate reader.

3.6. Apoptosis Analysis

The apoptosis assay was carried out with the Annexin V-FITC kit using the manufacturer's (BD Pharmingen) protocol. Treated and untreated 1×10^6 cells/mL were resuspended in cold binding buffer and staining simultaneously with 5 μ L FITC-Annexin V (green fluorescence) and 5 μ L propidium iodide (PI) in the dark, at room temperature for 15 min. Then, 400 μ L of Annexin V binding buffer was added and 10,000 cells/sample were acquired using a BD Canto II flow cytometer. The analysis was performed using DIVA 6.2 software in order to discriminate viable cells (FITC⁻PI⁻) from necrotic cells (FITC⁺PI⁺) and early apoptosis (FITC⁺PI⁻) from late apoptosis [56,57].

3.7. Cell Cycle Analysis by Flow Cytometry

For analysis of cell-cycle distribution, the cells were collected after treatment, fixed with 70% ethanol for at least one hour at 4 °C. The cells were stained with propidium iodide (PI) an agent which intercalates into the major groove of double-stranded DNA and produces a highly fluorescent adduct that can be excited at 488 nm with a broad emission around 600 nm. Since PI can also bind to double-stranded RNA, it is necessary to treat the cells with RNase for optimal DNA resolution. Cells

(1×10^6 cells/mL) were washed in PBS and centrifuge at $300 \times g$, 5 min at 4°C . The pellet of the cells were incubated for 10 min at 37°C with 0.5 mg/sample RNase A and then was added 10 μg /sample of PI staining solution to cell pellet, mix well and incubated 10 min at 37°C . The samples stored at 4°C until analyzed by flow cytometry. A minimum of 20,000 events for each sample were collected using a FACS CantoII flow cytometer and ModFIT software (Becton Dickinson) and used to determine the cell cycle phase distribution after debris exclusion [58,59].

3.8. RT-PCR [60,61]

3.8.1. RNA Isolation with TRIzol

In order to isolate of total RNA from treated or untreated cells was used TRIzol reagent (Invitrogen)-a monophasic solution of phenol and guanidine isothiocyanate. During the isolation phases, the TRIzol reagent maintains RNA integrity, while disrupting cells and dissolving cell components. The addition of chloroform followed by centrifugation ensures the separation phase of the solution into an aqueous phase and an organic phase. RNA remains in the aqueous phase and is recovered by isopropanol precipitation. The RNA pellet washed once with 75% ice-cold ethanol and entrifuged at $10,000 \times g$ for 5 min at 4°C . The RNA pellet is redissolved in nuclease-free water and incubating in a 60°C water bath for 10 min. The concentration of isolated RNA was assessed using a NanoDrop spectrophotometer (NanoDrop Technologies, Montchanin, DE, USA). RNA purity was determined by A_{260}/A_{280} ratios (an A_{260}/A_{230} ratio as close as possible to 2 indicates the presence of highly purified RNA).

Reverse transcription of messenger RNA molecules was performed using the High-capacity cDNA Reverse Transcription Kit from Applied Biosystems, using non-specific, randomic primers, following the manufacturer's instructions (Table 1). To perform cDNA synthesis $1 \mu\text{g}$ of total RNA was used. The obtained cDNA was stored at 4°C and further used in the amplification reaction Real-Time PCR (RT-PCR) [60,61].

Table 1. Preparation of the reaction mixture/reaction.

Reaction Components	Volume
RT-Buffer 10 \times	2.0 μL
Mix dNTP 25 \times (100 mM)	0.8 μL
Randomics RT-primeri 10 \times	2.0 μL
MultiScribe™ Reverse Transcriptase	1.0 μL
Ultrapure water	4.2 μL
Total Volume/reaction	10 μL

3.8.2. Real-Time PCR

The analysis of the CDKN1A gene (P21) expression level was performed by real time PCR using a ViiA™ 7 Real-Time PCR System by setting the ABI 7500 Fast program (Applied Biosystems). The reference gene used in the experiments was hypoxanthine ribosyltransferase (HPRT1) because this gene is found in all cell types and has a stable, relatively constant expression regardless of experimental conditions. The reference gene is useful in calibrating and interpreting qRT-PCR. The products obtained after reverse transcription reaction were diluted to a final concentration of 100 ng/ μL with DEPC-treated water. The samples were prepared according to the standard protocol kit, in a reaction volume of 20 μL (Table 2):

Table 2. Real-Time PCR reaction components.

Reaction Components	Volume
QPCR master mix	10 μ L
Reference dye	0.3 μ L
cDNA	5 μ L
Ultrapure water	4.7 μ L
Total Volume/reaction	20 μ L

Each sample was performed in duplicate. Thermal cycling conditions of PCR were as follows: 95 °C for 10 min for amplification activation and 40 cycles at 95 °C for 12 s and 60 °C for 15 s.

The samples were analyzed using the formula $2^{-\Delta\Delta Ct}$. The value obtained indicates how many times the expression of the gene has increased or decreased compared to the control sample (untreated cells):

$$\Delta Ct1 = Ct(\text{gene of interest}) - Ct(\text{reference gene})(\text{treated cells})$$

$$\Delta Ct2 = Ct(\text{gene of interest}) - Ct(\text{reference gene})(\text{control cells})$$

$$\Delta\Delta Ct = \Delta Ct1 - \Delta Ct2$$

$$\text{gene expression} = 2^{-\Delta\Delta Ct}$$

3.9. Statistical Analysis

Data analyses were performed using GraphPad Prism 7 (GraphPad Software Inc., La Jolla, CA, USA). The differences between the treatment and control groups were statistically analysed using unpaired two tailed t-test and one-way ANOVA. Statistical significance was considered at $p < 0.05$.

4. Results

4.1. Effects of CisPt and/or Natural Compounds RSV, CRM on Cell Viability

The anticancer cytotoxic activity in vitro was evaluated by the MTT assay. The tumor cells (PE/CA-PJ49) and normal cells (HUVEC) were treated for 24 h with different concentrations of CisPt (1, 2.5, 5, 10, 20, 30, 40, 80 and 160 μ M) and/or natural compounds CRM or RSV (1, 5, 10, 20, 30, 40, 80 and 160 μ M). The most widely used and informative measure of a drug's efficacy is IC₅₀-the half-maximal inhibitory concentration. IC₅₀ was determined at half of the difference between the maximum (plateau) and minimum absorbance values, by plotting the absorbance value at 570 nm (Y axis) versus the concentration of the compound analysed (X axis). The IC₅₀ values were reported as a mean of three independent experiments \pm standard deviation (S.D.). In addition, we also determined IC 25 for both CisPt and CRM and ESV in order to choose the optimal working concentrations for these compounds (Table 3). Results showed that in comparison to the control, both CisPt and CRM or RSV caused dose-dependent toxicity. The IC₅₀ values (\pm SEM) for CisPt were $9.72 \pm 1.7 \mu$ M on PE/CA-PJ49 cells and $20.93 \pm 2.1 \mu$ M on HUVEC cells (Table 3a). RSV, under our experimental conditions, had an IC₅₀ of $46.8 \pm 2.6 \mu$ M on PE/CA-PJ49 cells and $110.4 \pm 8.6 \mu$ M on HUVEC cells (Table 3a). CRM treatment for 24 h reduced the cellular viability to an IC₅₀ = $16.3 \pm 3.4 \mu$ M on PE/CA-PJ49 tumor cells and IC₅₀ = $59.3 \pm 6.1 \mu$ M on normal cells HUVEC (Table 3a).

Table 3. Inhibitory concentration (IC₂₅ and IC₅₀) values of the CisPt, RSV and CRM were performed using a linear regression equation for the cytotoxicity curve for PE/CA-PJ49 tumor cells and for normal cells HUVEC. IC₂₅ and IC₅₀ values are presented as mean ± SEM according to two independent assays, each done in triplicate (a). The selectivity index (SI), which indicates the cytotoxic selectivity for CisPt, RSV or CRM against cancer cells versus normal cells, and, SI values over 2 were considered as high selectivity (b).

(a)				
Treatment (24 h)	HUVEC		PE/CA-PJ49	
	IC 25	IC 50	IC 25	IC 50
CisPt (μM)	5.82 ± 1.1	20.93 ± 2.1	3.95 ± 1.2	9.72 ± 1.7
RSV (μM)	40.6 ± 3.3	110.4 ± 8.6	17.6 ± 1.5	46.8 ± 2.6
CRM (μM)	19.2 ± 2.1	59.3 ± 6.1	7.9 ± 1.8	16.3 ± 3.4
(b)				
	CisPt (μM)	RSV (μM)	CRM (μM)	
HUVEC (IC 50)	20.93 ± 2.1	110.4 ± 8.6	59.3 ± 6.1	
PE/CA-PJ49 (IC 50)	9.72 ± 1.7	46.8 ± 2.6	16.3 ± 3.4	
Selectivity Index (SI)	2.15	2.36	3.66	

Selectivity index (SI) values were also calculated for RSV or CRM on both cell lines and compared to those calculated for CisPt. The results are presented in Table 3b. The SI value calculated for RSV (2.36) was close to the SI value for CisPt (2.15), but the highest SI value was obtained for CRM (3.66). Knowing that the greater the SI value is, the more selective it is and SI values less than 2 indicate general toxicity [62], we concluded that compared to CisPt, the common chemotherapy drug, RSV (SI = 2.36), works in a similar manner as CisPt, while CRM exhibits a high degree of cytotoxic selectivity (SI = 3.66).

The aim of our study was to use natural compounds capable of potentiating the cytostatic effects of CisPt without having a toxic effect on their own on normal cells. For this purpose, we also determined IC₂₅ for CisPt, CRM or RSV treatments in order to select the optimal concentrations used in the combined treatment. The optimal time for cell-treatment was 24 h and the used concentrations for the natural compounds were 15 μM for CRM and 40 μM for RSV for treatment of both cell lines as shown in Figure 1. For CisPt treatment, the choice to use 2 concentrations was made (5 μM and 20 μM) in order to determine if the modulatory effects induced by the two natural compounds were dependent by the CisPt dose (Figure 1).

The obtained results showed that the cisplatin treatment affects the viability of both normal HUVEC cells and PE/CA-PJ49 tumor cells. As shown in Figure 1, the viability of tumor cells PE/CA-PJ49 is significantly affected by CisPt treatment 5 μM (** *p* = 0.002) or 20 μM (***) *p* < 0.0001), compared to untreated cells. Analysis of the effect of CisPt treatment on the viability of PE/CA-PJ49 tumor cells showed that the difference between the effect induced by 20 μM CisPt treatment is significantly higher than the one induced by 5 μM CisPt treatment (** *p* = 0.0058).

CisPt treatment of normal human HUVEC cells showed that regardless of the chosen concentration CisPt 5 μM (** *p* = 0.0055) and CisPt 20 μM (***) *p* = 0.0002) the cell viability was significantly reduced compared to untreated cells. In addition, CisPt 20 μM treatment of HUVEC cells led to a decrease cell viability compared to the effect induced by treatment with 5 μM CisPt (** *p* = 0.0081). Comparative analysis of the effect of CisPt treatment on the two cell lines led to the following observation—both the low-concentration 5 μM CisPt (non-significant, *p* = 0.287) and the high-concentration 20 μM CisPt (non-significant, *p* = 0.105) treatment acted similarly on the viability of tumor and normal cells.

The viability of tumor cells PE/CA-PJ49 (***) *p* = 0.0004) or normal HUVEC cells (** *p* = 0.0077) is significantly affected by RSV 40 μM treatment compared to untreated cells (Figure 1). The effect of the 40 μM RSV treatment on cell viability does not significantly differ from the effect induced by 5 μM CisPt on both normal cells (non-significant, *p* = 0.578) and tumor cells viability (non-significant, *p* = 0.0891).

When analyzing the effect of the 40 μM RSV treatment on PE/CA-PJ49 tumor cells, compared to the induced effect on normal HUVEC cells, it was observed that RSV reduced the viability of tumor cells more than in the case of normal cells (* $p < 0.013$) (Figure 1).

Treatment with 15 μM CRM reduced tumor cell viability compared to normal cells HUVEC (* $p < 0.015$). The effect induced by CRM treatment on tumor cells PE/CA-PJ49 was not different from the effect induced by treatment with 5 μM CisPt (non-significant, $p = 0.578$), but was different compared to the effects induce by the 20 μM CisPt treatment (** $p = 0.0077$), (Figure 1).

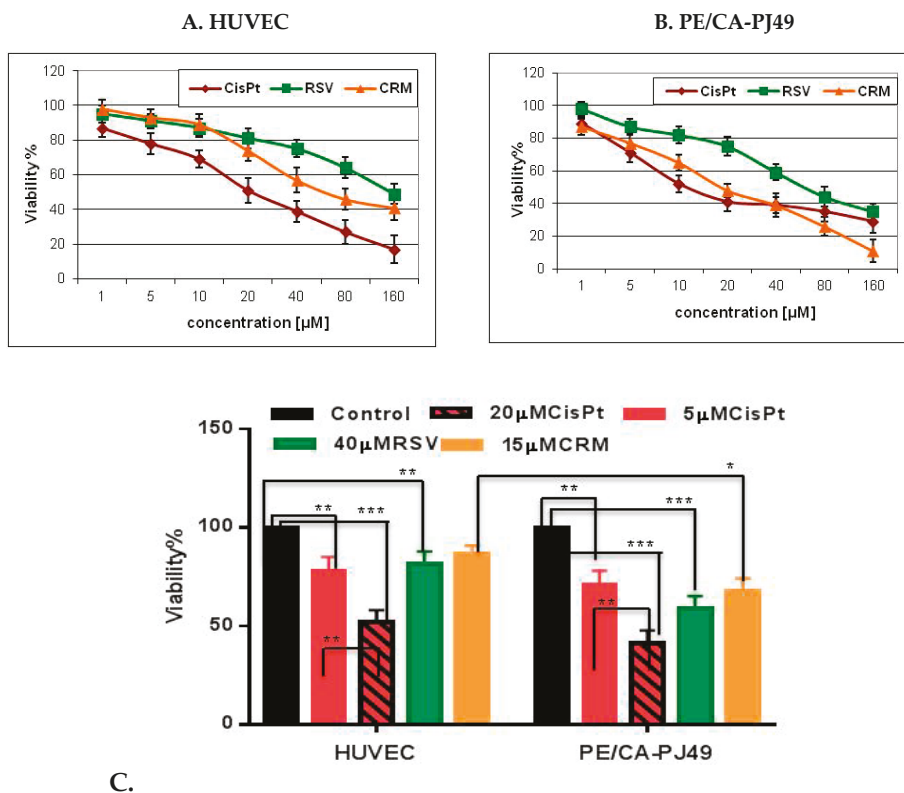


Figure 1. Cisplatin or natural compounds effects on cells viability. (A) HUVEC and (B) PE/CA-PJ49 cells were either left untreated or treated 24 h with different concentrations of CisPt, CRM. Data shown are representative of three independent experiments and are expressed as mean of three replicates \pm SD ($n = 3$). Untreated cells were considered to have 100% viability. Viability% = $(T - B)/(U - B) \times 100$, (where T, absorbance of treated cells; U, absorbance of untreated cells; and B, absorbance of blank). (C) Tumor cell viability compared to normal HUVEC cell viability after treatment with CisPt and / or RSV, CRM; (* $p < 0.05$, ** $p < 0.005$; *** $p < 0.0005$).

4.2. Effects of CisPt and/or Natural Compounds RSV or CRM on the Cell Proliferation Process

PE/CA-PJ49 and HUVEC cells were treated with 5 μM and 20 μM CisPt and/or 40 μM RSV, 15 μM CRM for 24 h. Analysis of the effect induced by the individual treatment with CisPt, RSV or CRM on the proliferation process of the PE/CA-PJ49 tumor cells and of the normal HUVEC cells are shown in Figure 2A,B. Treatment with 20 μM CisPt for 24 h determined a significant decrease of the proliferation process compared to the 5 μM CisPt treatment, both in the case of tumor cells PE/CA-PJ49 (** $p = 0.0065$) and that of normal cells HUVEC (** $p = 0.0011$). Treatment with 40 μM RSV for 24 h affected the

proliferation of tumor cells PE/CA-PJ49 much more than the one of normal cells HUVEC (** $p = 0.0063$) (Figure 2A).

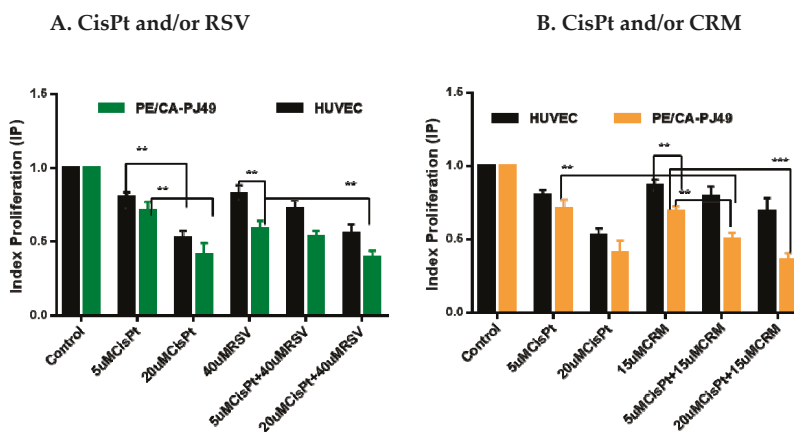


Figure 2. The index proliferation (IP) of HUVEC and PE/CA-PJ49 cells treated with CisPt and/or (A) RSV (B) CRM was calculated as IP = absorbance of treated cells/absorbance of untreated cells. Results are expressed as DO mean values of three determinations \pm standard deviation (SD). Untreated cells were considered to have IP equal 1. (** $p < 0.005$; *** $p < 0.0005$).

Analysis of the effect induced by the combined treatment of 5 μM CisPt + 40 μM RSV on PE/CA-PJ49 tumor cells showed that RSV can amplify the effect induced by lower CisPt concentration by recording a decrease of the IP (5 μM CisPt + 40 μM RSV vs. 5 μM CisPt; * $p = 0.0145$). In case of applying the same treatment on the normal HUVEC cells no significant changes of IP were registered (5 μM CisPt + 40 μM RSV vs. 5 μM CisPt; non-significant, $p = 0.105$). Using a high concentration of CisPt, the proliferative response of tumor cells to the combined treatment of 20 μM CisPt + 40 μM RSV recorded a significant decrease in IP (20 μM CisPt + 40 μM RSV vs. 40 μM RSV; ** $p = 0.0093$). Treatment of normal cells with 20 μM CisPt + 40 μM RSV led to a response similar to that induced by treatment with 20 μM CisPt (non-significant, $p = 0.53$), but there was a significant decrease in IP compared to the response induced by treatment with 40 μM RSV alone (** $p = 0.005$) (Figure 2A). These results show that the effect of treatment with 20 μM CisPt is dominant in the treatment of normal or tumor cells. Treatment with 15 μM CRM for 24 h on tumor cells PE/CA-PJ49 led to a much more intense decrease of the proliferative process compared to the effect induced on normal HUVEC cell proliferation (** $p = 0.0065$) (Figure 2B). Applying the combined 5 μM CisPt + 15 μM CRM treatment to normal cells did not alter the proliferative process compared to the effect induced by individual treatment with 5 μM CisPt (non-significant, $p = 0.784$) or 15 μM CRM (non-significant, $p = 0.209$). IP of tumor cells PE/CA-PJ49 treated with 5 μM CisPt + 15 μM CRM suggested a significant inhibition of the proliferative process compared to the effect induced by treatment with 5 μM CisPt (** $p = 0.008$) or 15 μM CRM (** $p = 0.0042$). The combined treatment of 20 μM CisPt + 15 μM CRM very strongly inhibited the proliferation of tumor cells compared to the effect induced by treatment only with CRM (** $p = 0.0006$) (Figure 2B). The combined treatment applied to normal cells HUVEC led to a decrease in IP, but the dominant effect on cell proliferation appears to be due to the high concentration of CisPt (20 μM CisPt + 15 μM CRM vs. 15 μM CRM; * $p = 0.0424$). Comparative analysis of the proliferative response of PE/CA-PJ49 tumor cells versus the normal HUVEC cells to the combined CisPt + CRM treatment shown a significantly different cellular behavior (** $p = 0.004$ – 5 μM CisPt + 15 μM CRM; ** $p = 0.0051$ – 20 μM CisPt + 15 μM CRM) (Figure 2B).

4.3. Modulation of p21 Protein Expression by Natural Compounds and/or Cisplatin Treatment

In cancer development and evolution p21 protein might acts as an oncogene or tumor suppressor and for this reason it could be an important player in processes such as the cancer aggressiveness or the response to chemotherapy [63,64]. In this study, using ELISA assay we analyzed the expression level of p21 in the tumor cells (PE-CA/PJ49) compared to a normal cells (HUVEC). In addition, we looked at how treatment with CisPt, RSV or CRM applied individually or in combination could affect cell p21 protein expression. The data showed that the p21 protein is expressed more (3.4×) in the untreated tumor cells of the PE-CA/PJ49 vs. normal cells of the HUVEC line (625/184 pg/mL). Individually applied treatment with CisPt, 40 μM RSV or 15 μM CRM did not significantly affect the expression of p21 protein ($p = \text{non-significant}$) in normal HUVEC cells. Treatment of normal cells with 20 μM CisPt + 40 μM RSV induced an increase of p21 protein expression compared to untreated cells ($p < 0.029$) or to cells treated only with RSV (** $p < 0.0085$). A significant increase in p21 protein expression of HUVEC cells was recorded in the case of the combined treatment 5 μM CisPt + 15 μM CRM compared to untreated cells (** $p < 0.0048$) (Figure 3 and Table 4).

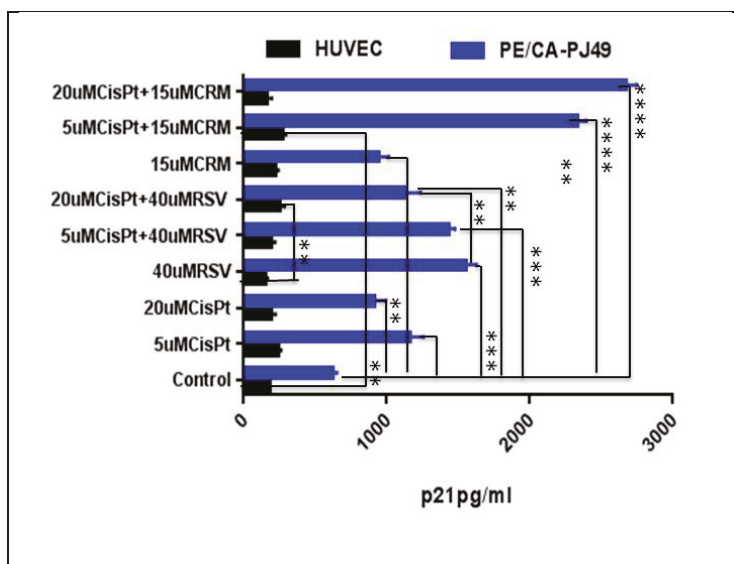


Figure 3. The total p21 protein expression (pg/mL) in normal cell line-HUVEC and in tumor cell line-PE/CA-PJ49 cells treated 24 h with CisPt and/or RSV, CRM. The experiments were performed in triplicates. Results are expressed as mean values of three determinations \pm standard deviation (SD). (** $p < 0.005$, *** $p < 0.0005$, **** $p < 0.00005$).

PE/CA-PJ49 tumour cells were treated 24 h with 5 μM CisPt (** $p = 0.0039$) or 20 μM CisPt (** $p = 0.0039$) showed a significant increase of total p21 protein expression compared to untreated cells (control). 40 μM RSV (**** $p < 0.0001$) applied alone, determined a significant increase of the total p21 protein expression in PE/CA-PJ49 cells versus control (Figure 3). On the contrary, after combined treatment with 5 μM CisPt + 40 μM RSV (* $p < 0.014$) versus treatment with 5 μM CisPt alone the results showed a slight increase in p21 expression of PE/CA-PJ49 cells. As shown in Figure 3 and Table 4 the simultaneous treatment with 20 μM CisPt + 40 μM RSV induced a significant decrease of p21 protein expression comparatively with the effect induced by RSV alone (** $p = 0.0058$). These results support the notion that the dominant effect is attributed to the high concentration of CisPt. Thus we can say that RSV can potentiate the induced effect of 5 μM CisPt but cannot counteract

the induced effects of treatment with a much higher concentration of CisPt on p21 protein expression in tumor cells.

Table 4. The effects of CisPt, RSV, CRM treatment applied alone or in combination for 24 h on the level of p21 protein expression (n-fold p21protein expression) in normal cell line-Huvec and in tumor cell line-PE/CA-PJ49. The n-fold p21expression was calculated using the formula: n-fold p21expression = p21 pg/mL treatment/p21 pg/mL control.

Treatment	p21 pg/mL HUVEC	n-fold p21 Protein Expression HUVEC	p21 pg/mL PE/CA-PJ49	n-fold p21 Protein Expression PE/CA-PJ49
Control	183	1	625	1
5 μ M CisPt	238	1.3	1157	1.85
20 μ M CisPt	195	1.07	915	1.46
40 μ M RSV	148	0.81	1550	2.48
5 μ M CisPt + 40 μ M RSV	196	1.07	1429	2.29
20 μ M CisPt + 40 μ M RSV	253	1.38	1124	1.80
15 μ M CRM	221	1.21	941	1.51
5 μ M CisPt + 15 μ M CRM	272	1.49	2335	3.74
20 μ M CisPt + 15 μ M CRM	164	0.90	2675	4.28

PE/CA-PJ49 tumor cells treatment with 15 μ M CRM led to a significant increase of the p21 protein expression compared to control (** $p = 0,0022$). Combined treatment 15 μ M CRM and 5 μ M CisPt (**** $p = 0.0001$) or 20 μ M CisPt (**** $p = 0.0001$) led to a much higher amplification of p21 protein expression compared to CisPt only-treated cells (Figure 3 and Table 4). Our data showed that in PE/CA-PJ49 tumor cells the effect induced by the CisPt and CRM was cumulative. In addition, the analysis reveal the potential of CRM to sustain and amplify the effect induced by CisPt treatment, regardless of the CisPt concentration used.

4.4. Modulation of P21 Gene Expression by Natural Compounds and/or Cisplatin Treatment

Changes of the P21 gene expression have been found in various types of malignancy including head and neck [65–67] but the impact of the P21 level on the disease progression and prognosis remains controversial. Therefore, we performed in vitro experiments to assess how natural compounds (RSV or CRM) modulated the P21 expression in head and neck tumor cells PE/CA-PJ49 versus normal cells HUVEC. Analysis of the expression level of P21 was performed by real-time qPCR assay in order to identify their role in response to chemotherapeutic agent-CisPt. Obtained data from this study may help define how P21 acts in modulating the DNA repair processes of tumor cells, in hope of finding new effective strategies in the treatment of head and neck cancer. Using real-time qPCR assay, we evaluated the P21 gene expression induced by CisPt and/or RSV, CRM treatment of HUVEC and PE/CA-PJ49 tumor cells. The data showed that RSV treatment acts differently on the two cell lines analyzed. RSV induces a slight decrease in P21 gene expression in HUVEC cells and an increase in the PE/CA-PJ49 tumor cells. Treatment with 5 μ M CisPt (* $p = 0.027$) or 20 μ M CisPt (** $p = 0.016$) induces an antagonist response compared to the effect induced by RSV treatment alone in P21 gene expression of normal HUVEC cells. The results obtained from the combined CisPt + RSV treatment show that RSV did not significantly modify the P21 gene expression generated by CisPt treatment in normal cells. CRM treatment applied alone did not affected P21 expression in HUVEC cells. The combined 5 μ M CisPt + 15 μ M CRM treatment showed a significant increase in P21 expression in normal cells (** $p = 0.019$ versus 15 μ M CRM). On the contrary, 20 μ M CisPt + 15 μ M CRM treatment of HUVEC cells induced a decrease of P21 gene expression compared with the effect induced by CRM alone (* $p = 0.021$) or 20 μ M CisPt (* $p = 0.013$) (Figure 4 and Table 5).

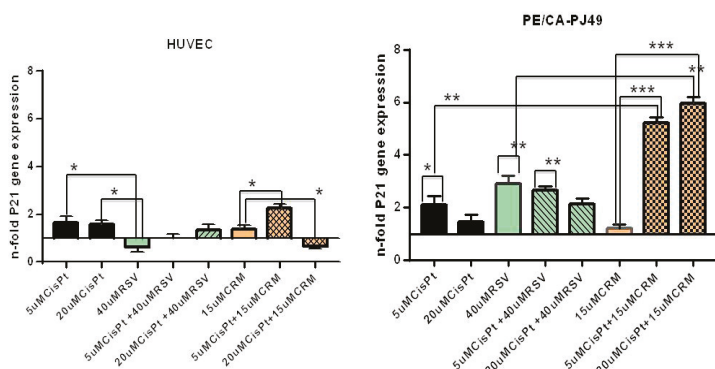


Figure 4. The effect of treatment with CisPt, RSV, CRM applied independently or in combination on P21 gene expression in tumor cells PE/CA-PJ49 compared to normal cells HUVEC. Each sample was performed in duplicate. The samples were analyzed using the formula $2^{-\Delta\Delta Ct}$ = gene expression. (* $p < 0.05$, ** $p < 0.005$, *** $p < 0.0005$).

Table 5. n-fold P21 gene expression in PE/CA-PJ49 tumor cells versus normal cells HUVEC treated 24 h with CisPt and/or RSV, CisPt and/or CRM. The results were obtained using gene reference HPRT.

Treatment	HUVEC	PE/CA-PJ49
Control	1	1
5 μM CisPt	1.64	2.0
20 μM CisPt	1.54	1.46
40 μM RSV	0.36	3.1
5 μM CisPt + 40 μM RSV	0.97	2.68
20 μM CisPt + 40 μM RSV	1.34	2.31
15 μM CRM	1.39	1.2
5 μM CisPt + 15 μM CRM	2.26	5.24
20 μM CisPt + 15 μM CRM	0.54	6.03

RSV alone induced a significant increase of P21 expression (** $p = 0.006$) while 5 μM CisPt ($p =$ non-significant) applied individually induced a slight increase of the P21 gene expression compared to untreated PE/CA-PJ49 tumor cells. The application of the combined treatment 5 μM CisPt + 40 μM RSV in tumor cells led to a significant increase in P21 gene expression compared to untreated cells (** $p = 0.002$). When using a higher concentration of CisPt together with RSV, a significant increase in P21 gene expression was observed in tumor cells versus control (** $p = 0.009$) or versus RSV (* $p = 0.046$) (Figure 4 and Table 5). These data support the modulatory role of RSV in tumor cells on the effect induced by 20 μM CisPt on the gene expression of P21 without influencing the effect induced by 5 μM CisPt.

Although CRM appears to induce a slight increase in P21 gene on the PE/CA-PJ49 tumor cells, this is not significantly different from P21 expression in untreated cells. The use of combination treatment with 5 μM CisPt + 15 μM CRM showed a significant increase in P21 in tumor cells (** $p = 0.0014$) compared to the effect induced by individual treatment with CRM. Analysis of the induced effect of 20 μM CisPt + 15 μM CRM in PE/CA-PJ49 tumor cells also showed a significant increase in P21 gene expression compared to the induced effect of CRM alone (** $p = 0.0009$) or compared to the 20 μM CisPt effect (** $p = 0.0018$) (Figure 4 and Table 5). These data demonstrate the ability of CRM to support the effect induced by CisPt treatment on P21 gene expression levels.

In conclusion, CisPt treatment led to an increase of the P21 gene expression level of in both lines. RSV treatment for 24 h had a different effect in PE-CA/PJ49 tumor cells (inducing an increase) versus the effect induced in normal HUVEC cells (induced a decrease) in P21 gene expression. CRM

alone amplified slightly P21 gene expression in both lines. Applied in combination with CisPt, CRM amplified the effect induced by 5 μ M CisPt in both lines, the effect being twice as high in tumor cells. When the high concentration of 20 μ M CisPt was used, the effects induced by CRM in tumor cells are the same as those recorded at CRM + 5 μ M CisPt. However, in the case of normal cells, 20 μ M CisPt + CRM treatment caused a drastic decrease in P21 gene expression, probably due to the toxic effect of CisPt, which killed a large number of normal HUVEC cells.

4.5. Effects of the Natural Compounds (RSV,CRM) on Cell Cycle Phases Distribution in Cisplatin Treated Cells

Cell cycle phases distribution was evaluated to further characterise the cytotoxic effect of CisPt and/or RSV, CRM on tumor cells PE-CA/PJ49 compared with HUVEC normal cells.

PE/CA-PJ49 tumor cells and HUVEC normal cells were treated with 5 μ M or 20 μ M CisPt in the presence or absence of 40 μ M RSV or 15 μ M CRM for 24 h. The progression through the cell cycle phases induced by treatment were evaluated by flow cytometry using a FACSCanto II flow cytometer. Data analysis was performed using the ModFit 3.2 program which offers the possibility of evaluating the cell cycle phases distribution (G0/G1, S, G2 + M).

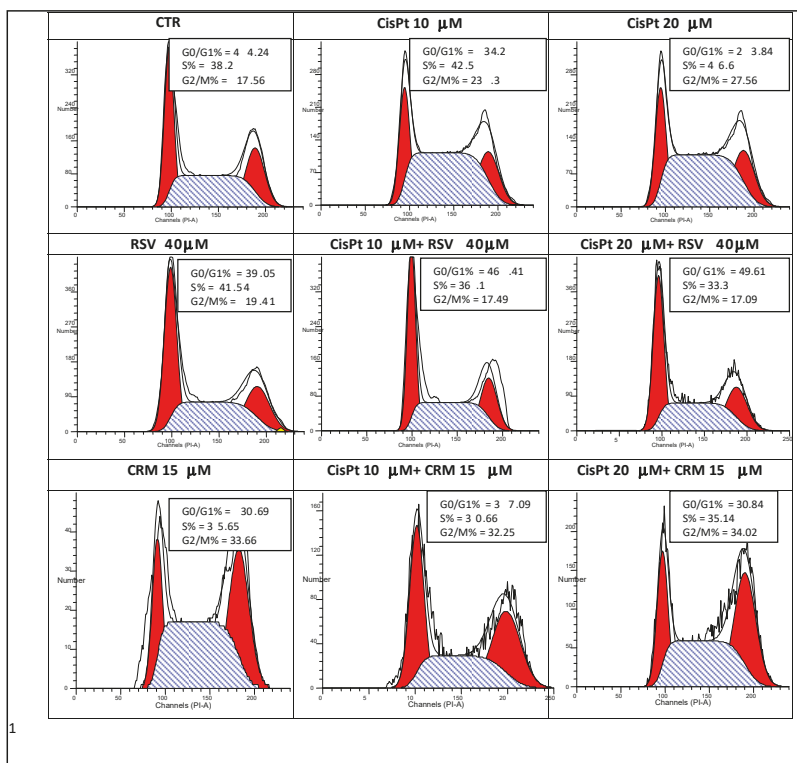
The results obtained in the case of the tumor cells PE-CA/PJ49 revealed that single 5 μ M or 20 μ M CisPt applied treatment decreased of the phase G0/G1 (24.2% or 22.84% versus 41.24 in untreated cells) associated with a slight increase of the synthesis phase (50.5% or 49.6% versus 43.2% in control cells) and followed by the increase of G2+M phase (25.3% or 27.5% versus 15.5% in untreated cells) (Figure 5A,B). The effects induced by the 40 μ M RSV treatment in PE/CA-PJ49 tumor cells shown a small decrease of G0/G1 phase (41.24 to 39.05%) associated with an increase in phase S (38.1 to 41.52%) and phase G2 + M (17.56 to 19.41%) compared to untreated cells (Control). Combined CisPt treatment with RSV applied to PE/CA-PJ49 induced an increase of G0/G1 phase (48.4% compared with the untreated cells 41.2%) and a decrease of the synthesis phase (34.1% versus 43.2% in control). Cell cycle phases distribution did not differ significantly when use different concentration of CisPt (5 or 20 μ M) and RSV 40 μ M are combined. Treatment of PE/CA-PJ49 tumor cells with 15 μ M CRM alone or in combination with CisPt induced a decrease in synthesis phase (CRM = 38.6%; CisPt 5 μ M + CRM = 33.6%; CisPt 20 μ M + CRM = 35.14%; versus control = 43.2%) accompanied by an increase of the G2 + M phase (CRM=33.6%; CisPt 5 μ M + CRM = 32.2%; CisPt 20 μ M + CRM = 34.02%; versus control = 15.5%) (Figure 5A,B). These results suggested that the combined CisPt treatment with CRM induced a tendency to block the cell cycle in G2+M phase in tumor cells.

The HUVEC cells used as the normal line showed a distribution in the synthesis phase of less than 20% (untreated cells). The treatments applied individually 5 μ M or 20 μ M CisPt caused an increase of the synthesis phase to 29.2% and 39.65%, respectively, compared to 19.1% recorded in untreated cells (Control). These data show that treatment with CisPt affects normal HUVEC cells especially at higher concentrations. 40 μ M RSV and 15 μ M CRM did not appear to significantly affect the cell cycle when applied individually, and cannot influence the effect induced by CisPt treatment when used in combination (Figure 6A,B).

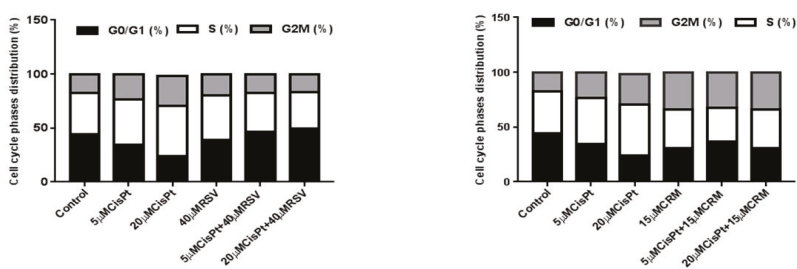
4.6. Effects of the Natural Compounds (RSV,CRM) on the Apoptotic Process in Cisplatin-Treated Cells

Apoptosis can be seen as an efficient method of preventing malignant transformation, as it ensures the removal of cells which present with genetic alterations. Deficient apoptosis can promote the development of cancer, both through the accumulation of cells found during division and the blocking of the removal of cells with high malignant potential genetic variations. The factors which determine the cells to follow one of three possible pathways are not yet known – the start of apoptosis after cellular injury, the repair of the lesion or the continuation of the cellular cycle. Many therapeutical agents have anti-tumoral effects generated by their capacity to activate the apoptotic process [68]. Tumoral cells PE/CA-PJ49 and normal cells HUVEC were treated for 24 h with CisPt, RSV, CRM in order to detect the effect induced by treatment with CisPt on tumor cells in the presence or absence of natural compounds (RSV or CRM). The flow cytometric analysis was performed using DIVA 6.2

software and allowed to discriminate viable cells (FITC⁻PI⁻ = Q3) from necrotic cells (FITC⁻PI⁺ = Q1) and early apoptosis (FITC⁺PI⁻ = Q4) from late apoptosis (FITC⁺PI⁺ = Q2).



(A)



CisPt and/or RSV treatments

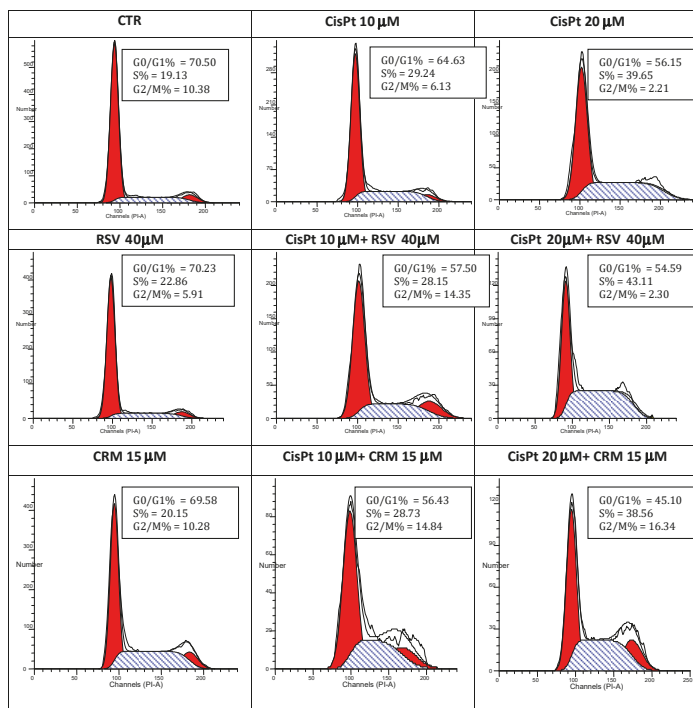
CisPt and/or CRM treatments

(B)

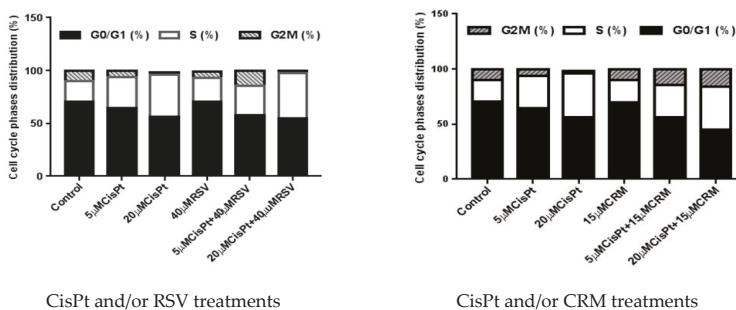
Figure 5. The effect of treatments with CisPt, RSV, CRM applied independently or in combination on tumor cells PE/CA-PJ49 on cell cycle phases distribution. (A) flow cytometry histograms; (B) cell cycle phases distribution (%).

Analysis the RSV or CRM effects on the apoptotic process of tumor cells PE/CA-PJ49 is shown in the Table 6 and Figure 7. Our results show that the untreated tumor cells PE/CA-PJ49 (Control) had low total apoptosis (Q2 + Q4 = 2%). Treatment with 40 μM RSV induced a raise of total apoptosis to

27.2%, much higher than the total apoptosis induced by 5 μ M CisPt (12.5%) or 20 μ M CisPt (17.4%). In the case of simultaneous treatment with CisPt and RSV a raise of the total apoptosis was registered (5 μ M CisPt + RSV = 31.1%; 20 μ M CisPt + RSV = 34.9%) and it seems to have been generated by the presence of RSV.



(A)



(B)

Figure 6. The effect of treatments with CisPt, RSV, CRM applied independently or in combination on normal cells HUVEC on the cell cycle phases distribution. (A) flow cytometry histograms; (B) cell cycle phases distribution (%).

Table 6. Apoptosis of PE/CA-PJ49 tumor cells induced by 24 h treatment with CisPt and/or RSV, CRM.

Treatment	Necrosis = Q1 (%)	Early Apoptosis = Q4 (%)	Late Apoptosis = Q2 (%)	Total Apoptosis = Q2 + Q4 (%)
Control	0.2	1.8	0.3	2.1
5 μM CisPt	2.1	11.3	1.2	12.5
20 μM CisPt	1.2	15.3	2.1	17.4
40 μM RSV	5.4	17.7	9.5	27.2
5 μM CisPt + 40 μM RSV	9.4	19.9	11.2	31.1
20 μM CisPt + 40 μM RSV	6.5	21.2	13.7	34.9
15 μM CRM	6.7	19.1	9.1	28.2
5 μM CisPt + 15 μM CRM	7.7	26.4	12.3	38.7
20 μM CisPt + 15 μM CRM	6.8	28.4	11.9	40.3

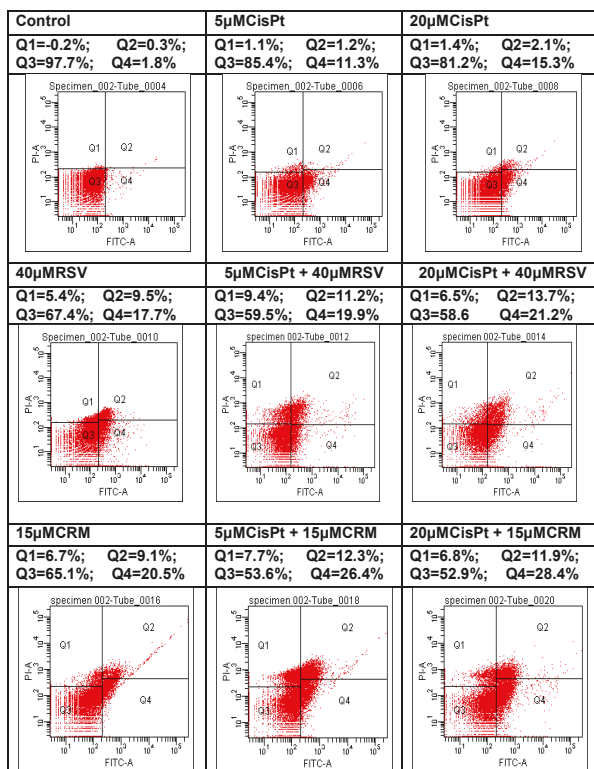


Figure 7. Natural compounds (RSV or CRM) effects on the apoptotic process of PE/CA-PJ49 tumor cells treated 24 h with CisPt and/or RSV or CRM (Dot-plot analysis).

Treatment for 24 h with 15μMCRM (29.6%) has determined an increase of the total apoptosis in the tumor cells PE/CA-PJ49. Combined treatment CRM with CisPt applied to the PE/CA-PJ49 cells for 24 h has determined a raise of total apoptosis to 28,7% when using 5 μM CisPt or to 40,3% when using 20 μM CisPt (Table 6 and Figure 7).

Effects of the natural compounds RSV or CRM on apoptosis process in normal HUVEC cells were analyzed after applying the same treatment scheme used in the case of PE/CA-PJ49 tumor cells. As shown in Table 7 and Figure 8, treatment with 5 μM or 20 μM CisPt, RSV or CRM did not significantly modify the apoptosis, compared to untreated HUVEC cells (Control). However, combined treatment led to an increase of the apoptotic process. Thus, 5 μM and 20 μM CisPt combined with RSV have determined apoptosis in 14% and 21.6% of the analysed cellular population, a value that was double the one obtained when using individual stimuli (Table 7 and Figure 8). Combined treatment CRM with 5 μM or 20 μM CisPt has induced a raise of apoptosis in 19,7% or 23.9% of the analysed cellular

population (Table 7 and Figure 8). Comparative analysis of the obtained data shows that both RSV and CRM have the capacity to stimulate the apoptosis of PE/CA-PJ49 tumor cells without significantly affecting the apoptotic process of normal HUVEC cells (RSV-PE/CA-PJ49 versus RSV HUVEC = 27.2% versus 5.1%; CRM-PE/CA-PJ49 versus CRM-HUVEC = 28.2% versus 7.2%). In conclusion, the two analyzed natural compounds (RSV and CRM) have the ability to amplify the apoptotic process induced by CisPt treatment in PE/CA-PJ49 tumor cells.

Table 7. Apoptosis of HUVEC cells induced by 24 h treatment with CisPt and/or RSV, CRM.

Treatment	Necrosis = Q1 (%)	Early Apoptosis = Q4 (%)	Apoptoza Tarzie = Q2 (%)	Apoptoza Totala = Q2+Q4 (%)
Control	1.1	4.5	0.2	4.7
5 μM CisPt	1.6	5.6	0.5	6.1
20 μM CisPt	1.5	7.7	0.5	8.2
40 μM RSV	1.2	4.8	0.3	5.1
5 μM CisPt + 40 μM RSV	0.4	12.8	1.2	14
20 μM CisPt + 40 μM RSV	2.5	14.9	6.7	21.6
15 μM CRM	2.6	6.7	0.5	7.2
5 μM CisPt + 15 μM CRM	5.7	13.4	6.3	19.7
20 μM CisPt + 15 μM CRM	3.3	19.5	4.4	23.9

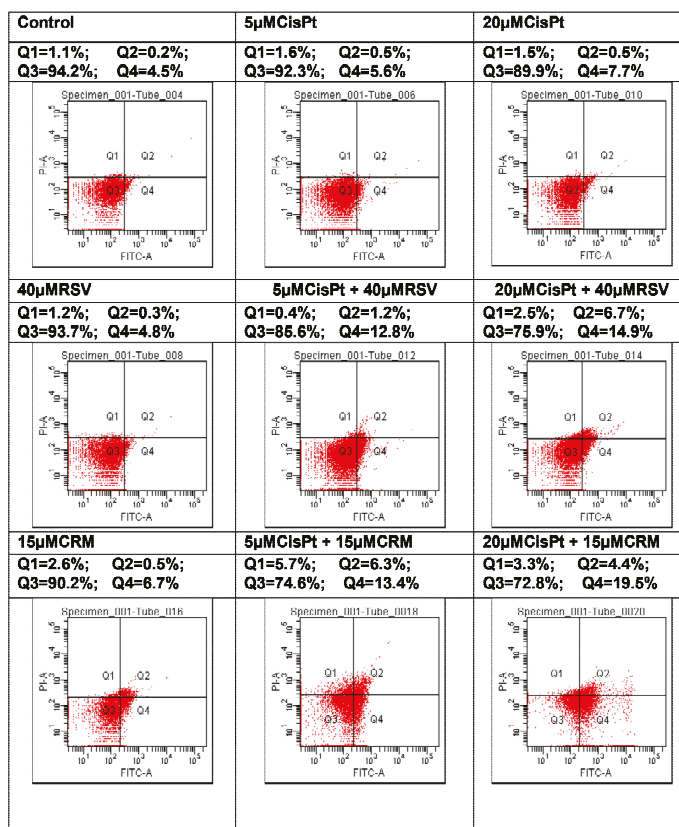


Figure 8. Natural compounds (RSV or CRM) effects on the apoptotic process on normal HUVEC cells treated 24 h with CisPt (Dot-plot analysis.).

5. Discussion

The toxic effects of CisPt are dose-dependent and affect the kidneys and bone marrow, which are accompanied by an increase in transaminases and serum creatinine. In addition, CisPt therapy alone has not been found to be effective in treating patients with HNSCC. Cisplatin efficacy appear to be more increased in combination with other chemotherapeutic agents and/or radiation therapy, but side effects or resistance to these drugs are often mentioned [69,70]. This observation suggests that the combination of cisplatin with other anti-tumor agents could be much more effective in the treatment and evolution of head and neck cancer. Some natural compounds due to their chemosensitizing potential, antitumoral activity and ability to reduce the side effects of drugs used in conventional cancer therapy protocols promise to be one of the important components of combinatorial therapy [71,72]. Natural compounds must be well tolerated and have long-lasting benefits. They can also act at the level of different signaling pathways responsible for the tumorigenesis process in HNSCC, which recommends them as agents with multiple molecular targets [73,74]. The experimental approach of this study focused on the enhancing chemotherapy response while lowering side effects and the incidence of drug resistance. To design novel combinatorial therapeutic strategy for improving the patients' prognosis and response to chemotherapy is needed. To streamline the response to chemotherapy, we analyzed how the use of CisPt in combination with CRM and RSV may influence some cellular processes such as proliferation, P21 gene expression, apoptotic process, and cell cycle development in HNSCC cell line (PE/CA-PJ49) compared to a normal cell line (HUVEC). The results showed that the viability of the tumor and normal cells was affected by CisPt treatment in the same way in both cell lines in a concentration-dependent manner. RSV or CRM treatment affected the viability of tumor cells PE/CA-PJ49 more than of normal HUVEC cells. RSV and CRM have the ability to amplify the inhibitory effect of 5 μ M CisPt induced on PE-CA/PJ49 tumor cells without significantly affecting the 5 μ M CisPt-induced effect in normal cells. The use of a high concentration of CisPt (20 μ M) together with a natural compound (CRM or RSV) led to the observation that the effect induced by CisPt on cell proliferation is dominant in both tumor cells and normal cells. Because p21 can act as a tumor suppressor or a tumor-promoting protein [75], and this makes more difficult to establish its function in the evolution of cancer we analysed the role of P21 in response to chemotherapy. Using ELISA and RT-PCR were evaluated protein and gene P21 expression in tumor PE/CA-PJ49 cells and normal HUVEC cells treated with CisPt in presence of RSV or CRM. A significant increase of total p21 protein expression was recorded in PE/CA-PJ49 tumor cells treated with 5 μ M CisPt and 20 μ M CisPt compared with the effect induced by RSV applied alone. However, it was observed that RSV can potentiate the induced effect of 5 μ M CisPt but cannot influence the effects induced by 20 μ M CisPt treatment on p21 protein expression in tumor cells. In PE/CA-PJ49 the CRM treatment amplified the increase of p21 protein expression induced by CisPt treatment, regardless the CisPt concentration. Increased p21 expression was correlated with a decreased of proliferative activity of tumor cells and a good response to CisPt therapy.

Analysis of P21 gene expression level showed that CisPt treatment induced an increase of P21 expression in both lines. RSV treatment influenced in a different manner P21 expression, inducing an increase in PE/CA-PJ49 and a decrease in normal HUVEC cells. In combination with CisPt, RSV did not influence the CisPt-induced effect in HUVEC cells. On the contrary in PE/CA-PJ49 tumor cells, using the combination CisPt+RSV induced an increase in P21 gene expression and this way, RSV can modulate the effect induced by 20 μ M CisPt. CRM alone did not modify the P21 gene expression in both lines. In combination with CisPt, CRM amplified the effect induced by 5 μ M CisPt in both lines, the effect being higher in tumor cells. Not significant differences were observed in P21 expression in tumor cells when used the high concentrations of CisPt (20 μ M). In normal cells was recorded a drastic decrease in P21 gene expression upon treatment with 20 μ M CisPt + CRM. These data support the toxic effect of CisPt used in high concentration on normal cells. The treatment of tumor cells with RSV or CRM in the presence of CisPt induced an increase in protein and gene expression levels of p21.

These results may be associated with a more effective response of tumor cells to treatment with lower concentrations of CisPt using RSV or CRM as therapeutic adjuvants.

The cell cycle ensures the cell can proliferate and grow by passing through the G1, S, G2 and M phases. Cancer cells reveal disorders in the cell cycle progression which contributes to exacerbate cell proliferation and to loss of genomic integrity. Treatment with 5 μ M or 20 μ M CisPt applied alone on tumor cells induced a slight transition from G1 to S phases accompanied by the increase of the G2+M phase (25.3% or 27.5% versus 15.5% in untreated cells). Cell cycle phases distribution did not differ significantly when different concentrations of CisPt (5 or 20 μ M) were used. Treatment of PE/CA-PJ49 tumor cells with 40 μ M RSV did not affect significantly the cell cycle phases compared to untreated cells. PE/CA-PJ49 cells treated with CisPt + RSV showed an increase of the G0/G1 phase and a decrease in the S phase. Treatment of PE/CA-PJ49 tumor cells with 15 μ M CRM alone or in combination with CisPt induced a decrease the number of cells in S phase which was accompanied the massive blockage of cells in G2/M phase. In addition, the results provide evidence that RSV and CRM induce an increase in the apoptotic process of tumor cells. Interaction of RSV or CRM with CisPt in triggering tumor cells apoptosis indicated the amplifier role of the used natural compounds with respect to cisplatin effect. Therefore, associated chemotherapy of CisPt with natural compounds (RSV or CRM) as adjuvants might have a beneficial effect in decreasing the CisPt doses and in reducing its adverse reactions.

6. Conclusions

In conclusion, the results suggest that RSV and CRM act against proliferation and sustain the effects of cisplatin by the induction of cell cycle arrest, amplification of DNA damage and contributing to cancer cell destruction by increasing the apoptotic process. In addition, RSV and CRM amplify the expression of P21 in tumor cells and might contribute to increasing the sensitivity to cisplatin.

Author Contributions: G.G.P.-M. had equal contribution with M.B. in designed the research, data acquisition, analysis and interpretation of data, and wrote the manuscript. V.R., R.H. and C.D.S. performed the experiments, data acquisition, analysis and interpretation of data and manuscript drafting. N.R. and C.C.D. contributed to statistical analysis, critical revision of the manuscript for important intellectual content. All authors have read and agreed to the published version of the manuscript.

Funding: This research was funded by Grant PN-III-P1-1.2-PCCDI-2017-0341/2018 and Competitiveness Operational Programme (COP) A1.1.4. Grant ID: P_37_798 MyeloAL-EDiaProT, Contract 149/26.10.2016, (SMIS: 106774) and ERAPerMed_Joint Transnational Call for Proposal (2019) for Personalised Medicine: Multidisciplinary Research Towards Implementation, BronchoBOC, Contract 140/2020.

Acknowledgments: Competitiveness Operational Programme (COP) A1.1.4. ID: P_37_798 MyeloAL-EDiaProT, Contract 149/26.10.2016, (SMIS: 106774), MyeloAL

Conflicts of Interest: The authors declare no conflict of interest.

References

1. Lawrence, M.S. Comprehensive genomic characterization of head and neck squamous cell carcinomas. *Nature* **2015**, *517*, 576–582.
2. Siegel, R.L.; Miller, K.D.; Jemal, A. Cancer statistics, 2017. *CA Cancer J. Clin.* **2017**, *67*, 7–30. [[CrossRef](#)] [[PubMed](#)]
3. Leemans, C.R.; Snijders, P.J.F.; Brakenhoff, R.H. The molecular landscape of head and neck cancer. *Nat. Rev. Cancer* **2018**, *18*, 269–282. [[CrossRef](#)] [[PubMed](#)]
4. Achkar, I.W.; Abdulrahman, N.; Al-Sulaiti, H.; Joseph, J.M.; Uddin, S.; Mraiche, F. Cisplatin based therapy: The role of the mitogen activated protein kinase signaling pathway. *J. Transl. Med.* **2018**, *16*, 96. [[CrossRef](#)] [[PubMed](#)]
5. Thai, A.A.; Rischin, D. High-dose cisplatin for head and neck cancer lives on. *J. Clin. Oncol.* **2018**, *36*, 1055–1057. [[CrossRef](#)]
6. Yang, Z.; Liao, J.; Carter-Cooper, B.A.; Lapidus, R.G.; Cullen, K.J.; Dan, H. Regulation of cisplatin-resistant head and neck squamous cell carcinoma by the SRC/ETS-1 signaling pathway. *BMC Cancer* **2019**, *19*, 485. [[CrossRef](#)]

7. Gerhards, N.M.; Rottenberg, S. New tools for old drugs: Functional genetic screens to optimize current chemotherapy. *Drug Resist. Updat.* **2018**, *36*, 30–46. [[CrossRef](#)]
8. Vermorken, J.B.; Remenat, E.; Van Herpen, C.; Gorlia, T.; Mesia, R.; Degardin, M.; Stewart, J.S.; Jelić, S.; Betka, J.; Preiss, J.H.; et al. Cisplatin, fluorouracil, and docetaxel in unresectable head and neck cancer. *N. Engl. J. Med.* **2007**, *357*, 1695–1704. [[CrossRef](#)]
9. Zhang, Q.Y.; Wang, F.X.; Jia, K.K.; Kong, L.D. Natural product interventions for chemotherapy and radiotherapy-induced side effects. *Front. Pharmacol.* **2018**, *9*. [[CrossRef](#)]
10. Abotaleb, M.; Kubatka, P.; Caprnda, M.; Varghese, E.; Zolakova, B.; Zubor, P.; Opatřilová, R.; Kruzliak, P.; Stefanicka, P.; Büsselberg, D. Chemotherapeutic agents for the treatment of metastatic breast cancer: An update. *Biomed. Pharmacother.* **2018**, *101*, 458–477. [[CrossRef](#)]
11. Ion, G.; Fazio, K.; Akinsete, J.A.; Hardman, W. Effects of canola and corn oil mimetic on Jurkat cells. *Lipids Health Dis.* **2011**, *10*, 90. [[CrossRef](#)] [[PubMed](#)]
12. Hotnog, D.; Mihaila, M.; Botezatu, A.; Matei, G.G.; Hotnog, C.; Anton, G.; Bostan, M.; Brasoveanu, L.I. Genistein potentiates the apoptotic effect of 5-fluorouracil in colon cancer cell lines. *Rom. Biotech. Lett.* **2013**, *18*, 8751–8760.
13. Radu, N.; Roman, V.; Bostan, M.; Radu, E.; Tanasescu, C. Influence of some spice food based bioproducts on human monocytic cells line type THP-1. *Mol. Cryst. Liq. Cryst.* **2017**, *655*, 114–123. [[CrossRef](#)]
14. Chiou, C.T.; Wang, K.C.; Yang, Y.C.; Huang, C.L.; Yang, S.H.; Kuo, Y.H.; Huang, N.K. Liu Jun Zi Tang—A potential, multi-herbal complementary therapy for chemotherapy-induced neurotoxicity. *Int. J. Mol. Sci.* **2018**, *19*, 1258. [[CrossRef](#)] [[PubMed](#)]
15. Zhou, Y.; Zheng, J.; Li, Y.; Xu, D.P.; Li, S.; Chen, Y.M.; Li, H.B. Natural polyphenols for prevention and treatment of cancer. *Nutrients* **2016**, *8*, 515. [[CrossRef](#)]
16. Grosso, G.; Bella, F.; Godos, J.; Sciacca, S.; Del Rio, D.; Ray, S.; Galvano, F.; Giovannucci, E.L. Possible role of diet in cancer: Systematic review and multiple meta-analyses of dietary patterns, lifestyle factors, and cancer risk. *Nutr. Rev.* **2017**, *75*, 405–419. [[CrossRef](#)]
17. Kumar, G.; Mittal, S.; Sak, K.; Tuli, H.S. Molecular mechanisms underlying chemopreventive potential of curcumin: Current challenges and future perspectives. *Life Sci.* **2016**, *148*, 313–328. [[CrossRef](#)]
18. Teow, S.Y.; Liew, K.; Ali, S.A.; Khoo, A.S.B.; Peh, S.C. Antibacterial action of curcumin against staphylococcus aureus: A brief review. *J. Trop. Med.* **2016**, *2016*, 1–10. [[CrossRef](#)]
19. Farhood, B.; Mortezaee, K.; Goradel, N.H.; Khanlarkhani, N.; Salehi, E.; Nashtaei, M.S.; Najafi, M.; Sahebkar, A. Curcumin as an anti-inflammatory agent: Implications to radiotherapy and chemotherapy. *J. Cell. Physiol.* **2019**, *234*, 5728–5740. [[CrossRef](#)]
20. Liu, Z.; Huang, P.; Law, S.; Tian, H.; Leung, W.; Xu, C. Preventive effect of curcumin against chemotherapy-induced side-effects. *Front. Pharmacol.* **2018**, *9*. [[CrossRef](#)]
21. Shanmugam, M.K.; Rane, G.; Mathi, K.M.; Arfuso, F.; Chinnathambi, A.; Zayed, M.E.; Alharbi, S.A.; Tan, B.K.H.; Kumar, A.P.; Sethi, G. The multifaceted role of curcumin in cancer prevention and treatment. *Molecules* **2015**, *20*, 2728–2769. [[CrossRef](#)] [[PubMed](#)]
22. Teiten, M.H.; Eifes, S.; Dicato, M.; Diederich, M. Curcumin—The paradigm of a multi-target natural compound with applications in cancer prevention and treatment. *Toxins* **2010**, *2*, 128–162. [[CrossRef](#)] [[PubMed](#)]
23. Rahmani, A.H.; Alsahli, M.A.; Aly, S.M.; Khan, M.A.; Aldebasi, Y.H. Role of curcumin in disease prevention and treatment. *Adv. Biomed. Res.* **2018**, *7*, 38. [[CrossRef](#)] [[PubMed](#)]
24. Garg, T.; Yadav, V.K. Effects of resveratrol as an anticancer agent—A systematic review. *Int. J. Pharm. Bio. Sci.* **2014**, *5*, 534–542.
25. Aluyen, J.K.; Ton, Q.N.; Tran, T.; Yang, A.E.; Gottlieb, H.B.; Bellanger, R.A. Resveratrol: Potential as anticancer agent. *J. Diet. Suppl.* **2012**, *9*, 45–56. [[CrossRef](#)]
26. Crandall, J.P.; Barzilai, N. Exploring the promise of resveratrol: Where do we go from here? *Diabetes* **2013**, *62*, 1022–1023. [[CrossRef](#)]
27. Santandreu, F.M.; Valle, A.; Oliver, J.; Roca, P. Resveratrol potentiates the cytotoxic oxidative stress induced by chemotherapy in human colon cancer cells. *Cell. Physiol. Biochem.* **2011**, *28*, 219–228. [[CrossRef](#)]
28. Fouad, M.; Agha, A.; Al Merzabani, M.; Shouman, S.A. Resveratrol inhibits proliferation, angiogenesis and induces apoptosis in colon cancer cells. *Hum. Exp. Toxicol.* **2013**, *32*, 1067–1080. [[CrossRef](#)]

29. Mihaila, M.; Bostan, M.; Hotnog, D.; Ferdes, M.; Brasoveanu, L.I. Real-time analysis of quercetin, resveratrol and/or doxorubicin effects in MCF-7 cells. *Rom. Biotech. Lett.* **2013**, *18*, 8106–8114.
30. McCubrey, J.A.; Lertpiriyapong, K.; Steelman, L.S.; Abrams, S.L.; Yang, L.V.; Murata, R.M. Effects of resveratrol, curcumin, ber-berine and other nutraceuticals on aging, cancer development, cancer stem cells and microRNAs. *Aging* **2017**, *9*, 1477–1536. [[CrossRef](#)]
31. Fillies, T.; Woltering, M.; Brandt, B.; Van Diest, J.P.; Werkmeister, R.; Joos, U.; Buerger, H. Cell cycle regulating proteins p21 and p27 in prognosis of oral squamous cell carcinomas. *Oncol. Rep.* **2007**, *17*, 355–359. [[CrossRef](#)] [[PubMed](#)]
32. Huang, Y.; Corbley, M.J.; Tang, Z.; Yang, L.; Peng, Y.; Zhang, Z.Y.; Tong, T.J. Down-regulation of p21WAF1 promotes apoptosis in senescent human fibroblasts: Involvement of retinoblastoma protein phosphorylation and delay of cellular aging. *J. Cell. Physiol.* **2004**, *201*, 483–491. [[CrossRef](#)] [[PubMed](#)]
33. Kreis, N.N.; Louwen, F.; Yuan, J. Less understood issues: P21Cip1 in mitosis and its therapeutic potential. *Oncogene* **2015**, *34*, 1758–1767. [[CrossRef](#)] [[PubMed](#)]
34. Gartel, A.L. Is p21 an oncogene? *Mol. Cancer Ther.* **2006**, *5*, 1385–1386. [[CrossRef](#)]
35. Efeyan, A.; Collado, M.; Velasco-Miguel, S.; Serrano, M. Genetic dissection of the role of p21Cip1/Waf1 in p53-mediated tumour suppression. *Oncogene* **2007**, *26*, 1645–1649. [[CrossRef](#)]
36. Ishida, M.; Morita, M.; Saeki, H.; Ohga, T.; Sadanaga, N.; Watanabe, M.; Kakeji, Y.; Maehara, Y. Expression of p53 and p21 and the clinical response for hyperthermochemoradiotherapy in patients with squamous cell carcinoma of the esophagus. *Anticancer. Res.* **2007**, *27*, 3501–3506.
37. Fisher, C.A.; Jung, M.; Zlobec, I.; Green, E.; Storck, C.; Tornillo, L.; Lugli, A.; Wolfensberger, M.; Terracciano, L.M. Co-overexpression of P21 and Ki67 in Head and Neck squamous cell carcinoma relative to a significant poor prognosis. *Head Neck* **2011**, *33*, 267–273. [[CrossRef](#)]
38. Sadaf, S.; Loya, A.; Mushtaq, S.; Akhter, N.; Hussain, R.; Jamshed, A. Correlation of P21 expression in head and neck squamous cell carcinoma with clinicopathologic and prognostic parameters. *J. Cancer Allied Spec.* **2015**, *1*, 5. [[CrossRef](#)]
39. Shamlou, B.; Usluer, S. P21 in cancer research. *Cancers* **2019**, *11*, 1178. [[CrossRef](#)]
40. Staalesen, V.; Leirvaag, B.; Lillehaug, J.R.; Lonning, P.E. Genetic and epigenetic changes in p21 and p21B do not correlate with resistance to doxorubicin or mitomycin and 5-fluorouracil in locally advanced breast cancer. *Clin. Cancer Res.* **2004**, *10*, 3438–3443. [[CrossRef](#)]
41. Gottifredi, V.; McKinney, K.; Poyurovsky, M.V.; Prives, C. Decreased p21 levels are required for efficient restart of DNA synthesis after S phase block. *J. Biol. Chem.* **2004**, *279*, 5802–5810. [[CrossRef](#)] [[PubMed](#)]
42. Alsahafi, E.; Begg, K.; Amelio, I.; Raulf, N.; Lucarelli, P.; Sauter, T.; Tavassoli, M. Clinical update on head and neck cancer: Molecular biology and ongoing challenges. *Cell Death Dis.* **2019**, *10*, 540. [[CrossRef](#)] [[PubMed](#)]
43. Rahman, M.A.; Amin, A.R.M.R.; Shin, D.M. Chemopreventive potential of natural compounds in head and neck cancer. *Nutr. Cancer* **2010**, *62*, 973–987. [[CrossRef](#)] [[PubMed](#)]
44. Saba, N.F.; Haigentz, M.; Vermorken, J.B.; Strojjan, P.; Bossi, P.; Rinaldo, A.; Takes, R.P.; Ferlito, A. Prevention of head and neck squamous cell carcinoma: Removing the “chemo” from “chemoprevention”. *Oral Oncol.* **2015**, *51*, 112–118. [[CrossRef](#)] [[PubMed](#)]
45. Crooker, K.; Aliani, R.; Ananth, M.; Arnold, L.; Anant, S.; Thomas, S.M. A review of promising natural chemopreventive agents for head and neck cancer. *Cancer Prev. Res.* **2018**, *11*, 441–450. [[CrossRef](#)]
46. Petrica-Matei, G.G.; Roman, V.; Mihaila, M.; Hotnog, C.M.; Brasoveanu, L.I.; Bostan, M. Role of p38-mitogen-activated protein kinase in modulation of response to therapy in FaDu human pharyngeal carcinoma cell line. *Rom. Biotech. Lett* **2019**, *24*, 118–128. [[CrossRef](#)]
47. Bostan, M.; Petrica-Matei, G.G.; Ion, G.; Radu, N.; Mihaila, M.; Hainarosie, R.; Brasoveanu, L.I.; Roman, V.; Constantin, C.; Neagu, M.T. Cisplatin effect on head and neck squamous cell carcinoma cells is modulated by ERK1/2 protein kinases. *Exp. Ther. Med.* **2019**, *18*, 5041–5051. [[CrossRef](#)]
48. Sylvester, P.W. Optimization of the tetrazolium dye (MTT) colorimetric assay for cellular growth and viability. *Methods Mol. Biol.* **2011**, *716*, 157–168. [[CrossRef](#)]
49. Bostan, M.; Radu, N.; Babeanu, N.; Zaharie, M.G.; Horatiu Tanasescu, C.A. Biological properties of a biomaterial obtained from Syzygiumaromaticum. *Mol. Cryst. Liq. Cryst.* **2019**, *695*, 45–52. [[CrossRef](#)]
50. Machana, S.; Weerapreeyakul, N.; Barusrux, S.; Nonpunya, A.; Sripanidkulchai, B.; Thitimetharoch, T. Cytotoxic and apoptotic effects of six herbal plants against the human hepatocarcinoma (HepG2) cell line. *Chin. Med.* **2011**, *6*, 39. [[CrossRef](#)]

51. Prayong, P.; Barusux, S.; Weerapreeyakul, N. Cytotoxic activity screening of some indigenous Thai plants. *Fitoterapia* **2008**, *79*, 598–601. [[CrossRef](#)] [[PubMed](#)]
52. Hotnog, C.M.; Mihaila, M.; Puiu, L.; Botezatu, A.; Roman, V.; Popescu, I.D.; Bostan, M.; Brasoveanu, L.I. Modulation of the interplay between p53, ICAM-1 and VEGF in drug-treated LoVo colon cancer cells. *Rom. Biotechnol. Lett.* **2019**, *24*, 261–270. [[CrossRef](#)]
53. Ciulu-Costinescu, F. Antimicrobial assay of a capsaicin— α -cyclodextrin inclusion complex against planktonic and adherent cells. *Farmacia* **2019**, *67*, 496–503. [[CrossRef](#)]
54. Zhao, G.; Bae, J.Y.; Zheng, Z.; Park, H.S.; Chung, K.Y.; Roh, M.R.; Jin, Z. Overexpression and implications of melanoma-associated antigen A12 in pathogenesis of human cutaneous squamous cell carcinoma. *Anticancer. Res.* **2019**, *39*, 1849–1857. [[CrossRef](#)] [[PubMed](#)]
55. Tak, J.; Sabarwal, A.; Shyanti, R.K.; Singh, R.P. Berberine enhances posttranslational protein stability of p21/cip1 in breast cancer cells via down-regulation of Akt. *Mol. Cell. Biochem.* **2019**, *458*, 49–59. [[CrossRef](#)]
56. Bundscherer, A.C.; Malsy, M.; Lange, R.; Hofmann, P.; Metterlein, T.; Graf, B.M.; Gruber, M. Cell harvesting method influences results of apoptosis analysis by annexin V staining. *Anticancer. Res.* **2013**, *33*, 3201–3204.
57. Roman, V.; Radu, N.; Bostan, M.; Popa, O.; Tanasescu, C.A.H. Effect of *Melaleuca alternifolia* bioproduct on acute monocytic leukemia cells line. *Mol. Cryst. Liq. Cryst.* **2019**, *695*, 29–36. [[CrossRef](#)]
58. Iancu, I.V.; Botezatu, A.; Plesa, A.; Huica, I.; Fudulu, A.; Albulescu, A.; Bostan, M.; Mihaila, M.; Grancea, C.; Manda, D.A.; et al. Alterations of regulatory factors and DNA methylation pattern in thyroid cancer. *Cancer Biomarkers* **2020**, *28*, 255–268. [[CrossRef](#)]
59. Petrică-Matei, G.G.; Iordache, F.; Hainăroșie, R.; Bostan, M. Characterization of the tumor cells from human head and neck cancer. *Rom. J. Morphol. Embryol.* **2016**, *57*, 791–799.
60. Botezatu, A.; Iancu, I.V.; Plesa, A.; Manda, D.; Popa, O.; Bostan, M.; Mihaila, M.; Albulescu, A.; Fudulu, A.; Vladoiu, S.V.; et al. Methylation of tumour suppressor genes associated with thyroid cancer. *Cancer Biomarkers* **2019**, *25*, 53–65. [[CrossRef](#)]
61. Kim, D.K.; Lee, J.H.; Lee, O.J.; Park, C.H. Expression and mutational analysis of Cip/Kip family in early glottic cancer. *J. Laryngol. Otol.* **2015**, *129*, 168–173. [[CrossRef](#)] [[PubMed](#)]
62. Badisa, R.B.; Darling-Reed, S.F.; Joseph, P.; Cooperwood, J.S.; Latinwo, L.M.; Goodman, C.B. Selective cytotoxic activities of two novel synthetic drugs on human breast carcinoma MCF-7 cells. *Anticancer. Res.* **2009**, *29*, 2993–2996. [[PubMed](#)]
63. Georgakilas, A.G.; Martin, O.A.; Bonner, W.M. P21: A two-faced genome guardian. *Trends Mol. Med.* **2017**, *23*, 310–319. [[CrossRef](#)]
64. Parveen, A.; Akash, M.S.H.; Rehman, K.; Kyunn, W.W. Dual role of p21 in the progression of cancer and its treatment. *Crit. Rev. Eukaryot. Gene Expr.* **2016**, *26*, 49–62. [[CrossRef](#)] [[PubMed](#)]
65. Liu, Y.W.; Xia, R.; Lu, K.; Xie, M.; Yang, F.; Sun, M.; De, W.; Wang, C.; Ji, G. LincRNAFEZF1-AS1 represses p21 expression to promote gastric cancer proliferation through LSD1-Mediated H3K4me2 demethylation. *Mol. Cancer* **2017**, *16*, 39. [[CrossRef](#)] [[PubMed](#)]
66. Yin, D.; Lu, X.; Su, J.; He, X.; De, W.; Yang, J.; Li, W.; Han, L.; Zhang, E. Long noncoding RNA AFAP1-AS1 predicts a poor prognosis and regulates non-small cell lung cancer cell proliferation by epigenetically repressing p21 expression. *Mol. Cancer* **2018**, *17*, 92. [[CrossRef](#)]
67. Li, G.; Liu, Z.; Sturgis, E.M.; Shi, Q.; Chamberlain, R.M.; Spitz, M.R.; Wei, Q. Genetic polymorphisms of p21 are associated with risk of squamous cell carcinoma of the head and neck. *Carcinogenesis* **2005**, *26*, 1596–1602. [[CrossRef](#)]
68. Kang, M.R.; Park, K.H.; Yang, J.O.; Lee, C.W.; Oh, S.J.; Yun, J.; Lee, M.Y.; Han, S.B.; Kang, J.S. MiR-6734 up-regulates p21 gene expression and induces cell cycle arrest and apoptosis in colon cancer cells. *PLoS ONE* **2016**, *11*, e0160961. [[CrossRef](#)]
69. Szturz, P.; Cristina, V.; Gómez, R.G.; Bourhis, J.; Simon, C.; Vermorken, J.B. Cisplatin eligibility issues and alternative regimens in locoregionally advanced head and neck cancer: Recommendations for clinical practice. *Front. Oncol.* **2019**, *9*, 464. [[CrossRef](#)]
70. Mehanna, H.; Robinson, M.; Hartley, A.; Kong, A.; Foran, B.; Fulton-Lieuw, T.; Dalby, M.; Mistry, P.; Sen, M.; O'Toole, L.; et al. Radiotherapy plus cisplatin or cetuximab in low-risk human papillomavirus-positive oropharyngeal cancer (De-ESCALaTE HPV): An open-label randomised controlled phase 3 trial. *Lancet* **2019**, *393*, 51–60. [[CrossRef](#)]

71. Kunnumakkara, A.B.; Anand, P.; Aggarwal, B.B. Curcumin inhibits proliferation, invasion, angiogenesis and metastasis of different cancers through interaction with multiple cell signaling proteins. *Cancer Lett.* **2008**, *269*, 199–225. [[CrossRef](#)] [[PubMed](#)]
72. Leischner, C.; Burkard, M.; Pfeiffer, M.M.; Lauer, U.M.; Busch, C.; Venturelli, S. Nutritional immunology: Function of natural killer cells and their modulation by resveratrol for cancer prevention and treatment. *Nutr. J.* **2016**, *15*, 47. [[CrossRef](#)]
73. Baharuddin, P.; Satar, N.; Fakiruddin, K.S.; Zakaria, N.; Lim, M.N.; Yusoff, N.M.; Zakaria, Z.; Yahaya, B.H. Curcumin improves the efficacy of cisplatin by targeting cancer stem-like cells through p21 and cyclin D1-mediated tumour cell inhibition in non-small cell lung cancer cell lines. *Oncol. Rep.* **2015**, *35*, 13–25. [[CrossRef](#)] [[PubMed](#)]
74. Osman, A.M.M.; Al-Malki, H.S.; Al-Harathi, S.E.; El-Hanafy, A.A.; Elashmaoui, H.M.; ElShal, M.F. Modulatory role of resveratrol on cytotoxic activity of cisplatin, sensitization and modification of cisplatin resistance in colorectal cancer cells. *Mol. Med. Rep.* **2012**, *12*, 1368–1374. [[CrossRef](#)] [[PubMed](#)]
75. Ling, Z.; Guan, H.; You, Z.; Wang, C.; Hu, L.; Zhang, L.; Wang, Y.; Chen, S.; Xu, B.; Chen, M. Aloperine executes antitumor effects through the induction of apoptosis and cell cycle arrest in prostate cancer in vitro and in vivo. *OncoTargets Ther.* **2018**, *11*, 2735–2743. [[CrossRef](#)] [[PubMed](#)]



© 2020 by the authors. Licensee MDPI, Basel, Switzerland. This article is an open access article distributed under the terms and conditions of the Creative Commons Attribution (CC BY) license (<http://creativecommons.org/licenses/by/4.0/>).

Article

Dietary Supplements for Male Infertility: A Critical Evaluation of Their Composition

Andrea Garolla ^{1,*}, Gabriel Cosmin Petre ^{1,†}, Francesco Francini-Pesenti ^{2,†}, Luca De Toni ¹, Amerigo Vitagliano ^{3,4}, Andrea Di Nisio ¹ and Carlo Foresta ¹

¹ Unit of Andrology and Reproductive Medicine & Centre for Male Gamete Cryopreservation, Department of Medicine, University of Padova, 35128 Padova, Italy; gabriel.petre@rocketmail.com (G.C.P.); detoni.luca@gmail.com (L.D.T.); andrea.dinisio@gmail.com (A.D.N.); carlo.foresta@unipd.it (C.F.)

² Department of Medicine, Clinical Nutrition Unit University of Padova, 35128 Padova, Italy; francescofrancini@yahoo.it

³ Department of Women and Children's Health, University of Padua, 35122 Padua, Italy; amerigovitagliano.md@gmail.com

⁴ Unit of Obstetrics and Gynecology, Madonna della Navicella Hospital, Chioggia, 30015 Venice, Italy

* Correspondence: andrea.garolla@unipd.it

† First co-author.

Received: 17 April 2020; Accepted: 18 May 2020; Published: 19 May 2020

Abstract: Dietary supplements (DS) represent a possible approach to improve sperm parameters and male fertility. A wide range of DS containing different nutrients is now available. Although many authors demonstrated benefits from some nutrients in the improvement of sperm parameters, their real effectiveness is still under debate. The aim of this study was to critically review the composition of DS using the Italian market as a sample. Active ingredients and their minimal effective daily dose (mED) on sperm parameters were identified through a literature search. Thereafter, we created a formula to classify the expected efficacy of each DS. Considering active ingredients, their concentration and the recommended daily dose, DS were scored into three classes of expected efficacy: higher, lower and none. Twenty-one DS were identified. Most of them had a large number of ingredients, frequently at doses below mED or with undemonstrated efficacy. Zinc was the most common ingredient of DS (70% of products), followed by selenium, arginine, coenzyme Q and folic acid. By applying our scoring system, 9.5% of DS fell in a higher class, 71.4% in a lower class and 19.1% in the class with no expected efficacy. DS marketed in Italy for male infertility frequently includes effective ingredients but also a large number of substances at insufficient doses or with no reported efficacy. Manufacturers and physicians should better consider the scientific evidence on effective ingredients and their doses before formulating and prescribing these products.

Keywords: fertility; ingredients; male reproduction; semen parameters; supplements

1. Introduction

Infertility is a pathological condition defined as the inability of a sexually active, non-contracepting couple to achieve pregnancy in one year [1]. Both male and female factors can lead to infertility. In particular, according to the causes, it has been reported that 29.3% is due to a male factor, 37.1% to a female factor, 17.6% to both male and female factors, with the remaining percentage considered as idiopathic [2].

It is estimated that around 10%–15% of all couples are affected by infertility, thus representing a global concern in most developed countries [3].

Among male infertility causes, many recent studies have emphasized the role of genital tract inflammation, incorrect lifestyles and malnutrition [4]. On this regard, weight excess and other

conditions such as metabolic syndrome, alcohol abuse, cigarette smoking, exposure to environmental pollutants etc. have been strongly related to a decrease in sperm quality and fertility. A major driving hypothesis is that these conditions, by inducing an elevation of reactive oxygen species (ROS) and nitrogen species (RONS), are able to alter the balance of the redox status of both the steroidogenic cell population and the germ line cell populations, leading to the impairment of the hypothalamic–pituitary–testicular axis and the reduction of sperm quality [5].

A large number of recent studies have focused on the ability of many substances, generally termed as *nutraceuticals*, to improve the hormonal status and sperm parameters by different mechanisms [6]. Nutraceuticals are used as ingredients of dietary supplements (DS), widely marketed for the prevention or treatment of the most disparate pathological conditions. From a legislative point of view, the European Food Safety Agency (EFSA) defines that DS are not intended for the treatment or prevention of disease in humans, but only to support specific physiological function [7]. Currently, DS are widely prescribed to improve physiological aspects related to male fertility.

Many DS are available on the market with various formulations, containing both nutrients and botanicals at different doses. Despite many authors demonstrating positive effects of some ingredients on semen parameters and fertility outcomes [8], many others have also shown a lack of efficacy and even potentially harmful side effects [9]. In a recent position statement, the Italian Society of Andrology and Sexual Medicine (SIAMS) summarized the state of the art on each single ingredient currently used in the andrological field. In this paper, authors concluded that there was still limited scientific evidence on the possible role of any nutraceutical in andrology and the use of antioxidants could be suggested in patients with idiopathic infertility in the presence of documented abnormal sperm parameters only after a specific diagnostic workup. However, to date, no regulation or guidelines are available for the use of these products, generating confusion for both prescribers and patients [10]. Moreover, several factors make it difficult to empirically address the right ingredient for the right patient. In particular, it is difficult to identify the correct DS since each product contains different ingredients at different doses.

The purpose of this study was to critically evaluate the composition of DS employed in male infertility, using the Italian market as a sample.

2. Materials and Methods

In order to evaluate the potential efficacy of DS, a systematic literature review on substances used to improve sperm parameters was preliminarily performed. The literature search was conducted in MEDLINE, Scopus, EMBASE, and Cochrane Library registers until 31 March 2020. Only randomized clinical trials (RCTs) and systematic reviews or meta-analysis of RCTs were considered eligible. With the aim to rule out possible interactions between ingredients, only studies that used active substances alone or in combination with at most the other three ingredients were considered. The key terms used for the search were: fertility or male reproduction or semen parameters and supplements or ingredients. Figure 1 displays the flow diagram of the selection of eligible papers.

To establish the efficacy of each ingredient we considered only those having at least one RCT or systematic review or meta-analysis of RCTs, demonstrating a significant effect on any sperm parameters involved in male fertility. Significance was set at p -value < 0.05 . When evaluating the findings of meta-analyses, we verified whether statistical methods incorporated substantial heterogeneity (Higgins $I^2 > 30\%$) into a random-effects model, as appropriate. Regarding the daily dose of each active ingredient with nutrient characteristics, we referred to the tolerable Upper Intake Levels (UL) as reported in Dietary Reference Intake (DRI) [11].

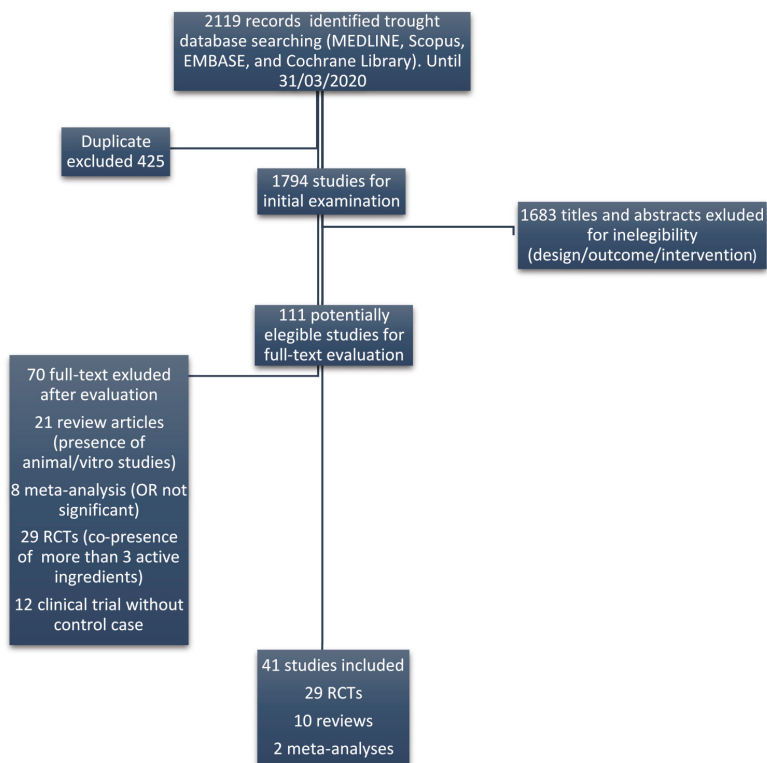


Figure 1. Flow diagram of the selection of eligible papers.

Based on the results of available articles, we were able to identify, for each active ingredient, the minimal effective daily dose (mED) able to improve sperm parameters. To define mED we used the lowest effective dose reported in RCTs, systematic review or meta-analysis of RCTs. Therefore, we classified the ingredients contained in each supplement and suggested daily dose into three categories: reported efficacy with a dose achieving the mED (A), reported efficacy but with a dose below mED (B) and unreported data of efficacy (C). To classify DS, we created a formula taking into consideration the three classes of ingredients and their number:

$$Score = \frac{(2A + B - C)}{2N} \times (A + B/2)$$

In particular, the above formula was conceived based on the following sequential steps:

- (1) Each class of ingredients was given an arbitrary value: $A = +2$, $B = +1$ and $C = -1$;
- (2) These values were multiplied for the respective number of ingredients within each supplement (A , B and C respectively), obtaining a total score given by the sum of each category ($2A + B - C$);
- (3) As the number of ingredients highly differed between supplements, we standardized the above total score by dividing it for the maximum possible score for that supplement, by assuming that each ingredient was of class A ($=2N$, where N is the total number of ingredients in each supplement);
- (4) In order to correct this value for the number of ingredients of only categories A and B , the relative score was multiplied for the sum of high efficacy ingredients plus half (as a proxy of their lower

efficacy) the number of moderate efficacy ingredients ($A + B/2$), finally obtaining a corrected score for each supplement.

- (5) Given the distribution of the scores resulted in three main clusters, we classified DS into three categories, resembling the efficacy of the ingredients: higher expected efficacy (corrected score ≥ 4), lower expected efficacy ($4 < \text{corrected score} > 1$) and no expected efficacy (corrected score ≤ 1).

We collected the names and formulations of the DS registered in Italy by referring to the register of the Italian Ministry of Health [12].

3. Results

The literature search on active ingredients allowed us to identify 41 studies (RCTs or meta-analyses) reporting their efficacy on sperm parameters (Figure 1). By this analysis we found that 18 of these ingredients had a reported efficacy. The complete list of ingredients with clinical evidence of efficacy, the respective references, evaluated sperm parameters and employed daily doses, are summarized in Table 1. In the right column, the mED of each ingredient is reported. In some studies, marked with an asterisk, the employed dose exceeded the reported UL. In particular, all the studies involving zinc evaluated the effect of this ingredient at a dose exceeding UL. For each active ingredient, the evidence of efficacy was supported by at least two RCTs or meta-analysis, excluding astaxanthin, D-aspartic acid and L-citrulline, which had only one reference.

Table 1. Active ingredients with evidence of efficacy, references, evaluated sperm parameters, employed daily doses and minimal effective dose (mED).

Active Ingredients	References	Evaluated Sperm Parameters	Employed Daily Dose	Minimal Effective Dose (mED)
Zinc	[13] * (Rev)	concentration	50 mg	50 mg
	[14] * (RCT)	concentration	66 mg	
	[15] * (RCT)	morphology	66 mg	
Selenium	[13] (Rev)	linear progression	50 µg	50 µg
	[16] (Met)	concentration	100 µg	
	[17] (RCT)	concentration/motility	200 µg	
Vitamin B12	[18] (Rev)	count	25 µg	25 µg
	[19] (RCT)	count	1500 µg	
	[20] (RCT)	count	6000 µg	
Folic Acid	[21] (RCT)	count/motility	400 µg	400 µg
	[22] (RCT)	volume/motility	500 µg	
	[23] (Met)	DNA damage	500 µg	
L-Arginine	[24] (RCT)	progressive motility	1.4 g	1.4 g
	[25] (RCT)	concentration/motility	1.4 g	
L-Citrulline	[26] (RCT)	volume/concentration motility/vitality	1.2 g	1.2 g
α-Lipoic Acid	[27] (RCT)	concentration/motility	600 mg	600 mg
	[28] (Rev)	motility/morphology	600 mg	
L-Carnitine (LC/LAC)	[29] (RCT)	motility	1 g	1 g
	[30] (RCT)	count/motility	2 g	
	[31] (RCT)	concentration/motility	2 g	
	[32] (Rev)	motility	3 g	
N-Acetyl Cysteine (NAC)	[33] (Rev)	motility/DNA damage	600 mg	600 mg
	[34] (RCT)	motility/DNA damage	600 mg	
	[17] (RCT)	motility/morphology	600 mg	
Coenzyme Q10	[35] (RCT)	motility	200 mg	200 mg
	[36] (RCT)	count/motility	200 mg	
	[37] (RCT)	concentration/morphology	300 mg	

Table 1. *Cont.*

Active Ingredients	References	Evaluated Sperm Parameters	Employed Daily Dose	Minimal Effective Dose (mED)
Astaxanthin	[38] (RCT)	motility	16 mg	16 mg
D-Aspartic Acid (DAA)	[39] (RCT)	count/motility	2.7 g	2.7 g
Tribulus Terrestris DE	[40] (RCT) [41] (RCT) [42] (Rev)	count/motility morphology/motility count/morphology	250 mg 500 mg 6000 mg	250 mg
Myoinositol	[43] (Rev) [44] (Rev)	motility concentration	2 g 4 g	2 g
α-Tocopherol	[45] (RCT) [32] (Rev) [46] (RCT) [47] * (RCT)	motility/DNA damage motility/morphology motility/lipid oxidation DNA damage	20 mg 268.46 mg 300 mg 1000 mg	20 mg
Vitamin C	[48] (RCT) [49] (Rev) [47] (RCT)	concentration/motility DNA damage	0.5 g 1 g 1 g	0.5 g
EPA + DHA	[50] (RCT)	concentration/motility	0.72 g + 0.48 g	DHA 0.48 g
EPA + DHA	[51] (RCT)	DNA damage	0.14 g + 1 g	
Lycopene	[52] (RCT) [53] (Rev)	concentration/motility count/morphology	4 mg 8 mg	4 mg

* The employed dose exceeded/reach UL. LC: L-Carnitine; LAC: Acetyl L-Carnitine; EPA: Eicosapentaenoic acid; DE: Dry Extract; DHA: docosahexaenoic acid. Rev: Review; Met: Meta-analysis.

Ingredients without clinical evidence in the improvement of sperm parameters (no RCT or meta-analyses) are listed in Table 2.

Table 2. Ingredients without clinical evidence of efficacy.

- Astragalus DE
- Damiana DE
- Nettle DE
- Catuba DE
- Ecklonia bicyclis DE
- L-Taurine
- Glutathione
- Glucosamine
- SOD
- Vitamin D3
- Vitamin B1
- Riboflavin
- Niacin
- Vitamin B5
- Vitamin B6
- Biotin
- Manganese

DE: Dry Extract; SOD: super oxide dismutase.

We found 21 DS marketed in Italy for male infertility. Their composition and the daily doses of their active ingredients are summarized in Table 3. Moreover, for each supplement, the scores of expected efficacy and the symbols summarizing the efficacy of their ingredients are reported.

Table 3. List of dietary supplements (DS) and relative composition.

Active Ingredients	DS 1		DS 2		DS 3		DS 4		DS 5		DS 6		DS 7	
	Daily Dose	EV	Daily Dose	EV	Daily Dose	EV	Daily Dose	EV	Daily Dose	EV	Daily Dose	EV	Daily Dose	EV
Zinc	7.5 mg	B	10 mg	B	12.5 mg	B	1.5 mg	B	13 mg	B	30 µg	B	55 µg	A
Selenium	60 µg	A			83 µg	A								
Vitamin B12							33 mg	A						
Folic Acid	200 µg	B					400 µg	A			400 µg	A	200 µg	B
L-Arginine	100 mg	B			1000 mg	B			2500 mg	A	125 mg	B	30 mg	B
L-Citrulline														
α-Lipoic Acid							50 mg	B						
L-Carnitine					1000 mg	A					200 mg	B	30 mg	B
N-Acetyl Cysteine (NAC)														
Coenzyme Q10	10 mg	B	200 mg	A	10 mg	B			200 mg	A	7.5 mg	B		
Astaxanthin	15 mg	B												
D-Aspartic Acid (DAAA)			2660 mg	A										
Tribulus terrestris DE					800 mg	A								
Myoinositol													1000 mg	A
α-Tocopherol	30 mg	A			12 mg	B			30 mg	A	36 mg	A	30 mg	A
Vitamin C	60 mg	B							180 mg	B				
DHA														
Lycopene					15 mg	A								
Astragalus DE					300 mg	C								
Damiana DE														
Nettle DE														
Catuba DE														
Ecklonia bicyclis DE														
L-Iaurine									500 mg	C				
Glutathione							30 mg	C			40 mg	C		
Glucosamine														
SOD							154 UI	C						
Vitamin D3														
Vitamin B1														

Table 3. *Contt.*

Active Ingredients	DS 8		DS 9		DS 10		DS 11		DS 12		DS 13		DS 14	
	Daily Dose	EV	Daily Dose	EV	Daily Dose	EV	Daily Dose	EV	Daily Dose	EV	Daily Dose	EV	Daily Dose	EV
Nettle DE														
Catuba DE	50 mg	C												
Ecklonia bicyclis DE									200 mg	C				
L-Taurine														
Glutathione			80 mg	C										
Glucosamine									150 mg	C				
SOD														
Vitamin D3														
Vitamin B1											1.1 mg	C		
Vitamin B2											1.4 mg	C	2.8 mg	C
Vitamin B3											16 mg	C		
Vitamin B5											6 mg	C		
Vitamin B6											1.4 mg	C	2.8 mg	C
Biotin											100 µg	C		
Manganese											2 mg	C		
Active Ingredients	DS 15		DS 16		DS 17		DS 18		DS 19		DS 20		DS 21	
	S = 4.33		S = 2.45		S = 2.06		S = 2.06		S = 1		S = 1.05		S = 2	
Zinc	15 mg	B	22.5 mg	B	10 mg	B	10 mg	B	6.5 mg	B	10 mg	B	10 mg	B
Selenium	50 µg	A			80 µg	A	50 µg	A			55 µg	A		
Vitamin B12	2.5 µg	B					1.5 µg	B						
Folic Acid	400 µg	A	300 µg	B	200 µg	B	200 µg	B					400 µg	A
L-Arginine			2500 mg	A			200 mg	B			30 mg	B		
L-Citrulline	3000 mg	A							200 mg	B				
α-Lipoic Acid														
L-Carnitine	1000 mg	A	200 mg	B			400 mg	B			44.7 mg	B		
N-Acetyl Cysteine (NAC)														
Coenzyme Q10	200 mg	A					100 mg	B	90 mg	B				
Asaxanthin														
D-Aspartic Acid (DAAA)			16 mg	A	10 mg	B					1000 mg	B		

Table 3. *Cont.*

Active Ingredients	DS 15		DS 16		DS 17		DS 18		DS 19		DS 20		DS 21	
	Daily Dose	EV	Daily Dose	EV	Daily Dose	EV	Daily Dose	EV	Daily Dose	EV	Daily Dose	EV	Daily Dose	EV
Tribulus terrestris DE														
Myoinositol					50 mg	B					500 mg	B	4000 mg	A
α -Tocopherol	40 mg	A	30 mg	A			12 mg	B						
Vitamin C	80 mg	B					100 mg	B			180 mg	B		
DHA					100 mg	B								
Lycopen	10 mg	A												
Astragalus DE														
Damiana DE	400 mg	C												
Nettle DE	300 mg	C												
Cattaba DE														
Ecklonia bicyclis DE														
L-Taurine													300 mg	B
Glutathione	40 mg	C					40 mg	C						
Glucosamine														
SOD					150 mg	C								
Vitamin D3														
Vitamin B1											3.75 μ g	C		
Vitamin B2														
Vitamin B3														
Vitamin B5														
Vitamin B6														
Biotin														
Mangense														

S: score of supplement's potential efficacy; EV: efficacy value of active ingredients; evidence of ingredients and dose efficacy: (A) reported efficacy and achievement of mED, (B) reported efficacy but below mED and (C) unreported efficacy. DE: Dry Extract; SOD: super oxide dismutase; DHA: docosahexaenoic acid.

A detailed analysis of this table raised the following considerations: (i) all supplements were mixtures of active ingredients; (ii) in each supplement the number of ingredients ranged from 2 up to 17, with a mean number higher than 7; (iii) 13 of 21 supplements contained at least one ingredient without reported efficacy; (iv) 19 supplements had ingredients below mED; (v) indeed, 1 supplement contained seven ingredients dosed below mED; (vi) 1 supplement contained only active ingredients satisfying mED; (vii) the product number 9 had a nutrient reaching UL (zinc 40 mg/day); (viii) zinc was the most used ingredient, followed by selenium, arginine, coenzyme Q, folic acid and carnitine. These substances were present in more than 50% of DS, whereas all the remaining ingredients were represented in 10% or less of products.

The distribution of DS into the three classes of efficacy is reported in Figure 2. Two DS out of 21 (9.5%) were included in the higher expected efficacy group. The majority of remaining products (71.4%) fell in the lower expected efficacy group, and four (19.1%) in the group with no efficacy.

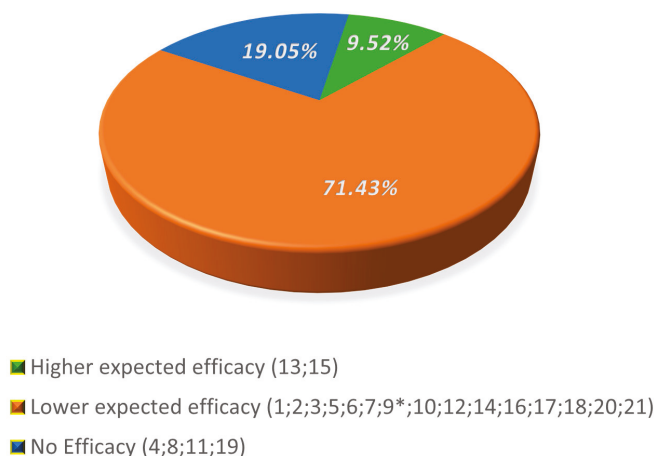


Figure 2. Distribution of supplements in classes of expected efficacy. * This supplement has a content of Zinc reaching the UL. Numbers refer to a specific supplement.

4. Discussion

This critical review aimed to evaluate the formulation of supplements for male infertility using the Italian market as a sample. In general, there is still poor evidence in terms of large well-designed randomized and placebo-controlled trials availability, supporting the efficacy of nutraceutical products in the field of male reproductive health [54,55]. Nevertheless, these products are commonly administered to infertile patients [8,56]. Since a medical prescription is not necessary to purchase dietary supplements, subjects seeking fertility may have easy access to these products [10,57]. As a proof of concept, the Italian market of supplements generated 3.3 billion euros in 2019, with an increase of 4.3% compared to 2018 [58].

Whilst a rational use of supplements may be potentially beneficial for the improvement of sperm parameters, we need to stress that their uncontrolled use is potentially harmful for patients' health due to direct toxic effects and interaction with drugs or nutrients [59]. In this respect, we were surprised to point out that all RCTs and meta-analyses on zinc for male infertility relied on doses always exceeding the UL. Over this background, in the near future it would be desirable to better define thoughtful criteria for each supplement in use.

Our analysis found that beside the gap of literature, the market of food supplements is still supported by poor scientific evidence. The majority of DS contained a huge number of ingredients, up to 17. The mixture of such a high number of ingredients may generate different issues, including a low

concentration of each substance (i.e., necessitating of two or more administrations to reach the daily effective dose), a large volume of pills and a high risk of interactions. What is more, we found that some ingredients included in many DS had no scientific evidence of efficacy (i.e., astragalus, vitamin D3, taurine and riboflavin). The formulation of pills with a large number of ingredients, some of which cause uncertain benefits, denotes a gap of knowledge of potential biologic targets by manufacturers. Moreover, it has been reported that some plant extracts, present in many of these supplements, are likely to interact with drug metabolism [60,61]. This aspect raises further concerns on the safety of these products.

Very frequently, nutrients were present in DS at a dosage below mED. This situation was more common among products with a high number of ingredients. The administration of any active substance with a dose below mED appears as scientifically unjustified due to uncertainties in the therapeutic results. Differently, when the number of ingredients was small, the dose often satisfied mED. Another major aspect in the evaluation of supplements concerns safety. Some ingredients, particularly when administered in high doses, are not free from risks when used as dietary supplements. For example, folates can mask the B12 deficiency favoring the progression of neurological damage [62]. The combination of these two vitamins could have a synergic effect in improving homocysteine metabolism hence the sperm quality. It should be noted that vitamin B12, when present, was rarely associated to folic acid [63,64]. Furthermore, zinc reduces the copper intestinal absorption interfering with its carrier [65]. With respect to this, we want to stress that one supplement on the market contained a dose of zinc reaching the UL.

On a positive note, our analysis revealed that some active ingredients with reported efficacy are frequently present in analyzed supplements. Previous studies demonstrated that some ingredients are particularly effective in specific patients' conditions. Substances with antioxidant properties are indicated in inflammation of the male accessory glands, both related to microbial and non-microbial origin. Several studies performed in asthenozoospermic infertile patients, showed that the positive effect of selenium supplementation is dependent on the correct structure of the mitochondrial capsule [66,67]. Carnitine supplementation induced a significant increase in sperm motility in cases of asthenozoospermia with preserved mitochondrial function [68,69]. Due to the key role of zinc in the processes of DNA compaction, administration of this micronutrient was successful in improving sperm morphology and DNA integrity in patients with prostate abnormalities [70,71].

Based on active ingredients reaching mED we created a grading scale of supplements distinguishing three classes of expected efficacy. Three products were present in the higher class, some of which contained ineffective or underdosed ingredients. Most of the supplements fell in the lower group of expected efficacy. In this class, a large number of ineffective or underdosed products were also present. For an adequate evaluation of these classes, we considered the number of the effective ingredients as the most important criterion of efficacy. A relevant aspect was the use of ineffective or underdosed ingredients that should be absent or less than possible. Another parameter to evaluate a product was the presence of a lower number of ingredients.

We acknowledge the application of a non-validated statistical method to calculate scores for each DS may represent a point of weakness in this study. Very recently, a validated formula to score supplements was suggested by Kuchakulla et al. [72], based on the Budoff's score, previously conceived by cardiologists to evaluate their procedures [73]. However, this scoring system when applied to DS, does not take into account the effective dose of ingredients, a crucial point in the evaluation of their efficacy. For example, using this approach, a DS containing ingredients at ineffective or toxic doses would be considered useful. As a point of strength, our scoring system relied on high quality evidence coming from RCTs or a systematic review and meta-analyses of RCTs, which represents a reliable approach to critically weighing the expected efficacy of dietary supplements. The same approach could be applied to evaluate products used in other clinical conditions.

In conclusion, this study showed that most DS marketed in Italy for male infertility contain ingredients with reported efficacy in the improvement of sperm parameters. Nevertheless, a

non-negligible number of DS are mixtures of substances with uncertain or unreported benefits, whose administration may be unhelpful or even harmful for infertile patients. On that basis, we believe manufacturers should carefully scrutinize scientific evidence before delivering each supplements' formulation. Accordingly, physicians should evaluate the composition of DS and the dose of each single constituent before considering their clinical use. Finally, the choice for DS should be tailored to the specific patient's fertility problem.

Author Contributions: A.G. and G.C.P. contributed to the conception/design of the research and acquisition/analysis of the literature data; A.G., G.C.P. and F.F.-P. equally contributed and drafted the manuscript; A.D.N. conceived and performed data analyses; L.D.T., A.V. and C.F. critically revised the paper for important intellectual content. All authors revised and approved the final manuscript, and agreed to be fully accountable for ensuring the integrity and accuracy of the work. All authors had full access to all the data in the study and are able to take responsibility for the integrity of them and the accuracy of the analysis.

Funding: This research received no external funding.

Acknowledgments: The authors thank Marco Ghezzi for helpful discussion.

Conflicts of Interest: The authors declare no conflicts of interest.

References

- World Health Organization. Task Force on Methods for the Regulation of Male Fertility. Contraceptive efficacy of testosterone-induced azoospermia in normal men. *Lancet* **1990**, *336*, 955–959. [CrossRef]
- Istituto Superiore di Sanità. Available online: http://old.iss.it/binary/rpma/cont/7_2017_Report.pdf (accessed on 20 March 2020).
- Winters, B.R.; Walsh, T.J. The Epidemiology of Male Infertility. *Urol. Clin. N. Am.* **2014**, *41*, 195–204. [CrossRef]
- Lotti, F.; Maggi, M. Ultrasound of the male genital tract in relation to male reproductive health. *Hum. Reprod. Updat.* **2014**, *21*, 56–83. [CrossRef] [PubMed]
- Ferlin, A.; Foresta, C. New genetic markers for male infertility. *Curr. Opin. Obstet. Gynecol.* **2014**, *26*, 193–198. [CrossRef] [PubMed]
- Falsig, A.L.; Gleerup, C.S.; Knudsen, U.B. The influence of omega-3 fatty acids on semen quality markers: A systematic PRISMA review. *Andrology* **2019**, *7*, 794–803. [CrossRef] [PubMed]
- EUR-Lex. Available online: <http://data.europa.eu/eli/reg/2006/1924/2012-11-29> (accessed on 20 March 2020).
- Cui, T.; Kovell, R.C.; Brooks, D.C.; Terlecki, R.P. A Urologist's Guide to Ingredients Found in Top-Selling Nutraceuticals for Men's Sexual Health. *J. Sex. Med.* **2015**, *12*, 2105–2117. [CrossRef]
- Henkel, R.; Sandhu, I.S.; Agarwal, A. The excessive use of antioxidant therapy: A possible cause of male infertility? *Andrologia* **2019**, *51*, 303–4569. [CrossRef]
- Calogero, A.E.; Aversa, A.; La Vignera, S.; Corona, G.; Ferlin, A. The use of nutraceuticals in male sexual and reproductive disturbances: Position statement from the Italian Society of Andrology and Sexual Medicine (SIAMS). *J. Endocrinol. Investig.* **2017**, *40*, 1389–1397. [CrossRef]
- Otten, J.J.; Hellwig, J.P.; Meyers, D.L. *Dietary Reference Intakes: The Essential Guide to Nutrient Requirements*; The National Academies Press: Washington, DC, USA, 2006; pp. 529–542.
- Bardelli, P.; Bardelli, M. Commento alle linee guida emanate dal Ministero della Salute sulle disfunzioni posturali. *Med. Chir. Caviglia Piede* **2019**, *43*. [CrossRef]
- Agarwal, A.; Majzoub, A. Antioxidant therapy in idiopathic oligoasthenoatozoospermia. *Indian J. Urol.* **2017**, *33*, 207–214. [CrossRef]
- Ebisch, I.M.W.; Pierik, F.H.; De Jong, F.H.; Thomas, C.M.G.; Steegers-Theunissen, R.P.M. Does folic acid and zinc sulphate intervention affect endocrine parameters and sperm characteristics in men? *Int. J. Androl.* **2006**, *29*, 339–345. [CrossRef] [PubMed]
- Azizollahi, G.; Azizollahi, S.; Babaei, H.; Kianinejad, M.; Baneshi, M.M.; Nematollahi-Mahani, S.N. Effects of supplement therapy on sperm parameters, protamine content and acrosomal integrity of varicocelectomized subjects. *J. Assist. Reprod. Genet.* **2013**, *30*, 593–599. [CrossRef] [PubMed]
- Smits, R.M.; Mackenzie-Proctor, R.; Yazdani, A.; Stankiewicz, M.T.; Jordan, V.; Showell, M.G. Antioxidants for male subfertility. *Cochrane Database Syst. Rev.* **2019**, *3*, CD007411. [CrossRef]

17. Safarinejad, M.R.; Safarinejad, S. Efficacy of Selenium and/or N-Acetyl-Cysteine for Improving Semen Parameters in Infertile Men: A Double-Blind, Placebo Controlled, Randomized Study. *J. Urol.* **2009**, *181*, 741–751. [[CrossRef](#)] [[PubMed](#)]
18. Banihani, S.A. Vitamin B12 and Semen Quality. *Biology* **2017**, *7*, 42. [[CrossRef](#)] [[PubMed](#)]
19. Kumamoto, Y.; Maruta, H.; Ishigami, J.; Kamidono, S.; Orikasa, S.; Kimura, M.; Yamanaka, H.; Kurihara, H.; Koiso, K.; Okada, K. Clinical efficacy of mecobalamin in the treatment of oligozoospermia—Results of double-blind comparative clinical study. *Hinyokika kyo. Acta Urol. Jpn.* **1988**, *34*, 1109–1132.
20. Moriyama, H.; Nakamura, K.; Sanda, N.; Fujiwara, E.; Seko, S.; Yamazaki, A.; Mizutani, M.; Sagami, K.; Kitano, T. Studies on the usefulness of a long-term, high-dose treatment of methylcobalamin in patients with oligozoospermia. *Hinyokika kyo. Acta Urol. Jpn.* **1987**, *33*, 151–156.
21. Calogero, A.E.; Gullo, G.; La Vignera, S.; Condorelli, R.A.; Vaiarelli, A. Myoinositol improves sperm parameters and serum reproductive hormones in patients with idiopathic infertility: A prospective double-blind randomized placebo-controlled study. *Andrology* **2015**, *3*, 491–495. [[CrossRef](#)]
22. Wong, W.Y.; Merkus, H.M.W.M.; Thomas, C.M.G.; Menkveld, R.; Zielhuis, G.A.; Steegers-Theunissen, R.P. Effects of folic acid and zinc sulfate on male factor subfertility: A double-blind, randomized, placebo-controlled trial. *Fertil. Steril.* **2002**, *77*, 491–498. [[CrossRef](#)]
23. Showell, M.G.; Brown, J.; Yazdani, A.; Stankiewicz, M.T.; Hart, R.J. Antioxidants for male subfertility. *Cochrane Database Syst. Rev.* **2011**. [[CrossRef](#)]
24. Stanislavov, R.; Nikolova, V.; Rohdewald, P. Improvement of seminal parameters with Prelox®: A randomized, double-blind, placebo-controlled, cross-over trial. *Phytother. Res.* **2009**, *23*, 297–302. [[CrossRef](#)]
25. Nikolova, V.; Stanislavov, R.; Vatev, I.; Nalbanski, B.; Pünevskva, M. Sperm parameters in male idiopathic infertility after treatment with prelox. *Akush Ginekol (Sofia)* **2007**, *46*, 7–12. [[PubMed](#)]
26. Stanislavov, R.; Rohdewald, P. Sperm quality in men is improved by supplementation with a combination of L-arginine, L-citrullin, roburins and Pycnogenol®. *Minerva Urol. Nefrol.* **2014**, *66*, 217–223.
27. Haghghian, H.K.; Haidari, F.; Mohammadi-Asl, J.; Dadfar, M. Randomized, triple-blind, placebo-controlled clinical trial examining the effects of alpha-lipoic acid supplement on the spermatogram and seminal oxidative stress in infertile men. *Fertil. Steril.* **2015**, *104*, 318–324. [[CrossRef](#)] [[PubMed](#)]
28. Dong, L.; Zhang, X.; Yang, F.; Li, J.; Yu, X.; Li, Y. Effect of oral alpha-lipoic acid (ALA) on the treatment of male infertility. *Medicine (Baltimore)* **2019**, *98*, e18453. [[CrossRef](#)] [[PubMed](#)]
29. Mehni, N.M.; Ketabchi, A.A.; Hosseini, E. Combination effect of Pentoxifylline and L-carnitine on idiopathic oligoasthenoteratozoospermia. *Iran. J. Reprod. Med.* **2014**, *12*, 817–824.
30. Peivandi, S.; Abasali, K.; Narges, M. Effects of L-carnitine on infertile men's spermogram; a randomised clinical trial. *J. Reprod. Infertil.* **2010**, *10*, 331.
31. Lenzi, A.; Lombardo, F.; Sgrò, P.; Salacone, P.; Caponecchia, L.; Dondero, F.; Gandini, L. Use of carnitine therapy in selected cases of male factor infertility: A double-blind crossover trial. *Fertil. Steril.* **2003**, *79*, 292–300. [[CrossRef](#)]
32. Ahmadi, S.; Bashiri, R.; Ghadiri-Anari, A.; Nadjarzadeh, A. Antioxidant supplements and semen parameters: An evidence based review. *Int. J. Reprod. BioMed.* **2016**, *14*, 729–736. [[CrossRef](#)]
33. Walczak-Jedrzejowska, R.; Wolski, J.K.; Slowikowska-Hilczer, J. The role of oxidative stress and antioxidants in male fertility. *Central Eur. J. Urol.* **2013**, *66*, 60–67. [[CrossRef](#)]
34. Çiftçi, H.; Verit, A.; Savas, M.; Yeni, E.; Erel, O. Effects of N-acetylcysteine on Semen Parameters and Oxidative/Antioxidant Status. *Urology* **2009**, *74*, 73–76. [[CrossRef](#)] [[PubMed](#)]
35. Nadjarzadeh, A.; Sadeghi, M.R.; Amirjannati, N.; Vafa, M.; Motevalian, S.A.; Gohari, M.R.; Akhondi, M.A.; Yavari, P.; Shidfar, F. Coenzyme Q₁₀ improves seminal oxidative defense but does not affect on semen parameters in idiopathic oligoasthenoteratozoospermia: A randomized double-blind, placebo controlled trial. *J. Endocrinol. Investig.* **2011**, *34*, 224–228.
36. Safarinejad, M.R.; Safarinejad, S.; Shafiei, N.; Safarinejad, S. Effects of the Reduced Form of Coenzyme Q₁₀ (Ubiquinol) on Semen Parameters in Men with Idiopathic Infertility: A Double-Blind, Placebo Controlled, Randomized Study. *J. Urol.* **2012**, *188*, 526–531. [[CrossRef](#)] [[PubMed](#)]
37. Safarinejad, M.R. Efficacy of Coenzyme Q₁₀ on Semen Parameters, Sperm Function and Reproductive Hormones in Infertile Men. *J. Urol.* **2009**, *182*, 237–248. [[CrossRef](#)] [[PubMed](#)]

38. Comhaire, F.H.; El Garem, Y.; Mahmoud, A.; Eertmans, F.; Schoonjans, F. Combined conventional/antioxidant “Astaxanthin” treatment for male infertility: A double blind, randomized trial. *Asian J. Androl.* **2005**, *7*, 257–262. [[CrossRef](#)] [[PubMed](#)]
39. D’Aniello, A.; Ronsini, S.; Notari, T.; Grieco, N.; Infante, V.; D’Angel, N.; Mascia, F.; Fiore, M.; Fisher, G. D-Aspartate, a Key Element for the Improvement of Sperm Quality. *Adv. Sex. Med.* **2012**, *2*, 45–53. [[CrossRef](#)]
40. Ismail, S.B.; Bakar, M.B.; Nik Hussain, N.H.; Norhayati, M.N.; Sulaiman, S.A.; Jaafar, H.; Draman, S.; Ramli, R.; Wan Yusoff, W.Z. Comparison on the effects and safety of tualang honey and tribestaan in sperm parameters, erectile function and hormonal profile among oligospermia males. *Evid.-Based Complement. Altern. Med.* **2014**, *2014*, 126138.
41. Setiawan, L. *Tribulus terrestris* L. extract improves spermatozoa motility and increases the efficiency of acrosome reaction in subjects diagnosed with oligoastheno-teratozoospermia. *Adv. Male. Reprod. Physiol.* **1996**, *2*, 105–114.
42. Sanagoo, S.; Oskouei, B.S.; Abdollahi, N.G.; Salehi-Pourmehr, H.; Hazhir, N.; Farshbaf-Khalili, A. Effect of *Tribulus terrestris* L. on sperm parameters in men with idiopathic infertility: A systematic review. *Complement. Ther. Med.* **2018**, *42*, 95–103. [[CrossRef](#)]
43. Vazquez-Levin, M.H.; Verón, G.L. Myo-inositol in health and disease: Its impact on semen parameters and male fertility. *Andrology* **2019**, *8*, 277–298. [[CrossRef](#)]
44. Condorelli, R.A.; La Vignera, S.; Mongioi, L.M.; Vitale, S.G.; Laganà, A.S.; Cimino, L.; Calogero, A.E. Myo-inositol as a male fertility molecule: Speed them up! *Eur. Rev. Med. Pharmacol. Sci.* **2017**, *21*, 30–35. [[PubMed](#)]
45. Omu, A.E.; Al-Azemi, M.; Kehinde, E.; Anim, J.; Oriowo, M.; Mathew, T. Indications of the Mechanisms Involved in Improved Sperm Parameters by Zinc Therapy. *Med Princ. Pr.* **2008**, *17*, 108–116. [[CrossRef](#)] [[PubMed](#)]
46. Suleiman, S.A.; Ali, M.E.; Zaki, Z.M.; El-Malik, E.M.; Nasr, M.A. Lipid peroxidation and human sperm motility: Protective role of vitamin E. *J. Androl.* **1996**, *17*, 530–537. [[PubMed](#)]
47. Greco, E.; Iacobelli, M.; Ferrero, S.; Tesarik, J.; Rienzi, L.; Ubaldi, F. Reduction of the Incidence of Sperm DNA Fragmentation by Oral Antioxidant Treatment. *J. Androl.* **2005**, *26*, 349–353. [[CrossRef](#)] [[PubMed](#)]
48. Cyrus, A.; Kabir, A.; Goodarzi, D.; Moghimi, M. The effect of adjuvant vitamin C after varicocele surgery on sperm quality and quantity in infertile men: A double blind placebo controlled clinical trial. *Int. Braz. J. Urol.* **2015**, *41*, 230–238. [[CrossRef](#)]
49. Dawson, E.B.; Harris, W.A.; Powell, L.C. Relationship between ascorbic acid and male fertility. *World Rev. Nutr. Diet.* **1990**, *62*, 1–26.
50. Safarinejad, M.R. MP-11.10: Effect of Omega-3 Polyunsaturated Fatty Acid Supplementation on Semen Profile and Enzymatic Anti-Oxidant Capacity of Seminal Plasma in Infertile Men with Idiopathic Oligoastheno-teratozoospermia: A Double Blind, Placebo-Controlled, Randomized Study. *Urology* **2009**, *74*, S96. [[CrossRef](#)]
51. Martinez-Soto, J.; Domingo, J.; Cordobilla, B.; Palbero, L.; Pellicer, A.; Landeras, J. Effect of dietary DHA supplementation on sperm DNA integrity. *Fertil. Steril.* **2010**, *94*, S235–S236. [[CrossRef](#)]
52. Gupta, N.P.; Kumar, R. Lycopene therapy in idiopathic male infertility—A preliminary report. *Int. Urol. Nephrol.* **2002**, *34*, 369–372. [[CrossRef](#)]
53. Agarwal, A.; Durairajanayagam, D.; Ong, C.; Prashast, P. Lycopene and male infertility. *Asian J. Androl.* **2014**, *16*, 420–425. [[CrossRef](#)]
54. Nassan, F.L.; Chavarro, J.E.; Tanrikut, C. Diet and men’s fertility: Does diet affect sperm quality? *Fertil. Steril.* **2018**, *110*, 570–577. [[CrossRef](#)] [[PubMed](#)]
55. Terai, K.; Horie, S.; Fukuhara, S.; Miyagawa, Y.; Kobayashi, K.; Tsujimura, A. Combination therapy with antioxidants improves total motile sperm counts: A Preliminary Study. *Reprod. Med. Boil.* **2019**, *19*, 89–94. [[CrossRef](#)] [[PubMed](#)]
56. Kumalic, S.I.; Pinter, B. Review of Clinical Trials on Effects of Oral Antioxidants on Basic Semen and Other Parameters in Idiopathic Oligoastheno-teratozoospermia. *BioMed Res. Int.* **2014**, *2014*, 1–11. [[CrossRef](#)] [[PubMed](#)]
57. Keszthelyi, M.; Sofikitis, N. Administration of Antioxidants in the Infertile Male: When it may have a Beneficial Effect? *Curr. Pharm. Des.* **2020**, *26*, 1. [[CrossRef](#)]

58. Federsalus. Available online: <https://www.federsalus.it/il-mercato-degli-integratori-dinamiche-aggiornate-a-marzo-2019/> (accessed on 20 March 2020).
59. Ronis, M.J.; Pedersen, K.B.; Watt, J. Adverse Effects of Nutraceuticals and Dietary Supplements. *Annu. Rev. Pharmacol. Toxicol.* **2018**, *58*, 583–601. [[CrossRef](#)]
60. Szewczyk, K.; Zidorn, C. Ethnobotany, phytochemistry, and bioactivity of the genus *Turnera* (Passifloraceae) with a focus on damiana—*Turnera diffusa*. *J. Ethnopharmacol.* **2014**, *152*, 424–443. [[CrossRef](#)]
61. Jung, H.A.; Roy, A.; Jung, J.H.; Choi, J.S. Evaluation of the inhibitory effects of eckol and dieckol isolated from edible brown alga *Eisenia bicyclis* on human monoamine oxidases A and B. *Arch. Pharmacol. Res.* **2017**, *40*, 480–491. [[CrossRef](#)]
62. Naderi, N.; House, J.D. Recent Developments in Folate Nutrition. *Adv. Food Nutr. Res.* **2018**, *83*, 195–213. [[CrossRef](#)]
63. Najafipour, R.; Moghbelinejad, S.; Aleyasin, A.; Jalilvand, A. Effect of B9 and B12 vitamin intake on semen parameters and fertility of men with *MTHFR* polymorphisms. *Andrology* **2017**, *5*, 704–710. [[CrossRef](#)]
64. Qi, Y.-N.; Ma, J.; Han, R.-Y.; Liu, W.-J.; Wang, S.-S. Correlation of the levels of seminal plasma homocysteine, folate and cobalamin with semen parameters in obese men. *Zhonghua Nan Ke Xue* **2018**, *24*, 883–886.
65. Duncan, A.; Yacoubian, C.; Watson, N.; Morrison, I. The risk of copper deficiency in patients prescribed zinc supplements. *J. Clin. Pathol.* **2015**, *68*, 723–725. [[CrossRef](#)] [[PubMed](#)]
66. Foresta, C.; Flohé, L.; Garolla, A.; Roveri, A.; Ursini, F.; Maiorino, M. Male fertility is linked to the selenoprotein phospholipid hydroperoxide glutathione peroxidase. *Boil. Reprod.* **2002**, *67*, 967–971. [[CrossRef](#)] [[PubMed](#)]
67. Berger, M.M. Do micronutrient deficiencies contribute to mitochondrial failure in critical illness? *Curr. Opin. Clin. Nutr. Metab. Care* **2020**, *23*, 102–110. [[CrossRef](#)] [[PubMed](#)]
68. Garolla, A.; Maiorino, M.; Roverato, A.; Roveri, A.; Ursini, F.; Foresta, C. Oral carnitine supplementation increases sperm motility in asthenozoospermic men with normal sperm phospholipid hydroperoxide glutathione peroxidase levels. *Fertil. Steril.* **2005**, *83*, 355–361. [[CrossRef](#)]
69. Zhang, X.; Cui, Y.; Dong, L.; Sun, M.; Zhang, Y. The efficacy of combined l-carnitine and l-acetyl carnitine in men with idiopathic oligoasthenoteratozoospermia: A systematic review and meta-analysis. *Andrology* **2019**, *52*, e13470. [[CrossRef](#)]
70. Foresta, C.; Garolla, A.; Cosci, I.; Menegazzo, M.; Ferigo, M.; Gandin, V.; De Toni, L. Role of zinc trafficking in male fertility: From germ to sperm. *Hum. Reprod.* **2014**, *29*, 1134–1145. [[CrossRef](#)]
71. Fallah, A.; Mohammad-Hasani, A.; Colagar, A.H. Zinc is an Essential Element for Male Fertility: A Review of Zn Roles in Men’s Health, Germination, Sperm Quality, and Fertilization. *J. Reprod. Infertil.* **2018**, *19*, 69–81.
72. Manish, K.; Yash, S.; Premal, P.; Neel, P.; Ranjith, R. A Systematic Review and Evidence-based Analysis of Ingredients in Popular Male Fertility Supplements. *Urology* **2020**, *136*, 133–141.
73. Budoff, M.J.; Achenbach, S.; Blumenthal, R.S.; Carr, J.J.; Goldin, J.; Greenland, P.; Guerci, A.D.; Lima, J.A.; Rader, D.J.; Rubin, G.D.; et al. Assessment of Coronary Artery Disease by Cardiac Computed Tomography. *Circulation* **2006**, *114*, 1761–1791. [[CrossRef](#)]



© 2020 by the authors. Licensee MDPI, Basel, Switzerland. This article is an open access article distributed under the terms and conditions of the Creative Commons Attribution (CC BY) license (<http://creativecommons.org/licenses/by/4.0/>).



Review

ω -3 and ω -6 Polyunsaturated Fatty Acids, Obesity and Cancer

Stefania D'Angelo, Maria Letizia Motti and Rosaria Meccariello *

Dipartimento di Scienze Motorie e del Benessere, Università di Napoli Parthenope, via Medina 40, 80133 Napoli, Italy; stefania.dangelo@uniparthenope.it (S.D.); motti@uniparthenope.it (M.L.M.)

* Correspondence: rosaria.meccariello@uniparthenope.it; Tel.: +39-081-5474668

Received: 5 August 2020; Accepted: 7 September 2020; Published: 10 September 2020

Abstract: Recently, nutraceutical bioactive compounds in foods have been discovered for their potential health benefits regarding the prevention of chronic disorders, such as cancer, and inflammatory, cardiovascular, and metabolic diseases. Dietary omega-3 polyunsaturated fatty acids (ω -3PUFAs), including alpha-linolenic acid, docosapentaenoic acid, and eicosapentaenoic acid, are mostly attractive. They are available for the customers worldwide from commonly used foods and/or as components of commercial food supplements. The anti-inflammatory and hypotriglyceridemic effects of these fatty acids are well known, whereas pro-inflammatory properties have been recognized in their dietary counterparts, the ω -6PUFAs. Both ω -3 and ω -6PUFAs contribute to the production of lipid mediators such as endocannabinoids that are notably involved in control of food intake, energy sensing, and food-related disorders. In this review, we present ω -3 and ω -6PUFAs and their derivatives, endocannabinoids; discuss the anti-obesity effects of ω -3PUFAs; their roles in inflammation and colorectal cancer development; and how their action can be co-preventative and co-therapeutic.

Keywords: obesity; ω -3PUFAs; ω -6PUFAs; endocannabinoids; CRC; fatty acids

1. Introduction

The prevalence of obesity has increased worldwide. Obesity represents a major health challenge because it substantially increases the risk of comorbidities, including cardiovascular disease, hypertension, type 2 diabetes, dyslipidemia, nonalcoholic fatty liver disease, obstructive sleep apnea, and some cancers, thereby contributing to a decline in both quality of life and life expectancy [1]. This syndrome is a complex condition involving social, biological, and psychosocial factors. The genesis of obesity is multifactorial: it is characterized by chronic low-grade inflammation, primarily due to an imbalance between the production/secretion of pro-inflammatory cytokines vs. anti-inflammatory cytokines [2]; deregulated lipid and glucose metabolism in metabolic organs is thought to be a critical factor. High-calorie diets and sedentary lifestyles are the most important factors in the development of obesity. As a consequence, global anti-obesity strategies focus on dietary and lifestyle modifications. In fact, weight loss, energy restriction, and nutrient dense diets can restore this imbalance, at least in part [3]. Therefore, the most used approaches aim at suppressing appetite, normalizing lipid metabolism, and increasing energy expenditure [4], through limitation of sugar and fat consumption, promotion of physical activity, consumption of fruits and vegetables, and pharmacological approaches.

Dietary interventions using natural bioactive food compounds have emerged as promising therapeutic tools for metabolic diseases, with limited deleterious side effects. Composition of the diet may affect metabolic and endocrine functions and overall energy balance [5]. Studies conducted in both animal models and humans support the assertion that dietary bioactive compounds can increase energy expenditure and thermogenesis, providing benefits in preventing/limiting obesity. Most health

recommendations emphasize diets rich in fruits and vegetables, which have lower caloric density and higher nutrient density [6]. Such diets would provide significant amounts of phytochemicals, bioactive components with nutraceutical effects due in part to their anti-oxidant and anti-inflammatory properties [7]. Natural bioactive compounds, for example, the polyphenols (epigallocatechin, resveratrol, curcumin, quercetin, oleuropein, anthocyanins, ellagic acid, and others), have been studied as factors with possible indirect or direct impacts on specific molecular pathways, associated with the pathophysiology of different syndromes [8,9] due to their well-documented anti-oxidant [10–12], anti-proliferative [13–16], anti-inflammatory, anti-cancer, anti-aging, and anti-obesity effects [17–21]. In addition to polyphenols, other nutraceuticals with anti-obesity effects are the dietary ω -3 polyunsaturated fatty acids (PUFAs), which can act on adipose tissue inflammation, in contrast to ω -6 (ω -6) PUFAs, which exhibit pro-inflammatory properties. Both ω -3 and ω -6 PUFAs contribute to the production of lipid mediators such as endocannabinoids, which are notably involved in control of food intake, energy sensing, and food-related disorders; reproduction; inflammation; the stress response; and cancer, among other things [22–28].

Therefore, in this review article we present ω -3 and ω -6 PUFAs and their derivatives, endocannabinoids; discuss the anti-obesity effects of ω -3 PUFAs; their role in inflammation and colorectal cancer (CRC) development; and co-preventative and co-therapeutic applications.

2. ω -3. and ω -6 PUFAs

The amount and type of dietary fat in the diet are important factors influencing adipose tissue function and whole-body metabolism, with important health ramifications. Fatty acids (FA) are hydrocarbon chains with a carboxyl group at one end and a methyl group at the other. FA species are classified by their varying degrees of saturation into three main classes: saturated fatty acids (SFA), monounsaturated fatty acids (MUFA), and polyunsaturated fatty acids (PUFA) [29].

SFAs have a simple carbon chain containing no double bonds; MUFAs contain one double bond; and PUFAs are classified as carbon chains containing two or more double bonds. The variations in the chemical structures of these diverse classes can lead to dissimilar physiological activities. For example, SFA has been linked to the development of metabolic dysfunction; contrariwise, MUFAs and PUFAs have helpful activities in metabolism [30].

PUFAs are additionally classified into ω -3 and ω -6 groups, based on the position of the first double bond from the methyl end of the fatty acid. The structural dissimilarities of these FAs also give rise to functional differences, in terms of their actions on inflammation and metabolism [5].

ω -3 FAs are PUFAs with more than one carbon-carbon double bond in their backbones. They are polyunsaturated because their chains have numerous double bonds. One way in which a FA is named derives from the position of the first double bond, counted from the tail, that is, the omega (ω -) or the n-end. Thus, in ω -3 FAs, the first double bond is between the third and fourth carbon atoms from the tail end; then, they have a double bond at the third carbon from the methyl end of the carbon chain.

Humans do not own the essential ω -3 desaturase to add a double bond at the 15th carbon of a long chain FAs, and are, therefore, unable to endogenously synthesize α -linoleic acid (ALA 18:3n-3) and linoleic acid (LA 18:2n-6), making them vital FAs.

In addition to ALA, ω -3 PUFAs can be defined as a heterogeneous mix of FAs, among which eicosapentaenoic acid (EPA, 20:5n-3) and docosapentaenoic acid (DHA, 22:6n-3) are presently thought to be the most bioactive of the ω -3 species; however, docosapentaenoic acid (DPA, 22:5), an intermediate of EPA and DHA, may also have positive health properties [30,31].

ω -6 PUFAs are also essential fatty acids and normally have metabolically distinct properties to ω -3 PUFAs. While the human body cannot synthesize ω -3 and ω -6 PUFAs, it does have the capability to further metabolize these FAs through stages of elongation and desaturation. ALA can be metabolized to EPA and DHA by Δ 6 desaturase and Δ 5 desaturase correspondingly, while LA is transformed to arachidonic acid (AA 22:4n-6). However, the change of ALA to DHA is very inefficient with <10% transformation in females and <3% in males [30,32]. While ALA is the favorite substrate for

$\Delta 6$ desaturase, plenty of dietary linoleic acid has been observed to suppress the change of ALA to DHA, which may be a confounding factor in these data. Evidence suggests that supplementing with stearidonic acid (18:3n-3) may increase the efficiency of transformation to DHA, demonstrating $\Delta 6$ desaturase as a rate limiting step. There is also a degree of individual change in the lipidome following ω -3 integration in humans, which may be a factor in the equivocal metabolic conversion measured in many human integration trials [30,33].

The structural differences of the FAs give rise to functional dissimilarities, in terms of their actions on inflammation and metabolism. For example, due to the pro-inflammatory actions of saturated FAs, intake of these molecules is associated with an increase in cardiovascular disease risk. In contrast, ω -3PUFAs have anti-inflammatory capability, and their intake is connected to a decrease of in cardiovascular disease risk. Dietary FAs are involved in glucose-insulin homeostasis and modulating adipose tissue properties [5]. High saturated-fat intake causes adipose tissue inflammation and obesity in mice; those effects can be partially reduced when these high-fat diets are energy-restricted [29]. Instead, dietary EPA supplementation ameliorates adipose tissue inflammation, regardless of adipose tissue mass. These data, taken as a whole, demonstrate the importance of AF in modulating the adipose tissue properties [34].

Saturated FA, generally, contributes to adipose tissue inflammation, probably due to TLR-2 and TLR-4 activation, and switching of downstream pro-inflammatory signaling pathways comprising the nuclear factor kappa-light-chain-enhancer of activated B cells (NF- κ B) pathway [29]. In contrast, ω -3 FA, primarily DHA and EPA, mitigate adipose tissue inflammation in diverse animal models of obesity [34]. Compared to ω -6PUFAs such as AA, ω -3PUFAs generate less eicosanoids with inflammatory properties. Additionally, ω -3PUFAs competitively decrease AA-mediated inflammatory eicosanoid prostaglandin E2 (PGE2) synthesis. As a whole, food sources rich in healthy fats can provide health benefits in both the long and short term.

Figure 1 summarizes the essential fatty acids and their dietary sources. In general, the primary source of ω -3PUFAs in the human diet is marine products, in particular phytoplankton that enters at multiple levels in the food chain [34], fatty fish, and cod liver oil, food rich in DHA and EPA [35,36].

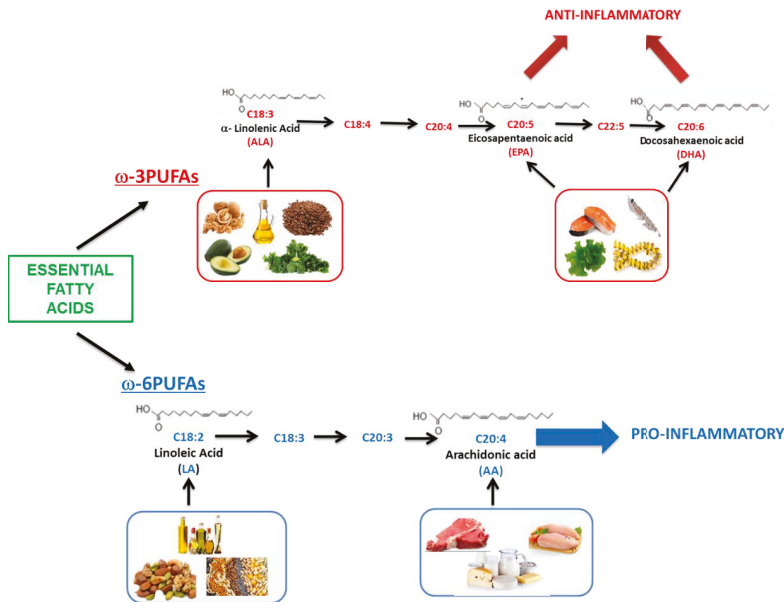


Figure 1. Essential fatty acids and dietary source (AA: arachidonic acid; ALA: α -linolenic acid; DHA: docosahexaenoic acid; EPA: eicosapentaenoic acid; LA: linoleic acid; PUFA: polyunsaturated fatty acid).

In plants, ALA can be extracted from seeds such as flaxseed (linseed), green leafy vegetables, legumes, and nuts. Vegetable oils such as sunflower, corn, perilla, canola, and soybean are the principal sources of LA, and they provide a small amount of ALA [31].

2.1. Endocannabinoids: PUFAs Derivatives Involved in the Central and Peripheral Control of Food Intake

The endocannabinoid system (ECS) comprises lipid mediators capable of binding to and activating cannabinoid receptors—traditionally, the central and the peripheral cannabinoid receptor, CB1 and CB2 respectively, membrane G-coupled receptors originally found to be mainly expressed in the brain and peripheral tissues. The system also includes a large set of biosynthetic and metabolizing enzymes and transporters [37]. Since the discovery in the 1990s of the first endocannabinoids, anandamide (AEA) and 2-arachidonoylglycerol (2-AG), the relevance of ECS has been progressively widening due to the inclusion in the system of non-canonical cannabinoid receptors (i.e., the transient receptor potential cation channel subfamily V member 1 (TRPV1); the orphan G-coupled receptors GPR18, GPR119, and GPR55; and also peroxisome proliferator-activated receptors (PPARs) such as PPAR α and γ), the discovery of several “endocannabinoid-like” compounds, and the large spectrum of biological functions [38]. Currently ECS represents a conserved, widely-expressed signaling system involved in the control of most biological activities within the brain and peripheral tissues, from food intake to reproduction, the immune response, and cancer, among others [22–28,39], and it is susceptible to epigenetic modulation by diet [40].

Traditionally, AEA and 2-AG are the N-ethanolamide and the glyceryl ester of ω -6PUFA AA respectively, and represent the main endogenous ligands of CB1 and CB2, with AEA having low CB2 affinity, and 2-AG capable of binding both receptors [41]. The endocannabinoids N-docosahexaenoyl ethanolamine (DHEA) and N-eicosapentaenoyl ethanolamine (EPEA) are ω -3 DHA and ω -3 EPA derivatives respectively; docosahexaenoylglycerol (DHG) and eicosapentaenoyl glycerol (EPG) are the glycerol esters of ω -3 DHA and EPA derivatives and have been discovered following the investigations on 2-AG analogues. While ω -6 AA derivatives AEA and 2-AG bind the canonical receptors [41], ω -3 EPA/DHA derived endocannabinoids, and endocannabinoid-like compounds exhibit lower affinity binding to CB1/CB2 than AEA/2-AG, and in some cases bind the aforementioned non canonical cannabinoid receptors [42]. Currently, ω -3 derived endocannabinoids are known at lesser extent than canonical ones, and their basic characterizations support possible involvement in inflammation, neuroprotection, and cancer [42]. Details concerning the metabolic/hydrolyzing pathways linking ω -3 and ω -6, endocannabinoids, and inflammatory mediators are summarized in Figure 2.

Endocannabinoids, via CB1, have a recognized role as orexigenic factors, in that they stimulate food intake and body fat deposition [26,43]; at the periphery ECS activity is largely reported in the gastrointestinal tract, and liver and adipose tissue, along with possible involvement in the microbiota–gut–brain axis and obesity onset, as excellently reviewed in [23]. Obese subjects display high endocannabinoid tone in the plasma and brain; furthermore, altered expression of CB1 and higher endocannabinoid levels in the muscle, adipose tissue, pancreas, and liver have been reported ([23] for a recent review). Consistently, CB1 activation increases food intake [44], whereas its pharmacological and genetic impairment reduces food assumption, protecting against the development of obesity, liver steatosis, and related inflammation [45,46]. Traditionally endocannabinoid signaling via CB1 is involved in the central control of food intake exerting its activity within the hypothalamus. This brain region catches and integrates the environmental cues, including fuel availability, in order to maintain energy homeostasis [47], projects neuronal networks towards different nuclei within the hypothalamus or in the brain stem controlling both the homeostatic regulation of energy balance, and biological functions deeply related to energy homeostasis and availability, such as reproduction [26]. Appetite inhibiting neuropeptides, such as proopiomelanocortin (POMC) precursor and cocaine-amphetamine regulated transcript (CART), and appetite stimulating neuropeptides such as neuropeptide Y (NPY), melanin-concentrating hormone (MCH), and agouti related protein (AgRP), are produced within the hypothalamic arcuate nucleus (ARC) to mediate the adaptive changes in food intake and energy

expenditure in response to nutrient availability and peripherally produced “metabolic sensors” (i.e., glucose from liver, interleukin-6 (IL-6) from muscle, leptin from white adipose tissue, insulin, amylin and pancreatic polypeptide from pancreas, glucagon-like peptide-1, ghrelin, cholecystokinin and peptide YY from the gastro-intestinal tract, and lastly gut microbiome-derived signals) [23,26,47]. ECS activity may be affected by metabolic sensors and may modulate neuronal population producing orexigenic/anorexigenic-peptides [26]. Among “metabolic sensors,” leptin is the major peripheral indicators of body metabolic reserves acting as satiety signal [48]. In the natural mutant mice for *Leptin* gene, the Ob/Ob mice, over activation of ECS has been reported in the hypothalamus whereas leptin inhibits the hypothalamic activity of ECS [49]. Additionally leptin resistance, a condition causing food intake alteration and consequent obesity development, has been linked to the over-activation of the ECS [49], with a sex-specific epigenetic modulation of *cnr1*, the gene encoding CB1, following maternal high fat diet (HFD) [50]. Therefore, CB1 antagonist-based therapy has been used for the treatment of obesity, but, in spite the promising anti-obesity effects, the treatment caused severe psychiatric side effects and has been discontinued in patients [51].

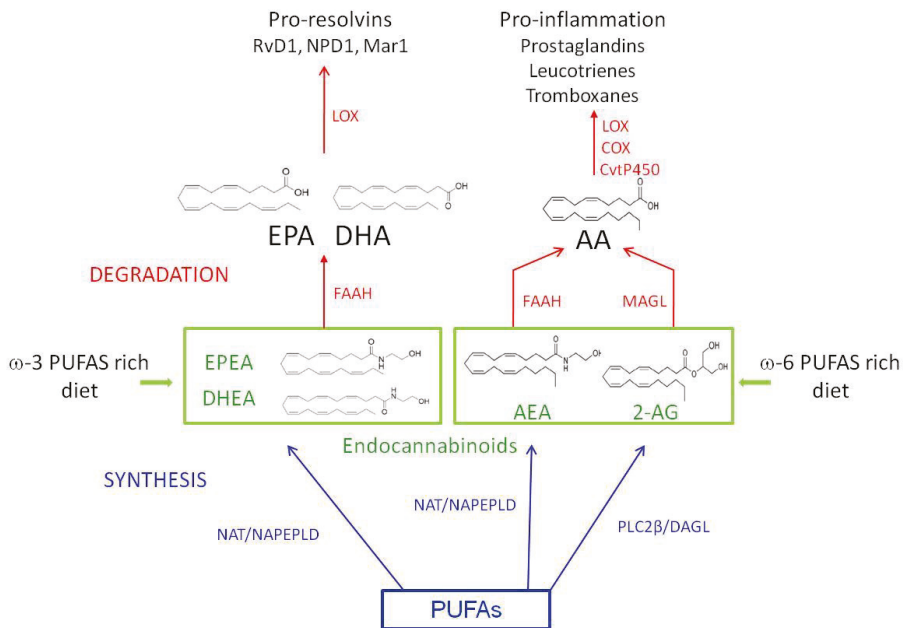


Figure 2. A schematic representation of the metabolic/hydrolyzing pathways linking ω-3 and ω-6, endocannabinoids, and inflammatory mediators. The syntheses of DHEA and EPEA, and AEA from ω-3 and ω-6 PUFAs respectively, requires the activity of N-acetyltransferase (NAT) followed by N-acyl phosphatidylethanolamine-specific phospholipase D (NAPEPLD). The synthesis of 2-AG from ω-6 PUFAs requires the subsequent activity of phospholipase Cβ (PLCâ) and diacylglycerol lipase (DAGL). The hydrolysis of the endocannabinoids requires the activity of the fatty acid amide hydrolase (FAAH) and monoacylglycerol lipase (MAGL). The activity of lipoxygenases (LOX), cyclooxygenase (COX), and cytochrome P450 enzymes (CyP450) drives the production of inflammation mediators. AA: arachidonic acid; AEA: anandamide; 2-AG: 2-arachinonylglycerol; DHA: docosahexaenoic acid; DHEA: N-docosahexaenoyl ethanolamine; EPA: eicosapentaenoic acid; EPEA: N-eicosapentanoyl ethanolamine; Mar1: maresin 1; NPD1: neuroprotectin D1; PUFA: polyunsaturated fatty acid; RvD1: resolvins D1.

A deep interplay between the synthesis and actions of the AA, DHA, and EPA-derived endocannabinoids and ECS occurred, as recently reviewed [52]. In this respect, many authors suggest that dietary PUFAs and in particular the ω -6/ ω -3 ratio may affect the endogenous tone of endocannabinoids with consequences on health [26,53]. For example, in animal models fed for three or four months with a ω -3 deficient diet, low DHA levels in the brain with effects on ECS and synaptic plasticity have been discovered [54,55]; similarly, long-term EPA and DHA supplementation reduces AEA and 2-AG levels, with reciprocal increases in levels of the corresponding endocannabinoid-like EPA- and DHA-derived molecules [52].

Lastly, dietary intervention may epigenetically affect ECS in animal models, and cell lines [40]; and at present, a recurrent process potentially influencing the development of eating disorders such as binge-eating has been related to the epigenetic modulation of FAAH [56], the gene encoding for the main endocannabinoid hydrolyzing enzyme.

3. The Antiobesity Effects of ω -PUFAs

DHA and EPA exert numerous beneficial effects, and they act as natural hypolipidemics, decrease risk of cardiovascular syndromes and could prevent the progress of insulin resistance and obesity [57].

Human dietary intervention trials suggest that fish oil (EPA and DHA) supplementation might decrease waist circumference. ω -3PUFAs decrease adiposity by numerous effects. For example, DHA and EPA start AMP-activated protein kinase (AMPK), which in turn activates FA β -oxidation in adipose tissue [5]. DHA and EPA are also promoting mitochondrial biogenesis, which can increase energy metabolism [58].

In rodents, DHA and EPA also raise FA oxidation in the small intestine and liver in vivo experiments. DHA and EPA prevent hepatic lipogenesis in an AMPK and PPAR α -dependent manner [5]. PPARs are transcription factors that form heterodimers with retinoid X receptors in the promoter regions of different genes implicated in glucose and lipid metabolism [59]. PPAR γ works as a main regulator of adipogenesis and checks numerous genes and adipokines in glucose and lipid metabolism. ω -3PUFAs work as ligands for PPAR γ , and it has been observed that PPAR γ plays a evident role in the capability of ω -3PUFAs, particularly DHA, to prompt M2 macrophage polarization and thereby decrease inflammation since these data are not detected in PPAR γ -knockdown RAW264.7 cells [60]. The EPA- and DHA-mediated increment in FA oxidation and decrease in lipogenesis could be accountable for their anti-obesity actions [61].

In Figure 3, some signaling mechanism-mediating effects of ω -3PUFAs are summarized.

DHA and EPA may act as anti-inflammatory agents directly. EPA improves adipose tissue inflammation and decreases insulin resistance. The ameliorations in adipokines' profiles are characterized by rises in anti-inflammatory adipokines, such as adiponectin, and reductions in pro-inflammatory cytokines, such as IL-6, tumor necrosis factor- α (TNF- α), monocyte chemo attractant protein 1 (MCP-1), and plasminogen activator inhibitor 1 (PAI-1). EPA and DHA's action of normalizing plasma adiponectin concentrations appears to be largely responsible for their insulin sensitizing action. This favorable activity on adiponectin secretion seems to be PPAR γ -dependent, because fish oil fails to raise plasma adiponectin in PPAR γ -null mice [62].

Prostaglandins, eicosanoids with pro-inflammatory action, are secreted by adipocytes. AA-originated eicosanoids such as thromboxane A2 and PGE2 possess stronger inflammatory action than EPA-originated ones. Since EPA contends with AA for incorporation into cell membranes, it is possible that enhancement dietary EPA intake decreases synthesis of AA-originated eicosanoids. Indeed, EPA hinders AA-induced secretion of PGE2 from 3T3-L1 adipocytes in vitro [63].

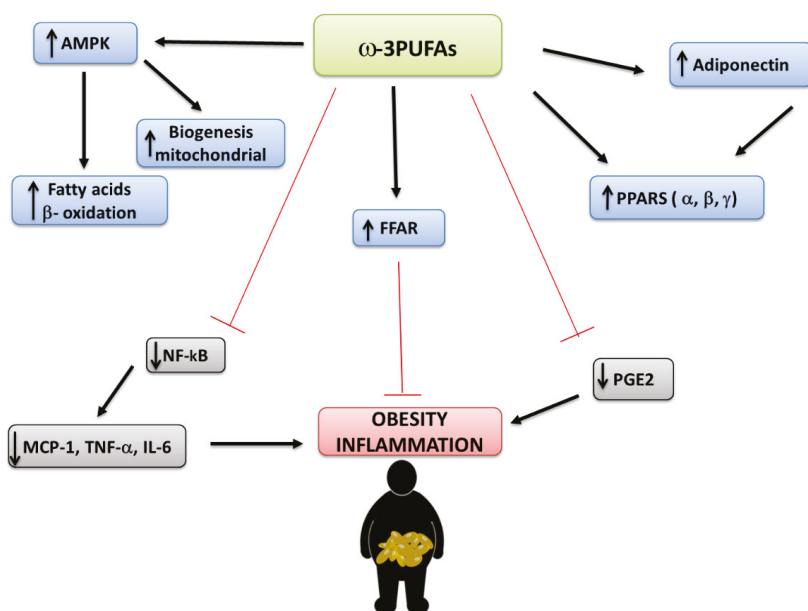


Figure 3. Some signaling mechanisms mediating effects of ω -3 PUFAs (AMPK: AMP-activated protein kinase; FFAR: free fatty acid receptor; IL-: Interleukin-; MCP-1: Monocyte chemo attractant protein 1; NF- κ B: nuclear factor- κ B; PGE2: Prostaglandin E2; PPAR: Peroxisome proliferator-activated receptor; PUFA: polyunsaturated fatty acid; TNF- α : Tumor necrosis factor- α).

A close link was observed between inflammatory markers, BMI, and body fat percentage. NF- κ B, a key transcription factor in gene expression and cytokine inflammation is inhibited by ω -3 PUFAs. Studies in humans and in vitro have shown that ω -3 PUFAs are involved in the reduction of cytokines, such as IL-1, IL-6, and TNF- α , whose concentrations are high in cases of obesity [64]. The ω -3 PUFAs behave as agonists for numerous free fatty acid receptors (FFARs) typical of different cell types, involved in both the inflammatory response and energy homeostasis. Some unsaturated and saturated long-chain fatty acids can activate FFAR1 and FFAR4 [65]. For example, FFAR4 stimulation prevents lipopolysaccharide (LPS)-mediated release of inflammatory cytokines, such as TNF- α and IL-6 in the macrophage-type RAW264.7 cell line [64].

Current data show that reduction of inflammation is an active process. EPA and DHA-derived resolvins and protectins are key examples of inflammation resolution agonists. Experiments involving treatment with resolvins or transgenic restoration of protectins have shown a slowdown of the adipose tissue macrophage infiltration, and enhanced insulin resistance in rodents. Secretion of these mediators could be another mechanism by which DHA and EPA ameliorate the inflammation in adipose tissue [5].

Human clinic trials have been organized to evaluate the effects of the intake of ω -3 PUFAs (using as food different types of fish with different contents of DHA and EPA) on the variation of composition and body weight, and also on the evaluation of the caloric content of food intake. Fish oil and fishes have also been used in dietetic interventions of different duration and with or without associated physical activity, to evaluate a possible weight loss.

Participant-reported diet diaries show evident decreases in fat, carbohydrate, and total caloric intake with ω -3 PUFAs integration [66], but others reported no variation in energy intake [29,67]. Since most trials only indicated total caloric intake, the action of ω -3 PUFAs integration on macronutrient and energy intake should be repeated in larger trials to conclusively establish the action of these PUFAs on weight reduction in humans. Weight reduction data appear more encouraging when ω -3 PUFA

integration and calorie restriction are combined, but it is problematic to draw deductions due to the diversity of calorie limit programs in dissimilar trials. Combined ω -3PUFAs supplementation and calorie restriction compared to calorie restriction alone or replacement of saturated fatty acids determined a major amelioration in insulin resistance and reduction of TGs [68,69]. ω -3PUFAs could decrease body weight, thereby improving the metabolic profile through various mechanisms: alteration in adipokines release; modification of gene expression in adipose tissue; adipokine-mediated or adipokine-connected pathways; variation in carbohydrate metabolism; appetite suppression; rise in fat oxidation; intensification in energy expenditure (probably by thermogenesis); initiation of mechanisms related to muscle anabolism; and, lastly, epigenetic actions.

The adipose tissue increase in obesity happens via hyperplasia (augmentation in adipocyte number due to adipogenesis) and adipocyte hypertrophy (growth of adipocytes). Both ω -3 and ω -6 PUFAs can bind and/or control transcriptional factors that regulate genes implicated in pre-adipocyte differentiation. Principally, AA and its derivatives act as ligands for PPAR γ and PPAR δ to cause fat cell differentiation and quicken maturation by increasing lipoprotein lipase expression in vitro [70]. Importantly, concentrations of ω -6 and ω -3PUFAs in human subcutaneous tissue are associated with less adipocyte size; improved saturated FA concentrations lead to amplified fat cell size. Considering all these data, it is possible to propose that ω -3PUFAs stimulate adipogenesis and a healthy expansion of adipose tissue during positive energy balance, stimulating a metabolically healthy phenotype [70].

Numerous trials have observed that ω -3PUFAs modulate adipokine secretion. Obese individuals have high plasma leptin values indicative of leptin resistance. Weight-loss-connected to decrease in leptin could act on hunger and a lower metabolic rate and ultimately lead to weight regaining [71]. EPA integration reduces the decrease in blood leptin values, which happens during weight loss in obese women, proposing a potentially prominent role of EPA in weight loss conservation [72]. ω -3PUFA-mediated consequences on leptin are related to a various factors, such as energy balance and kind of diet, which could determine incompatible data anyway [29]. It has been suggested that the anti-inflammatory capacities of ω -3PUFAs integration cause a rise in adipocyte adiponectin synthesis and get better leptin sensitivity. This interaction could have a substantial influence on body weight control.

A study described evident sensations of fullness in the attendees who took higher ω -3 PUFA content food compared to those who took lower ω -3PUFA content meals both immediately and 2 h after eating the meal. [73]. Consequently, it is possible that an increase in the feeling of satiety after a meal rich in ω -3PUFA content can help weight loss by reducing the next food intake. Additionally, FFAR4 could mediate appetite reduction. ω -3PUFAs are agonists for FFAR4, which provokes the secretion of cholecystokinin, a hormone that is synthesized, is freed from the small intestine, and is related to appetite suppression [74].

Brown adipose tissue (BAT) is a particular fat that disperses excess energy into heat (non-shivering thermogenesis) through mitochondrial uncoupling protein 1 (UCP1). Current studies confirm the metabolic activity of BAT by revealing BAT as a crucial regulator in ensuring energy balance by rising thermogenic energy consumption. An important quantity of BAT is dose in healthy adults and most children and adolescents, but not in the obese adults, indicating that loss of operative BAT depots is a contributing obesity factor. Cold- and diet-induced thermogenesis mediated by UCPs in the presence of ω -3PUFA have been analyzed in some studies [75]. UCPs are inner mitochondrial proteins moving hydrogen ions across the mitochondrial inner membrane [76]. ω -3PUFAs enhance mitochondrial oxidative capability in skeletal muscle and WAT, probably through UCP-3 up-regulation, but not in liver or BAT. Nevertheless, because most trials were carried out at 20 °C, it is uncertain whether increment in mitochondrial oxidative capability is ω -3PUFA-mediated or cold caused. Mechanisms relating the role of ω -3PUFAs in probable induction of energy expense and reduction of body fat should be investigated further at different temperatures since thermogenic markers act even at 22 °C [76].

Control of lipid metabolism may change by ω -3PUFA type, and by fat store. For example, EPA is preferably aimed to β -oxidation, while DHA and DPA avoid catabolism and are stored

in tissues. Furthermore, hormone-sensitive lipase, and gene expressions of fatty acid synthase, phosphoenol-pyruvate carboxykinase, and lipoprotein lipase, in retroperitoneal fat, are reduced with DHA and mixed EPA/DHA integration but not with EPA integration alone [77]. Additionally, ultimately, ω -3 PUFAs control lipid metabolism, encouraging fatty acid oxidation and repression of lipogenesis, causing a positive lipid profile and adipocyte metabolism.

The determination of ω -6 and ω -3PUFAs composition in the cell membrane of red blood cells (RBC) represents a biomarker of dietary intake and endogenous metabolism; in addition, it is a precise way to perform estimated studies and clinical trials in order to value their effects in weight increase and obesity. Harris et al. led a prospective study to observe the link between baseline RBC membrane phospholipids of ω -3PUFAs, ω -6PUFAs, ω -6/ ω -3 ratio, and *trans* FA with the variations in body weight and the risk of becoming obese or overweight during a mean of 10.5 years follow up in the NIH Women's Health Initiative Study. This prospective analysis provided a strongly suggestive sign that ω -3PUFAs in RBC membrane phospholipids are reversely connected, while *cis* ω -6, ω -6/ ω -3 ratio and *trans* fatty acids are favorably related with weight gain [78].

Recommendations for PUFAs Intake

The recommended intake for ω -3PUFAs is based on governing body. The Dietary Guidelines for Americans recommend consuming about 230 g/week of fish, corresponding to approximately 250 mg/day of EPA and DHA [29]. This recommended intake corresponds to consuming fish twice weekly, including one serving of oily fish. The U.S. Food and Drug Administration claimed that levels up to 3 g/day are considered as safe, while other authorities suggested at up to 5–6 g/day [79].

However, in intervention studies reporting a favorable health effect, the intake of fish oils or their derivatives resulted in long chain ω -3PUFAs daily intakes well above those "suggested" 200 mg/day and ranged from 0.5 to 9 g/day. Consequently, this justifies readjustments of nutritional guidelines to an upper level. Governments (UK, Belgium, The Netherlands, France, New Zealand, and Australia) and health organizations (American Heart Association, FAO/WHO, American Dietetic Association,) now advise dietary consumption for total ω -3 PUFA of 1.4 to 2.5 g/day, with EPA and DHA ranging from 140 to 600 mg/day depending on the authority issuing guidelines, FOA/WHO making a relatively low recommendation of 250 mg/day, the average being around 500 mg/day [80]. This means minimum of 2 intake of fish/week (30–40 g/day), including one of oily fish (tuna salmon, sardine, and mackerel). In the light of the literature and inter individual changeability in PUFA metabolism and requirement, perhaps the minimal EPA+DHA supplies for healthy adults should reach 0.5–1 g/day (2–4 servings per week of fish, half of oily fish); that is minimal intake proved to reduce obesity and, in general, metabolic syndrome [81], with a total serving of ω -3 PUFA of 5–6 g/day as found in ancestral nutrition to which our metabolism is best fit [82]. Such levels are met in the traditional Japanese diet as it contains 80–100 g fish and shellfish/d/capita [81,83].

Numerous studies have discussed the actions of ω -3 PUFAs integration on obesity, in both animal and human models, highlighting possible mechanisms for ω -3PUFAs in decreasing body weight, improving body composition and counteracting the contrary metabolic effects of obesity [28,84]. However, clearly, findings of prospective studies concerning the favorable actions of ω -3 intake on obesity are far from agreement. The manifest discrepancies may have arisen due to differing or inadequate methods of data collection on food intake (food frequency questionnaires), changes in cooking procedures and other unaccounted for lifestyle behaviors (exercise, etc.) from study to study and among diverse study populations [29]. Therefore it is not possible at present to decide the ω -3-dose to hinder obesity, neither through food, nor through integration. The advice is to act through nutritional interventions. In general, it is recommendable to replace the intake of SFAs with PUFAs. The World Health Organization (WHO) prompts eating at least two servings of oily fish per week, which is rich in the ω -3PUFAs (DHA and EPA) [85]. International and national guidelines on healthy eating agree in advising the intake of ω -3, both marine and vegetable, with a diverse and balanced diet, containing foods in which they are naturally present. In subjects at cardiovascular risk and on a

diet low in these fatty acids, or in patients in secondary prevention, integration at diverse levels should be estimated with the specialized doctor [81]. Human intervention trials indicate potential benefits of ω -3PUFAs supplementation, especially when combined with energy-restricted diets or exercise, but more well-controlled and long-term trials are needed to confirm these effects and identify doses for antiobesity-action.

ω -6PUFAs are pro-inflammatory and commonly occur in poultry, eggs, corn, and most vegetable oils, and also in processed and fast foods. ω -6PUFAs have pro-inflammatory capability and are considered to be the counterpart of ω -3PUFAs, which are anti-inflammatory [18]. A high-fat diet and the Western dietary pattern feature high quantities of ω -6PUFAs and low amounts of ω -3PUFAs. Instead, a low-fat diet (e.g., traditional Japanese diet) is low in ω -6PUFAs and high in ω -3PUFAs [86]. Data show that a higher ratio of ω -6/ ω -3PUFAs increases inflammation and the probability of chronic inflammatory syndromes, including cardiovascular disease, obesity, and nonalcoholic fatty liver syndrome [18]. Preclinical studies show that ω -6 PUFAs have a tumor-enhancing effect. In a recent Japanese cohort study, incorporating 38,200 women, ω -6PUFA intake was positively associated with breast cancer risk [81,87].

Many data discussed the importance of preserving a low omega-6/omega-3 ratio for decreasing inflammation. Decreasing the ω -6/ ω -3 ratio seems to reduce the inflammatory response to a high-fat meal [88]. A stable ω -6/ ω -3 is one of the most significant dietary factors in the inhibition of obesity: a lower ω -6/ ω -3 ratio should be reputed in the management of obesity [89]. A high omega-6 fatty acid intake and a high ω -6/ ω -3 ratio are connected with weight gain in both animal and human investigations, whereas a high ω -3 FAs intake reduces the risk for weight gain [89].

Several sources of information recommend that human beings evolved on a diet that had a ratio of ω -6 to ω -3PUFA of about 1/1; whereas today, Western diets have a ratio of 10/1 to 20–25/1, demonstrating that Western diets are lacking in ω -3PUFA related with the diet on which humans evolved and their genetic patterns were established [90,91].

Due to agribusiness and modern agriculture western diets enclose unnecessary levels of omega-6 PUFAs but very low levels of ω -3PUFAs, leading to an unhealthy ω -6/ ω -3 proportion, instead of 1:1 that was during evolution [90]. It is thought that hominids' foods during the Paleolithic era were high in seafood and low in seeds and vegetable oils, which led to a ω -6/ ω -3 proportion of about 1:1 [30,92,93]. ω -6PUFAs are related to the synthesis of pro-inflammatory mediators while omega-3 PUFAs produce less powerful inflammatory mediators and inflammatory resolving proteins, so manipulating this proportion may bring about helpful health outcomes.

A balanced ω -6/ ω -3 FA ratio (1:1 to 2:1 is optimal) is vital for homeostasis and regular development throughout the lifespan [92,94,95]. However, there are significant genetic variables in fatty acid biosynthesis including desaturase 1 and desaturase 2, which encode rate-limiting enzymes for FA metabolism. Data connected to genotyping of the desaturase region analyzed in human populations show that present-day humans vary dramatically in their capability to produce long-chain PUFAs [89,96].

In clinical investigations and intervention trials it is indispensable that the background diet is precisely determined in terms of the ω -6 and ω -3 FAs content. Because the concluding concentrations of ω -6 and ω -3PUFAs are defined by both dietary intake and endogenous metabolism, it is important that in all clinical investigations and intervention trials the ω -6 and ω -3 FAs are precisely defined in the red blood cell membrane phospholipids [89].

Mice fed the lowest ω -6/ ω -3 ratio had the lowest non-HDL (i.e., atherogenic lipoproteins) and inflammation (IL-6). Mice fed lower ω -6/ ω -3 ratio diets also had less macrophage cholesterol increase and less aortic atherosclerotic lesions. The lowest ω -6/ ω -3 ratio (1:1) diet led to the least atherosclerotic formation and the severity of atherosclerosis augmented as the ω -6/ ω -3 proportion increased [97].

Using long-chain ω -3PUFAs to suppress low-grade inflammation may advantage numerous chronic syndromes such as atherosclerosis, rheumatoid arthritis, diabetes, dyslipidaemia, obesity and heart failure. The ingesting of ω -6 seed oils may have the contrary action [98].

The consequences of extreme ω -6PUFAs remain controversial: ω -6PUFAs have intrinsic cardiovascular protective actions, justifying the latest FAO/WHO recommendations on maintaining high ω -6PUFAs consumptions if ω -3PUFA ones are fulfilled [99]. However, ω -6PUFAs compete with ω -3PUFAs for processing to eicosanoids, thereby limiting synthesis of anti-inflammatory ω -3PUFA derived mediators [100]. Moreover, there are convincing proofs that a low ω -6/ ω -3PUFA ratio is determinant for the inhibition of pathologies connected to the metabolic syndrome, as colorectal cancer [101].

Deduced from ancestral nutrition, in an ideal balanced diet, fat should represent no more than 20–30% of total energy intake amongst which 5–6 g/day of ω -3PUFAs with a great percentage of EPA+DHA and the ω -6-to- ω -3 proportion should average 1 [102,103]. To keep in with a developmental approach and with the epigenetic consequences of the diet, a proportion of ω -6/ ω -3 around 1 in breast milk should serve as a bench mark to decide the correct dietary requirements during pregnancy, lactation, and infant feeding [81,104].

4. Role of ω -3PUFAs in Inflammation and Colorectal Cancer Development

A large body of literature highlights the importance of dietary intake for the risk and progression of chronic disorders including inflammatory and neoplastic disease [105]. Nowadays it is well known that inflammation is a predisposing factor for cancer capable to promote the insurgence of several types of tumors [106], and that an inflammatory microenvironment is an essential component of all tumors. During metastasis development it has been shown that microenvironment modulates the capability of tumor cells and cancer stem cells to evade the innate immune response and survive. The metastatic niche is a complex system including several cell types, as vascular, stromal, and above all inflammatory and immune cells, in addition to many other molecules which provide survival, immune surveillance protection and metabolic requirements. The interaction among all these factors determines metastatic dissemination [107].

Only a few of all cancers depend on germline mutations, while the majority is determined by somatic mutations and environmental factors. Most often cancer is caused by chronic inflammation such as chronic infections, tobacco smoke, inhalation pollutants (such as silica and asbestos), and dietary factors (some forms of cancer are linked to obesity) [108]. Furthermore, in some cases exogenous diet-derived miRNAs might substantially contribute to the pool of circulating miRNAs, regulating tissue homeostasis and interfering with human health [109].

CRC is a multifactorial disease caused by multiple genetic and environmental factors. These include the type of diet, the lifestyle, the intake of alcoholic beverages, smoking, obesity, genomic abnormalities, alterations in the signaling pathways, chronic activation of the inflammatory response, oxidative stress, dysbiosis, etc. These factors work by altering intestinal homeostasis [110]. In fact, despite still lacking extensive epidemiological studies to date, most cases of early-onset colorectal cancer (EO-CRC) arise sporadically and are attributable to environmental factors [111]. In recent years, due to the activation of preventive screening activated in the population aged ≥ 50 years, the incidence of CRC in Western countries has stabilized and even decreased. In contrast, the incidence of CRC among people under the age of 50 has increased in both Europe and the United States, thereby representing a major public health problem [112,113]. However, CRC remains the fourth leading cause of cancer death in the world dependent on a close relationship between inflammation and environmental factors [114].

The gastrointestinal tract is not only responsible for digestion and absorption of nutrients but also represents a powerful barrier against pathogens and toxins harmful to the individual. It also has an endocrine function responsible for maintaining the metabolic homeostasis of the whole organism. Since the intestine comes into direct contact with food, it is very sensitive to dietary factors which directly influence both its structure and function [115]. In fact, the crypts and intestinal villi are structurally influenced by external factors by changing their size in response to changes in the diet [116].

Since chronic inflammation has been shown to promote the onset of CRC in humans, ω -3PUFAs, due to their strong anti-inflammatory function, have been shown to be protective against colon cancer [117,118].

Some studies have been conducted on the efficacy of ω -3PUFAs in the prevention of CRC through the integration of purified EPA with DHA or fish oil (FO). These studies have shown the importance of ω -3PUFAs in inhibiting the uncontrolled proliferation of CRC cells both when administered in large quantities for short times (8–9 g of EPA+DHA/day for 2 weeks) and in smaller quantities for longer times (2.5–4 g of EPA+DHA/day for 3–6 months). However, the effect on the control of intestinal cell proliferation was not seen in patients with the same supplementation but with a high-fat basal diet and a low ω -3/ ω -6PUFAs ratio. For this reason, the effectiveness of ω -3PUFAs depends on both the total lipid content and the ω -3/ ω -6PUFAs ratio [119].

Many studies have been conducted in CRC models to explain the molecular mechanisms to the base of the anti-inflammatory and anti-neoplastic activity of ω -3PUFAs. First of all, ω -3PUFAs are incorporated in phospholipid membrane inducing an alteration in structure, fluidity and function of lipid rafts. These membrane changes influence the activity of membrane receptors leading at the inhibition of signaling pathways involved in the activation of pro-inflammatory molecules of cell survival and apoptosis [120–122]. Moreover, in CRC, ω -3PUFAs modulate inflammatory pathways, generating lipid mediators implicated in the resolution of inflammation including resolvine, protectin, and maresins [123].

The ω -3PUFAs exert their antitumor actions through different mechanisms, involving proliferation, apoptosis, and migration. Their effects involve COX-dependent or COX-independent mechanisms, and they act on different pathways such as Wnt/ β -catenin and Hippo or by regulation of oxidative stress and the expression of Granzyme B. To date, there are numerous papers in the literature that describe different mechanisms of action of ω -3PUFAs in CRC, as summarized in Table 1.

Table 1. ω -3PUFAs target different molecular pathways acting on classical hallmarks of cancer, i.e., proliferation, apoptosis, and migration.

Mechanism of Action	Effects	References
Regulation of oxidative stress	Activation of apoptosis	[124]
Regulation of COX metabolism	Activation of apoptosis	[125,126]
Regulation of Hippo pathway via GPRs-G α s-PKA cascade	Activation of apoptosis, cell proliferation inhibition	[127,128]
Wnt/ β -catenin pathway regulation	Cell proliferation inhibition	[129,130]
Inhibition of Granzyme B expression	Inhibition of EMT, Inhibition of migration	[131]

Abbreviations: COX: cyclooxygenase, GPR: G-coupled receptor, G α s: G-protein alpha subunit, PKA: protein kinase A, EMT: epithelial mesenchymal transition.

Multiple molecular mechanisms causing an increased apoptosis of CRC cells depend on the action of ω -3PUFAs. First of all, ω -3PUFAs influence the redox state of the cells: indeed, there is a link between anti-tumor effects of ω -3PUFAs and oxidative stress. PUFAs may induce an increase in apoptotic potential of CRC cells by enhancing the concentration of intracellular reactive oxygen species (ROS), inducing an elevated cancer cells apoptosis by the loss of mitochondrial membrane potential, ROS generation, activation of caspase 3 and 9, and by an increase of Bax/Bcl2 ratio [124].

Another important anti-inflammatory mechanism involves COX, a major player in inflammation. COX hyperactivation in the CRC, induces in turn the production of PGE2, a powerful pro-inflammatory and pro-carcinogenic agent [125]. ω -3PUFAs exert their anti-inflammatory role by modulating COX activity. In this respect, EPA, acting as an alternative substrate for COX-2, induces a switch in production from pro-tumorigenic PGE2 to three series PGs (PGE3) that abrogate the antiapoptotic activity of PGE2 in CRC cells [126]. However, the anti-cancer mechanism of ω -3PUFAs in CRC could also be explained

by a COX2-independent mechanism. Indeed, DHA and EPA inhibit the proliferation and induce the apoptosis of CRC cells *in vitro* and in animal models. At molecular level, involvement of the Hippo pathway, cytoplasmic retention of phosphorylated YAP by GPRs (GPR40 and GPR120)-G α s-PKA cascade has been reported [127]. Moreover, the GPR120 is expressed on macrophages and regulates their polarization reducing inflammation [128].

In addition to apoptosis, ω -3PUFAs can also influence proliferation and migration capability of CRC cells. In colorectal cancer, the Wnt- β -catenin signaling pathway is the key regulator of tumor development, and alterations in this cellular signaling pathway can be found in most patients [129]. It has been shown that dietary ω -3PUFAs are able to inhibit significantly intestinal polyp growth in mice, correlating with the ECS described in Section 2.1. In fact, CB1 up-regulation reduces β -catenin and its transcriptional target c-myc, both involved in regulation of cell proliferation. In CRC patients, cancer tissue shows a significant inhibition of CB1 expression levels, compared to adjacent normal tissue, demonstrating that the “protective” action of endocannabinoids via CB1 is lost in the tumor [130]. Moreover, D’Eliseo and colleagues have studied the effect of DHA on migration of CRC cells and demonstrated that DHA inhibits Granzyme B expression, reducing CRC cells capacity to undergo epithelial mesenchymal transition (EMT) and invade matrigel [131].

Finally, ω -3PUFAs regulate the expressions of genes involved in inflammation and colon cancer development also through epigenetic modifications [132–134]. In fact, more recently, ω -3PUFAs have been attributed the ability to influence the epigenetic regulation of genes involved in the polarization of macrophages, negatively regulating the colorectal carcinogenesis; however, the interesting topic is not fully understood [135].

Taken together, although the many different mechanisms, ω -3PUFAs play anti-inflammatory and anticancer effects acting on the classic hallmarks of cancer, *i.e.*, cell proliferation, apoptosis and migration.

To date, one of the most important problems in the treatment of tumors, including sporadic colorectal cancer, is the development of resistance to anti-tumor treatments and tumor relapse that can be related to self-renewing of cancer stem/stem-like cells (CSC/CSLC) within a tumor mass. Many groups have studied the effects exerted by ω -3PUFAs on cancer stem-like cells.

With the immunophenotyping of CSLC, the anti-CD133 antibody was found to be effective for isolating a population of colon cancer cells that retained the properties of stem cells (CSLC), while anti-cytokeratin 20 (CK20) and anti-Mucin-2 (MUC2) were specific epithelium colonic differentiation markers. EPA treatment induces an increase in of CK2 and MUC2 and an inhibition of CD133 expression. This means that the EPA could induce a more differentiated state of most cancer cells and could trigger the reduction of the stem state of the CSLC, as demonstrated by the reduction of the expression of the CD133 marker [136].

Moreover, Yang and colleagues showed an antiproliferative and proapoptotic effect on the dedifferentiated SW620 colon cell line, treated with DHA and EPA [137].

Additionally Sam *et al.*, evaluating the effects of DHA and EPA treatments on LS174T cells, a model for colorectal cancer initiating cells with stem cell-like properties, demonstrated that ω -3PUFAs induce cell growth inhibition and promote cell death by down-regulating survivin expression and activating caspase-3 [138].

The effect of ω -3PUFAs on CSLC may be an important goal for cancer therapy and will constitute an interesting challenge for future studies. Anyway, the anti-tumor activity of ω -3PUFAs, shown through multiple mechanisms, suggests that they could have an important therapeutic role in the management of CRC.

5. Conclusions

Obesity is a preventable disease that can be treated through proper diet and exercise. A balanced ω -6/ ω -3 ratio 1–2/1 is an important dietary factor in the prevention of obesity, along with physical activity. Different pro- and anti-inflammatory properties are exerted by ω -6 and ω -3PUFAs themselves

and by their derivatives, such as endocannabinoids, lipid mediators deeply involved in the control of many biological functions, including the inflammatory response and the central and local control of food intake and energy homeostasis. Therefore, appropriate dietary intervention has primarily relevance in the prevention and the treatment of obesity in that it maintains the efficiency of key signaling pathways and avoids long term/chronic inflammatory states.

Inflammation is a predisposing factor for cancer, CRC included, with ω -3PUFAs exhibiting anti-cancer properties, once again confirming the need for a balanced ω -6/ ω -3 ratio for health preservation.

The discovery of cancer stem cells offers a new perspective in cancer therapy. Since CSCs contribute to cancer onset and relapse after conventional therapy, they can represent a unique fundamental therapeutic target to completely cure cancer. Thus, the effect of ω -3s on CSLC may be an important goal for cancer therapy and will constitute an interesting challenge for future studies. Anyway, the anti-tumor activity of ω -3s, performed through multiple mechanisms, suggests that they could have an important therapeutic role in the management of CRC.

Author Contributions: Conceptualization, M.L.M., S.D., and R.M.; writing—original draft preparation, M.L.M., S.D., and R.M.; supervision, R.M.; funding acquisition, R.M. All authors have read and agreed to the published version of the manuscript.

Funding: This research was funded by Prin-Miur 2017 to R.M. project code 20175MT5EM.

Conflicts of Interest: The authors declare no conflict of interest.

Abbreviations

AA	arachidonic acid
AEA	anandamide
2-AG	2-arachinonoylglycerol
AgRP	agouti related protein
ALA	α -linolenic acid
AMPK	AMP-activated protein kinase
ARC	hypothalamic arcuate nucleus
BAT	brown adipose tissue
BMI	body mass index
CART	cocaine-amphetamine regulated transcript
CB	cannabinoid receptor
CK	cytokeratin
COX	cyclooxygenase
CRC	colorectal cancer
CSC	cancer stem cell
CSLC	cancer stem-like cell
DHA	docosahexaenoic acid
DHEA	N-docosahexaenoyl ethanolamine
DPA	decosapentaenoic acid
ECS	endocannabinoids system
EMT	epithelial mesenchymal transition
EO-CRC	early-onset colorectal cancer
EPA	eicosapentaenoic acid
EPEA	N-eicosapentanoyl ethanolamine
EPG	eicosapentaenoyl glycerol

FA	fatty acid
FFAR	free fatty acid receptor
GPR	G-coupled receptor
HFD	high fat diet
IL-	Interleukin-
LA	linoleic acid
LPS	lipopolysaccharide
MCH	melanin-concentrating hormone
MCP-1	monocyte chemo attractant protein 1
MUC	mucin
NPY	neuropeptides like neuropeptide Y
PAI-1	plasminogen activator inhibitor
PGE2	prostaglandin E2
POMC	proopiomelanocortin
PPAR	peroxisome proliferator-activated receptor
PUFA	polyunsaturated fatty acid
RBC	red blood cells
ROS	reactive oxygen species
SFA	saturated fatty acid
TNF- α	tumor necrosis factor-alpha
TRPV1	transient receptor potential cation channel subfamily V member 1
UCP1	uncoupling protein 1
WAT	white adipose tissue

References

1. Salvestrini, V.; Sell, C.; Lorenzini, A. Obesity May Accelerate the Aging Process. *Front. Endocrinol.* **2019**, *10*, 266. [[CrossRef](#)] [[PubMed](#)]
2. Hotamisligil, G.S. Inflammation and metabolic disorders. *Nature* **2006**, *444*, 860–867. [[CrossRef](#)] [[PubMed](#)]
3. Galland, L. Diet and inflammation. *Nutr. Clin. Pract.* **2010**, *25*, 634–640. [[CrossRef](#)] [[PubMed](#)]
4. Torres-Fuentes, C.; Schellekens, H.; Dinan, T.G.; Cryan, J.F. A natural solution for obesity: Bioactives for the prevention and treatment of weight gain. A review. *Nutr. Neurosci.* **2015**, *18*, 49–65. [[CrossRef](#)] [[PubMed](#)]
5. Siriwardhana, N.; Kalupahana, N.S.; Cekanova, M.; LeMieux, M.; Greer, B.; Moustaid-Moussa, N. Modulation of adipose tissue inflammation by bioactive food compounds. *J. Nutr. Biochem.* **2013**, *24*, 613–623. [[CrossRef](#)]
6. Djuric, Z. The Mediterranean diet: Effects on proteins that mediate fatty acid metabolism in the colon. *Nutr. Rev.* **2011**, *69*, 730–744. [[CrossRef](#)]
7. Rosa, F.T.; Zulet, M.A.; Marchini, J.S.; Martinez, J.A. Bioactive compounds with effects on inflammation markers in humans. *Int. J. Food Sci. Nutr.* **2012**, *63*, 749–765. [[CrossRef](#)]
8. Konstantinidi, M.; Koutelidakis, A.E. Functional Foods and Bioactive Compounds: A Review of Its Possible Role on Weight Management and Obesity’s Metabolic Consequences. *Medicines* **2019**, *6*, 94. [[CrossRef](#)]
9. Mounien, L.; Tourniaire, F.; Landrier, J.F. Anti-Obesity Effect of Carotenoids: Direct Impact on Adipose Tissue and Adipose Tissue-Driven Indirect Effects. *Nutrients* **2019**, *11*, 1562. [[CrossRef](#)]
10. Zappia, V.; Galletti, P.; Manna, C.; D’Angelo, S.; Napoli, D.; De Bonis, M.L.; Capasso, G. Effects of Hydroxytyrosol on Cyclosporine Nephrotoxicity. In *Olives and Olive Oil in Health and Disease Prevention*; Preedy, V., Watson, R., Eds.; Academic Press: Oxford, UK, 2010; pp. 1245–1252. [[CrossRef](#)]
11. D’Angelo, S.; Sammartino, D. Protective effect of Annurca apple extract against oxidative damage in human erythrocytes. *Curr. Nutr. Food Sci.* **2015**, *11*, 248–256. [[CrossRef](#)]
12. D’Angelo, S. Polyphenols: Potential beneficial effects of these phytochemicals in athletes. *Curr. Sports Med. Rep.* **2020**, *19*, 260–265. [[CrossRef](#)] [[PubMed](#)]
13. D’Angelo, S.; Martino, E.; Ilisso, C.P.; Bagarolo, M.L.; Porcelli, M.; Cacciapuoti, G. Pro-oxidant and pro-apoptotic activity of polyphenol extract from Annurca apple and its underlying mechanisms in human breast cancer cells. *Int. J. Oncol.* **2017**, *51*, 939–948. [[CrossRef](#)] [[PubMed](#)]
14. D’Angelo, S.; Martino, E.; Cacciapuoti, G. Effects of Annurca Apple (*Maluspumila* cv Annurca) Polyphenols on Breast Cancer Cells. *Curr. Nutr. Food Sci.* **2019**, *15*, 745–751. [[CrossRef](#)]

15. Martino, E.; Vuoso, D.C.; D'Angelo, S.; Mele, L.; D'Onofrio, N.; Porcelli, M.; Cacciapuoti, G. Annurca apple polyphenol extract selectively kills MDA-MB-231 cells through ROS generation, sustained JNK activation and cell growth and survival inhibition. *Sci. Rep.* **2019**, *10*, 13045. [[CrossRef](#)] [[PubMed](#)]
16. Del Monaco, G.; Officioso, A.; D'Angelo, S.; Cara, F.L.; Ionata, E.; Marcolongo, L.; Squillaci, G.; Maurelli, L.; Morana, A. Characterization of extra virgin olive oils produced with typical Italian varieties by their phenolic profile. *Food Chem.* **2015**, *184*, 220–228. [[CrossRef](#)] [[PubMed](#)]
17. Jayarathne, S.; Kobozev, I.; Park, O.H.; Oldewage-Theron, W.; Shen, C.L.; Moustaid-Moussa, N. Anti-Inflammatory and Anti-Obesity Properties of Food Bioactive Components: Effects on Adipose Tissue. *Prev. Nutr. Food Sci.* **2017**, *22*, 251–262. [[CrossRef](#)] [[PubMed](#)]
18. Seiler, A.; Chen, M.A.; Brown, R.L.; Fagundes, C.P. Obesity, Dietary Factors, Nutrition, and Breast Cancer Risk. *Curr. Breast Cancer Rep.* **2018**, *10*, 14–27. [[CrossRef](#)]
19. D'Angelo, S.; Rosa, R. The impact of supplementation with Pomegranate fruit (*Punica granatum*, L.) on sport performance. *Sport Sci.* **2020**, *13*, 29–37.
20. D'Angelo, S. Current Evidence on the Effect of Dietary Polyphenols Intake on Brain Health. *Curr. Nutr. Food Sci.* **2020**, *16*, 1170–1182. [[CrossRef](#)]
21. Boccellino, M.; D'Angelo, S. Anti-Obesity Effects of Polyphenol Intake: Current Status and Future Possibilities. *Int. J. Mol. Sci.* **2020**, *21*, 5642. [[CrossRef](#)]
22. Pagotto, U.; Marsicano, G.; Cota, D.; Lutz, B.; Pasquali, R. The emerging role of the endocannabinoid system in endocrine regulation and energy balance. *Endocr. Rev.* **2006**, *27*, 73–100. [[CrossRef](#)] [[PubMed](#)]
23. Forte, N.; Fernández-Rilo, A.C.; Palomba, L.; Di Marzo, V.; Cristino, L. Obesity Affects the Microbiota-Gut-Brain Axis and the Regulation Thereof by Endocannabinoids and Related Mediators. *Int. J. Mol. Sci.* **2020**, *21*, 1554. [[CrossRef](#)] [[PubMed](#)]
24. Laezza, C.; Pagano, C.; Navarra, G.; Pastorino, O.; Proto, M.C.; Fiore, D.; Piscopo, C.; Gazzero, P.; Bifulco, M. The Endocannabinoid System: A Target for Cancer Treatment. *Int. J. Mol. Sci.* **2020**, *21*, 747. [[CrossRef](#)] [[PubMed](#)]
25. Meccariello, R.; Battista, N.; Bradshaw, H.B.; Wang, H. Updates in reproduction coming from the endocannabinoid system. *Int. J. Endocrinol.* **2014**, *2014*, 412354. [[CrossRef](#)] [[PubMed](#)]
26. Chianese, R.; Coccurello, R.; Viggiano, A.; Scafuro, M.; Fiore, M.; Coppola, G.; Operto, F.F.; Fasano, S.; Laye, S.; Pierantoni, R.; et al. Impact of Dietary Fats on Brain Functions. *Curr. Neuropharmacol.* **2018**, *16*, 1059–1085. [[CrossRef](#)] [[PubMed](#)]
27. Meccariello, R. Endocannabinoid System in Health and Disease: Current Situation and Future Perspectives. *Int. J. Mol. Sci.* **2020**, *21*, 3549. [[CrossRef](#)]
28. Turcotte, C.; Blanchet, M.R.; Lavolette, M.; Flamand, N. The CB₂ receptor and its role as a regulator of inflammation. *Cell. Mol. Life Sci.* **2016**, *73*, 4449–4470. [[CrossRef](#)]
29. Schulte, K.; Kalupahana, N.S.; Ramalingam, L.; Wang, S.; Rahman, S.M.; Robert-McComb, J.; Moustaid-Moussa, N. Omega-3 fatty acids in obesity and metabolic syndrome: A mechanistic update. *J. Nutr. Biochem.* **2018**, *58*, 1–16. [[CrossRef](#)]
30. Jeromson, S.; Gallagher, I.J.; Galloway, S.D.; Hamilton, D.L. Omega-3 Fatty Acids and Skeletal Muscle Health. *Mar. Drugs* **2015**, *13*, 6977–7004. [[CrossRef](#)]
31. Gammone, M.A.; Riccioni, G.; Parrinello, G.; D'Orazio, N. Omega-3 Polyunsaturated Fatty Acids: Benefits and Endpoints in Sport. *Nutrients* **2019**, *11*, 46. [[CrossRef](#)]
32. Burdge, G.C.; Jones, A.E.; Wootton, S.A. Eicosapentaenoic and docosapentaenoic acids are the principal products of alpha-linolenic acid metabolism in young men. *Br. J. Nutr.* **2002**, *88*, 355–363. [[CrossRef](#)] [[PubMed](#)]
33. Nording, M.L.; Yang, J.; Georgi, K.; Karbowski, C.H.; German, J.B.; Weiss, R.H.; Hogg, R.J.; Trygg, J.; Hammock, B.D.; Zivkovic, A.M. Individual variation in lipidomic profiles of healthy subjects in response to omega-3 Fatty acids. *PLoS ONE* **2013**, *8*, e76575. [[CrossRef](#)] [[PubMed](#)]
34. Cholewski, M.; Tomczykowa, M.; Tomczyk, M. A Comprehensive Review of Chemistry, Sources and Bioavailability of Omega-3 Fatty Acids. *Nutrients* **2018**, *10*, 1662. [[CrossRef](#)] [[PubMed](#)]
35. Ratnayake, W.M.; Galli, C. Fat and fatty acid terminology, methods of analysis and fat digestion and metabolism: A background review paper. *Ann. Nutr. Metab.* **2009**, *55*, 8–43. [[CrossRef](#)]
36. D'Angelo, S.; Madonna, G. Effects of fish oil supplementation in the sport performance. *J. Phys. Educ. Sport.* **2020**, *20* (Suppl. 4), 2322–2329. [[CrossRef](#)]

37. Lu, H.-C.; Mackie, K. An Introduction to the Endogenous Cannabinoid System. *Biol. Psychiatr.* **2016**, *79*, 516–525. [[CrossRef](#)]
38. Marzo, V.D.; Silvestri, C. Lifestyle and metabolic syndrome: Contribution of the endocannabinoidome. *Nutrients* **2019**, *11*, 1956. [[CrossRef](#)]
39. Bovolín, P.; Cottone, E.; Pomatto, V.; Fasano, S.; Pierantoni, R.; Cobellis, G.; Meccariello, R. Endocannabinoids are involved in male vertebrate reproduction: Regulatory mechanisms at central and gonadal level. *Front. Endocrinol.* **2014**, *5*, 54. [[CrossRef](#)]
40. Meccariello, R.; Santoro, A.; D'Angelo, S.; Morrone, R.; Fasano, S.; Viggiano, A.; Pierantoni, R. The Epigenetics of the Endocannabinoid System. *Int. J. Mol. Sci.* **2020**, *21*, 1113. [[CrossRef](#)]
41. Reggio, P.H. Endocannabinoid Binding to the Cannabinoid Receptors: What Is Known and What Remains Unknown. *Curr. Med. Chem.* **2010**, *17*, 1468–1486. [[CrossRef](#)]
42. Watson, J.E.; Kim, J.S.; Das, A. Emerging class of omega-3 fatty acid endocannabinoids & their derivatives. *Prostaglandins Other Lipid Mediat.* **2019**, *143*, 106337. [[CrossRef](#)] [[PubMed](#)]
43. Cristino, L.; Becker, T.; Marzo, V.D. Endocannabinoids and energy homeostasis: An update. *Biofactors* **2014**, *40*, 389–397. [[CrossRef](#)] [[PubMed](#)]
44. Quarta, C.; Bellocchio, L.; Mancini, G.; Mazza, R.; Cervino, C.; Braulke, L.J.; Fekete, C.; Latorre, R.; Nanni, C.; Bucci, M.; et al. CB1 signaling in forebrain and sympathetic neurons is a key determinant of endocannabinoid actions on energy balance. *Cell. Metab.* **2010**, *11*, 273–285. [[CrossRef](#)] [[PubMed](#)]
45. Trillou, C.R.; Delgorge, C.; Menet, C.; Arnone, M.; Soubrié, P. CB1 cannabinoid receptor knockout in mice leads to leanness, resistance to diet-induced obesity and enhanced leptin sensitivity. *Int. J. Obes. Relat. Metab. Disord.* **2004**, *28*, 640–648. [[CrossRef](#)]
46. Després, J.P.; Golay, A.; Sjöström, L. Rimonabant in Obesity-Lipids Study Group. Effects of rimonabant on metabolic risk factors in overweight patients with dyslipidemia. *N. Engl. J. Med.* **2005**, *353*, 2121–2134. [[CrossRef](#)]
47. Roh, E.; Song, D.K.; Kim, M.S. Emerging role of the brain in the homeostatic regulation of energy and glucose metabolism. *Exp. Mol. Med.* **2016**, *48*, e216. [[CrossRef](#)]
48. Halaas, J.L.; Gajiwala, K.S.; Maffei, M.; Cohen, S.L.; Chait, B.T.; Rabinowitz, D.; Lallone, R.L.; Burley, S.K.; Friedman, J.M. Weight-reducing effects of the plasma protein encoded by the obese gene. *Science* **1995**, *269*, 543–546. [[CrossRef](#)]
49. Marzo, V.D.; Goparaju, S.K.; Wang, L.; Liu, J.; Bátkai, S.; Járαι, Z.; Fezza, F.; Miura, G.I.; Palmiter, R.D.; Sugiura, T.; et al. Leptin-regulated endocannabinoids are involved in maintaining food intake. *Nature* **2001**, *410*, 822–825. [[CrossRef](#)]
50. Almeida, M.M.; Dias-Rocha, C.P.; Reis-Gomes, C.F.; Wang, H.; Atella, G.C.; Cordeiro, A.; Pazos-Moura, C.C.; Joss-Moore, L.; Trevenzoli, I.H. Maternal high-fat diet impairs leptin signaling and up-regulates type-1 cannabinoid receptor with sex-specific epigenetic changes in the hypothalamus of newborn rats. *Psychoneuroendocrinology* **2019**, *103*, 306–315. [[CrossRef](#)]
51. Sam, A.H.; Salem, V.; Ghati, M.A. Rimonabant: From RIO to Ban. *J. Obes.* **2011**, *2011*, 432607. [[CrossRef](#)]
52. Dyal, S.C. Interplay Between n-3 and n-6 Long-Chain Polyunsaturated Fatty Acids and the Endocannabinoid System in Brain Protection and Repair. *Lipids* **2017**, *52*, 885–900. [[CrossRef](#)]
53. Bosch-Bouju, C.; Layé, S. Dietary Omega-6/Omega-3 and Endocannabinoids: Implications for Brain Health and Diseases. In *Cannabinoids in Health and Disease*; Meccariello, R., Chianese, R., Eds.; IntechOpen: London, UK, 2016; pp. 111–142. [[CrossRef](#)]
54. Rao, J.S.; Ertley, R.N.; dEmAR, J.C.; Rapoport, S.I.; Bazinet, R.P.; Lee, H.-J. Dietary n-3 PUFA deprivation alters expression of enzymes of the arachydonic and docosahexaenoic acid cascade in rat frontal cortex. *Mol. Psychiatry* **2007**, *2*, 151–157. [[CrossRef](#)]
55. Igarashi, M.; Kim, H.-W.; Chang, L.; Ma, K.; Rapoport, S.I. Dietary n-6 polyunsaturated fatty acid deprivation increases docosahexaenoic acid metabolism in rat brain. *J. Neurochem.* **2012**, *120*, 985–997. [[CrossRef](#)]
56. Pucci, M.; Bonaventura, M.V.M.D.; Zaplatić, E.; Bellia, F.; Maccarrone, M.; Cifani, C.; D'Addario, C. Transcriptional regulation of the endocannabinoid system in a rat model of binge-eating behavior reveals a selective modulation of the hypothalamic fatty acid amide hydrolase gene. *Int. J. Eat Disord.* **2019**, *52*, 51–60. [[CrossRef](#)]
57. Flachs, P.; Rossmel, M.; Bryhn, M.; Kopecky, J. Cellular and molecular effects of n-3 polyunsaturated fatty acids on adipose tissue biology and metabolism. *Clin. Sci.* **2009**, *116*, 1–16. [[CrossRef](#)]

58. Hensler, M.; Bardova, K.; Jilkova, Z.M.; Wahli, W.; Meztger, D.; Chambon, P.; Kopecky, J.; Flachs, P. The inhibition of fat cell proliferation by n-3 fatty acids in dietary obese mice. *Lipids Health Dis.* **2011**, *10*, 128–135. [\[CrossRef\]](#)
59. Bougarne, N.; Weyers, B.; Desmet, S.J.; Deckers, J.; Ray, D.W.; Staels, B.; De Bosscher, K. Molecular Actions of PPAR α in Lipid Metabolism and Inflammation. *Endocr. Rev.* **2018**, *39*, 760–802. [\[CrossRef\]](#)
60. Chang, H.Y.; Lee, H.N.; Kim, W.; Surh, Y.J. Docosahexaenoic acid induces M2 macrophage polarization through peroxisome proliferator-activated receptor gamma activation. *Life Sci.* **2015**, *120*, 39–47. [\[CrossRef\]](#)
61. Hein, G.J.; Bernasconi, A.M.; Montanaro, M.A.; Pellon-Maison, M.; Finarelli, G.; Chicco, A.; Lombardo, Y.B.; Brenner, R.R. Nuclear receptors and hepatic lipidogenic enzyme response to a dyslipidemic sucrose-rich diet and its reversal by fish oil n-3 polyunsaturated fatty acids. *Am. J. Physiol. Endocrinol. Metab.* **2010**, *298*, E429. [\[CrossRef\]](#)
62. Neschen, S.; Morino, K.; Rossbacher, J.C.; Pongratz, R.L.; Cline, G.W.; Sono, S.; Gillum, M.; Shulman, G.I. Fish oil regulates adiponectin secretion by a peroxisome proliferator-activated receptor-gamma-dependent mechanism in mice. *Diabetes* **2006**, *55*, 924–928. [\[CrossRef\]](#)
63. Wortman, P.; Miyazaki, Y.; Kalupahana, N.S.; Kim, S.; Hansen-Petrik, M.; Saxton, A.M.; Claycombe, K.J.; Voy, B.H.; Whelan, J.; Moustaid-Moussa, N. n3 and n6 polyunsaturated fatty acids differentially modulate prostaglandin E secretion but not markers of lipogenesis in adipocytes. *Nutr. Metab.* **2009**, *6*, 5. [\[CrossRef\]](#) [\[PubMed\]](#)
64. Kalupahana, N.S.; Claycombe, K.J.; Moustaid-Moussa, N. (n-3) Fatty acids alleviate adipose tissue inflammation and insulin resistance: Mechanistic insights. *Adv. Nutr.* **2011**, *2*, 304–316. [\[CrossRef\]](#) [\[PubMed\]](#)
65. Ichimura, A.; Hasegawa, S.; Kasubuchi, M.; Kimura, I. Free fatty acid receptors as therapeutic targets for the treatment of diabetes. *Front. Pharmacol.* **2014**, *5*, 1–6. [\[CrossRef\]](#) [\[PubMed\]](#)
66. Harden, C.J.; Dible, V.A.; Russell, J.M.; Garaiova, I.; Plummer, S.F.; Barker, M.E.; Corfe, B.M. Long-chain polyunsaturated fatty acid supplementation had no effect on body weight but reduced energy intake in overweight and obese women. *Nutr. Res.* **2014**, *34*, 17–24. [\[CrossRef\]](#)
67. Albert, B.B.; Derraik, J.G.; Brennan, C.M.; Biggs, J.B.; Garg, M.L.; Cameron-Smith, D.; Hofman, P.L.; Cutfield, W.S. Supplementation with a blend of krill and salmon oil is associated with increased metabolic risk in overweight men. *Am. J. Clin. Nutr.* **2015**, *102*, 49–57. [\[CrossRef\]](#)
68. Lee, H.C.; Chenga, W.C.; Hsu, Y.H.; Su, H.; Huang, B.; Lin, Y. Effects of calorie restriction with n-3 long-chain polyunsaturated fatty acids on metabolic syndrome severity in obese subjects: A randomized-controlled trial. *J. Funct. Foods* **2015**, *19*, 929–940. [\[CrossRef\]](#)
69. Razny, U.; Kiec-Wilk, B.; Polus, A.; Goralska, J.; Malczewska-Malec, M.; Wnek, D.; Zdzienicka, A.; Gruca, A.; Childs, C.E.; Kapusta, M.; et al. Effect of caloric restriction with or without n-3 polyunsaturated fatty acids on insulin sensitivity in obese subjects: A randomized placebo controlled trial. *BBA Clin.* **2015**, *4*, 7–13. [\[CrossRef\]](#)
70. Martínez-Fernández, L.; Laiglesia, L.M.; Huerta, A.E.; Martínez, J.A.; Moreno-Aliaga, M.J. ω -3 fatty acids and adipose tissue function in obesity and metabolic syndrome. *Prostaglandins Other Lipid Mediat.* **2015**, *121*, 24–41. [\[CrossRef\]](#)
71. Arent, S.M.; Walker, A.J.; Pellegrino, J.K.; Sanders, D.J.; McFadden, B.A.; Ziegenfuss, T.N.; Lopez, H.L. The combined effects of exercise, diet, and a multi-ingredient dietary supplement on body composition and adipokine changes in overweight adults. *J. Am. Coll. Nutr.* **2017**, *37*, 1–10. [\[CrossRef\]](#)
72. Huerta, A.E.; Navas-Carretero, S.; Prieto-Hontoria, P.L.; Martínez, J.A.; Moreno-Aliaga, M.J. Effects of alpha-lipoic acid and eicosapentaenoic acid in overweight and obese women during weight loss. *Obesity* **2015**, *23*, 313–321. [\[CrossRef\]](#)
73. Thorsdottir, I.; Tomasson, H.; Gunnarsdottir, I.; Gisladottir, E.; Kiely, M.; Parra, M.D.; Bandarra, N.M.; Schaafsma, G.; Martínéz, J.A. Randomized trial of weight-loss-diets for young adults varying in fish and fish oil content. *Int. J. Obes.* **2007**, *31*, 1560–1566. [\[CrossRef\]](#) [\[PubMed\]](#)
74. Hilgendorf, K.I.; Johnson, C.T.; Mezger, A.; Rice, S.L.; Norris, A.M.; Demeter, J.; Greenleaf, W.J.; Reiter, J.F.; Kopinke, D.; Jackson, P.K. ω -3 Fatty Acids Activate Ciliary FFAR4 to Control Adipogenesis. *Cell* **2019**, *179*, 1289–1305. [\[CrossRef\]](#) [\[PubMed\]](#)

75. Bertrand, C.; Pignalosa, A.; Wanecq, E.; Rancoule, C.; Batut, A.; Deleruyelle, S.; Lionetti, L.; Valet, P.; Castan-Laurell, I. Effects of dietary eicosapentaenoic acid (EPA) supplementation in high-fat fed mice on lipid metabolism and apelin/AP system in skeletal muscle. *PLoS ONE* **2013**, *8*, e78874. [[CrossRef](#)] [[PubMed](#)]
76. Pahlavani, M.; Razafimanjato, F.; Ramalingam, L.; Kalupahana, N.S.; Moussa, H.; Scoggin, S.; Moustaid-Moussa, N. Eicosapentaenoic acid regulates brown adipose tissue metabolism in high-fat-fed mice and in clonal brown adipocytes. *J. Nutr. Biochem.* **2017**, *39*, 101–109. [[CrossRef](#)]
77. Lucero, D.; Miksztoewicz, V.; Gualano, G.; Longo, C.; Landeira, G.; Álvarez, E.; Zago, V.; Brites, F.; Berg, G.; Fassio, E.; et al. Nonalcoholic fatty liver disease associated with metabolic syndrome: Influence of liver fibrosis stages on characteristics of very low-density lipoproteins. *Clin. Chim. Acta* **2017**, *473*, 1–8. [[CrossRef](#)]
78. Harris, W.S.; Luo, J.; Pottala, J.V.; Espeland, M.A.; Margolis, K.L.; Manson, J.E.; Wang, L.; Brasky, T.M.; Robinson, J.G. Red blood cell polyunsaturated fatty acids and mortality in the Women’s Health Initiative Memory Study. *J. Clin. Lipidol.* **2017**, *11*, 250–259. [[CrossRef](#)]
79. EFSA Panel on Dietetic Products, Nutrition and Allergies (NDA). Scientific opinion on the tolerable upper intake level of eicosapentaenoic acid (EPA), docosahexaenoic acid (DHA) and docosapentaenoic acid (DPA). *EFSA J.* **2012**, *10*, 2815–2882. [[CrossRef](#)]
80. Harris, W.S. International recommendations for consumption of long-chain omega-3 fatty acids. *J. Cardiovasc. Med.* **2007**, *8*, 50–52. [[CrossRef](#)]
81. Molendi-Coste, O.; Legry, V.; Leclercq, I.A. Why and How Meet n-3 PUFA Dietary Recommendations? *Gastroenterol. Res. Pract.* **2011**, *2011*, 364040. [[CrossRef](#)]
82. Eaton, S.B.; Konner, M.J.; Cordain, L. Diet-dependent acid load, Paleolithic [corrected] nutrition, and evolutionary health promotion. *Am. J. Clin. Nutr.* **2010**, *91*, 295–297. [[CrossRef](#)]
83. Nagata, C.; Takatsuka, N.; Shimizu, H. Soy and fish oil intake and mortality in a Japanese community. *Am. J. Epidemiol.* **2002**, *156*, 824–831. [[CrossRef](#)] [[PubMed](#)]
84. Buckley, J.D.; Howe, P.R. Long-chain omega-3 polyunsaturated fatty acids may be beneficial for reducing obesity—a review. *Nutrients* **2010**, *2*, 1212–1230. [[CrossRef](#)] [[PubMed](#)]
85. Kris-Etherton, P.M.; Grieger, J.A.; Etherton, T.D. Dietary reference intakes for DHA and EPA. *Prostaglandins Leukot. Essent. Fatty Acids* **2009**, *81*, 99–104. [[CrossRef](#)]
86. Ogura, T.; Takada, H.; Okuno, M.; Kitade, H.; Matsuura, T.; Kwon, M.; Arita, S.; Hamazaki, K.; Itomura, M.; Hamazaki, T. Fatty acid composition of plasma, erythrocytes and adipose: Their correlations and effects of age and sex. *Lipids* **2010**, *45*, 137–144. [[CrossRef](#)]
87. Kiyabu, G.Y.; Inoue, M.; Saito, E.; Abe, S.K.; Sawada, N.; Ishihara, J.; Iwasaki, M.; Yamaji, T.; Shimazu, T.; Sasazuki, S.; et al. Fish, n-3 polyunsaturated fatty acids and n-6 polyunsaturated fatty acids intake and breast cancer risk: The Japan Public Health Center-based prospective study. *Int. J. Cancer* **2015**, *137*, 2915–2926. [[CrossRef](#)] [[PubMed](#)]
88. DiNicolantonio, J.J.; O’Keefe, J.H. Importance of maintaining a low omega-6/omega-3 ratio for reducing inflammation. *Open Heart* **2018**, *5*, e000946. [[CrossRef](#)]
89. Simopoulos, A.P. An increase in the omega-6/omega-3 fatty acid ratio increases the risk for obesity. *Nutrients* **2016**, *8*, 128–145. [[CrossRef](#)]
90. Simopoulos, A.P. The importance of the omega-6/omega-3 fatty acid ratio in cardiovascular disease and other chronic diseases. *Exp. Biol. Med.* **2008**, *233*, 674–688. [[CrossRef](#)]
91. Simopoulos, A.P. Evolutionary aspects of diet: The omega-6/omega-3 ratio and the brain. *Mol. Neurobiol.* **2011**, *44*, 203–215. [[CrossRef](#)]
92. Simopoulos, A.P. Evolutionary aspects of diet, the omega-6/omega-3 ratio and genetic variation: Nutritional implications for chronic diseases. *Biomed. Pharmacother.* **2006**, *60*, 502–507. [[CrossRef](#)]
93. Harris, W.S.; Mozaffarian, D.; Lefevre, M.; Toner, C.D.; Colombo, J.; Cunnane, S.C.; Whelan, J. Towards establishing dietary reference intakes for eicosapentaenoic and docosahexaenoic acids. *J. Nutr.* **2009**, *139*, 804S–819S. [[CrossRef](#)] [[PubMed](#)]
94. Vessby, B. Dietary fat, fatty acid composition in plasma and the metabolic syndrome. *Curr. Opin. Lipidol.* **2003**, *14*, 15–19. [[CrossRef](#)] [[PubMed](#)]
95. Patterson, E.; Wall, R.; Fitzgerald, G.F.; Ross, R.P.; Stanton, C. Health implications of high dietary omega-6 polyunsaturated Fatty acids. *J. Nutr. Metab.* **2012**, *2012*, 539426. [[CrossRef](#)]

96. Ameer, A.; Enroth, S.; Johansson, A.; Zaboli, G.; Igl, W.; Johansson, A.C.; Rivas, M.A.; Daly, M.J.; Schmitz, G.; Hicks, A.A.; et al. Genetic Adaptation of Fatty-Acid Metabolism: A Human-Specific Haplotype Increasing the Biosynthesis of Long-Chain ω -3 and ω -6 Fatty Acids. *Am. J. Hum. Genet.* **2012**, *90*, 809–820. [[CrossRef](#)] [[PubMed](#)]
97. Wang, S.; Wu, D.; Matthan, N.R.; Lamon-Fava, S.; Lecker, J.L.; Lichtenstein, A.H. Reduction in dietary omega-6 polyunsaturated fatty acids: Eicosapentaenoic acid plus docosahexaenoic acid ratio minimizes atherosclerotic lesion formation and inflammatory response in the LDL receptor null mouse. *Atherosclerosis* **2009**, *204*, 147–155. [[CrossRef](#)]
98. Barceló-Coblijn, G.; Murphy, E.J. Alpha-linolenic acid and its conversion to longer chain n-3 fatty acids: Benefits for human health and a role in maintaining tissue n-3 fatty acid levels. *Prog. Lipid Res.* **2009**, *48*, 355–374. [[CrossRef](#)]
99. Harris, W.S.; Mozaffarian, D.; Rimm, E.; Kris-Etherton, P.; Rudel, L.L.; Appel, L.J.; Engler, M.M.; Engler, M.B.; Sacks, F. Omega-6 fatty acids and risk for cardiovascular disease: A science advisory from the American Heart Association nutrition subcommittee of the council on nutrition, physical activity, and metabolism; council on cardiovascular nursing; and council on epidemiology and prevention. *Circulation* **2009**, *119*, 902–907. [[CrossRef](#)]
100. Bannenberg, G.L. Therapeutic applicability of anti-inflammatory and proresolving polyunsaturated fatty acid-derived lipid mediators. *ScientificWorldJournal* **2010**, *10*, 676–712. [[CrossRef](#)]
101. Simopoulos, A.P. The importance of the ratio of omega-6/omega-3 essential fatty acids. *Biomed. Pharmacother.* **2002**, *56*, 365–379. [[CrossRef](#)]
102. Simopoulos, A.P. n-3 fatty acids and human health: Defining strategies for public policy. *Lipids* **2001**, *36*, S83–S89. [[CrossRef](#)]
103. Sanders, T.A. Polyunsaturated fatty acids in the food chain in Europe. *Am. J. Clin. Nutr.* **2000**, *71*, 176S–178S. [[CrossRef](#)] [[PubMed](#)]
104. Simopoulos, A.P. Nutrigenetics/Nutrigenomics. *Annu. Rev. Public Health* **2010**, *31*, 53–68. [[CrossRef](#)] [[PubMed](#)]
105. Pietrzyk, L.; Torres, A.; Maciejewski, R.; Torres, K. Obesity and obese-related chronic low-grade inflammation in promotion of colorectal cancer development. *Asian Pac. J. Cancer Prev.* **2015**, *16*, 4161–4168. [[CrossRef](#)] [[PubMed](#)]
106. Grivnickov, S.I.; Greten, F.R.; Karin, M. Immunity, inflammation and cancer. *Cell* **2010**, *140*, 883–899. [[CrossRef](#)] [[PubMed](#)]
107. Ingangi, V.; Minopoli, M.; Ragone, C.; Motti, M.L.; Carriero, M.V. Role of Microenvironment on the Fate of Disseminating Cancer Stem Cells. *Front. Oncol.* **2019**, *9*, 82. [[CrossRef](#)] [[PubMed](#)]
108. Aggarwal, B.B.; Gehlot, P. Inflammation and cancer: How friendly is the relationship for cancer patients? *Curr. Opin. Pharmacol.* **2009**, *9*, 351–369. [[CrossRef](#)]
109. Motti, M.L.; D'Angelo, S.; Meccariello, R. MicroRNAs, Cancer and Diet: Facts and New Exciting Perspectives. *Curr. Mol. Pharmacol.* **2018**, *11*, 90–96. [[CrossRef](#)]
110. Colace, L.; Boccia, S.; De Maria, R.; Zeuner, A. Colorectal cancer: Towards new challenges and concepts of preventive healthcare. *Ecancermedicalscience* **2017**, *11*, ed74. [[CrossRef](#)]
111. Mauri, G.; Sartore-Bianchi, A.; Russo, A.G.; Marsoni, S.; Bardelli, A.; Siena, S. Early-Onset colorectal cancer in young individuals. *Mol. Oncol.* **2019**, *13*, 109–113. [[CrossRef](#)]
112. Sung, H.; Siegel, R.L.; Rosenberg, P.S.; Jemal, A. Emerging cancer trends among young adults in the USA: Analysis of a population-based cancer registry. *Lancet Public Health* **2019**, *4*, e137–e147. [[CrossRef](#)]
113. Vuik, F.E.; Nieuwenburg, S.A.; Bardou, M.; Lansdorp-Vogelaar, I.; Dinis-Ribeiro, M.; Bento, M.J.; Zadnik, V.; Pellise, M.; Esteban, L.; Kaminski, M.F.; et al. Increasing incidence of colorectal cancer in young adults in Europe over the last 25 years. *Gut* **2019**, *68*, 1820–1826. [[CrossRef](#)]
114. Favoriti, P.; Carbone, G.; Greco, M.; Pirozzi, F.; Pirozzi, R.E.M. Worldwide Burden of Colorectal Cancer: A Review. *Updates Sur.* **2016**, *68*, 7–11. [[CrossRef](#)] [[PubMed](#)]
115. Alonso, S.; Yilma, O.H. Nutritional Regulation of Intestinal Stem Cells. *Annu. Rev. Nutr.* **2018**, *38*, 273–301. [[CrossRef](#)] [[PubMed](#)]
116. O'Brien, L.E.; Soliman, S.S.; Li, X.; Bilder, D. Altered modes of stem cell division drive adaptive intestinal growth. *Cell* **2011**, *147*, 603–614. [[CrossRef](#)]

117. Hodge, A.M.; Williamson, E.J.; Bassett, J.K.; MacInnis, R.J.; Giles, G.G.; English, D.R. Dietary and biomarker estimates of fatty acids and risk of colorectal cancer. *Int. J. Cancer* **2015**, *137*, 1224–1234. [[CrossRef](#)]
118. Itzkowitz, S.H.; Yio, X. Inflammation and cancer, IV. Colorectal cancer in inflammatory bowel disease: The role of inflammation. *Am. J. Physiol. Gastrointest. Liver Physiol.* **2004**, *287*, 7–17. [[CrossRef](#)] [[PubMed](#)]
119. Weylandt, K.H.; Serini, S.; Chen, Y.Q.; Su, H.; Lim, K.; Cittadini, A.; Calviello, G. Omega-3 Polyunsaturated Fatty Acids: The Way Forward in Times of Mixed Evidence. *BioMed Res. Int.* **2015**, *2015*. [[CrossRef](#)] [[PubMed](#)]
120. Schley, P.D.; Brindley, D.N.; Field, C.J. (n-3) PUFA Alter Raft Lipid Composition and Decrease Epidermal Growth Factor Receptor Levels in Lipid Rafts of Human Breast Cancer Cells. *J. Nutr.* **2007**, *137*, 548–553. [[CrossRef](#)]
121. Collett, E.D.; Davidson, L.A.; Fan, Y.Y.; Lupton, J.R.; Chapkin, R.S. n-6 and n-3 polyunsaturated fatty acids differentially Modulate Oncogenic Ras Activation in Colonocytes. *Am. J. Physiol.* **2001**, *280*, 1066–1075. [[CrossRef](#)]
122. Calder, P.C. Omega-3 fatty acids and inflammatory processes: From molecules to man. *Biochem. Soc. Trans.* **2017**, *45*, 1105–1115. [[CrossRef](#)]
123. Janakiram, N.B.; Mohammed, A.; Rao, C.V. Role of lipoxins, resolvins, and other bioactive lipids in colon and pancreatic cancer. *Cancer Metastasis Rev.* **2011**, *30*, 507–523. [[CrossRef](#)] [[PubMed](#)]
124. Zhang, C.; Yu, H.; Shen, Y.; Ni, X.; Shen, S.; Das, U.N. Polyunsaturated Fatty Acids Trigger Apoptosis of Colon Cancer Cells Through a Mitochondrial Pathway. *Arch. Med. Sci.* **2015**, *11*, 1081–1094. [[CrossRef](#)] [[PubMed](#)]
125. Calviello, G.; Nicuolo, F.D.; Gragnoli, S.; Piccioni, E.; Serini, S.; Maggiano, N.; Tringali, G.; Navarra, P.; Ranelletti, F.O.; Palozza, P. n-3 PUFAs reduce VEGF expression in human colon cancer cells modulating the COX-2/PGE2 induced ERK-1 and -2 and HIF-1 α induction pathway. *Carcinogenesis* **2004**, *25*, 2303–2310. [[CrossRef](#)] [[PubMed](#)]
126. Hawcroft, G.; Loadman, P.M.; Belluzzi, A.; Hull, M.A. Effect of eicosapentaenoic acid on E-type prostaglandin synthesis and EP4 receptor signaling in human colorectal cancer cells. *Neoplasia* **2010**, *12*, 618–627. [[CrossRef](#)]
127. Zhang, K.; Hu, Z.; Qi, H.; Shi, Z.; Chang, Y.; Yao, Q.; Cui, H.; Zheng, L.; Han, Y.; Han, X.; et al. G-protein-coupled receptors mediate ω -3 PUFAs-inhibited colorectal cancer by activating the Hippo pathway. *Oncotarget* **2016**, *7*, 58315–58330. [[CrossRef](#)]
128. Oh, D.Y.; Talukdar, S.; Bae, E.J.; Imamura, T.; Morinaga, H.; Fan, W.; Li, P.; Lu, W.J.; Watkins, S.M.; Olefsky, J.M. GPR120 is an omega-3 fatty acid receptor mediating potent anti-inflammatory and insulin-sensitizing effects. *Cell* **2010**, *142*, 687–698. [[CrossRef](#)]
129. Sebio, A.; Kahn, M.; Lenz, H.J. The Potential of Targeting Wnt/ β -catenin in Colon Cancer. *Expert Opin. Ther. Targets* **2014**, *18*, 611–615. [[CrossRef](#)]
130. Notarnicola, M.; Tutino, V.; De Nunzio, V.; Dituri, F.; Caruso, M.G.; Giannelli, G. Dietary ω -3 Polyunsaturated Fatty Acids Inhibit Tumor Growth in Transgenic Apc^{Min/+} Mice, Correlating with CB1 Receptor Up-Regulation. *Int. J. Mol. Sci.* **2017**, *18*, 485. [[CrossRef](#)]
131. D'Eliseo, D.; Rocco, G.D.; Loria, R.; Soddu, S.; Santoni, A.; Velotti, F. Epithelial-to-mesenchymal Transition and Invasion Are Upmodulated by Tumor-Expressed Granzyme B and Inhibited by Docosahexaenoic Acid in Human Colorectal Cancer Cells. *J. Exp. Clin. Cancer Res.* **2016**, *35*, 24. [[CrossRef](#)]
132. Cho, Y.; Turner, N.D.; Davidson, L.A.; Chapkin, R.S.; Carroll, R.J.; Lupton, J.R. A chemoprotective fish oil/pectin diet enhances apoptosis via Bcl-2 promoter methylation in rat azoxymethane-induced carcinomas. *Exp. Biol. Med.* **2012**, *237*, 1387–1393. [[CrossRef](#)]
133. Cho, Y.; Turner, N.D.; Davidson, L.A.; Chapkin, R.S.; Carroll, R.J.; Lupton, J.R. Colon cancer cell apoptosis is induced by combined exposure to the n-3 fatty acid docosahexaenoic acid and butyrate through promoter methylation. *Exp. Biol. Med.* **2014**, *239*, 302–310. [[CrossRef](#)] [[PubMed](#)]
134. Tsoukas, M.A.; Ko, B.J.; Witte, T.R.; Dincer, F.; Hardman, W.E.; Mantzoros, C.S. Dietary walnut suppression of colorectal cancer in mice: Mediation by miRNA patterns and fatty acid incorporation. *J. Nutr. Biochem.* **2015**, *26*, 776–783. [[CrossRef](#)] [[PubMed](#)]
135. Serini, S.; Vasconcelos, R.O.; Fasano, E.; Calviello, G. Epigenetic regulation of gene expression and M2 macrophage polarization as new potential omega-3 polyunsaturated fatty acid targets in colon inflammation and cancer. *Expert Opin. Ther. Targets* **2016**, *20*, 843–858. [[CrossRef](#)] [[PubMed](#)]

136. De Carlo, F.; Witte, T.R.; Hardman, W.E.; Claudio, P.P. Omega-3 eicosapentaenoic acid decreases CD133 colon cancer stem-like cell marker expression while increasing sensitivity to chemotherapy. *PLoS ONE* **2013**, *8*, e69760. [[CrossRef](#)] [[PubMed](#)]
137. Yang, T.; Fang, S.; Zhang, H.X.; Xu, L.X.; Zhang, Z.Q.; Yuan, K.T.; Xue, C.L.; Yu, H.L.; Zhang, S.; Li, Y.F.; et al. N-3 PUFAs have antiproliferative and apoptotic effects on human colorectal cancer stem-like cells in vitro. *J. Nutr. Biochem.* **2013**, *24*, 744–753. [[CrossRef](#)] [[PubMed](#)]
138. Sam, M.R.; Ahangar, P.; Nejati, V.; Habibi, R. Treatment of LS174T colorectal cancer stem-like cells with n-3 PUFAs induces growth suppression through inhibition of survivin expression and induction of caspase-3 activation. *Cell. Oncol.* **2016**, *39*, 69–77. [[CrossRef](#)]



© 2020 by the authors. Licensee MDPI, Basel, Switzerland. This article is an open access article distributed under the terms and conditions of the Creative Commons Attribution (CC BY) license (<http://creativecommons.org/licenses/by/4.0/>).

Review

The Crosstalk between Prostate Cancer and Microbiota Inflammation: Nutraceutical Products Are Useful to Balance This Interplay?

Felice Crocetto ^{1,†}, Mariarosaria Boccellino ^{2,†}, Biagio Barone ¹, Erika Di Zazzo ^{3,*}, Antonella Sciarra ⁴, Giovanni Galasso ², Giuliana Settembre ², Lucio Quagliuolo ², Ciro Imbimbo ¹, Silvia Boffo ⁵, Italo Francesco Angelillo ⁶ and Marina Di Domenico ^{2,5}

¹ Department of Neuroscience, Reproductive Sciences and Dentistry, School of Medicine, University of Naples “Federico II”, 80135 Naples, Italy; felice.crocetto@unina.it (F.C.); biagio.barone@unina.it (B.B.); ciro.imbimbo@unina.it (C.I.)

² Department of Precision Medicine, University of Campania “Luigi Vanvitelli”, 80135 Naples, Italy; mariarosaria.boccellino@unicampania.it (M.B.); giovanni.galasso@unicampania.it (G.G.); giulianasettembre@gmail.com (G.S.); lucio.quagliuolo@unicampania.it (L.Q.); marina.didomenico@unicampania.it (M.D.D.)

³ Department of Health Science “V. Tiberio”, 86100 Campobasso, Italy

⁴ Department of Translational Medical Sciences, University of Campania Luigi Vanvitelli, 80135 Naples, Italy; Antonella.sciarra@unicampania.it

⁵ Sbarro Institute for Cancer Research and Molecular Medicine, Center for Biotechnology, College of Science and Technology, Temple University, Philadelphia, 19122 PA, USA; silvia.boffo@temple.edu

⁶ Department of Experimental Medicine, University of Campania Luigi Vanvitelli, 80135 Naples, Italy; italofrancesco.angelillo@unicampania.it

* Correspondence: erika.dizazzo@unimol.it

† These authors contributed equally.

Received: 31 July 2020; Accepted: 26 August 2020; Published: 31 August 2020

Abstract: The human microbiota shows pivotal roles in urologic health and disease. Emerging studies indicate that gut and urinary microbiomes can impact several urological diseases, both benign and malignant, acting particularly on prostate inflammation and prostate cancer. Indeed, the microbiota exerts its influence on prostate cancer initiation and/or progression mechanisms through the regulation of chronic inflammation, apoptotic processes, cytokines, and hormonal production in response to different pathogenic noxae. Additionally, therapies’ and drugs’ responses are influenced in their efficacy and tolerability by microbiota composition. Due to this complex potential interconnection between prostate cancer and microbiota, exploration and understanding of the involved relationships is pivotal to evaluate a potential therapeutic application in clinical practice. Several natural compounds, moreover, seem to have relevant effects, directly or mediated by microbiota, on urologic health, posing the human microbiota at the crossroad between prostatic inflammation and prostate cancer development. Here, we aim to analyze the most recent evidence regarding the possible crosstalk between prostate, microbiome, and inflammation.

Keywords: prostate cancer; microbiota; nutraceutical compounds

1. Introduction

Prostate cancer (PCa) is the second most commonly diagnosed malignancy in men and the fifth leading cause of tumor-associated death worldwide [1].

Global estimations are approximating 800,000 new PCa cases and 300,000 deaths per year [2], and this condition poses a significant health concern in the future due to the gradual aging of the

population. Genetics, family history, African descent, advanced age, diet, and environment are well-established risk factors for PCa development. However, the relevant pathways accounting for PCa development are not fully clarified [3–5]. The role of androgenic stimulation and the deficit of apoptosis of prostate cells are well-known explanations regarding the incidence and progression of PCa. Recent studies have also hypothesized a crucial role of microenvironment, infections, inflammation, and cytoskeletal changes induced by steroid integrating signals [6,7], influencing patients' outcomes and the rationale for the immunological treatment of PCa [8–12].

Chronic inflammation is a prominent contributing factor to the benign and malignant prostatic growth; however, the potential stimulus that induces or maintains this chronic inflammation remains poorly characterized [13]. Inflammation, sex hormones, and many other factors (e.g., infections, diet, physical activity, drugs), are known to affect the microbiota. The microbiota is a complex community composed of fungi, parasites, bacteria and viruses living within the human body. Microbiota components interact with each other and with the host, impacting, eventually, the overall human health. The purpose of this study is to summarize and analyze the most recent evidence regarding the possible crosstalk among prostate, microbiota, and inflammation.

2. Prostate and Chronic Inflammation

The role of inflammation in the carcinogenesis of a solid tumor is an accustomed aspect [13]. In fact, two key inflammatory cytokines, IL-6 and IL-2, have been convincingly implicated in prostate cancer pathogenesis. Inflammation may also contribute to impairing immune surveillance mechanisms, which are partially mediated by NK cells [14,15]. Repeated tissue damage and regeneration produce highly reactive nitrogen species (RNS) and oxygen species (ROS), which are responsible of cancer development and progression [16–19]. The underlying biological mechanism relies on DNA modifications of cells caused by this continuous process of damage and repair [20–22]. However, if there is a strong and proven connection between solid tumors and inflammation, the role of this condition in PCa development is still debatable and under revision. Different studies have suggested how chronic prostatitis could induce proliferation of stromal and glandular cells in response to ROS production, eliciting general tissue damage, and vascular injury [23,24]. ROS, moreover stimulate NF- κ B and TNF- α pathways by activating their proper kinases [25]. The morphological modification in the prostate tissue, associated with chronic and acute inflammation, is a glandular atrophy with hyperplasia called proliferative inflammatory atrophy (PIA) [26]. Up to 40% of PIA lead to the transition to a high-grade prostatic intraepithelial neoplasia (PIN), a precursor of PCa. Although some evidence of molecular changes has been observed in PIA, no certain clonal genetic alterations have been found in this condition [27]. However, genes such as NKX3.1 and CDKN1B have been shown to be downregulated in PIA, as in PIN and PCa, while the increased transcription of Hsp27 and PRDX6 could promote processes leading to tumorigenesis [28]. Several PCa susceptibility genes, such as MIC1, RNASEL, MSR1, PON1, TLR4, OGG, BRCA2 and CHEK2, are involved in prostate carcinogenesis and in other critical processes, as a host response to steroids, infection, inflammation and oxidative stress [29,30]. Furthermore, despite significant changes in inflammatory cellular infiltration between prostatitis, benign prostatic hyperplasia (BPH) and PCa have been found; the role of innate and adaptive immunity has not been completely cleared [13] (Figure 1). Chronic inflammation could have, moreover, a significant effect on cancer progression and metastatic invasion due to neo-angiogenesis and activation of epithelial–mesenchymal transitions (EMTs) [31,32]. These biologic and pathogenic processes are correlated to various molecules defined as biomarkers/indicators of normal, or pharmacologic, responses to a therapeutic intervention [33]. The control of these phenomena triggers pathways, as migration, proliferation, cell growth, apoptosis, and adhesion through various downstream effectors. The first key element that regulates cell proliferation, migration, and invasion in PCa is p85 α PI 3Kinase [34–38]. Evidence from the literature supports the role of angiogenesis in human cancer progression, including PCa. The vascular endothelial growth factor (VEGF) is a potent angiogenic factor [39,40]. Several miRNAs, functioning as tumor suppressors or oncogenes

are deregulated in prostate tumorigenesis. miRNA dysregulation progress has a key role in prostate cancer [41]. Anti-VEGF therapy and combined chemotherapy treatments trigger apoptosis in cancer and, in particular, in prostate cancer [42–50].

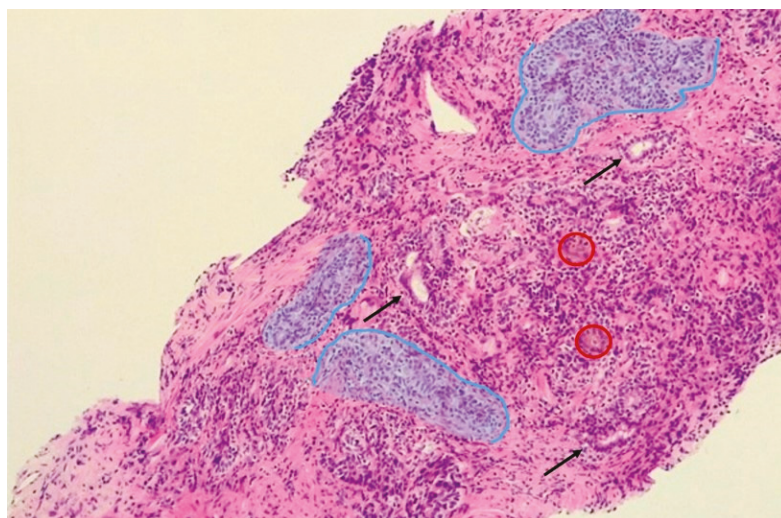


Figure 1. Chronic prostatitis and immune cell infiltration. Outlined in blue are aggregates of lymphocytes, plasmacells and istiocytes, which surround damaged glands (black arrows). In red circles, multinucleated giant cells are outlined.

Different cancer types (i.e., lung cancer, pancreatic cancer, glioblastoma, meningioma, myeloma, and myeloma) are characterized by distinct patterns revealed by corona composition, constituting a “fingerprint” for each cancer type [51–54].

Classically, the peripheral zone of the prostate gland is a common site of PCa development, while the transitional zone is mostly affected by benign prostatic hyperplasia [55]. However, in about 20% of cases, the two conditions subsist in the same zone and, despite different pathogenic pathways, several well-established epidemiologic studies confirm that both conditions are hormone-dependent and could be associated with a previous chronic prostatic inflammation [56]. A certain degree of inflammation is almost always present when prostate specimens are sampled: the REDUCE trial demonstrated on 8224 men that, indeed, 77.6% of biopsies are positive for some grade of inflammation, with the majority (>80%) showing a mild chronic inflammation [57]. To further support these findings, men diagnosed with prostatitis have an increased risk of developing, in the future, PCa compared to those without any grade of prostate inflammation. Specifically, 18% of those patients will develop PCa [58]. Chronic and acute inflammation is also frequently found in prostate tumor specimens obtained from prostatectomies and transurethral resections [59]. A study conducted by Daniels et al. on 5821 men >65 years old reported a positive association between a previous history of prostatitis and PCa (OR 5.4, 95% CI = 4.4–6.6) [60]. Similarly, Cheng et al. showed that protracted prostatitis symptoms could significantly increase the odds of PCa in 68,675 men (RR 1.3, 95% CI = 1.10–1.54) [61]. In addition, Dennis et al. reported, in a meta-analysis of 11 case-control studies, the evidence of a statistically significant risk of developing PCa in patients with a previous history of prostatitis (OR 1.6, 95% CI = 1–2.4) [62] and analogous results were found by a similar meta-analysis on 20 case-control studies (OR 1.50, 95% CI 1.39–1.62) [63]. Finally, a recent and wide meta-analysis by Perletti et al. reported, in 422,943 patients, a significant association between PCa and previous prostatitis (OR 1.83, 95% CI = 1.43–2.35) [4]. However, despite those data, the real impact of chronic inflammation on prostate carcinogenesis has been challenging to define. In particular, it is not easy to estimate the real

incidence of prostatitis due to the asymptomatic majority of cases (5–10%) [64]. Moreover, evidence that seems to show an increased risk for acute prostatitis rather than for chronic prostatitis, is influenced by the same potential detection bias.

Etiology of Prostate Chronic Inflammation

The etiology of chronic inflammation preceding PCa development remains unknown, however, infections and chemical trauma are often correlated to chronic inflammation.

Several putative etiological agents have been identified, from the xenotropic murine leukemia virus related-virus XMRV to different strains of bacteria [58,65–67]. Several studies support the potential role of infectious agents in PCa etiology with evidence that up to 87% of PCa patients show microbial DNA in their prostate [68,69]. However, if no clear association had been shown with HPV or other sexually transmitted viruses, men with previous gonorrhea or syphilis infections had a 60% increased risk of developing PCa [70]. A study based on animal models reported a mutagenic activity of inflammation caused by *Escherichia coli* in the prostatic gland, with the induction of epithelial hyperplasia, an increased tendency to apoptosis, and somatic mutations [71]. Moreover, the presence of an induced prostatic infection with *Escherichia coli*, in addition to the consumption of a diet enriched with a cyclic amine, the 2-amino-1-methyl-6-phenylimidazo [4,5-b]pyridine (PhIP) (a well-known prostatic carcinogen in rodents), further increased the risk of PCa development in mice with a marked drop in survival rate compared with PhIP-alone-treated animals, thus suggesting chronic inflammation as an enabling characteristic of PCa [72]. Cai et al., reported a significant increase in Gram-positive strains in patients with chronic prostatitis and a successively diagnosed PCa [73], while other significant associations between cancer development and infection were shown also for *Mycoplasma hominis* [74] and *Trichomonas vaginalis* [75,76]. In particular, previous *Trichomonas vaginalis* infection could create a favorable microenvironment, promoting PCa cell proliferation and invasiveness (activating the epithelial–mesenchymal transition), in addition to an increased overall inflammatory state of the gland [77]. Twu et al. reported, in fact, how *Trichomonas vaginalis* secretes a protein (TvMIF), which is 47% similar to the human macrophage migration inhibitory factor (HuMIF), which is reported to be elevated in PCa [78]. *Propionibacterium acnes*, which is frequently isolated in prostate tissue, has also been thought to have an influence on the development of PCa due to the association with reported histological inflammation in prostate-derived tissue models and prostatectomy specimens [79]. To further outline the role of *Propionibacterium acnes* in prostate carcinogenesis, Ugge et al. retrospectively analyzed the association between the presence of acne vulgaris during adolescence and the occurrence of PCa in 243,187 men for a median follow up of 36.7 years; 1633 of those patients developed PCa, reporting an adjusted OR of 1.43 (95% CI = 1.06–1.92) [80]. However, a recent meta-analysis by Zhang et al. did not find a significant association between acne and PCa, questioning this relation [81]. An EPICAP study reported instead the association between sexually transmitted and urinary tract infections and PCa, with an increased risk of developing this malignancy in patients with a previous history of prostatitis (OR 2.95, 95% CI = 1.26–6.92) and in patients who did not assume non-steroidal anti-inflammatory drugs (OR 2.00, 95% CI = 1.37–2.91) [82]. To further support the role of chronic inflammation in increased PCa risk, St. Hill et al. showed how EBV, HIV, HBV, HCV, or HSV chronic infections were associated with an increased risk of occurrence of PCA. Similarly, the risk was also increased in men with other chronic inflammatory diseases or conditions such as osteoporosis, diabetes mellitus, arthritis, or cardiovascular disease; however, currently, no inflammation marker could be associated with a higher risk of PCa development [83].

3. Microbiota in Urological Disease

3.1. Urinary and Prostate Microbiota

Commensal microorganisms colonize barrier surfaces of all multicellular organisms, coevolving and adapting with the host for more than 500 million years. As result, the commensal microbiota

affects many processes of their hosts via biologically active molecules, playing critical roles in human diseases, in particular cancers and autoimmune conditions, influencing the innate and adaptive immune response [84]. The discovery of communities of bacteria in the genitourinary tract and their role in urologic diseases has introduced novel factors and implications in the pathophysiology of these conditions. The advent of such molecular-based methods as the quantitative real-time PCR and amplification of 16S rRNA for the identification and characterization of microbial populations has permitted the discovery of previously unrevealed microbial populations. Historically, the bladder, and generally the urinary tract, has always been considered sterile, however, recent studies have revealed important evidence of the presence of microbes in bladders of patients without clinical infection [85,86]. Human urinary microbiota characteristics depend on the age, gender, and disease status of individuals [87–92], and understanding its role in urological diseases is of particular interest. Moreover, novel molecular methods have made it possible to characterize the bladder microbiota formed by *Burkholderia cenocepacia* and different strains of *Lactobacilli* in urologic chronic pelvic pain syndrome (UCPSS), which was considered to be defined as “the absence of identifiable bacterial infection” [93]. Particularly interesting is that, in the same condition, an increased rate of *Lactobacilli*, compared to the remaining flora, was instead revealed in the urine of patients with Interstitial Cystitis (IC) [94]. Furthermore, *Lactobacillus casei* and *Lactobacillus rhamnosus* could also have interesting applications in the treatment of bladder cancer, demonstrating a decreasing effect on rates of metastasis and recurrence due to an enhanced recruiting of natural killer cells, both in vitro and in vivo [95]. Accordingly, different studies have hypothesized a link between prostate microbiota and pro-inflammatory bacterial species. In 2016, Mandar et al. reported a lower rate of *Lactobacilli* in patients with chronic prostatitis, while Shoskes et al. reported, for the same condition, higher rates of *Clostridia* and *Bacteroides* compared with controls [96,97]. In 2015, Yu et al. described how bacterial strains present in prostatic secretions, seminal fluid and voided urine are different among patients with BPH and PCa. Specifically, there are lower rates of *Eubacterium* and *Defluviococcus* and higher rates of *Bacteroidetes* in patients with PCa, hypothesizing the role of certain bacteria in the induction of chronic inflammatory states, with enhanced production of factors favoring tumorigenesis [98]. An analogous study conducted on 135 PCa patients by Shrestha et al. in 2018, reported an increased presence of *Anaerococcus lactolyticus* and *obesiensis*, *Streptococcus anginosus*, *Varibaculum cambriense*, *Actinobaculum schaalii*, and *Propionimicrobium lymphophilum*. All patients were previously diagnosed with urinary tract infection caused by *Enterobacteriaceae*, which were instead more abundant in patients with BPH [99]. Similar conclusions were reported by Alane et al., confirming the possible association between urinary and fecal microbiota with PCa after examination of prostate biopsies, which were characterized by higher rates of *Streptococcus anginosus*, *Anaerococcus lactolyticus*, and *Varibaculum cambriense* [100]. Analogously, Bhudia et al., reported increased rates of *Staphylococcus epidermidis*, *Streptococci*, *Corynebacterium amycolatum*, *Peptoniphilus harei*, and *Fusobacterium nucleatum* in prostate secretions of PCa patients [101]. Cavarretta et al. reported an abundance of *Propionibacterium* spp. and *Staphylococcus* spp. in 16 tumoral and peritumoral prostatectomy specimens [102]. Similarly, Feng et al. examined 65 radical prostatectomy specimens, reporting an increased rate of *Escherichia coli*, *Propionibacterium acnes*, *Pseudomonas* spp. and *Acinetobacter*; in particular, *Pseudomonas* has a gene expression profile that strongly correlates with human small RNA’s profile, and that could be also related to metastasis [68]. Moreover, the same authors identified increased bacterial content (especially *Escherichia* spp. and *Acidovorax* spp.) in prostate specimens of African men, which were also associated with elevated tumor hypermutation, suggesting the possibility of a bacterially driven oncogenic transformation [69].

3.2. Gut Microbiota

The role of microbiota in urological diseases and PCa is, however, not limited to bacteria related to the urinary tract. Modification of the gut microbiota could modify the risk of incurring PCa and be influenced by the tumorigenesis process itself [103] (Table 1). Liss et al. reported significant differences

in bacteria obtained via rectal swab between PCa and healthy patients, with an increase in certain genera such as *Bacteroides* and *Streptococci* and impoverishment of bacteria related to folate and biotin production [104]. Golombos et al., similarly, confirmed the abundance of *Bacteroides* in PCa patients and reported an increased presence of *Faecalibacterium prausnitzii* and *Eubacterium rectale* in BPH patients [105]. Potential alterations of gut microbiota could influence, both directly and indirectly, prostate health via bacterial metabolites, and influence the enteric endocrine system [106]. Multiple studies have shown that gut microbiota also modulates the response to chemotherapy acting on the translocation, immunomodulation, metabolism, and enzymatic degradation of drugs [107]. This consideration, moreover, is valid also for androgen axis-targeted therapy in PCa treatment, which is influenced in its clinical response and antitumoral efficiency by gut microbiota. Conversely, androgen axis-targeted therapy enhances *Bacteroides* and *Streptococci* rates in the gastrointestinal tract while lowering overall bacterial diversity [108]. Besides, an analysis of the fecal microbiota of healthy volunteers and PCa patients by 16S rDNA sequencing, showed a greater abundance of *Akkermansia muciniphila* and *Ruminococcaceae* spp. in the microbioma of patients treated with oral androgen receptor axis-targeted therapies such as enzalutamide, bicalutamide and abiraterone acetate [109]. Finally, there are suggestions that butyrate, an anti-inflammatory micronutrient produced by *Faecalibacterium prausnitzii* and *Eubacterium rectale*, could be implicated in one of the pathways for the prevention of PCa, although further studies are required [105].

Table 1. Summary of bacteria increased in prostate diseases.

Bacterium	Localization	Findings	References
<i>Burkholderia cenopacia</i>	Bladder	Increased in UCPSS	[93]
<i>Lactobacillus casei/rhannosus</i>	Bladder/Prostate	Increased in IC. Enhanced the recruitment of natural killer cells. Decreased in chronic prostatitis	[94–96]
<i>Clostridia</i> spp.	Prostate	Increased in chronic prostatitis	[97]
<i>Anaerococcus lactolyticus/obesiensis</i>	Prostate	Increased in PCa	[99,100]
<i>Actinobaculum schaalii</i>	Prostate	Increased in PCa	[99]
<i>Varibaculum cambriense</i>	Prostate	Increased in PCa	[99,100]
<i>Propionimicrobium lymphophilum</i>	Prostate	Increased in PCa	[99]
<i>Enterobacteriaceae</i>	Prostate	Increased in BPH	[99]
<i>Propionibacterium acnes</i>	Prostate	Increased in PCa	[39,102]
<i>Escherichia coli</i>	Prostate	Increased in PCa. Associated with elevated tumour hypermutation	[39]
<i>Pseudomonas</i> spp.	Prostate	Increased in PCa. Expression profile related to metastasis	[39]
<i>Acinetobacter</i>	Prostate	Increased in PCa	[39]
<i>Acidovorax</i>	Prostate	Increased in PCa. Associated with elevated tumour hypermutation	[39]
<i>Bacteroides</i> spp.	Prostate/Gut	Increased in chronic prostatitis. Increased in the gut in PCa. Further increased in ADT.	[97,104,105,108]
<i>Staphylococcus epidermidis</i>	Prostate/Prostatic secretions	Increased in PCa	[101,102]
<i>Streptococcus anginosus</i>	Prostate/Prostatic secretions/Gut	Increased in PCa. Increased in the gut in PCa	[99–101,104,108]
<i>Peptoniphilus hareii</i>	Prostatic secretions	Increased in PCa	[101]
<i>Fusobacterium nucleatum</i>	Prostatic secretions	Increased in PCa	[101]

Table 1. Cont.

Bacterium	Localization	Findings	References
<i>Corynebacterium amycolatum</i>	Prostatic secretions	Increased in PCa	[101]
<i>Bacteroidetes</i> spp.	Prostatic secretions	Increased in PCa	[98]
<i>Deftluviococcus</i>	Prostatic secretions	Decreased in PCa	[98]
<i>Eubacterium rectal</i>	Prostatic secretion/Gut	Decreased in PCa. Increased in the gut in BPH. Could prevent PCa via increasing butyrate	[98,105]
<i>Faecalibacterium prausnitzii</i>	Gut	Increased in BPH. Could prevent PCa via increasing butyrate	[105]

Abbreviations: PCa (prostate cancer), BPH (benign prostatic hyperplasia), ADT (androgen deprivation therapy), UCPS (urologic chronic pelvic pain syndrome), IC (interstitial cystitis).

4. Nutraceutical Aspects in the Interplay between Prostate and Microbiota

4.1. Unsaturated Fatty Acids

Olive oil and unsaturated fats, high vegetable consumption, fruit intake, and allium vegetables, typical aspects of the Mediterranean diet, were related to a decreased risk of several cancer types. In particular, countries following the Mediterranean Diet have lower PCa incidence and mortality compared to other European regions. However, there are few studies that have assessed the effect of the Mediterranean diet on PCa incidence. Further large-scale studies are required to clarify the effect of the Mediterranean diet in order to establish the role of this diet in the PCa prevention [110,111]. PCa has a well-known association with food and, in particular, with fat intake; moreover, there is a relationship between PCa and gut microbiota that changes based on the diet [112]. A low-fat diet and/or intensive exercise involves changes in serum hormones and growth factors in vivo, which could reduce growth and induce apoptosis of LNCaP prostate tumor cells in vitro [113]. Low-fat diet-fed mice show significantly lower levels of prostate-specific serum antigen (PSA), insulin and Igf1 mRNA levels compared to mice with a high-fat diet, as well as a delayed tumor-growth rate in LAPC4 xenografts [114]. A high-fat diet induces, in fact, lipid accumulation in PCa and promotes metastasis via abnormal sterol regulatory element-binding protein (SREBP)-dependent lipid metabolism [115]. Several epidemiological studies suggest that an increased intake of saturated fatty acids and a sedentary lifestyle decreases the survival rate of PCa patients, whilst unsaturated fatty acids and physical activity reduce the risk of PCa [116,117]. In recent years, *n*-3 fatty acids, eicosapentaenoic acid (EPA) and docosahexaenoic acid (DHA), present in fish oil, have been found to influence cancer cell proliferation. EPA and DHA were, moreover, effective in decreasing the proliferation, invasion, and migration of prostate PC3 cancer cells as well [118]. As known, sex hormones also play an important role in the development and progression of PCa. In prostate-specific Pten^{-/-} mice, the reduction in serum cholesterol lowers intraprostatic androgens and suppresses tumor progression, although it does not change the incidence of PCa [119]. In transgenic mice, the consumption of high amounts of unsaturated fatty acid ω -3, produces a significant slow-down of prostate tumorigenesis by affecting estradiol, testosterone, and androgen receptor levels, suggesting a specific role of unsaturated fatty acids in the regulation of sex hormones, which may be the basis of fat-induced PCa progression [120].

4.2. Carnitine

Carnitine, and in particular its acetylated derivative, Acetyl-L-Carnitine (ALCAR) is involved in mitochondrial membrane trafficking in catabolic and anabolic pathways. Several studies have documented the antioxidant and scavenger activity of this compound, utilized in clinical settings related to disorders where the oxidative stress acts as a promoting factor (e.g., diabetes, Alzheimer's disease, and other neurometabolic disorders) [121,122]. ALCAR reduces PCa cell viability and induces apoptosis; moreover, ALCAR impairs the adhesion, invasion and migration of PC3, DU145, LNCaP, and BPH cells, eliciting a decreasing effect on TNF- α and other proinflammatory cytokines, such as

IL-6, CCL2 and CXCL12 [123]. Besides, ALCAR was able to limit inflammatory angiogenesis, in vitro and in vivo, downregulating the VEGF/VEGFR2, CXCL12/CXCR4, and FAK pathways [124].

4.3. N-acetylcysteine (NAC)

N-acetylcysteine (NAC) is an exogenous antioxidant primarily used as a mucolytic agent and as an antidote of acetaminophen toxicity. Its effects on increasing glutathione levels and scavenging free radicals pose NAC as a powerful antioxidant. The association of NAC with phenethyl isothiocyanate (PEITC) and sulforaphane (SFN), two compounds present in cruciferous vegetables (cauliflower, cabbage, and broccoli) inhibit LNCaP and DU145 cell growth in a dose-dependent manner, increasing p21, a potent inhibitor of cyclin-dependent kinases mediating cell replication, up to apoptosis. Besides, SFN-NAC reduces PSA and the expression of the androgen receptor [125,126]. NAC alone inhibits the growth of PC3 cells suppressing the transcription of nuclear factor (NF)- κ B, while increasing Cyr61 levels and activating the Erk pathway [127]. Finally, NAC shows a significant anti-migration and anti-invasion activity on DU145 and PC3 cells, limiting the metastatic ability of those cells [128].

4.4. Monoterpenes

Terpenoids are natural constituents of plants and animals. The most common form occurs as monoterpenes, components of essential oils of herbs and spices. D-Limonene, the most abundant monoterpene present in orange, lemon, and peppermint essential oil, has been shown to inhibit PCa cell growth via Erk pathway activation and the induction of WAF1 and p21 [129]. Geraniol, another monoterpene found in geranium and citronella plants, inhibits tumor cell growth via the induction of apoptosis in PC3 cells, activating caspase-3, reducing Bcl-2 expression and increasing Bax and BNIP3 levels. Besides, geraniol has been found to inhibit AKT-mTOR signaling without influencing mitogen-activated protein kinase (MAPK) activity [130]. A thyme honey component, the trihydroxy ketone E-4-(1,2,4-trihydroxy-2,6,6-trimethylcyclohexyl)-but-3-en-2-one exerted significant apoptotic activity in PC3 cells, through a reduction in NF- κ B activity and IL-6 secretion [131].

4.5. Polyphenols

Polyphenols are widely studied for their beneficial effects on human health, particularly in cancer prevention. Several studies associate, in particular, catechin and isoflavone with beneficial effects on PCa. The epigallocatechin-3-gallate (EGCG), the most common catechin in green tea (>50% of the total polyphenol content), shows a great physiological activity: EGCG arrests cell growth in the G0/G1-phase and induces apoptosis in both androgen-sensitive and insensitive human PCa cells [132]. Moreover, EGCG, in both androgen-sensitive and insensitive human PCa cells, attenuated the effects of arachidonic acid (AA) in increasing cell growth and prostaglandin E2 levels by reducing the concentration of the enzyme cyclooxygenase 2 (COX-2) [133]. EGCG also acts through different mechanisms in order to arrest cell cycle and induce apoptosis, in fact in 12-week-old TRAMP mice, contrary to 28-week-old mice, it suppressed PCa development at an early stage after oral intake of EGCG by regulating IGF-1-related signaling and COX-2 levels [134]. Green tea has, therefore, an inhibitory effect on PCa tumorigenesis when assumed in large quantities. Kurahashi et al. examined the relationship among green tea consumption and PCa risk, in a large-scale prospective study of 49,920 Japanese men, reporting how subjects who drank five or more cups of green tea each day had a lower risk of advanced PCa than those who drank less than one cup per day (RR 0.52, 95% CI = 0.28–0.96) [135]. More recently, a meta-analysis on ten large studies on the incidence of green tea and PCa has shown how the risk of PCa decreases in a dose-dependent manner, with a significant reduction in the risk for subjects who drank more than seven cups a day (RR 0.81, 95% CI = 0.67–0.97 for 7 cups/day; RR 0.74, 95% CI = 0.59–0.93 for 9 cups/day; RR 0.56, 95% CI = 0.35–0.92 for 15 cups/day) [136]. Isoflavones also play an important role in the prevention of PCa, with a reduction in PCa risk related to the intake of soy isoflavone [137]. Soy isoflavones, having a structure similar to 17 β -estradiol, can bind to the estrogen receptor (ER), behaving as phytoestrogens with a binding affinity and transcriptional activity stronger

on ER- β than on ER- α and thus having more likely estrogenic effects in prostate tissue, which expresses higher levels of ER- β . Genistein, another isoflavone contained in fava beans, soy, and coffee, induces apoptosis of PC3 cells by suppressing NF- κ B via the AKT signaling pathway [138]. In DU145 cells, genistein, EGCG, and Silymarin, a flavonolignan contained in *Cardus marianus*, induced the inhibition of erbB1 membrane receptor activation caused by TGF α , provoking a dose-dependent inhibition of cell growth [139]. In addition, EGCG could induce apoptosis in LNCaP cells by two pathways: the first acted on the stabilization of tumor suppressor gene p53 and on the reduction in MDM2 protein expression; the second was related to the negative regulation of NF- κ B activity, leading to a decreased expression of the anti-apoptotic protein Bcl-2 [140]. In TRAMP mice, food genistein reduced PCa development in a dose-dependent manner [141]. Parallel studies in TRAMP-FVB mice showed that a low-dose genistein diet (250 mg/kg) promoted PCa growth and metastasis compared to control and a high-dose genistein diet (1000 mg/kg), showing a biphasic effect of isoflavones on PCa [142]. Paller et al. found that an increase in quercetin intake, another well-known isoflavone contained in capers, leads to a reduced risk of PCa, in African-Americans with vitamin D deficiency, while Sun et al. showed that its use, associated with metformin, inhibits the growth, migration, and invasion on PC3 and LNCaP cells by inhibiting the VEGF/AKT/PI3K signaling pathway [143,144]. Similarly, fisetin has been suggested to act as a dual inhibitor on PI3K/AKT and mTOR metabolic pathways in PCa cell lines. In addition, this compound could be used, alone or as an adjunctive drug in the chemotherapeutic treatment of PCa [145]. In two different prostate cancer cell lines, androgen-sensitive (LNCaP) and androgen-independent (DU145), cyanidin-3-O-beta-glucopyranoside (C3G), the most abundant anthocyanin in the diet, produced anti-proliferative effects through the activation of caspase-3 and the induction of p21 protein expression. Besides, treatment with C3G increased the levels of tumor suppressor P75 NGFR, indicating a possible role of C3G in the acquisition of a normal-like cell phenotype. C3G may, therefore, be considered a new therapeutic agent with both anti-proliferative and pro-differentiation properties [146]. The DU-145 cells treatment with anthocyanins extracted from black soybean provoked a significant increase in apoptosis and a significant decrease in p53, Bcl-2 and AR expressions with, in addition, a further decrease in PSA levels. Moreover, the anthocyanin treatment showed a significant inhibition of tumor growth in xenograft models [147]. Gallic acid (GA) induced apoptosis in DU145 and 22Rv1 cell lines, demonstrating, in nude mice fed with GA, inhibition of tumor growth [148]. In addition, GA reduces survival, proliferation, and invasion in PC3 cells [149]. Gallotannins, polymers formed by the esterification of GA, produce an apoptotic effect in DU145 and PC3 cell lines by decreasing the expression of different genes, such as Mcl-1, and inhibiting caspase activation [150]. Similarly, the ellagitannins of the pomegranate, named punicalagin (PN), have elicited the induction of apoptosis in PC-3 and LNCaP cells [151]. In the pomegranate, as well as juice, extract, or oil, in addition to the ellagitannins, there are also large quantities of anthocyanins that have powerful antioxidant and anticancer activities in different tumors, including PCa [152]. Caffeic acid and its natural ester-caffeic acid phenethyl ester (CAPE) are potent inhibitors of the androgen-dependent PCa lines [153]. Caffeic acid and CAPE from bee propolis showed a synergistic effect with chemotherapeutics and radiotherapy, repressing, moreover, tumor growth and AKT signals in human PCa cells [154]. Esters of cinnamic acid induce apoptosis and inhibit the growth of prostate and breast cancer [155]. Chlorogenic acid inhibits benign prostatic hyperplasia growth, probably via the inhibition of 5 α R, in the animal model [156]. Ferulic acid induced the arrest of cell cycle in PC3 cells while, in LNCaP cells, it provoked apoptosis [157]. Resveratrol treatment of LNCaP cells led to the phosphorylation and the nuclear translocation of ERK1/2 (mitogen-activated protein kinase) and the accumulation of nuclear COX-2, and subsequently to the complex formation with pERK1/2 and p53 [158]. In addition, curcumin, a polyphenolic molecule extracted from the rhizome of the plant *Curcuma longa*, inhibits the proliferation of androgen-dependent and androgen-independent prostate cell lines [159]. Curcumin increases, in fact, the sensitivity of PCa cell cultures to gamma-radiation, reduces the trans-activation and the expression of AR (acting also as its antagonist), reduces the expression of EGF receptors, induces the degradation of HER2, reduces angiogenesis in vivo and the expression of VEGF [160]. Curcumin acts,

moreover, as an inhibitor of the tumor necrosis factor (TNF- α) and prostaglandin E2 (PGE2) production, but increases the caspase activity (3, 8, 9) in HL-60 PCa [161]. A recent study by Chen et al. examined the anti-carcinoma potential of curcumin, treating PC3 and DU145 cells with a series of curcumin analogs of the second generation, in concentrations of 0–10 μ M, founding the ability of curcumin to decrease the expression of NF- κ B, mTOR (mammalian target of rapamycin), AKT and p-AKT [162]. Colonic metabolites may participate in the chemoprevention of PCa by varied polyphenol-rich diet or composite polyphenol preparations. The gut microbiota-derived metabolites of ellagitannins and green tea catechins, urolithin A (uroA) and 5-(3',4',5'-trihydroxyphenyl)- γ -valerolactone (M4), respectively, are, in fact, the main compounds absorbed by the human system and derived from the metabolism of these polyphenols. Stanisławska et al. established the effects of M4, uroA, and their combinations on LNCaP cells: M4 showed modest antiproliferative activity in LNCaP cells (IC50 = 117 μ M; CI: 81–154), while uroA decreased proliferation (IC50 = 32.7 μ M; CI: 24.3–41.1) and induced apoptosis in the same line of cells with, furthermore, a synergistic antiproliferative activity of M4 plus uroA. Besides, M4 potentiated the inhibition of PSA secretion and enhanced AR retention in cytoplasm caused by uroA [163]. Urolithins induced apoptosis in LNCaP cells, negatively influencing the levels of Bcl-2 protein and probably decreasing the expression of AR and the PSA synthesis [164]. Moreover, the gut microbiota itself is influenced by those colonic metabolites, eliciting beneficial effects on intestinal probiotic bacteria [165]. The dietary pattern has, indeed, an important and direct influence on gut bacteria composition [166]. The western diet, consisting of high-fat content and high sugar content, reduces the diversity of the gut microbiota in mice, increasing in *Bacteroides* spp. and *Ruminococcus torques* [167] while, in humans, increasing *Enterobacteriaceae* rates and significantly decreasing short-chain fatty acids in feces, one of the metabolites generated by bacteria [168].

5. Conclusions

Although the prostate is not an organ directly affected by gut microbiota, a wealth of evidence suggests an indirect influence of cytokines and immune changes derived by different bacterial metabolites and gut microbiota modifications. The previously reported studies support a potential role of diet and nutrition in PCa pathogenesis, partially mediated by the gut microbiota itself. The gut microbiota could be targeted to improve therapies while attenuating adverse reactions. The influence of diet and nutrients on PCa pathogenesis and progression have received increasing attention. Several animal studies have reported how certain nutrients, including fat and polyphenols, are indeed involved through a variety of mechanisms, which include inflammation, antioxidant activity, and influence on sex hormones (Table 2). Generally, a healthy dietary pattern (e.g., low in meat and high in vegetables) could help in the prevention of PCa and lifestyle-related diseases. Due to such considerations, the close relationship between gut microbiota and cancer is a research area that is receiving considerable attention. Based on recent findings, gut microbiota alterations, which are caused by various external factors such as dietary composition, are involved in all stages of cancer, including initiation, progression, treatment outcomes, and adverse reactions [169]. The mechanism by which gut microbiota may influence PCa has not been elucidated. Therefore, it is challenging to understand how microbiota and host influence each other. It could be speculated that while microbiota could affect the natural cancer history, cancer itself could change the microbiota composition. However, it is undeniable that colonic metabolites may contribute to the chemoprevention of PCa by varied polyphenol-rich diet or composite polyphenol preparations. Understanding the specifics of gut microbiota in the context of PCa is needed in the era of precision medicine for the development of personalized treatments. However, a further investigation and understanding of the relationships between microbiota and PCa pathogenesis, development, and progression are warranted.

Table 2. Summary of the effects of several natural compounds.

Substance	Source	Findings	References
Eicosapentaenoic acid (EPA)	Fish oil	Decreases proliferation, invasion and migration of PC3 cells.	[118]
Docosahexaenoic acid (DHA)	Fish oil	Decreases proliferation, invasion and migration of PC3 cells.	[118]
Acetyl L-Carnitine (ALCAR)	Meat, tempeh, cod	Induces apoptosis and impairs migration and invasion of PC3, DU145, LNCaP cells decreasing TNF- α , IL-6, CCL2, CXCL12. Limits angiogenesis downregulating VEGF and FAK.	[123,124]
N-Acetylcysteine (NAC)	Allium plants	Inhibits invasion and migration of DU145 and PC3 cells.	[128]
N-Acetyl-S-(N'-phenethylthiocarbamoyl)-L-cysteine (PEIT-NAC)	Cauliflower, cabbage and broccoli	Inhibits LNCaP and DU145, increasing p21.	[125,126]
DL-Sulforaphane N-acetyl-L-cysteine (SFN-NAC)	Cauliflower, cabbage and broccoli	Inhibits LNCaP and DU145 cells, increasing p21. Reduces AR and PSA.	[125,126]
D-Limonene	Essential oil of orange, lemon, peppermint	Inhibits PCa cells, activating ERK and inducing WAF1 and p21.	[129]
Geraniol	Essential oil of geranium and citronella	Induces apoptosis of PC3 cells, activating caspase-3, reducing bcl-2 and increasing Bax and BNIP3. Inhibits AKT-mTOR.	[130]
Trihydroxy ketone E-4-(1,2,4-trihydroxy-2,6,6-trimethylcyclohexyl)-but-3-en-2-one	Thyme honey	Induces apoptosis of PC3 cells via reduction in NF- κ B and IL-6.	[131]
Epigallocatechin-3-gallate (EGCG)	Green tea	Induces apoptosis of PCa cells, reduces COX-2, regulates IGF-1. Inhibits via erbB1 DU145 cells growth. Induces apoptosis of LNCaP, stabilizing p53, reducing MDM2 and downregulating NF- κ B.	[132,133,139,140]
Soy Isoflavone	Soy	Binds ERs, with a stronger activity on ER- β .	[137]
Genistein	Fava beans, soy, coffee	Induces apoptosis of PC3 cells through the suppression of NF- κ B via AKT. Inhibits via erbB1 DU145 cells growth.	[138,139]
Silymarin	Cardus marianus	Inhibits via erbB1 DU145 cells growth.	[139]
Quercetin	Capers	Reduces PCa risk in vit.D deficiency, inhibits growth, migration and invasion of PC3 and LNCaP cells, inhibiting VEGF, AKT, PI3K in combination with metformin.	[143,144]
Fisetin	Strawberries, apples, onions	Inhibits PI3K, AKT and mTOR in PCa cells.	[145]
Cianidina-3-O-beta-glucopiranoside (C3G)		Inhibits proliferation of LNCaP and DU145 cells through activation of caspase-3 and induction of p21. Increases P75NGFR.	[146]
Gallic acid (GA)	Gallnuts, sumac, tea	Induces apoptosis of DU145 and 22Rv1 cells. Reduces proliferation of PC3 cells. Its polymers (gallotannins) decrease Mcl-1.	[148–150]

Table 2. Cont.

Substance	Source	Findings	References
Punicalagin (PN)	Pomegranate	Induces apoptosis of PC3 and LNCaP cells.	[151]
Caffeic acid phenethyl ester (CAPE)	Bee propolis	Reduces AKT in PCA cells.	[154]
Ferulic acid	Cereals	Causes cell cycle arrest in PC3 cells while inducing apoptosis in LNCaP cells.	[157]
Resveratrol	Grapes, blueberries	Inhibits LNCaP cells via ERK1/2 and inducing p53.	[158]
Curcumin	Curcuma longa	Reduces AR, EGF, VEGF while inhibiting TNF- α and PGE2 in PCA cells. Inhibits NF- κ B, mTOR, AKT and p-AKT expression.	[160–162]

Author Contributions: Conceptualization, F.C., B.B., M.B.; writing—original draft preparation, F.C., B.B., M.B., G.G., E.D.Z.; writing—review and editing, F.C., B.B., M.B., E.D.Z., M.D.D., C.I., I.F.A., A.S., G.G., G.S., L.Q., S.B. All authors have read and agreed to the published version of the manuscript.

Funding: This research received no external funding.

Conflicts of Interest: The authors declare no conflict of interest.

References

1. Wong, M.C.S.; Goggins, W.B.; Wang, H.H.; Fung, F.D.H.; Leung, C.; Wong, S.Y.S.; Fai Ng, C.; Sung, J.J.Y. Global Incidence and Mortality for Prostate Cancer: Analysis of Temporal Patterns and Trends in 36 Countries. *Eur. Urol.* **2016**, *70*, 862–874. [[CrossRef](#)] [[PubMed](#)]
2. Fitzmaurice, C.; Dicker, D.; Pain, A.; Hamavid, H.; Moradi-Lakeh, M.; MacIntyre, M.F.; Allen, C.; Hansen, G.; Woodbrook, R.; Wolfe, C.; et al. The Global Burden of Cancer 2013. *JAMA Oncol.* **2015**, *1*, 505–527. [[CrossRef](#)] [[PubMed](#)]
3. Rebbeck, T.R. Prostate Cancer Genetics: Variation by Race, Ethnicity and Geography. *Semin. Radiat. Oncol.* **2017**, *27*, 3–10. [[CrossRef](#)] [[PubMed](#)]
4. Di Zazzo, E.; Galasso, G.; Giovannelli, P.; Di Donato, M.; Di Santi, A.; Cerneria, G.; Rossi, V.; Abbondanza, C.; Moncharmont, B.; Sinisi, A.A.; et al. Prostate cancer stem cells: The role of androgen and estrogen receptors. *Oncotarget* **2016**, *1*, 193–208. [[CrossRef](#)] [[PubMed](#)]
5. Di Zazzo, E.; Galasso, G.; Giovannelli, P.; Di Donato, M.; Castoria, G. Estrogens and Their Receptors in Prostate Cancer: Therapeutic Implications. *Front Oncol.* **2018**, *8*, 2. [[CrossRef](#)]
6. Caraglia, M.; Alaia, C.; Grimaldi, A.; Boccellino, M.; Quagliuolo, L. MiRNA as prognostic and therapeutic targets in tumor of male urogenital tract. In *Molecular Targets and Strategies in Cancer Prevention*; Springer: Cham, Switzerland, 2016; pp. 151–171.
7. Castoria, G.; Migliaccio, A.; D'Amato, L.; Di Stasio, R.; Ciociola, A.; Lombardi, M.; Bilancio, A.; Di Domenico, M.; De Falco, A.; Auricchio, F. Integrating signals between cAMP and MAPK pathways in breast cancer. *Front. Biosci.* **2008**, *13*, 1318–1327. [[CrossRef](#)]
8. Mazaris, E.; Tsiotras, A. Molecular pathways in prostate cancer. *Nephro-Urol. Mon.* **2013**, *5*, 792–800. [[CrossRef](#)]
9. Di Domenico, M.; Giordano, A. Signal transduction growth factors: The effective governance of transcription and cellular adhesion in cancer invasion. *Oncotarget* **2017**, *8*, 36869–36884. [[CrossRef](#)]
10. Castoria, G.; Lombardi, M.; Barone, M.V.; Bilancio, A.; Di Domenico, M.; Bottero, D.; Vitale, F.; Migliaccio, A.; Auricchio, F. Androgen-stimulated DNA synthesis and cytoskeletal changes in fibroblasts by a nontranscriptional receptor action. *J. Cell Biol.* **2003**, *161*, 547–556. [[CrossRef](#)]

11. Nardone, V.; Botta, C.; Caraglia, M.; Martino, E.C.; Ambrosio, M.R.; Carfagno, T.; Tini, P.; Semeraro, L.; Misso, G.; Grimaldi, A.; et al. Tumor infiltrating T lymphocytes expressing FoxP3; CCR7 or PD-1 predict the outcome of prostate cancer patients subjected to salvage radiotherapy after biochemical relapse. *Cancer Biol. Ther.* **2016**, *17*, 1213–1220. [[CrossRef](#)]
12. Migliaccio, A.; Castoria, G.; Di Domenico, M.; De Falco, A.; Bilancio, A.; Lombardi, M.; Barone, M.V.; Ametrano, D.; Zannini, M.S.; Abbondanza, C.; et al. Steroid-induced androgen receptor-oestradiol receptor β -Src complex triggers prostate cancer cell proliferation. *EMBO J.* **2000**, *19*, 5406–5417. [[CrossRef](#)] [[PubMed](#)]
13. Grivennikov, S.I.; Greten, F.R.; Karin, M. Immunity, inflammation and cancer. *Cell* **2010**, *140*, 883–899. [[CrossRef](#)] [[PubMed](#)]
14. Vidal, A.C.; Howard, L.E.; Wiggins, E.; De Hoedt, A.M.; Shiao, S.L.; Knott, S.; Taioli, E.; Fowke, J.H.; Freedland, S.J. Natural killer cell activity and prostate cancer risk in veteran men undergoing prostate biopsy. *Cancer Epidemiol.* **2019**, *62*, 101578. [[CrossRef](#)] [[PubMed](#)]
15. Engelhardt, P.F.; Seklehner, S.; Brustmann, H.; Lusuardi, L.; Riedl, C.R. Immunohistochemical expression of interleukin-2 receptor and interleukin-6 in patients with prostate cancer and benign prostatic hyperplasia: Association with asymptomatic inflammatory prostatitis NIH category IV. *Scand. J. Urol.* **2015**, *49*, 120–126. [[CrossRef](#)] [[PubMed](#)]
16. Fiorelli, A.; Ricciardi, C.; Pannone, G.; Santoro, A.; Bufo, P.; Santini, M.; Serpico, R.; Rullo, R.; Pierantoni, G.M.; Di Domenico, M. Interplay between steroid receptors and neoplastic progression in sarcoma tumors. *J. Cell Physiol.* **2011**, *226*, 2997–3003. [[CrossRef](#)] [[PubMed](#)]
17. Liou, G.Y.; Storz, P. Reactive oxygen species in cancer. *Free Radic. Res.* **2010**, *44*, 479–496. [[CrossRef](#)]
18. Di Domenico, M.; Pinto, F.; Quagliuolo, L.; Contaldo, M.; Settembre, G.; Romano, A.; Coppola, M.; Ferati, K.; Bexheti-Ferati, A.; Sciarra, A.; et al. The Role of Oxidative Stress and Hormones in Controlling Obesity. *Front. Endocrinol.* **2019**, *10*, 540. [[CrossRef](#)]
19. Vanacore, D.; Messina, G.; Lama, S.; Bitti, G.; Ambrosio, P.; Tenore, G.; Messina, A.; Monda, V.; Zappavigna, S.; Boccellino, M.; et al. Effect of Restriction Vegan Diet's on Muscle Mass, Oxidative Status and Myocytes Differentiation: A Pilot Study. *J. Cell Physiol.* **2018**, *12*, 9345–9353. [[CrossRef](#)]
20. Davidsson, S.; Fiorentino, M.; Andrén, O.; Fang, F.; Mucci, A.L.; Varenhorst, E.; Fall, K.; Rider, J.R. Inflammation, focal atrophic lesions, and prostatic intraepithelial neoplasia with respect to risk of lethal prostate cancer. *Cancer Epidemiol. Prev. Biomark.* **2011**, *20*, 2280–2287. [[CrossRef](#)]
21. De Nunzio, C.; Kramer, G.; Marberger, M.; Montironi, R.; Nelson, W.; Schröder, F.; Sciarra, A.; Tubaro, A. The controversial relationship between benign prostatic hyperplasia and prostate cancer: The role of inflammation. *Eur. Urol.* **2011**, *60*, 106–117. [[CrossRef](#)]
22. Brawer, M.K. Prostatic intraepithelial neoplasia: An overview. *Rev. Urol.* **2005**, *7*, S11. [[PubMed](#)]
23. Roumequère, T.; Delree, P.; Van Antwerpen, P.; Rorive, S.; Vanhamme, L.; de la Kethulle de Ryhove, L.; Serteyn, D.; Wespes, E.; Vanhaerberbeek, M.; Zouaoui Boudjeltia, K. Intriguing location of myeloperoxidase in the prostate: A preliminary immunohistochemical study. *Prostate* **2012**, *72*, 507–513. [[CrossRef](#)]
24. Staal, J.; Beyaert, R. Inflammation and NF-kappaB Signaling in Prostate Cancer: Mechanisms and Clinical Implications. *Cells* **2018**, *7*, 122. [[CrossRef](#)] [[PubMed](#)]
25. Roberts, R.O.; Bergstralh, E.J.; Bass, S.E.; Lieber, M.M.; Jacobsen, S.J. Prostatitis as a risk factor for prostate cancer. *Epidemiology* **2004**, *15*, 93–99. [[CrossRef](#)] [[PubMed](#)]
26. Sfanos, K.S.; Hempel, H.A.; De Marzo, A.M. The role of inflammation in prostate cancer. *Adv. Exp. Med. Biol.* **2014**, *816*, 153–181. [[PubMed](#)]
27. Stark, T.; Livas, L.; Kyprianou, N. Inflammation in prostate cancer progression and therapeutic targeting. *Transl. Androl. Urol.* **2015**, *4*, 455–463. [[PubMed](#)]
28. Liu, W. DNA alterations in the tumor genome and their associations with clinical outcome in prostate cancer. *Asian J. Androl.* **2016**, *18*, 533–542. [[CrossRef](#)]
29. Castoria, G.; Lombardi, M.; Barone, M.V.; Bilancio, A.; Di Domenico, M.; De Falco, A.; Varricchio, L.; Bottero, D.; Nanayakkara, M.; Migliaccio, A.; et al. Rapid signalling pathway activation by androgens in epithelial and stromal cells. *Steroids* **2004**, *69*, 517–522. [[CrossRef](#)]
30. Rizzo, A.; Di Domenico, M.; Romano Carratelli, C.; Mazzola, N.; Paolillo, R. Induction of proinflammatory cytokines in human osteoblastic cells by Chlamydia pneumoniae. *Cytokine* **2011**, *56*, 450–457. [[CrossRef](#)]

31. Di Zazzo, E.; Galasso, G.; Giovannelli, P.; Di Donato, M.; Bilancio, A.; Perillo, B.; Sinisi, A.A.; Migliaccio, A.; Castoria, G. Estrogen Receptors in Epithelial-Mesenchymal Transition of Prostate Cancer. *Cancers* **2019**, *11*, 1418. [[CrossRef](#)]
32. Ricci, S.; Pinto, F.; Auletta, A.; Giordano, A.; Giovane, A.; Settembre, G.; Boccellino, M.; Boffo, S.; Di Carlo, A.; Di Domenico, M. The enigmatic role of matrix metalloproteinases in epithelial-to-mesenchymal transition of oral squamous cell carcinoma: Implications and nutraceutical aspects. *J. Cell. Biochem.* **2019**, *120*, 6813–6919. [[CrossRef](#)] [[PubMed](#)]
33. Santini, A.C.; Giovane, G.; Auletta, A.; Di Carlo, A.; Fiorelli, A.; Cito, L.; Astarita, C.; Giordano, A.; Alfano, R.; Feola, A.; et al. Translational Research and Plasma Proteomic in Cancer. *J. Cell. Biochem.* **2016**, *117*, 828–835. [[CrossRef](#)] [[PubMed](#)]
34. Cosentino, C.; Di Domenico, M.; Porcellini, A.; Cuzzo, C.; De Gregorio, G.; Santillo, M.R.; Agnese, S.; Di Stasio, R.; Feliciello, A.; Migliaccio, A.; et al. p85 regulatory subunit of PI3K mediates cAMP-PKA and estrogens biological effects on growth and survival. *Oncogene* **2007**, *26*, 2095–2103. [[CrossRef](#)] [[PubMed](#)]
35. Feola, A.; Cimini, A.; Migliucci, F.; Iorio, R.; Zuchegna, C.; Rothenberger, R.; Cito, L.; Porcellini, A.; Unteregger, G.; Tombolini, V.; et al. The inhibition of p85 α PI3KSer83 phosphorylation prevents cell proliferation and invasion in prostate cancer cells. *J. Cell. Biochem.* **2013**, *114*, 2114–2119. [[CrossRef](#)] [[PubMed](#)]
36. Di Zazzo, E.; Feola, A.; Zuchegna, C.; Romano, A.; Donini, C.F.; Bartollino, S.; Costagliola, C.; Frunzio, R.; Laccetti, P.; Di Domenico, M.; et al. The p85 regulatory subunit of PI3K mediates cAMP-PKA and insulin biological effects on MCF-7 cell growth and motility. *Sci. World J.* **2014**, *2014*, 565839. [[CrossRef](#)]
37. Donini, C.F.; Di Zazzo, E.; Zuchegna, C.; Di Domenico, M.; D’Inzeo, S.; Nicolussi, A.; Avvedimento, E.V.; Coppa, A.; Porcellini, A. The p85 α regulatory subunit of PI3K mediates cAMP-PKA and retinoic acid biological effects on MCF7 cell growth and migration. *Int. J. Oncol.* **2012**, *40*, 1627–1635.
38. Castoria, G.; Migliaccio, A.; Bilancio, A.; Di Domenico, M.; De Falco, A.; Lombardi, M.; Fiorentino, R.; Varricchio, L.; Barone, M.V.; Auricchio, F. PI3-kinase in concert with Src promotes the S-phase entry of oestradiol-stimulated MCF-7 cells. *EMBO J.* **2001**, *20*, 6050–6059. [[CrossRef](#)]
39. Fiorelli, A.; Vicidomini, G.; Di Domenico, M.; Napolitano, F.; Messina, G.; Morgillo, F.; Ciardiello, F.; Santini, M. Vascular endothelial growth factor in pleural fluid for differential diagnosis of benign and malignant origin and its clinical applications. *Interact. Cardiovasc. Thorac. Surg.* **2011**, *12*, 420–424. [[CrossRef](#)]
40. Saber-Karimian, M.; Katsiki, N.; Caraglia, M.; Boccellino, M.; Majeed, M.; Sahebkar, A. Vascular endothelial growth factor: An important molecular target of curcumin. *Crit. Rev. Food Sci. Nutr.* **2019**, *59*, 299–312. [[CrossRef](#)]
41. Vanacore, D.; Boccellino, M.; Rossetti, S.; Cavaliere, C.; D’Aniello, C.; Di Franco, R.; Romano, F.J.; Montanari, M.; La Mantia, E.; Piscitelli, R.; et al. Micronas in prostate cancer: An overview. *Oncotarget* **2017**, *30*, 50240–50251. [[CrossRef](#)]
42. Grimaldi, A.; Santini, D.; Zappavigna, S.; Lombardi, A.; Misso, G.; Boccellino, M.; Desiderio, V.; Vitiello, P.; Di Lorenzo, G.; Zoccoli, A.; et al. Antagonistic effects of chloroquine on autophagy occurrence potentiate the anticancer effects of everolimus on renal cancer cells. *Cancer Biol. Ther.* **2015**, *16*, 567–579. [[CrossRef](#)] [[PubMed](#)]
43. Franco, R.; Nicoletti, G.; Lombardi, A.; Di Domenico, M.; Botti, G.; Zito Marino, F.; Caraglia, M. Current treatment of cutaneous squamous cancer and molecular strategies for its sensitization to new target-based drugs. *Expert Opin. Biol. Ther.* **2013**, *13*, 51–66. [[CrossRef](#)] [[PubMed](#)]
44. Di Domenico, M.; Ricciardi, C.; Fusco, A.; Pierantoni, G.M. Anti-VEGF therapy in breast and lung mouse models of cancers. *J. Biomed. Biotechnol.* **2011**, *2011*, 947928.
45. Alaia, C.; Boccellino, M.; Zappavigna, S.; Amler, E.; Quagliuolo, L.; Rossetti, S.; Facchini, G.; Caraglia, M. Ipilimumab for the treatment of metastatic prostate cancer. *Expert Opin. Biol. Ther.* **2018**, *18*, 205–213. [[CrossRef](#)] [[PubMed](#)]
46. Cardillo, I.; Spugnini, E.P.; Galluzzo, P.; Contestabile, M.; Dell’Anna, M.L.; Picardo, M.; Crispi, S.; Calogero, R.A.; Piccolo, M.T.; Arigoni, M.; et al. Functional and pharmacodynamic evaluation of metronomic cyclophosphamide and docetaxel regimen in castration-resistant prostate cancer. *Future Oncol.* **2013**, *9*, 1375–1388. [[CrossRef](#)]
47. Boccellino, M.; Pedata, P.; Castiglia, L.; La Porta, R.; Pieri, M.; Quagliuolo, L.; Acampora, A.; Sannolo, N.; Miraglia, N. Doxorubicin can penetrate nitrile gloves and induces apoptosis in keratinocytes cell lines. *Toxicol. Lett.* **2010**, *197*, 61–68. [[CrossRef](#)]

48. Boccellino, M.; Alaia, C.; Misso, G.; Cossu, A.M.; Facchini, G.; Piscitelli, R.; Quagliuolo, L.; Caraglia, M. Gene interference strategies as a new tool for the treatment of prostate cancer. *Endocrine* **2015**, *49*, 588–605. [[CrossRef](#)]
49. Boccellino, M.; Di Domenico, M.; Donniacuo, M.; Bitti, G.; Gritti, G.; Ambrosio, P.; Quagliuolo, L.; Rinaldi, B. AT1-receptor blockade: Protective effects of irbesartan in cardiomyocytes under hypoxic stress. *PLoS ONE* **2018**, *13*, e0202297. [[CrossRef](#)]
50. Fiorelli, A.; Vitiello, F.; Morgillo, F.; Santagata, M.; Spuntarelli, C.; Di Domenico, M.; Santini, M.; Bianco, A. Pembrolizumab monotherapy in advanced NSCLC patients with low PD-L1 expression: Is there real evidence? *Transl. Cancer Res.* **2019**, *8*, S618–S620. [[CrossRef](#)]
51. Caracciolo, G.; Safavi-Sohi, R.; Malekzadeh, R.; Poustchi, H.; Vasighi, M.; Chiozzi, R.Z.; Capriotti, A.L.; Laganà, A.; Hajipour, M.; Di Domenico, M.; et al. Disease-specific protein corona sensor arrays may have disease detection capacity. *Nanoscale Horiz.* **2019**, *4*, 1063–1076. [[CrossRef](#)]
52. Di Domenico, M.; Pozzi, D.; Palchetti, S.; Digiaco, L.; Iorio, R.; Astarita, C.; Fiorelli, A.; Pierdiluca, M.; Santini, M.; Barbarino, M.; et al. Nanoparticle-biomolecular corona: A new approach for the early detection of non-small-cell lung cancer. *J. Cell. Physiol.* **2019**, *234*, 9378–9386. [[CrossRef](#)] [[PubMed](#)]
53. Papi, M.; Palmieri, V.; Palchetti, S.; Pozzi, D.; Digiaco, L.; Guadagno, E.; Del Basso De Caro, M.; Di Domenico, M.; Ricci, S.; Pani, R.; et al. Exploitation of nanoparticle-protein interactions for early disease detection. *Appl. Phys. Lett.* **2019**, *114*, 163702. [[CrossRef](#)]
54. Borghese, C.; Casagrande, N.; Pivetta, E.; Colombatti, A.; Boccellino, M.; Amler, E.; Normanno, N.; Caraglia, M.; De Rosa, G.; Aldinucci, D. Self-assembling nanoparticles encapsulating zoledronic acid inhibit mesenchymal stromal cells differentiation; migration and secretion of proangiogenic factors and their interactions with prostate cancer cells. *Oncotarget* **2017**, *8*, 42926–42938. [[CrossRef](#)] [[PubMed](#)]
55. McNeal, J.E. Normal histology of the prostate. *Am. J. Surg. Pathol.* **1988**, *12*, 619–633. [[CrossRef](#)]
56. Alcaraz, A.; Hammerer, P.; Tubaro, A.; Schröder, F.H.; Castro, R. Is there evidence of a relationship between benign prostatic hyperplasia and prostate cancer? Findings of a literature review. *Eur. Urol.* **2009**, *55*, 864–873. [[CrossRef](#)]
57. Nickel, J.C.; Roehrborn, C.G.; O’Leary, M.P.; Bostwick, D.G.; Somerville, M.C.; Rittmaster, R.S. The relationship between prostate inflammation and lower urinary tract symptoms: Examination of baseline data from the REDUCE trial. *Eur. Urol.* **2008**, *54*, 1379–1384. [[CrossRef](#)]
58. Sfanos, K.S.; Isaacs, W.B.; De Marzo, A.M. Infections and inflammation in prostate cancer. *Am. J. Clin. Exp. Urol.* **2013**, *1*, 3–11.
59. Di Silverio, F.; Gentile, V.; De Matteis, A.; Mariotti, G.; Voria, G.; Pastore, A.L.; Sciarra, A. Distribution of inflammation, pre-malignant lesions, incidental carcinoma in histologically confirmed benign prostatic hyperplasia: A retrospective analysis. *Eur. Urol.* **2003**, *43*, 164–175. [[CrossRef](#)]
60. Daniels, A.N.; Ewing, S.K.; Zmuda, J.M.; Wilt, T.J.; Bauer, D.C. Correlates and prevalence of prostatitis in a large community-based cohort of older men. *Urology* **2005**, *66*, 964–970. [[CrossRef](#)]
61. Cheng, I.; Witte, J.S.; Jacobsen, S.J.; Haque, R.; Quinn, V.P.; Quesenberry, C.P.; Caan, B.J.; Van Den Eeden, S.K. Prostatitis, sexually transmitted diseases, and prostate cancer: The California Men’s Health Study. *PLoS ONE* **2010**, *5*, e8736. [[CrossRef](#)]
62. Dennis, L.K.; Lynch, C.F.; Torner, J.C. Epidemiologic association between prostatitis and prostate cancer. *Urology* **2002**, *60*, 78–83. [[CrossRef](#)]
63. Jiang, J.; Li, J.; Zhang, Y.; Zhu, H.; Liu, J.; Pumill, C. The role of prostatitis in prostate cancer: Meta-analysis. *PLoS ONE* **2013**, *8*, e85179. [[CrossRef](#)] [[PubMed](#)]
64. Roberts, R.O.; Lieber, M.M.; Rhodes, T.; Girman, C.J.; Bostwick, D.J.; Jacobsen, S.J. Prevalence of a physician-assigned diagnosis of prostatitis: The Olmsted County Study of Urinary Symptoms and Health Status Among Men. *Urology* **1998**, *51*, 578–584. [[CrossRef](#)]
65. De Luca, L.; Crocetto, F.; Barone, B.; Creta, M.; Pesce, S.; Aveta, A.; Campanino, M.R.; Imbimbo, C.; Longo, N. Granulomatous prostatitis mimicking prostate cancer in a patient with psoriatic arthritis: A case report. *Future Sci. OA* **2020**, *6*, FSO591. [[CrossRef](#)] [[PubMed](#)]
66. Crocetto, F.; Barone, B.; De Luca, L.; Creta, M. Granulomatous prostatitis: A challenging differential diagnosis to take into consideration. *Future Oncol.* **2020**, *16*, 805–806. [[CrossRef](#)]

67. Feng, Y.; Ramnarine, V.R.; Bell, R.; Volik, S.; Davicioni, E.; Hayes, V.M.; Ren, S.; Collins, C.C. Metagenomic and metatranscriptomic analysis of human prostate microbiota from patients with prostate cancer. *BMC Genom.* **2019**, *20*, 14. [[CrossRef](#)]
68. Feng, Y.; Jaratlerdsiri, W.; Patrick, S.M.; Lyons, S.J.; Haynes, A.; Collins, C.C.; Stricker, P.D.; Bormman, M.S.R.; Hayes, V.M. Metagenomic analysis reveals a rich bacterial content in high-risk prostate tumors from African men. *Prostate* **2019**, *79*, 1731–1738. [[CrossRef](#)]
69. Gao, Y.; Wei, L.; Wang, C.; Huang, Y.; Li, W.; Li, T.; Mo, C.; Qin, H.; Zhong, X.; Wang, Y.; et al. Chronic prostatitis alters the prostatic microenvironment and accelerates preneoplastic lesions in C57BL/6 mice. *Biol. Res.* **2019**, *52*, 30. [[CrossRef](#)]
70. Sfanos, K.S.; Aloia, L.A.; De Marzo, A.M.; Rein, A. XMRV and prostate cancer—A ‘final’ perspective. *Nat. Rev. Urol.* **2012**, *9*, 111–118. [[CrossRef](#)]
71. Sfanos, K.S.; Canene-Adams, K.; Hempel, H.; Yu, S.; Simons, B.W.; Schaeffer, A.J.; Schaeffer, A.J.; Nelson, W.J.; De Marzo, A.M. Bacterial Prostatitis Enhances 2-Amino-1-Methyl-6-Phenylimidazo[4,5-b]Pyridine (PhIP)-Induced Cancer at Multiple Sites. *Cancer Prev. Res. (Phila.)* **2015**, *8*, 683–692. [[CrossRef](#)]
72. Cai, T.; Tamanini, I.; Kulchavenya, E.; Perepanova, T.; Köves, B.; Wagenlehner, F.M.E.; Tandogdu, Z.; Bonkat, G.; Bartoletti, R.; Johansen, T.E.B. The role of nutraceuticals and phytotherapy in the management of urinary tract infections: What we need to know? *Arch. Ital. Urol. Androl.* **2017**, *89*, 1–6. [[CrossRef](#)]
73. Barykova, Y.A.; Logunov, D.Y.; Shmarov, M.M.; Vinarov, A.Z.; Fiev, D.N.; Vinarova, N.A.; Rakovskaya, I.V.; Baker, P.S.; Shyshynova, I.; Stephenson, A.J.; et al. Association of Mycoplasma hominis infection with prostate cancer. *Oncotarget* **2011**, *2*, 289–297. [[CrossRef](#)]
74. Han, I.M.; Kim, J.H.; Kim, S.S.; Ahn, M.H.; Ryu, J.S. Signalling pathways associated with IL-6 production and epithelial-mesenchymal transition induction in prostate epithelial cells stimulated with *Trichomonas vaginalis*. *Parasite Immunol.* **2016**, *38*, 678–687. [[CrossRef](#)] [[PubMed](#)]
75. Kim, J.; Moon, H.; Kim, S.; Hwang, S.; Ryu, S.; Park, S. Comparison of Seropositivity to *Trichomonas vaginalis* between Men with Prostatic Tumor and Normal Men. *Korean J. Parasitol.* **2019**, *57*, 21–25. [[CrossRef](#)] [[PubMed](#)]
76. Langston, M.E.; Bhalla, A.; Alderete, J.F.; Nevin, R.; Pakpahan, R.; Hansen, J.; Elliott, D.; De Marzo, A.M.; Gaydos, C.A.; Isaacs, W.B.; et al. *Trichomonas vaginalis* infection and prostate-specific antigen concentration: Insights into prostate involvement and prostate disease risk. *Prostate* **2019**, *79*, 1622–1628. [[CrossRef](#)] [[PubMed](#)]
77. Twu, O.; Dessi, D.; Vu, A.; Mercer, F.; Stevens, G.C.; de Miguel, N.; Rappelli, P.; Cocco, A.R.; Clubb, R.T.; Fiori, P.L.; et al. *Trichomonas vaginalis* homolog of macrophage migration inhibitory factor induces prostate cell growth, invasiveness, and inflammatory responses. *Proc. Natl. Acad. Sci. USA* **2014**, *111*, 8179–8184. [[CrossRef](#)]
78. Davidsson, S.; Mölling, P.; Rider, J.R.; Unemo, M.; Karlsson, M.G.; Carlsson, J.; Andersson, S.O.; Elgh, F.; Söderquis, B.; Andrén, O. Frequency and typing of *Propionibacterium acnes* in prostate tissue obtained from men with and without prostate cancer. *Infect. Agents Cancer* **2016**, *11*, 26. [[CrossRef](#)]
79. Ugge, H.; Udumyan, R.; Carlsson, J.; Andrén, O.; Montgomery, S.; Davidsson, S.; Fall, K. Acne in late adolescence and risk of prostate cancer. *Int. J. Cancer* **2018**, *142*, 1580–1585. [[CrossRef](#)]
80. Zhang, X.; Lin, Y.; Xie, X.; Shen, M.; Huang, G.; Yang, Y. Is acne in adolescence associated with prostate cancer risk? Evidence from a meta-analysis. *PLoS ONE* **2018**, *13*, e0206249. [[CrossRef](#)]
81. Doat, S.; Cénéte, S.; Trétarre, B.; Rebillard, X.; Lamy, P.J.; Bringer, J.P.; Iborra, F.; Murez, T.; Sanchez, M.; Menegaux, F. Nonsteroidal anti-inflammatory drugs (NSAIDs) and prostate cancer risk: Results from the EPICAP study. *Cancer Med.* **2017**, *6*, 2461–2470. [[CrossRef](#)]
82. St Hill, C.A.; Lutfiyya, M.N. An epidemiological analysis of potential associations between C-reactive protein; inflammation; and prostate cancer in the male US population using the 2009–2010 National Health and Nutrition Examination Survey (NHANES) data. *Front. Chem.* **2015**, *3*, 55. [[CrossRef](#)] [[PubMed](#)]
83. Dzutsev, A.; Goldszmid, R.S.; Viaud, S.; Zitvogel, L.; Trinchieri, G. The role of the microbiota in inflammation, carcinogenesis, and cancer therapy. *Eur. J. Immunol.* **2015**, *45*, 17–31. [[CrossRef](#)] [[PubMed](#)]
84. Boomer, S.M.; Lodge, D.P.; Dutton, B.E. Bacterial Diversity Studies Using the 16S rRNA Gene Provide a Powerful Research-Based Curriculum for Molecular Biology Laboratory. *Microbiol. Educ.* **2002**, *3*, 18–25. [[CrossRef](#)] [[PubMed](#)]

85. Singhal, N.; Kumar, M.; Kanaujia, P.K.; Viridi, J.S. MALDI-TOF mass spectrometry: An emerging technology for microbial identification and diagnosis. *Front. Microbiol.* **2015**, *6*, 791. [[CrossRef](#)]
86. Hilt, E.E.; McKinley, K.; Pearce, M.M.; Rosenfeld, A.B.; Zilliox, M.J.; Mueller, E.R.; Brubaker, L.; Gai, X.; Wolfe, A.J.; Schreckenberger, P.C. Urine is not sterile: Use of enhanced urine culture techniques to detect resident bacterial flora in the adult female bladder. *J. Clin. Microbiol.* **2014**, *52*, 871–876. [[CrossRef](#)]
87. Dong, Q.; Nelson, D.E.; Toh, E.; Diao, L.; Gao, X.; Fortenberry, J.D.; Van der Pol, B. The microbial communities in male first catch urine are highly similar to those in paired urethral swab specimens. *PLoS ONE* **2011**, *6*, e19709. [[CrossRef](#)]
88. Lewis, D.A.; Brown, R.; Williams, J.; White, P.; Jacobson, S.K.; Marchesi, J.R.; Drake, M.J. The human urinary microbiome; bacterial DNA in voided urine of asymptomatic adults. *Front. Cell. Infect. Microbiol.* **2013**, *3*, 41. [[CrossRef](#)]
89. Nelson, D.E.; Dong, Q.; Van der Pol, B.; Toh, E.; Fan, B.; Katz, B.P.; Mi, D.; Rong, R.; Weinstock, G.M.; Sodergren, E.; et al. Bacterial communities of the coronal sulcus and distal urethra of adolescent males. *PLoS ONE* **2012**, *7*, e36298. [[CrossRef](#)]
90. Nelson, D.E.; Van Der Pol, B.; Dong, Q.; Revanna, K.V.; Fan, B.; Easwaran, S.; Sodergren, E.; Weinstock, G.M.; Diao, L.; Fortenberry, J.D. Characteristic male urine microbiomes associate with asymptomatic sexually transmitted infection. *PLoS ONE* **2010**, *5*, e14116. [[CrossRef](#)]
91. Pearce, M.M.; Hilt, E.E.; Rosenfeld, A.B.; Zilliox, M.J.; Thomas-White, K.; Fok, C.; Kliethermes, S.; Schreckenberger, P.C.; Brubaker, L.; Gai, X.; et al. The female urinary microbiome: A comparison of women with and without urgency urinary incontinence. *MBio* **2014**, *5*, e01283-14. [[CrossRef](#)] [[PubMed](#)]
92. Nickel, J.C.; Stephens, A.; Landis, J.R.; Chen, J.; Mullins, C.; van Bokhoven, A.; Lucia, M.S.; Melton-Kreft, R.; Ehrlich, G.D. Search for Microorganisms in Men with Urologic Chronic Pelvic Pain Syndrome: A Culture-Independent Analysis in the MAPP Research Network. *J. Urol.* **2015**, *194*, 127–135. [[CrossRef](#)] [[PubMed](#)]
93. Siddiqui, H.; Lagesen, K.; Nederbragt, A.J.; Jeansson, S.L.; Jakobsen, K.S. Alterations of microbiota in urine from women with interstitial cystitis. *BMC Microbiol.* **2012**, *12*, 205. [[CrossRef](#)] [[PubMed](#)]
94. Whiteside, S.A.; Razvi, H.; Dave, S.; Reid, G.; Burton, J.P. The microbiome of the urinary tract—a role beyond infection. *Nat. Rev. Urol.* **2015**, *12*, 81–90. [[CrossRef](#)] [[PubMed](#)]
95. Mändar, R.; Punab, M.; Korrovits, P.; Türk, S.; Ausmees, K.; Lapp, E.; Preem, J.K.; Oopkaup, K.; Salumets, A.; Truu, J. Seminal microbiome in men with and without prostatitis. *Int. J. Urol.* **2017**, *24*, 211–216. [[CrossRef](#)]
96. Shoskes, D.A.; Altemus, J.; Polackwich, A.S.; Tucky, B.; Wang, H.; Eng, C. The Urinary Microbiome Differs Significantly Between Patients With Chronic Prostatitis/Chronic Pelvic Pain Syndrome and Controls as Well as Between Patients With Different Clinical Phenotypes. *Urology* **2016**, *92*, 26–32. [[CrossRef](#)]
97. Yu, H.; Meng, H.; Zhou, F.; Ni, X.; Shen, S.; Das, U.N. Urinary microbiota in patients with prostate cancer and benign prostatic hyperplasia. *Arch. Med. Sci.* **2015**, *11*, 385–394. [[CrossRef](#)]
98. Shrestha, E.; White, J.R.; Yu, S.; Kulac, I.; Ertunc, O.; De Marzo, A.M.; Yegnasubramanian, S.; Mangold, L.A.; Partin, A.W.; Sfanos, K.S. Profiling the Urinary Microbiome in Men with Positive versus Negative Biopsies for Prostate Cancer. *J. Urol.* **2018**, *199*, 161–171. [[CrossRef](#)]
99. Alane, S.; El-Zawahry, A.; Dynda, D.; McVary, K.; Karr, M.; Braundmeier-Fleming, A. Prospective examination of the changes in the urinary microbiome induced by transrectal biopsy of the prostate using 16S rRNA gene analysis. *Prostate Cancer Prostatic Dis.* **2019**, *22*, 446–452. [[CrossRef](#)]
100. Bhudia, R.; Ahmad, A.; Akpenyi, O.; Whiley, A.; Wilks, M.; Oliver, T. Identification of low oxygen-tolerating bacteria in prostate secretions of cancer patients and discussion of possible aetiological significance. *Sci. Rep.* **2017**, *7*, 15164. [[CrossRef](#)]
101. Cavarretta, I.; Ferrarese, R.; Cazzaniga, W.; Saita, D.; Lucianò, R.; Ceresola, E.R.; Locatelli, I.; Visconti, L.; Lavorgna, G.; Brigant, A.; et al. The Microbiome of the Prostate Tumor Microenvironment. *Eur. Urol.* **2017**, *72*, 625–631. [[CrossRef](#)]
102. Sha, S.; Ni, L.; Stefil, M.; Dixon, M.; Mouraviev, V. The human gastrointestinal microbiota and prostate cancer development and treatment. *Investig. Clin. Urol.* **2020**, *61*, S43–S50. [[CrossRef](#)] [[PubMed](#)]
103. Liss, M.A.; White, J.R.; Goros, M.; Gelfond, J.; Leach, R.; Johnson-Pais, T.; Lai, Z.; Rourke, E.; Basler, J.; Ankerst, D.; et al. Metabolic Biosynthesis Pathways Identified from Fecal Microbiome Associated with Prostate Cancer. *Eur. Urol.* **2018**, *74*, 575–582. [[CrossRef](#)] [[PubMed](#)]

104. Golombos, D.M.; Ayangbesan, A.; O'Malley, P.; Lewicki, P.; Barlow, L.A.; Barbieri, C.E.; Chan, C.; DuLong, C.; Abu-Ali, G.; Huttenhower, C.; et al. The Role of Gut Microbiome in the Pathogenesis of Prostate Cancer: A Prospective, Pilot Study. *Urology* **2018**, *111*, 122–128. [[CrossRef](#)] [[PubMed](#)]
105. Bruggemann, H.; Al-Zeer, M.A. Bacterial signatures and their inflammatory potentials associated with prostate cancer. *APMIS* **2020**, *128*, 80–91. [[CrossRef](#)]
106. Pouncey, A.L.; Scott, A.J.; Alexander, J.L.; Marchesi, J.; Kinross, J. Gut microbiota, chemotherapy and the host: The influence of the gut microbiota on cancer treatment. *Ecancermedicalscience* **2018**, *12*, 868. [[CrossRef](#)]
107. Sfanos, K.S.; Markowski, M.C.; Peiffer, L.B.; Ernst, S.E.; White, J.R.; Pienta, K.J.; Antonarakis, E.S.; Ross, A.E. Compositional differences in gastrointestinal microbiota in prostate cancer patients treated with androgen axis-targeted therapies. *Prostate Cancer Prostatic Dis.* **2018**, *21*, 539–548. [[CrossRef](#)]
108. Liss, M.A.; Al-Bayati, O.; Gelfond, J.; Goros, M.; Ullevig, S.; DiGiovanni, J.; Hamilton-Reeves, J.; O'Keefe, D.; Bacich, D.; Weaver, B.; et al. Higher baseline dietary fat and fatty acid intake is associated with increased risk of incident prostate cancer in the SABOR study. *Prostate Cancer Prostatic Dis.* **2019**, *22*, 244–251. [[CrossRef](#)]
109. Massari, F.; Mollica, V.; Di Nunno, V.; Gatto, L.; Santoni, M.; Scarpelli, M.; Cimadamore, A.; Lopez-Beltran, A.; Cheng, L.; Battelli, N.; et al. The Human Microbiota and Prostate Cancer: Friend or Foe? *Cancers* **2019**, *11*, 459. [[CrossRef](#)]
110. López-Guarnido, O.; Álvarez-Cubero, M.J.; Saiz, M.; Lozano, D.; Rodrigo, L.; Pascual, M.; Cozar, J.M.; Rivas, A. Mediterranean diet adherence and prostate cancer risk. *Nutr. Hosp.* **2015**, *31*, 1012–1019.
111. Pelucchi, C.; Bosetti, C.; Rossi, M.; Negri, E.; La Vecchia, C. Selected Aspects of Mediterranean Diet and Cancer Risk. *J. Nutr. Cancer* **2009**, *61*, 756–766. [[CrossRef](#)]
112. Barnard, R.J.; Ngo, T.H.; Leung, P.S.; Aronson, W.J.; Golding, L.A. A low-fat diet and/or strenuous exercise alters the IGF axis in vivo and reduces prostate tumor cell growth in vitro. *Prostate* **2003**, *56*, 201–206. [[CrossRef](#)] [[PubMed](#)]
113. Ngo, T.H.; Barnard, R.J.; Cohen, P.; Freedland, S.; Tran, C.; De Gregorio, F.; Elshimali, Y.I.; Heber, D.; Aronson, W.J. Effect of isocaloric low-fat diet on human LAPC-4 prostate cancer xenografts in severe combined immunodeficient mice and the insulin-like growth factor axis. *Clin. Cancer Res.* **2003**, *9*, 2734–2743. [[PubMed](#)]
114. Chen, M.; Zhang, J.; Sampieri, K.; Clohessy, J.G.; Mendez, L.; Gonzalez-Billalabeitia, E.; Liu, X.S.; Lee, Y.R.; Fung, J.; Katon, J.M.; et al. An aberrant SREBP-dependent lipogenic program promotes metastatic prostate cancer. *Nat. Genet.* **2018**, *50*, 206–218. [[CrossRef](#)] [[PubMed](#)]
115. Epstein, M.M.; Kasperzyk, J.L.; Mucci, L.A.; Giovannucci, E.; Price, A.; Wolk, A.; Håkansson, N.; Fall, K.; Andersson, S.O.; Andrén, O. Dietary fatty acid intake and prostate cancer survival in Örebro county, Sweden. *Am. J. Epidemiol.* **2012**, *176*, 240–252. [[CrossRef](#)]
116. Capece, M.; Creta, M.; Calogero, A.; La Rocca, R.; Napolitano, L.; Barone, B.; Sica, A.; Fusco, F.; Santangelo, M.; Dodaro, C. Does Physical Activity Regulate Prostate Carcinogenesis and Prostate Cancer Outcomes? *A Narrative Review. Int. J. Environ. Res. Public Health* **2020**, *17*, 1441. [[CrossRef](#)] [[PubMed](#)]
117. Oono, K.; Takahashi, K.; Sukehara, S.; Kurosawa, H.; Matsumura, T.; Taniguchi, S.; Ohta, S. Inhibition of PC3 human prostate cancer cell proliferation, invasion and migration by eicosapentaenoic acid and docosahexaenoic acid. *Mol. Clin. Oncol.* **2017**, *7*, 217–220.
118. Allott, E.H.; Masko, E.M.; Freedland, A.R.; MacLus, E.; Pelton, K.; Solomon, K.R.; Mostaghel, E.A.; Thomas, G.V.; Pizzo, S.V.; Freeman, M.R.; et al. Serum cholesterol levels and tumor growth in a PTEN-null transgenic mouse model of prostate cancer. *Prostate Cancer Prostatic Dis.* **2018**, *21*, 196–203. [[CrossRef](#)] [[PubMed](#)]
119. Akinsete, J.A.; Ion, G.; Witte, T.R.; Hardman, W.E. Consumption of high ω -3 fatty acid diet suppressed prostate tumorigenesis in C3(1) Tag mice. *Carcinogenesis* **2012**, *33*, 140–148. [[CrossRef](#)]
120. Lee, B.J.; Lin, J.S.; Lin, Y.C.; Lin, P.T. Effects of L-carnitine supplementation on oxidative stress and antioxidant enzymes activities in patients with coronary artery disease: A randomized, placebo-controlled trial. *Nutr. J.* **2014**, *13*, 79. [[CrossRef](#)] [[PubMed](#)]
121. Baci, D.; Bruno, A.; Cascini, C.; Gallazzi, M.; Mortara, L.; Sessa, F.; Pelosi, G.; Albin, A.; Noonan, D.M. Acetyl-L-Carnitine downregulates invasion (CXCR4/CXCL12, MMP-9) and angiogenesis (VEGF, CXCL8) pathways in prostate cancer cells: Rationale for prevention and interception strategies. *J. Exp. Clin. Cancer Res.* **2019**, *38*, 464. [[CrossRef](#)]

122. Baci, D.; Bruno, A.; Bassani, B.; Tramacere, M.; Mortara, L.; Albini, A.; Noonan, D.M. Acetyl-L-carnitine is an anti-angiogenic agent targeting the VEGFR2 and CXCR4 pathways. *Cancer Lett.* **2018**, *429*, 100–116. [[CrossRef](#)] [[PubMed](#)]
123. Chiao, J.W.; Chung, F.; Krzeminski, J.; Amin, S.; Arshad, R.; Ahmed, T.; Conaway, C.C. Modulation of growth of human prostate cancer cells by the N-acetylcysteine conjugate of phenethyl isothiocyanate. *Int. J. Oncol.* **2000**, *16*, 1215–1219. [[CrossRef](#)] [[PubMed](#)]
124. Chiao, J.W.; Chung, F.L.; Kancherla, R.; Ahmed, T.; Mittelman, A.; Conaway, C.C. Sulforaphane and its metabolite mediate growth arrest and apoptosis in human prostate cancer cells. *Int. J. Oncol.* **2002**, *20*, 631–636. [[CrossRef](#)] [[PubMed](#)]
125. Lee, Y.J.; Lee, D.M.; Lee, C.O.; Heo, S.H.; Won, S.Y.; Im, J.H.; Cho, M.K.; Nam, H.S.; Lee, S.H. Suppression of human prostate cancer PC-3 cell growth by N-acetylcysteine involves over-expression of Cyr61. *Toxicol. In Vitro* **2011**, *25*, 199–205. [[CrossRef](#)]
126. Supabphol, A.; Supabphol, R. Antimetastatic potential of N-acetylcysteine on human prostate cancer cells. *J. Med. Assoc. Thai.* **2012**, *95*, S56–S62.
127. Rabi, T.; Gupta, S. Dietary terpenoids and prostate cancer chemoprevention. *Front. Biosci.* **2008**, *13*, 3457–3469. [[CrossRef](#)] [[PubMed](#)]
128. Cho, M.; So, I.; Chun, J.N.; Jeon, J.H. The antitumor effects of geraniol: Modulation of cancer hallmark pathways (Review). *Int. J. Oncol.* **2016**, *48*, 1772–1782. [[CrossRef](#)]
129. Kassi, E.; Chinou, I.; Spilioti, E.; Tsiapara, A.; Graikou, K.; Karabournioti, S.; Manoussakis, M.; Moutsatsou, P. A monoterpene, unique component of thyme honeys, induces apoptosis in prostate cancer cells via inhibition of NF- κ B activity and IL-6 secretion. *Phytomedicine* **2014**, *21*, 1483–1489. [[CrossRef](#)]
130. Gupta, S.; Ahmad, N.; Nieminen, A.L.; Mukhtar, H. Inibizione della crescita; disregolazione del ciclo cellulare e induzione dell'apoptosi da parte del componente del tè verde (–)—Epigallocatechina-3-gallato in cellule di carcinoma prostatico umano sensibili agli androgeni e insensibili agli androgeni. *Toxicol. Appl. Pharmacol.* **2000**, *164*, 82–90. [[CrossRef](#)]
131. Hussain, T.; Gupta, S.; Adhami, V.M.; Mukhtar, H. L'epigallocatechina-3-gallato costituente il tè verde inibisce selettivamente la COX-2 senza influenzare l'espressione della COX-1 nelle cellule di carcinoma prostatico umano. *Int. J. Cancer* **2005**, *113*, 660–669. [[CrossRef](#)]
132. Harper, C.E.; Patel, B.B.; Wang, J.; Eltoum, I.A.; Lamartiniere, C.A. Epigallocatechin-3-gallate suppresses early stage; but not late stage prostate cancer in TRAMP mice: Mechanisms of action. *Prostate* **2007**, *67*, 1576–1589. [[CrossRef](#)]
133. Giudice, A.; Montella, M.; Boccellino, M.; Crispo, A.; D'Arena, G.; Bimonte, S.; Facchini, G.; Ciliberto, G.; Botti, G.; Quagliuolo, L.; et al. Epigenetic Changes Induced by Green Tea Catechins are Associated with Prostate Cancer. *Curr. Mol. Med.* **2017**, *6*, 405–420. [[CrossRef](#)]
134. Kurahashi, N.; Sasazuki, S.; Iwasaki, M.; Inoue, M.; Tsugane, S.; JPHC Study Group. Green tea consumption and prostate cancer risk in Japanese men: A prospective study. *Am. J. Epidemiol.* **2008**, *167*, 71–77. [[CrossRef](#)] [[PubMed](#)]
135. Guo, Y.; Zhi, F.; Chen, P.; Zhao, K.; Xiang, H.; Mao, Q.; Wang, X.; Zhang, X. Green tea and the risk of prostate cancer: A systematic review and meta-analysis. *Med. Baltim.* **2017**, *96*, e6426. [[CrossRef](#)] [[PubMed](#)]
136. Mahmoud, A.M.; Yang, W.; Bosland, M.C. Soy isoflavones and prostate cancer: A review of molecular mechanisms. *J. Steroid Biochem. Mol. Biol.* **2014**, *140*, 116–132. [[CrossRef](#)]
137. Li, Y.; Sarkar, F.H. Inhibition of nuclear factor kappaB activation in PC3 cells by genistein is mediated via Akt signaling pathway. *Clin. Cancer Res.* **2002**, *8*, 2369–2377. [[PubMed](#)]
138. Agarwal, R. Cell signaling and regulators of cell cycle as molecular targets for prostate cancer prevention by dietary agents. *Biochem. Pharmacol.* **2000**, *60*, 1051–1059. [[CrossRef](#)]
139. Hastak, K.; Gupta, S.; Ahmad, N.; Agarwal, M.K.; Agarwal, M.L.; Mukhtar, H. Role of p53 and NF-kappaB in epigallocatechin-3-gallate-induced apoptosis of LNCaP cells. *Oncogene* **2003**, *22*, 4851–4859. [[CrossRef](#)]
140. Mentor-Marcel, R.; Lamartiniere, C.A.; Eltoum, I.E.; Greenberg, N.M.; Elgavish, A. Genistein in the diet reduces the incidence of poorly differentiated prostatic adenocarcinoma in transgenic mice (TRAMP). *Cancer Res.* **2001**, *61*, 6777–6782.
141. El Touny, L.H.; Banerjee, P.P. Identification of a biphasic role for genistein in the regulation of prostate cancer growth and metastasis. *Cancer Res.* **2009**, *69*, 3695–3703. [[CrossRef](#)]

142. Paller, C.J.; Kanaan, Y.M.; Beyene, D.A.; Naab, T.J.; Copeland, R.L.; Tsai, H.L.; Kanarek, N.F.; Hudson, T.S. Risk of prostate cancer in African-American men: Evidence of mixed effects of dietary quercetin by serum vitamin D status. *Prostate* **2015**, *75*, 1376–1383. [[CrossRef](#)] [[PubMed](#)]
143. Rossi, V.; Di Zazzo, E.; Galasso, G.; De Rosa, C.; Abbondanza, C.; Sinisi, A.A.; Altucci, L.; Migliaccio, A.; Castoria, G. Estrogens Modulate Somatostatin Receptors Expression and Synergize With the Somatostatin Analog Pasireotide in Prostate Cells. *Front Pharmacol.* **2019**, *10*, 28. [[CrossRef](#)] [[PubMed](#)]
144. Sun, S.; Gong, F.; Liu, P.; Miao, Q. Metformin combined with quercetin synergistically repressed prostate cancer cells via inhibition of VEGF/PI3K/Akt signaling pathway. *Gene* **2018**, *664*, 50–57. [[CrossRef](#)]
145. Adhami, V.M.; Syed, D.N.; Khan, N.; Mukhtar, H. Dietary flavonoid fisetin: A novel dual inhibitor of PI3K/Akt and mTOR for prostate cancer management. *Biochem. Pharmacol.* **2012**, *84*, 1277–1281. [[CrossRef](#)] [[PubMed](#)]
146. Sorrenti, V.; Vanella, L.; Acquaviva, R.; Cardile, V.; Giofrè, S.; Di Giacomo, C. Cyanidin induces apoptosis and differentiation in prostate cancer cells. *Int. J. Oncol.* **2015**, *47*, 1303–1310. [[CrossRef](#)]
147. Ha, U.S.; Bae, W.J.; Kim, S.J.; Yoon, B.I.; Hong, S.H.; Lee, J.Y.; Hwang, T.K.; Hwang, S.Y.; Wang, Z.; Kim, S.W. Anthocyanin induces apoptosis of DU-145 cells in vitro and inhibits xenograft growth of prostate cancer. *Yonsei Med. J.* **2015**, *56*, 16–23. [[CrossRef](#)]
148. Kaur, M.; Velmurugan, B.; Rajamanickam, S.; Agarwal, R.; Agarwal, C. Gallic acid, an active constituent of grape seed extract, exhibits anti-proliferative, pro-apoptotic and anti-tumorigenic effects against prostate carcinoma xenograft growth in nude mice. *Pharm. Res.* **2009**, *26*, 2133–2140. [[CrossRef](#)]
149. Heidarian, E.; Keloushadi, M.; Ghatreh-Samani, K.; Valipour, P. The reduction of IL-6 gene expression; pAKT; pERK1/2; pSTAT3 signaling pathways and invasion activity by gallic acid in prostate cancer PC3 cells. *Biomed. Pharmacother.* **2016**, *84*, 264–269. [[CrossRef](#)]
150. Park, E.; Kwon, H.Y.; Jung, J.H.; Jung, D.B.; Jeong, A.; Cheon, J.; Kim, B.; Kim, S.H. Inhibition of Myeloid Cell Leukemia 1 and Activation of Caspases Are Critically Involved in Gallotannin-induced Apoptosis in Prostate Cancer Cells. *Phytother. Res.* **2015**, *29*, 1225–1236. [[CrossRef](#)]
151. Adaramoye, O.; Erguen, B.; Nitzsche, B.; Höpfner, M.; Jung, K.; Rabien, A. Punicalagin, a polyphenol from pomegranate fruit, induces growth inhibition and apoptosis in human PC-3 and LNCaP cells. *Chem. Biol. Interact.* **2017**, *274*, 100–106. [[CrossRef](#)]
152. Sharma, P.; McClees, S.F.; Afaq, F. Pomegranate for prevention and treatment of cancer: An update. *Molecules* **2017**, *22*, 177. [[CrossRef](#)] [[PubMed](#)]
153. Sanderson, J.T.; Clabault, H.; Patton, C.; Lassalle-Claux, G.; Jean-François, J.; Paré, A.F.; Hébert, M.J.; Surette, M.E.; Touaibia, M. Antiproliferative, antiandrogenic and cytotoxic effects of novel caffeic acid derivatives in LNCaP human androgen-dependent prostate cancer cells. *Bioorg. Med. Chem.* **2013**, *21*, 7182–7193. [[CrossRef](#)] [[PubMed](#)]
154. Liu, C.C.; Hsu, J.M.; Kuo, L.K.; Chuu, C.P. Caffeic acid phenethyl ester as an adjuvant therapy for advanced prostate cancer. *Med. Hypotheses* **2013**, *80*, 617–619. [[CrossRef](#)] [[PubMed](#)]
155. Imai, M.; Yokoe, H.; Tsubuki, M.; Takahashi, N. Growth inhibition of human breast and prostate cancer cells by cinnamic acid derivatives and their mechanism of action. *Biol. Pharm. Bull.* **2019**, *42*, 1134–1139. [[CrossRef](#)] [[PubMed](#)]
156. Huang, Y.; Chen, H.; Zhou, X.; Wu, X.; Hu, E.; Jiang, Z. Inhibition effects of chlorogenic acid on benign prostatic hyperplasia in mice. *Eur. J. Pharmacol.* **2017**, *809*, 191–195. [[CrossRef](#)]
157. Eroğlu, C.; Seçme, M.; Bağcı, G.; Dodurga, Y. Assessment of the anticancer mechanism of ferulic acid via cell cycle and apoptotic pathways in human prostate cancer cell lines. *Tumor Biol.* **2015**, *36*, 9437–9446. [[CrossRef](#)]
158. Cheng, T.M.; Chin, Y.T.; Ho, Y.; Chen, Y.R.; Yang, Y.N.; Yang, Y.C.; Shih, Y.J.; Lin, T.I.; Lin, H.Y.; Davis, P.J. Resveratrol induces sumoylated COX-2-dependent anti-proliferation in human prostate cancer LNCaP cells. *Food Chem. Toxicol.* **2017**, *112*, 67–75. [[CrossRef](#)]
159. Teiten, M.H.; Gaascht, F.; Eifes, S.; Dicato, M.; Diederich, M. Chemopreventive potential of curcumin in prostate cancer. *Genes Nutr.* **2010**, *5*, 61–74. [[CrossRef](#)]
160. Aggarwal, B.B. Prostate cancer and curcumin: Add spice to your life. *Cancer Biol. Ther.* **2008**, *7*, 1436–1440. [[CrossRef](#)]
161. Mohebbati, R.; Anaiegoudari, A.; Khazdair, M.R. The effects of Curcuma longa and curcumin on reproductive systems. *Endocr. Regul.* **2017**, *51*, 220–228. [[CrossRef](#)]

162. Chen, S.; Nimick, M.; Cridge, A.G.; Hawkins, B.C.; Rosengren, R.J. Anticancer potential of novel curcumin analogs towards castrate-resistant prostate cancer. *Int. J. Oncol.* **2018**, *52*, 579–588. [[CrossRef](#)] [[PubMed](#)]
163. Stanisławska, I.J.; Granica, S.; Piwowski, J.P.; Szawkało, J.; Wiązecki, K.; Czarnocki, Z.; Kiss, A.K. The Activity of Urolithin A and M4 Valerolactone, Colonic Microbiota Metabolites of Polyphenols, in a Prostate Cancer in Vitro Model. *Planta Med.* **2019**, *85*, 118–125. [[CrossRef](#)] [[PubMed](#)]
164. Sánchez-González, C.; Ciudad, C.J.; Noé, V.; Izquierdo-Pulido, M. Walnut polyphenol metabolites, urolithins A and B, inhibit the expression of the prostate-specific antigen and the androgen receptor in prostate cancer cells. *Food Funct.* **2014**, *5*, 2922–2930. [[CrossRef](#)] [[PubMed](#)]
165. Kawabata, K.; Yoshioka, Y.; Terao, J. Role of Intestinal Microbiota in the Bioavailability and Physiological Functions of Dietary Polyphenols. *Molecules* **2019**, *24*, 370. [[CrossRef](#)] [[PubMed](#)]
166. Rinninella, E.; Cintoni, M.; Raoul, P.; Lopetuso, L.R.; Scaldaferri, F.; Pulcini, G.; Miggiano, G.A.D.; Gasbarrini, A.; Mele, M.C. Food components and dietary habits: Keys for a healthy gut microbiota composition. *Nutrients* **2019**, *11*, 2393. [[CrossRef](#)]
167. Martínez-Medina, M.; Denizot, J.; Dreux, N.; Robin, F.; Billard, E.; Bonnet, R.; Darfeuille-Michaud, A.; Barnich, N. Western diet induces dysbiosis with increased *E coli* in CEABAC10 mice, alters host barrier function favouring AIEC colonisation. *Gut* **2014**, *63*, 116–124. [[CrossRef](#)]
168. De Filippo, C.; Cavalieri, D.; Di Paola, M.; Ramazzotti, M.; Poullet, J.B.; Massart, S.; Collini, S.; Pieraccini, G.; Lionetti, P. Impact of diet in shaping gut microbiota revealed by a comparative study in children from Europe and rural Africa. *Proc. Natl. Acad. Sci. USA* **2010**, *107*, 14691–14696. [[CrossRef](#)]
169. Dzutsev, A.; Badger, J.H.; Perez-Chanona, E.; Roy, S.; Salcedo, R.; Smith, C.K.; Trinchieri, G. Microbes and Cancer. *Annu. Rev. Immunol.* **2017**, *35*, 199–228. [[CrossRef](#)]



© 2020 by the authors. Licensee MDPI, Basel, Switzerland. This article is an open access article distributed under the terms and conditions of the Creative Commons Attribution (CC BY) license (<http://creativecommons.org/licenses/by/4.0/>).

Review

Lactoferrin from Bovine Milk: A Protective Companion for Life

Fabiana Superti

National Centre for Innovative Technologies in Public Health, National Institute of Health,
Viale Regina Elena 299, 00161 Rome, Italy; fabiana.superti@iss.it; Tel.: +39-06-4990-3149

Received: 30 July 2020; Accepted: 20 August 2020; Published: 24 August 2020

Abstract: Lactoferrin (Lf), an iron-binding multifunctional glycoprotein belonging to the transferrin family, is present in most biological secretions and reaches particularly high concentrations in colostrum and breast milk. A key function of lactoferrin is non-immune defence and it is considered to be a mediator linking innate and adaptive immune responses. Lf from bovine milk (bLf), the main Lf used in human medicine because of its easy availability, has been designated by the United States Food and Drug Administration as a food additive that is generally recognized as safe (GRAS). Among the numerous protective activities exercised by this nutraceutical protein, the most important ones demonstrated after its oral administration are: Antianemic, anti-inflammatory, antimicrobial, immunomodulatory, antioxidant and anticancer activities. All these activities underline the significance in host defence of bLf, which represents an ideal nutraceutical product both for its economic production and for its tolerance after ingestion. The purpose of this review is to summarize the most important beneficial activities demonstrated following the oral administration of bLf, trying to identify potential perspectives on its prophylactic and therapeutic applications in the future.

Keywords: lactoferrin; bovine milk; nutraceutical; human health

1. Introduction

Lactoferrin, an 80 kDa iron-binding glycoprotein belonging to the family of transferrin proteins, was first isolated in 1939 from cow's milk [1] and in 1960 was shown to be the main iron-binding protein in human milk [2]. Lactoferrin is also found in mucosal secretions such as tears, saliva, vaginal mucus, seminal plasma, nasal and bronchial secretions, bile, gastrointestinal fluids and urine [3]. It is present in plasma in relatively low concentrations, where it is predominantly neutrophil derived [4].

Bovine lactoferrin (bLf) has been extensively studied in the past 60 years, as research on this protein actually started around the 1960s, when technological progress had allowed its correct extraction from milk and its complete characterization [5].

Its role in numerous and varied biological functions is now accepted by the scientific community. Indeed, it has been shown that bLf is involved in various physiological and protective actions, among which some of the most studied to date are antioxidant, anti-tumour, anti-inflammatory and antimicrobial activities [6–13].

In this review on bLf, both the main characteristics and the major biological functions of this pleiotropic nutraceutical protein will be summarized. In particular, the use of exogenous bLf as a therapeutic agent and the mechanisms responsible for its various actions will be taken into consideration in order to identify new research perspectives.

2. Bioavailability, Metabolism, Absorption and Delivery of Bovine Lactoferrin

As previously mentioned, bLf, from milk or whey, is used to improve immunity, resistance to infection, control of non-communicable diseases, iron absorption and human health in general.

Since many of these functional properties are highly dependent on the structural integrity of the protein, it must be remembered that when bLf is taken orally it can be largely digested in the stomach [14]. In particular, since bLf receptors are found in the intestinal mucosa and in the cells of the lymphatic tissue of the intestine [15,16], it is important that bLf maintain its structural integrity to bind its receptors. However, it has been shown that bLf directly induces the growth and proliferation of enterocytes, depending on its concentration [17], so intestinal absorption of lactoferrin can be different in different periods of life. It is noteworthy that at the beginning of life the intestinal lumen of the baby who is breastfed or fed with infant formula fortified with bLf will have a high concentration of lactoferrin attributable to very limited proteolytic degradation and high cell proliferation [18]. The mucosal development induced by lactoferrin can, thus, increase the mucosal surface and not only improve the absorption of iron but also of other nutrients. Later, as the baby grows, the digestion of proteins will be more efficient and the lactoferrin concentration will be much lower, resulting in increased differentiation. Hence, in adulthood, as previously mentioned, bLf administered orally will be largely digested into small molecules. Since many functions of bLf (such as the ability to bind iron) are highly dependent on the integrity of the protein structure, its gastrointestinal digestion causes a loss of many of these properties. However, protein degradation also has positive aspects as some peptides produced by its digestion, such as lactoferricin, a 25-residue peptide (Lf amino acid residues 17–41) [19], and lactoferrampin, a 20-residue peptide (Lf amino acid residues 265–284) [20], display potent defensive activity. These peptides possess antimicrobial activity due to their hydrophobicity and cationic charge that make them amphipathic molecules. Lactoferricin that in some cases displays a more potent antibacterial and anti-fungal activity than intact bLf [19,21] possess antimicrobial [22–24], anticancer [24–27] and anti-inflammatory properties [28], while lactoferrampin shows a wide antimicrobial action against bacteria, viruses, yeasts and parasites [22,24]. Finally, it has been reported that lactoferricin, incorporated in food supplements, could provide health benefits and reduce the risk of chronic disease [29]. Additional studies are needed to identify all biological activities (together with the molecular mechanisms involved) of these bioactive peptides derived from the digestion of bLf. This is essential in order to optimize their use for human health and well-being. Further insights into the multiple activities of these two peptides can be found in the reviews of Gifford et al. [24], Bruni et al. [30] and Drago-Serrano et al. [31].

As mentioned above, bLf receptors are found in the intestine [15,16], so the orally administered protein must be protected to pass through the stomach and reach the intestine without being degraded. In order to improve its oral bioavailability, the formulation of bLf oral delivery systems has been approached with different approaches. Among the most commonly used methods to protect bLf during the oral and gastric passage phases we find: Iron saturation, microencapsulation, PEGylation and absorption enhancers [14,32]. While it is believed that iron saturation is one of the methods for slowing the enzymatic hydrolysis of bLf, it is not considered an effective method of delivering bLf in its structurally intact form to small intestine by oral administration [33]. Microencapsulation is a commonly used method to protect bLf from protease digestion. This method involves the formation of a protective structure (protein or polysaccharide shell) around the bLf core. This core-shell system effectively protects the bLf from gastric digestion and, by using appropriate shell materials, can also allow for specific and controlled release of the protein. In addition to microencapsulation with proteins or carbohydrates, liposomes have also been shown to prevent gastric degradation of bLf [34]. PEGylation, i.e., the covalent attachment of polyethylene glycol (PEG) to therapeutic proteins, is used to protect bLf from the gastric environment. This technique increases bLf resistance to proteases through steric hindrance and, by increasing molecular mass, inhibits renal clearance [32]. As for absorption stimulators, these are a group of chemicals that increase the permeability or transport of molecules across biological membranes. In the field of bLf, research on absorption stimulators focused on chitosan, a linear polysaccharide composed of randomly distributed beta-(1→4)-linked D-glucosamine (deacetylated unit) and N-acetyl-D-glucosamine (acetylated unit). Chitosan has been reported to increase bLf uptake in the gut by opening the intercellular junctions [35]. However, chitosan tends

to dissolve at acidic gastric pH, so, to overcome this problem, chitosan derivatives which are poorly soluble in acidic conditions, such as chitosan-succinate and chitosan-phthalate, have been used [32]. Therefore, regarding the oral bioavailability of bLf, we can conclude that, at present, microencapsulation and PEGylation appear to be the most efficient methods to deliver bLf to gut absorption sites.

3. Lactoferrin, Iron, Oxidative Stress and Anaemia

Lactoferrin, as the other transferrins, has a molecular weight of about 80 kDa and its structure includes two lobes, each capable of reversibly chelating two Fe^{+3} ions per molecule. Both lobes have the same fold, consistent with their sequence identity of ~40%. In each lobe, two domains, referred to as N1 and N2, or C1 and C2, enclose a deep fissure containing the conserved iron-binding site [36]. It is usually only about 15% saturated with iron, indicating that the two lobes are not entirely occupied by iron. bLf, possessing twice the serum transferrin's affinity for iron, is also able to act on systemic iron homeostasis by modulating the synthesis of the two key proteins hepcidin and ferroportin through the down-regulation of interleukin-6 (IL-6) [37]. Figure 1 shows the two Fe^{+3} binding domains of bLf.

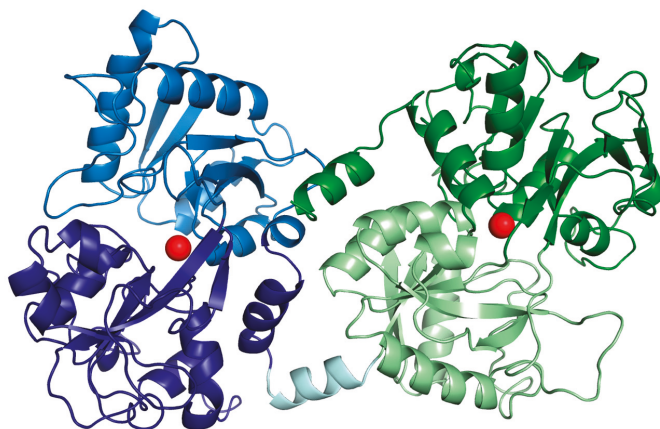


Figure 1. Cartoon representation of bovine lactoferrin. N-lobe is blue (N1 pale blue and N2 dark blue) and C-lobe is green (C1 dark green and C2 pale green). The hinge helix is represented in a pale cyan. Iron ions are reported as red spheres.

3.1. bLf Protection against Iron Deregulation and Oxidative Stress

Iron, an essential nutrient for cell growth, can become toxic when too abundant, leading to the generation of free radicals by interconverting between its most common oxidative forms, ferrous (Fe^{2+}) and ferric (Fe^{3+}) forms [38]. Free iron is toxic because it can donate or receive an electron from adjacent molecules, causing damage to cellular components or generating reactive oxygen species (ROS) that are themselves cytotoxic.

bLf controls the physiological balance of ROS production and their elimination rate through iron sequestration. Many researchers have demonstrated that bLf is able to modulate the adaptive immune system, and that it possesses significant regulation activity on cellular redox via upregulation of key antioxidant enzymes [39–42]. Oxidative stress plays a role in numerous chronic degenerative processes, such as those that affect tumour development, inflammation and aging [12]. Notwithstanding factors responsible for the ROS production imbalance having not been fully elucidated, it is known that the rate and extent of ROS development removal is dependent on the efficiency of superoxide dismutase (SOD), glutathione peroxidase (GPx) and catalase (CAT). SOD converts the superoxide radical ($\bullet\text{O}_2^-$) into hydrogen peroxide (H_2O_2); GPx or CAT transform H_2O_2 into water (H_2O) or into H_2O and molecular oxygen (O_2), respectively. In the presence of free ferric ions (Fe^{3+}) the superoxide radical ($\bullet\text{O}_2^-$) can be

degraded through two phases: In the first, a superoxide molecule reacts with Fe^{3+} to form ferrous ion (Fe^{2+}) and O_2 ; in the second (Fenton reaction), Fe^{2+} reacts with H_2O_2 to form Fe^{3+} , a hydroxyl radical ($\bullet\text{OH}$) and a hydroxide ion (OH^-). The reaction of the hydroxyl radical with polyunsaturated fatty acids, causing the removal of a hydrogen atom, starts the lipid peroxidation and the production of new radicals.

bLf by sequestering Fe^{3+} , is able to prevent the harmful effects of oxidative stress and many studies have demonstrated that it contributes to general homeostasis by disrupting the production of these dangerous radicals [12]. Figure 2 shows Fenton and Haber–Weiss reactions.

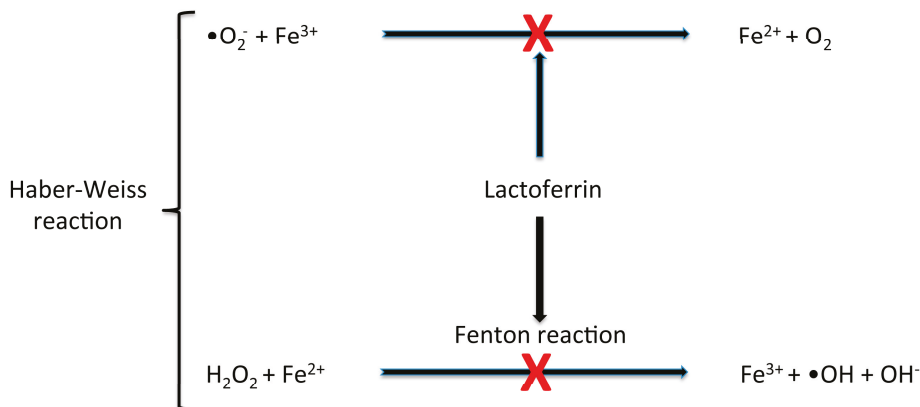


Figure 2. Lactoferrin protects against cellular damage induced by oxidative stress. It inhibits free ferric ion reactivity with superoxide molecules, thus limiting the formation of ferrous salt and ground state oxygen. This effect prevents the Fenton reaction in which the ferrous ion is oxidized by hydrogen peroxide to ferric ion, forming a hydroxyl radical and a hydroxide ion.

An example of these studies on bLf protection against iron deregulation and oxidative stress is the one conducted by Okazaki et al. [43] that examined the antioxidant property of bLf oral administration in a rat model of ferric nitrilotriacetate-induced renal tubular oxidative injury. Results of this research showed that bLf pre-treatment suppressed elevation of either serum creatinine or blood urea nitrogen levels and exerted protective effects against renal oxidative tubular damage. These results not only demonstrated the antioxidative effect of bLf but also indicate that lactoferrin consumption is useful in the prevention of iron-mediated renal tubular oxidative damage [43].

3.2. bLf in the Prevention and Treatment of Iron Deficiency Anaemia

Homeostasis is the maintenance of balance in a biological system and is controlled by several factors including bLf which, for its ability to bind ferric ions, plays a central role. Indeed, iron homeostasis is regulated in part by bLf which plays a safety role by protecting against oxidative stress and reducing the amount of cell damage induced by insult. An increasing amount of data have shown the association between disruption of iron homeostasis and different pathophysiological conditions such as anaemia and, in particular, Fe-overload related disorders [44].

Anaemia, defined as number of red blood cells or haemoglobin concentration below established cut-off levels [45], is a worldwide disease that should not be underestimated as it has important consequences for human health. Its prevalence in pre-school aged children, pregnant women and women of reproductive age is approximately 50%, 40% and 30%, respectively [46]. WHO has estimated that about 50% of all cases of anaemia can be attributed to iron deficiency [47]. It is well known that iron, an essential component of haemoglobin, is found both in plant and animal foods but it is

better absorbed from animal sources [48]. In this view, lactoferrin, being one of the main iron-binding proteins also responsible for its transport and release into cells, represents a key element of the iron absorption process.

On the basis of these considerations, several studies have been carried out to evaluate the efficacy of oral administration of bLf for the treatment of iron deficiency anaemia (IDA). In these researches the effectiveness of bLf has often been compared to that of ferrous iron preparations, sometimes leading to partially conflicting results.

Fransson et al. in 1983 [49] analysed the efficacy of bLf supplementation in iron-deficient and iron-sufficient young mice demonstrating that this transferrin represents a useful vehicle for iron supplementation. In this research, the efficacy of lactoferrin supplementation was compared with that of iron chloride and no significant differences were observed. Successively, as IDA during pregnancy represents a risk factor for preterm delivery, the effect of bLf supplementation was studied in women at different trimesters of pregnancy and compared with that of ferrous sulphate. Unlike what was previously observed in mice, in this study haemoglobin and total serum iron values increased to a greater extent in women treated with bLf compared to those who received ferrous sulphate [50]. In a subsequent clinical study by the same authors on pregnant women with IDA, it has been demonstrated that the number of red blood cells, haemoglobin and serum iron increased when they received bLf and decreased when they received ferrous sulphate [51]. In particular, during bLf therapy, serum IL-6 concentrations decreased. So, since IL-6 induces hypoferrremia and causes anaemia, bLf is likely to improve serum iron and haemoglobin concentrations, rather than providing more absorbable iron [9]. These results of Paesano et al. [51] are partially in disagreement with those obtained by Nappi et al. [52] who, in a prospective, randomized, controlled, double blind trial, compared the effects of bLf with ferrous sulphate on iron nutritional status in 100 pregnant women with IDA. In fact, the results of this trial showed that bLf and ferrous sulphate had the same efficacy in restoring iron deposits. However, it is important to note that bLf had significantly lower gastrointestinal side effects than ferrous sulphate. Recently, a systematic review and meta-analysis performed to evaluate the efficacy of daily oral bLf compared to daily oral ferrous iron preparations for the treatment of IDA in pregnancy confirmed results reported above, suggesting lactoferrin as the iron replacement agent of choice for IDA treatment in pregnancy [53].

Anaemia is also often observed in endurance athletes (sports anaemia). Especially, female long distance runners, who menstruate and accurately control their weight, can easily develop this type of anaemia. Hence, Koikawa et al. [54] conducted a study to verify whether taking bLf could improve or prevent anaemia in these athletes. The results of this study have shown that bLf increases iron absorption among female long distance runners, suggesting that it can be helpful in preventing sports anaemia.

Concerning pre-school aged children, a prospective, multicentre, controlled intervention study on 260 infants (ages 4 to 6 months) evaluated and compared the effect of an iron-fortified formula containing bLf and an iron-fortified formula without bLf on hematologic indexes and iron status in term infants [55]. Results of this study demonstrated that significant increases in total body iron content and iron absorption in the intestine were observed only in infants fed with lactoferrin fortified formula milk. Further information on the role of lactoferrin in the fight against iron deficiency and IDA in newborns and infants are available in the reviews of Ochoa et al. [56] and Cerami [57].

4. Lactoferrin in the Defences of the Babies: Decreased Risk of Sepsis and Necrotizing Enterocolitis in Preterm Infants

As just mentioned at the end of the previous paragraph, lactoferrin is fundamental in the infant's diet. It is important to note that lactoferrin also plays important functions both in protecting the newborn infants from infections and in promoting the maturation of their innate and adaptive immune system. In fact, term and, in particular, preterm infants are at risk of infections. In preterm neonates, necrotizing enterocolitis (NEC), a destructive inflammatory bowel condition and sepsis are causes

of severe morbidity and represent the most common motives of death in the first weeks of life and breastfeeding is known to reduce the risks of these serious conditions.

Based on the numerous activities of bLf, in particular the antimicrobial, antioxidant and anti-inflammatory ones, some of which will be better described later, and on the observation that bLf is well tolerated, several clinical studies were conducted that examined the usefulness of the administration of lactoferrin (in general commercial bLf added to infant formula) in the prevention of infections in preterm and term neonates as well as in the reduction of mortality or major morbidity [58–64]. Results of these clinical trials are summarized in Table 1.

Table 1. Effect of bovine lactoferrin (bLf) in neonates: Clinical trials.

Infants	Study Design	Intervention	Main Results	References
VLBW neonates (<1000 g at birth)	Multicentre, double-blind, placebo-controlled, randomized trial	bLf (100 mg/d) or bLf + LGG 6.10 ⁹ CFU/d) or placebo.	bLf alone or in combination with LGG reduced the incidence of a first episode of late-onset sepsis in VLBW neonates.	[58]
VLBW neonates (<1500 g)	Multicentre, double-blind, placebo-controlled, randomized trial	bLf (100 mg/d), or bLf + LGG 6.10 ⁹ CFU/d) or placebo.	NEC or death incidence was significantly lower in groups bLf and bLf + LGG. No adverse effects or intolerances to treatment occurred.	[59]
VLBW (<1500 g) or <32 weeks neonates	Single-centre, double-blind, placebo-controlled, randomized trial	bLf (200 mg/d) or placebo, during hospitalization period	bLf prophylaxis decreased nosocomial sepsis episodes and increased Treg levels. Treg level increasing is suggested to be responsible for decreased sepsis.	[60]
VLBW (neonates <2000 g)	Placebo-controlled, double-blind, randomized rial	bLf 80–140 mg/kg/d or placebo for 4 weeks	bLf supplementation decreased the incidence of first episode of LOS.	[61]
Neonates, (<2500 g at birth)	Placebo-controlled, double-blind, randomized trial	bLf 200 mg/kg/d or placebo for 4 weeks	bLf supplementation decreased nosocomial sepsis episodes, especially in VLBW neonates.	[62]
Neonates <32 weeks or <1500 g	Placebo-controlled, double-blind, randomized trial	bLf (100 mg/d) or bLf + LGG 1.10 ⁶ CFU/d) or placebo.	bLf supplementation decreased the incidence of severe NEC.	[63]
VLBW preterm neonates	Multicentre, double-blind, placebo-controlled, randomized trial	bLf (100 mg/d) or bLf + LGG 1.10 ⁶ CFU/d) or placebo.	bLf supplementation, alone or in combination with LGG, reduced the risk for infections related to inhibitors of gastric acidity. bLf decreased the incidence of LOS and NEC.	[64]

LGG: *Lactobacillus rhamnosus* GG; VLBW: Very low birth weight; CFU: Colony-forming units; Tregs: T-regulatory cells; LOS: Late-onset sepsis; NEC: Necrotizing enterocolitis.

These clinical studies are particularly interesting, not only because they were targeted to the critical VLBW infants, but above all because both mortality and morbidity following sepsis and NEC remain high despite the use of powerful antimicrobial agents [65]. The results of these trials have shown that the administration of bLf in preterm infants, in the absence or in the presence of the probiotic LGG strain, was able to reduce blood infection without adverse effects.

While these results are extremely encouraging, studies are still needed to establish more precisely the dosage, duration of treatment and development of premature babies.

The data obtained so far support the usefulness of further examining the effects of bLf supplementation on the immune response, in particular to infections, in highly vulnerable infants. It is hoped that the results of the numerous on-going studies will definitively demonstrate the benefits of integrating bLf into the preterm baby's diet leading the way the use of bLf in a clinical setting. More insights into the role of lactoferrin in neonatology can be found in the review by Sharma et al. [66].

5. Antimicrobial Activity of bLf

The antimicrobial effect was the first identified lactoferrin protective activity and has been widely demonstrated both in vitro and in vivo [8,10,67]. The bacteriostatic and bactericidal activity of lactoferrin against a large number of gram-positive and gram-negative bacteria is due to two distinct mechanisms [8,10,67,68]. bLf primary role involves the binding and sequestration of free iron at the infection sites, thus depriving microorganisms of this essential substrate for their growth

and inducing a bacteriostatic effect [36]. Differently, bactericidal activity is independent of iron and involves direct interaction with the infectious agent: Specific interactions have been described both with lipoteichoic acid (LTA) of gram-positive bacteria and with lipopolysaccharide (LPS) of gram-negative bacteria [67]. Iron sequestration by bLf also prevents biofilm formation that represents a crucial step in the development and persistence of infection [69].

Further mechanisms of the antimicrobial action of bLf are: Rupture of the cell membrane of pathogens, proteolysis of microbial virulence factors, inhibition of microbial adhesion to host cells by binding with glycosaminoglycans (GAGs) and improvement of the growth of normal commensal probiotic microflora in the intestine [67,70].

Concerning in vivo preclinical studies, twenty years ago Wada et al. [71] demonstrated in germfree BALB/c mice that the administration of 10 mg bLf for 3–4 weeks significantly reduced the number of *Helicobacter pylori* in the stomach and also inhibited the attachment of bacteria to it. Numerous in vivo studies have been conducted since then, many of which are described in the review of Teraguchi et al. [72]. The satisfactory results obtained in animal models then led to clinical trials. For example in 2005 Okuda et al. [73] confirmed the activity of bLf in inhibiting colonization by *Helicobacter pylori* in humans. In this double-blind placebo-controlled randomized trial, healthy subjects positive for *Helicobacter pylori* received bLf tablets (200 mg/day) or placebo tablets for 12 weeks. After treatments the decrease of the (13) C-urea breath test values in the bLf group was significantly higher than that in the control group suggesting that bLf administration is effective to suppress *Helicobacter pylori* colonization. *Helicobacter pylori* infection, still very frequent, causes chronic active gastritis and can have serious complications such as gastric malignancies. Since antibiotic treatment (mainly clarithromycin and levofloxacin) has led to an increase in antibiotic-resistant strains in recent decades, these results are of particular interest for the development of a new eradication therapy. This represents only one example of the applications of bLf as an antimicrobial agent in humans since many other studies have shown that oral administration of bLf can reduce bacterial and fungal infections mainly in the gastrointestinal tract [74].

Among the many activities carried out by bLf to fight infections, it should be remembered that bLf also acts as a prebiotic by promoting the growth of beneficial bacteria for the host such as probiotics. So, concerning in vivo preclinical and clinical studies, there are a number of experimental observations that oral administration of bLf, alone or in association with probiotic strains, is able to counteract bacterial and fungal vaginal infections [70].

The antiviral activity of bLf has been extensively studied in in vitro systems [67,75,76] and two main mechanisms have been identified by which bLf inhibits viral infection: (i) Competition with the virus for the binding to cell receptors [77,78]; (ii) direct interaction with capsid or viral envelope proteins [67,75,76,79]. An in vivo preclinical study by Shin et al. [80] demonstrated that orally administered bLf reduced pneumonia in mice infected with the Influenza virus by suppressing the infiltration of inflammatory cells in the lung.

Concerning the effects of lactoferrin oral administration against viral infections in humans, its beneficial action has been demonstrated for different viruses such as hepatitis C virus (HCV) [81,82], rotavirus [83], norovirus [84] and common cold infections [85]. Very recently, clinical use of liposomal bLf in seventy-five patients affected by SARS-CoV-2 infection has been reported [86]. The use of liposomes arises from the observation that liposomes loaded with bLf improved the resistance of bLf to digestive enzymes thus enhancing the effect of orally administered bLf [87]. All 75 COVID-19 positive patients were successfully treated with the oral administration of liposomal bLf, which allowed a complete and fast recovery. As aerosol liposomal therapy is widely employed with good results [88,89], in some patients with headache, dry cough and nasal congestions liposomal bLf was also administered by aerosol that was very useful to relieve not only the respiratory symptoms but also the cough, the headache and the smell and taste dysfunction. The results of this study are very encouraging as they indicated that oral treatment with liposomal bLf induces a fast recovery in 100% of patients and that lower dose of the same treatment (half doses) seems to exert a potential preventive effect against

COVID-19 in healthy family members in direct contact with the affected patients [86]. The use of bLf trapped in liposomes will be better discussed in the section on the anticancer activity of bLf. Given the emergence of containing this terrible pandemic, further studies are underway on the use of different forms of Lf to treat COVID-19 patients.

Regarding the antifungal activity of bLf, most of the studies involved *Candida albicans*, known as one of the most dangerous opportunistic pathogens. As for bacteria, bLf can act effectively on a broad spectrum of fungal species due to its strong iron-absorbing property. It has been shown that bLf is capable of killing *Candida albicans* [90]. However, in addition to the iron-depriving effect, bLf is able to directly bind the surface of fungal cells, resulting in increased membrane permeability and inducing their death. The combination of bLf with other antifungal compounds (such as fluconazole) significantly enhanced the inhibitory activity against *Candida albicans* [91] and *Cryptococcus neoformans* [92]. Concerning in vivo studies, it has been reported that, in guinea pigs infected with *Trichophyton mentagrophytes*, orally administered bLf did not prevent development of symptoms during the early phase of infection, but facilitated clinical improvement of skin lesions after the peak of the symptoms [93]. These results indicate the potential utility of bLf as a food component to promote the treatment of dermatophytosis. Other authors developed an experimental model of reproducible oral candidiasis, with immunosuppressed mice, showing local symptoms characteristic of oral thrush in humans and, using this model, demonstrated the efficacy of bLf against experimental *Candida albicans* oral infection [94]. For further information see also the reviews from Superti and De Seta [70] and Fernandes and Carter [95].

In summary, numerous in vivo studies have shown that oral administration of bLf is able to counteract various bacterial, viral and fungal infections. With regard to communicable diseases in general, it is important to remember that, due to the frequent use of antimicrobial drugs, numerous pathogens have become prone to drug resistance which represents the main cause of the unsatisfactory results of some conventional antimicrobial treatments. Consequently, research and development of new therapeutic have become urgent. From this point of view, bLf can represent a very promising tool as an alternative or complementary therapeutic approach to conventional therapy.

6. Anti-Inflammatory Activity of bLf

Inflammation is a complex pathophysiological process involving numerous mediators and various cell types in response to microbial or non-microbial injury [12]. If inflammation is not promptly limited, it can cause damage to the host by establishing systemic and even chronic inflammatory conditions. It is well known that the production of principal immune mediators, such as cytokines and chemokines, depends on the recruitment of inflammatory cells and, in particular, innate immune cells.

Several studies demonstrated that lactoferrin, being a natural immunomodulator, exerts an anti-inflammatory effect [96] supported by the strong increase of its content in body secretions during inflammation [97,98]. There are numerous evidences concerning the capability of lactoferrin to improve injury induced by insult and protect the integrity of organs during the development of inflammation. The anti-inflammatory activity of bLf can be partially ascribed to its positive charge through which it interacts with negatively charged groups (for example proteoglycans) present on the surface of the immune cells. This interaction can activate signalling pathways that induce a physiological anti-inflammatory reaction [41]. bLf is also able to enter cells and translocate to the nucleus [99], so regulating pro-inflammatory gene expression [100]. The anti-inflammatory effect of lactoferrin during bacterial infection is also due to its ability to neutralize negatively charged microbial molecules such as LPS, thus preventing the interaction of the LPS-binding protein with the endotoxin and blocking the binding of LPS with the membrane protein CD14 and the subsequent activation of monocytes and macrophages [101].

It is also likely that lactoferrin controls inflammatory response by preventing iron-mediated free radical injury at inflamed sites [9] so, through the control of oxidative stress, it modulates innate immune responsiveness that alters production of immune regulatory mediators that are important for

directing development of adaptive immune function [39,102]. Several mechanisms are involved in the immunomodulating activity of lactoferrin [103,104]. Lactoferrin acts on B cells to allow their successive interaction with T cells, promotes the maturation of T cell precursors into T helper cells and induces the differentiation of immature B cells into antigen presenting cells [103]. It has been also suggested that lactoferrin may play a role in T cell activation through modulation of dendritic cell function [105]. The anti-inflammatory effect is probably due to the inhibition of production of proinflammatory cytokines such as interleukin-1 beta (IL-1 beta), IL-6 and TNF-alpha. This, as mentioned before, can be obtained by the translocation of lactoferrin to the nucleus, where it blocks NF-kB (nuclear factor kappa-light-chain-enhancer of activated B cells) activation. It has long been known that bLf is able to limit irritation both at the level of the skin and within the subcutaneous tissues and internal organs and many studies on the immunomodulatory effects of orally administered bLf have been carried out [106]. For further information see also the reviews from Kruzel et al. [12] and Drago-Serrano et al. [107].

6.1. Lactoferrin and Dermatitis

Allergic contact dermatitis is an inflammation of the skin resulting from exposure to irritants and allergens present in the environment. The main therapeutic approaches to limit the symptoms of skin allergies include the use of topical corticosteroids and calcineurin inhibitors, which have side effects [108]. Consequently, to overcome the limitations of the currently available treatments, new therapeutic categories including biological ones were considered [109]. In this view, Zimecki et al. [110] carried out a study in BALB/c mice to compare the immunomodulatory actions of bLf on the elicitation phases of the cellular and humoral cutaneous immune responses to oxazolone and toluene diisocyanate, respectively. This study showed that bLf is able to differentially influence the stimulation phases of humoral and cellular immune responses in mouse skin models and that the inhibition of the cellular immune response is probably due to the suppression of Th1 cells.

6.2. Lactoferrin and Inflammatory Bowel Diseases

Togawa et al. [111] examined the potential ability of bLf to attenuate colitis utilising a 2,4,6-trinitrobenzenesulfonic acid (TNBS)-induced colitis model in rats. This is a well-established model very similar to human inflammatory bowel disease characterized by mucosal infiltration of neutrophils mediated, at least in part, by tumour necrosis factor-alpha (TNF-alpha) and IL-1beta activation [112]. Results obtained showed that bLf administration is able to suppress the activation of proinflammatory cytokines, such as TNF-alpha, IL-1beta and IL-6 in rats with TNBS-induced colitis. Similar results have been obtained by the same research group in a dextran sulphate sodium (DSS) induced-colitis rat model [113]. The ability of bLf to relieve the inflammatory conditions of DSS-induced experimental colitis was later confirmed in BALB/c mice as well [114]. Since, as expected, iron-free bLf (apo-bLf) treatment was better than iron saturated bLf (holo-bLf) treatment, the results of this study suggested therapy with apo-bLf as a helpful tool in clinical management of ulcerative colitis. More recently, it has been demonstrated in *in vitro* and *ex vivo* systems that bLf markedly inhibited expression of pro-inflammatory cytokines, such as TNF-alpha, interleukin-8 (IL-8) and IL-6, both in cultured and Crohn-derived intestinal cells [100]. Investigating the dose-dependent effects of bLf, it has been also observed that it is able to modulate neonatal intestinal inflammation [115]. In this study, the effects of bLf at doses comparable to the levels of lactoferrin in bovine and human milk were analysed using intestinal epithelial cells, as the *in vitro* system, and immature pig intestine, as the *in vivo* system. Results obtained demonstrated beneficial effects of bLf at low doses (0.1–1 g/L, close to its levels in cow and human milk, respectively) and harmful effects at a high dose (10 g/L, close to hLf levels in colostrum). These researches, demonstrating that moderate doses of bLf increase the proliferation of intestinal cells while high doses trigger inflammation, are fundamental for establishing effective doses of bLf for the integration of formula in preterm infants, in order to support intestinal maturation and prevent inflammation. This study has important biological significance because it shows that bLf

does not always have a beneficial effect but, at high doses and under certain conditions, it can exert a proinflammatory effect.

6.3. Lactoferrin and Pulmonary Inflammation Disorders

Over the past decades, asthma and allergic lung inflammation diseases have become increasingly common. Asthma is a long-term inflammatory disease of the lungs characterized by airway eosinophilia, mucin secretion, IgE production and airway hyperresponsiveness.

In bronchial asthma, oxidative stress exacerbates airway inflammation by inducing different proinflammatory mediators, enhancing bronchial hyperresponsiveness, stimulating bronchospasm and increasing mucin production. Oxidative stress is a consequence of enhanced ROS production by eosinophils recruited into the lungs during exposure to pro-oxidant environmental molecules or to respiratory viruses [116]. It has been demonstrated that ROS generated by reduced nicotinamide adenine dinucleotide phosphate (NADPH) oxidase from environmental molecules, such as pollen grains or their extracts, provide a signal that enhances antigen-induced allergic airway inflammation in mouse [117]. Successively, it has been shown that bLf, as an iron-binding protein, is able to reduce pollen extract-induced airway inflammation [118]. It is interesting to note that apo-bLf, but not holo-bLf, significantly reduced the accumulation of inflammatory cells and the formation of mucin-producing cells in the inflamed respiratory tract of mice.

Zimecki et al. [119] studied the efficacy of both bLf and human lactoferrin (hLf) to decrease allergen (ovalbumin)-induced pleurisy in BALB/c mice. bLf was given either orally or was administered by gavage intragastrically or by an intraperitoneal injection. The results demonstrated the efficacy of Lfs, bLf more than hLf, in reducing pleurisy in a well-established experimental mouse model of ovalbumin-induced pleurisy. This study is of particular interest as it has increased knowledge of the suppressive efficacy of bLf in allergy, suggesting that oral administration of bLf may be effective in improving allergy symptoms in patients.

bLf has also been used successfully in a cystic fibrosis (CF) mouse model [120]. CF is a multifactorial genetic disease that affects several organs, including the respiratory tract, in which iron imbalance, inflammation as well as bacterial infection, play an important role in the chronicity and gravity of lung disease. Results of this study demonstrated that aerosolized bLf was able to reduce infiltrated leukocytes in CF mice and pulmonary iron overload in both control and CF mice. Above all, a significant reduction was observed in ferroportin (the iron-regulated transporter 1), ferritin (the intracellular protein that stores and releases iron in a regulated manner) and in the luminal iron content.

6.4. Lactoferrin and Hepatitis

Orally ingested bLf has been shown to provide a wide range of benefits in animal models with inflamed liver [121,122] and clinical use of bLf has also produced several promising outcomes, such as the inhibition of hepatic inflammation in chronic hepatitis C (CHC) patients [81,123].

Concerning in vivo studies, Tsubota et al. [121] utilized Long–Evans Cinnamon rats, which spontaneously develop fulminant-like hepatitis, to evaluate the effect of oral administration of bLf on oxidative liver damage. This study showed that bLf allows the recovery of the reduced base excision repair capacity and reduces the accumulation levels of 8-hydroxy-2-deoxyguanosine (a reliable marker of ROS-induced DNA modifications) and mutations in hepatic mitochondrial DNA, possibly thereby protecting Long–Evans Cinnamon rats from lethal hepatic insufficiency. Based on these observations, it has been suggested that bLf could potentially be useful for the treatment of inflammatory liver diseases induced by oxidative stress.

Successively Kuhara et al. [122] utilized four mouse models of hepatitis induced by D-galactosamine, carbon tetrachloride, D-galactosamine plus lipopolysaccharide and zymosan plus lipopolysaccharide to evaluate the efficacy of oral administration of bLf against hepatitis and to identify its mechanism. Results of this research demonstrated that bLf is able to improve the expression of interleukin 11

(IL-11) and bone morphogenetic protein 2 in the small intestine and to protect mice with hepatitis against inflammation.

Regarding clinical trials, Tanaka et al. [81] carried out a first pilot clinical study demonstrating that lactoferrin could be one potential candidate as an anti-HCV reagent that may be effective for the treatment of CHC patients with low serum concentrations of HCV RNA. Finally, Konishi et al. [123] evaluated the effect of bLf on lipid peroxidation, hepatic inflammation and iron metabolism in patients with CHC. Results of this clinical trial demonstrated that bLf therapy allows improvement in lipid peroxidation and alanine aminotransferase (ALT) levels suggesting its oral administration as a promising therapeutic approach for suppressing oxidative stress and inflammation in patients with CHC non-responders to antiviral therapy.

In conclusion, bLf performs its anti-inflammatory action through different cellular receptors and the activation of various cellular signalling pathways, often via iron-dependent mechanisms. Indeed, its ability to sequester iron and to inhibit ROS formation is a key factor in reducing the damage caused to excessive inflammatory responses. The interaction of bLf with its receptors can trigger several protective effects due to the regulation of enzymatic activities and ROS production, the modification of cell phenotype and cytokine profile, the binding to LPS or the competition with its receptors and the prevention of apoptosis.

7. Anticancer Activity of bLf

The World Health Organization [124] reported that, in 2018, 18.1 million people around the world had cancer, 9.6 million cancer patients died and cancer was the cause of about 30% of all premature deaths from non-communicable diseases (NCDs) among adults aged 30–69. So the incidence of cancer is getting higher and there is still no fully efficacious cure for all different forms of the disease. Therefore, preventing the development of carcinomas and treating them is critical to reduce current cancer mortality.

The anti-tumour activity of hLf and bLf has been extensively studied for both prevention and treatment, and several mechanisms have been suggested such as intra- and extra-cellular effects or immunoregulatory and anti-inflammatory functions.

In vitro studies showed that the intracellular effects are generally associated with the arrest of tumour cell growth, while the extracellular ones are mainly related to the interaction between bLf and cell membranes, and the immunoregulatory action of bLf is obtained through the activation of the cells of the immune system that release tumour cytotoxic effectors [11].

Numerous in vivo studies have provided evidence that oral administration of bLf is effective in reducing the development of chemically induced tumours [125–129]. The chemopreventive anticancer effects are probably due to the multiple functions of bLf and, in particular, to the stimulation of the immune response, to the modulation of the carcinogenic metabolic enzymes [127], to the antioxidant activity [129], the induction of cell death in tumour tissue and to the inhibition of angiogenesis [128,130]. Regulation of the immune system is a key factor in the action of bLf against cancer [11] and both innate and adaptive immunity are involved in immunostimulation induced by bLf [131–134].

It has been demonstrated that orally administered bLf exhibits high bioavailability and selectivity towards tumour cells by inhibiting tumour proliferation, survival, migration, invasion and metastasis [131,135–139]. It is important to underline that bLf is able to promote or inhibit cell proliferation by acting selectively on normal or cancerous cells, respectively [139]. The first study on the suppressive effect of bLf in rat carcinogenesis was carried out by Sekine et al. [125]. These authors demonstrated in male F344 rats treated with azoxymethane that oral administration of bLf (diet containing 2 or 0.2% bLf) induced a significant reduction in the incidence and in the number of adenocarcinomas of the large intestine. Results of this study suggested that bLf might be a promising chemopreventor of colon carcinogenesis. In 1999 Igo et al. [136] examined the effects on tumor growth and metastasis of bLf administered orally to BALB/c mice bearing subcutaneous implants of the highly metastatic colon carcinoma 26. Results of this study showed that bLf demonstrated

significant inhibition of lung metastatic colony formation from subcutaneous implanted tumours without appreciable effects on tumor growth. Subsequently, Kuhara et al. [131] investigated the effects of oral administration of bLf on the lung colonization by the same colon carcinoma 26. In this study bLf was efficacious before and after tumor implantation, demonstrating a significant inhibitory effect on experimental metastasis. bLf oral administration increased CD4+ and CD8+ cells in the spleen and peripheral blood and enhanced their cytotoxic activity against colon carcinoma 26. Moreover, bLf induced an increase of CD4+ and CD8+ cells and of interleukin-18 production in the small intestinal epithelium. The results of this study indicate that the inhibition of metastases by oral administration of bLf could be due to an increase in cellular immunity, probably mediated by the increase in IL-18 production in the intestinal epithelium. As previously described, in addition to modulating cellular immunity, bLf carries out anti-inflammatory activity by eliminating ROS, pro-oxidant agents capable of contributing to the development of cancer. bLf protects the host from ROS-mediated cell and tissue damage by both binding free iron and regulating key antioxidant enzymes [39–43]. In this regard, a recent study has shown in a mouse model of hepatocarcinogenesis induced by diethylnitrosamine that oral treatment with bLf, by inhibiting in a dose-dependent manner the elevation in serum markers of liver carcinoma and inflammation, induces a significant improvement in hepatic histological structures [138]. This study demonstrated that bLf is effective in inhibiting the oncogenic activity of diethylnitrosamine in a mouse model of hepatocarcinogenesis through its ability to alleviate the hepatic inflammation and apoptosis. As regard the selectivity of bLf towards transformed cells, Chea et al. [137] demonstrated, in oral squamous cell carcinoma cell lines, that bLf is able to reverse programming of epithelial-to-mesenchymal transition (a biological process of invasion and metastasis in cancers) to mesenchymal-to-epithelial transition and observed in vivo both inhibition of tumor cell infiltration and increased E-cadherin expression in xenografts of mice administered orally with bLf.

Since one of the desired properties of an ideal anticancer drug is the ability to selectively target transformed cancer cells, an appropriate delivery system can be extremely useful in releasing bLf into the tumour site. From this point of view, liposomes represent an efficient drug delivery system that can significantly improve the therapeutic potential of the encapsulated compounds. For instance, apo-bLf trapped in positively charged liposomes composed of phosphatidylcholine, dioleoyl phosphatidylethanolamine, cholesterol and stearylamine (ratio 6:1:2:1 M) has been shown to have a greater capacity, compared to protein alone, to inhibit the growth of B16-F10 melanoma cells [140]. In addition, it has been demonstrated, in a brain-targeted chemotherapeutic delivery system, that doxorubicin (DOX)-loaded bLf-modified procationic liposome (PCL), effectively improved both uptake and cytotoxicity of bLf against the glioma C6 cell proliferation, as well as the anti-glioma activity in vivo, compared with DOX solution or DOX-loaded conventional liposomes [141]. In this study, a cholesterol derivative (CHETA, C36H61N3O4S2) was used to prepare negatively charged PCLs and, subsequently, bLf (positively charged at physiological pH) was absorbed onto their surface via electrostatic interaction. This study showed that DOX-Lf-PCLs delivery system was effective and feasible for systemic administration in chemotherapy of glioma. These results confirmed and supported previous researches of the same authors in which this drug carrier for brain delivery, PCLs, was evaluated both in vitro and in vivo. In this study an in vitro model of the blood–brain barrier was developed to assess the ability and mechanisms of PCLs and Lf-PCLs to cross endothelial cells whereas the uptake of PCLs and Lf-PCLs by the mouse brain in vivo was detected by HPLC-fluorescence analysis. Results obtained demonstrated that, compared with the conventional liposomes, PCL and Lf-PCL-8 (CHETA/Lf ratio = 1:8, w/w) showed an improved performance in the uptake efficiency and in the cytotoxicity as well as much improved localization in the brain [142]. Taken together, these results encourage further investigation for the application of Lf-PCLs to treat other brain diseases.

Other authors investigated whether natural bLf or its different iron-saturated forms, as dietary supplements, were able to increase the anti-tumour activity of different recognized anticancer drugs [143]. In this study, bLf was added to the diet of mice that were then challenged with cancer cells and treated with chemotherapy. Results obtained demonstrated that tumours in holo-bLf-fed

mice were totally eradicated with a single injection of known chemotherapy agents whereas apo-bLf (4% iron saturated) or native bLf (about 15% iron saturated) were ineffective. To be fully effective in eradicating tumours, iron-saturated bLf (holo-bLf) had to be administered to mice for more than two weeks before the chemotherapy, indicating that it functions as a competence factor. In particular holo-bLf decreased tumour vascularity and increased anti-tumour cytotoxicity, apoptosis and infiltration of leukocytes in tumours. Holo-bLf bound to intestinal epithelium and enhanced the production of cytokines within the intestine and tumour, as well as nitric oxide that are known to sensitize cancer to chemotherapy. These results that may seem paradoxical are related to the fact that holo-bLf can release iron and trigger an inflammatory reaction. Holo-bLf also restored peripheral blood cell numbers depleted by chemotherapy, thus defending mice from cancer [143].

A subsequent study, based on emerging nanotechnologies, has been carried out to further improving the bioavailability of holo-bLf to tumour sites by developing polymeric-ceramic nanocarriers (NCs) [144]. The authors validated the preclinical efficacies of novel NC oral formulations for the delivery of holo-bLf in colon cancer therapy. Further insights into the therapeutic application of lactoferrin encapsulated in NCs can be found in the review of Sabra and Agwa [145].

In summary, iron-saturated bLf is a powerful natural adjuvant and a fortifying agent capable of improving cancer chemotherapy. As already said, currently the extraction of Lf from cow's milk and its use in various products represents an industrial reality and it is therefore likely that, in the future, the consumption of bLf containing dietary products could be suggested to inhibit or delay the onset of cancer.

8. Other Therapeutic Properties of Lactoferrin

There are many other potential uses of bLf for improving human health and some of them will be discussed below.

8.1. Lactoferrin and Obesity

Obesity represents a serious public health problem and is a strong predictor of chronic diseases. It is now recognized that the intestine and its commensal microflora play an important role in the development of chronic inflammation related to obesity. In fact, obesity and a diet rich in fats are associated with an alteration of the gut microbiota and an increase in intestinal permeability that allows the translocation of LPS into the circulation contributing to systemic inflammation. bLf has been used successfully in the prevention and treatment of obesity and inflammation by inducing the reduction of visceral fat, the neutralization of bacteria in the mucous membrane and the reduction of intestinal permeability.

Concerning the control of fat accumulation, it has been demonstrated that bLf oral administration during caloric restriction in mice was able to enhance weight loss and induced a significant reduction in the total fat pad weight and adipocyte size [146]. Moreover, it has been shown in a mice model with unrestricted food intake that bLf administration induced visceral fat reduction and affected mesenteric adipocytes and fatty acid metabolism in the liver, decreasing the size of mesenteric fat without modulating body weight [147].

Based on the observation that the intestinal commensal microflora plays an important role in the obesity control [148], Sun et al. [149] investigated the role of bLf in obesity as a probiotic compound, demonstrating that oral administration of 100 mg/kg BW bLf for 12 weeks in high-fat diet induced obese mice was able to positively modulate gut microbiota, inhibited inflammation, reduced body weight and fat accumulation, regulated glucose metabolism and relieved liver steatosis. These results are in agreement with previous reports suggesting a healthy role for the supplementation of bLf in the prevention of metabolic complications related to obesity [150].

More recently, Xiong et al. [151] have confirmed the modulatory effects of bLf on lipid metabolism, however the regulatory mechanisms still remain unclear. Moreover, this study has been carried out on high-fat diet-induced obese C57BL/6J mice in which oral administration of bLf for 15 weeks significantly

decreased fat tissue weight, visceral adiposity and hepatic lipid accumulation. These effects are probably due to the suppression of lipogenic gene expression and to the improvement of liver and epididymal adipose tissue inflammation.

The effect of bLf administration has also been studied in association with other safe and effective substances. For example, since bLf and metformin both exhibit beneficial effects on body weight management and fat accumulation, their effects, alone or in combination, on lipid accumulation and metabolism in mice fed with high fat diet has been also studied [152]. Results obtained showed that bLf and metformin, both alone or in combination, prevented high fat diet induced obesity and improved lipid metabolism. The actions bLf and metformin that significantly decreased body weight, waist circumference, Lee's index and visceral fat but had no effect on liver weight were partially due to a key kinase regulating cellular energy homeostasis, the AMP-activated protein kinase.

Regarding the administration of bLf in humans, the effect of enteric-coated bLf was also studied in a randomised double-blind placebo-controlled trial. This human clinical trial also reported that eight-week bLf consumption decreased total adiposity and visceral fat accumulation in male and female subjects with abdominal obesity [153].

In conclusion, numerous studies have shown that dietary bLf consumption represents a favourable agent for the control of lipid accumulation however, prospective as well as mechanistic analyses are still necessary to explain the lipolytic role of bLf in the diet and its potential applications for the obesity treatment. Results of these preclinical studies are summarized in Table 2.

Table 2. Impact of bLf on the metabolic syndrome components or obesity: Preclinical studies.

Animal Species (Male)	Dose	Administration	Treatment Length	Outcomes	References
ICR mice	100 mg/kg	Gastric intubation	4 weeks	Reduced mesenteric fat tissue and hepatic lipid accumulation	[147]
High-fat diet induced obese C57BL/6j mice	(190 mL/kg) 100 mg/kg	Oral	7 weeks	Reduced body weight, obesity, adipose tissue (visceral, abdominal) and plasma glucose	[146]
High-fat diet induced obese C57BL/6j mice	100 mg/kg	Oral	12 weeks	Reduced body weight, fat accumulation, inflammation and relieve liver steatosis	[149]
High-fat diet induced obese C57BL/6j mice	100 mg/kg	Oral	15 weeks	Reduced weight gain, visceral adiposity, serum glucose, inflammation and improved hepatic steatosis	[151]
High-fat diet induced obese C57BL/6j mice	100 mg/kg	Oral	50 days	Ameliorated fatty liver formation, exerted beneficial effects on glucose tolerance and adipocyte tissue inflammation without interfering energy intake.	[150]
C57BL/6 mice	2 g/100 mL alone or in combination with metformin	Oral	12 weeks	Improved high-fat diet-induced obesity and lipid metabolism.	[152]

Lastly, an important aspect to consider is the relationships between adiposity and serum iron as hypoferrremia could be either an actual iron deficiency or a functional iron deficiency mediated by inflammation. In particular, the link among iron levels, bLf and obesity needs further investigations. This is very important, as it is now clear that iron deficiency and obesity are closely linked [154]. It still remains to be clarified the role of bLf in the two aspects of the relationship between iron and obesity: What is the mechanism that leads to an imbalance of iron in the presence of excess adipose tissue and how iron participates in the pathogenesis linked to obesity.

8.2. Lactoferrin and Bone Metabolism

It is established that the bones and the immune system are closely connected. Both tissues possess common progenitors and produce common cytokines and inflammation and bone loss coexist in several diseases such as arthritis, osteoporosis and periodontitis.

It is also known that both bLf and hLf are anabolic factor for skeletal tissue as they are able to exert strong proliferative and anti-apoptotic actions in osteoblasts, and a reducing or even inhibitory effect on osteoclastogenesis [155–158]. Lactoferrin also stimulated proliferation of primary chondrocytes [156,157].

It has been demonstrated *in vitro* that, at physiological concentrations, bLf not only stimulates the proliferation of bone forming cells, osteoblasts and cartilage cells, but it is also an effective osteoblast survival factor. In addition, lactoferrin is able to decrease osteoclast in a murine bone marrow culture system as well as in rabbit mixed bone cell culture [155] and, concerning *in vivo* systems, local injection of bLf in adult mice resulted in increased calvary bone growth [159]. Subsequent research was conducted to evaluate the effects of oral administration of bLf on bone physiology in an osteopenic rat model (ovariectomized rats) [160]. The results of this study showed that bLf oral administration protected osteopenic rats against the ovariectomy-induced reduction of bone volume, trabecular number and thickness. bLf administration also prevented the elevation of trabecular separation and increased bone mineral density in osteopenic rats. Moreover, after bLf treatment, serum TNF-alpha and IL-6 production was suppressed and serum calcitonin increased [160]. Finally, it has been demonstrated that oral administration of bLf in ovariectomized rats strongly stimulated the bone healing following tibial fracture [161].

Lactoferrin, as mentioned above, is also one of the many defence proteins present in saliva where it exerts a defensive activity against both periodontal bacteria and inflammatory processes.

Concerning periodontitis, it has been shown that orally administered liposomal bLf in Wistar rats is an effective preventive and therapeutic agent in decreasing alveolar bone destruction [87] significantly inhibiting LPS-induced alveolar bone reabsorption without interrupting orthodontic tooth movement [162]. Results of this study suggest that liposomal bLf could represent a powerful preventive or therapeutic agent to control periodontal inflammation. In fact, when liposomal bLf was administered orally to periodontitis subjects, a significant improvement in probing depth and a considerable reduction in the production of LPS-induced cytokines from peripheral blood mononuclear cells were obtained [163]. To clarify the mechanism by which bLf is able to prevent LPS-induced osteoclastogenesis without interrupting tooth movement, the same authors investigated its effects on compressive stress (CS)-induced osteoclastogenesis in comparison with those on LPS-induced osteoclastogenesis via osteoblasts *in vitro* [164]. Results obtained demonstrated that bLf fights bone destruction associated with periodontitis without inhibiting bone remodelling by CS-loading suggesting that its oral administration could be highly beneficial for control of periodontitis in orthodontic patients [164].

All these studies have shown that bLf plays an important physiological role in bone growth and healing and exerts a therapeutic role in various bone diseases. We can therefore conclude that bLf can be considered a useful therapeutic agent both for bone regeneration and for destructive bone diseases.

8.3. Lactoferrin and Dry Eye Disease

As mentioned above, lactoferrin is secreted into tears by the lacrimal gland. Dry eye, a multifactorial disease causing visual disturbances and instability of the tear film with potential lesion and inflammation of the ocular surface, is a very common condition with a high prevalence among the elderly. Tear lactoferrin level is an indicator of lacrimal secretory function and correlated with the severity of conjunctivocorneal epithelial lesions in patients with primary, secondary and non-Sjögren's syndrome dry eyes [165].

Kawashima et al. [166] studied in a mouse model whether oral administration of bLf was able to influence age-related tear dysfunction. The results obtained showed that lactoferrin, administered orally, can preserve the function of the lacrimal gland in elderly mice by mitigating oxidative damage and suppressing subsequent inflammation of the gland.

Concerning investigations on human subjects, it has been demonstrated that oral administration of bLf (270 mg/day for one month) represents an efficient treatment modality to improve tear stability and

preserve ocular surface epithelium in dry eye patients with Sjögren's syndrome. The authors attribute the tear function and ocular surface improvements to the suppression of inflammatory mediators by bLf [167]. More likely these effects of bLf on tear secretion are due to the combination of its direct action on the tear glands and the overall improvement of body metabolism.

Taken together these results suggest that the use of bLf as a dietary supplement may be a new and safe therapeutic alternative for patients with dry eye syndrome. Moreover, as it has been described in the section on bone metabolism, bLf could also prove useful in the prevention and therapy of other age-related diseases such as autoimmune, neurodegenerative and immune hypersensitivity disorders [168].

9. bLf on the Market

Large-scale preparation of bLf from cheese whey or skim milk has made this protein accessible commercialized health product for human and animals. The first important application of bLf in a commercial product was its supplementation in infant formula and has been subsequently used for the supplementation of various foods (such as probiotic foods to enhance the beneficial intestinal flora or functional foods to increase iron absorption), for skin care (in cosmetics as antioxidant) and oral care products (to provide oral hygiene), and as nutraceutical, to improve the immune system and to inhibit the inflammatory response. bLf is also used for the conservation and safety of food as it delays lipid oxidation [169] and inhibits microbial growth. The use of bLf in the food industry includes: Meat and wine industry, fat process and dairy industry [170]. The increased demand for natural foods has also increased the importance of natural inhibitors such as bLf. Therefore, the applications of bLf in the food sector are growing remarkably. In all these applications, bLf is expected to express its natural antioxidant, anti-inflammatory, immunomodulatory and anticancer properties.

10. Conclusions

Lactoferrin is an extremely adaptable protein that has been designated by natural selection to be a first-line defence in mammals. This key protein of natural immunity shows many kinds of marvellous biological activities in vitro and in vivo and helps us to defend against external aggressions both of infectious and non-infectious origin. In fact, being positively charged, it can bind numerous surface molecules or metal ions inducing the host's immunomodulatory activation, which in turn affects both adaptive and innate immunity.

The focus of the present review was on several important health-promoting effects of this multi-functional nutraceutical protein although, given the growing array of applications of lactoferrin in the field of human health, coverage is certainly not complete.

Still, the (intentionally diverse) application domains here reviewed should substantiate the main message I meant to convey: This pleiotropic substance accompanies us and defends us throughout our life, from birth to old age, it is safe and is considered by the United States Food and Drug Administration as a GRAS product with no contraindications in patients of all ages. Besides, it represents an ideal nutraceutical product, cheaply produced from bovine milk, and numerous products containing bLf alone or in association with other nutraceuticals, supplements or probiotics are currently being commercialized.

Taken together, the evidence summarized in this review indicate that it would be advisable to embrace a more comprehensive and integrated approach to various diseases, whereby improvement in the patient's quality of life, and even the clinical outcome, may be obtained by combining bLf with conventional therapies, as suggested by the studies examined here.

Such a perspective should motivate the collection of more data in order to improve our understanding of the protective role of bLf, in relation to both non-communicable diseases and infectious diseases.

I hope to have kindled the interest of the reader in the numerous and often interconnected beneficial activities of this surprisingly versatile milk protein.

Funding: This research received no external funding.

Acknowledgments: Mariangela Agamennone (University “G. d’Annunzio”, Chieti, Italy) was kind enough to provide the artwork of Figure 1, for which I thank her warmly.

Conflicts of Interest: The author declares no conflict of interest.

References

1. Sorensen, M.; Sorensen, S.P.L. The proteins in whey. *Comptes-rendus des Trav. du Lab. Carlsberg Ser. Chim.* **1939**, *23*, 55–99.
2. Groves, M.L. The isolation of a red protein from milk. *J. Am. Chem. Soc.* **1960**, *82*, 3345–3350.
3. Levay, P.F.; Viljoen, M. Lactoferrin: A general review. *Haematologica* **1995**, *80*, 252–267. [[PubMed](#)]
4. Iyer, S.; Lönnnerdal, B. Lactoferrin, lactoferrin receptors and iron metabolism. *Eur. J. Clin. Nutr.* **1993**, *47*, 232–241. [[PubMed](#)]
5. Johanson, B. Isolation of an iron-containing red protein from human milk. *Acta Chem. Scand.* **1960**, *14*, 510–512. [[CrossRef](#)]
6. Mayeur, S.; Spahis, S.; Pouliot, Y.; Levy, E. Lactoferrin, a pleiotropic protein in health and disease. *Antioxid. Redox Signal.* **2016**, *24*, 813–836. [[CrossRef](#)] [[PubMed](#)]
7. Tsuda, H.; Sekine, K.; Fujita, K.; Iigo, M. Cancer prevention by bovine lactoferrin and underlying mechanisms—A review of experimental and clinical studies. *Biochem. Cell Biol.* **2002**, *80*, 131–136. [[CrossRef](#)] [[PubMed](#)]
8. Lönnnerdal, B.; Iyer, S. Lactoferrin: Molecular structure and biological function. *Annu. Rev. Nutr.* **1995**, *15*, 93–110. [[CrossRef](#)]
9. Lönnnerdal, B. Nutritional roles of lactoferrin. *Curr. Opin. Clin. Nutr. Metab. Care* **2009**, *12*, 293–297. [[CrossRef](#)] [[PubMed](#)]
10. Vorland, L.H. Lactoferrin: A multifunctional glycoprotein. *APMIS* **1999**, *107*, 971–981. [[CrossRef](#)] [[PubMed](#)]
11. Zhang, Y.; Lima, C.F.; Rodrigues, L.R. Anticancer effects of lactoferrin: Underlying mechanisms and future trends in cancer therapy. *Nutr. Rev.* **2014**, *72*, 763–773. [[CrossRef](#)] [[PubMed](#)]
12. Kruzel, M.L.; Zimecki, M.; Actor, J.K. Lactoferrin in a context of inflammation-induced pathology. *Front. Immunol.* **2017**, *8*, 1438. [[CrossRef](#)] [[PubMed](#)]
13. Kell, D.B.; Heyden, E.L.; Pretorius, E. The Biology of Lactoferrin, an Iron-Binding Protein That Can Help Defend Against Viruses and Bacteria. *Front. Immunol.* **2020**, *11*, 1221. [[CrossRef](#)] [[PubMed](#)]
14. Wang, B.; Timilsena, Y.P.; Blanch, E.; Adhikari, B. Lactoferrin: Structure, function, denaturation and digestion. *Crit. Rev. Food Sci. Nutr.* **2019**, *59*, 580–596. [[CrossRef](#)]
15. Jiang, R.; Lopez, V.; Kelleher, S.L.; Lönnnerdal, B. Apo- and holo- lactoferrin are both internalized by lactoferrin receptor via clathrin-mediated endocytosis but differentially affect ERK-signaling and cell proliferation in Caco-2 cells. *J. Cell Physiol.* **2011**, *226*, 3022–3031. [[CrossRef](#)] [[PubMed](#)]
16. Yao, X.; Bunt, C.; Cornish, J.; Quek, S.Y.; Wen, J. Oral Delivery of Bovine Lactoferrin Using Pectin- and Chitosan-Modified Liposomes and Solid Lipid Particles: Improvement of Stability of Lactoferrin. *Chem. Biol. Drug Des.* **2015**, *86*, 466–475. [[CrossRef](#)]
17. Buccigrossi, V.; de Marco, G.; Bruzzese, E.; Ombrato, L.; Bracale, I.; Polito, G.; Guarino, A. Lactoferrin induces concentration-dependent functional modulation of intestinal proliferation and differentiation. *Pediatr. Res.* **2007**, *61*, 410–414. [[CrossRef](#)]
18. Lönnnerdal, B. Bioactive Proteins in Human Milk: Health, Nutrition, and Implications for Infant Formulas. *J. Pediatr.* **2016**, *173* (Suppl. S4–S9). [[CrossRef](#)] [[PubMed](#)]
19. Bellamy, W.; Takase, M.; Wakabayashi, H.; Kawase, K.; Tomita, M.J. Antibacterial spectrum of lactoferricin B, a potent bactericidal peptide derived from the N-terminal region of bovine lactoferrin. *Appl. Bacteriol.* **1992**, *73*, 472–479. [[CrossRef](#)] [[PubMed](#)]
20. Van der Kraan, M.I.; Nazmi, K.; Teeken, A.; Groenink, J.; van’t Hof, W.; Veerman, E.C.; Bolscher, J.G.; Nieuw Amerongen, A.V. Lactoferrampin, an antimicrobial peptide of bovine lactoferrin, exerts its candidacidal activity by a cluster of positively charged residues at the C-terminus in combination with a helix-facilitating N-terminal part. *Biol. Chem.* **2005**, *386*, 137–142. [[CrossRef](#)] [[PubMed](#)]

21. Vorland, L.H.; Ulvatne, H.; Andersen, J.; Haukland, H.H.; Rekdal, Ø.; Svendsen, J.S.; Gutteberg, T.J. Lactoferricin of bovine origin is more active than lactoferricins of human, murine and caprine origin. *Scand. J. Infect. Dis.* **1998**, *30*, 513–517. [[CrossRef](#)] [[PubMed](#)]
22. Flores-Villaseñor, H.; Canizalez-Román, A.; Reyes-Lopez, M.; Nazmi, K.; de la Garza, M.; Zazueta-Beltrán, J.; León-Sicairos, N.; Bolscher, J.G. Bactericidal effect of bovine lactoferrin, LFcin, LFampin and LFchimera on antibiotic-resistant *Staphylococcus aureus* and *Escherichia coli*. *Biometals* **2010**, *23*, 569–578. [[CrossRef](#)] [[PubMed](#)]
23. Wakabayashi, H.; Bellamy, W.; Takase, M.; Tomita, M. Inactivation of *Listeria monocytogenes* by lactoferricin, a potent antimicrobial peptide derived from cow's milk. *J. Food Prot.* **1992**, *55*, 238–240.
24. Gifford, J.L.; Hunter, H.N.; Vogel, H.J. Lactoferricin: A lactoferrin-derived peptide with antimicrobial, antiviral, antitumor and immunological properties. *Cell. Mol. Life Sci.* **2005**, *62*, 2588–2598. [[CrossRef](#)] [[PubMed](#)]
25. Eliassen, L.T.; Berge, G.; Sveinbjørnsson, B.; Svendsen, J.S.; Vorland, L.H.; Rekdal, Ø. Evidence for a direct antitumor mechanism of action of bovine lactoferricin. *Anticancer Res.* **2002**, *22*, 2703–2710. [[PubMed](#)]
26. Chen, H.Y.; Mollstedt, O.; Tsai, M.H.; Kreider, R.B. Potential clinical applications of multi-functional milk proteins and peptides in cancer management. *Curr. Med. Chem.* **2014**, *21*, 2424–2437. [[CrossRef](#)] [[PubMed](#)]
27. Jiang, R.; Lönnerdal, B. Bovine lactoferrin and lactoferricin exert antitumor activities on human colorectal cancer cells (HT-29) by activating various signaling pathways. *Biochem. Cell Biol.* **2017**, *95*, 99–109. [[CrossRef](#)]
28. Yan, D.; Chen, D.; Shen, J.; Xiao, G.; van Wijnen, A.J.; Im, H.J. Bovine lactoferricin is anti-inflammatory and anti-catabolic in human articular cartilage and synovium. *J. Cell. Physiol.* **2013**, *228*, 447–456. [[CrossRef](#)] [[PubMed](#)]
29. Marcone, S.; Belton, O.; Fitzgerald, D.J. Milk-derived bioactive peptides and their health promoting effects: A potential role in atherosclerosis. *Br. J. Clin. Pharmacol.* **2017**, *83*, 152–162. [[CrossRef](#)] [[PubMed](#)]
30. Bruni, N.; Capucchio, M.T.; Biasibetti, E.; Pessione, E.; Cirrione, S.; Giraud, L.; Corona, A.; Dosio, F. Antimicrobial Activity of Lactoferrin-Related Peptides and Applications in Human and Veterinary Medicine. *Molecules* **2016**, *21*, 752. [[CrossRef](#)] [[PubMed](#)]
31. Drago-Serrano, M.E.; Campos-Rodriguez, R.; Carrero, J.C.; de la Garza, M. Lactoferrin and peptide-derivatives: Antimicrobial agents with potential use in nonspecific immunity modulation. *Curr. Pharm. Des.* **2018**, *24*, 1067–1078. [[CrossRef](#)] [[PubMed](#)]
32. Yao, X.; Bunt, C.; Cornish, J.; Quek, S.Y.; Wen, J. Oral Delivery of Lactoferrin: A Review. *Int. J. Pept. Res. Ther.* **2013**, *19*, 125–134. [[CrossRef](#)]
33. Wang, B.; Timilsena, Y.P.; Blanch, E.; Adhikari, B. Mild thermal treatment and in-vitro digestion of three forms of bovine lactoferrin: Effects on functional properties. *Int. Dairy J.* **2017**, *64*, 22–30. [[CrossRef](#)]
34. Liu, W.; Ye, A.; Liu, W.; Liu, C.; Singh, H. Stability during in vitro digestion of lactoferrin-loaded liposomes prepared from milk fat globule membrane-derived phospholipids. *J. Dairy Sci.* **2013**, *96*, 2061–2070. [[CrossRef](#)]
35. Hejazi, R.; Amiji, M. Chitosan-based gastrointestinal delivery systems. *J. Control. Release* **2003**, *89*, 151–165. [[CrossRef](#)]
36. Baker, E.N.; Baker, H.M. Molecular structure, binding properties and dynamics of lactoferrin. *Cell. Mol. Life Sci.* **2005**, *62*, 2531–2539. [[CrossRef](#)]
37. Fleming, R.E.; Bacon, B.R. Orchestration of Iron Homeostasis. *N. Engl. J. Med.* **2005**, *352*, 1741–1744. [[CrossRef](#)]
38. Eid, R.; Arab, N.T.; Greenwood, M.T. Iron mediated toxicity and programmed cell death: A review and a re-examination of existing paradigms. *Biochim. Biophys. Acta. Mol. Cell. Res.* **2017**, *1864*, 399–430. [[CrossRef](#)]
39. Zimecki, M.; Mazurier, J.; Spik, G.; Kapp, J.A. Human lactoferrin induces phenotypic and functional changes in murine splenic B cells. *Immunology* **1995**, *86*, 122–127. [[PubMed](#)]
40. Zimecki, M.; Kocieba, M.; Kruzel, M. Immunoregulatory activities of lactoferrin in the delayed type hypersensitivity in mice are mediated by a receptor with affinity to mannose. *Immunobiology* **2002**, *205*, 120–131. [[CrossRef](#)] [[PubMed](#)]
41. Legrand, D. Overview of Lactoferrin as a Natural Immune Modulator. *J. Pediatr.* **2016**, *173*, S10–S15. [[CrossRef](#)]

42. Kruzel, M.L.; Actor, J.K.; Zimecki, M.; Wise, J.; Ploszaj, P.; Mirza, S.; Kruzel, M.; Hwang, S.A.; Ba, X.; Boldogh, I. Novel recombinant human lactoferrin: Differential activation of oxidative stress related gene expression. *J. Biotechnol.* **2013**, *168*, 666–675. [[CrossRef](#)]
43. Okazaki, Y.; Kono, I.; Kuriki, T.; Funahashi, S.; Fushimi, S.; Iqbal, M.; Okada, S.; Toyokuni, S. Bovine lactoferrin ameliorates ferric nitrilotriacetate-induced renal oxidative damage in rats. *J. Clin. Biochem. Nutr.* **2012**, *51*, 84–90. [[CrossRef](#)] [[PubMed](#)]
44. Gozzellino, R.; Arosio, P. Iron Homeostasis in Health and Disease. *Int. J. Mol. Sci.* **2016**, *17*, 130. [[CrossRef](#)] [[PubMed](#)]
45. Beutler, E.; Waalen, J. The definition of anemia: What is the lower limit of normal of the blood hemoglobin concentration? *Blood* **2006**, *107*, 1747–1750. [[CrossRef](#)]
46. Scholl, T.O. Maternal iron status: Relation to fetal growth, length of gestation, and iron endowment of the neonate. *Nutr. Rev.* **2011**, *69*, S23–S29. [[CrossRef](#)] [[PubMed](#)]
47. World Health Organization. Conclusions and recommendations of the WHO Consultation on prevention and control of iron deficiency in infants and young children in malaria-endemic areas. *Food Nutr. Bull.* **2007**, *28*, S621–S627. [[CrossRef](#)] [[PubMed](#)]
48. Hunt, J.R. Bioavailability of iron, zinc, and other trace minerals from vegetarian diets. *Am. J. Clin. Nutr.* **2003**, *78*, 633S–639S. [[CrossRef](#)] [[PubMed](#)]
49. Fransson, G.B.; Keen, C.L.; Lönnerdal, B. Supplementation of milk with iron bound to lactoferrin using weanling mice: L. Effects on hematology and tissue iron. *J. Pediatr. Gastroenterol. Nutr.* **1983**, *2*, 693–700. [[CrossRef](#)] [[PubMed](#)]
50. Paesano, R.; Torcia, F.; Berlutti, F.; Pacifici, E.; Ebano, V.; Moscarini, M.; Valenti, P. Oral administration of lactoferrin increases hemoglobin and total serum iron in pregnant women. *Biochem. Cell. Biol.* **2006**, *84*, 377–380. [[CrossRef](#)] [[PubMed](#)]
51. Paesano, R.; Berlutti, F.; Pietropaoli, M.; Pantanella, F.; Pacifici, E.; Goolsbee, W.; Valenti, P. Lactoferrin efficacy versus ferrous sulfate in curing iron deficiency and iron deficiency anemia in pregnant women. *Biomaterials* **2010**, *23*, 411–417. [[CrossRef](#)] [[PubMed](#)]
52. Nappi, C.; Tommaselli, G.A.; Morra, I.; Massaro, M.; Formisano, C.; Di Carlo, C. Efficacy and tolerability of oral bovine lactoferrin compared to ferrous sulfate in pregnant women with iron deficiency anemia: A prospective controlled randomized study. *Acta Obstet. Gynecol. Scand.* **2009**, *88*, 1031–1035. [[CrossRef](#)] [[PubMed](#)]
53. Abu Hashim, H.; Foda, O.; Ghayaty, E. Lactoferrin or ferrous salts for iron deficiency anemia in pregnancy: A meta-analysis of randomized trials. *Eur. J. Obstet. Gynecol. Reprod. Biol.* **2017**, *219*, 45–52. [[CrossRef](#)] [[PubMed](#)]
54. Koikawa, N.; Nagaoka, I.; Yamaguchi, M.; Hamano, H.; Yamauchi, K.; Sawaki, K. Preventive effect of lactoferrin intake on anemia in female long distance runners. *Biosci. Biotechnol. Biochem.* **2008**, *72*, 931–935. [[CrossRef](#)] [[PubMed](#)]
55. Ke, C.; Lan, Z.; Hua, L.; Ying, Z.; Humina, X.; Jia, S.; Weizheng, T.; Ping, Y.; Lingying, C.; Meng, M. Iron metabolism in infants: Influence of bovine lactoferrin from iron-fortified formula. *Nutrition* **2015**, *31*, 304–309. [[CrossRef](#)]
56. Ochoa, T.J.; Pezo, A.; Cruz, K.; Chea-Woo, E.; Cleary, T.G. Clinical studies of lactoferrin in children. *Biochem. Cell. Biol.* **2012**, *90*, 457–467. [[CrossRef](#)] [[PubMed](#)]
57. Cerami, C. Iron Nutrition of the Fetus, Neonate, Infant, and Child. *Ann. Nutr. Metab.* **2017**, *71* (Suppl. 3), 8–14. [[CrossRef](#)]
58. Manzoni, P.; Rinaldi, M.; Cattani, S.; Pagni, L.; Romeo, M.G.; Messner, H.; Stolfi, I.; Decembrino, L.; Laforgia, N.; Vagnarelli, F.; et al. Italian Task Force for the Study and Prevention of Neonatal Fungal Infections, Italian Society of Neonatology. Bovine lactoferrin supplementation for prevention of late-onset sepsis in very low-birth-weight neonates: A randomized trial. *JAMA* **2009**, *302*, 1421–1428. [[CrossRef](#)]
59. Manzoni, P.; Meyer, M.; Stolfi, I.; Rinaldi, M.; Cattani, S.; Pagni, L.; Romeo, M.G.; Messner, H.; Decembrino, L.; Laforgia, N.; et al. Bovine lactoferrin supplementation for prevention of necrotizing enterocolitis in very-low-birth-weight neonates: A randomized clinical trial. *Early Hum. Dev.* **2014**, *90* (Suppl. 1), S60–S65. [[CrossRef](#)] [[PubMed](#)]

60. Akin, I.M.; Atasay, B.; Dogu, F.; Okulu, E.; Arsan, S.; Karatas, H.D.; Ikinogullari, A.; Turmen, T. Oral lactoferrin to prevent nosocomial sepsis and necrotizing enterocolitis of premature neonates and effect on T-regulatory cells. *Am. J. Perinatol.* **2014**, *31*, 1111–1120. [[CrossRef](#)] [[PubMed](#)]
61. Kaur, G.; Gathwala, G. Efficacy of Bovine Lactoferrin Supplementation in Preventing Late-onset Sepsis in low Birth Weight Neonates: A Randomized Placebo-Controlled Clinical Trial. *J. Trop. Pediatr.* **2015**, *61*, 370–376. [[CrossRef](#)] [[PubMed](#)]
62. Ochoa, T.J.; Zegarra, J.; Cam, L.; Llanos, R.; Pezo, A.; Cruz, K.; Zea-Vera, A.; Carcamo, C.; Campos, M.; Bellomo, S. Randomized controlled trial of lactoferrin for prevention of sepsis in peruvian neonates less than 2500 g. *Pediatr. Infect. Dis. J.* **2015**, *34*, 571–576. [[CrossRef](#)] [[PubMed](#)]
63. Meyer, M.P.; Alexander, T.J. Reduction in necrotizing enterocolitis and improved outcomes in preterm infants following routine supplementation with *Lactobacillus* GG in combination with bovine lactoferrin. *Neonatal Perinatal Med.* **2017**, *10*, 249–255. [[CrossRef](#)] [[PubMed](#)]
64. Manzoni, P.; García Sánchez, R.; Meyer, M.; Stolfi, I.; Pugni, L.; Messner, H.; Cattani, S.; Betta, P.M.; Memo, L.; Decembrino, L.; et al. Italian Task Force for the Study, and Prevention of Neonatal Fungal Infections and the Italian Society of Neonatology. Exposure to gastric acid inhibitors increases the risk of infection in preterm very low birth weight infants but concomitant administration of lactoferrin counteracts this effect. *J. Pediatr.* **2018**, *193*, 62–67.e1. [[CrossRef](#)] [[PubMed](#)]
65. Stoll, B.J.; Hansen, N.I.; Higgins, R.D.; Fanaroff, A.A.; Duara, S.; Goldberg, R.; Laptook, A.; Walsh, M.; Oh, W.; Hale, E.; et al. Very low birth weight preterm infants with early onset neonatal sepsis: The predominance of gram-negative infections continues in the National Institute of Child Health and Human Development Neonatal Research Network, 2002–2003. *Pediatr. Infect. Dis. J.* **2005**, *24*, 635–639. [[CrossRef](#)] [[PubMed](#)]
66. Sharma, D.; Shastri, S.; Sharma, P. Role of lactoferrin in neonatal care: A systematic review. *J. Matern. Fetal Neonatal Med.* **2017**, *30*, 1920–1932. [[CrossRef](#)] [[PubMed](#)]
67. Superti, F.; Berlutti, F.; Paesano, R.; Valenti, P. Structure and activity of lactoferrin—a multi functional protective agent for human health. In *Iron Metabolism and Disease*; Fuchs, H., Ed.; Publisher Research Signpost: Trivandrum, India, 2008; Volume 8, pp. 1–32.
68. Orsi, N. The antimicrobial activity of lactoferrin: Current status and perspectives. *Biometals* **2004**, *17*, 189–196. [[CrossRef](#)]
69. Singh, P.K.; Parsek, M.R.; Greenberg, E.P.; Welsh, M.J. A component of innate immunity prevents bacterial biofilm development. *Nature* **2002**, *417*, 552–555. [[CrossRef](#)] [[PubMed](#)]
70. Superti, F.; De Seta, F. Warding Off Recurrent Yeast and Bacterial Vaginal Infections: Lactoferrin and Lactobacilli. *Microorganisms* **2020**, *8*, 130. [[CrossRef](#)] [[PubMed](#)]
71. Wada, T.; Aiba, Y.; Shimizu, K.; Takagi, A.; Miwa, T.; Koga, Y. The therapeutic effect of bovine lactoferrin in the host infected with *Helicobacter pylori*. *Scand. J. Gastroenterol.* **1999**, *34*, 238–243. [[CrossRef](#)] [[PubMed](#)]
72. Teraguchi, S.; Wakabayashi, H.; Kuwata, H.; Yamauchi, K.; Tamura, Y. Protection against infections by oral lactoferrin: Evaluation in animal models. *Biometals* **2004**, *17*, 231–234. [[CrossRef](#)]
73. Okuda, M.; Nakazawa, T.; Yamauchi, K.; Miyashiro, E.; Koizumi, R.; Booka, M.; Teraguchi, S.; Tamura, Y.; Yoshikawa, N.; Adachi, Y.; et al. Bovine lactoferrin is effective to suppress *Helicobacter pylori* colonization in the human stomach: A randomized, double-blind, placebo-controlled study. *J. Infect. Chemother.* **2005**, *11*, 265–269. [[CrossRef](#)] [[PubMed](#)]
74. Giansanti, F.; Panella, G.; Leboffe, L.; Antonini, G. Lactoferrin from Milk: Nutraceutical and Pharmacological Properties. *Pharmaceuticals* **2016**, *9*, 61. [[CrossRef](#)] [[PubMed](#)]
75. Marchetti, M.; Superti, F. Recent developments in antiviral research. In *Antiviral Activity of Lactoferrin*; Pandalai, S.G., Ed.; Transworld Research Network: Trivandrum, India, 2001; pp. 193–203.
76. Seganti, L.; Di Biase, A.M.; Marchetti, M.; Pietrantonio, A.; Tinari, A.; Superti, F. Antiviral activity of lactoferrin towards naked viruses. *Biometals* **2004**, *17*, 295–299. [[CrossRef](#)] [[PubMed](#)]
77. Marchetti, M.; Trybala, E.; Superti, F.; Johansson, M.; Bergström, T. Inhibition of herpes simplex virus infection by lactoferrin is dependent on interference with the virus binding to glycosaminoglycans. *Virology* **2004**, *318*, 405–413. [[CrossRef](#)] [[PubMed](#)]
78. Pietrantonio, A.; Fortuna, C.; Remoli, M.E.; Ciufolini, M.G.; Superti, F. Bovine lactoferrin inhibits Toscana virus infection by binding to heparan sulphate. *Viruses* **2015**, *7*, 480–495. [[CrossRef](#)] [[PubMed](#)]

79. Pietrantoni, A.; Di Biase, A.M.; Tinari, A.; Marchetti, M.; Valenti, P.; Seganti, L.; Superti, F. Bovine lactoferrin inhibits adenovirus infection by interacting with viral structural polypeptides. *Antimicrob. Agents Chemother.* **2003**, *47*, 2688–2691. [[CrossRef](#)] [[PubMed](#)]
80. Shin, K.; Wakabayashi, H.; Yamauchi, K.; Teraguchi, S.; Tamura, Y.; Kurokawa, M.; Shiraki, K. Effects of orally administered bovine lactoferrin and lactoperoxidase on influenza virus infection in mice. *J. Med. Microbiol.* **2005**, *54*, 717–723. [[CrossRef](#)]
81. Tanaka, K.; Ikeda, M.; Nozaki, A.; Kato, N.; Tsuda, H.; Saito, S.; Sekihara, H. Lactoferrin inhibits hepatitis C virus viremia in patients with chronic hepatitis C: A pilot study. *Jpn. J. Cancer Res.* **1999**, *90*, 367–371. [[CrossRef](#)] [[PubMed](#)]
82. Ueno, H.; Sato, T.; Yamamoto, S.; Tanaka, K.; Ohkawa, S.; Takagi, H.; Yokosuka, O.; Furuse, J.; Saito, H.; Sawaki, A.; et al. Randomized, double-blind, placebo-controlled trial of bovine lactoferrin in patients with chronic hepatitis C. *Cancer Sci.* **2006**, *97*, 1105–1110.
83. Egashira, M.; Takayanagi, T.; Moriuchi, M.; Moriuchi, H. Does daily intake of bovine lactoferrin-containing products ameliorate rotaviral gastroenteritis? *Acta Paediatr.* **2007**, *96*. [[CrossRef](#)]
84. Ochoa, T.J.; Chea-Woo, E.; Baiocchi, N.; Pecho, I.; Campos, M.; Prada, A.; Valdiviezo, R.N.; Lluque, A.; Lai, D.; Cleary, T.G. Randomized double-blind controlled trial of bovine lactoferrin for prevention of diarrhea in children. *J. Pediatr.* **2013**, *162*, 349–356. [[CrossRef](#)] [[PubMed](#)]
85. Vitetta, L.; Coulson, S.; Beck, S.L.; Gramotnev, H.; Du, S.; Lewis, S. The clinical efficacy of bovine lactoferrin/whey protein Ig-rich fraction (Lf/IgF) for the common cold: A double blind randomized study. *Complement Ther. Med.* **2013**, *21*, 164–171. [[CrossRef](#)] [[PubMed](#)]
86. Serrano, G.; Kochergina, I.; Albors, A.; Diaz, E.; Oroval, M.; Hueso, G.; Serrano, J.M. Liposomal Lactoferrin as Potential Preventative and Cure for COVID-19. *Int. J. Res. Health Sci.* **2020**, *8*, 8–15. [[CrossRef](#)]
87. Yamano, E.; Miyauchi, M.; Furusyo, H.; Kawazoe, A.; Ishikado, A.; Makino, T.; Tanne, K.; Tanaka, E.; Takata, T. Inhibitory effects of orally administrated liposomal bovine lactoferrin on the LPS-induced osteoclastogenesis. *Lab. Investig.* **2010**, *90*, 1236–1246. [[CrossRef](#)] [[PubMed](#)]
88. Wyde, P.R.; Six, H.R.; Wilson, S.Z.; Gilbert, B.E.; Knight, V. Activity against rhinoviruses, toxicity, and delivery in aerosol of enviroxime in liposomes. *Antimicrob. Agents Chemother.* **1988**, *32*, 890–895. [[CrossRef](#)]
89. Taylor, K.M.G.; Fan, S.J. Liposomes for Drug Delivery to the Respiratory Tract. *Drug Dev. Ind. Pharm.* **1993**, *19*, 123–142.
90. Kirkpatrick, C.H.; Green, I.; Rich, R.R.; Schade, A.L. Inhibition of growth of *Candida albicans* by iron un saturated lactoferrin: Relation to host-defense mechanisms in chronic mucocutaneous candidiasis. *J. Infect. Dis.* **1971**, *124*, 539–544. [[CrossRef](#)]
91. Kobayashi, T.; Kakeya, H.; Miyazaki, T.; Izumikawa, K.; Yanagihara, K.; Ohno, H.; Yamamoto, Y.; Tashiro, T.; Kohno, S. Synergistic antifungal effect of lactoferrin with azole antifungals against *Candida albicans* and a proposal for a new treatment method for invasive candidiasis. *Jpn. J. Infect. Dis.* **2011**, *64*, 292–296. [[PubMed](#)]
92. Lai, Y.W.; Campbell, L.T.; Wilkins, M.R.; Pang, C.N.I.; Chen, S.; Carter, D.A. Synergy and antagonism between iron chelators and antifungal drugs in *Cryptococcus*. *Int. J. Antimicrob. Agents* **2016**, *48*, 388–394. [[CrossRef](#)] [[PubMed](#)]
93. Wakabayashi, H.; Uchida, K.; Yamauchi, K.; Teraguchi, S.; Hayasawa, H.; Yamaguchi, H. Lactoferrin given in food facilitates dermatophytosis cure in guinea pig models. *J. Antimicrob. Chemother.* **2000**, *46*, 595–602. [[CrossRef](#)] [[PubMed](#)]
94. Takakura, N.; Wakabayashi, H.; Ishibashi, H.; Teraguchi, S.; Tamura, Y.; Yamaguchi, H.; Abe, S. Oral lactoferrin treatment of experimental oral candidiasis in mice. *Antimicrob. Agents Chemother.* **2003**, *47*, 2619–2623. [[CrossRef](#)] [[PubMed](#)]
95. Fernandes, K.E.; Carter, D.A. The Antifungal Activity of Lactoferrin and Its Derived Peptides: Mechanisms of Action and Synergy with Drugs against Fungal Pathogens. *Front. Microbiol.* **2017**, *8*, 2. [[CrossRef](#)] [[PubMed](#)]
96. Ward, P.P.; Paz, E.; Conneely, O.M. Multifunctional roles of lactoferrin: A critical overview. *Cell. Mol. Life Sci.* **2005**, *62*, 2540–2548. [[CrossRef](#)] [[PubMed](#)]
97. Sagel, S.D.; Sontag, M.K.; Accurso, F.J. Relationship between antimicrobial proteins and airway inflammation and infection in cystic fibrosis. *Pediatr. Pulmonol.* **2009**, *44*, 402–409. [[CrossRef](#)]
98. Pfefferkorn, M.D.; Boone, J.H.; Nguyen, J.T.; Juliar, B.E.; Davis, M.A.; Parker, K.K. Utility of fecal lactoferrin in identifying Crohn disease activity in children. *J. Pediatr. Gastroenterol. Nutr.* **2010**, *51*, 425–428. [[CrossRef](#)]

99. Ashida, K.; Sasaki, H.; Suzuki, Y.A.; Lönnnerdal, B. Cellular internalization of lactoferrin in intestinal epithelial cells. *Biomaterials* **2004**, *17*, 311–315. [[CrossRef](#)]
100. Bertuccini, L.; Costanzo, M.; Iosi, F.; Tinari, A.; Terruzzi, F.; Stronati, L.; Aloï, M.; Cucchiara, S.; Superti, F. Lactoferrin prevents invasion and inflammatory response following *E. coli* strain LF82 infection in experimental model of Crohn's disease. *Dig. Liver Dis.* **2014**, *46*, 496–504. [[CrossRef](#)] [[PubMed](#)]
101. Ellass-Rochard, E.; Legrand, D.; Salmon, V.; Roseanu, A.; Trif, M.; Tobias, P.D.; Mazurier, J.; Genevieve Spik, G. Lactoferrin Inhibits the Endotoxin Interaction with CD14 by Competition with the Lipopolysaccharide-Binding Protein. *Infect. Immun.* **1998**, *66*, 486–491. [[PubMed](#)]
102. Zimecki, M.; Spiegel, K.; Własczyk, A.; Kübler, A.; Kruzel, M.L. Lactoferrin increases the output of neutrophil precursors and attenuates the spontaneous production of TNF-alpha and IL-6 by peripheral blood cells. *Arch. Immunol. Ther. Exp. (Warsz)* **1999**, *47*, 113–118. [[PubMed](#)]
103. Actor, J.K.; Hwang, S.A.; Kruzel, M.L. Lactoferrin as a natural immune modulator. *Curr. Pharm. Des.* **2009**, *15*, 1956–1973. [[CrossRef](#)]
104. Legrand, D.; Mazurier, J. A critical review of the roles of host lactoferrin in immunity. *Biomaterials* **2010**, *23*, 365–376. [[CrossRef](#)]
105. Hwang, S.A.; Kruzel, M.L.; Actor, J.K. Lactoferrin augments BCG vaccine efficacy to generate T helper response and subsequent protection against challenge with virulent *Mycobacterium tuberculosis*. *Int. Immunopharmacol.* **2005**, *5*, 591–599. [[CrossRef](#)]
106. Legrand, D.; Ellass, E.; Carpentier, M.; Mazurier, J. Lactoferrin: A modulator of immune and inflammatory responses. *Cell. Mol. Life Sci.* **2005**, *62*, 2549–2559. [[CrossRef](#)]
107. Drago-Serrano, M.E.; Campos-Rodríguez, R.; Carrero, J.C.; de la Garza, M. Lactoferrin: Balancing Ups and Downs of Inflammation Due to Microbial Infections. *Int. J. Mol. Sci.* **2017**, *18*, 501. [[CrossRef](#)]
108. Draelos, Z.D. Use of topical corticosteroids and topical calcineurin inhibitors for the treatment of atopic dermatitis in thin and sensitive skin areas. *Curr. Med. Res. Opin.* **2008**, *24*, 985–994. [[CrossRef](#)] [[PubMed](#)]
109. Katoh, N. Future perspectives in the treatment of atopic dermatitis. *J. Dermatol.* **2009**, *36*, 367–376. [[CrossRef](#)] [[PubMed](#)]
110. Zimecki, M.; Artym, J.; Kocieba, M.; Kruzel, M.L. Effects of lactoferrin on elicitation of the antigen-specific cellular and humoral cutaneous response in mice. *Postępy Hig. Med. Dosw.* **2012**, *66*, 16–22. [[CrossRef](#)] [[PubMed](#)]
111. Togawa, J.; Nagase, H.; Tanaka, K.; Inamori, M.; Umezawa, T.; Nakajima, A.; Naito, M.; Sato, S.; Saito, T.; Sekihara, H. Lactoferrin reduces colitis in rats via modulation of the immune system and correction of cytokine imbalance. *Am. J. Physiol. Gastrointest. Liver Physiol.* **2002**, *283*, G187–G195. [[CrossRef](#)] [[PubMed](#)]
112. Neurath, M.F.; Fuss, I.; Pasparakis, M.; Alexopoulou, L.; Haralambous, S.; Meyer zum Buschenfelde, K.H.; Strober, W.; Kollias, G. Predominant pathogenic role of tumor necrosis factor in experimental colitis in mice. *Eur. J. Immunol.* **1997**, *27*, 1743–1750. [[CrossRef](#)] [[PubMed](#)]
113. Togawa, J.; Nagase, H.; Tanaka, K.; Inamori, M.; Nakajima, A.; Ueno, N.; Saito, T.; Sekihara, H. Oral administration of lactoferrin reduces colitis in rats via modulation of the immune system and correction of cytokine imbalance. *J. Gastroenterol. Hepatol.* **2002**, *17*, 1291–1298. [[CrossRef](#)] [[PubMed](#)]
114. Li, L.; Ren, F.; Yun, Z.; An, Y.; Wang, C.; Yan, X. Determination of the effects of lactoferrin in a preclinical mouse model of experimental colitis. *Mol. Med. Rep.* **2013**, *8*, 1125–1129. [[CrossRef](#)] [[PubMed](#)]
115. Nguyen, D.N.; Jiang, P.; Stensballe, A.; Bendixen, E.; Sangild, P.T.; Chatterton, D.E.W. Bovine lactoferrin regulates cell survival, apoptosis and inflammation in intestinal epithelial cells and preterm pig intestine. *J. Proteomics* **2016**, *139*, 95–102. [[CrossRef](#)]
116. Holgate, S.T. The epidemic of allergy and asthma. *Nature* **1999**, *402*, B2–B4. [[CrossRef](#)]
117. Boldogh, I.; Bacsı, A.; Choudhury, B.K.; Dharajiya, N.; Alam, R.; Hazra, T.K.; Mitra, S.; Goldblum, R.M.; Sur, S. ROS generated by pollen NADPH oxidase provide a signal that augments antigen-induced allergic airway inflammation. *J. Clin. Investig.* **2005**, *115*, 2169–2179. [[CrossRef](#)]
118. Kruzel, M.L.; Bacsı, A.; Choudhury, B.; Sur, S.; Boldogh, I. Lactoferrin decreases pollenantigen-induced allergic airway inflammation in a murine model of asthma. *Immunology* **2006**, *119*, 159–166. [[CrossRef](#)]
119. Zimecki, M.; Artym, J.; Kocieba, M.; Kaleta-Kuratowicz, K.; Kruzel, M.L. Lactoferrin restrains allergen-induced pleurisy in mice. *Inflamm. Res.* **2012**, *61*, 1247–1255. [[CrossRef](#)] [[PubMed](#)]

120. Cutone, A.; Lepanto, M.S.; Rosa, L.; Scotti, M.J.; Rossi, A.; Ranucci, S.; De Fino, I.; Bragonzi, A.; Valenti, P.; Musci, G.; et al. Aerosolized Bovine Lactoferrin Counteracts Infection, Inflammation and Iron Dysbalance in A Cystic Fibrosis Mouse Model of *Pseudomonas aeruginosa* Chronic Lung Infection. *Int. J. Mol. Sci.* **2019**, *20*, 2128. [[CrossRef](#)]
121. Tsubota, A.; Yoshikawa, T.; Nariai, K.; Mitsunaga, M.; Yumoto, Y.; Fukushima, K.; Hoshina, S.; Fujise, K. Bovine lactoferrin potently inhibits liver mitochondrial 8-OHdG levels and retrieves hepatic OGG1 activities in Long-Evans Cinnamon rats. *J. Hepatol.* **2008**, *48*, 486–493. [[CrossRef](#)] [[PubMed](#)]
122. Kuhara, T.; Tanaka, A.; Yamauchi, K.; Iwatsuki, K. Bovine lactoferrin ingestion protects against inflammation via IL-11 induction in the small intestine of mice with hepatitis. *Br. J. Nutr.* **2014**, *111*, 1801–1810. [[CrossRef](#)]
123. Konishi, M.; Iwasa, M.; Yamauchi, K.; Sugimoto, R.; Fujita, N.; Kobayashi, Y.; Watanabe, S.; Teraguchi, S.; Adachi, Y.; Kaito, M. Lactoferrin inhibits lipid peroxidation in patients with chronic hepatitis C. *Hepatol. Res.* **2006**, *36*, 27–32. [[CrossRef](#)]
124. World Health Organization. *WHO Report on Cancer: Setting Priorities, Investing Wisely and Providing Care for All*; Technical Report; World Health Organization: Geneva, Switzerland, 2020.
125. Sekine, K.; Watanabe, E.; Nakamura, J.; Takasuka, N.; Kim, D.J.; Asamoto, M.; Krutovskikh, V.; Baba-Toriyama, H.; Ota, T.; Moore, M.A.; et al. Inhibition of azoxymethane-initiated colon tumor by bovine lactoferrin administration in F344 rats. *Jpn. J. Cancer Res.* **1997**, *88*, 523–526. [[CrossRef](#)]
126. Ushida, Y.; Sekine, K.; Kuhara, T.; Takasuka, N.; Iigo, M.; Maeda, M.H.; Tsuda, H. Possible chemopreventive effects of bovine lactoferrin on esophagus and lung carcinogenesis in the rat. *Jpn. J. Cancer Res.* **1999**, *90*, 262–267. [[CrossRef](#)] [[PubMed](#)]
127. Tanaka, T.; Kawabata, K.; Kohno, H.; Honjo, S.; Murakami, M.; Ota, T.; Tsuda, H. Chemopreventive effect of bovine lactoferrin on 4-nitroquinoline 1-oxide-induced tongue carcinogenesis in male F344 rats. *Jpn. J. Cancer Res.* **2000**, *91*, 25–33. [[CrossRef](#)] [[PubMed](#)]
128. Norrby, K.; Mattsby-Baltzer, I.; Innocenti, M.; Tuneberg, S. Orally administered bovine lactoferrin systemically inhibits VEGF(165)-mediated angiogenesis in the rat. *Int. J. Cancer* **2001**, *91*, 236–240. [[CrossRef](#)] [[PubMed](#)]
129. Chandra Mohan, K.V.; Kumaraguruparan, R.; Prathiba, D.; Nagini, S. Modulation of xenobiotic-metabolizing enzymes and redox status during chemoprevention of hamster buccal carcinogenesis by bovine lactoferrin. *Nutrition* **2006**, *22*, 940–946. [[CrossRef](#)] [[PubMed](#)]
130. Shimamura, M.; Yamamoto, Y.; Ashino, H.; Oikawa, T.; Hazato, T.; Tsuda, H.; Iigo, M. Bovine lactoferrin inhibits tumor-induced angiogenesis. *Int. J. Cancer* **2004**, *111*, 111–116. [[CrossRef](#)] [[PubMed](#)]
131. Kuhara, T.; Iigo, M.; Itoh, T.; Ushida, Y.; Sekine, K.; Terada, N.; Okamura, H.; Tsuda, H. Orally administered lactoferrin exerts an antimetastatic effect and enhances production of IL-18 in the intestinal epithelium. *Nutr. Cancer* **2000**, *38*, 192–199. [[CrossRef](#)]
132. Iigo, M.; Shimamura, M.; Matsuda, E.; Fujita, K.I.; Nomoto, H.; Satoh, J.; Kojima, S.; Alexander, B.D.; Moore, M.A.; Tsuda, H. Orally administered bovine lactoferrin induces caspase-1 and interleukin-18 in the mouse intestinal mucosa: A possible explanation for inhibition of carcinogenesis and metastasis. *Cytokine* **2004**, *25*, 36–44. [[CrossRef](#)]
133. Fischer, R.; Debbabi, H.; Dubarry, M.; Boyaka, P.; Tomé, D. Regulation of physiological and pathological Th1 and Th2 responses by lactoferrin. *Biochem. Cell. Biol.* **2006**, *84*, 303–311. [[CrossRef](#)]
134. Iigo, M.; Alexander, D.B.; Long, N.; Xu, J.; Fukamachi, K.; Fukamachi, M.; Takase, M.; Tsuda, H. Anticarcinogenesis pathways activated by bovine lactoferrin in the murine small intestine. *Biochimie* **2009**, *91*, 86–101. [[CrossRef](#)]
135. Yoo, Y.C.; Watanabe, S.; Watanabe, R.; Hata, K.; Shimazaki, K.; Azuma, I. Bovine lactoferrin and Lactoferricin inhibit tumor metastasis in mice. *Adv. Exp. Med. Biol.* **1998**, *443*, 285–291. [[CrossRef](#)]
136. Iigo, M.; Kuhara, T.; Ushida, Y.; Sekine, K.; Moore, M.A.; Tsuda, H. Inhibitory effects of bovine lactoferrin on colon carcinoma 26 lung metastasis in mice. *Clin. Exp. Metastasis* **1999**, *17*, 35–40. [[CrossRef](#)]
137. Chea, C.; Miyauchi, M.; Inubushi, T.; Okamoto, K.; Haing, S.; Thao Nguyen, P.; Imanaka, H.; Takata, T. Bovine lactoferrin reverses programming of epithelial-to-mesenchymal transition to mesenchymal-to-epithelial transition in oral squamous cell carcinoma. *Biochem. Biophys. Res. Commun.* **2018**, *507*, 142–147. [[CrossRef](#)] [[PubMed](#)]
138. Mohammed, M.M.; Ramadan, G.; Zoheiry, M.K.; El-Beih, N.M. Antihepatocarcinogenic activity of whey protein concentrate and lactoferrin in diethylnitrosamine-treated male albino mice. *Environ. Toxicol.* **2019**, *34*, 1025–1033. [[CrossRef](#)]

139. Cutone, A.; Rosa, L.; Ianiro, G.; Lepanto, M.S.; Bonaccorsi di Patti, M.C.; Valenti, P.; Musci, G. Lactoferrin's anti-cancer properties: Safety, selectivity, and wide range of action. *Biomolecules* **2020**, *10*, 456. [[CrossRef](#)]
140. Roseanu, A.; Florian, P.E.; Moisei, M.; Sima, L.E.; Evans, R.W.; Trif, M. Liposomalization of lactoferrin enhanced its anti-tumoral effects on melanoma cells. *Biomaterials* **2010**, *23*, 485–492. [[CrossRef](#)]
141. Chen, H.; Qin, Y.; Zhang, Q.; Jiang, W.; Tang, L.; Liu, J.; He, Q. Lactoferrin modified doxorubicin-loaded procationic liposomes for the treatment of gliomas. *Eur. J. Pharm. Sci.* **2011**, *44*, 164–173. [[CrossRef](#)]
142. Chen, H.; Tang, L.; Qin, Y.; Yin, Y.; Tang, J.; Tang, W.; Sun, X.; Zhang, Z.; Liu, J.; He, Q. Lactoferrin-modified procationic liposomes as a novel drug carrier for brain delivery. *Eur. J. Pharm. Sci.* **2010**, *40*, 94–102. [[CrossRef](#)]
143. Kanwar, J.R.; Palmano, K.P.; Sun, X.; Kanwar, R.K.; Gupta, R.; Haggarty, N.; Rowan, A.; Ram, S.; Krissansen, G.W. 'Iron-saturated' lactoferrin is a potent natural adjuvant for augmenting cancer chemotherapy. *Immunol. Cell. Biol.* **2008**, *86*, 277–288. [[CrossRef](#)]
144. Kanwar, J.R.; Mahidhara, G.; Kanwar, R.K. Novel alginate-enclosed chitosan-calcium phosphate-loaded iron-saturated bovine lactoferrin nanocarriers for oral delivery in colon cancer therapy. *Nanomedicine (Lond)* **2012**, *7*, 1521–1550. [[CrossRef](#)]
145. Sabra, S.; Agwa, M.M. Lactoferrin, a unique molecule with diverse therapeutical and nanotechnological applications. *Int. J. Biol. Macromol.* **2020**. [[CrossRef](#)]
146. Pilvi, T.K.; Harala, S.; Korpela, R.; Mervaala, E.M. Effects of high-calcium diets with different whey proteins on weight loss and weight regain in high-fat-fed C57BL/6J mice. *Br. J. Nutr.* **2009**, *102*, 337–341. [[CrossRef](#)] [[PubMed](#)]
147. Morishita, S.; Ono, T.; Fujisaki, C.; Ishihara, Y.; Murakoshi, M.; Kato, H.; Hosokawa, M.; Miyashita, K.; Sugiyama, K.; Nishino, H. Bovine lactoferrin reduces visceral fat and liver triglycerides in ICR mice. *J. Oleo Sci.* **2013**, *62*, 97–103. [[CrossRef](#)] [[PubMed](#)]
148. Baothman, O.A.; Zamzami, M.A.; Taher, I.; Abubaker, J.; Abu-Farha, M. The role of Gut Microbiota in the development of obesity and Diabetes. *Lipids Health Dis.* **2016**, *15*, 108. [[CrossRef](#)]
149. Sun, J.; Ren, F.; Xiong, L.; Zhao, L.; Guo, H. Bovine lactoferrin suppresses high-fat diet induced obesity and modulates gut microbiota in C57BL/6J mice. *J. Funct. Foods* **2016**, *22*, 189–200. [[CrossRef](#)]
150. Shi, J.; Finckenberg, P.; Martonen, E.; Ahiroos-Lehmus, A.; Pilvi, T.; Korpela, R. Metabolic effects of lactoferrin during energy restriction and weight regain in diet-induced obese mice. *J. Funct. Foods* **2012**, *4*, 66–78. [[CrossRef](#)]
151. Xiong, L.; Ren, F.; Lv, J.; Zhang, H.; Guo, H. Lactoferrin attenuates high-fat diet-induced hepatic steatosis and lipid metabolic dysfunctions by suppressing hepatic lipogenesis and down-regulating inflammation in C57BL/6J mice. *Food Funct.* **2018**, *9*, 4328–4339. [[CrossRef](#)] [[PubMed](#)]
152. Min, Q.Q.; Qin, L.Q.; Sun, Z.Z.; Zuo, W.T.; Zhao, L.; Xu, J.Y. Effects of metformin combined with lactoferrin on lipid accumulation and metabolism in mice fed with high-fat diet. *Nutrients* **2018**, *10*, 1628. [[CrossRef](#)] [[PubMed](#)]
153. Ono, T.; Murakoshi, M.; Suzuki, N.; Iida, N.; Ohdera, M.; Iigo, M.; Yoshida, T.; Sugiyama, K.; Nishino, H. Potent antiobesity effect of enteric-coated lactoferrin: Decrease in visceral fat accumulation in Japanese men and women with abdominal obesity after 8-week administration of enteric-coated lactoferrin tablets. *Br. J. Nutr.* **2010**, *104*, 1688–1695. [[CrossRef](#)]
154. Nikonorov, A.A.; Skalnaya, M.G.; Tinkov, A.A.; Skalny, A.V. Mutual interaction between iron homeostasis and obesity pathogenesis. *J. Trace Elem. Med. Biol.* **2015**, *30*, 207–214. [[CrossRef](#)] [[PubMed](#)]
155. Lorget, F.; Clough, J.; Oliveira, M.; Dauray, M.C.; Sabokbar, A.; Offord, E. Lactoferrin reduces in vitro osteoclast differentiation and resorbing activity. *Biochem. Biophys. Res. Commun.* **2002**, *296*, 261–266. [[CrossRef](#)]
156. Cornish, J.; Callon, K.E.; Naot, D.; Palmano, K.P.; Banovic, T.; Bava, U.; Watson, M.; Lin, J.M.; Tong, P.C.; Chen, Q.; et al. Lactoferrin is a potent regulator of bone cell activity and increases bone formation in vivo. *Endocrinology* **2004**, *145*, 4366–4374. [[CrossRef](#)]
157. Cornish, J.; Naot, D. Lactoferrin as an effector molecule in the skeleton. *Biomaterials* **2010**, *23*, 425–430. [[CrossRef](#)]
158. Inubushi, T.; Kawazoe, A.; Miyachi, M.; Yanagisawa, S.; Subarnbhesaj, A.; Chanbora, C.; Ayuningtyas, N.F.; Ishikado, A.; Tanaka, E.; Takata, T.; et al. Lactoferrin inhibits infection-related osteoclastogenesis without interrupting compressive force-related osteoclastogenesis. *Arch. Oral Biol.* **2014**, *59*, 226–232. [[CrossRef](#)]
159. Cornish, J. Lactoferrin promotes bone growth. *Biomaterials* **2004**, *17*, 331–335. [[CrossRef](#)] [[PubMed](#)]

160. Guo, H.Y.; Jiang, L.; Ibrahim, S.A.; Zhang, L.; Zhang, H.; Zhang, M.; Ren, F.Z. Orally administered lactoferrin preserves bone mass and microarchitecture in ovariectomized rats. *J. Nutr.* **2009**, *139*, 958–964. [[CrossRef](#)] [[PubMed](#)]
161. Li, W.; Hu, J.; Ji, P.; Zhu, S.; Zhu, Y. Oral administration of bovine lactoferrin accelerates the healing of fracture in ovariectomized rats. *J. Bone Miner. Metab.* **2020**. [[CrossRef](#)] [[PubMed](#)]
162. Kawazoe, A.; Inubushi, T.; Miyauchi, M.; Ishikado, A.; Tanaka, E.; Tanne, K.; Takata, T. Orally administered liposomal lactoferrin inhibits inflammation-related bone breakdown without interrupting orthodontic tooth movement. *J. Periodontol.* **2013**, *84*, 1454–1462. [[CrossRef](#)] [[PubMed](#)]
163. Ishikado, A.; Uesaki, S.; Suido, H.; Nomura, Y.; Sumikawa, K.; Maeda, M.; Miyauchi, M.; Takata, T.; Makino, T. Human trial of liposomal lactoferrin supplementation for periodontal disease. *Biol. Pharm. Bull.* **2010**, *33*, 1758–1762. [[CrossRef](#)] [[PubMed](#)]
164. Inubushi, T.; Kosai, A.; Yanagisawa, S.; Chanbora, C.; Miyauchi, M.; Yamasaki, S.; Sugiyama, E.; Ishikado, A.; Makino, T.; Takata, T. Bovine lactoferrin enhances osteogenesis through Smad2/3 and p38 MAPK activation. *J. Oral Biosci.* **2020**, *62*, 147–154. [[CrossRef](#)]
165. Danjo, Y.; Lee, M.; Horimoto, K.; Hamano, T. Ocular surface damage and tear lactoferrin in dry eye syndrome. *Acta Ophthalmol. (Copenh.)* **1994**, *72*, 433–437. [[CrossRef](#)] [[PubMed](#)]
166. Kawashima, M.; Kawakita, T.; Inaba, T.; Okada, N.; Ito, M.; Shimmura, S.; Watanabe, M.; Shinmura, K.; Tsubota, K. Dietary lactoferrin alleviates age-related lacrimal gland dysfunction in mice. *PLoS ONE* **2012**, *7*, e33148. [[CrossRef](#)] [[PubMed](#)]
167. Dogru, M.; Matsumoto, Y.; Yamamoto, Y.; Goto, E.; Saiki, M.; Shimazaki, J.; Takebayashi, T.; Tsubota, K. Lactoferrin in Sjögren’s syndrome. *Ophthalmology* **2007**, *114*, 2366–2367. [[CrossRef](#)] [[PubMed](#)]
168. Cardoso, A.L.; Fernandes, A.; Aguilar-Pimentel, J.A.; de Angelis, M.H.; Guedes, J.R.; Brito, M.A.; Ortolano, S.; Pani, G.; Athanasopoulou, S.; Gonos, E.S.; et al. Towards frailty biomarkers: Candidates from genes and pathways regulated in aging and age-related diseases. *Ageing Res. Rev.* **2018**, *47*, 214–277. [[CrossRef](#)]
169. Medina, I.; Tombo, I.; Satué-Gracia, M.T.; German, J.B.; Frankel, E.N. Effects of natural phenolic compounds on the antioxidant activity of lactoferrin in liposomes and oil-in-water emulsions. *J. Agric. Food Chem.* **2002**, *50*, 2392–2399. [[CrossRef](#)]
170. Duran, A.; Kahve, H.I. The use of lactoferrin in food industry. *Acad. J. Sci.* **2017**, *7*, 89–94.



© 2020 by the author. Licensee MDPI, Basel, Switzerland. This article is an open access article distributed under the terms and conditions of the Creative Commons Attribution (CC BY) license (<http://creativecommons.org/licenses/by/4.0/>).

Review

Abscisic Acid: A Conserved Hormone in Plants and Humans and a Promising Aid to Combat Prediabetes and the Metabolic Syndrome

Mirko Magnone ^{1,2,*}, Laura Sturla ², Lucrezia Guida ², Sonia Spinelli ², Giulia Begani ²,
Santina Bruzzone ², Chiara Fresia ³ and Elena Zocchi ^{2,*}

¹ Nutravis S.r.l., Via Corsica 2/19, 16128 Genova, Italy

² Department of Experimental Medicine, University of Genova, 16132 Genova, Italy; laurasturla@unige.it (L.S.); l.guida@unige.it (L.G.); sonia.spinelli94@libero.it (S.S.); giulia.begani@gmail.com (G.B.); santina.bruzzone@unige.it (S.B.)

³ Molecular and Cell Biology Laboratory, Salk Institute for Biological Studies, 10010 N Torrey Pines Rd, La Jolla, CA 92037, USA; chiara.fresia.8@gmail.com

* Correspondence: m.magnone@nutravis.it (M.M.); ezocchi@unige.it (E.Z.);
Tel.: +39-10-3538131 (M.M.); +39-10-3538161 (E.Z.)

Received: 11 May 2020; Accepted: 3 June 2020; Published: 9 June 2020

Abstract: Abscisic acid (ABA) is a hormone with a very long evolutionary history, dating back to the earliest living organisms, of which modern (ABA-producing) cyanobacteria are likely the descendants, well before separation of the plant and animal kingdoms, with a conserved role as a signal regulating cell responses to environmental challenges. In mammals, nanomolar ABA controls the metabolic response to glucose availability by stimulating glucose uptake in skeletal muscle and adipose tissue with an insulin-independent mechanism and increasing energy expenditure in the brown and white adipose tissues. Activation by ABA of AMP-dependent kinase (AMPK), in contrast to the insulin-induced activation of AMPK-inhibiting Akt, is responsible for stimulation of GLUT4-mediated muscle glucose uptake, and for the browning effect on white adipocytes. Intake of micrograms per Kg body weight of ABA improves glucose tolerance in both normal and in borderline subjects and chronic intake of such a dose of ABA improves blood glucose, lipids and morphometric parameters (waist circumference and body mass index) in borderline subjects for prediabetes and the metabolic syndrome. This review summarizes the most recent results obtained in vivo with microgram amounts of ABA, the role of the receptor LINC8 in the hormone's action and the significance of the endowment by mammals of two different hormones controlling the metabolic response to glucose availability. Finally, open issues in need of further investigation and perspectives for the clinical use of nutraceutical ABA are discussed.

Keywords: abscisic acid; prediabetes; type 2 diabetes mellitus; metabolic syndrome; insulin resistance; adipocyte browning; AMP-activated protein kinase; food supplement

1. Introduction

1.1. Abscisic Acid (ABA), A Stress Hormone in Plants and Animals

2-cis, 4-trans-Abscisic acid (ABA) is a 15-carbon weak acid (pKa 4.8) terpenoid hormone (Figure 1) that regulates several pivotal physiological functions in plants, mainly involved in the response to abiotic and biotic stress (water and nutrient availability, UV irradiation; pathogen attack) [1].

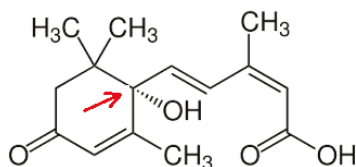


Figure 1. Structure of ABA. 2-cis, 4-trans-Abscisic acid has an asymmetric carbon atom (arrow) generating two enantiomers S-(+)-ABA and R-(-)-ABA. (+)-ABA is the naturally-occurring form in plants, although (-)-ABA is active in some vegetal functional assays [2].

The function of ABA as a stress signal and its signaling pathway are conserved in all plants, including mosses, and are believed to be the result of the very early adaptation of life to the terrestrial environment. Although the study of ABA in plants has been ongoing for several decades, also in view of its industrial application to improve stress tolerance in crops, it is only in the past decade that evidence has mounted regarding the presence and physiological significance of ABA also in animals. Le Page-Degivry et al. first described the presence of ABA in mammalian tissues, particularly brain [3], but their interesting observation remained isolated. Our group became interested in ABA in our quest for the animal hormonal signal upstream of the second messenger cyclic ADP-ribose (cADPR), a universal Ca^{2+} mobilizer from intracellular stores that had been discovered to be involved in insulin release [4]. Intracellular Ca^{2+} movements are arguably the most ancient and conserved signaling mechanism throughout the animal and plant kingdoms. Indeed, cADPR had been reported to mediate the effect of ABA in guard cells [5]. Thus, we hypothesized a role for ABA as an animal, as well as a plant hormone, and started our investigation on the simplest and most ancient Metazoa, marine sponges and hydroids; the physiological functions of these animals are limited to water filtration and respiration. However, being sessile, they are particularly exposed to environmental stress (e.g., changes in water temperature or light exposure). We discovered that temperature and light stimulated ABA production in sponges and hydroids, respectively, and that ABA stimulated specific functional responses to these environmental challenges (an increase in water filtration and oxygen consumption in sponges, tissue regeneration in hydroids). These functional responses were mediated by a signaling pathway sequentially involving cAMP, PKA, cADPR and intracellular Ca^{2+} movements [6–8]. These discoveries warranted further investigations into the role of ABA in cell-specific functions of higher Metazoa.

1.2. Micromolar ABA Has Pro-Inflammatory and Insulin-Releasing Activity In Vitro and In Vivo

In several different innate immune cell types exogenous ABA elicits pro-inflammatory functional responses and endogenous ABA is released when cells are challenged with environmental (physical, chemical) stimuli. Briefly, human granulocytes release ABA in response to heat stress or phorbol myristate acetate and exogenous micromolar ABA stimulates cell migration, phagocytosis, ROS and NO production [9]. ABA is released by rat alveolar macrophages stimulated with quartz particles and exogenous micromolar ABA induces the release of pro-inflammatory PGE2 and TNF- α [10]. Micromolar ABA stimulates NO and TNF- α production and cell migration of the mouse microglial cell line N9 and endogenous ABA is released when cells are challenged with bacterial lipopolysaccharide, phorbol myristate acetate, the chemoattractant peptide f-MLP, or β -amyloid [11]. Thus, a plethora of data suggest that ABA in the micromolar concentration range has pro-inflammatory effects on mammalian innate immune cells: a conserved signaling pathway involves the activation of the ADP-ribosyl cyclase CD38 and the production of the Ca^{2+} -mobilizing second messenger cADPR. Starting from the observation that cADPR was involved in the Ca^{2+} signaling leading to insulin release, the effect of ABA on β -pancreatic cells was explored. Indeed, micromolar ABA stimulated insulin release in vitro, from rat insulinoma cells and from isolated human islets [12], and also in vivo, in the perfused rat pancreas [13]. In the in vitro study, the role of cADPR as the second messenger of ABA was confirmed, similarly to what observed on innate immune cells.

1.3. ABA Is an Endogenous Mammalian Hormone: Nanomolar ABA Peaks in Human Plasma after Glucose Load

The studies described above provided ample demonstration that ABA exerts cell-specific functional effects on mammalian cells through the Ca^{2+} -mobilizing second messenger cADPR. However, a clear indication that ABA is indeed an endogenous animal hormone was still missing. In their study, Le Page-Degivry et al. observed that ABA was present in the brain of mice fed a synthetic, ABA-free diet at even higher concentrations compared with mice fed a normal (ABA-containing) chow, arguing in favor of the endogenous origin of ABA [3]. A credible indication that ABA is indeed an endogenous animal hormone came from the observation that plasma ABA increases after a glucose load in normal human subjects, reaching concentrations in the low nanomolar range [14]. Moreover, in the same study, the authors showed that nanomolar ABA stimulated glucose uptake, quantitatively similarly to insulin, in rat L6 myoblasts and in murine 3T3-L1 cells differentiated to adipocytes, by increasing GLUT-4 translocation to the plasma membrane. This study provided the first evidence that endogenous ABA could be involved in glycemia homeostasis at hormone-like concentrations.

1.4. ABA Reduces Glycemia without Increasing Insulinemia

The observations that nanomolar ABA stimulates glucose transport in myocytes and adipocytes in vitro and that endogenous nanomolar ABA increases in the blood of normal subjects after glucose load suggested a role for endogenous ABA in the control of glycemia. Insulin and GLP-1 are the only two peptide hormones known so far to stimulate tissue glucose uptake under conditions of hyperglycemia, and GLP-1 acts by stimulating insulin release. Thus, insulin represents a sort of bottleneck in the response to high blood glucose, apparently a weak spot in glycemia control and a conspicuous example contrary to the principle of redundancy that governs most (if not all) biochemical mechanisms fundamental for cell and organism survival. These considerations suggested to explore the possibility that the effect of ABA on tissue glucose uptake could occur independently of insulin. Several experiments were performed in vivo and ex vivo to address this issue.

In a study performed on rats, the animals were administered an oral glucose load without (control) or with synthetic ABA (at a dose of 1 $\mu\text{g}/\text{Kg}$ body weight), or with an aqueous fruit extract yielding the same dose of ABA. The animals receiving the extract and those treated with synthetic ABA showed similar and significantly lower values of the area under the curve (AUC) of the glycemia and insulinemia profiles compared with the control group, suggesting that the active molecule present in the extract and responsible for the observed metabolic effects was indeed ABA [15]. The same fruit extract, providing a dose of approximately 0.5 $\mu\text{g}/\text{Kg}$ body weight, was also tested on human volunteers as an adjunct to carbohydrate-rich meals (breakfast and lunch): a significant reduction of the AUC of glycemia and of insulinemia was observed in each subject when the meals were taken with the extract compared with the same meals taken without extract [15]. The plasma ABA concentration measured after intake of the extract in humans increased significantly compared with basal (fasting) values for several hours, but remained in the nanomolar range. The sparing effect on insulinemia of ABA at a dose of 0.5–1 $\mu\text{g}/\text{Kg}$ was unexpected, since micromolar ABA had been reported to stimulate insulin release from human β -pancreatic cells and from rat insulinoma cells in vitro [12]. Indeed, when rats were subjected to an OGTT with synthetic ABA at 100 mg/Kg , the AUC of insulinemia was not reduced compared with controls, indicating that at this pharmacological dose ABA did not spare insulin release, although it reduced glycemia [15], in line with previously reported results obtained on mice [16].

The most convincing evidence of the insulin-independent activity of ABA on glycemia control was derived in ex vivo experiments: in mouse skeletal muscle samples taken from fasted animals uptake of ^{18}F -deoxyglucose (FDG) increased two-fold in the presence of nanomolar ABA compared with untreated controls [17]. Stimulation by nanomolar ABA of muscle glucose uptake was confirmed in vivo, on rats undergoing an oral glucose load; as detected by micro-PET, animals receiving a dose of

1 µg/Kg ABA with the glucose load showed a two-fold increase of FDG uptake in skeletal muscle and consequently a significantly reduced glycemia profile after glucose load [17].

A reduction of plasma insulin levels in response to a carbohydrate load would be desirable since insulin stimulates the conversion of glucose into triglycerides in the adipose tissue. Indeed, hyperinsulinemia, either endogenously produced as a result of reduced insulin sensitivity, or exogenously administered as an anti-diabetic drug, is a major factor contributing to an increase in body weight and hepatic steatosis in the pre-diabetic and diabetic patient [18]. Could (endogenous) ABA be a safeguard against excess insulin release?

An indication that ABA can substitute in part for insulin comes from studies on insulin-deficient mice. Administration of 1 µg/Kg ABA together with an oral glucose load reduced the AUC of glycemia in wild-type and also in TRPM2^{-/-} mice [17], which have a significantly reduced insulin secretion in response to glucose [19]. The AUC of insulin during the OGTT with ABA was also significantly reduced in the TRPM2^{-/-} animals, as in the wild-type mice, compared with the respective OGTT without ABA [17], indicating that the effect of ABA was independent of insulin in both genotypes. Finally, the daily intake of 1 µg/Kg ABA increased muscle glycogen content in TRPM2^{-/-} mice fed a high-glucose diet similarly to what observed in wild-type animals, indicating that ABA stimulated muscle glucose uptake also in insulin-deficient animals.

1.5. ABA Improves Lipidemia and Reduces Body Weight and Cardiovascular Risk in Borderline Subjects

In a recently published human study, the daily intake of a food supplement containing a vegetal extract titrated in ABA in its composition GSECM-50[®], sufficient to yield a dose of ABA of approximately 1 µg/Kg body weight, for 75 days significantly improved the metabolic (fasting glycemia, glycated hemoglobin, total, LDL and HDL cholesterol) and morphometric parameters (waist circumference and body mass index) currently employed to evaluate the risk for metabolic syndrome and diabetes. At the end of treatment, fasting blood glucose, glycated hemoglobin, total, LDL and HDL cholesterol, body mass index and waist circumference had significantly improved compared to values at time zero, particularly in those subjects with starting borderline values. The Framingham point score and the 10-year percentage risk calculated for each subject before and at the end of treatment were both significantly reduced in all subjects. In the same study, the daily intake of the same dose of synthetic ABA for four months improved glucose tolerance, and reduced glycated hemoglobin, blood lipids and body weight in mice fed a high-glucose diet [20]. The human and murine parts of the study, taken together, allow to conclude that the improvement of metabolic and bodily parameters observed in the clinical study, performed with the food supplement, can be attributed to ABA present in the vegetal extract of the composition, because similar results were observed on mice fed the synthetic, pure molecule. In addition, mice have certainly not changed their feeding behavior during the study, allowing to rule out this possibility as an explanation for the improvement of the parameters investigated in both studies.

In another set of experiments, the effect of a single dose of the same ABA-containing food supplement used in the chronic study was tested on the glycemia profile after intake of a standardized carbohydrate-rich breakfast. A significant reduction of the mean glycemia profile and of the mean AUC of glycemia (measured over 120 min) was observed in each subject when breakfast was taken with the food supplement compared with the same breakfast taken without supplement [20]. Intake of the ABA-rich food supplement significantly increased ABAP 5- to 16-fold over fasting levels (5–15 nM), indicating that oral ABA was readily absorbed and contributed to increase endogenous ABAP [20].

A similar significant reduction of the AUC of glycemia as observed with the formulated food supplement was observed when the same standardized carbohydrate-rich breakfast was taken with the ABA-containing vegetal extract alone (ABAMET[®]), indicating that the active ingredient of the food supplement was indeed the ABA-containing vegetal extract (Figure 2).

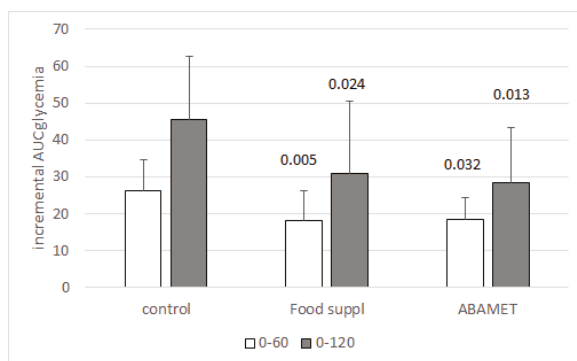


Figure 2. The active ingredient of the food supplement is the ABA-containing vegetal extract. Six volunteers introduced a standardized carbohydrate-rich breakfast, one without any supplement (control), one with one tablet of the formulated food supplement (Food suppl) and another taking only the amount of vegetal extract (ABAMET[®]) present in one tablet of the food supplement. The three experiments were performed one week apart. The food supplement or ABAMET[®] were taken before the meal [20] Mean \pm SD values of the incremental AUC of glycemia in the time frames 0–60 and 0–120 min are shown. *p* values by paired, two-tailed *t*-test of the comparison between each bar with the respective control bar are shown.

A daily dose of 0.5–1 μg ABA/Kg body weight, sufficient to improve glucose tolerance in humans in the nanomolar range, is approximately 1 log higher than the amount of hormone that can be ingested daily with a fruit- and vegetable-rich diet [15]. The nutraceutical composition GSECM-50[®] containing the ABA-rich vegetal extract ABAMET[®] can provide the optimal daily dose of ABA sufficient to increase endogenous ABAp levels to the extent producing a beneficial effect on human metabolism [20].

1.6. ABA Stimulates White Adipocyte Browning and BAT Activity

The reduction in body weight in the face of unchanged dietary habits observed in humans and mice treated with low-dose ABA could be attributed to the sparing effect of ABA on insulin release; however, adipose tissue also seems to be a direct target of ABA, along with skeletal muscle, as suggested by *in vitro* and *in vivo* studies. Unlike insulin, ABA does not induce preadipocyte differentiation into triglyceride-rich adipocytes *in vitro*; instead, treatment with ABA induces adipocyte remodeling in differentiated cells, reducing cell size and increasing mitochondrial content, O₂ consumption and expression of the brown adipocyte-specific genes UCP-1, PGC-1 α , TMEM26, PRDM16 and CIDE-A. *In vivo*, a single oral dose of ABA 1 $\mu\text{g}/\text{Kg}$ increased BAT glucose uptake 2-fold in rats, as detected by micro-PET, and treatment of mice for 30 days with the same dose significantly increased expression of BAT genes in the WAT and in WAT-derived preadipocytes, isolated from the treated animals [21]. Mitochondrial DNA increased 20-fold in the WAT from ABA-treated mice compared with untreated controls and expression of UCP-1 in the BAT was also significantly higher in ABA-treated as compared with control animals [21]. Thus, oral low-dose ABA stimulates BAT activity and induces browning features in the WAT of chronically treated mice. These actions of ABA on AT could be responsible for the observed reduction of body weight in chronically ABA-treated mice compared with controls: female C57Bl/6 mice fed a high-fat diet and treated with ABA (1 $\mu\text{g}/\text{Kg}$ body weight/day) for 12 weeks showed a significantly lower weight gain compared with untreated controls, in the face of a higher food intake in the ABA-treated animals: the body weight relative to time zero was 1.30 ± 0.1 vs. 1.53 ± 0.1 in ABA-treated vs. untreated animals ($n = 5$; $p < 0.01$ by two-tailed, unpaired *t* test); the daily food intake during the period of observation was 2.7 ± 0.2 vs. 2.4 ± 0.2 g/animal/day in ABA-treated vs. untreated animals ($n = 5$; $p < 0.01$ by two-tailed, unpaired *t* test) (Magnone M. unpublished result).

1.7. The Plasma ABA Response to A Glucose Load Is Impaired in T2D and in GDM

Plasma ABA increases in normal human subjects after an oral glucose load [14], but not in patients with type 2 diabetes mellitus (T2D) nor in pregnant women with gestational diabetes mellitus (GDM). Resolution of GDM one month after childbirth coincides with a restoration of the normal ABAP response to glucose load [22].

Interestingly, a significant increase of ABAP relative to pre-surgical values was observed in obese patients one month after bilio-pancreatic diversion (BPD), a type of bariatric surgery performed to reduce body mass and improve glucose tolerance [22]. The increase of fasting ABAP was observed both in normal glucose tolerant (NGT) and in T2D obese subjects, in parallel with a reduction of fasting blood glucose and a significant decrease of the HOMA-IR and fasting insulinemia in the diabetic subjects [22]. Another difference observed between T2D and NGT subjects regarded the fasting ABAP levels, which were significantly higher in T2D compared with NGT subjects; the respective median values were 1.15 (0.19–4.77) vs. 0.66 (0.13–1.72) ($n = 21$ T2D and 27 NGT; $p = 0.013$ by Mann–Whitney test). Moreover, the distribution of the ABAP values was normal in NGT, but not in T2D subjects [22]. These abnormalities may be caused by a heterogeneity of ABA-related dysfunctions occurring in T2D, such as resistance to the effect of ABA (inducing an increase of ABAP, as occurs with insulin in insulin-resistant subjects), or the inability of ABAP to increase in response to hyperglycemia (causing ABAP levels to be in the normal range despite hyperglycemia).

Collectively, these observations on diabetic patients suggest a role for ABAP dysfunction in the development of glucose intolerance and obesity and a beneficial effect of elevated ABAP on glycemic control; indeed, one can expect that insufficiency of either one of the hormones regulating tissue glucose uptake and its metabolic disposal (insulin and ABA) should negatively affect glycemia control.

1.8. The ABA Signaling Pathway Is Different from That of Insulin

Conservation of ABA between plant and animal kingdoms suggested to explore whether the ABA receptor could be also conserved. Among the several receptors identified in different plant tissues, a putative G-protein coupled receptor (GCR2) [23] indeed showed a significant amino acid sequence identity with a mammalian family of proteins, the lanthionine synthetase C-like protein (LANCL) family. GCR2 has since been disputed as a G protein-coupled receptor, and its homology with the bacterial lanthionine synthetase protein superfamily has instead been advocated [24], a homology that also pertains to the mammalian LANCL proteins. Although the current general consensus is that the PYR/PYL/RCAR family of intracellular receptors are the principal ABA receptors in land plants [25], the homology between mammalian LANCL proteins and plant GCR2 suggested to explore the possibility that they were implicated in ABA sensing. A role for the LANCL protein family in lanthionine biosynthesis has since been ruled out [26]. The LANCL family comprises three proteins: LANCL1 is the most highly expressed in mammals, particularly in the brain, and is a cytosolic protein, LANCL2 is membrane-anchored through its myristoylated N-terminal [27] and LANCL3 has the lowest expression levels of the LANCL proteins and appears to be cytosolic. The membrane-bound location of LANCL2 first attracted interest in this protein as a putative mammalian ABA receptor; indeed, several *in vitro* studies indicate that human recombinant LANCL2 binds ABA with a high affinity (Kd 2.6 nM) [28,29] and is required for ABA action in several different mammalian cell types [30]. LANCL2 has an unusual behavior as a hormone receptor as it is coupled to a G protein when membrane bound, but can also detach from the membrane when de-myristoylated and accumulate in the cell nucleus [27]. Indeed, the nuclear translocation of LANCL2 occurs following ABA binding [31]. This behavior appears to combine features typical of the receptors for peptide (G protein coupling) and for steroid hormones (nuclear translocation), perhaps a heritage of the primordial origin of the hormone, or the result of the solubility features of ABA.

ABA is a weak acid ($pK_a = 4.8$). Protonated ABA can diffuse through the lipid bilayer [32]; however, a very low percentage of ABA is protonated at the near-neutral pH of plasma and interstitial liquid. For this reason, the presence of a transport system is essential for ABA trafficking between

extra- and intracellular fluids. Conversely, the strongly acidic pH present in the stomach probably allows the diffusion of protonated ABA through the gastric lipid bilayer, accounting for the rapid absorption of the hormone after oral intake [15].

Binding of ABA to LANCL2 bound to the inner plasma membrane layer requires influx of the hormone through the plasma membrane, which occurs through transporters of the anion exchanger (AE) superfamily [33].

The signaling pathway downstream of LANCL2 has been studied in the target cells of the immune (monocytes, macrophages and T lymphocytes) [34], and of the metabolic actions of the hormone (adipocytes and muscle cells) [17,21]. In innate immune cells, ABA binding to its receptor leads to the activation of adenylate cyclase and the subsequent phosphorylation and activation of the ADP-ribosyl cyclase CD38 by protein kinase A (PKA). The product of the enzyme action of CD38 on its substrate NAD⁺, cADPR, then triggers an intracellular Ca²⁺ rise due to both intracellular Ca²⁺ release from ryanodine-sensitive endoplasmic Ca²⁺ channels and to extracellular Ca²⁺ influx due to ADPR-gated plasma membrane Ca²⁺ channels [9]. This sequence of events closely parallels the ABA signaling pathway first described in marine sponges [6]. The transcriptional effects of ABA observed on hemopoietic progenitors are also likely mediated by the observed increase of intracellular cAMP and the consequent activation of the cAMP-responsive transcription factor CREB [35]. A role for NFκB in the micromolar ABA-induced activation of the transcription of cyclooxygenase-2 has also been observed in quartz-stimulated rat alveolar macrophages [10], again pointing to intracellular Ca²⁺ movements as an important feature of the ABA signaling pathway in inflammatory cells. The effect of ABA on cells of the hemopoietic lineage (progenitors and innate immune cells) occurs at low micromolar concentrations, thus it is possible that a different signaling pathway is activated by the low nanomolar concentrations exerting its metabolic actions. The signaling pathway downstream of LANCL2 in macrophages and Treg was studied in silico by Leber et al., suggesting a role for LANCL2 in the induction of regulatory responses in macrophages and T cells during *H. pylori* infection [36].

In adipocytes, stimulation by ABA of glucose uptake via GLUT4 involves the activation of phosphoinositide 3-kinases (PI3K). Interestingly, the N-terminal sequence of LANCL2 has been shown to bind to phosphatidylinositol phosphates (PIPs), particularly PI3P, on the plasma membrane, suggesting a spatial as well as functional correlation between LANCL2-dependent and PI3P-mediated signaling. In muscle cells, AMP-activated protein kinase (AMPK) appears to mediate the nanomolar ABA-induced increase of glucose transport, since the effect of ABA is abrogated by pre-treatment of cultured myocytes and of murine muscle biopsies with the AMPK inhibitor dorsomorphin [17]. Activation of AMPK in the ABA-signaling pathway is in sharp contrast with the signal transduction activated by insulin, which results in the inactivation of AMPK by Akt/PKB-mediated phosphorylation.

Indeed, the effect of ABA on energy metabolism appears to be different from that of insulin, pointing to non-overlapping physiological functions of these hormones.

Glucose intake induces an increase of ABAP and one could hypothesize that this hormone provides the first response to nutrient availability, stimulating muscle glucose uptake and thermogenic energy expenditure. Persistence of hyperglycemia, despite the action of ABA and in excess of muscle energy requirement, then results in insulin release and in the activation of the metabolic responses to nutrient abundance (glycogen and fatty acid synthesis, adipocyte differentiation and accumulation of triglycerides) (Figure 3). Interestingly, in 3T3-L1-derived murine adipocytes the siRNA-mediated downregulation of LANCL2 expression reduces both the ABA- and insulin-induced glucose uptake and downregulates Akt phosphorylation after insulin treatment [21], suggesting that levels of LANCL2 expression in adipocytes could affect insulin sensitivity.

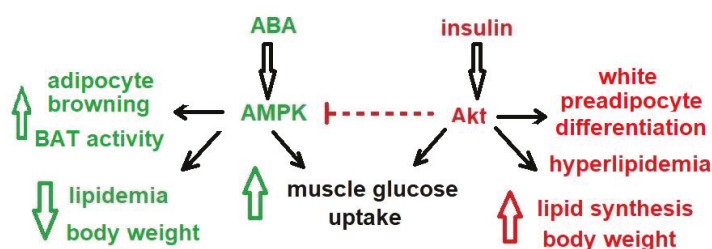


Figure 3. Non-overlapping roles of ABA and insulin in the regulation of energy metabolism. Insulin, via the kinase Akt, stimulates glucose uptake in skeletal muscle and white adipose tissue (WAT), triglyceride synthesis in adipocytes, preadipocyte differentiation into WAT and increased hepatic triglyceride synthesis and lipoprotein export into the blood. Nanomolar ABA, via the AMP-dependent protein kinase (AMPK), stimulates muscle glucose uptake similarly to insulin, but the effect on adipose tissue is different. ABA does not induce preadipocytes differentiation; instead, it stimulates the expression of browning genes in the WAT and increases glucose uptake and mitochondrial uncoupling in brown adipose tissue (BAT). The effect of insulin and of ABA on body weight (BW) is opposite, with insulin inducing an increase and ABA instead favoring a decrease. The relative plasma concentrations of these hormones is likely to affect BW homeostasis and energy metabolism. Via Akt, insulin inhibits AMPK and the metabolic responses to low cell energy levels.

Activation by ABA of the transcription and phosphorylation of AMPK opens new perspectives on the signaling pathways activated by the hormone. AMPK phosphorylates and inhibits the transcriptional activity of PPAR- γ , the master regulator of adipogenesis, thereby preventing the differentiation of preadipocytes [37] and triglyceride accumulation [38]. AMPK is also an upstream positive regulator of p38 MAPK [39], which promotes PPAR- γ phosphorylation on Ser122, thus preventing PPAR- γ mediated inhibition of GLUT4 expression [40]. The partial suppression of the transcriptional activity of PPAR- γ in heterozygous PPAR- γ -deficient mice results in an improved insulin sensitivity and in a reduced tendency to obesity [41,42] and mice chimeric for wild-type and PPAR- γ null cells exhibit little or no contribution to adipose tissue formation by null cells [43]. The observations that low-dose ABA significantly reduces body weight in mice fed a high-glucose diet and in humans [20] and improves muscle glucose uptake are in agreement with the activation of AMPK in adipocytes and muscle cells.

1.9. LANCL2 Is Not the Only Mammalian ABA Receptor

The role of LANCL2 in mediating the stimulatory effect of ABA on innate immune cell function and on energy metabolism appears to be somewhat different.

Unlike inflammatory cells, where LANCL2 silencing abrogates the response to ABA [30] in adipocytes and muscle cells, silencing of LANCL2 reduces, but does not eliminate, the effect of ABA [14,17], suggesting a role for other receptors in the metabolic action of the hormone. A more direct indication that other receptors could contribute to mediate the metabolic actions of ABA comes from studies on LANCL2 knock-out mice. Indeed, in C57Bl/6 mice, the genetic ablation of LANCL2 did not modify fasting glycemia values but resulted in the reduction of glucose tolerance compared with wild-type siblings, as indicated by a significantly increased AUC of glycemia after an oral glucose load; however, LANCL2^{-/-} mice were still responsive to exogenous ABA, which significantly reduced the AUC of glycemia after glucose load, to values similar to those of wild-type animals (Figure 4) (Magnone M., unpublished results).

This result clearly indicates that the genetic ablation of LANCL2 negatively affects glucose tolerance. The fact that exogenous low-dose ABA (1 $\mu\text{g}/\text{Kg}$ body weight) improved glucose tolerance in LANCL2^{-/-} mice suggests that another receptor can substitute for LANCL2 in the stimulation of muscle and AT glucose transport, although at higher ABA concentrations than those reached by

the endogenous hormone (Magnone M., unpublished results). Indeed, intake of ABA at a dose of 1 µg/Kg body weight increases ABAP between 10 and 50 times compared to basal, endogenous levels in humans [15]. These high plasma concentrations, obtained by pharmacologic intervention, could activate a low-affinity receptor not normally participating in endogenous ABA signaling.

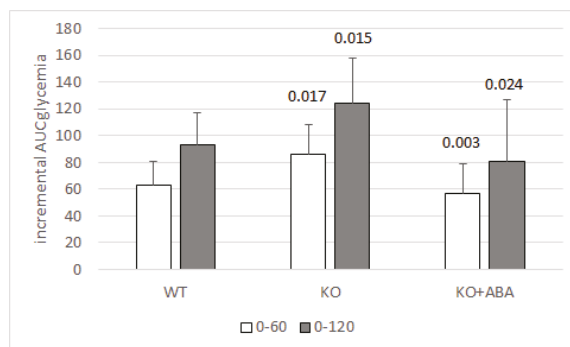


Figure 4. LANCL2^{-/-} mice have a reduced glucose tolerance, but respond to ABA. Eight-hour fasted, male LANCL2^{-/-} (KO) and wild-type (WT) mice (6/group) were subjected to OGTT (2 g glucose/Kg body weight) without or with ABA (1 µg/Kg body weight). Glycemia was measured before gavage (time zero) and at 30, 60 and 120 min thereafter. The incremental AUC of glycemia was calculated in the time frames 0–60 and 0–120 min by the trapezoidal rule on values relative to time zero. *p* values by two-tailed unpaired *t*-test (KO vs. WT) or by two-tailed paired *t*-test (KO + ABA vs. KO). The genetic ablation of LANCL2 in KO mice was confirmed by genotyping. Absence of LANCL2 protein expression in skeletal muscle, liver, WAT and BAT of KO mice was confirmed by Western blot (not shown), (Magnone M., unpublished results).

The identity of this receptor remains to be determined; however, the high sequence identity (54%) between LANCL2 and LANCL1 is highly suggestive of a role for LANCL1 as a second ABA receptor, in addition to LANCL2. These results suggest a redundancy in ABA-sensing molecules in mammals too, as occurs in plants, which could be expected given the strategic role of the hormone in the response to nutrients. Nonetheless, absence of LANCL2 negatively affects glucose tolerance in mice, indicating that the other ABA receptor(s) do not wholly substitute for this protein. Further studies are definitely needed to deepen our understanding of the physiology of mammalian ABA receptors, their tissue distribution and affinity for the hormone.

He et al. published a study on the triple knock out of LANCL1-2-3 in mice, demonstrating that these proteins are not involved in the synthesis of lanthionine, which conversely could have been hypothesized based on their homology with bacterial LanC enzymes. It would be informative to compare glucose tolerance and insulin sensitivity on the LANCL2 KO and on the double (LANCL1 + 2) KO [26].

2. Conclusions and Future Perspectives

In this review, we focused our attention on the metabolic function of the ABA/LANCL2 system on glycemic and lipidemic control, neglecting other important aspects of ABA physiology in mammals, such as its regulatory role in inflammation, for which we redirect the reader to the excellent review by Lievens et al. [44].

The results summarized in this review allow to draw some conclusions, but also provide the starting point for future investigations, both clinical and preclinical.

The significant beneficial effect of micrograms of oral ABA observed in volunteers with metabolic and morphometric parameters borderline with the metabolic syndrome allows to forecast similar positive results in trials of the ABA-containing nutraceutical on a higher number of prediabetic subjects

and of subjects with the metabolic syndrome. The primary outcomes of this study would be the improvement of glucose and lipid tolerance and the reduction of body weight.

In addition, studies on murine model(s) of insulin-dependent diabetes could provide preclinical evidence supporting the use of oral low-dose ABA to improve glycemia control in combination with insulin. This result in turn would warrant clinical studies aimed at confirming whether ABA-containing nutraceuticals could represent an adjunctive therapy in insulin-dependent diabetic patients (both T1D and T2D), improving the daily glycemia profile, reducing blood lipids and contributing to the control of body weight by reducing the amount of insulin required for glycemic control.

The physiology and possible dysfunction of LANCL2 and of other ABA receptors still to be identified is another important area of research. Do LANCL2 mutations or constitutively low expression levels, particularly in skeletal muscle, predispose to “ABA resistance” and to diabetes? In this case, intake of the ABA-containing nutraceutical would provide the amount of ABA sufficient to increase ABAP 5- to 10-fold over endogenous levels, overtaking ABA resistance.

Another issue requiring further study is the identity of the ABA-producing cells in mammals. Results obtained on T1D patients seem to indicate that β -pancreatic cells are the main ABA producers, since ABAP is reduced by approximately 90% compared to values measured in healthy controls. In addition, rat insulinoma cells and human pancreatic islets release ABA after stimulation with GLP-1 [14]. In mice, a very high ABA concentration has been measured in the BAT, but not in the WAT, suggesting that BAT could be another source of endogenous ABA in mammals. The identification of the main ABA-releasing cells in humans is relevant to understand which physiological stimuli induce an ABA response in humans. In particular, if β -pancreatic cells were indeed the main ABA producers, the demise of these cells in T1D would compromise secretion of both hormones regulating glycemia, insulin and ABA, of which only one is currently replaced by therapy.

Finally, a field of exploration on mammalian ABA physiology which lies at the crossroad between metabolism and inflammation is the role of ABA in the central nervous system. The fact that brain has the highest ABA content among the various tissues, as first reported by Le Page-Degivry et al. [3], raises the possibility that ABA is produced and acts locally in the brain. ABA administration improves neuroinflammation and cognitive impairment and anxiety in rodents [45,46]. Interestingly, phaseic acid, the principal ABA metabolite in plants, is apparently endogenously produced in the brain and protects from ischemic injury by acting as a non-competitive inhibitor of glutamate receptors [47].

Author Contributions: M.M. and E.Z. wrote the review and performed the experiments on the LANCL2 KO mice; C.F. generated the LANCL2 KO mouse strain; L.S., G.B., S.S., S.B. and L.G. contributed to performing the experiments reported herein. All authors have read and agreed to the published version of the manuscript.

Funding: This study was supported by Nutraviv S.r.l., which provided the ABA-containing food supplement and ABAMET[®] tested in the clinical studies and by the University of Genova (FRA).

Acknowledgments: This study was supported in part by the University of Genova (FRA) and by the Italian Ministry of Research (FIRB RBFR1299KO_002).

Conflicts of Interest: M.M. is also the C.E.O. of Nutraviv S.r.l., a University spin-off whose mission is the development of nutraceuticals; L.S., L.G., S.S., G.B., C.F. and E.Z. declare no conflicts of interest.

References

1. Hey, S.J.; Byrne, E.; Halford, N.G. The interface between metabolic and stress signalling. *Ann. Bot.* **2010**, *105*, 197–203. [[CrossRef](#)]
2. Cutler, S.R.; Rodriguez, P.L.; Finkelstein, R.R.; Abrams, S.R. Abscisic acid: Emergence of a core signaling network. *Ann. Rev. Plant Biol.* **2010**, *61*, 651–679. [[CrossRef](#)]
3. Le Page-Degivry, M.T.; Bidard, J.N.; Rouvier, E.; Bulard, C.; Lazdunski, M. Presence of abscisic acid, a phytohormone, in the mammalian brain. *Proc. Natl. Acad. Sci. USA* **1986**, *83*, 1155–1158. [[CrossRef](#)]
4. Togashi, K.; Hara, Y.; Tominaga, T.; Higashi, T.; Konishi, Y.; Mori, Y.; Tominaga, M. TRPM2 activation by cyclic ADP-ribose at body temperature is involved in insulin secretion. *EMBO J.* **2006**, *25*, 1804–1815. [[CrossRef](#)]

5. Leckie, C.P.; McAinsh, M.R.; Allen, G.J.; Sanders, D.; Hetherington, A.M. Abscisic acid-induced stomatal closure mediated by cyclic ADP-ribose. *Proc. Natl. Acad. Sci. USA* **1998**, *95*, 15837–15842. [[CrossRef](#)] [[PubMed](#)]
6. Zocchi, E.; Carpaneto, A.; Cerrano, C.; Bavestrello, G.; Giovine, M.; Bruzzone, S.; Guida, L.; Franco, L.; Usai, C. The temperature-signaling cascade in sponges involves a heat-gated cation channel, abscisic acid and cyclic ADP-ribose. *Proc. Natl. Acad. Sci. USA* **2001**, *98*, 14859–14864. [[CrossRef](#)]
7. Zocchi, E.; Basile, G.; Cerrano, C.; Bavestrello, G.; Giovine, M.; Bruzzone, S.; Guida, L.; Carpaneto, A.; Magrassi, R.; Usai, C. ABA- and cADPR-mediated effects on respiration and filtration downstream of the temperature-signaling cascade in sponges. *J. Cell Sci.* **2003**, *116*, 629–636. [[CrossRef](#)] [[PubMed](#)]
8. Puce, S.; Basile, G.; Bavestrello, G.; Bruzzone, S.; Cerrano, C.; Giovine, M.; Arillo, A.; Zocchi, E. Abscisic acid signaling through cyclic ADP-ribose in hydroid regeneration. *J. Biol. Chem.* **2004**, *279*, 39783–39788. [[CrossRef](#)] [[PubMed](#)]
9. Bruzzone, S.; Moreschi, I.; Usai, C.; Guida, L.; Damonte, G.; Salis, A.; Scarfi, S.; Millo, E.; De Flora, A.; Zocchi, E. Abscisic acid is an endogenous cytokine in human granulocytes with cyclic ADP-ribose as second messenger. *Proc. Natl. Acad. Sci. USA* **2007**, *104*, 5759–5764. [[CrossRef](#)] [[PubMed](#)]
10. Magnone, M.; Sturla, L.; Jacchetti, E.; Scarfi, S.; Bruzzone, S.; Usai, C.; Guida, L.; Salis, A.; Damonte, G.; De Flora, A.; et al. Autocrine abscisic acid plays a key role in quartz-induced macrophage activation. *FASEB J.* **2012**, *26*, 1261–1271. [[CrossRef](#)] [[PubMed](#)]
11. Bodrato, N.; Franco, L.; Fresia, C.; Guida, L.; Usai, C.; Salis, A.; Moreschi, I.; Ferraris, C.; Verderio, C.; Basile, G.; et al. Abscisic acid activates the murine microglial cell line N9 through the second messenger cyclic ADP-ribose. *J. Biol. Chem.* **2009**, *284*, 14777–14787. [[CrossRef](#)]
12. Bruzzone, S.; Bodrato, N.; Usai, C.; Guida, L.; Moreschi, I.; Nano, R.; Antonioli, B.; Fruscione, F.; Magnone, M.; Scarfi, S.; et al. Abscisic acid is an endogenous stimulator of insulin release from human pancreatic islets with cyclic ADP-ribose as second messenger. *J. Biol. Chem.* **2008**, *283*, 32188–32197. [[CrossRef](#)]
13. Booz, V.; Christiansen, C.B.; Kuhre, R.E.; Saltiel, M.Y.; Sociali, G.; Schaltenberg, N.; Fischer, A.W.; Heeren, J.; Zocchi, E.; Holst, J.J.; et al. Abscisic acid stimulates the release of insulin and of GLP-1 in the rat perfused pancreas and intestine. *Diabetes Metab. Res. Rev.* **2019**, *35*, e3102. [[CrossRef](#)]
14. Bruzzone, S.; Ameri, P.; Briatore, L.; Mannino, E.; Basile, G.; Andraghetti, G.; Grozio, A.; Magnone, M.; Guida, L.; Scarfi, S.; et al. The plant hormone abscisic acid increases in human plasma after hyperglycemia and stimulates glucose consumption by adipocytes and myoblasts. *FASEB J.* **2012**, *26*, 1251–1260. [[CrossRef](#)]
15. Magnone, M.; Ameri, P.; Salis, A.; Andraghetti, G.; Emionite, L.; Murialdo, G.; De Flora, A.; Zocchi, E. Microgram amounts of abscisic acid in fruit extracts improve glucose tolerance and reduce insulinemia in rats and in humans. *FASEB J.* **2015**, *29*, 4783–4793. [[CrossRef](#)]
16. Guri, A.J.; Hontecillas, R.; Si, H.; Liu, D.; Bassaganya-Riera, J. Dietary abscisic acid ameliorates glucose tolerance and obesity-related inflammation in db/db mice fed high-fat diets. *Clin. Nutr.* **2007**, *26*, 107–116. [[CrossRef](#)]
17. Magnone, M.; Emionite, L.; Guida, L.; Vigliarolo, T.; Sturla, L.; Spinelli, S.; Buschiazzi, A.; Marini, C.; Sambuceti, G.; De Flora, A.; et al. Insulin-independent stimulation of skeletal muscle glucose uptake by low-dose abscisic acid via AMPK activation. *Sci. Rep.* **2020**, *10*, 1454. [[CrossRef](#)]
18. Vatner, D.F.; Majumdar, S.K.; Kumashiro, N.; Petersen, M.C.; Rahimi, Y.; Gattu, A.K.; Bears, M.; Camporez, J.P.; Cline, G.W.; Jurczak, M.J.; et al. Insulin-independent regulation of hepatic triglyceride synthesis by fatty acids. *Proc. Natl. Acad. Sci. USA* **2015**, *112*, 1143. [[CrossRef](#)]
19. Uchida, K.; Dezaki, K.; Damdindorj, B.; Inada, H.; Shiuchi, T.; Mori, Y.; Yada, T.; Minokoshi, Y.; Tominaga, M. Lack of TRPM2 impaired insulin secretion and glucose metabolisms in mice. *Diabetes* **2011**, *60*, 119–126. [[CrossRef](#)]
20. Magnone, M.; Leoncini, G.; Vigliarolo, T.; Emionite, L.; Sturla, L.; Zocchi, E.; Murialdo, G. Chronic intake of micrograms of abscisic acid improves glycemia and lipidemia in a human study and in high-glucose fed mice. *Nutrients* **2018**, *10*, 1495. [[CrossRef](#)]
21. Sturla, L.; Mannino, E.; Scarfi, S.; Bruzzone, S.; Magnone, M.; Sociali, G.; Booz, V.; Guida, L.; Vigliarolo, T.; Fresia, C.; et al. Abscisic acid enhances glucose disposal and induces brown fat activity in adipocytes in vitro and in vivo. *Biochim. Biophys. Acta* **2017**, *1862*, 131–144. [[CrossRef](#)]

22. Ameri, P.; Bruzzone, S.; Mannino, E.; Sociali, G.; Andraghetti, G.; Salis, A.; Ponta, M.L.; Briatore, L.; Adami, G.F.; Ferraiolo, A.; et al. Impaired increase of plasma abscisic acid in response to oral glucose load in type 2 diabetes and in gestational diabetes. *PLoS ONE* **2015**, *10*, e0115992. [[CrossRef](#)]
23. Liu, X.; Yue, Y.; Li, B.; Nie, Y.; Li, W.; Wu, W.H.; Ma, L. A G protein-coupled receptor is a plasma membrane receptor for the plant hormone abscisic acid. *Science* **2007**, *315*, 1712–1716. [[CrossRef](#)]
24. Johnston, C.A.; Temple, B.R.; Chen, J.G.; Gao, Y.; Moriyama, E.N.; Jones, A.M.; Siderovski, D.P.; Willard, F.S. Comment on “A G protein coupled receptor is a plasma membrane receptor for the plant hormone abscisic acid”. *Science* **2007**, *318*, 914. [[CrossRef](#)]
25. Klingler, J.P.; Batelli, G.; Zhu, J.K. ABA receptors: The START of a new paradigm in phytohormone signalling. *J. Exp. Bot.* **2010**, *61*, 3199–3210. [[CrossRef](#)]
26. He, C.; Zeng, M.; Dutta, D.; Koh, T.H.; Chen, J.; van der Donk, W.A. LanCL proteins are not Involved in Lanthionine Synthesis in Mammals. *Sci. Rep.* **2017**, *7*, 40980. [[CrossRef](#)] [[PubMed](#)]
27. Landlinger, C.; Salzer, U.; Prohaska, R. Myristoylation of human LanC-like protein 2 (LANCL2) is essential for the interaction with the plasma membrane and the increase in cellular sensitivity to adriamycin. *Biochim. Biophys. Acta* **2006**, *1758*, 1759–1767. [[CrossRef](#)]
28. Sturla, L.; Fresia, C.; Guida, L.; Grozio, A.; Vigliarolo, T.; Mannino, E.; Millo, E.; Bagnasco, L.; Bruzzone, S.; De Flora, A.; et al. Binding of abscisic acid to human LANCL2. *Biochem. Biophys. Res. Commun.* **2011**, *415*, 390–395. [[CrossRef](#)]
29. Cichero, E.; Fresia, C.; Guida, L.; Booz, V.; Millo, E.; Scotti, C.; Iamele, L.; de Jonge, H.; Galante, D.; De Flora, A.; et al. Identification of a high affinity binding site for abscisic acid on human lanthionine synthetase component C-like protein 2. *Int. J. Biochem. Cell Biol.* **2018**, *97*, 52–61. [[CrossRef](#)]
30. Sturla, L.; Fresia, C.; Guida, L.; Bruzzone, S.; Scarfi, S.; Usai, C.; Fruscione, F.; Magnone, M.; Millo, E.; Basile, G.; et al. LANCL2 is necessary for abscisic acid binding and signaling in human granulocytes and in rat insulinoma cells. *J. Biol. Chem.* **2009**, *284*, 28045–28057. [[CrossRef](#)]
31. Fresia, C.; Vigliarolo, T.; Guida, L.; Booz, V.; Bruzzone, S.; Sturla, L.; Bona, M.D.; Pesce, M.; Usai, C.; De Flora, A.; et al. G-protein coupling and nuclear translocation of the human abscisic acid receptor LANCL2. *Sci. Rep.* **2016**, *6*, 26658. [[CrossRef](#)]
32. Boursiac, Y.; L eran, S.; Corratg e-Faillie, C.; Gojon, A.; Krouk, G.; Lacombe, B. ABA transport and transporters. *Trends Plant Sci.* **2013**, *18*, 325–333. [[CrossRef](#)] [[PubMed](#)]
33. Vigliarolo, T.; Zocchi, E.; Fresia, C.; Booz, V.; Guida, L. Abscisic acid influx into human nucleated cells occurs through the anion exchanger AE2. *Int. J. Biochem. Cell Biol.* **2016**, *75*, 99–103. [[CrossRef](#)]
34. Bassaganya-Riera, J.; Guri, A.J.; Lu, P.; Climent, M.; Carbo, A.; Sobral, B.W.; Horne, W.T.; Lewis, S.N.; Bevan, D.R.; Hontecillas, R. Abscisic acid regulates inflammation via ligand-binding domain-independent activation of peroxisome proliferator-activated receptor. *J. Biol. Chem.* **2011**, *286*, 2504–2516. [[CrossRef](#)] [[PubMed](#)]
35. Scarfi, S.; Fresia, C.; Ferraris, C.; Bruzzone, S.; Fruscione, F.; Usai, C.; Benvenuto, F.; Magnone, M.; Podest a, M.; Sturla, L.; et al. The plant hormone abscisic acid stimulates the proliferation of human hemopoietic progenitors through the second messenger cyclic ADP-ribose. *Stem Cells* **2009**, *27*, 2469–2477. [[CrossRef](#)]
36. Leber, A.; Bassaganya-Riera, J.; Tubau-Juni, N.; Zoccoli-Rodr iguez, V.; Viladomiu, M.; Abedi, V.; Lu, P.; Hontecillas, R. Modeling the Role of Lanthionine Synthetase C-Like 2 (LANCL2) in the Modulation of Immune Responses to Helicobacter pylori Infection. *PLoS ONE* **2016**, *11*, e0167440. [[CrossRef](#)]
37. Feng, S.; Reuss, L.; Wang, Y. Potential of natural products in the inhibition of adipogenesis through regulation of PPAR  expression and/or its transcriptional activity. *Molecules* **2016**, *21*, 1278. [[CrossRef](#)]
38. Seo, J.B.; Choe, S.S.; Jeong, H.W.; Park, S.W.; Shin, H.J.; Choi, S.M.; Park, J.Y.; Choi, E.W.; Kim, J.B.; Seen, D.S.; et al. Anti-obesity effects of Lysimachia foenum-graecum characterized by decreased adipogenesis and regulated lipid metabolism. *Exp. Mol. Med.* **2011**, *43*, 205–215. [[CrossRef](#)]
39. Xi, X.; Han, J.; Zhang, J.Z. Stimulation of glucose transport by AMP-activated protein kinase via activation of p38 mitogen-activated protein kinase. *J. Biol. Chem.* **2001**, *276*, 4129–41034. [[CrossRef](#)]
40. Armoni, M.; Kritz, N.; Harel, C.; Bar-Yoseph, F.; Chen, H.; Quon, M.J.; Karnieli, E. Peroxisome proliferator-activated receptor-  represses GLUT4 promoter activity in primary adipocytes, and rosiglitazone alleviates this effect. *J. Biol. Chem.* **2003**, *278*, 30614–30623. [[CrossRef](#)]

41. Kubota, N.; Terauchi, Y.; Miki, H.; Tamemoto, H.; Yamauchi, T.; Komeda, K.; Satoh, S.; Nakano, R.; Ishii, C.; Sugiyama, T.; et al. PPAR gamma mediates high-fat diet-induced adipocyte hypertrophy and insulin resistance. *Mol. Cell* **1999**, *4*, 597–609. [[CrossRef](#)]
42. Miles, P.D.; Barak, Y.; He, W.; Evans, R.M.; Olefsky, J.M. Improved insulin-sensitivity in mice heterozygous for PPAR-gamma deficiency. *J. Clin. Investig.* **2000**, *105*, 287–292. [[CrossRef](#)]
43. Rosen, E.D.; Sarraf, P.; Troy, A.E.; Bradwin, G.; Moore, K.; Milstone, D.S.; Spiegelman, B.M.; Mortensen, R.M. PPAR γ is required for the differentiation of adipose tissue in vivo and in vitro. *Mol. Cell* **1999**, *4*, 611–617. [[CrossRef](#)]
44. Lievens, L.; Pollier, J.; Goossens, A.; Beyaert, R.; Staal, J. Abscisic Acid as Pathogen Effector and Immune Regulator. *Front. Plant Sci.* **2017**, *8*, 587. [[CrossRef](#)] [[PubMed](#)]
45. Khorasani, A.; Abbasnejad, M.; Esmaeili-Mahani, S. Phytohormone abscisic acid ameliorates cognitive impairments in streptozotocin-induced rat model of Alzheimer’s disease through PPAR β/δ and PKA signaling. *Int. J. Neurosci.* **2019**, *129*, 1053–1065. [[CrossRef](#)] [[PubMed](#)]
46. Naderi, R.; Esmaeili-Mahani, S.; Abbasnejad, M. Extracellular calcium influx through L-type calcium channels, intracellular calcium currents and extracellular signal-regulated kinase signaling are involved in the abscisic acid-induced precognitive and anti-anxiety effects. *Biomed. Pharmacother.* **2019**, *109*, 582–588. [[CrossRef](#)]
47. Hou, S.T.; Jiang, S.X.; Zaharia, L.I.; Han, X.; Benson, C.L.; Slinn, J.; Abrams, S.R. Phaseic acid, an endogenous and reversible inhibitor of glutamate receptors in mouse brain. *J. Biol. Chem.* **2016**, *291*, 27007–27022. [[CrossRef](#)]



© 2020 by the authors. Licensee MDPI, Basel, Switzerland. This article is an open access article distributed under the terms and conditions of the Creative Commons Attribution (CC BY) license (<http://creativecommons.org/licenses/by/4.0/>).

MDPI
St. Alban-Anlage 66
4052 Basel
Switzerland
Tel. +41 61 683 77 34
Fax +41 61 302 89 18
www.mdpi.com

Nutrients Editorial Office
E-mail: nutrients@mdpi.com
www.mdpi.com/journal/nutrients



MDPI
St. Alban-Anlage 66
4052 Basel
Switzerland

Tel: +41 61 683 77 34
Fax: +41 61 302 89 18

www.mdpi.com



ISBN 978-3-0365-0445-2